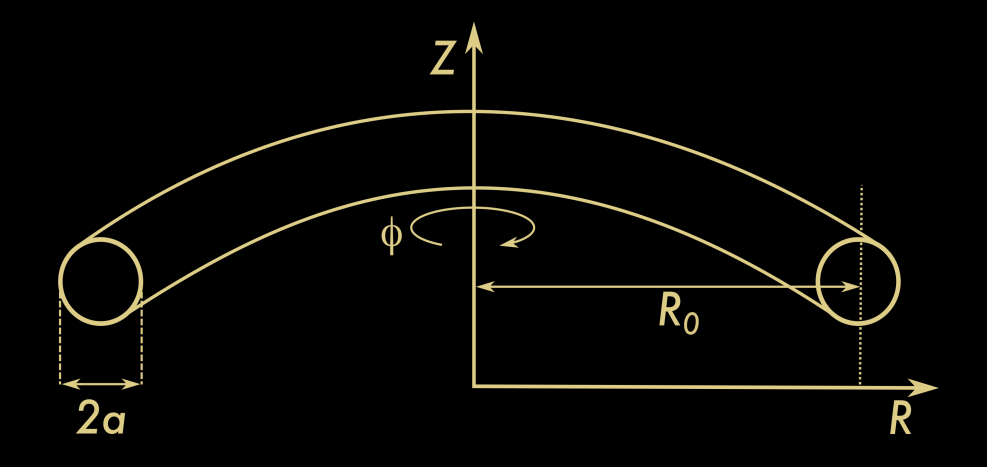
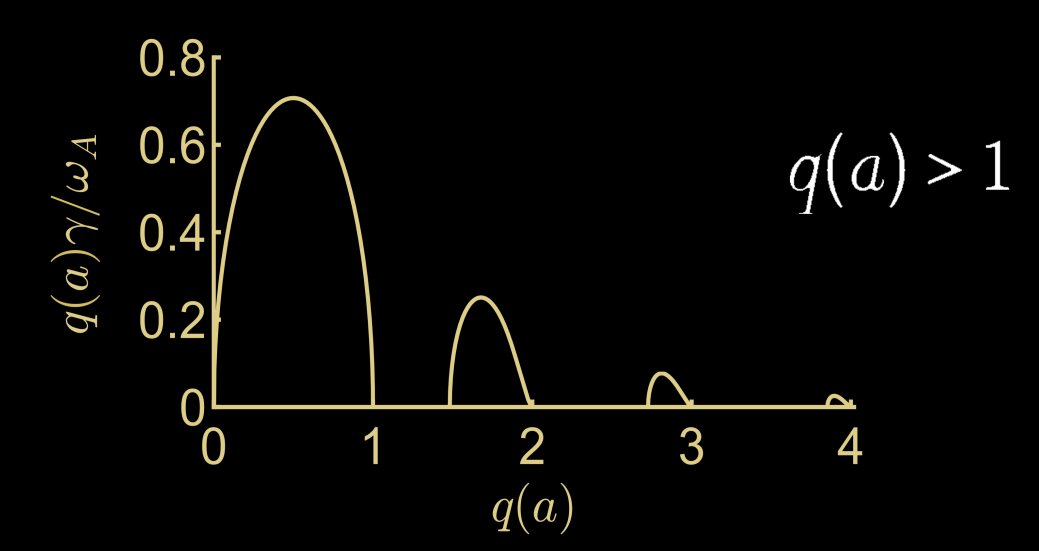
BASICS OF MHD IN TOKAMAKS

$$\Delta^* \psi \equiv R^2 \nabla \cdot \left(\frac{1}{R^2} \nabla \psi \right) = -F \frac{dF}{d\psi} - \mu_0 R^2 \frac{dp}{d\psi}$$



$$\frac{\gamma}{\omega_A} = \frac{\pi}{r_s^2 n s \sqrt{1 + \frac{2}{n^2}}} \int_0^{r_s - \epsilon} r U dr.$$



UKAEA-CCFE-RE(25)03

Daniele BRUNETTI

United Kingdom Atomic Energy Authority

UKAEA-CCFE-RE(25)03

© UKAEA

Report: Basics of MHD in Tokamaks

Contents

Pr	eface	•		ix
Ι	BA	SIC CO	ONCEPTS .	1
1	Nuc	lear fu	sion and plasma confinement	3
	1.1	Funda	mentals on nuclear fusion	3
	1.2	Magn	etic cages	5
		1.2.1	Open and closed systems	5
		1.2.2	Tokamaks	7
2	The	MHD	framework	11
	2.1	Ideal	MHD	11
		2.1.1	Freezing of the magnetic field	14
		2.1.2	Energy conservation	15
		2.1.3	Momentum conservation	15
		2.1.4	The virial theorem	16
	2.2	Resist	ive MHD	17
	2.3	Doma	in of validity of the MHD model	18
	2.4	Advar	nced MHD models	18
		2.4.1	Drift-MHD	19
		2.4.2	Guiding centre plasma	20
3	Cur	vilinea	r coordinate systems	23
	3.1	Gener	al properties	23
		3.1.1	Orthogonal cylindrical coordinates	26
		3.1.2	Orthogonal toroidal coordinates	27
II	EÇ	QUILII	BRIUM	29
4	Tok	amak e	equilibrium	31
•	4.1		etic surfaces, safety factor and plasma β	31
	•	4.1.1	The safety factor q	33
		4.1.2	Plasma β	34
	4.2		Grad-Shafranov equation	35
		4.2.1	The Solov'ev equilibrium	36
	4.3	1	aspect ratio expansion: The plasma solution	37

		4.3.1 ε -ordering	39
		4.3.2 Equilibrium at leading orders	41
		4.3.3 Tyre tube and hoop forces	44
		4.3.4 Equilibrium with local steep gradients	45
		4.3.5 An almost intuitive derivation of the Shafranov shift	
	4.4	Large aspect ratio expansion: The vacuum solution	47
		4.4.1 External vertical field	49
_	Stra	aight field line coordinates	
5	5.1	Higher order tokamak equilibrium	55 56
	5.2	The rectifying parameter	59
	5.3	The metric tensor coefficients	59 61
	5·4	Metric of the $s - \alpha$ equilibrium model	64
II	I <u>I</u>	DEAL STABILITY	67
6	Ger	neral remarks on ideal MHD stability	69
Ū	6.1	Linearised MHD	70
	0.1	6.1.1 Boundary conditions in linearised MHD	70 71
		6.1.2 Eigenvalue properties	72
		6.1.3 Self-adjointness of the force operator F	73
	6.2	Parallel gradient and magnetic shear	75
	6.3	Mode coupling	77
7	Die	tilled stability equations	70
/	7.1	Convenient form of the linearised MHD equations	79 80
	7.2	Orderings	81
	/	7.2.1 Equilibrium	82
		7.2.2 Perturbations	82
	7.3	Auxiliary quantities: Global modes	85
	7.0	7.3.1 Behaviour far from resonance	85
		7.3.2 Layer ordering	88
	7.4	Auxiliary quantities: Localised modes	90
	, 1	7.4.1 Small scale modes far from resonances	90
		7.4.2 The inertial layer of small scale modes	91
	7.5	General form of the eigenmode equations	92
	, 0	7.5.1 Equation for the main mode	93
		7.5.2 Equations for the neighbouring sidebands	97
8	The	m = 1 internal kink mode	99
	8.1	The general form of the growth rate	
		8.1.1 Inertia enhancement	
	8.2	Equations for the satellite harmonics	
		8.2.1 Lower $\ell = 0$ sideband	
		8.2.2 Upper $\ell = 2$ sideband	
		8.2.3 Integrations across a point	

	0	C C'S TI	
	8.3	Evaluation of $\int_0^{r_s} r U_{TC} dr$	
	8.4	Integrals involving the function U_0	
	8.5	The stability criterion	
	8.6	The $m = 1$ internal kink with a hollow $q \ldots \ldots \ldots$	115
9	Infe	rnal modes	119
J	9.1	High-shear region equations	•
	9.2	Low-shear region equations	
	J	9.2.1 Sidebands	
		9.2.2 Dominant harmonic	
	9.3	The dispersion relation	
	9.4	Infernal modes with a reversed $q > 1 \dots \dots$	
	9.5	Hybrid kink—infernal perturbations	
10	Exte	ernal kinks	133
		Eigenmode equations	
		Necessary condition for instability	
		Marginal boundaries	
	U	10.3.1 $m = 1$ external kinks	
		10.3.2 $m \ge 2$ external kinks	
	10.4	Growth rates	
11	Mer	cier modes	143
		Eigenmode equation	
		The Mercier stability criterion	
		Dispersion relation and growth rate	
10	Rall	ooning modes	1
12		The ballooning equation	155
	12.1	12.1.1 Extending to the $s-\alpha$ equilibrium	
	10.0	Fourier space representation	
		The small shear case	_
		The large shear case	
	12.4	The large shear case	109
IV	<u>R</u> .	ESISTIVE STABILITY	17 3
19	Resi	stive MHD in tokamaks: the basics	175
-3		Fundamental equations	
		Where resistivity matters	
		Resistive layer orderings	
		Solution of the resistive layer equations	
14	Теат	ring modes	189
-4		The reconnected flux	•
		The tearing equation	
		Eigenfunction and growth rate for the step current model	
	44.5	Engomenton and growin rate for the Step current fillout	-411

C General proof of the self-adjointness of the ideal MHD for operator	r <mark>ce</mark> 260
B Tokamak GCP equilibrium	263
A Particle motion in a tokamak-like magnetic field	257
V APPENDICES	255
17.5.3 Tearing modes	. 250
17.5.2 Resistive interchange modes	
17.5.1 $m = 1$ resistive kink	
17.5 Stability criteria modified by curvature	
17.4 The eigensolution	
17.3.2 Vorticity equation	
17.3.1 Induction equation	_
17.3 The resistive layer equations	
17.2.3 Perturbed pressure	_
17.2.2 Poloidal and toroidal displacements	
17.2.1 Perturbed magnetic field	
17.2 Fields, displacements and pressure	_
17.1 Toroidal layer orderings	. 234
17 Curvature effects in the resistive layer	233
16.3.3 Growth rate and stability boundary	. 229
16.3.2 $k \gg 1$ eigenfunction	
16.3.1 $k \lesssim 1$ eigenfunction	
16.3 Resistive interchange modes	_
16.2.2 The growth rate	
16.2.1 The eigenmode equation	
16.2 Resistive ballooning modes	
16.1 Governing equations	
16 Localised resistive instabilities	217
	, 212
solutions	
15.1.4 On the relative amplitude of the even and odd	
15.1.3 The $m = 1$ reconnecting mode	_
15.1.2 The $m = 1$ resistive internal kink	
15.1.1 The ideal limit	
15.1 The dispersion relation	
15 The $m = 1$ resistive mode	205
14.5 2 caste teating medes 1 1 1 1 1 1 1 1 1 1 1 1 1 1 1 1 1 1 1	00
14.5 Double tearing modes	_
profiles	
14.4 The numerical solution of the tearing equation for generic	3

D	The screw-pinch eigenmode equation	275
E	External kinks in a cylinder with a resistive wall	281
F	A more general derivation of the resistive layer equations	285
Sy	mbols	293
Su	mmary table for internal ideal MHD	297
Inc	dex	301

Preface

The goal of this report is to provide the basic analytic tools necessary to describe magnetohydrodynamic (MHD) instabilities in toroidally symmetric devices known as tokamaks.

Although an extensive literature is available on the subject, it is quite difficult to find a thorough explanation of the mathematical techniques employed in MHD tokamak physics. Some of the fundamental results are often only briefly mentioned, and their derivation is usually referred either to the original works, or to very few highly technical references, which, most of the times due to the compactness of the exposition, are a very challenging reading. This, combined with the fact that at times some topics are better developed in certain references than others, results in a rather fragmented literature typically scattered over several books or research articles.

Hence, my hope with this report is to present in an unified and clear manner such techniques, detailing the derivation of some of the relevant results in tokamak MHD without omitting the salient mathematical steps involved. In some instances the mathematical manipulations do not follow the standard textbook approaches but, in my personal opinion, have the advantage to being more transparent in terms of logical methodology and applicability. I also tried to emphasize the connection between theory and experiment: a short mention to an experimentally observed phenomenon, stressing the relevance/motivation behind the development of the theory, is usually given.

The report is divided into four main parts. In the first part I give a very brief account of the tokamak device, with a discussion on the physical model and the mathematical tools used to describe the macroscopic plasma dynamics in curved geometries. In the second part, the theory of tokamak equilibrium is developed. The third and fourth parts are dedicated to the exposition of the linear stability properties within the ideal and resistive MHD frameworks respectively. The list of the MHD instabilities treated in this report is not exhaustive. These however have been chosen in such a way that many of the MHD phenomena observed in experiments can either be interpreted by combining appropriately the results here discussed, or analysed by using the mathematical techniques we present. The appendices include optional material (not strictly necessary for the comprehension of the main text), and some technical derivations which resulted to be too heavy to be included in the main body of

the report. *Boxes* in chapters contain some physical or mathematical highlights.

Despite the fact that there has been a tremendous effort in the last decades in the development of numerical tools for the analysis of MHD equilibrium and stability in toroidal devices, this subject, although proven to be of great importance for the understanding of tokamak behaviour, is not discussed apart from very few instances. More advanced topics such as multi-fluid effects, the interaction of global instabilities with highly energetic particles, or non-linear behaviours are not addressed either.

We employ the International System of Units (SI) as system of measurement. In the stability calculation however, we will normalise the vacuum permeability to unity. It is not uncommon to use the same symbol with different meanings. However, the meaning of the symbol, unless made explicit, should be clear from the context.

This report is intended for a graduate and post-graduate audience. Basic results in magnetohydrodynamics are assumed to be known as well as some knowledge of Fourier transform, special functions, asymptotic analysis and matching theory. Familiarity with MHD theory in cylindrical confinement systems, namely pinches, is highly desirable.

Culham, 12th May 2025.

Part I BASIC CONCEPTS

1

Nuclear fusion and plasma confinement

This short chapter introduces the fundamental concepts of nuclear fusion and plasma confinement. Particular emphasis is given to the description of the main components of the *tokamak* device (from the Russian acronym for toroidal chamber with magnetic coils) which is one of the most promising configurations for achieving controlled thermonuclear fusion, and whose dynamics (from the macroscopic plasma point of view) is the subject of this report.

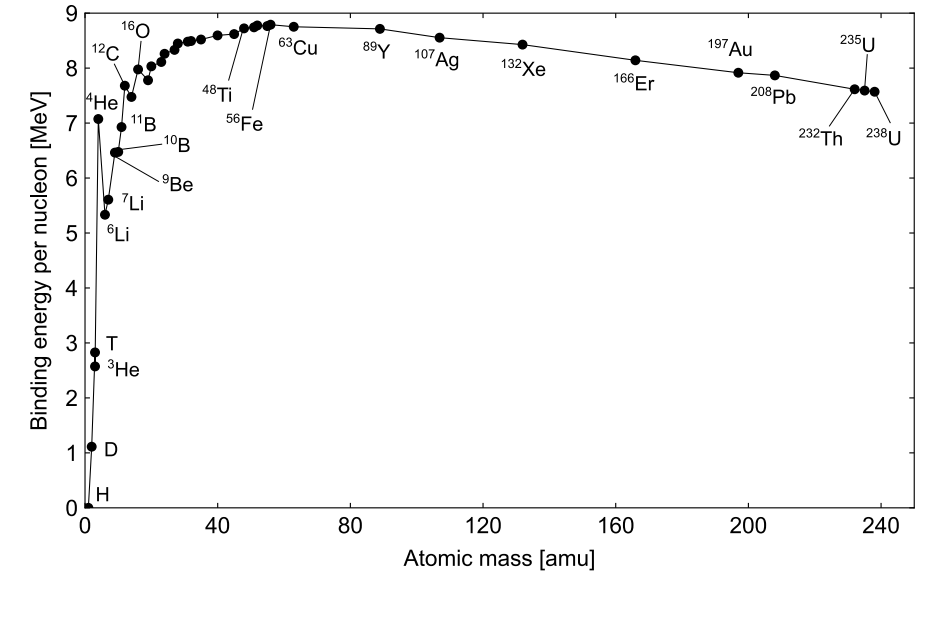
1.1 Fundamentals on nuclear fusion

Contrarily to nuclear fission, in which a heavy nucleus breaks up into two lighter ones, nuclear fusion is a reaction in which two or more atomic nuclei combine to form heavier elements. Let us introduce the average binding energy per nucleon (denoted by B/A), i.e. the energy required to separate an atomic nucleus completely into its constituent protons and neutrons. Energy is released, either from fission or fusion, when the final products of the nuclear reaction have larger B/A than the reacting nuclei (see figure 1.1).

Nuclear fusion releases million times more energy than a chemical reaction (e.g. from burning coal, oil or gas) and four times as much as nuclear fission reactions (at equal mass). Therefore it has the potential to be a sustainable and abundant energy source, with no greenhouse gas emissions and modest radioactive waste production. Although nuclear fusion regularly occurs in the universe, as it powers most of the stars in the sky, reproducing the process in a **controlled way** has been proven to be extraordinarily difficult.

Of all the many possible fusion reactions (cf. Fig. 1.2), the most

Figure 1.1: Nuclear binding energy curve. Generally, energy is released by the nuclear fusion process when atomic nuclei lighter than iron-56 or nickel-62 are produced.



promising to be used in a reactor, that is the one with the largest cross-section and therefore probability to occur at lower temperatures, is the reaction between Deuterium (D) and Tritium (T):

$$D + T \rightarrow {}^{4}He(3.5MeV) + {}^{1}n(14.1MeV).$$

The released energy is contained in the kinetic energy of the reaction products, namely an *alpha* particle (4 He) and a neutron (1n). Deuterium is plentiful on Earth, and Tritium can be obtained from nuclear capture of a neutron by an atom of either 6 Li or 7 Li (both of which are abundant elements)

$$^{1}n + ^{6}\text{Li} \rightarrow \text{T} + ^{4}\text{He} + 4.8\text{MeV},$$
 $^{1}n + ^{7}\text{Li} \rightarrow \text{T} + ^{4}\text{He} + ^{1}n - 2.5\text{MeV}.$

In order to overcome the mutual Coulomb repulsion, and therefore to have an appreciable probability of undergoing fusion, the D and T positively charged nuclei must be heated to a sufficiently large temperature. At such temperatures, D and T atoms are stripped of their electrons and a **plasma** is formed. Furthermore, to reach the so called **ignition** condition, in which the plasma temperature is maintained at a steady level only by the internal heating generated by the helium particles, the rate of energy production has to be higher than the rate of loss, and enough of that energy must be captured by the system. This condition is expressed by the **Lawson criterion** which, for plasma temperatures in the range of 10-20 keV, takes the form¹

$$n\tau_E T \gtrsim 3 \times 10^{21} m^{-3} skeV$$

where n and T are the plasma density and temperature, and τ_E is the energy confinement time defined as the ratio of the plasma stored energy W over the rate of energy loss P_L ($\tau_E = W/P_L$). The quantity on the left-hand-side of the Lawson criterion is know as **fusion triple product**. For

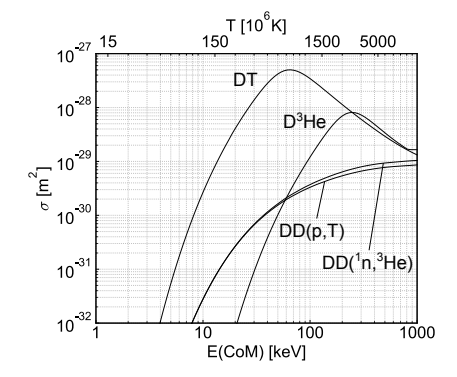


Figure 1.2: Fusion cross sections, as a function of the energy of the centre of mass, for the reactions D-T, D- 3 He and D-D (with the two D-D branches). The letters in brackets indicate the reaction products, p for proton and 1n for neutron.

¹ This condition is achieved for e.g. $n = 10^{20} m^{-3}$, T = 10 keV, $\tau_E = 3 s$.

temperatures in the range of some tens of keV, the ignition condition expressed by the Lawson criterion states that the plasma, i.e. the nuclear fuel, has to be confined either for long times at low density, or for short times at high density. The latter approach is pursued by the so called inertial confinement schemes which mainly use lasers for fuel heating and compression, whereas the former by magnetic confinement approaches, in which the plasma is trapped by powerful magnetic fields. The table below summarises the orders of magnitude for temperature, density and confinement times for magnetic confinement fusion (MCF) and inertial confinement fusion (ICF) approaches.

	MCF	ICF
T	10~keV	10~keV
n	$10^{20} \ m^{-3}$	$10^{31} \ m^{-3}$
$ au_E$	1 <i>s</i>	$10^{-10} \ s$

The difficult part in nuclear fusion research is keeping the fuel in the plasma state hot and dense enough for the required time (tokamak experiments reached a fusion triple product of the order of $\sim 1 \times$ $10^{21} m^{-3} skeV$). This report focusses on a specific MCF device, namely the tokamak, and the following sections will provide a brief introduction to the main ideas underlying the magnetic confinement approach.

Magnetic cages

Open and closed systems

Magnetic confinement relies on the application of strong fields in order to enclose the hot plasma in a magnetic bottle. Since currents flowing in the plasma cannot self-confine the plasma itself (this is a consequence of the virial theorem which is discussed in the next chapter), these fields must be applied externally.

Due to the Lorentz force, to lowest approximation, a charged particle with velocity v undergoing the effect of external electric and magnetic fields gyrates along the line of force, being essentially "glued" to the field lines. Several concepts have been developed during the past fifty years based on this basic idea, with the two main families of magnetic confinement devices grouped in the so called open configurations and closed configurations.

The basic design of open configurations, known as magnetic mirrors (or simply mirrors), consists of two parallel coils which carry the same current in the same direction separated by a small distance, producing a magnetic bottle between them (see Fig. 1.3) with an increased density of magnetic field lines near the coils region. From orbit theory, in absence

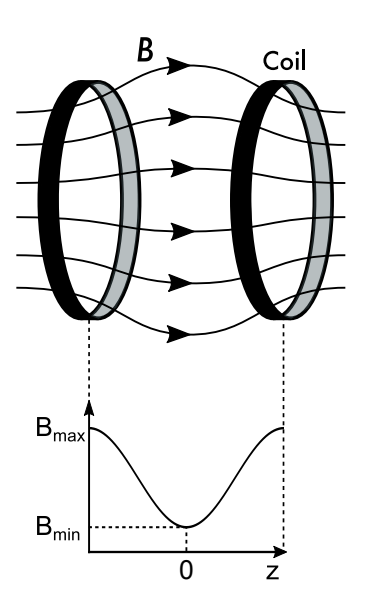


Figure 1.3: Magnetic mirror geometry.

of electric fields one has for the energy $\mathscr E$ and magnetic moment μ of a particle of mass m_s and charge e_s

$$\mathscr{E} = \frac{1}{2}m_s v_{||}^2 + \mu B = const, \quad \mu = \frac{m_s v_{\perp}^2}{2B} = const, \quad (1.1)$$

where v_{\perp} and $v_{||}$ denote, respectively, the perpendicular and parallel particle velocity to the magnetic field of strength B. The invariance of the magnetic moment holds, with a good degree of accuracy, even if electric fields are present. These relations are exact to leading order in the particle **gyro-radius** $r_{L,s} = m_s v_{\perp}/(e_s B)$ (also known as **Larmor radius**),² and $v_{||}$ is in first approximation the parallel velocity of the **guiding centre**, that is the point at the centre of the circle about which the particle gyrates.

Because of energy and magnetic moment conservation, particles near the coils where the magnetic field is stronger drop their parallel velocity and eventually bounce back towards the plasma centre. The reflection of the sign of $v_{||}$ arises from the force due to the parallel gradient of the magnetic field which, in case of a vanishing electric field, determines the parallel motion:

$$m_s \frac{dv_{||}}{dt} = -\mu \frac{\boldsymbol{B} \cdot \boldsymbol{\nabla} B}{B}.$$
 (1.2)

The force on the right-hand-side increases as ∇B increases and is independent of the particle charge, hence is the same for both ions and electrons. Particles with appropriate speeds spiral repeatedly back and forth from one end to the other.³

For a particle with energy \mathscr{E} and moment μ , the mirror field, which is required to be smaller than the maximum one (B_{\max}) , is

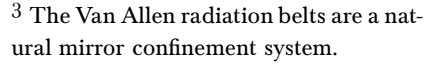
$$B_{\text{mirror}} = \frac{\mathscr{E}}{\mu} < B_{\text{max}}, \quad \text{or} \quad \frac{\mathscr{E}}{B_{\text{max}}} < \mu.$$
 (1.3)

Referring to figure 1.3, at z=0 we have $\mu=m_s v_\perp^2/(2B_{\min})$ so that we find that mirror configurations cannot confine particles which have

$$\left|\frac{v_{||}}{v_{\perp}}\right| > \sqrt{\frac{B_{\max}}{B_{\min}} - 1}.$$

This relation, known as **mirror criterion**, identifies the so called **particle loss cones**, i.e. regions in the velocity space for which particles that are lying inside are not reflected within the ends of the magnetic bottle (see Fig. 1.4).

These particle losses along the field lines can be eliminated by *closing* the system. Closed configurations typically have a shape which resembles the one of a doughnut and are characterised by a strong longitudinal field. Examples of closed configurations include tokamaks and reversed field pinches (RFPs), both of which are symmetric in the longitudinal direction,⁴ and stellarators, which instead exhibit helical symmetry. The material discussed in this report will be focusing on tokamaks.



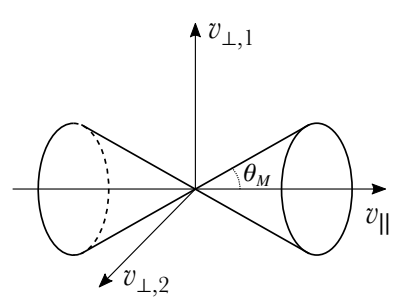
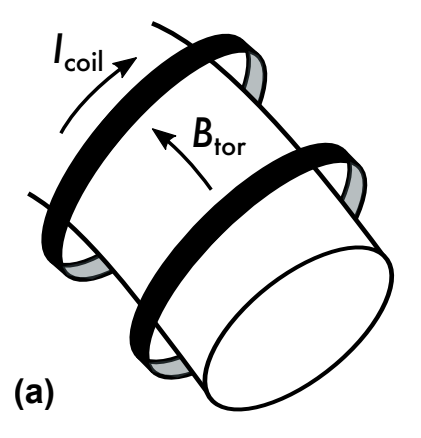


Figure 1.4: Geometry of the magnetic mirror loss cones in the velocity space. Particles with a pitch angle in velocity space less than $\theta_M = \arctan(v_\perp/v_{||})$ are lost.

² That is the radius of the particle gyration around the magnetic field.

⁴ In real experiments perfect axisymmetry is never fully achieved due to inhomogeneities induced by external structures such as coils, vessel components, etc.



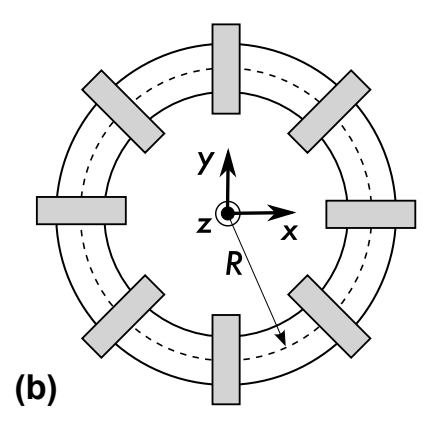


Figure 1.5: Toroidal magnetic field and toroidal field coil geometry. (a) sideview, (b) top-view.

1.2.2 **Tokamaks**

A tokamak device, which confines a toroidally symmetric doughnutshaped plasma in a vacuum vessel, consists essentially of four major elements:

- toroidal field coils,
- iron core (or solenoid in modern machines),
- external heating systems,
- · poloidal field coils.

We shall now briefly describe the purpose of each of these components.

The current flowing in the coils linking the plasma (see Fig. 1.5-(a)) produces the longitudinal (or **toroidal**) magnetic field denoted by B_{tor} . From Ampére's law, taking the line integral along a circuit inside the coils as indicated by the dashed line in figure 1.5-(b) shows that such a field decays proportionally to 1/R, where R is the radial distance from the symmetry axis. The outer midplane where the field is weaker is usually referred to as **low-field-side**, while the inner region where B is stronger is called **high-field-side**. With **stationary** but spatially inhomogeneous B and weak E, the equation of motion for the position vector r of the **guiding centre** of a particle with charge e_s and mass m_s is

$$\frac{d\mathbf{r}}{dt} = v_{||}\frac{\mathbf{B}}{B} + \frac{\mathbf{E} \times \mathbf{B}}{B^2} + \frac{m_s v_{\perp}^2}{2e_s B^3} \mathbf{B} \times \nabla B + \frac{m_s v_{||}^2}{e_s B^4} \mathbf{B} \times (\mathbf{B} \cdot \nabla \mathbf{B}). \tag{1.4}$$

Apart from the contribution parallel to the magnetic field, the righthand-side of (1.4) is composed of three drifts: the $E \times B$ -drift

$$v_{E\times B}=rac{E\times B}{B^2},$$

the ∇B -drift

$$\boldsymbol{v}_{\boldsymbol{\nabla}B} = \frac{m_s v_{\perp}^2}{2e_s B^3} \boldsymbol{B} \times \boldsymbol{\nabla}B,$$

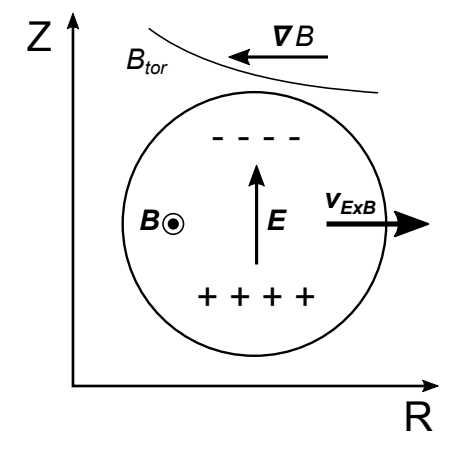


Figure 1.6: ∇B drift induced electric field, and corresponding outward $E \times B$ drift.

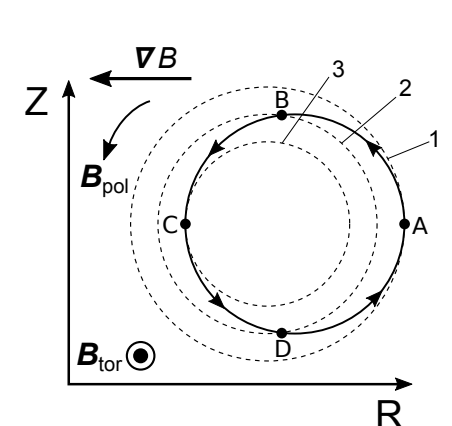


Figure 1.7: Qualitative ion projected trajectory in the presence of a helical field. Starting off from point A on surface 1, the particle moving along the field line undergoes a downward shift crossing the surface 2 at B. As the particle keeps its helical trajectory, it will meet surface 3 at point C (downward shift with respect to surface 2). Continuing in its path, the ion crosses surface 2 again in D (downward shift with respect to 3), and finally will return at point A.

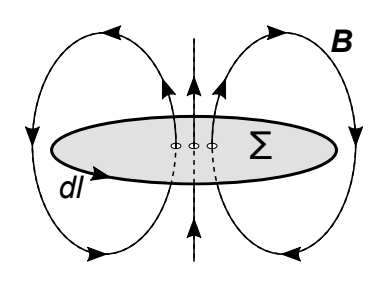


Figure 1.8: Schematic representation of the current induction in a tokamak due to a varying field generated by a central solenoid: from Faraday's law, a time varying magnetic field flux through the surface Σ induces a linking electric field. A plasma current then appears due to Ohm's law.

and the curvature drift

$$v_{\text{curv}} = \frac{m_s v_{||}^2}{e_s B^4} \boldsymbol{B} \times (\boldsymbol{B} \cdot \nabla \boldsymbol{B}).$$

With E=0 and a purely toroidal magnetic field ($\nabla \times B=0$), the particle experiences a vertical motion due to the ∇B and curvature drifts. These depend on the particle charge, and because ions will drift in the opposite direction with respect to electrons, this motion produces charge separation. As a consequence, an electric field is generated, and its interaction with the toroidal field drives a further drift, the $E \times B$ one. Contrarily to the ∇B or curvature drifts, this is independent of the electric charge so that is the same for both ions and electrons. Since it points in the outward direction along R, this drift keeps expanding the plasma eventually leading to its loss (see figure 1.6). Therefore, the toroidal field alone is not sufficient to confine the particles, and an additional field in the poloidal direction $B_{\rm pol}$ must be added.

With this supplementary poloidal field, usually much smaller than the longitudinal one $(B_{\rm pol} \ll B_{\rm tor})$, the magnetic field lines become helical, winding around the plasma and lying on nested surfaces. The particles which gyrate around the field lines, slowly drift vertically up and down. An intuitive pictorial explanation of this behaviour is depicted in Fig. 1.7, while a more detailed, although not exhaustive, analysis of the particle motion in a complex magnetic field is given in appendix A. Charge separation is therefore prevented and individual particles are confined. The additional poloidal field is sustained by letting a current, usually denoted by I_p , flowing in the plasma along the longitudinal direction. To generate this current old tokamaks used an iron core with the plasma acting as the secondary winding of the transformer: by varying a current in the primary winding, a plasma current is induced. Modern machines employ a central solenoid to generate the magnetic flux change needed to initiate the plasma current (see Fig. 1.8). A diagram of a tokamak configuration, showing the direction of the poloidal and toroidal fields with the associated sustaining currents and the iron core, is depicted in figure 1.9.

The plasma current, apart from generating the poloidal field required for particle confinement, also serves as a heating source. Indeed, since the plasma is not a perfect conductor, as it has a finite resistivity, it can be heated-up by the flowing current thanks to the Joule effect. This is known as **Ohmic heating**. The power of heating P_H generated by the current I_P is

$$P_H = R_p I_p^2,$$

where R_p is the plasma resistance. However, as the plasma temperature T increases, the plasma resistivity (and thus its resistance) decreases, typically with a dependence of the form $T^{-3/2}$ (more details on this will be given in §2.2 and chapter 13). Therefore, the Ohmic heating

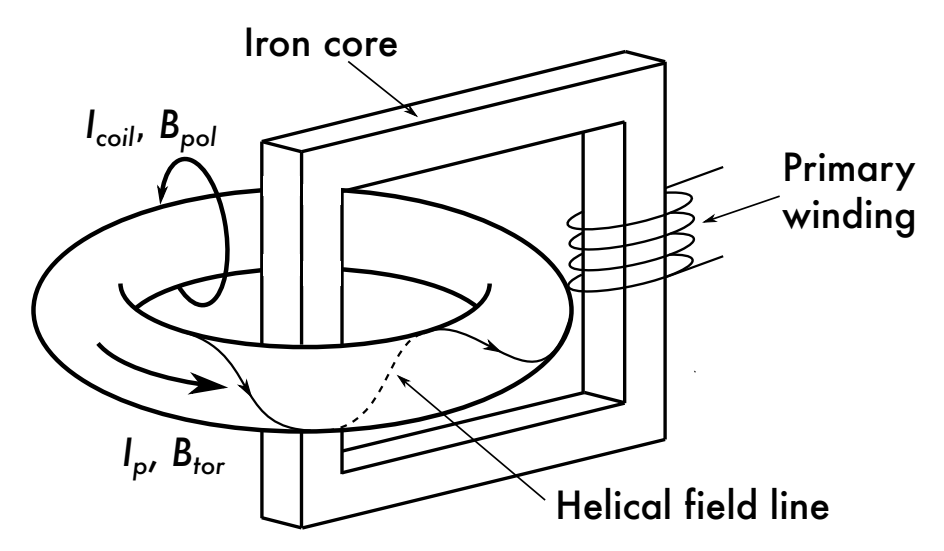


Figure 1.9: Diagram of a tokamak with an iron core. A varying current in the primary winding creates a varying magnetic flux. This induces a current I_P in the secondary winding (the plasma itself), and in turn generates the poloidal magnetic field $B_{\rm pol}$. The toroidal field B_{tor} is sustained by a poloidally flowing current in the toroidal coils (cf. Fig. 1.5).

becomes gradually less effective, and eventually negligible at sufficiently high plasma temperatures. This means that the heat transferred through the plasma current is limited to a defined level. If the temperatures required to sustain thermonuclear fusion conditions are much larger than those achieved by Ohmic heating alone, additional means of heating are required to reach the threshold where fusion can occur: these include the injection of electromagnetic waves (RF, from radio-frequency) or energetic neutral particles (NBI, from neutral beam injection).

The last element which is essential for tokamak operation is the set of coils mounted around the exterior of the mechanical shell, i.e. the vessel in which the plasma is contained. These coils, known as poloidal field coils, are used to control the plasma position (both horizontal and vertical) and shape (the latter has a strong impact on plasma stability). They also provide the vertical field required to maintain the radial force balance. A more detailed discussion on the plasma tendency to expand radially is given in chapter 4. A sketch of the positioning of vacuum vessel, toroidal and poloidal field coils (including the primary winding or central solenoid) is shown in figure 1.10.

This concludes our brief description of the main elements and key features which characterise the tokamak device. In the next chapter we shall focus our attention on the physical models employed for describing the very core of the tokamak, i.e. the superheated gas contained in the magnetic cage.

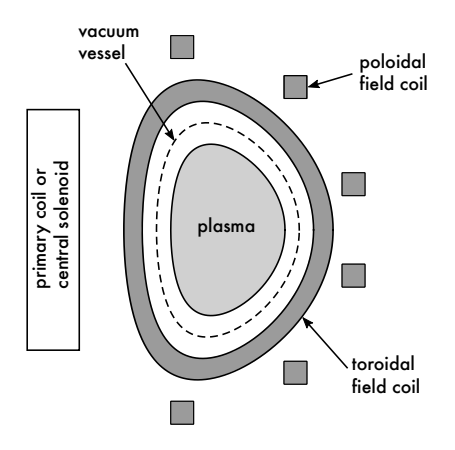


Figure 1.10: External coils positioning in a tokamak.

References

- L. A. Artsimovitch, **A Physicist's ABC on Plasma**, Mir Publishers (Moscow, USSR), 1978.
- S. Atzeni & J. Meyer-ter-Vehn, Physics of Inertial Fusion: Beam Plasma Interaction, Hydrodynamics, Hot Dense Matter, Oxford University Press (Oxford, UK), 2009.
- J. P. Freidberg, **Ideal MHD**, Cambridge University Press (Cambridge, UK), 2014.
- P. Helander and D. J. Sigmar, Collisional Transport in Magnetized Plasmas, Cambridge University Press (Cambridge, UK), 2005.
- J. D. Lawson, Proc. Phys. Soc. B 70, 6 (1957).
- A. I. Morozov and L. S. Solov'ev, Reviews of Plasma Physics Vol. 2 p. 201 (Ed. M. A. Leontovich), Consultants Bureau (New York, US), 1966.
- J. A. Wesson, Tokamaks, Oxford University Press (Oxford, UK), 2011.

The MHD framework

The main goal of this chapter is to provide the essential information on the magnetohydrodynamic (MHD) model. This consists of a set of fluid equations coupled to Maxwell equations. Despite its mathematical simplicity, it is capable of describing a large variety of phenomena observed in experiments, and therefore is widely used in modelling the dynamics of tokamak plasmas. We do not attempt to present a complete and detailed derivation of the MHD equations, for which the reader is referred to other excellent sources listed at the end of this chapter. Rather, we outline which are the main steps and ideas involved in the derivation of the magnetohydrodynamic equations, and provide an intuitive discussion about the physical consequences and limitations associated with this framework. Some more advanced beyond-MHD models, which are of interest in tokamak physics, are also briefly presented.

2.1 Ideal MHD

The MHD model gives a description of the long-wavelength and low-frequency dynamics of a macroscopic single fluid plasma. Faster phenomena associated with smaller length-scales¹ are not captured by the MHD equations. For these dynamics different approaches are needed, which however are not discussed in this report.

The starting point of the derivation of the MHD model are the microscopic kinetic equations. The plasma kinetic description is based upon the concept of **distribution function**. We associate to each particle species labelled by s, e.g. electrons and ions, a different distribution function f_s . This function, which is defined in a 7-dimensional space (3 spatial coordinates, 3 velocity coordinates plus time), gives the number

Unless otherwise specified, the time dependence will always be denoted by the variable t.

¹ These are typically associated with micro-instabilities, whose non-linear evolution determines energy and particle transport.

of particles of the species s per m³ at position x and time t with velocity components between v_x and $v_x + dv_x$, v_y and $v_y + dv_y$, v_z and $v_z + dv_z$ (here the triplet (x, y, z) indicates the familiar Cartesian coordinates) through the relation

$$f_s(x, y, z, v_x, v_y, v_z, t) dv_x dv_y dv_z$$
.

Its time evolution obeys the Boltzmann kinetic equation

$$\frac{\partial f_s}{\partial t} + \boldsymbol{v} \cdot \boldsymbol{\nabla} f_s + \frac{\boldsymbol{F}}{m} \cdot \frac{\partial f_s}{\partial \boldsymbol{v}} = \left(\frac{\partial f_s}{\partial t}\right)_c,$$

where F is the force acting on particles and $(\partial f_s/\partial t)_c$ is the time rate of change of f_s due to collisions. When collisions are ignored and forces between particles are electromagnetic, the equation above takes the name of **Vlasov equation**. Thus, in order to solve the evolution of the electric and magnetic fields, we must couple the Boltzmann/Vlasov equation to Maxwell's equations. For the sake of simplicity, we assume a fully ionised globally neutral plasma consisting of electrons and positive hydrogen or isotopes ions with charge number $Z_i = 1$. As a matter of notation the subscript e(i) refers to electron(ion) related quantities.

The fluid variables of each species s such as e.g. particle density $n_s(x,t)$ and fluid velocity $u_s(x,t)$ are defined as the integral over the velocity space of the product of f_s with a function $\phi(v)$ of the microscopic velocity v, that is

$$n_s(\mathbf{x},t) = \int f_s(\mathbf{x},v,t)d^3v,$$

$$n_s(\mathbf{x},t)\mathbf{u}_s(\mathbf{x},t) = \int f_s(\mathbf{x},v,t)vd^3v.$$

These are called **moments** of the distribution function f_s . The temporal evolution of these moments is obtained by multiplying the Boltzmann equation by the function $\phi(v)$ and then integrating it over the microscopic velocity variables v. This yields a set of equations for each species s which are usually referred to as the **multi-fluid** equations. Unfortunately, the system of equations obtained from this procedure is not closed, in that the time evolution of any moment of the distribution function will depend upon the next higher order moments (e.g., the density evolution depends on the flow velocity, the flow velocity evolution depends on the viscosity tensor, etc.). The process in which additional information is used to express the latter quantities in terms of the former yielding a complete set of equations is known as **closure**. There are several types of closures, and one of the simplest involves a truncation in which higher order moments are assumed to vanish, or simply prescribed in terms of lower moments.

In the closure scheme employed for deriving standard MHD, the plasma is assumed to be collisional (fluid limit), so that the pressure tensor becomes isotropic with a negligible heat flux. Furthermore, displacement currents and net charges $(\varepsilon_0 \nabla \cdot E)$ are set to zero in Maxwell's

² In a plasma consisting of electrons and a single ion species this set of equations forms the so called **two-fluid** model.

equations. Neglecting displacement currents implies that the electromagnetic wave phase velocity is much smaller than the speed of light, and the characteristic thermal velocities of ions and electrons are non-relativistic. Neglecting the net charge implies that i) the characteristic frequency of plasma behaviour is much smaller than the plasma frequency ω_{pe} , ii) the plasma characteristic length is much longer than the Debye length λ_D , and iii) the ion and electron number densities are equal i.e. $n_e = n_i = n$. The latter condition is known as **quasineutrality** approximation. As a final assumption electron inertia is neglected, that is $m_e \to 0$ (m_e is the electron mass), and dissipation effects as well.

Thus, after defining macroscopic one-fluid variables as linear combinations of the two-fluid variables,⁴ one obtains the following system

$$\frac{\partial \rho}{\partial t} + \nabla \cdot (\rho \mathbf{u}) = 0, \tag{2.1}$$

$$\rho \left(\frac{\partial \boldsymbol{u}}{\partial t} + \boldsymbol{u} \cdot \nabla \boldsymbol{u} \right) = -\nabla p + \boldsymbol{J} \times \boldsymbol{B}, \tag{2.2}$$

$$\boldsymbol{E} + \boldsymbol{u} \times \boldsymbol{B} = 0, \tag{2.3}$$

$$\nabla \times \boldsymbol{E} = -\frac{\partial \boldsymbol{B}}{\partial t},\tag{2.4}$$

$$\nabla \times \boldsymbol{B} = \mu_0 \boldsymbol{J},\tag{2.5}$$

$$\nabla \cdot \boldsymbol{B} = 0, \tag{2.6}$$

where the energy equation, which provides the closure, is⁵

$$\frac{d}{dt}\left(\frac{p}{\rho^{\Gamma}}\right) = 0,\tag{2.7}$$

which, by means of (2.1), can also be expressed as

$$\frac{\partial \boldsymbol{p}}{\partial t} + \boldsymbol{u} \cdot \boldsymbol{\nabla} \boldsymbol{p} + \Gamma \boldsymbol{p} \boldsymbol{\nabla} \cdot \boldsymbol{u} = 0. \tag{2.8}$$

These are referred to as **ideal MHD equations** which form the **ideal MHD model**. In the equations above, $\rho = m_i n$ is the plasma mass density, \boldsymbol{E} and \boldsymbol{B} the electric and magnetic field, $\boldsymbol{J} = e n(\boldsymbol{u}_i - \boldsymbol{u}_e)$ the current density with e the ion charge, $\boldsymbol{p} = p_i + p_e$ the plasma kinetic pressure, $\Gamma = 5/3$ the adiabatic index, and $d/dt = \partial/\partial t + \boldsymbol{u} \cdot \nabla$ is the convective derivative. In (2.5), μ_0 denotes the vacuum magnetic permeability. The momentum of the fluid is carried by the ions, i.e. $\boldsymbol{u} \approx \boldsymbol{u}_i$ with

$$\boldsymbol{u} = \frac{\boldsymbol{E} \times \boldsymbol{B}}{B^2} + u_{||} \frac{\boldsymbol{B}}{|B|} = \boldsymbol{u}_{\perp} + u_{||} \frac{\boldsymbol{B}}{|B|}.$$
 (2.9)

It is instructive to discuss briefly the physical interpretation and consequences for some of the equations of the system above. Equations (2.4)-(2.6) are pre-Maxwell equations, indicating low frequency electromagnetic behaviour. The mass density equation (2.1) implies that the number of particles is conserved (no ionisation or recombination phenomena, etc.). Equation (2.2) which is referred to as the **momentum**

- ³ The plasma frequency and Debye length are $\omega_p = \sqrt{n_0 e^2/m_e \varepsilon_0}$ and $\lambda_D = V_{T_e/\omega_p e}$ respectively, with the **thermal velocity** defined as $V_{T_s} = \sqrt{2k_B T_s/m_s}$. n_0 is the plasma density, e the ion charge, k_B the Boltzmann constant, T_s and m_s the temperature and mass associated with the s species.
- ⁴ The one-fluid evolution equations are obtained by adding pairs of the two-fluid equations multiplied by mass and charge factors.

⁵ This is the **equation of state**.

- ⁶ Here $p = nk_B(T_i + T_e)$ with T_s the temperature of the species s.
- ⁷ The convective derivative, also known as total derivative, gives the time rate of change of a physical quantity in an element of fluid moving with the local flow.

Magnetic helicity is conserved too.

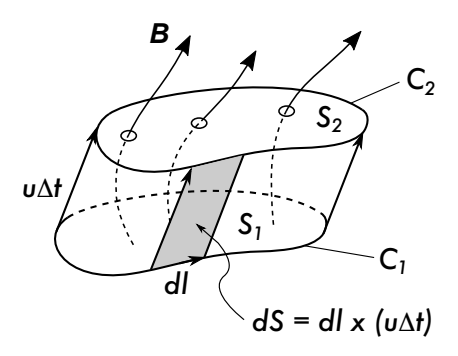


Figure 2.1: Volume element swept out by a surface S moving with the fluid in a magnetic field with velocity u viewed at time t and $t + \Delta t$. The shaded area is the side surface spanned by the length element dl of the contour C_1 .

equation describes the momentum balance. Equation (2.3) tells that the plasma is a perfect conductor, i.e. the electric field in the moving plasma frame is zero. This equation has an important consequence: it implies that the motion of the fluid element is *glued* to the one of the magnetic field lines. This is known as **frozen-in theorem**, or flux freezing, meaning that if a fluid element is displaced, the magnetic field will follow it accordingly and *vice versa*. Total energy and momentum are also conserved. These are the so called ideal MHD **conservations laws**, whose proofs are outlined in the next subsections.

2.1.1 Freezing of the magnetic field

Consider a surface $S_1 = S(t)$ of contour C_1 at time t crossed by a magnetic field B. As S moves in time, each line element comprising it moves by a distance $u\Delta t$, so that at time $t + \Delta t$ we have $S(t) \to S(t + \Delta t) = S_2$ with contour C_2 , as shown in figure 2.1.

The flux Φ_M across the surface S is defined as

$$\Phi_M = \int_S \mathbf{B} \cdot \mathbf{n} dS,$$

where n is the unit vector normal to the surface S. The rate of change of the magnetic flux through the open surface S can be written as

$$\frac{d\Phi_M}{dt} = \lim_{\Delta t \to 0} \frac{1}{\Delta t} \left[\int_{S_2} \boldsymbol{B}(t + \Delta t) \cdot \boldsymbol{n} dS - \int_{S_1} \boldsymbol{B}(t) \cdot \boldsymbol{n} dS \right].$$

We Taylor expand $\boldsymbol{B}(t+\Delta t)=\boldsymbol{B}(t)+\frac{\partial \boldsymbol{B}}{\partial t}\Delta t+\ldots$, and obtain

$$\frac{d\Phi_{M}}{dt} = \lim_{\Delta t \to 0} \left[\int_{S_{2}} \frac{\partial \mathbf{B}}{\partial t} \cdot \mathbf{n} dS + \frac{1}{\Delta t} \left(\int_{S_{2}} \mathbf{B}(t) \cdot \mathbf{n} dS - \int_{S_{1}} \mathbf{B}(t) \cdot \mathbf{n} dS \right) \right]. \tag{2.10}$$

Let us consider the **closed** surface delimited by the surfaces S_1 , S_2 and the lateral side spanned by the surface dS of length $u\Delta t$ as in Fig. 2.1. Because of (2.6), from the Gauss divergence theorem, the flux through this surface is zero, i.e.

$$0 = \int_{S_2} \mathbf{B}(t) \cdot \mathbf{n} dS - \int_{S_1} \mathbf{B}(t) \cdot \mathbf{n} dS + \oint_{C_1} \mathbf{B} \cdot d\mathbf{l} \times \mathbf{u} \Delta t,$$

where the minus sign in the term with S_1 is because the unit vector normal to that surface is not pointing outwards, and dl is the infinitesimal element of the contour C_1 (see Fig. 2.1). Using the result above into (2.10) gives

$$\frac{d\Phi_M}{dt} = \lim_{\Delta t \to 0} \left[\int_{S_2} \frac{\partial \mathbf{B}}{\partial t} \cdot \mathbf{n} dS - \oint_{C_1} \mathbf{B} \cdot d\mathbf{l} \times \mathbf{u} \right].$$

The first term on the right hand side can be evaluated using (2.4) and Stoke's theorem. Thus, taking the limit $\Delta t \to 0$ one has $S_1 = S_2 = S$ with $C_1 = C_2 = C$, so that

$$\frac{d\Phi_{M}}{dt} = -\oint_{C} d\boldsymbol{l} \cdot (\boldsymbol{E} + \boldsymbol{u} \times \boldsymbol{B}). \tag{2.11}$$

Therefore, using (2.3) and assuming that the velocity \boldsymbol{u} coincides with the plasma velocity, one has that $d\Phi_M/dt = 0$. This demonstrates that in ideal MHD the total magnetic flux is conserved, i.e. the magnetic field lines move following the plasma motion, being frozen into the fluid.

2.1.2 Energy conservation

Another quantity that is conserved in ideal MHD is the total energy.⁸ Dotting (2.2) with u and using (2.1) yields

$$\frac{\partial}{\partial t} \left(\frac{\rho u^2}{2} \right) + \nabla \cdot \left(\rho \frac{u^2}{2} u \right) = -u \cdot \nabla p + u \cdot J \times B = -u \cdot \nabla p + J \cdot E,$$

where use of (2.3) has been made in the last passage. By means of Faraday's law we easily have

$$\boldsymbol{J} \cdot \boldsymbol{E} = \frac{1}{\mu_0} \boldsymbol{E} \cdot \boldsymbol{\nabla} \times \boldsymbol{B} = -\frac{1}{\mu_0} \boldsymbol{\nabla} \cdot (\boldsymbol{E} \times \boldsymbol{B}) - \frac{1}{2\mu_0} \frac{\partial B^2}{\partial t}.$$

Finally, equation (2.8) gives

$$\boldsymbol{u} \cdot \boldsymbol{\nabla} \boldsymbol{p} = \frac{\partial}{\partial t} \left(\frac{\boldsymbol{p}}{\Gamma - 1} \right) + \boldsymbol{\nabla} \cdot \left(\frac{\Gamma}{\Gamma - 1} \boldsymbol{p} \boldsymbol{u} \right).$$

Therefore, by collating these results together we get

$$\frac{\partial}{\partial t} \left(\frac{\rho u^2}{2} + \frac{p}{\Gamma - 1} + \frac{B^2}{2\mu_0} \right) = -\nabla \cdot \left(\rho \frac{u^2}{2} u + \frac{p}{\Gamma - 1} u + \rho u + \frac{1}{\mu_0} E \times B \right). \tag{2.12}$$

The left-hand-side is the rate of change in time of the sum of kinetic, internal and magnetic energies, whereas the divergence term on the right-hand-side represents the flux of kinetic and internal energy, the mechanical work due to pressure forces and flux of electromagnetic energy through the Poynting vector.⁹

We now integrate the expression above over a volume V (which may include a vacuum region) such that the normal and tangential components of \boldsymbol{u} and \boldsymbol{E} are vanishing on the surface enclosing this volume. This shows that the total energy (dV) is the infinitesimal volume element)

$$U = \int \left(\frac{\rho u^2}{2} + \frac{p}{\Gamma - 1} + \frac{B^2}{2\mu_0}\right) dV$$

is conserved in time.

2.1.3 Momentum conservation

Proving that the global momentum is conserved is a rather simple task. We first observe that by means of (2.1)

$$\rho \frac{\partial \mathbf{u}}{\partial t} = \frac{\partial (\rho \mathbf{u})}{\partial t} - \mathbf{u} \frac{\partial \rho}{\partial t} = \frac{\partial (\rho \mathbf{u})}{\partial t} + \mathbf{u} \nabla \cdot (\rho \mathbf{u})$$
$$= \frac{\partial (\rho \mathbf{u})}{\partial t} + \nabla \cdot (\rho \mathbf{u} \mathbf{u}) - \rho \mathbf{u} \cdot \nabla \mathbf{u}.$$

⁸ This conservation law will be exploited when certain properties of equations (2.1)-(2.8) will be discussed in the context of the stability of an equilibrium subject to small perturbations.

⁹ The quantity $\frac{p}{\Gamma-1}u + pu = \frac{\Gamma}{\Gamma-1}pu$ can be interpreted as the enthalpy flux.

This tensor has diagonal elements equal to unity, while the off-diagonal ones are

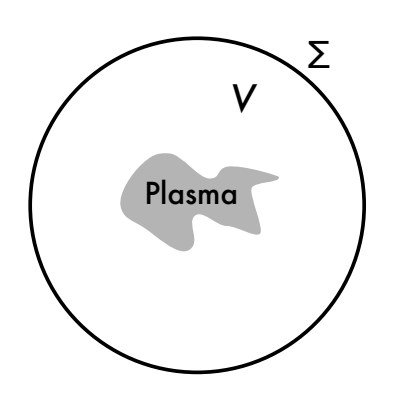


Figure 2.2: Plasma volume V enclosed by the surface Σ used in the proof of the virial theorem.

The current term is rearranged as follows

$$(\nabla \times \boldsymbol{B}) \times \boldsymbol{B} = -\nabla \left(\frac{\boldsymbol{B}^2}{2}\right) + \boldsymbol{B} \cdot \nabla \boldsymbol{B} = -\nabla \cdot \left(\frac{\boldsymbol{B}^2}{2} \underline{\boldsymbol{I}}\right) + \nabla \cdot (\boldsymbol{B}\boldsymbol{B}),$$

with $I_{ij} \equiv (\underline{\underline{I}})_{ij} = \delta_{ij}$ is the **diagonal unit tensor**. Finally, $\nabla p = \nabla \cdot (p\underline{\underline{I}})$. Plugging the results above into (2.2) gives

$$\frac{\partial(\rho \mathbf{u})}{\partial t} = -\nabla \cdot \left(p \underline{\mathbf{I}} + \frac{B^2}{2\mu_0} \underline{\mathbf{I}} + \rho \mathbf{u} \mathbf{u} - \frac{1}{\mu_0} \mathbf{B} \mathbf{B} \right), \tag{2.13}$$

which has the same structure of (2.12) where the left-side describes the acceleration. We thus conclude that the total momentum is conserved if the same boundary conditions as those used in the derivation of the energy conservation are fulfilled. Relation (2.13) is used for the derivation of pressure jump conditions at the plasma-vacuum interface.

2.1.4 The virial theorem

This theorem states that it is not possible to confine a plasma only with currents flowing within the plasma itself. We prove it by contradiction. Assume a plasma at equilibrium to occupy a bounded area enclosed by a surface Σ associated with a volume V as shown in figure 2.2. There are no rigid current-carrying conductors inside or outside the plasma. From (2.13), the equilibrium condition is $\nabla \cdot \underline{\underline{T}} = 0$, i.e. no forces, with the tensor $\underline{\underline{T}}$ given by

$$\underline{\underline{T}} = \left(p + \frac{B^2}{2\mu_0}\right)\underline{\underline{I}} - \frac{1}{\mu_0}BB + \rho uu.$$

It is immediate to see that $T_{ij} = T_{ji}$ and

$$T_{ii} = p + \frac{B^2}{2\mu_0} - \frac{B_i^2}{\mu_0} + \rho u_i^2.$$

The following relation holds

$$\nabla \cdot \left(\boldsymbol{x} \cdot \underline{\underline{\boldsymbol{T}}} \right) = \frac{\partial}{\partial x_i} \left(x_i T_{ij} \right) = T_{ij} \frac{\partial x_i}{\partial x_j} + x_i \frac{\partial T_{ji}}{\partial x_j} = T_{ii} + \boldsymbol{x} \cdot \nabla \cdot \underline{\underline{\boldsymbol{T}}} = \operatorname{Tr}(\underline{\underline{\boldsymbol{T}}}),$$

where the symbol Tr denotes the trace of the associated tensor. It follows that $\text{Tr}(\underline{T}) = 3p + \frac{B^2}{2\mu_0} + \rho u^2$. Therefore, one has

$$0 < \int_{V} \left(3p + \frac{B^2}{2\mu_0} + \rho u^2 \right) dV = \int_{\Sigma} x \cdot \left[\left(p + \frac{B^2}{2\mu_0} \right) \underline{\underline{I}} - \frac{1}{\mu_0} BB + \rho u u \right] \cdot n d\Sigma,$$

where \mathbf{n} is the unit vector normal to the surface Σ . Let the volume be a sphere of radius r with $r \to \infty$. Since Σ encloses the plasma, we have $p|_{\Sigma} = \mathbf{u}|_{\Sigma} = 0$. The magnetic field decays at large radii at least as a dipole field, i.e. $B \sim 1/r^3$ whereas in spherical coordinates (r, θ, ϕ) we have $d\Sigma \sim r^2$ and $\mathbf{x} \sim r$. Thus, in the equation above the integral on the left takes some positive value while the one on the right is vanishing, hence the contradiction.

Resistive MHD 2.2

The condition of magnetic field freezing can be violated, i.e. the magnetic field can diffuse through the fluid element, if the ideal constraint is relaxed and the plasma is allowed to be resistive. In such a case equation (2.3) is modified by including resistive dissipation effects: in its simplest form it becomes

$$\boldsymbol{E} + \boldsymbol{u} \times \boldsymbol{B} = \eta \boldsymbol{J},\tag{2.14}$$

where η is the plasma resistivity which, generally, can depend upon xand t. Equation (2.14) is called the **Ohm's law**. The system of equations (2.1), (2.2), (2.4)-(2.6), (2.8) and (2.14) forms the so called **resistive** MHD model. Using Faraday's law, equation (2.14) can be cast as

$$\frac{\partial \boldsymbol{B}}{\partial t} = \nabla \times (\boldsymbol{u} \times \boldsymbol{B}) - \nabla \times (\eta \boldsymbol{J}),$$

which is called the **induction equation**.

By comparing with (2.11), the inclusion of resistivity allows the magnetic flux to diffuse, i.e. is not glued anymore to the fluid element. As a consequence, in a resistive plasma oppositely directed magnetic field lines can break and reconnect (see Fig. 2.3). During this process, called magnetic reconnection, the magnetic field energy is converted into kinetic and thermal energy. Magnetic reconnection in tokamaks is invoked to explain certain phenomena associated with severe confinement degradation (e.g. the formation of the so-called magnetic islands whose analysis will be addressed in chapter 14).

We point out that there are many ways to model plasma resistivity, and one of the most widely used is the so called Spitzer model. In this model plasma resistivity arises from electron-ion collisions, and is a decreasing function of the electron temperature¹⁰

$$\eta \sim T_e^{-3/2}$$
.

In summary, accounting for the plasma response through the induction equation, the MHD model system describing ideal and resistive plasmas can be written in a compact way as

$$\frac{\partial \rho}{\partial t} + \nabla \cdot (\rho \mathbf{u}) = 0,$$

$$\rho \left(\frac{\partial \mathbf{u}}{\partial t} + \mathbf{u} \cdot \nabla \mathbf{u} \right) = -\nabla p + \mathbf{J} \times \mathbf{B},$$

$$\frac{\partial \mathbf{B}}{\partial t} = \nabla \times (\mathbf{u} \times \mathbf{B}) - \nabla \times (\eta \mathbf{J}),$$

$$\frac{\partial p}{\partial t} + \mathbf{u} \cdot \nabla p + \Gamma p \nabla \cdot \mathbf{u} = 0,$$

$$\nabla \times \mathbf{B} = \mu_0 \mathbf{J}, \quad \nabla \cdot \mathbf{B} = 0,$$

where the ideal limit is obtained by setting $\eta \to 0$. This is the set of equations that will be used throughout the following chapters.

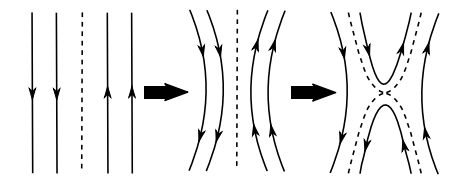


Figure 2.3: Typical reconnection event for oppositely directed field lines.

¹⁰ Under certain conditions, the resistivity of a plasma tends to be much higher than the Spitzer resistivity. In such a case we talk about anomalous resistivity.

¹¹ Recalling the discussion in §2.1, this means that collisions are so frequent that the plasma is assumed to behave as a perfect gas such that (2.7) or (2.8) hold.

2.3 Domain of validity of the MHD model

The MHD model assumes a collision-dominated plasma, for which¹¹

$$V_{T_i}\tau_{ii}/a \sim V_{T_e}\tau_{ee}/a \ll 1,$$

where τ_{ss} is the s-s particle collision time, and a is the characteristic length of the system, much longer than the Debye length (thermal velocities V_{T_s} have been defined in **sidenote 3**). This implies that the distribution function for both ions and electrons is nearly Maxwellian and the macroscopic length scale is much longer than the mean-free-path. The validity of the MHD model can be summarised by the following conditions (Freidberg (2014)):

$$\begin{split} &1 - \text{High collisionality, } \left(\frac{m_i}{m_e}\right)^{1/2} \frac{V_{T_i} \tau_{ii}}{a} \ll 1 \\ &2 - \text{Small gyro-radius, } \frac{r_{L_i}}{a} \ll 1 \\ &3 - \text{Small resistivity, } \frac{r_{L_i}^2}{a} \left(\frac{m_e}{m_i}\right)^{1/2} \frac{1}{V_{T_i} \tau_{ii}} \ll 1 \end{split}$$

where $r_{L_i} = V_{T_i}/\Omega_i$ is the ion gyro-radius (cf. section 1.2.1) and $\Omega_i = e_i B/m_i$ is the ion cyclotron frequency (e_i and m_i are the charge and mass of the ion). The small gyro-radius condition is normally fulfilled in tokamaks as long as the magnetic field is sufficiently strong. The third condition implies that, despite the high collisionality, resistive diffusion is still small or negligible. In tokamak plasmas resistivity is usually a small quantity so that this condition is safely fulfilled as well. The main issue is caused by the first requirement: in fusion relevant plasmas the assumption of high collisionality is never fulfilled. Nevertheless empirical evidence during many years of fusion plasma research has shown that the ideal MHD model provides an excellent theoretical framework for the description of several phenomena observed in experiments.

To resolve this issue modified kinetic MHD models are introduced (see e.g. Freidberg (2014)).¹² A brief account of a hybrid framework in which the plasma response parallel or perpendicular to the magnetic field is treated kinetically or fluid-like respectively, is given in the next section where two beyond-MHD models are discussed. We also highlight the discussion on closure in magnetised plasmas by Fitzpatrick (2014).

2.4 Advanced MHD models

In the next two subsections we sketch the basic equations which characterise two extensions to the MHD framework, namely the **drift-MHD** and **guiding centre plasma** models. The former attempts to capture the effects arising from the two plasma populations, namely ion and electron drifts¹³, whereas the latter aims to describe kinetically the dynamics

The fluid-kinetic model studied in Bondeson (1989) recovers the standard (ideal) MHD marginal stability boundaries (i.e. loci in some appropriate parameter space for which the growth rate of a perturbation is vanishing) in the limit of a cylindrical static plasma with a **Maxwellian distribution function** for both ions and electrons

¹³ Diamagnetic drifts represent fluid flows for which there is no corresponding motion of the particle guiding centres.

along the magnetic field while retaining the fluid description across it. These two models are widely employed in describing tokamak physics, however they are not always presented in a transparent way. Thus, although these are not used in the following chapters, we think it is helpful to provide a concise summary of their corresponding fundamental equations.

2.4.1 **Drift-MHD**

The drift-MHD (or FLR from finite Larmor radius) model is suitable for describing phenomena which are slower compared with the ones predicted by the fast ordering employed for deriving standard MHD. Many of the approximations used to derive the drift-MHD model are extremely crude, but the resulting set of equations has the great advantage to be simple enough to be manageable analytically, and yet contains several important physical effects such as diamagnetic drifts, temperature gradients and field curvature. Many FLR models are available in the literature: these are scattered across many references, and sometimes they are presented in some obscure fashion. Below we report a ready to be used model set of drift-MHD equations adapted from several references (see Hazeltine (1992), Ara (1978), Kadomtsev (1970), Mikhailovskii (1998)) which, in the authors' opinion, is fairly physically transparent and simple enough to be handled analytically. This is

$$\begin{split} \frac{\partial \rho}{\partial t} + \boldsymbol{\nabla} \cdot \left[\rho(\boldsymbol{u} + \boldsymbol{u}^*) \right] &= 0, \\ \rho \left(\frac{\partial \boldsymbol{u}}{\partial t} + \boldsymbol{u} \cdot \boldsymbol{\nabla} \boldsymbol{u} + \boldsymbol{u}^* \cdot \boldsymbol{\nabla} \boldsymbol{u}_{\perp} \right) &= -\boldsymbol{\nabla} p + \boldsymbol{J} \times \boldsymbol{B}, \\ \boldsymbol{E} + \boldsymbol{u} \times \boldsymbol{B} + \frac{\boldsymbol{\nabla}_{||} p}{2en} &= \eta \boldsymbol{J}, \\ \frac{\partial p}{\partial t} + \boldsymbol{u} \cdot \boldsymbol{\nabla} p + \Gamma p \boldsymbol{\nabla} \cdot \boldsymbol{u} &= 0, \end{split}$$

having defined $\nabla_{||} = \boldsymbol{b}(\boldsymbol{b} \cdot \nabla)$ with $\boldsymbol{b} = \boldsymbol{B}/|\boldsymbol{B}|$ and

$$\boldsymbol{u}^* = \frac{\boldsymbol{B} \times \boldsymbol{\nabla} \boldsymbol{p}}{2e \, n B^2},$$

with \boldsymbol{u} and \boldsymbol{u}_{\perp} given by (2.9). To close the system, the equations above are augmented, as usual, by Maxwell's equations (2.4)-(2.6). Note that in the drift model just presented, FLR corrections enter the density, momentum and Ohm's law equations. An approximation that is commonly used is the so called *hydrodynamic* ions limit (Hazeltine (1978)), in which temporal changes of the ion pressure are balanced by convection yielding

$$\nabla \cdot \boldsymbol{u}_i \equiv \nabla \cdot (\boldsymbol{u} + \boldsymbol{u}^*) \approx 0.$$

This turns out to be quite handy for evaluating inertia arising from plasma compressibility.

Other drift-MHD models which appear in the literature retain the same structure of equations above but have different expressions for e.g. the Ohm's law equation or the pressure evolution.

2.4.2 Guiding centre plasma

As previously mentioned, the high collisionality condition is normally violated in tokamaks. Moreover, the presence of a strong toroidal magnetic field decouples the parallel dynamics from the perpendicular one. Indeed, a particle may do several turns along the field line before undergoing a collision so that, although the fluid motion across the magnetic field can be regarded as fluid-like, the fluid description is not appropriate to describe the parallel dynamics.

One of the models that have been proposed to solve this problem is the **guiding centre plasma** (GCP) model developed by Grad (1967). In this model the dynamics along the magnetic field is described by a collisionless kinetic equation which serves as an equation of state providing the required closure.

Neglecting collisions, the Vlasov equation is expanded to first order in the gyro-phase angle φ_g (see Fig. 2.4) and then averaged over it. This eventually yields the drift-kinetic equation for the averaged distribution function $\bar{f}_{\rm c}$

$$\frac{\partial \bar{f_s}}{\partial t} + (\boldsymbol{u}_{\perp} + v_{||}\boldsymbol{b}) \cdot \nabla \bar{f_s} + [v_{||}\boldsymbol{u}_{\perp} \cdot (\boldsymbol{b} \cdot \nabla \boldsymbol{b}) - \boldsymbol{b} \cdot \nabla E_s] \frac{\partial \bar{f_s}}{\partial v_{||}} = 0, \quad (2.15)$$

with $E_s = \mu B + \frac{e_s}{m_s} \Phi_E - \frac{u_\perp^2}{2}$ where $\mu = v_\perp^2/2B$ is the particle magnetic moment (note that compared to the definition in Eq. (1.1) here we drop the particle mass), e_s the charge and the parallel electric field is given by $E_{||} = -\boldsymbol{b} \cdot \boldsymbol{\nabla} \Phi_E$. As before, we defined $\boldsymbol{b} = \boldsymbol{B}/|B|$ and denote the parallel and perpendicular projections of the velocities with respect to the magnetic field by $v_{||}$ and v_\perp respectively. Note that \boldsymbol{u}_\perp in the drift-kinetic equation is the perpendicular fluid velocity as given in (2.9), i.e. the fluid drift due to the electric field. In the derivation above use has been made of the conservation of the magnetic moment, i.e.

$$\frac{d\mu}{dt} = 0. (2.16)$$

Because of the gyro-averaging, $\bar{f_s}$ depends on 6 variables: the three spatial coordinates x along with $v_{||}$, μ and time.

Thus, assuming the plasma to be a perfect conductor, the resulting GCP equations are

$$\partial_{t}\rho + \nabla \cdot (\rho \mathbf{u}) = 0,$$

$$\rho \left(\frac{\partial \mathbf{u}}{\partial t} + \mathbf{u} \cdot \nabla \mathbf{u} \right) = -\nabla \cdot \underline{\underline{P}} + \mathbf{J} \times \mathbf{B},$$

$$\mathbf{E} + \mathbf{u} \times \mathbf{B} = 0,$$
(2.17)

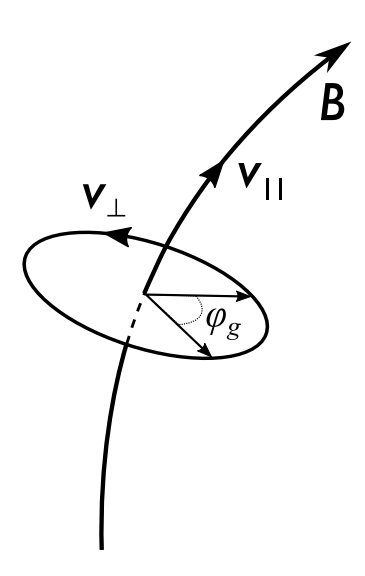


Figure 2.4: Schematic view of the particle motion in a magnetic field identified by its parallel and perpendicular velocities, $v_{||}$ and v_{\perp} , and by the gyro-phase angle φ_g . φ_g is the angle lying in the plane perpendicular to the magnetic field between a reference direction and the gyroradius vector.

21

where $\underline{\underline{P}} = p_{\perp}\underline{\underline{I}} + (p_{||} - p_{\perp})bb$ with $\underline{\underline{I}}$ the diagonal unit tensor. The parallel and perpendicular pressure are defined as moment averages according to

$$p_{||} = \sum_{s} m_{s} \int d^{3} \boldsymbol{v} \bar{f}_{s} (\boldsymbol{v}_{||} - \boldsymbol{b} \cdot \boldsymbol{u})^{2},$$

$$p_{\perp} = \sum_{s} m_{s} \int d^{3} \boldsymbol{v} \bar{f}_{s} v_{\perp}^{2} / 2,$$
(2.18)

where the sum is carried over all species s of mass m_s and the integration extends over the whole microscopic velocity space. The number and mass densities are given by

¹⁴
$$\int d^3v = 2\pi \int_0^\infty dv_\perp v_\perp \int_{-\infty}^\infty dv_{||}.$$

$$n_s = \int d^3 v \bar{f_s}, \quad \rho = \sum_s m_s n_s.$$

As before, the system is closed by Maxwell's equations (2.4)-(2.6). We will briefly mention the guiding centre model in Appendix B when discussing some properties of anisotropic tokamak equilibria.

Thus, having completed the presentation of tokamak-relevant MHD models, the next chapter will be devoted to the exposition of some useful mathematical tools which are needed to embed these models in complex geometries.

References

- G. Ara et al., Ann. Phys. 112, 443 (1978).
- J. A. Bittencourt, **Fundamentals of Plasma Physics**, Springer (Springer New York, NY), 2004.
- A. Bondeson and R. Iacono, Phys. Fluids B 1, 1431 (1989).
- T. J. M. Boyd and J. J. Sanderson, The Physics of Plasmas, Cambridge University Press (Cambridge, UK), 2003.
- S. Chandrasekhar, **Hydrodynamic and Hydromagnetic Stability**, Oxford University Press (Oxford, UK), 1961.
- F. F. Chen, Introduction to Plasma Physics and Controlled Fusion, Springer, 2016.
- R. Fitzpatrick, **Plasma Physics An Introduction**, CRC Press (Boca Raton, US), 2014.
- J. P. Freidberg, **Ideal Magnetohydrodynamics**, Plenum Press (New York, US), 1987.
- J. P. Freidberg, **Ideal MHD**, Cambridge University Press (Cambridge, UK), 2014.
- J. P. Goedbloed and S. Poedts, **Principles of Magnetohydrodynamics With Applications to Laboratory and Astrophysical Plasmas**, Cambridge University Press (Cambridge, UK), 2004.
- V. E. Golant, A. P. Zhilinsky and I. E. Sakharov, Fundamentals of Plasma Physics, Wiley (New York, US), 1980.
- H. Grad, Magneto-Fluid and Plasma Dynamics, Symposia in Applied Mathematics Vol 18 p. 162 (Ed. H. Grad), American Mathematical Society (Providence, RI), 1967.

- R. D. Hazeltine and D. Ross, Phys. Fluids 21, 1140 (1978).
- R. D. Hazeltine and J. D Meiss, **Plasma Confinement**, Addison-Wesley Publishing Company (Redwood City, US), 1992.
- B. B. Kadomtsev and O. P. Pogutse, **Reviews of Plasma Physics Vol.** 5 p. 249 (ed. M. A. Leontovich), Consultants Bureau (New York, US), 1970.
- R. M. Kulsrud, Handbook of Plasma Physics Vol. 1: Basic Plasma physics, edited by A. A. Galeev and R. N. Sudan p. 115 (Eds. M. N. Rosenbluth and R. Z. Sagdeev), North-Holland (Amsterdam, NL), 1983.
- A. B. Mikhailovskii, **Instabilities in a Confined Plasma**, Institute of Physics Publishing (Bristol, UK), 1998.
- V D. Shafranov, Reviews of Plasma Physics Vol. 2 p. 103 (Ed. M. A. Leontovich), Consultants Bureau (New York, US), 1966.
- D. D. Schnack, Lectures in Magnetohydrodynamics: With an Appendix on Extended MHD, Springer (Springer, Berlin Heidelbergk, DE), 2009.
- L. Spitzer Jr, Physics of Fully Ionized Gases, Dover Publications (New York, US), 2006.

3

Curvilinear coordinate systems

In this short chapter we introduce some basic concepts about the mathematical properties of curvilinear coordinate systems which will be extensively used in the following analyses when the problem of the equilibrium and stability of a tokamak will be addressed. The discussion broadly follows the excellent exposition by Balescu (1988) and is kept at a very basic level. All the results are presented without a proof, and the reader interested in a deeper exposition on this subject is referred to the book by D'haeseleer (1991), or any other book on tensor calculus. Although not particularly engaging, the properties listed here provide a fundamental and powerful tool widely used in modelling tokamak physics. Hence, unless already familiar with the topic, the reader is strongly encouraged not to skip the reading of this chapter.

3.1 General properties

A coordinate system is an arrangement of reference lines or curves (axes) used to identify the location of points in space. When the axes are pairwise perpendicular, the coordinates are said to be orthogonal. Otherwise, we generically refer to curvilinear coordinate systems when the orthogonality condition is not fulfilled. Depending on the intrinsic symmetries of the physical problem under consideration, certain coordinate systems can be preferred to others, and in some cases it is more convenient to work with non-orthogonal ones. This indeed proves to be particularly true for tokamak physics, as it will be clear in the next chapters. We shall thus provide a brief account of the properties of non-orthogonal coordinates.

Let us take a point P in space, characterised by its three Cartesian

It is simpler to describe a spherically symmetric problem in spherical rather than Cartesian coordinates.

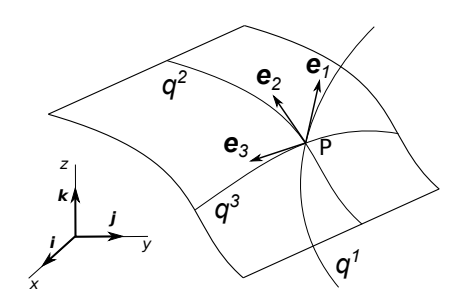


Figure 3.1: Curvilinear coordinate system (q^1, q^2, q^3) adapted on a constant q^1 surface.

coordinates x, y and z. The three unit vectors along the three axes, orthogonal to each other, are denoted by i, j and k. Assume that P lies on a surface. It is convenient to introduce two vectors e_2 and e_3 tangent to the surface and a third one denoted by e_1 pointing, say, outwards from the surface in P. It is possible to introduce three curves (q^1, q^2, q^3) passing through P, tangent to e_1 , e_2 , e_3 respectively. These lines are called coordinate lines and are shown in Fig. 3.1.

Therefore, we have a coordinate system in which any point in space is described by the following relation

$$\boldsymbol{x} = \boldsymbol{x} \left(q^1, q^2, q^3 \right),$$

where x = (x, y, z). We define the length $d\ell$ between two adjacent points by $(i = 1, 2, 3 \text{ not to be confused with the Cartesian unit vector along the <math>x$ axis)

$$d\ell^2 = dx^2 + dy^2 + dz^2 = g_{ij}dq^idq^j, (3.1)$$

having used the Einstein summation convention for repeated indices with i and j running from 1 to 3. The quantities g_{ij} are called the **covariant** elements of the metric tensor and are defined by

$$g_{ij} = \frac{\partial x}{\partial q^i} \frac{\partial x}{\partial q^j} + \frac{\partial y}{\partial q^i} \frac{\partial y}{\partial q^j} + \frac{\partial z}{\partial q^i} \frac{\partial z}{\partial q^j} = g_{ji}.$$

The **determinant** of this matrix, denoted by the letter g, has a simple physical interpretation: the infinitesimal volume element dV = dx dy dz transforms according to

$$dV = \sqrt{g}dq^1dq^2dq^3 (3.2)$$

in the frame identified by the coordinates q^i . We call the quantity \sqrt{g} the **Jacobian** associated with the system (q^1, q^2, q^3) .

Conversely, one can think of the coordinate lines q^i as function of x, namely the Cartesian coordinates, through the relation $q^i = q^i(x, y, z)$, and thus introduce the **contravariant** components of the metric tensor which are defined in an analogous manner:

$$g^{ij} = \frac{\partial q^i}{\partial x} \frac{\partial q^j}{\partial x} + \frac{\partial q^i}{\partial y} \frac{\partial q^j}{\partial y} + \frac{\partial q^i}{\partial z} \frac{\partial q^j}{\partial z} = g^{ji}.$$

It is easy to check that

$$\sum_{n=1}^{3} g_{in} g^{nj} = \delta_i^j \tag{3.3}$$

where δ_i^j is the Kronecker delta, and $\det(g^{ij}) = 1/g$. The covariant and contravariant components of the metric tensor are linked by the relations $g^{ij} = G^{ij}/g$ and $g_{ij} = gG_{ij}$ where G_{ij} (or G^{ij}) represents the cofactor of the matrix element g^{ij} (or g_{ij}).

Let us now define the two sets of three vectors (i = 1, 2, 3):

$$e_i = \frac{\partial x}{\partial q^i} i + \frac{\partial y}{\partial q^i} j + \frac{\partial z}{\partial q^i} k, \qquad e^i = \frac{\partial q^i}{\partial x} i + \frac{\partial q^i}{\partial y} j + \frac{\partial q^i}{\partial z} k.$$

These are not necessarily unit vectors. The set of vectors e_i is called the **covariant basis**, while the set e^i is the **contravariant basis**. The latter is also denoted as $e^i = \nabla q^i$. The contravariant basis vectors e^i are perpendicular to the constant coordinate surfaces whereas the covariant basis vectors e_i are tangent to the coordinate curves. This is sketched in Fig. 3.2.

It immediately follows that

$$e_i \cdot e_j = g_{ij},$$

$$\nabla q^i \cdot \nabla q^j = g^{ij}.$$

It is important to note that the covariant or contravariant vectors are **not necessarily mutually orthogonal**. If, however, e_3 is orthogonal to e_1 and e_2 we have $g_{i3} = g_{3i} = 0$ for $i \neq 3$ and

$$g_{ij} = g \begin{pmatrix} g^{22}g^{33} & -g^{12}g^{33} & 0\\ -g^{12}g^{33} & g^{11}g^{33} & 0\\ 0 & 0 & g^{11}g^{22} - g^{12}g^{12} \end{pmatrix}.$$
(3.4)

Also note that in this case by exploiting (3.3) one obtains

$$1/g_{33} = g^{33}$$
.

The following relations hold

$$\nabla q^1 = (\mathbf{e}_2 \times \mathbf{e}_3) / \sqrt{g},\tag{3.5}$$

$$e_1 = \sqrt{g}(\nabla q^2 \times \nabla q^3). \tag{3.6}$$

and equivalent expressions for the other basis vectors are obtained by circular permutations. The determinant of the metric tensor matrix g is computed by means of

$$\mathbf{e}_1 \cdot (\mathbf{e}_2 \times \mathbf{e}_3) = \sqrt{g},\tag{3.7}$$

$$\nabla q^1 \cdot \left(\nabla q^2 \times \nabla q^3\right) = 1/\sqrt{g},\tag{3.8}$$

with the triad (e_1, e_2, e_3) being right handed if $\sqrt{g} > 0$. Again, the remaining expressions are obtained through cyclic permutations of the indeces. Finally, we have $e_i \cdot \nabla q^j = \delta_i^j$.

We can now define for a generic vector A its covariant (A_i) and contravariant (A^i) components, that is

$$\boldsymbol{A} = A_i \boldsymbol{\nabla} q^i = A^i \boldsymbol{e}_i. \tag{3.9}$$

This gives the rule for raising and lowering indices, that is

$$A_i = g_{ij}A^j, \quad A^i = g^{ij}A_j,$$

 $e_i = g_{ij}\nabla q^j, \quad \nabla q^i = g^{ij}e_j.$

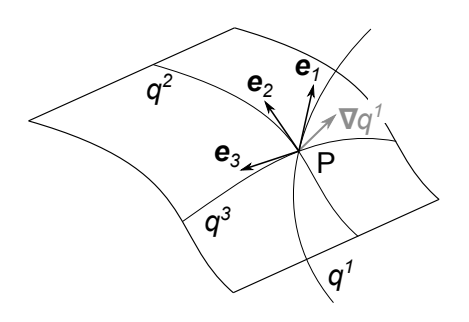


Figure 3.2: Example of the direction of contravariant and covariant basis vectors. ∇q^1 is perpendicular to the plane tangent to the vectors \boldsymbol{e}_2 and \boldsymbol{e}_3 at the point P.

The cross products can be written in a compact form as

$$(\mathbf{A} \times \mathbf{B})^i = \frac{1}{\sqrt{g}} \varepsilon^{ijk} A_j B_k,$$

$$(\boldsymbol{A}\times\boldsymbol{B})_i=\sqrt{g}\varepsilon_{ijk}A^jB^k,$$

where $\varepsilon^{ijk} = \varepsilon_{ijk}$ is the Levi-Civita symbol (a tensor) which is +(-)1 for any even (odd) permutation of the indices (ijk) and o otherwise. Other properties of the Levi-Civita symbol can be found in any tensor algebra textbook.

As a minor remark we point out that in Cartesian coordinates, vector operations are sometimes more easily handled by looking at vector components. As a simple example we consider the operation $A \cdot \nabla A$ where A = |A|a with a = A/|A|. Let the index i denote one of the x, y or z components, and ∂_i the derivative along one of the three coordinates. We find that

$$(\mathbf{A} \cdot \nabla \mathbf{A})_i = |A| a_i \partial_i (|A| a_j)$$
$$= |A|^2 a_i \partial_i a_j + a_j a_i \partial_i |A|^2 / 2,$$

which shows that $\mathbf{A} \cdot \nabla \mathbf{A} = |\mathbf{A}|^2 \mathbf{a} \cdot \nabla \mathbf{a} + \mathbf{a} (\mathbf{a} \cdot \nabla |\mathbf{A}|^2/2)$.

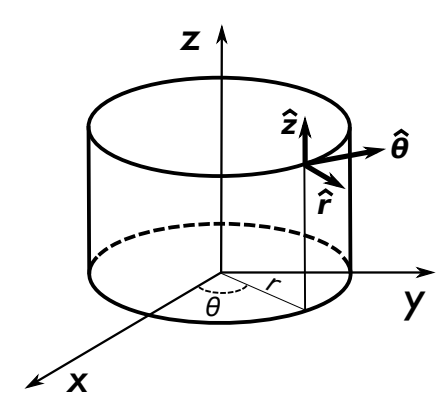


Figure 3.3: Cylindrical coordinate system (r, θ, z) with unit vectors $(\hat{r}, \hat{\theta}, \hat{z})$.

The scalar and cross products between two vectors \boldsymbol{A} and \boldsymbol{B} are given by

$$\mathbf{A} \cdot \mathbf{B} = A^j B_j = A_j B^j = g_{jk} A^k B^j, \tag{3.10}$$

$$(\mathbf{A} \times \mathbf{B})^i = \frac{1}{\sqrt{g}} \left(A_j B_k - A_k B_j \right), \tag{3.11}$$

$$(\mathbf{A} \times \mathbf{B})_i = \sqrt{g} \left(A^j B^k - A^k B^j \right). \tag{3.12}$$

Gradient, divergence and curl operators are written as follows:

$$(\nabla u)_i = \frac{\partial u}{\partial q^i},\tag{3.13}$$

$$\nabla \cdot \mathbf{A} = \frac{1}{\sqrt{g}} \frac{\partial}{\partial q^i} \left(\sqrt{g} A^i \right), \tag{3.14}$$

$$(\nabla \times \mathbf{A})^i = \frac{1}{\sqrt{g}} \left(\frac{\partial A_k}{\partial q^j} - \frac{\partial A_j}{\partial q^k} \right) = \frac{1}{\sqrt{g}} \varepsilon^{ijk} \frac{\partial A_k}{\partial q^j}. \tag{3.15}$$

Note that $\nabla \times \nabla q^i = 0$.

Finally, terms of the form ∇A are evaluated by using the Christoffel symbols (of the second kind)

$$\left(\frac{\partial \boldsymbol{A}}{\partial q^k}\right)_j = \frac{\partial A_j}{\partial q^k} - \Gamma^i_{jk} A_i, \quad \left(\frac{\partial \boldsymbol{A}}{\partial q^k}\right)^j = \frac{\partial A^j}{\partial q^k} + \Gamma^j_{ik} A^i,$$

where

$$\Gamma^{i}_{jk} = \frac{\partial \mathbf{e}_{j}}{\partial q^{k}} \cdot \mathbf{e}^{i} = \frac{g^{im}}{2} \left[\frac{\partial g_{mj}}{\partial q^{k}} + \frac{\partial g_{mk}}{\partial q^{j}} - \frac{\partial g_{jk}}{\partial q^{m}} \right].$$

Although the latter two identities will not be used in the calculations presented in this report, they prove to be particularly useful when dealing with flow convection problems in complex geometries.

In the next subsections we report a brief discussion on the particular case of cylindrical and toroidal coordinates, which are extensively used in the tokamak physics community.

3.1.1 Orthogonal cylindrical coordinates

Let's identify the triplet (q^1, q^2, q^3) with (r, θ, z) where r is the radius, θ the angular variable and z the azimuthal coordinate as sketched in figure (3.3). The length element $d\ell^2$ is given explicitly by

$$d\ell^2 = g_{rr}dr^2 + g_{\theta\theta}d\theta^2 + g_{zz}dz^2 + 2g_{r\theta}drd\theta + 2g_{rz}drdz + 2g_{\theta z}d\theta dz.$$

The Cartesian coordinates (x, y, z), when written as a function of (r, θ, z) become

$$x = r \cos \theta$$
, $y = r \sin \theta$, $z = z$.

It follows that $g_{rr}=1$, $g_{\theta\theta}=r^2$, $g_{zz}=1$, and $g_{r\theta}=g_{rz}=g_{\theta z}=0$. These are the proper **orthogonal cylindrical coordinates**. Note that the off-diagonal components of the metric tensor associated with variables along which the system exhibits symmetry vanish.

We now point out that tokamaks are often modelled as cylinders of length L and periodic in the azimuthal (z) direction. Hence, let us introduce the variable $\phi = z/R_0$ with $R_0 = L/2\pi$. Then, the parametrisation of (x, y, z) of a toroidally symmetric system with circular concentric surfaces of radius r is given by 1

$$x = (R_0 + r \cos \theta) \sin \phi,$$

$$y = (R_0 + r \cos \theta) \cos \phi,$$

$$z = r \sin \theta.$$
(3.16)

The quantity R_0 is called the **major radius** (or radius of curvature) and the length element becomes

$$d\ell^{2} = dr^{2} + r^{2}d\theta^{2} + (R_{0} + r\cos\theta)^{2}d\phi^{2}.$$

Intuitively, if we now think of stretching the torus to such an extent that the ratio R_0/r becomes infinite, we obtain the following metric coefficients

$$g_{rr} = 1$$
, $g_{\theta\theta} = r^2$, $g_{\phi\phi} = R_0^2$, $g_{r\theta} = g_{r\phi} = g_{\theta\phi} = 0$,

with $\sqrt{g} = rR_0$. It is immediate to convince ourselves that the resulting metric is equivalent to that obtained by working in proper cylindrical geometry. Approximating tokamaks as cylinders characterised by metric as the one given above is usually referred to as the cylindrical **approximation**. If the radius of curvature R is large enough, we may be tempted to employ the cylindrical limit. Unfortunately, this approximation is not adequate to describe most of tokamak MHD problems, either the equilibrium or stability ones, for which a fully toroidal analysis is required.

Orthogonal toroidal coordinates 3.1.2

Luckily, extending the coordinates just discussed to properly embody toroidicity, and yet avoiding the complication of the non-orthogonality of the basis vectors is immediate. Let the geometry of the system consist of nested concentric circular surfaces labelled by the variable r where θ and ϕ are the poloidal and toroidal angles respectively (cf. Fig. 3.4). The angle θ always increases counterclockwise in the poloidal plane. The relation to the Cartesian coordinates is given by (3.16) and the metric tensor coefficients are

$$g_{rr} = 1$$
, $g_{\theta\theta} = r^2$, $g_{r\theta} = g_{r\phi} = g_{\theta\phi} = 0$,
 $g_{\phi\phi} = (R_0 + r\cos\theta)^2$, $\sqrt{g} = r(R_0 + r\cos\theta)$.

The power of the orthogonal toroidal coordinates manifests itself when expressing the gradient, divergence and curl operators. Letting $(\hat{r}, \hat{\theta}, \hat{\phi})$ be the mutually orthogonal unit vectors along the radial, poloidal and

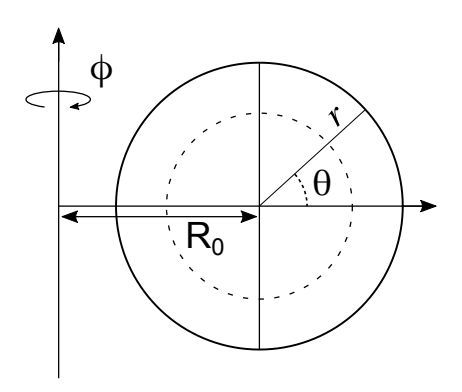


Figure 3.4: Concentric toroidal coordinates with a circular cross section.

¹ The angle θ is oriented counterclockwise and ϕ increases clockwise starting from the y axis.

toroidal directions, we have the following (fairly simple) representation for the above-mentioned differential operators

$$\begin{split} \boldsymbol{\nabla} \boldsymbol{A} &= \frac{\partial \boldsymbol{A}}{\partial r} \hat{\boldsymbol{r}} + \frac{1}{r} \frac{\partial \boldsymbol{A}}{\partial \theta} \hat{\boldsymbol{\theta}} + \frac{1}{R} \frac{\partial \boldsymbol{A}}{\partial \phi} \hat{\boldsymbol{\phi}}, \\ \boldsymbol{\nabla} \cdot \boldsymbol{A} &= \frac{1}{rR} \left(\frac{\partial (rRA_r)}{\partial r} + \frac{\partial (RA_\theta)}{\partial \theta} + \frac{\partial (rA_\phi)}{\partial \phi} \right), \\ \boldsymbol{\nabla} \times \boldsymbol{A} &= \frac{1}{rR} \left(\frac{\partial (RA_\phi)}{\partial \theta} - \frac{\partial (rA_\theta)}{\partial \phi} \right) \hat{\boldsymbol{r}} \\ &+ \frac{1}{R} \left(\frac{\partial A_r}{\partial \phi} - \frac{\partial (RA_\phi)}{\partial r} \right) \hat{\boldsymbol{\theta}} + \frac{1}{r} \left(\frac{\partial (rA_\theta)}{\partial r} - \frac{\partial A_r}{\partial \theta} \right) \hat{\boldsymbol{\phi}}, \end{split}$$

where $R = R_0 + r \cos \theta$. Finally, one has

$$\hat{r} \times \hat{\theta} = \hat{\phi}$$
.

with the remaining relations obtained by circular permutations. Although these coordinates capture many important features of toroidal systems, the majority of the problems arising in equilibrium and stability analyses are best tackled in non-orthogonal frames (we explicitly employ orthogonal toroidal coordinates when discussing particle orbits in complex magnetic fields in appendix A).

Summarising, we now have all the theoretical tools for understanding the principles of tokamak dynamics:

- i) A basic understanding of what a tokamak is and which key components characterise it
- ii) A physical model which can describe low-frequency, long-wavelength plasma dynamics
- iii) The mathematical tools needed to describe complex geometries, such as those of tokamak devices

The three tools listed above will be used in the next chapters first for the description of tokamak equilibrium, and then for assessing its stability against various types of perturbations (to each of which a chapter will be dedicated).

References

- R. Balescu, Transport Processes in Plasmas Vol. 2 Neoclassical Transport Theory, North-Holland (Amsterdam, NL), 1988.
- W. D. D'haeseleer *et al.*, Flux Coordinates and Magnetic Field Structure, Springer Berlin (Heidelberg, DE), 1991.
- L. S. Solov'ev and V. D. Shafranov, Reviews of Plasma Physics Vol. 5 p. 1 (Ed. M. A. Leontovich), Consultants Bureau (New York, US), 1970.

Part II EQUILIBRIUM

4

Tokamak equilibrium

This chapter is dedicated to the description of the equilibrium in a tokamak. The fundamental concepts of magnetic surfaces and safety factor are introduced and discussed. The derivation of the Grad-Shafranov equation, i.e. the force balance equation for a toroidally symmetric device, is then presented. This does not follow the usual textbook procedure, rather it exploits the power of the formalism of curvilinear coordinates written in such a way that the connection with the actual geometry of the physical system is more evident. A brief discussion on a particular analytically exact solution, namely the Solov'ev equilibrium, is given before introducing the approximate solution methods based on the thin torus ansazt. We discuss the ordering of the relevant physical quantities, and the order-by-order solution of the Grad-Shafranov equation. Finally, we address the equilibrium condition in the vacuum region separating the plasma from the surrounding vessel. Two additional "boxes" provide a more "intuitive" derivation of the Shafranov shift, and a brief discussion on the equilibrium condition for toroidally rotating plasmas.

4.1 Magnetic surfaces, safety factor and plasma β

A static equilibrium $(\partial/\partial t = 0 \text{ and } u = 0)$ is described by the force balance equation (cf. (2.2))

$$\nabla p = \boldsymbol{J} \times \boldsymbol{B}. \tag{4.1}$$

It is trivial to show that

$$\boldsymbol{B} \cdot \boldsymbol{\nabla} \boldsymbol{p} = 0, \tag{4.2}$$

$$\boldsymbol{J} \cdot \boldsymbol{\nabla} \boldsymbol{p} = 0, \tag{4.3}$$

Figure 4.1: Right handed cylindrical (R, Z, ϕ) and toroidal (r, θ, ϕ) coordinate systems. The dashed line lying on the surface of radius r indicates a B or J field line.

indicating that both magnetic field and current lines lie on constant pressure surfaces (**isobars**). A surface which is covered by a magnetic field line is called **magnetic** or **flux surface** (it will be described later the motivation behind this nomenclature). More rigorously, a given smooth surface S with normal vector \mathbf{n} is a flux surface of a smooth vector field \mathbf{B} when $\mathbf{B} \cdot \mathbf{n} = 0$ everywhere on S, that is the field \mathbf{B} does not cross the surface S anywhere. The relations above show that pressure is constant along the field (or current) lines.

Let us assume that closed toroidally symmetric nested isobaric surfaces exist. The innermost surface, which collapses to a single line, is called the magnetic axis. Each of these surfaces is labelled by the variable r (the so called **flux label**, also the reason for this will be clear later), which has the dimension of a length and is zero on the magnetic axis, so that p = p(r) and $\nabla p = \frac{dp}{dr} \nabla r$. We often refer to r as the radius (implicitly of the plasma column). We introduce the right handed coordinate system (r, θ, ϕ) as shown in figure 4.1, where θ and ϕ are the poloidal-like (short way around the torus) and geometric toroidal (long way around the torus) angles respectively. In this report we take the poloidal-like angle θ to be always counter-clockwise. It is important to stress the fact that constant θ curves may not necessarily be "straight". This reflects the freedom in choosing the poloidal angular variable: constant θ curves are indeed rays centred on the magnetic axis if θ is the geometric poloidal angle, but this might not hold true anymore if different definitions of the angular variable, which turn out to be more convenient for certain problems, are taken. Finally, toroidal symmetry requires that $\frac{\partial f}{\partial \phi} = 0$ for any scalar function f.

The coordinates (r, θ, ϕ) are associated with the basis vectors

$$(\boldsymbol{e}_r, \boldsymbol{e}_\theta, \boldsymbol{e}_\phi)$$
, covariant basis, $(\nabla r, \nabla \theta, \nabla \phi)$, contravariant basis.

The scalar product of these quantities yields the metric tensor coefficients discussed in chapter 3, and because of axisymmetry we have $g_{r\phi}=g_{\theta\phi}=g^{r\phi}=g^{\theta\phi}=0$ while $g_{\phi\phi}=1/g^{\phi\phi}=R^2$ (the exact expressions of the remaining terms is not required at this stage).² Let \sqrt{g} be the Jacobian associated with (r,θ,ϕ) . In this coordinate system, equations (4.2) and (4.3) read

$$\mathbf{B} \cdot \nabla r = B^r = 0,$$
$$\mathbf{J} \cdot \nabla r = J^r = 0.$$

We decompose the magnetic field into two components, one parallel and the other perpendicular to the toroidal direction. This leads to

$$\boldsymbol{B} = F \boldsymbol{\nabla} \phi - \boldsymbol{\nabla} \psi(r) \times \boldsymbol{\nabla} \phi \equiv F \boldsymbol{\nabla} \phi + \boldsymbol{B}_{p}. \tag{4.4}$$

The divergence-free condition is fulfilled by the equation above, as well as the requirement of vanishing radial magnetic field. i.e. Eq. (4.2).

¹ The toroidal derivative might not be zero for vector quantities.

² At fixed *R* and *Z*, i.e. $dr = d\theta = 0$, the square of the length element is $d\ell^2 = g_{\phi\phi} d\phi^2$ (see (3.1)).

Now consider a ring-shaped ribbon S_p stretched between the magnetic axis and the surface labelled by r at constant θ as in Fig. 4.2. The infinitesimal surface is

$$d\Sigma_p = 2\pi R d\ell,$$

where the length element $d\ell = \sqrt{g_{rr}}dr$ is obtained from (3.1).³ The unit vector normal to this surface is (see (3.4))

$$\boldsymbol{n}_p = \frac{\boldsymbol{e}_\phi \times \boldsymbol{e}_r}{|\boldsymbol{e}_\phi \times \boldsymbol{e}_r|} = \frac{\boldsymbol{\nabla} \theta}{|\boldsymbol{\nabla} \theta|} = \frac{\boldsymbol{\nabla} \theta}{\sqrt{g^{\theta \theta}}} = \frac{\sqrt{g}}{R \sqrt{g_{rr}}} \boldsymbol{\nabla} \theta.$$

We find that the quantity ψ measures the flux of the magnetic field through this ribbon, indeed $(\nabla r \cdot \nabla \theta \times \nabla \phi = 1/\sqrt{g})$

$$\int_{S_b} \boldsymbol{B} \cdot \boldsymbol{n}_p d\Sigma_p = 2\pi \int_0^r \boldsymbol{B} \cdot \boldsymbol{\nabla} \theta \sqrt{g} dr = 2\pi \bigg(\psi(r) - \psi(0) \bigg).$$

Hence, we refer to ψ as the **poloidal flux**. From (4.4) one sees that \boldsymbol{B} is invariant apart from an arbitrary additional constant in ψ . Thus, we set for convenience $\psi(0)=0$. We may therefore define the poloidal flux as

$$\psi(r) = \frac{1}{2\pi} \int_0^r \int_0^{2\pi} \mathbf{B} \cdot \nabla \theta \sqrt{g} dr d\theta. \tag{4.5}$$

It is then trivial to see that constant p surfaces correspond to constant ψ surfaces. From this, isobaric surfaces are also called **flux surfaces** and the variable r is referred to as **flux label**. As a matter of terminology, any function which is constant on a magnetic surface is called *surface quantity*.

Analogously, let now S_t be a surface in the (R, Z) plane at ϕ constant with normal unit vector $\mathbf{n}_t = \nabla \phi / |\nabla \phi| = R \nabla \phi$. Its associated infinitesimal surface is $d\Sigma_t = \frac{\sqrt{g}}{R} dr d\theta$. One can then introduce the **toroidal flux** function Φ via

$$2\pi\Phi(r) = \int_{S_t} \mathbf{B} \cdot \mathbf{n}_t d\Sigma_t = \int_0^r \int_0^{2\pi} \mathbf{B} \cdot \nabla \phi \sqrt{g} dr d\theta, \qquad (4.6)$$

having set $\Phi(0) = 0$. Finally, from (4.3), we have

$$0 = \mu_0 J^r = \frac{1}{\sqrt{g}} \left(\frac{\partial B_{\phi}}{\partial \theta} - \frac{\partial B_{\theta}}{\partial \phi} \right) = \frac{1}{\sqrt{g}} \frac{\partial F}{\partial \theta}$$

which shows that also F is a function of r, i.e. F = F(r).

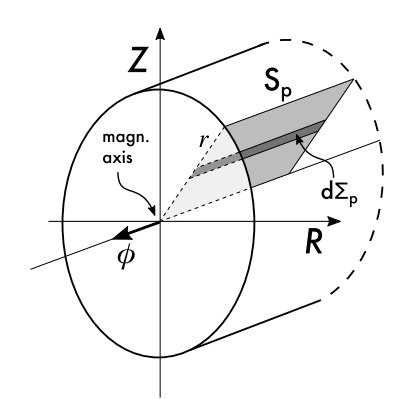
We shall now introduce two quantities of fundamental importance in tokamak physics: the safety factor and the plasma β .

4.1.1 The safety factor q

The equation for a magnetic field line, that is a line which is tangent to vector field \mathbf{B} at each point, reads

$$\mathbf{B} = c d\ell$$
.

³ Note that we work at θ fixed and the integration along the toroidal coordinate gives the factor $2\pi R$.



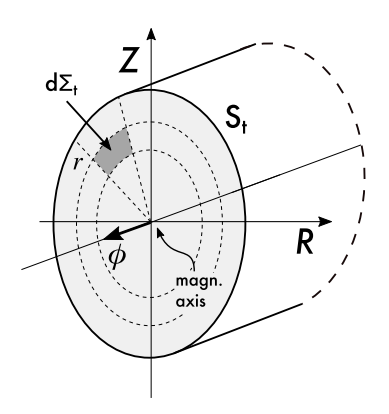


Figure 4.2: Surfaces S_p and S_t used to calculate the magnetic fluxes ψ and Φ . The surface S_p covers the full range $0 \le \phi \le 2\pi$ and it can be taken between the magnetic axis and any circle R = const, Z = const lying on the magnetic surface.

where c is a proportionality constant and $d\ell = dre_r + d\theta e_\theta + d\phi e_\phi$ is a differential vector tangent to the field line. This is equivalent to $\mathbf{B} \times d\ell = 0$. This yields

$$\frac{B^{\theta}}{d\theta} = \frac{B^{\phi}}{d\phi} = c,$$

which can be rearranged giving

$$\frac{d\phi}{d\theta} = \frac{B^{\phi}}{B^{\theta}}. (4.7)$$

Integration of the equation above over a poloidal circuit along the flux surface yields

$$q \equiv \frac{\Delta \phi}{2\pi} = \frac{1}{2\pi} \int_0^{2\pi} \frac{B^{\phi}}{B^{\theta}} d\theta. \tag{4.8}$$

Viewing the field line from the top of the torus, we select a toroidal angle ϕ_0 from which the field line starts off. After one poloidal turn, the field line will be at a different toroidal location, i.e. $\phi_0 + \Delta \phi$. This means that q measures the progression of the field line over the toroidal angle after one full poloidal revolution. If q = m/n with both m and n integers, the field line will return in its original position after m toroidal and n poloidal transits around the torus (see figure 4.3). If the value of q is irrational, the magnetic surface is covered ergodically by the field line. We call the quantity q the **safety factor**.⁴

The safety factor can also be expressed in terms of magnetic fluxes. Indeed, from (4.6) we readily have

$$\frac{d\Phi}{dr} = \frac{1}{2\pi} \int_0^{2\pi} B^{\phi} \sqrt{g} \, d\theta.$$

Thus, plugging $\sqrt{g}B^{\theta}=d\psi/dr$ into (4.8), and using the expression above, gives

$$q = \frac{d\Phi}{dv}$$

which is the rate of change of the toroidal flux with the poloidal flux. Later we will see how the safety factor relates to the current density profile.

4.1.2 Plasma β

The ratio of the kinetic pressure p over the magnetic pressure $B^2/2\mu_0$ can be used as an indicator of the plasma performance. This ratio is denoted by β . There are several definitions of β in the literature, and the one that we adopt in this report is

$$\beta = \frac{2\mu_0 p_V(a)}{B_0^2} \tag{4.9}$$

where B_0 is the magnetic field on the magnetic axis, a is the value of the flux label r at the plasma boundary and p_V is the volume averaged



Figure 4.3: Trajectory of a field line with q = 3/2.

⁴ In **cylindrical geometry** the safety factor takes the simple form

$$q=\frac{rB_T}{R_0B_p},$$

with B_T and B_p the physical toroidal and poloidal magnetic field, and R_0 the position of the magnetic axis.

pressure, that is⁵

$$p_{V}(r) = \frac{\int_{0}^{2\pi} d\theta \int_{0}^{r} \sqrt{g} p dr}{\int_{0}^{2\pi} d\theta \int_{0}^{r} \sqrt{g} dr}.$$
 (4.10)

As a matter of notation, in the remainder of this chapter B_0 will always denote the axis value of the magnetic field. In standard tokamaks β is usually a small number, ranging between 1% and 10%, while higher β values have been attained in more compact devices, although with a smaller magnetic field.

With a smooth pressure profile, one finds that β is typically proportional to the ratio of the pressure on the axis p(0) and B_0^2 , i.e.

$$\beta \sim \frac{2\mu_0 p(0)}{B_0^2}.$$

Notice that, according to definition (4.9), β is a global quantity, i.e. it does not capture the local features of the kinetic pressure. For cases in which the local structure of the pressure profile is needed, in particular information about its gradients, it is more convenient to use the local beta value

$$eta_{loc}(r) = rac{2\mu_0 p(r)}{B_0^2}.$$

Both β and β_{loc} play an important role in determining equilibrium and global MHD stability properties against small perturbation.

4.2 The Grad-Shafranov equation

The aim of this section is to derive an equilibrium equation for the plasma toroid, written in terms of p, ψ and F (or alternatively Φ). We start by noting that (4.1) gives a trivial identity 0 = 0 when dotted with either e_{θ} or e_{ϕ} . Thus, projecting (4.1) along the e_r direction and using (3.12) yields

$$\frac{dp}{dr} = \sqrt{g} \left(J^{\theta} B^{\phi} - J^{\phi} B^{\theta} \right). \tag{4.11}$$

As mentioned earlier, in an axisymmetric configuration we have $g_{r\phi}=g_{\theta\phi}=0$ and $R^2=g_{\phi\phi}=1/g^{\phi\phi}$, so that $B^{\phi}=F(r)/R^2$ and $\sqrt{g}J^{\theta}=-\frac{1}{\mu_0}dF/dr$. Using these results into (4.11) we obtain

$$\frac{dp}{dr} = -\frac{F}{\mu_0 R^2} \frac{dF}{dr} - J^{\phi} \frac{d\psi}{dr}.$$
 (4.12)

Furthermore, by means of (4.4) one has

$$\mu_0 J^{\phi} = \nabla \phi \cdot \nabla \times \boldsymbol{B} = \nabla \cdot (\boldsymbol{B} \times \nabla \phi) = \nabla \cdot \left(\frac{1}{R^2} \nabla \psi\right). \tag{4.13}$$

Since both p and F are function of r only, we can safely divide (4.12) by $d\psi/dr$. Thus, using the equation above we get⁶

$$\boldsymbol{\Delta}^* \psi \equiv R^2 \boldsymbol{\nabla} \cdot \left(\frac{1}{R^2} \boldsymbol{\nabla} \psi \right) = -F \frac{dF}{d\psi} - \mu_0 R^2 \frac{dp}{d\psi}, \tag{4.14}$$

⁵ The denominator corresponds to the volume enclosed by a flux surface of radius r.

If $J^{\phi}=0$, the left-hand-side of (4.12) is function of r only while the right-hand-side depends also on θ which indicates that no equilibrium with toroidal nested closed flux surfaces can exist.

⁶ Notice that $\nabla r = g^{rr}e_r + g^{r\theta}e_\theta$. Since the e_θ projection of (4.1) vanishes, then dotting it with e_r is equivalent to projecting along ∇r . Hence the Grad-Shafranov equation is an equation for the radial force balance.

⁷ This equation can be derived in a more general way without assuming nested flux surfaces by exploiting the divergenceless of the magnetic field and current density.

which is the celebrated **Grad-Shafranov equation**.⁷ This is a non-linear, second order elliptic partial differential equation for the equilibrium flux ψ . The geometry of the associated flux surfaces is computed after prescribing the functions $p(\psi)$ and $F(\psi)$ (or more specifically $FdF/d\psi$), namely the pressure and poloidal current distribution, and the boundary conditions or external constraints on ψ itself (these may be the shape of the last plasma surface).⁸ The way it is written is particularly powerful, in that the left-hand-side is independent of the system of coordinates on a given flux surface.

The solution of (4.14) can be tackled either numerically, usually involving an iterative procedure for the inversion of the operator Δ^* until convergence is reached, or analytically. Most of the analytical approaches are based on a series expansion in the small curvature ansatz. Before moving to the discussion of these approximate methods, which form the backbone of the tools employed in the stability analysis, it is instructive to present an exact solution of (4.14), although limited in its applicability.

4.2.1 The Solov'ev equilibrium

Let us write the operator Δ^* in cylindrical coordinates (R, Z, ϕ) as (cf. figure 4.1)

$$\mathbf{\Lambda}^* \psi = R \frac{\partial}{\partial R} \left(\frac{1}{R} \frac{\partial \psi}{\partial R} \right) + \frac{\partial^2 \psi}{\partial Z^2}.$$

The right-hand-side of (4.14) is simplified by choosing

$$\mu_0 \frac{dp}{d\psi} = -a, \quad F \frac{dF}{d\psi} = b,$$

where a and b are constants. This yields

$$R\frac{\partial}{\partial R}\left(\frac{1}{R}\frac{\partial\psi}{\partial R}\right) + \frac{\partial^2\psi}{\partial Z^2} = -b + R^2a. \tag{4.15}$$

We seek an up-down symmetric solution based on the expansion

$$\psi = \sum_{k=0}^{\infty} f_k(R) Z^{2k}.$$

Imposing $f_{k\geq 2}(R)=0$, a particular solution of (4.15) is given by

$$\psi = \frac{1}{2}(c_0R^2 - b)Z^2 + \frac{(a - c_0)}{8}(R^2 - R_0^2)^2,$$
 (4.16)

where c_0 is an arbitrary constant, and R_0 the position of the magnetic axis (i.e. the position for which $\partial \psi/\partial R|_{Z=0}=0$). This is the so called **Solov'ev equilibrium**. An example of the various $\psi=const$ surfaces parametrised by (4.16) is shown in figure 4.4. Despite the rather restrictive profiles for pressure and poloidal current, there is a wide degree of flexibility on the shape of the boundary surfaces that can be obtained.

⁸ Analogous equations can be derived for toroidal systems for which the axisymmetry constraint is relaxed. Note that in the numerical solution of the Grad-Shafranov equation one can prescribe as an input the shape of the toroidal current density or the safety factor instead of $FdF/d\psi$.

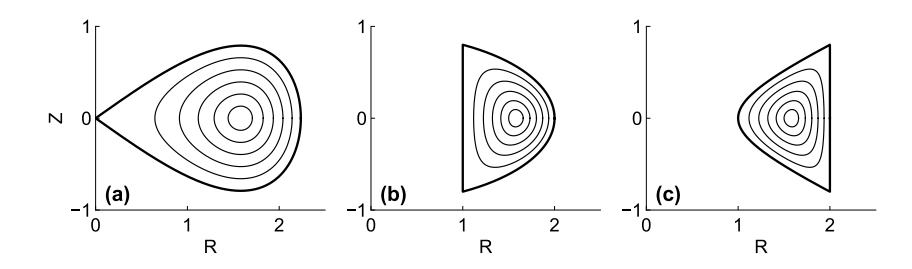


Figure 4.4: Constant flux surfaces computed with the Solov'ev solution Eq. (4.16) with parameters $R_0 = \sqrt{5/2}$ and (a) $c_0 = 0$, $a/b = -1/R_0^2$, (b) $c_0/b = 1$, a/b = 1.8533, (c) $c_0/b = 1/4$, a/b = 0.0367

The Solov'ev solution has also the pleasant property that R and Z can be explicitly written as functions of ψ and an appropriate angle-like variable Θ . Let us define

$$f^2 = \frac{(a-c_0)}{8}(R^2-R_0^2)^2$$
, $g^2 = \frac{1}{2}(c_0R^2-b)Z^2$,

and $\tan\Theta=g/f$ so that $\psi=f^2+g^2$. It easily follows that $f^2=\psi\cos^2\Theta$ and $g^2=\psi\sin^2\Theta$ which gives

$$\begin{split} R(r,\Theta) &= R_0 \sqrt{1 + \frac{2r}{R_0} \cos \Theta}, \\ Z(r,\Theta) &= \frac{r \sqrt{a - c_0} \sin \Theta}{\sqrt{c_0 \left(1 + \frac{2r}{R_0} \cos \Theta\right) - b/R_0^2}} \end{split}$$

where we introduced the "radial" variable $r=\sqrt{\frac{2\psi}{R_0^2(a-c_0)}}$. Letting r_b the value of r at the boundary surface, the quantities a, c_0, r_b and R_0 can be expressed in terms of $R_{in}=R(r_b,\pi), R_{out}=R(r_b,0), R_{mid}=R(r_b,\Theta_M)$ and $Z_{max}=Z(r_b,\Theta_M)$ (see figure 4.5) where Θ_M is determined by solving $\partial Z/\partial\Theta|_{r=r_b}=0$.

Although other exact solutions can be found, either by generalising the procedure above or with different p and F profiles, these usually lack the required flexibility to describe the broad variety of plasma scenarios encountered in the experiments. Therefore, an alternative method is devised which, despite the fact of being highly approximated, has the great advantage of providing algebraically simple results, yet complete of all the relevant physical ingredients.

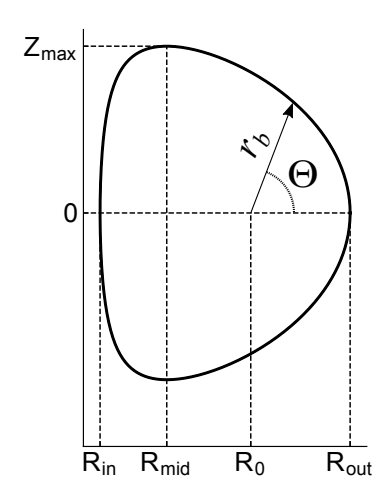


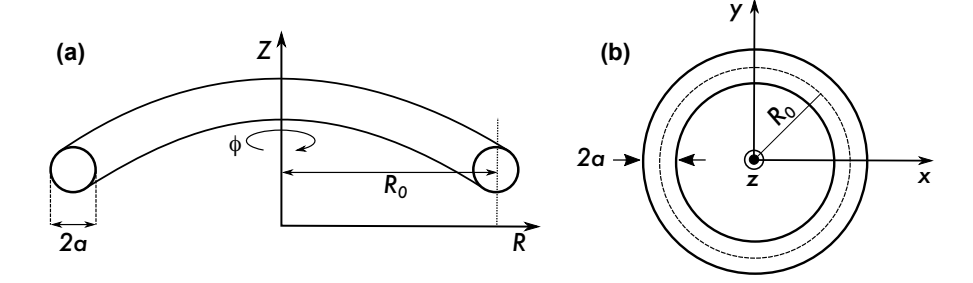
Figure 4.5: Definition of the geometric parameters for the Solov'ev equilibrium.

4.3 Large aspect ratio expansion: The plasma solution

We consider a torus of nearly circular up-down symmetric cross section with nested flux surfaces within. We further assume that the magnetic axis lies on the equatorial Z=0 plane. The R position of the magnetic axis, namely the **major radius**, is denoted by R_0 . As in the previous sections, we use the coordinate system $(r, \theta, \phi)^9$ with the toroidal symmetry constraint $\partial/\partial\phi=0$.

⁹ In this toroidal right-handed coordinate system, the poloidal angle is always **counterclockwise** (cf. Figs. 4.1 and 4.5). In old papers, though, this angle is often taken clockwise with the direction of ϕ flipped.

Figure 4.6: Sketch of a circular tokamak geometry: (a) cross section and (b) tokamak top view.



In early tokamak experiments it was found that the plasma underwent a displacement during the discharge, leading to a contact with the surrounding structures. This suggested to parametrise the R and Z coordinates of the flux surfaces with a Fourier series of the type

$$R(r,\theta) = R_0 + r\cos\theta - \Delta(r) + \sum_{m=1}^{\infty} R_{c,m}(r)\cos m\theta, \qquad (4.17)$$

$$Z(r,\theta) = r\sin\theta + \sum_{m=1}^{\infty} Z_{s,m}(r)\sin m\theta.$$
 (4.18)

with $\Delta(r)/r$, $R_{c,m}(r)/r$, $Z_{s,m}(r)/r \ll 1$. We refer to $R_{c,m}$ and $Z_{s,m}$ as the **shaping parameters**. This parametrisation relates to the Cartesian coordinates (x, y, z) through (cf. chapter 3)

$$x = R \sin \phi$$
, $y = R \cos \phi$, $z = Z$,

and the metric coefficients and Jacobian associated with the coordinate system (r, θ, ϕ) are

$$g_{rr} = \left(\frac{\partial R}{\partial r}\right)^{2} + \left(\frac{\partial Z}{\partial r}\right)^{2},$$

$$g_{\theta\theta} = \left(\frac{\partial R}{\partial \theta}\right)^{2} + \left(\frac{\partial Z}{\partial \theta}\right)^{2},$$

$$g_{r\theta} = \frac{\partial R}{\partial r}\frac{\partial R}{\partial \theta} + \frac{\partial Z}{\partial r}\frac{\partial Z}{\partial \theta},$$

$$g_{\phi\phi} = R^{2},$$

$$\sqrt{g} = \sqrt{g_{\phi\phi} \left[g_{rr}g_{\theta\theta} - (g_{r\theta})^{2}\right]}.$$

$$(4.19)$$

It is trivial to show that $g_{r\phi}=g_{\theta\phi}=0$ due to axisymmetry.

The quantity $\Delta(r)$, known as the **Shafranov shift**, measures the **inward** displacement of the flux surfaces with respect to R_0 .¹⁰ Equations (4.17) and (4.18) ensure the up-down symmetry with respect to the equatorial plane. If the up-down symmetry constraint is relaxed, we should allow for $\sin m\theta$ and $\cos m\theta$ terms in (4.17) and (4.18) respectively. The radial variable r extends up to r = a, and the radius a is called **minor radius**: it corresponds roughly to the distance of the outermost plasma flux surface from its geometric centre (cf. figure 4.6).

The metric tensor is (cf. (3.4))

$$g_{ij} = \begin{pmatrix} g_{rr} & g_{r\theta} & 0 \\ g_{r\theta} & g_{\theta\theta} & 0 \\ 0 & 0 & g_{\phi\phi} \end{pmatrix}$$

$$= g \begin{pmatrix} g^{\theta\theta} g^{\phi\phi} & -g^{r\theta} g^{\phi\phi} & 0 \\ -g^{r\theta} g^{\phi\phi} & g^{rr} g^{\phi\phi} & 0 \\ 0 & 0 & g^{rr} g^{\theta\theta} - (g^{r\theta})^2 \end{pmatrix}.$$

 $^{^{10}}$ Here Δ is zero on the axis and maximum at the plasma boundary, i.e. is a shift relative to the magnetic axis. Often in the literature the Shafranov shift refers to the displacement of the flux surfaces relative to the geometric centre of the outermost one. In this case the shift is zero at the plasma boundary and maximum on the magnetic axis.

We introduce the **large aspect ratio approximation**, which consists in assuming that the torus is thin, that is

$$\varepsilon \equiv \frac{a}{R_0} \ll 1.$$

The parameter ε is called the **inverse aspect ratio**.

Now, the aim is to solve perturbatively the force balance equation written as an appropriate power series in the small parameter ε . We recast Eq. (4.12) in a more convenient form as

$$\mu_0 \frac{dp/B_0^2}{dr} = -\frac{F}{B_0^2 R^2} \frac{dF}{dr} - \mu_0 J^{\phi} \frac{d\psi}{dr} / B_0^2, \tag{4.20}$$

where we recall that B_0 is the value of the magnetic field on the axis. This equation depends on the flux quantities p, F and ψ , and on the shape of the magnetic surfaces through the metric coefficients appearing in the toroidal current

$$\mu_0 J^{\phi} = \frac{1}{\sqrt{g}} \left[\frac{\partial}{\partial r} \left(\frac{g_{\theta\theta}}{\sqrt{g}} \frac{d\psi}{dr} \right) - \frac{\partial}{\partial \theta} \left(\frac{g_{r\theta}}{\sqrt{g}} \right) \frac{d\psi}{dr} \right]. \tag{4.21}$$

Hence, assuming that the profiles for the pressure p and the toroidal current J^{ϕ} are prescribed functions, from (4.20) we can derive the equations for F, Δ and the shaping parameters, whose solutions will determine the equilibrium. Note that this is slightly different compared to the approach employed for the Solov'ev solution, in which the pressure and toroidal field profiles were imposed.

Thus, the solution strategy consists in the following steps: i) deploy an appropriate ε -ordering of the equilibrium quantities and determine the approximate expressions of the metric coefficients, and ii) plug the resulting expressions into (4.20) and solve it order by order in ε . We shall now go through each of these steps one by one.

4.3.1 ε -ordering

Let us assume that the pressure is a regular and smooth function of r with no strong localised gradients. The first term on the left-hand-side of (4.20) is proportional to the ratio of the kinetic pressure over the magnetic pressure, i.e. β . As discussed before (cf. section 4.1.2), this quantity is typically a small number, ¹¹ so that we order

$$\mu_0 p/B_0^2 \sim \varepsilon^2$$
,

with the symbol \sim meaning "of the order of". The toroidal component of the magnetic field is 12

$$B_{tor} = rac{oldsymbol{B} \cdot oldsymbol{e}_{\phi}}{|oldsymbol{e}_{\phi}|} = rac{F}{R},$$

so that, letting $F_0 = F(r = 0)$, we obtain

$$F \sim F_0 = R_0 B_0$$
.

It will be clear that imposing the current density corresponds to giving the safety factor profile q.

¹¹ High- β tokamaks, for which $\beta \sim \varepsilon$, and their associated pressure limits are not discussed.

¹² Recall that $|e_{\phi}| = \sqrt{g_{\phi\phi}} = R$.

The toroidal field is usually stronger than the poloidal one. Thus under the assumption $B_{pol}/B_{tor}\sim \varepsilon$, and noting that $B_{tor}\sim F|\nabla\phi|$ and $B_{pol}\sim \frac{d\psi}{d\tau}|\nabla\phi|$, we obtain from (4.4)

$$\frac{d\psi}{dr}\sim \varepsilon R_0 B_0.$$

From this, the contravariant toroidal current density is ordered as

$$\mu_0 J^{\phi} \sim \varepsilon \frac{B_0}{aR_0}$$
.

The metric coefficients appearing in J^{ϕ} can be easily computed by noting that, normally, the experimentally measured shift of the flux surfaces is much smaller than the minor radius. Therefore, we let

$$\Delta \sim \varepsilon r,$$
 $R_{c,m} \sim Z_{s,m} \sim \varepsilon^2 r,$

yielding (hereafter we will use the notation $f'(r) \equiv \frac{df(r)}{dr}$ or $f'(r) \equiv \frac{\partial f(r,\theta,\phi)}{\partial r}$ for a generic function f)

$$g_{rr} = 1 - 2\Delta' \cos \theta + \dots,$$

$$g_{\theta\theta} = r^2 + \dots,$$

$$g_{r\theta} = r\Delta' \sin \theta + \dots,$$

$$g_{\phi\phi} = R_0^2 \left(1 + 2\frac{r}{R_0} \cos \theta + \dots \right),$$

$$\sqrt{g} = rR_0 \left[1 + \left(\frac{r}{R_0} - \Delta' \right) \cos \theta + \dots \right],$$

$$(4.22)$$

where the terms omitted in the ε expansion are of order ε^2 .

We shall note that by employing this ε ordering and using the expressions for the metric coefficients above, we can write the flux ψ as a function of the safety factor q. Indeed, since $B^{\theta} = \psi'/\sqrt{g}$ and $B^{\phi} = F/R^2$, by means of (4.8) we have

$$\psi' = \frac{F}{2\pi q} \int_0^{2\pi} \frac{\sqrt{g}}{R^2} d\theta. \tag{4.23}$$

Expanding R and the Jacobian in ε , it is immediate to obtain¹³

$$\frac{1}{2\pi} \int_0^{2\pi} \frac{\sqrt{g}}{R^2} d\theta \approx \frac{r}{R_0} \left(1 + o(\varepsilon^2) \right).$$

Therefore, to order ε we have

$$\psi' = \frac{rF}{gR_0} \left(1 + o(\varepsilon^2) \right). \tag{4.24}$$

Now we can proceed in solving (4.20) order by order in ε .

This corresponds to a weak plasma shaping for which the flux surfaces are nearly circular.

¹³ The meaning of the small oh notation should be clear, i.e. $o(\varepsilon) \sim \varepsilon$.

4.3.2 Equilibrium at leading orders

We impose that the pressure p and the safety factor q are known functions. By inspecting the pressure and toroidal current terms in (4.20), both of order ε^2/r , it is evident that

$$F = R_0 B_0 [1 + g(r) + h(r) + f(r) + \dots],$$

$$g(r) \sim \varepsilon^2, \quad h(r) \sim \varepsilon^3, \quad f(r) \sim \varepsilon^4.$$
(4.25)

Thus, plugging this into (4.24) yields

$$\psi' = \frac{rB_0}{q} \left(1 + o(\varepsilon^2) \right). \tag{4.26}$$

The expression for the term involving the toroidal current density is

$$\mu_0 J^{\phi} \psi' \approx \frac{\psi' (r\psi')'}{rR_0^2} + \frac{\psi'}{rR_0^2} \left[\left(\Delta' - \frac{r}{R_0} \right) (r\psi')' + \frac{\partial}{\partial r} \left(\left(\Delta' - \frac{r}{R_0} \right) r\psi' \right) - \Delta' \psi' \right] \cos \theta. \tag{4.27}$$

Since this does not have non-oscillating (in θ) terms of order ε^3 it follows that in Eq. (4.25) we must set h=0. Furthermore, at leading order one has $J^{\phi} \sim (r\psi')'/r$. In most experimentally relevant situations, J^{ϕ} has a finite value on the magnetic axis. Thus, in order to fulfil this condition, we must have $\psi' \sim r^{\alpha}$ with $\alpha \geq 1$ near the axis. In this report we restrict the analysis to the $\alpha=1$ case. Cases with $\alpha>1$, which will not be discussed, describe the so called *current-hole* configurations in which the toroidal current vanishes at r=0. Note that for $\alpha=1$ Eq. (4.26) yields a finite q at the magnetic axis, whereas $q(0) \to \infty$ when $\alpha>1$.

Hence, by means of (4.26) the current density can be expressed to order ε as a function of the safety factor q through the relation

$$\mu_0 J^{\phi} = \frac{B_0}{r R_0^2} \left(\frac{r^2}{q}\right)'. \tag{4.28}$$

From this, the total plasma toroidal current I_p is easily computed and reads

$$I_{p} = \int_{0}^{2\pi} d\theta \int_{0}^{a} dr \sqrt{g} J^{\phi} \propto \frac{1}{q(a)}, \tag{4.29}$$

where the latter estimate has been obtained by setting $\sqrt{g} \approx rR_0$. Figure 4.7 shows some experimentally relevant shapes of the safety factor and current density.

Thus, to leading order (4.20) gives

$$\frac{\mu_0 p'}{B_0^2} + g' + \frac{(r^2 \psi'^2)'}{2r^2 R_0^2 B_0^2} = 0, (4.30)$$

which is the radial force balance for a straight **screw-pinch**, namely a cylindrically symmetric configuration with a strong longitudinal field

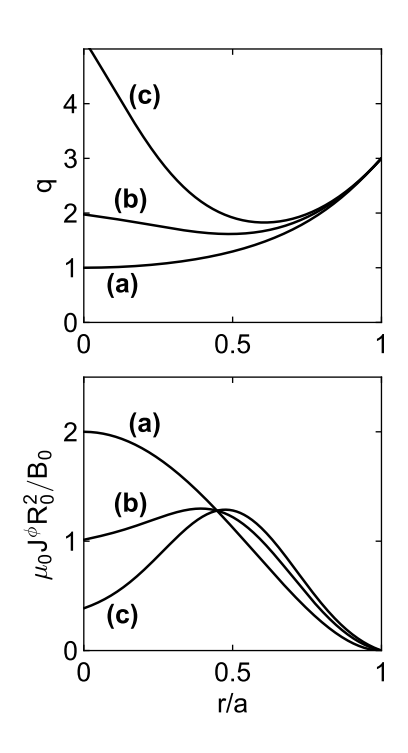


Figure 4.7: Typical safety factor and associated toroidal current density profiles in tokamaks: (a) monotonic, (b) hollow, and (c) strongly reversed configuration, the latter exhibiting a current-hole if $J^{\phi} \rightarrow 0$ on the axis.

We flag an abuse of notation for the function under the sign of integration. However, its meaning is obvious, and the same notation will be used in other integral expressions. and a small poloidal field (equivalent to a tokamak with an infinite radius of curvature). The equation above can be easily integrated, and using (4.26) we obtain an ε expansion of the function F correct to second order which reads

$$F = R_0 B_0 \left[1 - \frac{\mu_0 \left(p - p(0) \right)}{B_0^2} - \int_0^r \frac{r}{R_0^2 q^2} \left(2 - \frac{rq'}{q} \right) dr + \dots \right], \quad (4.31)$$

where p(0) = p(r = 0) and the constant of integration has been chosen such that $F_0 = R_0 B_0$. The quantity

$$s \equiv \frac{rq'}{q} \tag{4.32}$$

is known as **magnetic shear** and plays a key role in determining the tokamak stability properties (this will be discussed in the next chapters).

To next order in ε , equation (4.20) is oscillating in θ and yields

$$0 = \frac{2rg'}{R_0}\cos\theta - \left(\frac{\psi'}{R_0B_0}\right)^2 \left[\Delta'' + 2\frac{(r\psi')'}{r\psi'}\left(\Delta' - \frac{r}{R_0}\right) - \frac{1}{R_0} - \frac{\Delta'}{r}\right]\cos\theta.$$

Using (4.30) for expressing g', we obtain an equation for the radial displacement of the magnetic surfaces

$$0 = \Delta'' + \left(\frac{1}{r} + \frac{2\psi''}{\psi'}\right) \Delta' + \frac{2\mu_0 r R_0 p'}{(\psi')^2} - \frac{1}{R_0}$$

$$= \Delta'' + \left(\frac{3}{r} - \frac{2q'}{q}\right) \Delta' + \frac{2\mu_0 R_0 p' q^2}{r B_0^2} - \frac{1}{R_0}, \tag{4.33}$$

where the second equality has been obtained by means of (4.26). This expression is usually solved numerically, although exact analytical solutions can be found with simple p and q profiles. The two constants of integration appearing in the solution of (4.33) are determined by requiring that Δ vanishes on the magnetic axis. This implies that at the plasma boundary Δ has a finite value.

By means of the identity

$$\frac{1}{r} + \frac{2\psi''}{\psi'} = \frac{\left[r(\psi')^2\right]'}{r(\psi')^2},$$

we can integrate (4.33) once giving

$$\Delta' = \frac{1}{r(\psi')^2} \int_0^r r(\psi')^2 \left(\frac{1}{R_0} - \frac{2\mu_0 r R_0 p'}{(\psi')^2} \right) dr, \tag{4.34}$$

where the limits of integration have been chosen in order to avoid singularities at r = 0. Interestingly, we note that the toroidal field does not enter the expression above. Using (4.26), equation (4.34) can be recast (to leading order in ε) in a more compact form as

$$\Delta' = \frac{r}{R_0} \left(\beta_p(r) + \frac{\ell_i(r)}{2} \right), \tag{4.35}$$

having defined the poloidal plasma β

$$\beta_{p}(r) = \frac{2\mu_{0}R_{0}^{2}q^{2}}{r^{2}B_{0}^{2}} \left[p_{V}(r) - p(r) \right], \tag{4.36}$$

with p_V given by (4.10), and the internal inductance by

$$\ell_i(r) = 2\frac{q^2}{r^4} \int_0^r \frac{r^3}{q^2} dr. \tag{4.37}$$

Note that the quantity β_p is proportional to the ratio of the kinetic pressure over the poloidal magnetic field.

Intuitively, the shift of the flux surfaces, i.e. their compression in the low field side of the torus, balances the outward force in the ∇R direction due to the so called tyre tube (due to pressure) and hoop forces (due to the self-inductance of a current carrying circuit), represented by first and second terms on the right-hand-side of (4.35) respectively (both are briefly discussed in the next subsection).

By assuming ℓ_i to be small compared with the pressure term, one has $\Delta' \sim \frac{r}{R_0} \beta_p(r)$. Thus, as the magnetic pressure is increased, the shift compresses the surfaces on the outboard side so that the increasing of the magnetic pressure balances the outward force.

There is no limitation to the maximum β if the last closed surface enclosing the plasma is directly surrounded by a ideally conducting wall. However, in a realistic experimental situation a vacuum region separates the plasma from the neighbouring structures. In such a case, a **vertical field** is required to maintain the equilibrium (see section 4.4.1) which increases with β . Adding this field produces a separatrix with an X-point (a point of null poloidal field) on the inner side of the torus (cf. figure 4.14). Working at fixed current, as β is increased, the external vertical field must be increased. This moves the X-point closer to the plasma. A limit in β is reached when the X-point "touches" the outermost boundary plasma surface. Some estimates presented at the end of section 4.4.1 indicate that the critical β_p is of the order of $1/\varepsilon$. Since our analysis focusses on the low β case with $\beta_p \sim 1$ at most, we are not concerned with this equilibrium β limit.

In principle, however, such a limit could be eluded if the plasma is heated sufficiently rapidly (with respect to the magnetic skin-time scale) so that the magnetic fluxes would be frozen into the plasma. Additional net currents will be then induced, and the separatrix will be kept outside the plasma. This is the basis of the *flux conserving tokamak* concept. The interested reader is referred to Freidberg (2014) for its thorough discussion.

To summarise, the equilibrium of a circular tokamak whose flux surfaces are parametrised by (4.17) and (4.18) is completely defined to leading order by the relations (4.26), (4.30), (4.31) and (4.33). For shaped cross-sections (e.g. as in Fig. 4.8), the expressions listed above are mod-

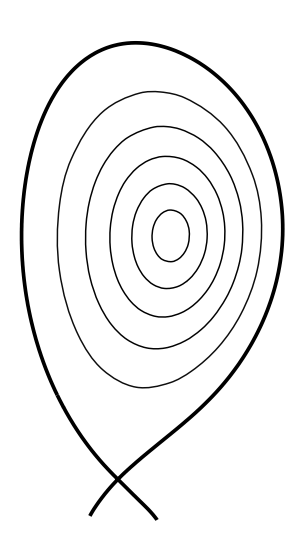


Figure 4.8: Typical cross-section of a tokamak plasma with divertor.

One of the most used flux surface parametrisation with the inclusion of shaping is

$$R = R_0 + r\cos(\theta + \frac{r}{a}\delta\sin\theta) - \Delta,$$

$$Z = \varkappa r\sin\theta.$$

where x and δ measure the plasma elongation and triangularity respectively.

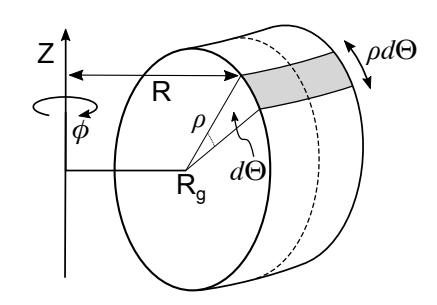


Figure 4.9: Toroidal ribbon surface for the computation of the tyre tube and hoop forces.

It is easy to see that $|\nabla R| = |\nabla Z| = 1$.

ified by the inclusion of the shaping parameters (primarily elongation and triangularity). 14

4.3.3 Tyre tube and hoop forces

Pressure is the amount of force applied perpendicular to the surface per unit area. Mathematically, for a surface Σ with normal vector \boldsymbol{n} such that $d\Sigma \equiv \boldsymbol{n} d\Sigma$ one has

$$d\mathbf{F} = p d\Sigma$$

where dF is the force applied to the surface $d\Sigma$ which is acting in the same direction of n. Assume that constant pressure nested circular flux surfaces centred in R_{ε} can be parametrised as

$$R = R_g + \rho \cos \Theta, \quad Z = \rho \sin \Theta.$$
 (4.38)

The metric tensor coefficients and Jacobian in the coordinate system (ρ, Θ, ϕ) associated with the parametrisation above read (see section 3.1.2)

$$g_{\rho\rho} = 1$$
, $g_{\Theta\Theta} = \rho^2$, $g_{\rho\Theta} = g_{\rho\phi} = g_{\Theta\phi} = 0$, $\sqrt{g} = \rho R$. (4.39)

From (3.4) it follows that $g^{\rho\rho} = 1$ and $g^{\Theta\Theta} = 1/\rho^2$.

We take $d\Sigma$ to be the infinitesimal toroidal ribbon with unit vector normal to the surface $\mathbf{n} = \nabla \rho$ such that $d\Sigma = 2\pi \rho R d\Theta \mathbf{n}$ (cf. (3.2) and figure 4.9). Projecting $d\mathbf{F}$ along the ∇R and ∇Z directions gives

$$\begin{split} dF_R &= d\boldsymbol{F} \cdot \boldsymbol{\nabla} R = 2\pi p \frac{\partial R}{\partial \rho} \rho R d\Theta, \\ dF_Z &= d\boldsymbol{F} \cdot \boldsymbol{\nabla} Z = 2\pi p \frac{\partial Z}{\partial \rho} \rho R d\Theta. \end{split}$$

By integrating in Θ the two expressions above and using (4.38), we obtain the net forces F_R and F_Z . It is immediate to see that $F_Z = 0$ whereas

$$F_R = 2\pi^2 p \rho^2,$$

which gives an outward force in the ∇R direction. This is the **tyre tube force**, which is analogous to the force experienced by a rubber tyre which tends to expand due to the air pressure within.

The hoop force is similar to the tyre tube one, with the kinetic pressure p replaced by the magnetic pressure B^2 . Using (4.4) and imposing $F = F(\rho)$ and $\psi = \psi(\rho)$, it is immediate to see that $B^2 \sim 1/R^2$. This yields

$$dF_R \propto rac{\partial R/\partial
ho}{R} d\Theta, \quad dF_Z \propto rac{\partial Z/\partial
ho}{R} d\Theta.$$

As before, integrating in Θ shows that there is a net force outwards in the radial direction.

4.3.4 Equilibrium with local steep gradients

We shall now briefly discuss the properties of equilibria characterised by the presence of localised steep pressure gradients. Let us consider a large aspect ratio tokamak with nearly circular cross section. We use Eqs. (4.17) and (4.18) to parametrise the flux surfaces adopting the same ordering employed earlier for the Shafranov shift, that is $\Delta/a \sim \varepsilon$. Other shaping parameters are assumed to be of higher order, and thus they will be dropped. We further assume that $\Delta' \sim \varepsilon$ with q a continuous function of the minor radius. It follows that we can still use (4.22) for the expressions of the metric tensor coefficients.

Now, suppose that the pressure $\mu_0 p \sim \varepsilon^2 B_0^2$ is locally a step function with the step located at some point r_p such that $p' \propto \delta(r - r_p)$. Deploying the same expansions for ψ and F, i.e. (4.24) and (4.25), the equilibrium condition is determined on the left and on the right of r_p by equations (4.26) and (4.30) whose solutions are (4.31) and (4.33) respectively. We must now compute the jumps across r_p . From (4.30), we expect g to be discontinuous at this point while ψ' is continuous at leading order. Hence, from (4.24) we infer that a discontinuity in ψ' appears at order ϵ^2 . Therefore, we may still approximate $\psi' \approx r B_0/q$, so that we are allowed to write the Shafranov shift as (4.34). Plugging the stepped pressure profile into this equation shows that Δ' is discontinuous at r_p while Δ itself remains continuous with both Δ/a and Δ' still of order ϵ as we assumed above. It follows that that $\Delta'' \propto \delta(r - r_p)$, i.e. it has a spike at r_p .

We shall now extend this highly idealised case to a more realistic situation in which the pressure is not a step function but decreases sufficiently rapidly in a narrow region such that $\mu_0 a p'/B_0^2 \sim \varepsilon$ (see Fig. 4.10). This means that we are locally "promoting" the order of the pressure gradient. Hence, following the discussion above, from balancing the terms in (4.33) we have at leading order

$$r\Delta'' = -\frac{2R_0\mu_0 p' q^2}{B_0^2} \sim 1,$$
(4.40)

whereas $\Delta/a \sim \Delta' \sim \varepsilon$. Upon introducing the quantity

$$\alpha = -\frac{2R_0\mu_0 p' q^2}{B_0^2},\tag{4.41}$$

which is known as the **ballooning parameter**, ¹⁵ equation (4.40) can be cast as $r\Delta'' = \alpha$.

Moreover, we may write (cf. (4.26))¹⁶

$$\psi' = \frac{rB_0}{q} (1+v), \tag{4.42}$$

with $v \sim \varepsilon r v' \sim \varepsilon^2$. Therefore, by means of (4.30) we see that $g \sim \varepsilon^2$ and $rg' \sim \varepsilon$ so that

$$F' = -\frac{\mu_0 R_0 p'}{B_0}. (4.43)$$

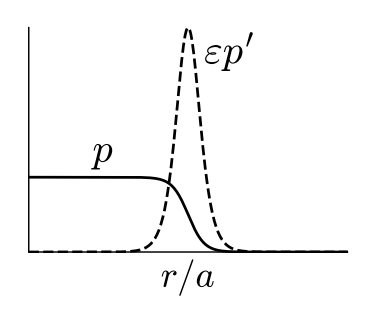


Figure 4.10: Example of localised steep pressure profile and its associated gradient

¹⁵ It was first introduced in the context of ballooning mode analysis, that we will address in the following chapters.

¹⁶ Note that this is a proportionality equation between the poloidal flux and the safety factor. Usually, when the equilibrium is solved numerically one can either impose q or the toroidal current. If the input is a smooth J^{ϕ} then q is expected to have a small jump, or *vice versa* if a smooth q is imposed as an input.

The equilibrium of a large aspect ratio tokamak with circular cross section and localised steep pressure gradients is known in the literature as $s - \alpha$ equilibrium model or $s - \alpha$ model in short. This equilibrium model will be extensively employed in chapter 12.

4.3.5 An almost intuitive derivation of the Shafranov shift

The parametrisation (4.17) and (4.18) has been chosen because we already knew, somehow, how the flux surfaces would look like. Here we show how the displacement of the flux surfaces naturally appears. Consider a coordinate system consisting of concentric nested toroidal surfaces centred in R_g with radius ρ as in (4.38). Here the variable ρ is not a flux label and R_g is not the magnetic axis. The associated metric tensor coefficients are given by (4.39). Hence, from (4.13) the toroidal current density is written as

$$\mu_{0}J^{\phi} = \frac{1}{\rho(R_{g} + \rho\cos\Theta)} \left[\frac{\partial}{\partial\rho} \left(\frac{\rho\partial\psi/\partial\rho}{R_{g} + \rho\cos\Theta} \right) + \frac{\partial}{\partial\Theta} \left(\frac{\partial\psi/\partial\Theta}{\rho(R_{g} + \rho\cos\Theta)} \right) \right]. \tag{4.44}$$

We plug this into (4.14) and expand for $\rho/R_g \ll 1$ giving

$$\begin{split} R_g^2 \left(1 + \frac{2\rho}{R_g} \cos \Theta \right) & \mu_0 \frac{dp}{d\psi} + F \frac{dF}{d\psi} + \frac{1 + \frac{\rho}{R_g} \cos \Theta}{\rho^2} \left[\rho \frac{\partial}{\partial r} \left(\rho \frac{\partial \psi}{\partial \rho} \right) + \frac{\partial^2 \psi}{\partial \theta^2} \right] \\ & - \frac{1}{\rho R_g} \left[\frac{\partial}{\partial \rho} \left(\rho^2 \frac{\partial \psi}{\partial \rho} \right) \cos \Theta + \frac{\partial}{\partial \theta} \left(\cos \Theta \frac{\partial \psi}{\partial \theta} \right) \right] = 0. \quad (4.45) \end{split}$$

We seek a solution of the form $\psi = \psi_0(\rho) + \psi_1(\rho, \Theta)$ with $\psi_1/\psi_0 \sim \rho/R_g$. Let us expand a generic quantity f as

$$f(\psi) = f(\psi_0) + \left(\frac{df}{d\psi}\right)_{\psi_0} \psi_1 + \dots$$

Thus, when the form of ψ given above is plugged into (4.45), it produces to first order in ρ/R_g

$$\begin{split} R_g^2 \mu_0 \left(\frac{d p}{d \psi} \right)_{\psi_0} + \frac{1}{2} \left(\frac{d F^2}{d \psi} \right)_{\psi_0} + \frac{1}{\rho} \frac{\partial}{\partial \rho} \left(\rho \frac{\partial \psi_0}{\partial \rho} \right) + \\ \left(R_g^2 \mu_0 \left(\frac{d^2 p}{d \psi^2} \right)_{\psi_0} + \frac{1}{2} \left(\frac{d^2 F^2}{d \psi^2} \right)_{\psi_0} \right) \psi_1 \\ + \frac{\cos \Theta}{R_g} \left(2 \rho R_g^2 \left(\frac{d p}{d \psi} \right)_{\psi_0} - \frac{\partial \psi_0}{\partial \rho} \right) + \frac{1}{\rho} \frac{\partial}{\partial \rho} \left(\rho \frac{\partial \psi_1}{\partial \rho} \right) + \frac{1}{\hat{\rho}^2} \frac{\partial^2 \psi_1}{\partial \Theta^2} = 0. \end{split}$$

By setting to zero the first line, we obtain (4.30), that is the radial pressure balance for the general screw-pinch. It is evident that for having the next order to vanish we must require $\psi_1 \sim \cos \Theta$, which shows that the constant ψ surfaces are shifted along R (cf. Fig. 4.11), at least to first

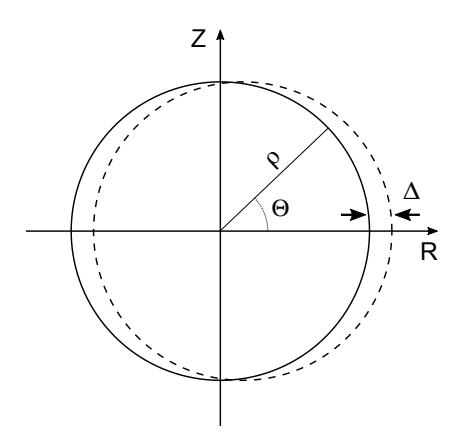


Figure 4.11: Forward shifted flux surface (dashed line) with flux $\psi = \psi_0(r) + \psi_1 \cos \theta$ with $\psi_0 > 0$ an increasing function of r and $|\psi_1/\psi_0| \ll 1$. On the equatorial plane for R > 0 we have $\psi_0(r) + \psi_1 = \psi_0(r - \Delta) \approx \psi_0(r) - \Delta \frac{\partial \psi_0}{\partial r}$, so that $\Delta = -\psi_1/(\frac{\partial \psi_0}{\partial r})$.

approximation. Therefore, writing $\psi_1 = -\Delta \frac{\partial \psi_0}{\partial \rho} \cos \Theta$ and using the radial pressure balance, after some algebra we get

$$\frac{\partial \psi_0}{\partial \rho} \left[\frac{\partial^2 \Delta}{\partial \rho^2} + \left(\frac{1}{\rho} + 2 \frac{\partial^2 \psi_0 / \partial \rho^2}{\partial \psi_0 / \partial \rho} \right) \frac{\partial \Delta}{\partial \rho} \right] - \frac{1}{R_g} \left(2\rho R_g^2 \left(\frac{dp}{d\psi} \right)_{\psi_0} - \frac{\partial \psi_0}{\partial \rho} \right) = 0,$$

which is equation (4.33). It is important to stress that, contrarily to the derivation presented earlier, here is the magnetic axis which undergoes the radial shift.

4.4 Large aspect ratio expansion: The vacuum solution

In experiments, in order to prevent the plasma from touching the surrounding structures, a vacuum region separates the plasma column from the containing vessel.¹⁷ The absence of currents in the vacuum yields the equilibrium condition

$$\nabla \times \boldsymbol{B} = 0. \tag{4.46}$$

The aim now is to determine the shape of the flux surfaces in this region.

Let us employ the coordinate system (r, θ, ϕ) with r labelling the surfaces of constant poloidal flux as defined in (4.5) and let the magnetic field to have the same form as in (4.4). The condition $J^r = J^\theta = 0$ implies that F is constant in the vacuum (this reflects the $\sim 1/R$ decay of the toroidal magnetic field). Thus, the magnetic equilibrium in the vacuum is determined by the equation

$$J^{\phi} = 0. \tag{4.47}$$

Because of the hoop force, the magnetic surfaces are expected to be displaced in the vacuum as well.¹⁸ Hence, we parametrise them with equations (4.17) and (4.18).

Assume for the moment that the metallic wall surrounding the plasma at distance r=b>a with $1-a/b\ll 1$ is a perfect conductor. Since $b\sim a$, we deploy the ordering $b/R_0\sim \varepsilon$. Therefore, the procedure for obtaining the vacuum solution consists in first expanding J^ϕ in ε and then solving (4.47) order by order in the inverse aspect ratio. Using (4.27), the leading order of (4.47) yields $r\psi'=const$, so that by means of (4.26) we obtain (compare with (4.28))

$$q \sim r^2, \tag{4.48}$$

which holds up to order ε^2 .

By combining (4.26) and (4.27) we get $rJ^{\phi} \sim (r^2/q)'$ which can be integrated across the plasma boundary r=a giving

$$\frac{1}{q(a+\delta)} - \frac{1}{q(a-\delta)} \sim \int_{a-\delta}^{a+\delta} r J^{\phi} dr,$$

¹⁷ Note that this is an approximation of a much more complex situation.

¹⁸ This is because the magnetic field is stronger on the inner side than on the outer side of the current carrying torus.

 19 This does not hold for diverted configurations, such as the one shown in Fig. 4.8 for which the plasma boundary identified by the separatrix is not smooth. In such a case, the q profile diverges logarithmically at the edge (see Wesson (2011)). Diverted geometries, however, are not analysed in this report, which only focusses on limited plasmas with a smooth boundary.

²⁰ Given the normal vector $\mathbf{n} = \nabla r/|\nabla r|$ from plasma to vacuum, the plasma-vacuum jump conditions are

$$\mathbf{n} \cdot (\mathbf{B}_{vac} - \mathbf{B}_{plasma}) = 0,$$

 $\mathbf{n} \times (\mathbf{B}_{vac} - \mathbf{B}_{plasma}) = 0,$

where we assumed no surface currents at the plasma boundary.

²¹ Note that often in the literature the coordinate system of 4.3.5 is used. In such a case $\Delta_a = 0$ and the substitution $\Delta'_a \to -\Delta'_a$ must be performed.

with $\delta \to 0$. The right-hand-side of the equation above can be made arbitrarily small if the function under the sign of integration is not singular at the boundary, i.e. there are no surface current densities (in short surface current). This shows that the safety factor profile is continuous at the plasma-vacuum interface.¹⁹

To the next order in ε , equation (4.47) yields

$$\Delta'' - \frac{\Delta'}{r} - \frac{1}{R_0} = 0, (4.49)$$

which is equivalent to (4.33) computed with p = 0 and $q \sim r^2$. This shows that (4.33) can be used both in the plasma and vacuum region. As discussed in the previous section, equation (4.33) can be cast as

$$\frac{d}{dr}\left[r(\psi')^2\Delta'\right] + r(\psi')^2\left(\frac{2\mu_0 r R_0 p'}{(\psi')^2} - \frac{1}{R_0}\right) = 0.$$

In analogy with the calculation above, without surface currents we integrate it across the plasma boundary giving

$$\frac{a^3}{q^2(a)} \left(\Delta'(a+\delta) - \Delta'(a-\delta) \right) = -\int_{a-\delta}^{a+\delta} \frac{r^3}{q^2} \left(\frac{2\mu_0 R_0 p' q^2}{r R_0^2} - \frac{1}{R_0} \right) dr,$$

where we made use of (4.26). The right-hand-side of this equation vanishes if p' is not singular, so that Δ' is continuous at a. This is equivalent to requiring that the poloidal component of the magnetic field is continuous a the plasma-vacuum interface. Finally, we impose the obvious constraint $\Delta(a+\delta)=\Delta(a-\delta)$. Thus, denoting with Δ_v the displacement of the magnetic surfaces in the vacuum region, the solution of (4.49) supplied with the interface conditions at the plasma edge given above reads

$$\Delta_v = \Delta_a + \frac{a^2}{4R_0} \left(1 - \frac{2R_0}{a} \Delta_a' \right) \left[1 - \left(\frac{r}{a} \right)^2 \right] + \frac{r^2}{2R_0} \ln \left(\frac{r}{a} \right), \tag{4.50}$$

having introduced the notation $\Delta_a = \Delta(a - \delta)$ and $\Delta'_a = \Delta'(a - \delta)$.

With a perfectly conducting wall at distance b from the plasma, the shift of the flux surfaces is written as²¹

$$\frac{\Delta_v(b) - \Delta_a}{b} = \frac{b}{2R_0} \left[\ln \left(\frac{b}{a} \right) + \left(\beta_p(a) + \frac{\ell_i(a)}{2} - \frac{1}{2} \right) \left(1 - \frac{a^2}{b^2} \right) \right].$$

Hence, letting the wall to be at distance b, expanding (4.50) for $b/a \approx 1$ yields

$$\Delta_n(b) \approx \Delta_a + \Delta'_a(b-a) + \dots$$

This indicates that the magnetic flux is compressed in the vacuum region right up to the vessel wall. Flux compression therefore prevents further plasma expansion (see Fig. 4.12). Here it is evident the importance of the poloidal field for the plasma confinement, in that the longitudinal

(toroidal) field does not enter the expression for the equilibrium position of the plasma in the vacuum chamber.

Unfortunately, in reality the vessel wall is not a perfect conductor, and the poloidal flux can only remain compressed for times typically much shorter compared to the ones of experimental interest. It turns out that an external vertical field B_{\perp} must be applied to maintain the plasma in equilibrium, preventing the expansion in R due to the radial force. Although not strictly necessary for the stability calculations of the next chapters, the evaluation of B_{\perp} is of high importance for experimental purposes, therefore we shall discuss it in the next section for a large aspect ratio tokamak with a circular cross section.

4.4.1 External vertical field

Assume that there is no conducting wall surrounding the plasma. In the vacuum, the condition of no currents implies that (4.46) holds. Let us employ polar coordinates (ρ, Θ, ϕ) which relate to the flux ones (r, θ, ϕ) through (cf. (4.38))

$$R_g + \rho \cos \Theta = R = R_0 + r \cos \theta - \Delta, \quad \rho \sin \Theta = Z = r \sin \theta.$$
 (4.51)

We choose R_g to be the geometric centre of the last surface enclosing the plasma labelled by ρ_b (see figure 4.13). This means that $R_g = R_0 - \Delta(a)$. The associated metric tensor coefficients are given by (4.39). By inverting (4.51), the flux coordinates are then written in terms of the polar ones via

$$r = \rho - (\Delta_a - \Delta)\cos\Theta + \dots, \quad \theta = \Theta + \frac{(\Delta_a - \Delta)}{\rho}\sin\Theta\dots,$$

where here Δ has to be considered as a function of ρ such that $\Delta(\rho_b) = \Delta_a$ with Δ_a following the notation introduced in (4.50).

With a magnetic field written as (4.4) where F is constant and $\psi = \psi(\rho,\Theta)$ (cf. §4.4), we exploit axisymmetry $(\nabla \rho \cdot \nabla \phi = \nabla \Theta \cdot \nabla \phi = 0)$ to obtain $J^{\rho} = J^{\Theta} = 0$, so that the equilibrium in the vacuum is determined by equation (4.47). Denoting the vacuum flux by ψ^{ext} , this becomes (cf. (4.44))

$$\frac{\partial}{\partial \rho} \left(\frac{\rho}{R_g + \rho \cos \Theta} \frac{\partial \psi^{ext}}{\partial \rho} \right) + \frac{1}{\rho} \frac{\partial}{\partial \Theta} \left(\frac{1}{R_g + \rho \cos \Theta} \frac{\partial \psi^{ext}}{\partial \Theta} \right) = 0.$$

Although this equation admits an exact solution expressed in terms of **toroidal (ring) functions**, we shall seek a simplified form for the flux which is valid in a region near the outermost plasma surface.

Expanding for $\rho/R_g \sim \varepsilon \ll 1$ and focusing on a solution of the form $\psi^{ext} = \psi_0(\rho) + \psi_1(\rho)\cos\Theta$ with $\psi_1 \sim \varepsilon\psi_0$, the equation above yields

$$\frac{\partial}{\partial \rho} \left(\rho \frac{\partial \psi_0}{\partial \rho} \right) = 0, \quad \frac{\partial}{\partial \rho} \left(\rho \frac{\partial \psi_1}{\partial \rho} \right) - \frac{\psi_1}{\rho} - \frac{\rho}{R_g} \frac{\partial \psi_0}{\partial \rho} = 0.$$

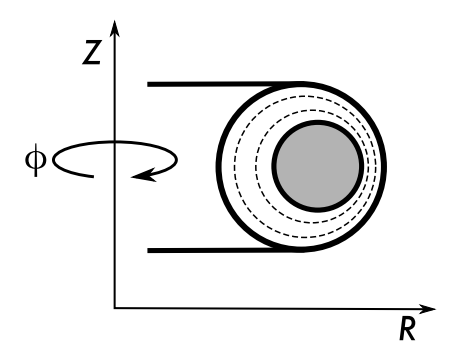


Figure 4.12: Sketch of the poloidal flux compression in the outer midplane for a plasma surrounded by a perfectly conducting wall.

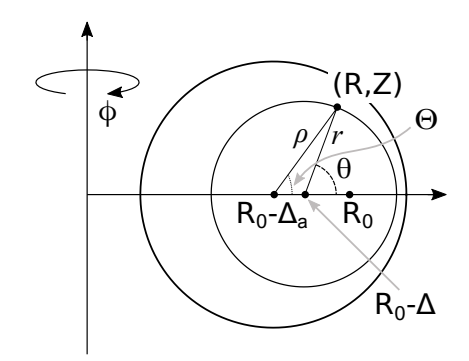


Figure 4.13: Polar (ρ, Θ, ϕ) and flux (r, θ, ϕ) coordinates.

Thus, the vacuum flux can be written not too far from the plasma as

$$\psi^{ext} = C_0 + C_1 \ln \frac{\rho}{a} + \left[C_2 \rho + \frac{C_3}{\rho} + \frac{C_1 \rho}{2R_g} \left(\ln \rho - \frac{1}{2} \right) \right] \cos \Theta. \tag{4.52}$$

The constants C_i (i=1,2,3) are determined by requiring that in absence of surface currents the normal and tangential components of the magnetic field are continuous at the plasma boundary. We denote with ψ^{in} the poloidal flux inside the plasma. Exploiting again axisymmetry and the fact that $\partial \psi^{in}/\partial \theta = 0$, it follows that at the plasma boundary one has at leading orders

$$\left. \frac{\partial \psi^{in}}{\partial \rho} \right|_{\rho_b} = \frac{d \psi^{in}}{dr} \Big|_a \frac{\partial r}{\partial \rho} \Big|_{\rho_b} \approx \frac{a B_0}{q(a)} \left[1 + \frac{a}{R_0} \left(\beta_p(a) + \frac{l_i(a)}{2} \right) \cos \Theta \right],$$

having used equation (4.26) and $\partial \Delta(\rho)/\partial \rho|_{\rho_b} \approx d\Delta(r)/dr|_a$ with $\frac{R_0}{a}\Delta_a' = \beta_p(a) + l_i(a)/2$ (cf. (4.35)). Since

$$B^{
ho} = -rac{1}{\sqrt{g}}rac{\partial \psi}{\partial \Theta}, \quad B^{\Theta} = rac{1}{\sqrt{g}}rac{\partial \psi}{\partial
ho}, \quad B^{\phi} = rac{F}{R^2},$$

the continuity of the tangential magnetic field implies $\partial \psi^{in}/\partial \rho|_{\rho_b} = \partial \psi^{ext}/\partial \rho|_{\rho_b}$ whereas the vanishing of the radial component of \boldsymbol{B} requires $B^{\rho}(\rho_b) = 0$.

Therefore, the interface conditions become

$$C_{2} + \frac{C_{3}}{a^{2}} + \frac{C_{1}}{2R_{g}} \left(\ln a - \frac{1}{2} \right) = 0,$$

$$\frac{C_{1}}{a} + \left[C_{2} - \frac{C_{3}}{a^{2}} + \frac{C_{1}}{2R_{g}} \left(\ln a + \frac{1}{2} \right) \right] \cos \Theta$$

$$= \frac{aB_{0}}{q(a)} \left[1 + \frac{a}{R_{0}} \left(\beta_{p}(a) + \frac{l_{i}(a)}{2} \right) \cos \Theta \right],$$

$$(4.54)$$

having approximated $\rho_b \approx a$. Defining $\Lambda = \beta_p(a) + l_i(a)/2 - 1$ with $R_g \approx R_0$, we easily obtain

$$C_1 = rac{a^2 B_0}{q(a)}, \quad C_2 = rac{a^2 B_0}{2 R_0 q(a)} \left(\Lambda - \ln a + 1 \right),$$
 $C_3 = -rac{a^4 B_0}{2 q(a) R_0} \left(\Lambda + rac{1}{2}
ight),$

so that the vacuum flux is 22

$$\psi^{ext} = C_0 + \frac{\mu_0 R_0 I_p}{2\pi} \ln \frac{\rho}{a} + \frac{\mu_0 I_p}{4\pi} \left[\ln \frac{\rho}{a} + \left(\Lambda + \frac{1}{2} \right) \left(1 - \frac{a^2}{\rho^2} \right) \right] \rho \cos \Theta.$$
(4.55)

The magnitude of the external field required to maintain the equilibrium is obtained by subtracting from ψ^{ext} the contribution due to the toroidal current itself. Let us write $\psi^{ext} = \psi^{cur} + \psi^{VF}$, where ψ^{cur} is the flux due to the plasma current and ψ^{VF} is the additional external

 22 We use the fact that

$$\frac{a^2B_0}{q(a)}\approx\frac{\mu_0R_0I_p}{2\pi},$$

where I_p is the plasma current.

one. For a current loop of radius R_g which carries a current I_p in the ϕ direction one has (Jackson (1999))²³

$$\begin{split} \psi^{cur} &= -\frac{\mu_0 R_g I_p}{2\pi} \sqrt{\frac{R}{R_g}} \left[\frac{(2-k^2)K(k) - 2E(k)}{k} \right], \\ k^2 &= \frac{4R/R_g}{\left(1 + R/R_g\right)^2 + Z^2/R_g^2}, \end{split}$$

where K(k) and E(k) are the complete elliptic integrals of the first and second kind respectively.²⁴ By means of (4.51), expanding in powers of ρ/R_g yields

$$k^2 = 1 - \frac{1}{4} \left(\frac{\rho}{R_g}\right)^2 + \frac{1}{4} \left(\frac{\rho}{R_g}\right)^3 \cos\Theta + \dots,$$

so that to the required accuracy we approximate

$$E(k) \approx 1, \quad K(k) \approx \ln \frac{4}{\sqrt{1-k^2}} \approx \ln \frac{8R_g}{\rho} + \frac{\rho}{2R_g} \cos \Theta.$$

Collating these results together and letting $R_g \approx R_0$ gives

$$\psi^{cur} \approx -\frac{\mu_0 R_0 I_p}{2\pi} \left[\ln \frac{8R_0}{\rho} - 2 + \frac{\rho}{2R_0} \left(\ln \frac{8R_0}{\rho} - 1 \right) \cos \Theta \right]. \tag{4.56}$$

When this flux is subtracted from (4.55), we obtain for $\rho \gg a$

$$\psi^{VF} \approx const + \frac{\mu_0 I_p}{4\pi} \left[\ln \frac{8R_0}{a} + \Lambda - \frac{1}{2} \right] (R - R_0) \,. \label{eq:psi_VF}$$

Since $B_Z = \frac{1}{R} \partial \psi^{VF} / \partial R$, the magnitude of the external vertical field needed to maintain the equilibrium is found to be

$$B_{\perp} pprox rac{\mu_0 I_p}{4\pi R_0} \left(\ln rac{8R_0}{a} + \Lambda - rac{1}{2}
ight).$$

Note that $B_{\perp} \sim \varepsilon^2 B_0$ (the logarithm is a slowly growing function of its argument so that we let $\ln(R_0/a) \sim 1$). The effect of such a field is sketched in Fig. 4.14. One notes the appearance of a point of poloidal field null (X-point) in the high-field-side.

Using this result, the equilibrium β limit discussed at the end of section 4.3.2 can be estimated as follows: let $\Theta=\pi$ so that $R=R_0-\rho$ with $\rho\ll R_0$ and assume $I_p>0$. From (4.56), the magnitude of the magnetic field at Z=0 and close to R_0 generated by the plasma current scales approximately as $\frac{\mu_0 I_p}{2\pi |R-R_0|}$. Let $a=|R-R_0|$ be the radius of the plasma. The X-point will intersect the outermost plasma surface when $B_\perp\sim\frac{\mu_0 I_p}{2\pi a}$, so that for R_0/a sufficiently large the critical β_p setting the equilibrium limit is

$$\beta_p(a) \sim R_0/a$$
.

²³ If $\mathbf{B} = -\nabla \psi \times \nabla \phi$ the associated vector potential is $\mathbf{A} = -\psi \nabla \phi$. From this

$$A_{tor} = \frac{\boldsymbol{A} \cdot \boldsymbol{\nabla} \phi}{|\boldsymbol{\nabla} \phi|} = -\psi/R.$$

The quantity A_{tor} is used in Jackson (1999).

The elliptic integrals K(k) and E(k) are defined as

$$K(k) = \int_0^{\pi/2} \frac{dt}{\sqrt{1 - k^2 \sin^2 t}}$$

$$= \frac{\pi}{2} {}_2F_1(\frac{1}{2}, \frac{1}{2}; 1; k^2),$$

$$E(k) = \int_0^{\pi/2} \sqrt{1 - k^2 \sin^2 t} dt$$

$$= \frac{\pi}{2} {}_2F_1(-\frac{1}{2}, \frac{1}{2}; 1; k^2),$$

where $_2F_1$ denotes the hypergeometric function.

We use a right handed cylindrical coordinate system (R, Z, ϕ) .

25 Note that

$$\frac{\partial \psi^{\varepsilon u r}}{\partial R} = \frac{\partial \psi^{\varepsilon u r}}{\partial \rho} \frac{\partial \rho}{\partial R} + \frac{\partial \psi^{\varepsilon u r}}{\partial \Theta} \frac{\partial \Theta}{\partial R},$$

and $\frac{\partial \psi^{cur}}{\partial \Theta} = 0$ for $\Theta = \pi$. We also take $\ln 8R_0/\rho \sim 1$.

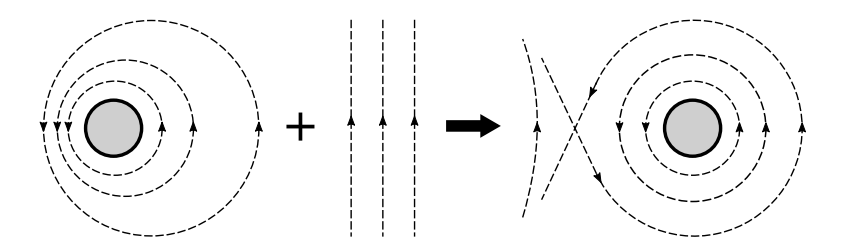


Figure 4.14: Total poloidal field due to the combination between the one generated by the plasma current and the externally applied one. Note the presence of the magnetic separatrix and the X-point.

Toroidally rotating plasmas

To increase the temperature, beams of neutral particles can be injected into the plasma. This may induce a rotation in the direction of the injection due to momentum transfer and if this rotation is sufficiently fast, it can impact the equilibrium. The equilibrium condition for a stationary rotating plasma is (cf. (2.2))

$$\rho \boldsymbol{v} \cdot \boldsymbol{\nabla} \boldsymbol{v} = -\boldsymbol{\nabla} \boldsymbol{p} + \boldsymbol{J} \times \boldsymbol{B},\tag{4.57}$$

where the magnetic field is given by (4.4) (we use the same coordinate system employed in §4.3). Let the variable r label isoflux surfaces such that $B^r=0$, i.e. $\psi=\psi(r)$ (isoflux surfaces may not correspond to isobars as it is shown below). The rotation is typically in the toroidal direction, so that $v=v^\phi e_\phi$. Hence, writing $E=-\nabla \Phi_E$ where Φ_E is the electric potential, the projection of (2.3) along B shows that Φ_E depends only on the flux variable r. Multiplying (2.3) by e_r shows that v^ϕ is a flux function as well. We call $\Omega(r) \equiv v^\phi$. Dotting (4.57) with e_ϕ gives $J^r=0$ showing that F=F(r) is a flux quantity, whereas the e_θ projection yields

$$\rho\Omega^2 \frac{R}{2} \frac{\partial R}{\partial \theta} = \frac{\partial p}{\partial \theta}.$$
 (4.58)

We assume strong parallel electron thermal conductivity which ensures isothermal flux surface, i.e.

$$\boldsymbol{B} \cdot \boldsymbol{\nabla} T = 0 \tag{4.59}$$

so that T = T(r). For the sake of simplicity $T = T_i = T_e$. Hence, writing $\rho = m_i n$ and p = 2nT, equation (4.58) can be integrated giving

$$\rho = \frac{p}{2T} = \rho_0 e^{\frac{m_i \Omega^2}{4T} (R^2 - R_0^2)} = \rho_0 e^{\frac{\mathcal{M}^2(\frac{R^2}{R_0^2} - 1)}{R_0^2}},$$
(4.60)

where ρ_0 is a function of r and $\mathcal{M}^2 = \rho \Omega^2 R_0^2/2p$ is the **Mach number**. Expanding in ε yields

$$\rho = \rho_0 \left(1 + 2\mathcal{M}^2 \frac{r}{R_0} \cos \theta + \ldots \right), \tag{4.61}$$

which shows that the constant density (or pressure) surfaces are radially shifted with respect to the flux surfaces (cf. Fig. 4.11). This is due to the centrifugal effects which also enter the expression of the Shafranov shift Δ through a modification of the pressure term. We see that rotation effects become significant when $\mathcal{M} \sim 1$.

References

- M. Abramowitz and I. A. Stegun (eds.), **Handbook of Mathematical Functions**, Dover Publications (New York, US), 1964.
- L. A. Artsimovitch, **A Physicist's ABC on Plasma**, Mir Publishers (Moscow, USSR), 1978.
- W. D. D'haeseleer et al., Flux Coordinates and Magnetic Field Structure, Springer Berlin (Heidelberg, DE), 1991.
- J. P. Freidberg, **Ideal MHD**, Cambridge University Press (Cambridge, UK), 2014.
- J. P. Goedbloed, R. Keppens and S. Poedts, Advanced Magnetohydrodynamics With Applications to Laboratory and Astrophysical Plasmas, Cambridge University Press (Cambridge, UK), 2010.
- J. D. Jackson, Classical Electrodynamics, Wiley (New York, US), 1999.
- C. Mercier and H. Luc, Lectures in Plasma Physics: The Magnetohydrodynamic Approach to the Problem of Plasma Confinement in Closed Magnetic Configurations (Commission of the European Communities, Luxembourg), 1974.
- A. B. Mikhailovskii, Instabilities in a Confined Plasma, Institute of Physics Publishing (Bristol, UK), 1998.
- V. S. Mukhovatov and V. D. Shafranov, Nucl. Fusion 11, 605 (1971).
- V. D. Shafranov, J. Nucl. Energy, Part C Plasma Phys. 5, 251 (1963).
- L. S. Solov'ev, Zh. Eksp. Teor. Fiz. **53**, 626 (1967) [Sov. Phys.-JETP **26**, 400 (1968)].
- J. A. Wesson, Tokamaks, Oxford University Press (Oxford, UK), 2011.
- S. B. Zheng et al., Phys. Plasmas 3, 1176 (1996).

5

Straight field line coordinates

In the previous chapter we mentioned that for a toroidal coordinate system (r, θ, ϕ) where the variable r labels the flux surfaces and ϕ is the geometric toroidal angle, there is a degree of freedom in choosing the definition of the poloidal angle θ , i.e. its definition is not unique. Depending on the problem under consideration, certain definitions turn out to be more useful, or easier to handle mathematically, than others: for example, for plasma diagnostics related problems the proper geometrical angle is often the preferred choice. This, however, is not the most convenient definition when dealing with analytic stability calculations.

We see from (4.7) that, given θ and ϕ the (generic) poloidal and toroidal angles, the infinitesimal increment of the field line position in the toroidal direction per increment in the poloidal one is

$$d\phi = rac{B^{\phi}}{B^{ heta}}d heta.$$

If we select a particular flux surface, the pitch of the field line, that is the ratio $d\phi/d\theta$, can depend upon the poloidal variable θ . For stability analyses, however, it is much more convenient to have a constant pitch angle on each flux surface of radius r. Hence, to remove such a dependence on the poloidal angle, we introduce a new angular variable θ such that the magnetic field lines on a given flux surface are straight (see figure 5.1), that is

$$\frac{d\phi}{dr} = q(r).$$

This new angle, namely ϑ , is called the **rectified poloidal angle**. Using the coordinates (r, ϑ, ϕ) , from (4.4) the **equilibrium magnetic** ¹ It is possible to introduce alternative definitions of the toroidal angle ϕ as well. In this report, however, ϕ will always denote the geometric toroidal one.

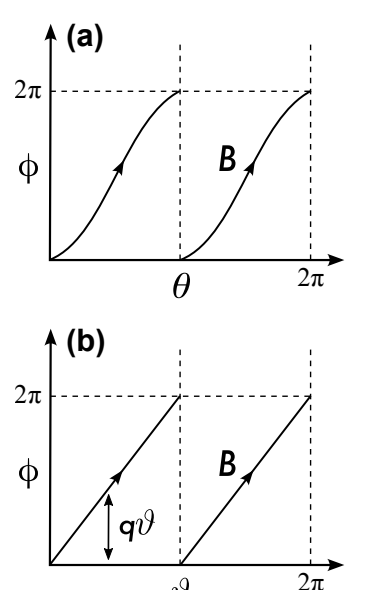


Figure 5.1: Field lines on a cut open magnetic surface for (a) arbitrary flux coordinates, and (b) straight field line coordinates.

field components are

$$B^r = 0, (5.1)$$

$$B^{\vartheta} = \frac{\psi'}{\sqrt{g}},\tag{5.2}$$

$$B^{\phi} = \frac{F}{R^2},\tag{5.3}$$

with \sqrt{g} denoting the Jacobian associated with this **straight field line coordinate system**.² This means that the ratio

$$\frac{B^{\phi}}{B^{\vartheta}} = \frac{F\sqrt{g}}{\psi'R^2} = q(r) \tag{5.4}$$

is a flux function (i.e. constant on a flux surface), yielding to the equivalent requirement that

$$\frac{\partial}{\partial \vartheta} \left(\frac{\sqrt{g}}{R^2} \right) = 0, \tag{5.5}$$

which also corresponds having $\sqrt{g}B^{\phi}$ to be a flux function. Relation (5.4) gives a very simple representation of the **safety factor**.

Because the mapping $\theta \to \vartheta$ is one-to-one, we can think of the angle θ as a function of r and ϑ (analogously ϑ can be viewed as a function of r and θ). Figure 5.2 shows the curves of constant straight angle (note that it can become highly distorted near the edge). Thus, the aim of this chapter is to find i) how to represent the equilibrium geometry in terms of this new straightened angular variable ϑ , and ii) derive the appropriate expressions for the covariant elements of the metric tensor. In doing so, we must first resolve some subtleties related to the higher order solution of a tokamak equilibrium. This initial step is discussed in the next section.

5.1 Higher order tokamak equilibrium

In the previous chapter the equilibrium was solved only to first order in ε . However, this is not sufficient for the correct computation of the metric tensor coefficients to the accuracy required for later analyses. This means that the equilibrium must be solved to the next order in ε . Let us use the (r, θ, ϕ) coordinate system introduced in chapter 4, and parametrise the flux surfaces as

$$R = R_0 + r\cos\theta - \Delta + E(r,\theta), \qquad Z = r\sin\theta + S(r,\theta), \tag{5.6}$$

with $E \sim S \sim \varepsilon^2 r$. The symbol \sqrt{g}_u identifies the Jacobian associated with these coordinates. Using (4.25), we see that

$$\frac{FF'}{B_0^2 R^2} = g' \left(1 - 2 \frac{r}{R_0} \cos \theta + g + 3 \frac{r^2}{R_0^2} \cos^2 \theta + \frac{2\Delta}{R_0} \right) + f' + \dots,$$

² Hereafter the symbol \sqrt{g} will always denote the Jacobian of the system (r, ϑ, ϕ)

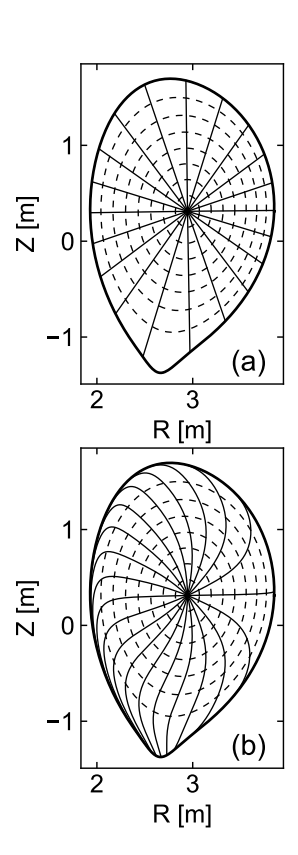


Figure 5.2: Cross section of a shaped plasma showing the levels of constant geometric (a), and straightened (b) poloidal angles. Dashed lines indicate isobaric surfaces.

where the prime indicates differentiation with respect to the radial variable. From an inspection of (4.20), it is thus clear that E and S must generate terms proportional to $\cos^2\theta$ when expanding the coefficients $g_{\theta\theta}/\sqrt{g}_u$ and $g_{r\theta}/\sqrt{g}_u$ appearing in (4.21) (cf. (4.27)) to higher order.

Let us introduce the quantities

$$C_1 = R' = \cos \theta - \Delta' + E', \quad C_2 = \frac{\partial R}{\partial \theta} = -r \sin \theta + \frac{\partial E}{\partial \theta}$$

 $D_1 = Z' = \sin \theta + S', \quad D_2 = \frac{\partial Z}{\partial \theta} = r \cos \theta + \frac{\partial S}{\partial \theta}.$

It follows that (cf. section 4.3.1)

$$g_{rr} = C_1^2 + D_1^2, \quad g_{r\theta} = C_1C_2 + D_1D_2, \quad g_{\theta\theta} = C_2^2 + D_2^2,$$

$$\sqrt{g}_u = R\sqrt{g_{rr}g_{\theta\theta} - g_{r\theta}^2} = R\left(C_1D_2 - D_1C_2\right).$$

From this it is fairly easy to see that

$$\begin{split} g_{r\theta} &\approx r\Delta' \sin \theta + \left(\frac{\partial E}{\partial \theta} + rS'\right) \cos \theta - \left(rE' - \frac{\partial S}{\partial \theta}\right) \sin \theta, \\ g_{\theta\theta} &\approx r^2 - 2r\frac{\partial E}{\partial \theta} \sin \theta + 2r\frac{\partial S}{\partial \theta} \cos \theta, \\ \sqrt{g}_u &\approx rR_0 \left[1 + \left(\frac{r}{R_0} - \Delta'\right) \cos \theta + \left(\frac{\partial S/\partial \theta}{r} + E'\right) \cos \theta + \left(\frac{\partial$$

so that the metric tensor coefficients that enter the equilibrium toroidal current density can be written to the first two leading orders as

$$\frac{g_{\theta\theta}}{\sqrt{g}_{u}} = \frac{r}{R_{0}} \left[1 + \left(\Delta' - \frac{r}{R_{0}} \right) \cos \theta + \left(\frac{\partial S/\partial \theta}{r} - E' \right) \cos \theta \right. \\
\left. - \left(S' + \frac{\partial E/\partial \theta}{r} \right) \sin \theta - \frac{r\Delta'}{R_{0}} \cos^{2} \theta + \frac{\Delta}{R_{0}} + \Delta'^{2} \cos^{2} \theta + \frac{r^{2}}{R_{0}^{2}} \cos^{2} \theta \right], \\
\frac{g_{r\theta}}{\sqrt{g}_{u}} = \frac{1}{R_{0}} \left[\Delta' \sin \theta + \left(\Delta' - \frac{r}{R_{0}} \right) \Delta' \sin \theta \cos \theta + \left(\frac{\partial S/\partial \theta}{r} - E' \right) \sin \theta + \left(S' + \frac{\partial E/\partial \theta}{r} \right) \cos \theta \right]. \tag{5.7}$$

When these expressions are plugged into (4.21), in order to have the required $\cos^2 \theta$ dependent terms, we must impose

$$E(r, \theta) = \bar{E}(r)\cos\theta, \quad S(r, \theta) = \bar{S}(r)\sin\theta.$$

An expression for $\bar{E}(r)$ and $\bar{S}(r)$ is now needed.

³ For $x \ll 1$ one has

$$\frac{1}{1+ax+bx^2}\approx 1-ax+(a^2-b)x^2.$$

Introducing $\Lambda_* = \Delta' - r/R_0$, from (5.7) we shall formally write³

$$\begin{split} \frac{1}{\sqrt{g}_u} &= \frac{1}{rR_0} \left[1 + \Lambda_* \cos \theta + t_0(r,\theta) \right], \quad \frac{g_{\theta\theta}}{\sqrt{g}_u} = \frac{r}{R_0} \left[1 + \Lambda_* \cos \theta + t_1(r,\theta) \right], \\ \frac{g_{r\theta}}{\sqrt{g}_u} &= \frac{1}{R_0} \left[\Delta' \sin \theta + t_2(r,\theta) \right], \end{split}$$

where t_0 , t_1 and t_2 are quantities of order ε^2 which are defined as follows:

$$t_{0} = -\left(\frac{\bar{S}}{r} + \bar{E}'\right)\cos^{2}\theta - \left(\bar{S}' + \frac{\bar{E}}{r}\right)\sin^{2}\theta + \left(\Delta'^{2} + \frac{r^{2}}{R_{0}^{2}} - \frac{r\Delta'}{R_{0}}\right)\cos^{2}\theta + \frac{\Delta}{R_{0}},$$

$$t_{1} = \left(\frac{\bar{S}}{r} - \bar{E}'\right)\cos^{2}\theta - \left(\bar{S}' - \frac{\bar{E}}{r}\right)\sin^{2}\theta + \left(\Delta'^{2} + \frac{r^{2}}{R_{0}^{2}} - \frac{r\Delta'}{R_{0}}\right)\cos^{2}\theta + \frac{\Delta}{R_{0}},$$

$$t_{2} = \left[\left(\Delta' - \frac{r}{R_{0}}\right)\Delta' + \frac{\bar{S} - \bar{E}}{r} + \bar{S}' - \bar{E}'\right]\sin\theta\cos\theta.$$

With a simple manipulation it can be shown that the toroidal current density at the two leading orders is written as

$$\mu_0 J^{\phi} = \frac{1}{rR_0^2} \Big[(r\psi')' + \{ (r\psi'\Lambda_*)' + \Lambda_*(r\psi')' - \psi'\Delta' \} \cos \theta + (r\psi't_1)' + \Lambda_*\{ (r\psi'\Lambda_*)' - \psi'\Delta' \} \cos^2 \theta + t_0(r\psi')' - \psi'\frac{\partial t_2}{\partial \theta} \Big].$$
 (5.8)

It is important to remind that for a given shape of the safety factor, the expression for the poloidal flux is given by (4.23) and includes contributions up to order ε^2 which enter the equation above.

By inspecting (5.7), we observe that no further corrections proportional to $\cos \theta$ appear in J^{ϕ} beyond the one originating from terms of order ε .⁴ Noting that $\cos^2 \theta = (1 + \cos 2\theta)/2$, Eq. (4.20) generates two equations to order ε^3 : one is obtained by averaging it in θ , whereas the other is obtained by multiplying by $\cos 2\theta$ and integrating in θ from 0 to 2π . The former provides an expression for f' while the latter, after plugging (5.7) and (5.8) into (4.20), yields

$$\bar{C}'' + \left(1 + 2\frac{r\psi''}{\psi'}\right)\frac{\bar{C}'}{r} - 3\frac{\bar{C}}{r^2} = \frac{3r^2R_0^2g'}{(\psi')^2} + \frac{6r}{R_0^2} - \frac{3\Delta'}{R_0} + 3\Delta'\Delta'' - \frac{2r}{R_0}\Delta'' + \frac{\psi''}{\psi'}\left(\frac{3r^2}{R_0^2} + 3\Delta'^2 - \frac{4r}{R_0}\Delta'\right),$$
(5.9)

having defined

$$\bar{C} = \bar{E} - \bar{S}.\tag{5.10}$$

The equations above determine, say, \bar{E} while \bar{S} remains a free function whose choice allows for several alternatives. Upon defining $\bar{P} = \bar{E} + \bar{S}$, we cast (5.6) as

$$R = R_0 + (r + \frac{1}{2}\bar{P})\cos\theta - \Delta + \frac{1}{2}\bar{C}\cos\theta,$$

$$Z = (r + \frac{1}{2}\bar{P})\sin\theta - \frac{1}{2}\bar{C}\sin\theta.$$

⁴ This indicates that there are no additional non-oscillating (in θ) terms of order ε^2 in (5.6).

It is clear that \bar{P} corresponds to a relabelling of the flux surfaces and \bar{C} determines their ellipticity.⁵

A particularly clever choice is to take a linear combination of \bar{E} and \bar{S} such that in the straightened coordinate system $g_{\phi\phi}/\sqrt{g}=R_0/r$ at all orders. This will be elaborated more in detail in the next sections.

5.2 The rectifying parameter

Let us assume that the pressure profile is smooth and does not present narrow regions of sharp gradients. Taking into account the results of the previous section, we take the parametrisation of the flux surfaces to be the one given by Eqs. (4.17) and (4.18), i.e.

$$R = R_0 + r \cos \theta - \Delta + \bar{E} \cos \theta,$$

$$Z = r \sin \theta + \bar{S} \sin \theta$$

where the expression of the Shafranov shift is given by (4.33) and $\bar{E} \sim \bar{S} \sim \varepsilon^2 a$. As discussed earlier, we can view the poloidal angle θ as a function of the rectified one ϑ and of the labelling variable r, that is

$$\theta = \theta(r, \vartheta)$$

with $0 \le \vartheta < 2\pi$. The aim of this section is to find an explicit form, though approximated, of θ expressed in terms of ϑ . Although most of the problems encountered in the stability analysis do not require an accuracy correct to order ε^2 , here we work out the full computation.

In analogy to what we did in the previous section, after introducing the coordinates (r, ϑ, ϕ) we define the quantities

$$C_{1} = R' = \left(1 + \bar{E}'\right)\cos\theta - r\theta'\left(1 + \frac{\bar{E}}{r}\right)\sin\theta - \Delta',$$

$$C_{2} = \dot{R} = -r\dot{\theta}\left(1 + \frac{\bar{E}}{r}\right)\sin\theta,$$

$$D_{1} = Z' = \left(1 + \bar{S}'\right)\sin\theta + r\theta'\left(1 + \frac{\bar{S}}{r}\right)\cos\theta,$$

$$D_{2} = \dot{Z} = r\dot{\theta}\left(1 + \frac{\bar{S}}{r}\right)\cos\theta,$$

having used the notation $f' = \partial f/\partial r$ and $\dot{f} = \partial f/\partial \vartheta$. The covariant components of the metric tensor are thus written as (cf. section 4.3.1)

$$g_{rr} = C_1^2 + D_1^2,$$

 $g_{r\theta} = C_1C_2 + D_1D_2,$ (5.11)
 $g_{\vartheta\vartheta} = C_2^2 + D_2^2,$

and the Jacobian associated with this coordinate system is

$$\sqrt{g} = R \sqrt{g_{rr} g_{\vartheta\vartheta} - g_{r\vartheta}^2} = R \left(C_1 D_2 - D_1 C_2 \right).$$

⁵ From (5.9) we infer that such an elongation is small as long as β is small.

⁶ Terms of the order of ε^2 are needed for the correct evaluation of the metric coefficients in the $s-\alpha$ equilibrium model with steep gradients. This will be discussed in Sec. 5.4.

It is immediate to verify that to leading order

$$\frac{\sqrt{g}}{R^2} = \frac{r}{R}\dot{\theta} \left[1 - \Delta' \cos \theta + \left(\bar{E}' + \frac{\bar{S}}{r} \right) \cos^2 \theta + \left(\bar{S}' + \frac{\bar{E}}{r} \right) \sin^2 \theta \right]. \quad (5.12)$$

According to (5.5), this quantity only depends on the flux label r. We then write

$$\theta = \vartheta + \lambda(r, \vartheta), \tag{5.13}$$

where $\lambda \sim \varepsilon \ll 1$ known as the **rectifying parameter** is a periodic function of ϑ such that $\lambda(r,0) = \lambda(r,2\pi) = 0$. The quantity λ is then expanded in ε as

$$\lambda = \lambda_1(r, \vartheta) + \lambda_2(r, \vartheta) + \dots, \tag{5.14}$$

where $\lambda_1 \sim \varepsilon$, $\lambda_2 \sim \varepsilon^2$ and the dots indicate higher order corrections. Plugging (5.13) and (5.14) into (5.12) yields

$$\begin{split} \frac{\sqrt{g}}{R^2} &= \frac{r}{R_0} \left[1 - \left(\frac{r}{R_0} + \Delta' \right) \cos \vartheta + \dot{\lambda}_1 + \left(\bar{E}' + \frac{\bar{S}}{r} \right) \cos^2 \vartheta + \left(\bar{S}' + \frac{\bar{E}}{r} \right) \sin^2 \vartheta \right. \\ &+ \left(\frac{r\Delta'}{R_0} + \frac{r^2}{R_0^2} \right) \cos^2 \vartheta + \frac{\Delta}{R_0} + \dot{\lambda}_2 + \left(\Delta' + \frac{r}{R_0} \right) \left(\lambda_1 \sin \vartheta - \dot{\lambda}_1 \cos \vartheta \right) \right]. \end{split}$$

Imposing the condition (5.5) and solving order by order in ε , after some algebra we obtain

$$\lambda_1 = \left(\frac{r}{R_0} + \Delta'\right) \sin \vartheta,$$

$$\lambda_2 = -\frac{\sin 2\vartheta}{4} \left[(\bar{E} - \bar{S})' - \frac{\bar{E} - \bar{S}}{r} - \frac{3r}{R_0} \Delta' - \frac{r^2}{R_0^2} - 2\Delta'^2 \right].$$
(5.15)

Note that to leading order we have

$$\frac{\sqrt{g}}{R^2} pprox \frac{r}{R_0}.$$

Therefore, we can finally write the angle θ in terms of r and ϑ as

$$\theta \approx \vartheta + \left(\frac{r}{R_0} + \Delta'\right) \sin \vartheta + \dots$$
 (5.16)

We have now all the elements to compute the metric tensor coefficients in these new straight field line coordinates. This is carried out in the next section for a tokamak equilibrium without steep pressure gradients. In such a case the accuracy of (5.16) proves to be sufficient for the correct evaluation of the metric tensor coefficients needed for the stability calculations. The stability analysis of equilibria which exhibit localised regions of sharp pressure variations requires a more careful computation of the geometric coefficients, and this will be detailed in §5.4.

If $\vartheta = \theta + \nu(r, \theta)$, one has

$$\frac{B^{\vartheta}}{B^{\phi}} = \frac{B^{\theta}}{B^{\phi}} \left(1 + \frac{\partial \nu}{\partial \theta} \right)$$

Recalling (5.4), in line with the notation employed in earlier sections this gives $1 + \frac{\partial v}{\partial \theta} = \sqrt{g}_u / \sqrt{g}$ and averaging it in θ yields $\sqrt{g}/R^2 = \frac{1}{2\pi} \int_0^{2\pi} \sqrt{g}_u / R^2 d\theta$, so that

$$\frac{\partial v}{\partial \theta} = \frac{2\pi \sqrt{g}_u/R^2}{\int_0^{2\pi} \sqrt{g}_u/R^2 d\theta} - 1.$$

 $\lambda(r,\vartheta)$ can be obtained perturbatively from the equation above.

The metric tensor coefficients 5.3

Let us assume that $\mu_0 p/B_0^2 \sim \mu_0 r p'/B_0^2 \sim \varepsilon^2$. By means of (5.11), the elements of the metric tensor in the straight field line coordinates introduced in the previous section can be easily obtained (cf. (4.22)) and their expressions at leading orders read

$$g_{rr} = 1 - 2\Delta' \cos \vartheta + \dots,$$

$$g_{r\vartheta} = \left(\frac{r^2}{R_0} + r\Delta' + r^2\Delta''\right) \sin \vartheta + \dots,$$

$$g_{\vartheta\vartheta} = r^2 + \frac{2r^3}{R_0} \cos \vartheta + 2r^2\Delta' \cos \vartheta + \dots,$$

$$g_{\phi\phi} = R_0^2 \left[1 + \frac{2r}{R_0} \cos \vartheta + \dots\right],$$

$$\frac{1}{\sqrt{g}} = \frac{1}{rR_0} \left[1 - \frac{2r}{R_0} \cos \vartheta + \dots\right].$$
(5.17)

We refer to the quantities g_{ij}/\sqrt{g} (the indices i and j run over (r, ϑ, ϕ)) as the **metric coefficients**. Unfortunately, the expressions of the metric coefficients computed from (5.17) are not, generally, accurate enough for what is required in the stability analysis. In (5.17), we must thus include higher order terms meaning, more specifically, that second order corrections in the smallness parameter ε have to be evaluated. The best strategy for tackling the problem, which is a rather long and boring procedure, and to avoid an unnecessary amount of algebra is divide et *impera*: we compute separately $1/\sqrt{g}$ and g_{ij} , and then we evaluate their product to the relevant orders in ε . Let us introduce the symbol of poloidal average

$$\langle f \rangle \equiv \frac{1}{2\pi} \int_0^{2\pi} f \, d\vartheta. \tag{5.18}$$

Exploiting the results of the previous section, a tedious calculation shows that to second order in ε we have

$$\frac{1}{\sqrt{g}} \approx \frac{1}{rR_0} \left[1 + \Lambda_* \cos \vartheta - \dot{\lambda} - \Lambda_* \lambda \sin \vartheta + \left(\Delta'^2 - \frac{r\Lambda_*}{R_0} \right) \cos^2 \vartheta \right. \\
+ \dot{\lambda}^2 - \Lambda_* \dot{\lambda} \cos \vartheta + \frac{\Delta}{R_0} - \left(\bar{E}' + \frac{\bar{S}}{r} \right) \cos^2 \vartheta - \left(\bar{S}' + \frac{\bar{E}}{r} \right) \sin^2 \vartheta \right], \tag{5.19}$$

where λ is given by (5.14) and we recall that $\Lambda_* = \Delta' - r/R_0$. We remark that one has to account appropriately for the correct orders of λ in the expansion above.

Now one notices that

$$R^{2} = R_{0}^{2} \left(1 + 2 \frac{r}{R_{0}} \cos \vartheta - \frac{2\Delta}{R_{0}} + \frac{r^{2}}{R_{0}^{2}} \cos^{2} \vartheta - 2 \frac{r}{R_{0}} \left(\Delta' + \frac{r}{R_{0}} \right) \sin^{2} \vartheta \right), \tag{5.20}$$

from which it immediately follows that

$$\langle R^2 \rangle' = -rR_0 \left(\Delta'' + 3\Delta' / r + 1 / R_0 \right).$$
 (5.21)

Since $R^2/\sqrt{g} = \langle R^2/\sqrt{g} \rangle$, by means of (5.19) and (5.20) we readily obtain

$$G \equiv \frac{R^2}{\sqrt{g}} = \frac{R_0}{r} \left(1 - \frac{\Delta}{R_0} - \frac{r^2}{2R_0^2} - \frac{r\Delta'}{2R_0} - \frac{(\bar{E} + \bar{S})'}{2} - \frac{\bar{E} + \bar{S}}{2r} \right).$$

We notice that one may think of r as a function of another labelling parameter \tilde{r} , i.e. $r=r(\tilde{r})$. Denoting with $\sqrt{g}_{\tilde{r}}$ the Jacobian in this new variable, we choose \tilde{r} such that $R^2/\sqrt{g}_{\tilde{r}}=R_0/\tilde{r}$. Since $\sqrt{g}_{\tilde{r}}=dr/d\tilde{r}\sqrt{g}$, from the equation above we have

$$\frac{R_0}{\tilde{r}} = \frac{R_0}{r} \left(1 - \frac{1}{2r} \left(\frac{r^2 \Delta}{R_0} + \frac{r^4}{4R_0^2} + r(\bar{E} + \bar{S}) \right)' \right) \frac{d\tilde{r}}{dr}.$$

This can be easily solved yielding

$$r=\tilde{r}-\Big(\frac{\tilde{r}\Delta}{2R_0}+\frac{\tilde{r}^3}{8R_0^2}+\frac{1}{2}(\bar{E}+\bar{S})\Big).$$

Therefore, in an equivalent manner, we conveniently choose \bar{E} and \bar{S} such that \bar{S}

$$\bar{E} + \bar{S} = -\frac{r\Delta}{R_0} - \frac{r^3}{4R_0^2},\tag{5.22}$$

so that

$$G = \frac{R_0}{r}. (5.23)$$

Now it remains to compute the expressions for the coefficients g_{rr}/\sqrt{g} , $g_{\theta\theta}/\sqrt{g}$ and $g_{r\theta}/\sqrt{g}$. We can write g_{ij}/\sqrt{g} as a sum of an averaged and a fluctuating (in ϑ) part as

$$\frac{g_{ij}}{\sqrt{g}} = \langle \frac{g_{ij}}{\sqrt{g}} \rangle + \left(\frac{g_{ij}}{\sqrt{g}} \right) ,$$

where

$$f_{\sim} = f - \langle f \rangle.$$

The analysis of MHD instabilities for equilibria without sharp pressure gradients⁸ requires knowledge of the expressions of $\langle g_{rr}/\sqrt{g}\rangle$ and $\langle g_{\vartheta\vartheta}/\sqrt{g}\rangle$ with an ε^2 accuracy, while it is sufficient to evaluate their fluctuating part to first order in ε . For this purpose only λ_1 is needed (cf. (5.15)). We anticipate, however, that cases with large p' will need the oscillating part of the metric coefficients to be computed with an accuracy of order ε^2 (this will be discussed in detail in the next section). Therefore, for the sake of clarity as we did for the computation of the rectifying parameter, we present below the full calculation correct to second order in ε .

⁷ It is often found in the literature $\bar{E} = -\bar{S}$.

⁸ Primarily for the computation of the m = 1 internal kink.

Let us start with g_{rr}/\sqrt{g} . A quick algebraic manipulation gives

$$g_{rr} \approx 1 - 2\Delta' \cos \vartheta + 2\Delta' \lambda \sin \vartheta + r^2 \lambda'^2 + \Delta'^2 + 2r\Delta' \lambda' \sin \vartheta + 2(\bar{E}' \cos^2 \vartheta + \bar{S}' \sin^2 \vartheta).$$

Thus, by using the results above, we obtain

$$\langle \frac{g_{rr}}{\sqrt{g}} \rangle = \frac{1}{rR_0} \left(1 + \frac{9}{4} \frac{r^2}{R_0^2} + 4 \frac{r\Delta'}{R_0} + \frac{\Delta}{R_0} + 2\Delta'^2 + \frac{r^2}{2} \Delta''^2 + \frac{r^2}{R_0} \Delta'' + r\Delta'\Delta'' \right),$$

for the averaged part, and⁹

$$\begin{split} \left(\frac{g_{rr}}{\sqrt{g}}\right)_{\sim} &= -\frac{2}{rR_0} \left(\Delta' + \frac{r}{R_0}\right) \cos \vartheta \\ &+ \left(\bar{C}' - \Delta'^2 - \frac{r\Delta'}{R_0} - \frac{r^2\Delta''^2}{2} - \frac{r^2\Delta''}{R_0} - r\Delta'\Delta''\right) \frac{\cos 2\vartheta}{rR_0} + \dots, \end{split}$$

for the fluctuating one where C is given by (5.10) and the dots indicate as usual higher order corrections. Hence, we write

$$L = \frac{g_{rr}}{\sqrt{g}} = \frac{1}{rR_0} \left[1 - 2\left(\Delta' + \frac{r}{R_0}\right) \cos\vartheta + \frac{9}{4} \frac{r^2}{R_0^2} + 4\frac{r\Delta'}{R_0} + \frac{\Delta}{R_0} + 2\Delta'^2 + \frac{r^2}{2}\Delta''^2 + \frac{r^2}{R_0}\Delta'' + r\Delta'\Delta'' + \left(\bar{C}' - \Delta'^2 - \frac{r\Delta'}{R_0} - \frac{r^2\Delta''^2}{2} - \frac{r^2\Delta''}{R_0} - r\Delta'\Delta''\right) \cos 2\vartheta \right]. \quad (5.24)$$

The derivation of $g_{\vartheta\vartheta}/\sqrt{g}$ is somehow simpler. Let us write

$$g_{\vartheta\vartheta} \approx r^2 \left(1 + 2\dot{\lambda} + \dot{\lambda}^2 \right) + 2r(\bar{E}\sin^2\vartheta + \bar{S}\cos^2\vartheta).$$

It easily follows that

$$\begin{split} \langle \frac{g_{\vartheta\vartheta}}{\sqrt{g}} \rangle &= \frac{r}{R_0} \left(1 + \frac{\Delta'^2}{2} + \frac{3r^2}{4R_0^2} + \frac{\Delta}{R_0} \right), \\ \left(\frac{g_{\vartheta\vartheta}}{\sqrt{g}} \right)_{\sim} &= \frac{2r}{R_0} \Delta' \cos\vartheta + \frac{r}{R_0} \left(\frac{r\Delta'}{R_0} + \frac{5}{2} \Delta'^2 - \bar{C}' \right) \cos 2\vartheta + \ldots. \end{split}$$

Thus, collating the two results together gives

$$N \equiv \frac{g_{\vartheta\vartheta}}{\sqrt{g}} = \frac{r}{R_0} \left[1 + 2\Delta' \cos\vartheta + \frac{\Delta'^2}{2} + \frac{3r^2}{4R_0^2} + \frac{\Delta}{R_0} + \left(\frac{r\Delta'}{R_0} + \frac{5}{2}\Delta'^2 - \bar{C}'\right) \cos 2\vartheta \right].$$
 (5.25)

9 A **periodic function** f in the variable ϑ can be written as a sine-cosine series

$$f = \langle f \rangle + \sum_{m=1}^{\infty} A_m \cos m\vartheta + B_m \sin m\vartheta,$$

where the coefficients A_m and B_m are given by

$$A_{m} = \frac{1}{\pi} \int_{-\pi}^{\pi} f \cos m\vartheta d\vartheta,$$

$$B_{m} = \frac{1}{\pi} \int_{-\pi}^{\pi} f \sin m\vartheta d\vartheta.$$

Computing $g_{r\vartheta}/\sqrt{g}$ also does not require a lot of algebra. We start from noting that

$$g_{r\vartheta} \approx r^2 \lambda' + r\Delta' \sin \vartheta + r^2 \lambda' \dot{\lambda} + r\Delta' \dot{\lambda} \sin \vartheta + r\Delta' \lambda \cos \vartheta$$

 $-\frac{r}{2} \left(\bar{E}' - \bar{S}' + \frac{\bar{E} - \bar{S}}{r} \right) \sin 2\vartheta,$

which shows that $g_{r\vartheta}/\sqrt{g}$ is ε times smaller compared to g_{rr}/\sqrt{g} and $g_{\vartheta\vartheta}/\sqrt{g}$. By multiplying the equation above by (5.19), it is immediate to see that $\langle g_{r\vartheta}/\sqrt{g} \rangle = 0$, so that we obtain

$$M = \frac{g_{r\vartheta}}{\sqrt{g}} = \frac{r}{R_0} \left[\left(\Delta'' + \frac{\Delta'}{r} + \frac{1}{R_0} \right) \sin \vartheta + \left(\frac{5}{2} \frac{\Delta'}{R_0} + \frac{r\Delta''}{2R_0} \right) + 3\Delta'\Delta'' + 2\frac{\Delta'^2}{r} - \frac{\bar{C}''}{2} - \frac{\bar{C}''}{2r} - \frac{3\bar{C}}{2r^2} \right] \frac{\sin 2\vartheta}{2} \right].$$
 (5.26)

Thus, for straight field line coordinates, the geometry of equilibria which satisfy the conditions $\mu_0 p/B_0^2 \sim \mu_0 r p'/B_0^2 \sim \varepsilon^2$ is completely determined by equations (5.21)-(5.26). To complete the framework which is required for the stability calculations presented in the next chapters, it only remains to account for modification of the metric coefficients in presence of localised steep pressure gradients. This is discussed in the next section.

5.4 Metric of the $s - \alpha$ equilibrium model

Let us assume that, globally, the ratio of the kinetic over magnetic pressure is of order ε^2 , but allow for localised strong pressure gradients. This is what characterises the so called $s-\alpha$ equilibrium model introduced in section 4.3.4 which is relevant for the discussion of ballooning modes addressed in chapter 12. Hence, the aim of this section is to derive the appropriate expressions of the metric coefficients in the narrow region where such gradients occur.

First notice that the enhancement of the pressure gradient can locally "promote" the order of some quantities like, for example, the second derivative of the Shafranov shift (see (4.40)-(4.43)). It follows, and this is a crucial subtlety, that care has to be taken any time the derivative operator acts on e.g. Δ' : if the differential operator acts on some expressions involving Δ' , then terms proportional to Δ'' may appear whose order would be lower than the one of the original expression prior to differentiation. Notice that this reflects the fact that Δ' becomes nearly discontinuous when large localised pressure gradients are allowed (see the discussion in section 4.3.4 and figure 5.3).

Hence, the expressions for the coefficients L, M and N, and their derivatives, must be modified accounting for such enhancements. Noticing that $G = R_0/r$ is guaranteed by the choice of the function \bar{S} (cf.

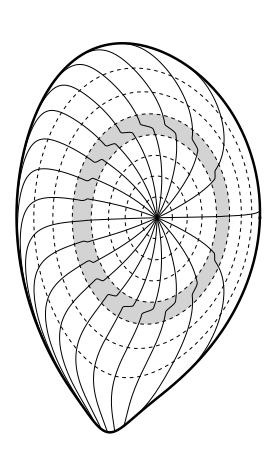


Figure 5.3: Example of the straight field poloidal angle distortion due to a steep pressure gradient radially localised within the shaded region. In such a case, θ becomes nearly discontinuous where the pressure gradient is large due to the discontinuity of the first derivative of the Shafranov shift (cf. (5.15) which can be inverted to write θ as a function of θ).

(5.23)), we anticipate that the quantities that will enter the stability analysis of the $s - \alpha$ model are

$$\langle N \rangle \quad \langle N \rangle' \quad \langle N \rangle'' \quad \langle M \rangle \quad \langle M \rangle' \quad \langle L \rangle$$

$$N_{\pm 1} \quad N'_{\pm 1} \quad N''_{\pm 1} \quad M_{\pm 1} \quad M'_{\pm 1} \quad L_{\pm 1}$$

$$N_{\pm 2} \quad N'_{\pm 2} \quad N''_{\pm 2} \quad M_{\pm 2} \quad M'_{\pm 2} \quad L_{\pm 2}$$

$$(5.27)$$

with the notation $A_{\pm \ell} = \frac{1}{2\pi} \int_0^{2\pi} A e^{\mp i \ell \vartheta} d\vartheta$.

The computation of the coefficients above is easily accomplished by means of equations (5.24)-(5.26). Following the discussion of section 4.3.4, we allow $r\mu_0 p_0'/B_0^2 \sim \varepsilon$ and let $\Delta'' \to \alpha/r$ with the assumption that α is constant and of the order of unity. By means of (4.40)-(4.43)and (5.0), we immediately see that $r\bar{C}'' \sim \varepsilon$ while $\bar{C}' \sim \bar{C}/r \sim \varepsilon^{2.10}$ We are now ready to evaluate the expressions of the metric coefficients for an $s - \alpha$ equilibrium.

Anticipating that only the leading ε order is needed, all the entries marked in light grey in the table above are at least of order ε^2 and thence they can be dropped (note that $\langle M \rangle = 0$). Quantities that will be employed explicitly are

$$\langle L \rangle \approx \frac{1}{rR_0} \left(1 + \frac{\alpha^2}{2} \right), \quad L_{\pm 2} \approx -\frac{\alpha^2}{4rR_0},$$

$$\langle N \rangle \approx \frac{r}{R_0}, \quad \langle N \rangle' \approx \frac{1}{R_0},$$

$$M_{\pm 1} \approx \mp \frac{i\alpha}{2R_0}.$$
(5.28)

All the remaining terms in (5.27) are of order ε at most whose explicit expression is not required.

We shall point out that the approximations above do not account for terms of the form α^k with k > 2 which may appear at higher orders in the ε -expansion of (5.24)-(5.26). Such terms, however, can be expected to be small under the assumption that, also in the case of locally steep profiles, the metric tensor coefficients can be written as a converging series in ε .¹¹

In conclusion, the expressions for the metric coefficients represented by (5.21), (5.23)-(5.26) and (5.28) will form the geometrical basis to be used in the stability analysis of the various MHD perturbations addressed in the following chapters.

References

- M. N. Bussac et al., Phys. Rev. Lett. 35, 1638 (1975).
- H. J. de Blank and T. J. Schep, Phys. Fluids B 3, 1136 (1991).
- J. M. Greene et al., Phys. Fluids 14, 671 (1971).
- J. M. Greene and M. S. Chance, Nucl. Fusion 21, 453 (1981).

Note that $r^2\bar{C}^{\prime\prime\prime}\sim 1$ at most, having assumed that $r^2\psi''' \sim \psi'$ (cf. (4.42)).

¹¹ This a rather heuristic argument.

- S. Hamada, Nucl. Fusion 2, 23 (1962).
- B. B. Kadomtsev and O. P. Pogutse Reviews of Plasma Physics Vol. ${\bf 5}$ (Ed. M. A. Leontovich), Consultants Bureau (New York, US), 1970.
- E. Lazzaro and P. Zanca, Phys. Plasmas 10, 2399 (2003).
- V. D. Shafranov, Nucl. Fusion 8, 253 (1968).
- V. D. Shafranov and E. I. Yurchenko, Nucl. Fusion 8, 329 (1968).
- V. D. Shafranov and E. I. Yurchenko, Zh. Eksp. Teor. Fiz. 53, 1157 (1967) [Sov. Phys.-JETP **26**, 682 (1968)].
- L. S. Solov'ev and V. D. Shafranov Reviews of Plasma Physics Vol. 5 (Ed. M. A. Leontovich), Consultants Bureau (New York, US), 1970.
- A. B. Mikhailovskii, Instabilities in a Confined Plasma, Institute of Physics Publishing (Bristol, UK), 1998.

Part III IDEAL STABILITY

General remarks on ideal MHD stability

It is inevitable that a plasma which is in its equilibrium state will be subject to some sort of perturbations: these can be, for example, a small fluctuation of the magnetic field caused by external conductors, or a modification of the temperature profile due to local power deposition, and so on. Thus, the natural question to ask is whether such an equilibrium is stable or unstable with respect to small deviations from its initial state. We say that the equilibrium is **unstable** if the perturbation grows in time pushing the system away from its original equilibrium state. Otherwise is **stable**. We refer to growing perturbations as **instabilities** (often we simply call them **perturbations** or **unstable modes**, the reason of the latter will become clear later).

In some cases plasma instabilities can be dangerous, either leading to a severe deterioration of the plasma performances or putting in danger the structural integrity of the device.¹ In other cases instead, they might have a beneficial effect, helping e.g. in controlling the plasma impurity content or enhancing the exhaust of the **fusion ashes** (namely the Helium fusion by-product).

Thus, with the aim of maximising tokamak performance, many efforts have been devoted to the understanding of the driving mechanisms of such events, and to the identification of their stability boundaries. MHD instabilities in tokamaks can be divided into two main families: ideal instabilities and resistive instabilities. We talk about ideal instabilities when the plasma is modelled as a perfect conductor, whereas we refer to resistive instabilities if a small amount of plasma resistivity is allowed. We shall focus on ideal instabilities first.

Before diving into the mathematical analysis of the various MHD perturbations, it is instructive to provide a brief account of the basic

¹ This happens when sudden and violent transients occur. Disruptions (a rapid collapse of the plasma column) and Edge Localised Modes (ELMs) are such a kind of phenomena. Both are associated with extremely high heat loads. Disruptions also induce severe structural mechanical loads.

The ideal instabilities discussed in this report are **internal** and **external kinks**, **infernal**, **Mercier** and **ballooning** modes. Their understanding provides the basic tools for the comprehension of many of MHD events observed in experiments.

concepts which the ideal MHD stability framework leans on. This is the aim of this chapter.

6.1 Linearised MHD

The whole MHD stability framework is based on the concept of **linearisation**. To explain it, let's take a generic physical quantity f, either a scalar or a vector, and assume that it can be written as the sum of an equilibrium (indicated by the subscript zero) and a fluctuating (denoted by a tilde) part, viz.

$$f = f_0 + \tilde{f}. \tag{6.1}$$

The linearisation approach basically expands the equations in which f appears to first order in the fluctuating part. All the physics of the interaction of the fluctuation with itself, the so called **non-linearities**, is neglected.

We start with the system of equations (2.1)-(2.6), and (2.8). Let us assume that the plasma is in a **static equilibrium state** (i.e. no equilibrium fluid flows), and add a small **fluid perturbation** ξ (also called **fluid displacement**). This quantity is related to the plasma velocity through the relation

$$\boldsymbol{u} = \frac{\partial \boldsymbol{\xi}}{\partial t}.\tag{6.2}$$

Plugging (6.2) into the MHD equations, and retaining only the first order fluctuating terms yields

$$\tilde{\rho} = -\nabla \cdot (\rho_0 \xi),$$

$$\rho_0 \frac{\partial^2 \xi}{\partial t^2} = -\nabla \tilde{p} + \tilde{J} \times B_0 + J_0 \times \tilde{B},$$

$$\tilde{B} = \nabla \times (\xi \times B_0),$$

$$\tilde{p} = -\xi \cdot \nabla p_0 - \Gamma p_0 \nabla \cdot \xi,$$

$$\nabla \times \tilde{B} = \mu_0 \tilde{J},$$

$$\nabla \cdot \tilde{B} = 0.$$
(6.3)

For the sake of simplicity, we assume isothermal flux surfaces (cf. (4.59)), so that both p_0 and ρ_0 are flux functions.

It is immediate to recognise that the equation for the perturbed mass density can be ignored.³ Thus, by combining equations (6.3) together, we easily obtain a single vector equation for ξ :

$$\rho_0 \frac{\partial^2 \boldsymbol{\xi}}{\partial t^2} = \nabla \left(\boldsymbol{\xi} \cdot \nabla \boldsymbol{p}_0 + \Gamma \boldsymbol{p}_0 \nabla \cdot \boldsymbol{\xi} \right) + \frac{1}{\mu_0} \nabla \times \left[\nabla \times (\boldsymbol{\xi} \times \boldsymbol{B}_0) \right] \times \boldsymbol{B}_0 + \frac{1}{\mu_0} \left(\nabla \times \boldsymbol{B}_0 \right) \times \nabla \times (\boldsymbol{\xi} \times \boldsymbol{B}_0) . \tag{6.4}$$

The equation above is often written in a compact form as

$$\rho_0 \frac{\partial^2 \boldsymbol{\xi}}{\partial t^2} = \boldsymbol{F}(\boldsymbol{\xi}),\tag{6.5}$$

² This is the ideal MHD model. The effects of plasma resistivity on the stability will be discussed in part four.

 $^{^3}$ This is because the plasma is static. With a stationary equilibrium flow, the equation for $\tilde{\rho}$ is needed.

where the linear operator F is known as MHD force operator. This equation must be supplied with the appropriate boundary conditions. These are discussed below.

Boundary conditions in linearised MHD

Let us assume that a vacuum region separates the plasma from an ideally conducting rigid wall,⁴ with the vacuum magnetic perturbation obeying

$$\nabla \times \widetilde{\boldsymbol{B}}_{n} = 0. \tag{6.6}$$

Hereafter the subscript v will indicate a vacuum quantity. We further impose that there are no electric fields at the equilibrium.

The physical quantities appearing in equations (6.5) and (6.6) have to fulfil the correct matching conditions at the plasma-vacuum interface and at the wall. These are computed from Maxwell's equations assuming that the displaced surface moves with a normal velocity $n \cdot u$, and choosing a reference frame comoving with the plasma surface. The quantities in the original fixed reference frame are obtained from those in the moving one by applying the Galilean transformations⁵ $p_M = p$, $B_M = B$ and $E_M = E + u \times B$, where we used the subscript M for denoting quantities in the moving frame. Hence, at the plasma-vacuum boundary we get

$$\boldsymbol{n} \cdot (\boldsymbol{B} - \boldsymbol{B}_{v}) = 0, \tag{6.7}$$

$$\boldsymbol{n} \times (\boldsymbol{B} - \boldsymbol{B}_{v}) = \mu_{0} \boldsymbol{K}, \tag{6.8}$$

$$\mathbf{n} \times (\widetilde{\mathbf{E}}_M - \widetilde{\mathbf{E}}_{n,M}) = 0, \tag{6.9}$$

with n being the unit vector perpendicular to the perturbed surface and **K** the surface current density.

Let us now consider an infinitesimal Gaussian pillbox lying across the plasma-vacuum surface as shown in figure fig. 6.1. For the case in which there is no flow across the plasma surface, integrating (2.13) over the pillbox and letting the width approaching zero but keeping the surface area finite (Jackson (1999), Boyd (2003)) gives

$$[\![p + B^2 / 2\mu_0]\!] = 0,$$
 (6.10)

where $[\![\cdot]\!] = (\cdot)_{r_b+\epsilon} - (\cdot)_{r_b-\epsilon}$ with $\epsilon \to 0$, and r_p denoting the plasmavacuum surface. Here we used the fact that since the plasma is modelled as an ideal conductor, the normal component of B on the plasma surface is vanishing (i.e. it remains a magnetic surface). This relation guarantees that in a region of a rapid variation of kinetic (p) and/or magnetic (B^2) pressure there is no infinite acceleration of the plasma element. Hence, equation (6.10) gives the jump condition of the total pressure (kinetic and magnetic) at the perturbed plasma-vacuum surface. We now notice that a scalar quantity f evaluated at the perturbed plasma-vacuum surface takes the form

$$f = f_0(r_{\text{pert}}) + \tilde{f}(r_{\text{pert}}) \approx f_0(r) + \boldsymbol{\xi} \cdot \boldsymbol{\nabla} f_0(r) + \tilde{f}(r), \tag{6.11}$$

⁴ The particular case of a plasma surrounded by a resistive wall is discussed in appendix E.

⁵ This is not strictly correct as one should use Lorentz transformations. However, for nonrelativistic systems this approximation proves to be very accurate.

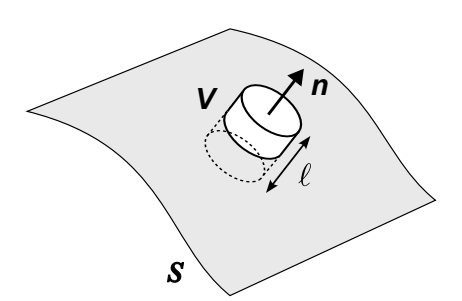


Figure 6.1: Pillbox of volume *V* extending across the plasma-vacuum surface S. The jump conditions are computed by letting $\ell \to 0$. Note that $\boldsymbol{n} = \nabla r/|\nabla r|$.

where r_{pert} and r denote the position of the perturbed and unperturbed surface respectively. It follows that (6.10) can be cast as

$$\begin{split} \left[\tilde{p}(r) + \frac{\boldsymbol{B}_{0}(r) \cdot \tilde{\boldsymbol{B}}(r)}{\mu_{0}} + \boldsymbol{\xi} \cdot \boldsymbol{\nabla} \left(p_{0}(r) + \frac{B_{0}^{2}(r)}{2\mu_{0}} \right) \right]_{\text{plasma}} \\ &= \left[\frac{\boldsymbol{B}_{0}(r) \cdot \tilde{\boldsymbol{B}}(r)}{\mu_{0}} + \boldsymbol{\xi} \cdot \boldsymbol{\nabla} \frac{B_{0}^{2}(r)}{2\mu_{0}} \right]_{\text{vacuum}}, \end{split}$$

having written explicitly the dependence upon the radial variable.

At the ideally conducting metallic wall surface we impose

$$\boldsymbol{n}_w \times \widetilde{\boldsymbol{E}}_v = 0, \tag{6.12}$$

$$\mathbf{n}_w \cdot \partial \mathbf{B}_v / \partial t = 0, \tag{6.13}$$

with n_w indicating the unit vector normal to the wall pointing towards the plasma. Equation (6.13) follows from (6.7) having used the fact that inside a perfect conductor the magnetic field can be non-zero but independent of time. Therefore, we can write (6.13) as $n_w \cdot \tilde{B}_v = 0$, where \tilde{B}_v is the fluctuating (perturbed) magnetic field.

If the ideal wall is facing directly the plasma, the appropriate boundary conditions at the **plasma-wall interface** are

$$\mathbf{n} \cdot \widetilde{\mathbf{B}} = 0, \tag{6.14}$$

$$\mathbf{n} \times \widetilde{\mathbf{E}} = 0, \tag{6.15}$$

from which, by combining with (2.3), one has

$$\boldsymbol{n} \cdot \boldsymbol{u} = 0, \tag{6.16}$$

where here n and n_w coincide apart from the direction along which they are pointing.

6.1.2 Eigenvalue properties

In order to resolve the time dependence in (6.5), we attempt a solution of the form

$$\tilde{\mathfrak{f}}(\boldsymbol{x},t) = \tilde{f}(\boldsymbol{x})e^{\gamma t} + c.c., \tag{6.17}$$

where γ is a complex number and c.c. stands for complex conjugate. This is the so called **normal mode analysis**, 6 which is the approach that will be used throughout this report to investigate MHD stability. The real part of γ is associated with the growth of the perturbation's amplitude, whereas the imaginary part to its rotation frequency. Hence, the study of stability basically boils down to the analysis of the real part of γ .

A remarkable property of the ideal MHD model is that for the case of a plasma directly surrounded by a perfectly conducting wall the operator

⁶ A more rigorous procedure for solving linearised equations involves using the Laplace transform.

F is self-adjoint, meaning that for two arbitrary functions ξ and η satisfying the boundary condition (6.14)-(6.16) one has

$$\int_{V} \bar{\boldsymbol{\eta}} \cdot \boldsymbol{F}(\boldsymbol{\xi}) dV = \int_{V} \boldsymbol{\xi} \cdot \boldsymbol{F}(\bar{\boldsymbol{\eta}}) dV,$$

where V is the volume enclosing the plasma with a corresponding infinitesimal volume element dV and the overbar indicates the complex conjugate.⁷ This is proved in the next subsection. The self-adjointness property of F also holds when a vacuum region separates the plasma from the ideal wall (a proof of this is given in appendix C.).

The operator F being self-adjoint implies that γ^2 , its **eigenvalue**, has to be real. Hence, if $\gamma^2 > 0$, we have two real solutions, one with $\gamma > 0$ (growing mode) and one with $\gamma < 0$ (damped mode). If the eigenvalue γ is positive, we call it the **growth rate** (for simplicity, we shall always use this terminology also when γ is not positive or real). The condition $\gamma = 0$ identifies the so called **marginal stability boundary** (or **marginal boundary** in short). If $\gamma^2 < 0$, then γ is purely imaginary indicating a stationary oscillation which does not grow in time. It is worth to point out that the spectrum of F contains both discrete eigenvalues and continua, the latter however only appearing for $\gamma^2 < 0$, i.e. in the stable domain (Freidberg (2014)). Therefore, within the normal mode approach, we may just focus on assessing the existence of exponentially growing modes.

Self-adjointness of the force operator F

We follow the proof in Bernstein (1958) which leverages the energy conservation (2.12) in ideal MHD. Let us assume that the plasma is directly surrounded by a perfectly conducting metallic wall. Using the results of section 2.1.2, the total energy U = K + W, where K and W are the kinetic and potential contributions, is conserved. This means that for small deviations from the equilibrium, which is supposed to be static, we have⁸

$$\frac{\partial}{\partial t} \left(\delta K + \delta W \right) = 0,$$

where

$$\delta K = \frac{1}{2} \int_{V} \rho_0 \left(\frac{\partial \boldsymbol{\xi}}{\partial t} \right)^2 dV.$$

with V the plasma volume and dV the infinitesimal volume element. Here the fluid displacement ξ is a real function.

By dotting (6.5) with $\frac{\partial \xi}{\partial t}$ and integrating over the plasma volume V we obtain

$$\frac{\partial \delta K}{\partial t} = \int_{V} \frac{\partial \xi}{\partial t} \cdot F(\xi) dV = -\frac{\partial \delta W}{\partial t}.$$
 (6.18)

We shall consider the integral in the expression above as a functional of the two functions ξ and $\frac{\partial \xi}{\partial t}$, that is

$$\int_{V} \frac{\partial \boldsymbol{\xi}}{\partial t} \cdot \boldsymbol{F}(\boldsymbol{\xi}) dV = \mathscr{F}\left(\frac{\partial \boldsymbol{\xi}}{\partial t}, \boldsymbol{\xi}\right).$$

⁷ Loosely speaking, F is an operator acting on fluid displacement functions f_i of a Hilbert space with inner product

$$(f_i, f_j) = \int_V \bar{f}_i \cdot f_j dV.$$

For a mathematical description of operator theory in MHD, the reader is referred to Lifshitz (1987). Note that the self-adjointness property of the force operator holds only in ideal MHD.

⁸ Take

$$K = K_0 + \delta K,$$

$$W = W_0 + \delta W.$$

with $K_0 = 0$ and W_0 constant.

Let W_0 be the potential energy at the equilibrium position r_{eq} , i.e. $W_0 = W(r_{eq})$. Taylor expanding W in ξ gives

$$W(\mathbf{r}_{eq} + \boldsymbol{\xi}) = W_0 + \boldsymbol{\xi} \cdot \nabla W|_{\mathbf{r}_{eq}} + \frac{1}{2}\boldsymbol{\xi} \cdot \left[\boldsymbol{\xi} \cdot \nabla (\nabla W)\right]|_{\mathbf{r}_{eq}} + \dots$$

Since we are in a neighbourhood of the equilibrium, we have $\nabla W|_{r_{eq}} = 0$. It follows that the functional δW is a quadratic form in ξ :

$$\delta W = \delta W(\xi,\xi), \quad \text{and} \quad \frac{\partial \delta W}{\partial t} = \delta W\left(\frac{\partial \xi}{\partial t},\xi\right) + \delta W\left(\xi,\frac{\partial \xi}{\partial t}\right).$$

Additionally, δW is symmetric in its arguments, i.e. for arbitrary $\pmb{\xi}$ and $\pmb{\eta}$

$$\delta W(\boldsymbol{\eta}, \boldsymbol{\xi}) = \delta W(\boldsymbol{\xi}, \boldsymbol{\eta}).$$

Hence

$$\frac{\partial \delta W}{\partial t} = 2\delta W \left(\frac{\partial \xi}{\partial t}, \xi \right) = 2\delta W \left(\xi, \frac{\partial \xi}{\partial t} \right).$$

Now, the crucial step is to recognise that ξ is algebraically independent of $\frac{\partial \xi}{\partial t}$. Thus, in (6.18) we replace $\frac{\partial \xi}{\partial t}$ by η , and readily obtain

$$\int_{V} \boldsymbol{\eta} \cdot \boldsymbol{F}(\boldsymbol{\xi}) dV = \mathscr{F}(\boldsymbol{\eta}, \boldsymbol{\xi}) = -2\delta W(\boldsymbol{\eta}, \boldsymbol{\xi}) =$$

$$-2\delta W(\boldsymbol{\xi}, \boldsymbol{\eta}) = \mathscr{F}(\boldsymbol{\xi}, \boldsymbol{\eta}) = \int_{V} \boldsymbol{\xi} \cdot \boldsymbol{F}(\boldsymbol{\eta}) dV,$$

showing that F is self-adjoint. Note also that

$$\delta W = -\frac{1}{2} \int_{V} \boldsymbol{\xi} \cdot \boldsymbol{F}(\boldsymbol{\xi}) dV$$

having omitted to write the arguments of the functional.

A "brute force" proof of the self adjointness of the force operator \boldsymbol{F} including a vacuum region separating the plasma from an ideally conducting wall is given in Appendix C. In the next sections we introduce three ideas which prove to be fundamental for the understanding of tokamak dynamics, namely the parallel gradient operator, the magnetic shear and mode coupling.

The energy principle

The self-adjointness property of F allows to derive a minimising principle, known as **energy principle**, which determines whether or not an equilibrium is stable without solving explicitly the differential equation $\rho_0 \partial^2 \xi / \partial t^2 = F(\xi)$. Focusing on the case of no vacuum region between plasma and ideal wall, the energy principle states that the equilibrium is stable if and only if

$$\delta W = -\frac{1}{2} \int_{V} \boldsymbol{\xi} \cdot \boldsymbol{F}(\boldsymbol{\xi}) dV \ge 0$$

 9 We use the definition $\delta W = W(\emph{r}_{eq} + \emph{E}) - W_0$

for all trial displacements ξ which satisfy the appropriate boundary conditions, with the integration carried over the plasma volume (the energy principle can be extended to the case of a vacuum region separating plasma and ideal wall). A very readable proof of the energy principle can be found in Biskamp (1993) and Goedbloed and Poedts (2004).

Although not used in the following calculations, the energy principle becomes quite handy when one has a guess on the form of ξ for an unstable perturbation. One can plug this trial function ξ , although not being the exact solution of the linearised equation of motion, into the integral above and check whether the result is negative proving that the equilibrium is not stable.

Furthermore, we can gain an intuitive physical understanding of the various stabilising and destabilising contributions by inspecting the terms appearing in δW . A little algebra shows that (ξ is taken to be a real quantity)

$$\delta W = \frac{1}{2} \int_{V} \left[\frac{|\tilde{B}^{2}|}{\mu_{0}} + \Gamma p_{0} |\nabla \cdot \boldsymbol{\xi}|^{2} + (\boldsymbol{\xi} \cdot \nabla p_{0}) \nabla \cdot \boldsymbol{\xi} - \boldsymbol{\xi} \cdot \boldsymbol{J}_{0} \times \nabla \times (\boldsymbol{\xi} \times \boldsymbol{B}_{0}) \right] dV.$$
(6.19)

The first and second terms, both positive and thus stabilising, are associated with magnetic field line bending and plasma compression respectively, the former due to the $|\tilde{\boldsymbol{B}}_{\perp}|^2$ term. The remaining terms can be negative, and hence acting as instability drives.

6.2 Parallel gradient and magnetic shear

In the previous chapter we introduced the straight field line coordinate system (r, ϑ, ϕ) , in which the ratio $q = B^{\phi}/B^{\vartheta}$ depends only on the flux label r. Because ϑ and ϕ are cyclic variables, any physical quantity \mathfrak{f} must be periodic in ϑ and ϕ so that it can be decomposed in a Fourier series

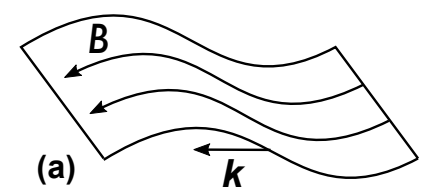
$$\tilde{f} = \sum_{m,n} f_{m,n}(r) e^{i(m\vartheta - n\varphi)}.$$
(6.20)

The quantities $f_{m,n}$ are called **Fourier harmonics** (or simply **harmonics** or **modes**), and m and n are the **poloidal** and **toroidal** mode numbers respectively. We refer to the pair (m, n) as the **mode helicity**, as these two numbers measure the angular twisting of the perturbation. For a fixed n, the various harmonics with different m's form the so called **poloidal spectrum**.

Very often terms of the form

$$R \cdot \nabla$$

appear (for sake of simplicity we drop the subscript o in writing equilibrium quantities). This is called the **parallel gradient** operator. We



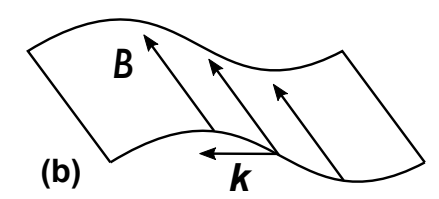


Figure 6.2: Field line movement following a displaced plasma flux surface associated with a wave vector k. (a): magnetic field parallel to the wave vector. (b): magnetic field perpendicular to the wave vector.

already saw in chapter 4 that equilibrium magnetic field lines lie on isobaric surfaces, this being expressed by the relation $\mathbf{B} \cdot \nabla p = 0$. In such a case, p can be viewed as a series of the form (6.20) for which all but the m = n = 0 terms are vanishing.

Let us now consider a perturbation of the form

$$\tilde{A} = A_{m,n}(r)e^{i(m\vartheta - n\varphi)} = A_{m,n}(r)e^{ik\cdot r},$$

having introduced the wave vector $\mathbf{k} = m\nabla \vartheta - n\nabla \phi$ with $\mathbf{r} = r\mathbf{e}_r + \vartheta \mathbf{e}_\vartheta + \phi \mathbf{e}_\phi$ (cf. Sec. 4.1.1). That is, we allow only a single harmonic in the expansion (6.20).

When we apply the parallel gradient to \tilde{A} , we obtain 10

$$\boldsymbol{B} \cdot \nabla \tilde{A} = i(\boldsymbol{k} \cdot \boldsymbol{B}) \tilde{A} = i B^{\phi} \left(\frac{m}{q} - n \right) \tilde{A}.$$

Because of the frozen-in theorem the field lines are either bent if $k \cdot B \neq 0$, or rigidly displaced if $k \cdot B = 0$ while following the fluid motion. This is schematically shown in figure 6.2. It turns out that the situation depicted in Fig. 6.2-(a) is energetically unfavourable compared to the case of Fig. 6.2-(b). This is because the magnetic energy term in (6.19) associated with **field line bending** is

$$|\tilde{\boldsymbol{B}}_{\perp}| \propto \boldsymbol{k} \cdot \boldsymbol{B}$$
.

For a given a perturbation with mode numbers m and n, it can be possible that its parallel gradient is zero for some values of q. The radii, namely the flux surfaces, for which $k \cdot B = 0$ are called **resonant surfaces** or **resonances**. We thus expect the perturbation to develop where the stabilisation associated with the bending of the field lines is minimised, i.e. where $k \cdot B \approx 0$.¹¹

The most dangerous case occurs when there is an extended region for which $q \approx m/n$. In such a situation the perturbation can develop over a large plasma portion. Things however are mitigated by the fact that q can be a varying function of the radius r. The magnetic shear is defined as (cf. Sec. 4.3)

$$s=\frac{rq'}{q},$$

and measures the radial rate of variation of q (cf. Fig. 6.3). Configurations with large values of magnetic shear generally exhibit improved

¹⁰ The power of the straight field line coordinates manifests clearly in the expression of the parallel gradient, having exploited the fact that the ratio B^{ϕ}/B^{ϑ} is a flux function.

¹¹ There are some special cases for which the field line bending stabilisation can be strongly reduced over a broad region even if $k \cdot B \neq 0$. This is what happens, e.g., with the m = 1 internal kink mode, which will be studied in detail later.

stability because of the reduced radial extension of the region where $k \cdot B$ is small for the helically resonant mode. Intuitively speaking, the fluid can "slip through" the magnetic cage when the wave vector is orthogonal to the field (cf. Fig 6.2-(b)). If one thinks of the magnetic field lines lying on each flux surface as a sequence of cords, then for a sufficiently strong twisting from one surface to another, the fluid element is less likely to escape. This provides a very efficient stabilising effect, although things might be slightly different when the ideal constraint is violated.

6.3 Mode coupling

In the two preceding sections, we introduced the perturbed MHD equations (see (6.3)) with appropriate boundary conditions, and provided an intuitive picture of the meaning of the parallel gradient operator and the effect of a sheared magnetic field. This discussion was developed by considering a fluid perturbation characterised by a single harmonic. The most general solution of (6.5), however, is typically a superposition of modes of the form given by equation (6.20).

Let us first notice that F depends on r and ϑ , and because of the equilibrium axisymmetry there is no dependence upon ϕ . This means that Fourier harmonics with different toroidal mode numbers behave, at least linearly, independently of each other. The situation is radically different when we consider the poloidal spectrum for a fixed n.

In order to make it more transparent, let us employ, instead of (6.5), the following model equation

$$\gamma^2 \rho_0 \xi = \mathscr{F} \xi, \tag{6.21}$$

where \mathscr{F} is a differential operator which depends on both r and ϑ , and ξ is of the form (6.20). We take ρ_0 to depend only on r.

As a matter of notation, for a generic quantity $A(r, \vartheta)$ one defines its mth (poloidal) **Fourier projection** as

$$A_m(r) = \frac{1}{2\pi} \int_0^{2\pi} A e^{-im\vartheta} d\vartheta.$$

The nth toroidal projection is computed similarly by replacing the poloidal angle with the toroidal one.

Hence, the (m, n) Fourier projection of (6.21) is

$$\gamma^2 \rho_0 \xi_{m,n} = \frac{1}{(2\pi)^2} \int \mathscr{F} \xi e^{-i(m\vartheta - n\phi)} d\vartheta d\phi,$$

with the integration carried out from 0 to 2π for both of the two angular variables. On the right hand side of this equation we have the convolution of \mathscr{F} and ξ . This leads to 13

$$\gamma^2 \rho_0 \xi_{m,n} = \mathscr{F}_{0,0} \xi_{m,n} + \sum_{m' \neq 0} \mathscr{F}_{m',0} \xi_{m-m',n}. \tag{6.22}$$

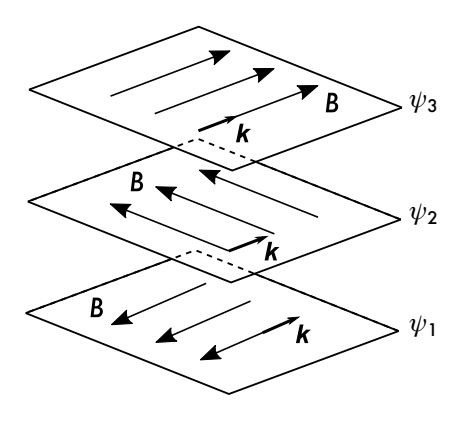


Figure 6.3: Highly exaggerated example of a sheared magnetic field across three flux surfaces. k indicates the wave vector of the perturbation.

In cylindrical geometry, in contrast, the dependence upon ϑ disappears.

¹² This makes n a good quantum number.

$$(fg)_m = \langle f \rangle g_m + \sum_{m' \neq 0} f_{m'} g_{m-m'}.$$

where the angular brackets indicate the poloidal average as defined in (5.18).

¹³ The convolution of two functions f and g of the poloidal angle ϑ is denoted by $(fg)_m$ and is given by

One then realises that the equation for the evolution of $\xi_{m,n}$ is not "monochromatic", in that it may include contributions from other harmonics. This is what we call **mode coupling** or **toroidal coupling** (because it is induced by toroidicity). This feature plays a crucial role in explaining the dynamics of several MHD instabilities and it will be thoroughly discussed in the next chapters.

We would like to stress that this effect is completely **absent in cylindrical plasmas**. Hence, care has to be taken when interpreting tokamak dynamics using results borrowed from analyses carried out in cylindrical geometry.

References

- I. B Bernstein et al., Proc. R. Soc. Lond. A 244, 17 (1958).
- D. Biskamp, Nonlinear Magnetohydrodynamics, Cambridge University Press (Cambridge, UK) 1993.
- T. J. M. Boyd and J. J. Sanderson, **The Physics of Plasmas**, Cambridge University Press (Cambridge, UK), 2003.
- J. P. Freidberg, **Ideal Magnetohydrodynamics**, Plenum Press (New York, US), 1987.
- J. P. Freidberg, Ideal MHD, Cambridge University Press (Cambridge, UK), 2014.
- J. P. Goedbloed and S. Poedts, Principles of Magnetohydrodynamics With Applications to Laboratory and Astrophysical Plasmas, Cambridge University Press (Cambridge, UK), 2004.
- J. D. Jackson, Classical Electrodynamics, Wiley (New York, US), 1999.
- B. B. Kadomtsev, Reviews of Plasma Physics Vol. 2 p. 153 (ed. M. A. Leontovich), Consultants Bureau (New York, US), 1966.
- G. Laval et al., Nucl. Fusion 5, 156 (1965).
- A. E. Lifschitz, Magnetohydrodynamics and Spectral Theory, Kluwer Academic Publishers (Dordrecht, NE) 1989.
- D. D. Schnack, Lectures in Magnetohydrodynamics: With an Appendix on Extended MHD, Springer Berlin (Heidelberg, DE) 2009.
- J. A. Wesson, Tokamaks, Oxford University Press (Oxford, UK), 2011.

Distilled stability equations

Although equation (6.5) encapsulates the whole physics of linearised MHD, it is not easy to handle in its form. We are thus interested in deriving a suitable set of coupled differential equations simple enough to be analytically manageable, and yet sufficiently flexible to describe a wide variety of phenomena. We show that, eventually, this set will consist of three equations only which, remarkably, are able to capture the fundamental physics of many phenomena observed in tokamaks.¹ These are called **eigenmode equations** or **stability equations**; they also form the basis for the development of the resistive theory. This chapter is thence devoted to their derivation.

We first rearrange the ideal MHD equations in a form easier to handle mathematically in a tokamak geometry. Then, specialising to the case of a **nearly circular plasma cross-sections**, a set of coupled differential equations is derived through a careful ordering of equilibrium and perturbed quantities.² The procedure for obtaining the stability equations is based on an **inverse aspect ratio expansion**. Particular emphasis is given to the effects of mode coupling induced by toroidicity: one finds that the dynamics of a specific poloidal harmonic is determined by the coupling with the first neighbouring **sidebands** (or **satellite harmonics**) while contributions arising from farther Fourier harmonics can, generally, be ignored. We work out the derivation in such a way to have a fairly easy comparison with the results obtained in cylindrical geometry for a screw-pinch (see appendix D).

The analysis presented in this and the following chapters is carried out in the straight field line coordinate system described in chapter 5. Salient equations and quantities, which will be extensively used in the rest of this report, are put in a box to facilitate their identi-

- ¹ MHD instabilities that are not modelled within the framework discussed in this report are those requiring a more advanced physics model (**Alfvén eigenmodes** are such of a kind for which kinetic extensions prove to be essential), or a more careful treatment of the plasma geometry (this is needed to describe shaping induced perturbations).
- ² Recall that in §5.1 we found that a small elongation is needed to satisfy the equilibrium at higher orders.

fication. In the remainder of the report it is always assumed that q takes positive values.

7.1 Convenient form of the linearised MHD equations

We shall first rearrange the linearised MHD equations in a form which is more convenient for simple analytic manipulations. As usual, the equilibrium is supposed to be **static**. For this purpose, the set of equations that we need are:

$$\rho\left(\frac{\partial \boldsymbol{u}}{\partial t} + \boldsymbol{u} \cdot \boldsymbol{\nabla} \boldsymbol{u}\right) = -\boldsymbol{\nabla} \boldsymbol{p} + \boldsymbol{J} \times \boldsymbol{B},\tag{7.1}$$

$$\frac{\partial \boldsymbol{B}}{\partial t} = \boldsymbol{\nabla} \times (\boldsymbol{u} \times \boldsymbol{B}), \tag{7.2}$$

$$\frac{\partial \boldsymbol{p}}{\partial t} + \boldsymbol{u} \cdot \boldsymbol{\nabla} \boldsymbol{p} + \Gamma \boldsymbol{p} \boldsymbol{\nabla} \cdot \boldsymbol{u} = 0, \tag{7.3}$$

$$\nabla \times \boldsymbol{B} = \mu_0 \boldsymbol{J},\tag{7.4}$$

$$\nabla \cdot \boldsymbol{B} = 0. \tag{7.5}$$

Allowing the perturbed quantities to have a $\exp(\gamma t)$ time dependence,³ the aim is to rearrange the equations above to obtain a single eigenvalue equation for the contravariant radial projection of the fluid displacement

$$\boldsymbol{\xi}^r = \boldsymbol{\xi} \cdot \boldsymbol{\nabla} r$$

with **eigenvalue** γ .

Let us write $\partial/\partial t \to \gamma$ and denote equilibrium quantities with the subscript 0. The dependence upon the perturbed current density can be eliminated by means of (7.4), that is

$$\mu_{0}\tilde{J}^{r} = \frac{1}{\sqrt{g}} \left(\frac{\partial \tilde{B}_{\phi}}{\partial \theta} - \frac{\partial \tilde{B}_{\theta}}{\partial \phi} \right),$$

$$\mu_{0}\tilde{J}^{\theta} = \frac{1}{\sqrt{g}} \left(\frac{\partial \tilde{B}_{r}}{\partial \phi} - \frac{\partial \tilde{B}_{\phi}}{\partial r} \right),$$

$$\mu_{0}\tilde{J}^{\phi} = \frac{1}{\sqrt{g}} \left(\frac{\partial \tilde{B}_{\theta}}{\partial r} - \frac{\partial \tilde{B}_{r}}{\partial \theta} \right).$$

$$(7.6)$$

We multiply by the Jacobian in order to eliminate the ϑ dependence in the parallel gradient.

Linearising (7.2) and dotting it by ∇r and $\nabla \phi$ yields respectively

$$\sqrt{g}\tilde{B}^r = \sqrt{g}\boldsymbol{B}_0 \cdot \boldsymbol{\nabla}\xi^r, \tag{7.7}$$

$$\sqrt{g}\tilde{B}^{\phi} = \sqrt{g}\boldsymbol{B}_{0} \cdot \nabla \xi^{\phi} - \sqrt{g}\nabla \cdot (\boldsymbol{\xi}\boldsymbol{B}_{0}^{\phi}). \tag{7.8}$$

From Eq. (7.3) and exploiting the fact that $p_0 = p_0(r)$ we get

$$\tilde{p} = -p_0' \xi^r + \Delta p \quad \text{with} \quad \Delta p = -\Gamma p_0 \nabla \cdot \xi. \tag{7.9}$$

³ This means that we are addressing stability via normal mode analysis.

Here Δp represents the **compressible contribution** to the perturbed pressure, or simply **compressibility**. We get an equation for Δp by dotting (7.1) with B and then perturbing it. Using (7.7), this gives

$$\rho_0 \gamma^2 \mathbf{B}_0 \cdot \boldsymbol{\xi} = -\widetilde{\mathbf{B}} \cdot \nabla \boldsymbol{p} = -\widetilde{\mathbf{B}}^r \boldsymbol{p}_0' + \mathbf{B}_0 \cdot \nabla \left(\boldsymbol{p}_0' \boldsymbol{\xi}^r - \Delta \boldsymbol{p} \right)$$
$$= -\mathbf{B}_0 \cdot \nabla \Delta \boldsymbol{p}. \tag{7.10}$$

Equations for \tilde{B}^{θ} and \tilde{B}^{ϕ} are obtained by means of (7.5) and projecting (7.1) along e_{θ} , so that one has

$$\frac{\partial \sqrt{g}\tilde{B}^{\vartheta}}{\partial \vartheta} = -\frac{\partial \sqrt{g}\tilde{B}^{r}}{\partial r} - \frac{\partial \sqrt{g}\tilde{B}^{\phi}}{\partial \phi}, \qquad (7.11)$$

$$\rho_{0}\gamma^{2}\xi_{\vartheta} = -\frac{\partial \tilde{p}}{\partial \vartheta} + \sqrt{g}J_{0}^{\phi}\tilde{B}^{r} - \sqrt{g}\tilde{J}^{r}B_{0}^{\phi}$$

$$= -\frac{\partial \tilde{p}}{\partial \vartheta} + J_{0}^{\phi}\left(\sqrt{g}\tilde{B}^{r}\right) - \frac{B_{0}^{\phi}}{\mu_{0}}\left(\frac{g_{\phi\phi}}{\sqrt{g}}\frac{\partial \sqrt{g}\tilde{B}^{\phi}}{\partial \vartheta} - \frac{\partial \tilde{B}_{\vartheta}}{\partial \phi}\right), \qquad (7.12)$$

where we recall that $B_0^r = 0$ and $g_{\phi\phi}/\sqrt{g}$ is independent of ϑ (cf. (5.5)). Finally, to close the system we first apply the operator $\nabla \phi \cdot \nabla \times \frac{1}{B_0^{\varphi}}$ to (7.1), and then linearise to obtain⁴

$$\frac{\gamma^{2}}{\sqrt{g}} \left[\frac{\partial}{\partial r} \left(\frac{\rho_{0}}{B_{0}^{\phi}} \xi_{\vartheta} \right) - \frac{\partial}{\partial \vartheta} \left(\frac{\rho_{0}}{B_{0}^{\phi}} \xi_{r} \right) \right] = \mathbf{B}_{0} \cdot \nabla \frac{\tilde{J}^{\phi}}{B_{0}^{\phi}} + \widetilde{\mathbf{B}} \cdot \nabla \frac{J_{0}^{\phi}}{B_{0}^{\phi}} - \mathbf{J}_{0} \cdot \nabla \frac{\tilde{B}^{\phi}}{B_{0}^{\phi}} - \nabla \phi \cdot \nabla \frac{1}{B_{0}^{\phi}} \times \nabla \tilde{p}, \tag{7.13}$$

having used the fact that $\nabla \cdot J_0 = 0$. This is known as the **vorticity** equation because of the analogy with its fluid-dynamical counterpart.

If a vacuum region is allowed, we must add Eq. (6.6) to the set of equations above and supply appropriate boundary conditions at the plasma-vacuum interface as discussed in the preceding chapter.

In summary, the equations that we need are formed by the system (7.6)-(7.13)⁵ which can be employed to address MHD stability both in cylindrical and toroidal configurations. In the next sections we will show how the desired equation for ξ^r with eigenvalue γ in toroidal geometry will be generated by combining Eqs. (7.6)-(7.12) with (7.13) whereas a brief account on the derivation of the eigenmode equation in a straight cylindrical screw-pinch is carried out in appendix D.

7.2 Orderings

For achieving the goal of obtaining a set of simplified equations, the first crucial step to take is to deploy an appropriate ordering of equilibrium and perturbed quantities. The aim of the next two subsections is thus to carefully detail such orderings.

 4 Rising or lowering indeces follow the rules given in chapter $_3$.

⁵ This set of equations forms the basis for the analysis of resistive instabilities as well, although some small but profound modifications will be required.

Recall that, for an axisymmetric system, the transformation rules from covariant to contravariant vector components are

$$A_r = g_{rr}A^r + g_{r\vartheta}A^{\vartheta},$$

$$A_{\vartheta} = g_{r\vartheta}A^r + g_{\vartheta\vartheta}A^{\vartheta},$$

$$A_{\phi} = g_{\phi\phi}A^{\phi}.$$

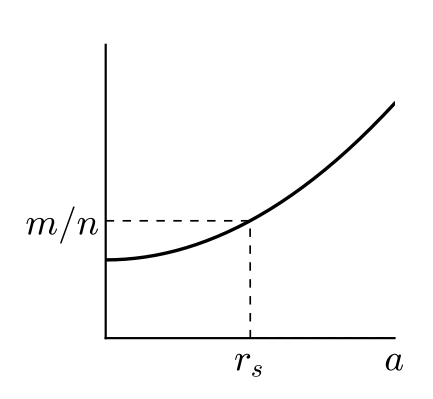


Figure 7.1: Example of q profile with a m/n resonance.

7.2.1 Equilibrium

The equilibrium analysis has already been discussed in chapter 4, hence we just summarise the most important results.

From (5.3), the contravariant toroidal component of the equilibrium magnetic field is written as⁶

$$B_0^{\phi} = \frac{f_0'}{\sqrt{g}}, \text{ with } f_0' = rB_0[1 + o(\varepsilon^2)],$$
 (7.14)

having made use of (4.25), with B_0 denoting the on axis equilibrium magnetic field. Furthermore, the following relation holds

$$\langle \frac{1}{B_0^{\phi}} \rangle' = \frac{\langle R^2 \rangle'}{F} - \frac{\langle R^2 \rangle F'}{F^2},\tag{7.15}$$

where we recall that angular brackets denote **poloidal average** as defined by (5.18).

The ε -ordering of the metric tensor coefficients is

$$g_{rr} \sim 1$$
, $g_{r\theta} \sim \varepsilon a$, $g_{\vartheta\vartheta} \sim a^2$, $\sqrt{g} \sim \frac{a^2}{\varepsilon}$, $g_{\phi\phi} \sim \frac{a^2}{\varepsilon^2}$,

with $g_{r\phi}=g_{\theta\phi}=0.7$ Other equilibrium quantities, such as pressure, follow the usual ordering introduced in section 4.3.1, and are assumed to fulfil the condition $r\mathfrak{f}_0'\sim\mathfrak{f}_0$ with \mathfrak{f}_0 denoting a generic equilibrium quantity.

The particular case for which $\mu_0 p_0/B_0^2 \sim \varepsilon^2$ and $\mu_0 r p_0'/B_0^2 \sim \varepsilon$ will be addressed separately in chapter 12 when the stability of ballooning modes will be investigated.

7.2.2 Perturbations

As mentioned earlier, for the sake of convenience in this report it is assumed that q > 0. Let us denote with r_s the radius at which q = m/n (cf. Fig. 7.1), that is the resonance, with both m and n positive integers different from zero. We take $q \sim 1$, a condition which is usually fulfilled in tokamaks, so that $m \sim n$. Moreover, the plasma cross section is assumed to be nearly circular in line with the analysis of chapters 4 and 5.

In a region sufficiently far from r_s we assume that for any perturbed quantity \tilde{f} one has

$$r\frac{\partial \tilde{f}}{\partial r} \sim m\tilde{f}.$$
 (7.16)

Letting Δr be the mode radial extension, the relation above states that $\Delta r \sim r/m$. Hence, if $m \sim 1$ the perturbation does not have strong gradients and extends over a broad region. This is what characterises **global modes**. On the contrary, **localised modes** (or **small-scale modes**) have $m \gg 1$ with Δr small enough so that $r\tilde{f}'/\tilde{f} \gg 1$.

⁸ All MHD instabilities, including the resistive ones, in tokamaks can be grouped into two families: **global** modes and **localised** modes.

Now, the crucial step for understanding tokamak instabilities is to realise that, as discussed in the preceding chapter, the spectrum of the perturbation is not necessarily monochromatic, but it may contain several harmonics whose **coupling** is induced by toroidicity. We first point out that since the equilibrium is toroidally symmetric, harmonics with different n numbers do not interact linearly, whereas coupling involves poloidal harmonics with different m's. We say that n is a **good quantum number**, and thus we focus on a single n at a time.

Let's imagine for the moment that experimental evidence shows some MHD activity in the form of a global helical fluid perturbation with dominant poloidal and toroidal mode numbers m and n, both of the order of unity (see e.g. figure 7.2). For a given n, we may Fourier expand the perturbed fluid displacement ξ as

$$\xi^{j} = \xi_{m}^{j} e^{i(m\vartheta - n\phi)} + \xi_{m+1}^{j} e^{i[(m+1)\vartheta - n\phi]} + \xi_{m-1}^{j} e^{i[(m-1)\vartheta - n\phi]} + \dots, \quad (7.17)$$

with the index j running over (r, ϑ, ϕ) . Since n is fixed, we omit to write the subscript n in the Fourier components. We recall that the set consisting of all the harmonics with different poloidal mode numbers is called the **poloidal spectrum**.

When the spectrum of the perturbation is dominated by the harmonic of helicity (m, n), we order

$$\xi_{m+1}^{j} \sim \xi_{m-1}^{j} \sim \varepsilon \xi_{m}^{j}. \tag{7.18}$$

We further assume that the contravariant projections of ξ for a given poloidal number are comparable in magnitude, that is

$$\frac{1}{a}\xi_{\ell}^{r} \sim \xi_{\ell}^{\vartheta} \sim \xi_{\ell}^{\phi},\tag{7.19}$$

where $\ell=m-1,m,m+1$. Harmonics with poloidal mode numbers $m\pm 1,\pm 2,\ldots$ are called **sidebands** or **satellite harmonics** whereas we refer to the one with mode number m as the **main (or dominant) mode**. We anticipate that mode coupling for global modes in a tokamak with circular cross section typically involves first neighbouring sidebands only.

We now discuss the ordering of the magnetic field. As long as $\ell - nq$ remains of the order of unity, ¹⁰ from (7.7) one has

$$rB_0\xi_\ell^r \sim (\sqrt{g}\tilde{B}^r)_\ell. \tag{7.20}$$

Therefore, the perturbed magnetic field can be expanded and ordered in a way similar to that of Eqs. (7.17)-(7.19), which is

$$(\sqrt{g}\tilde{B}^{j})_{m+1} \sim (\sqrt{g}\tilde{B}^{j})_{m-1} \sim \varepsilon(\sqrt{g}\tilde{B}^{j})_{m},$$

$$\frac{1}{\sigma}(\sqrt{g}\tilde{B}^{r})_{\ell} \sim (\sqrt{g}\tilde{B}^{\vartheta})_{\ell} \sim (\sqrt{g}\tilde{B}^{\phi})_{\ell}.$$
(7.21)

Any other perturbed quantity appearing in equations (7.6)-(7.13) can be written in terms of ξ or \widetilde{B} , so that similar arguments apply.

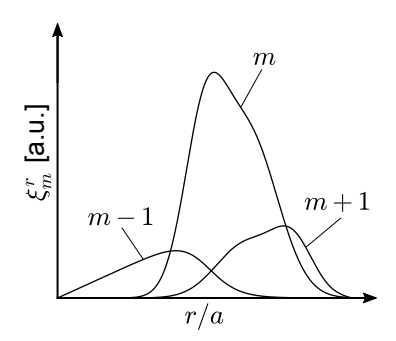


Figure 7.2: Example of the spectral structure vs normalised minor radius of a perturbation dominated by the harmonic with poloidal mode number m.

⁹ Plasma shaping induces couplings with higher order harmonics. For example elongation couples m and $m \pm 2$ modes.

¹⁰ This means far from the resonance $q = \ell/n$.

In the following sections we show how these orderings, which have been kept fairly general for the moment, can be further refined. ¹¹ In a tokamak, ω_A is typically of the order of MHz. The order of magnitude of the growth of MHD modes ranges from few milliseconds ($\lesssim 10^{-2}\omega_A$) to few microseconds ($\sim \omega_A$).

To transform back to SI units one has to replace $p \to \mu_0 p$. The same applies with ρ .

Having examined the orderings of the fluid and magnetic perturbations, we shall discuss the magnitude of the growth rates. Upon defining the Alfvén frequency ω_A and the Alfvén speed c_A as¹¹

$$\omega_A = \frac{B_0}{R_0 \sqrt{\mu_0 \rho_0}}, \quad c_A = R_0 \omega_A, \tag{7.22}$$

we distinguish between **fast-growing modes** that have characteristic growth rates comparable with ω_A and **slow-growing modes** which grow on slower time-scales. For fast-growing modes we may let

$$\frac{\gamma}{\omega_A} \sim 1,$$
 (7.23)

whereas the appropriate ordering for slow-growing instabilities is

$$\frac{\gamma}{\omega_A} \sim \varepsilon.$$
 (7.24)

Typically, $\gamma/\omega_A \ll \varepsilon$ which implies that we should take $\gamma/\omega_A \sim \delta$ with $\delta \ll \varepsilon$ some small parameter. Nevertheless, the ordering above works quite well without complicating the algebra, and therefore we stick to it.

We point out that the preceding remarks apply to **global modes**, i.e. instabilities with m and n of the order of unity, and far from resonances. Few modifications of the orderings given above are required when dealing with small scale modes, or when a resonant surface is approached. These are thoroughly detailed in section 7.3.2 in and §7.4.

Hence, we have now all the logical elements to derive the required stability equations for both global and localised perturbations in tokamaks. For the sake of simplicity, hereafter and in the remainder of the report we normalise $\mu_0 = 1$.

The structure of the eigenmode equations

The equilibrium of a large aspect ratio tokamak is determined by the moments of (4.20). The leading order solution has the form of a cylinder force balance equation (cf. (4.30)) and effects related to toroidicity, such as the Shafranov shift, appear to the next order.

Similarly, one can imagine that the eigenvalue equation of the fluid displacement is of the form (6.21) and its "moments", namely the Fourier projections, yield the following system of equations (see (6.22))

$$\begin{split} \gamma^2 \rho_0 \xi_m &= \mathcal{F}_0 \xi_m + \sum_{m' \neq 0} \mathcal{F}_{m'} \xi_{m-m'}, \\ \gamma^2 \rho_0 \xi_{m\pm 1} &= \mathcal{F}_0 \xi_{m\pm 1} + \sum_{m' \neq 0} \mathcal{F}_{m'} \xi_{m\pm 1-m'}, \\ &\vdots \end{split}$$

where \mathscr{F} is a differential operator which depends on r and ϑ . Here \mathscr{F}_0

represents its cylindrical part, i.e. roughly speaking the one which does not vanish when $\varepsilon \to 0$, while the "coefficients" $\mathscr{F}_{m'}$ with $m' \neq 0$ are toroidal corrections. One sees that if $\mathscr{F}_{m'}$ $(m' \neq 0)$ are not vanishing, the spectrum of the perturbation must be composed of several poloidal harmonics, i.e. **mode coupling** occurs. In a low- β tokamak with nearly circular cross section the following is expected to hold

$$\mathscr{F}_0 \sim \frac{1}{\varepsilon} \mathscr{F}_{m\pm 1} \sim \frac{1}{\varepsilon^2} \mathscr{F}_{m\pm 2} \sim \dots$$

Hence, given the decomposition of the fluid perturbation as in (7.17), stability is typically determined at leading order by the first two equations of the system above.

Auxiliary quantities: Global modes 7.3

To derive the eigenmode equations we require a more precise characterisation of the expressions for the perturbed fluid displacement, pressure and toroidal field. More specifically, here we want to determine ξ_m^{θ} , ξ_m^{ϕ} $\sqrt{g}\tilde{B}_{m}^{\phi}$, Δp_{m} and $\Delta p_{m\pm 1}$. This is the aim of this section. We focus on global modes first, assuming that the spectrum is dominated by a main harmonic of helicity (m, n) accompanied by ε times smaller sidebands with mode numbers $(m \pm 1, n)$, i.e. Eq. (7.18) holds. We point out that in a nearly circular tokamak only the first neighbouring sidebands contribute.

The analysis is carried out in two regions: one far from a resonant point r_s for which m - nq = 0, and one close to r_s if such a resonance occurs in the plasma. It will be shown that, with some appropriate approximations, the latter can be viewed as a limiting case of the former. The generalisation to localised instabilities is addressed in §7.4

Behaviour far from resonance 7.3.1

We select the poloidal and toroidal mode numbers m and n respectively, and assume to carry out the analysis sufficiently far from any resonance q = m/n, if this occurs within the plasma. We shall focus on cases with either $m-nq\sim 1$ or $m-nq\sim \varepsilon$. The latter is typical of plasmas with a safety factor flat and close to the value m/n over a broad region while the exact resonance is still avoided. The growth rate can conform to the ordering of either fast-growing or slow-growing modes. A summary of the orderings of m - nq and γ employed in this section is shown in table 7.1.

Let us start by Fourier analysing (7.11) which gives

$$(\sqrt{g}\tilde{B}^{\theta})_{\ell} = -\frac{1}{i\ell}(\sqrt{g}\tilde{B}^{r})_{\ell}' + \frac{n}{\ell}(\sqrt{g}\tilde{B}^{\phi})_{\ell}, \tag{7.25}$$

m-nq	γ/ω_A
1	ε
ε	$\boldsymbol{arepsilon}$
1	1

Table 7.1: Global modes orderings for m - nq and γ/ω_A .

¹² Hereafter we take $r \sim a$.

where the prime indicates, as usual, differentiation with respect to the radial variable and the subscript ℓ denotes a generic Fourier harmonic. According to (7.17), if m is the mode number of the dominant harmonic, from (7.9) it is immediate to recognise that $\tilde{p}_{m\pm 1} \sim \varepsilon \tilde{p}_m$, and by means of (7.19) it can be shown that $\Delta p \sim \varepsilon^2 B_0^2 \xi_m^r / a$ at most. Plugging this result, in conjunction with equation (7.25), into (7.12) shows that

$$\sqrt{g}\tilde{B}^{\phi} \sim \varepsilon^2 B_0 \xi_m^r. \tag{7.26}$$

Therefore, it follows from (7.8) and the fluid expansion (7.17) that to leading order we have

$$\frac{1}{r} (r\xi_{m}^{r})' + im\xi_{m}^{\vartheta} - i\frac{m}{q}\xi_{m}^{\varphi} = 0,
\frac{1}{r} (r\xi_{m\pm 1}^{r})' + i(m\pm 1)\xi_{m\pm 1}^{\vartheta} - i\frac{m\pm 1}{q}\xi_{m\pm 1}^{\varphi} = 0,$$
(7.27)

where we implicitly used (7.16). Exploiting (7.27) we can write

$$(\nabla \cdot \boldsymbol{\xi})_{m} \approx \frac{1}{r} \left(r \boldsymbol{\xi}_{m}^{r} \right)' + i m \boldsymbol{\xi}_{m}^{\theta} - i n \boldsymbol{\xi}_{m}^{\phi} = i \left(\frac{m}{q} - n \right) \boldsymbol{\xi}_{m}^{\phi},$$

$$(\nabla \cdot \boldsymbol{\xi})_{m \pm 1} = i \left[\frac{1}{q} (m \pm 1) - n \right] \boldsymbol{\xi}_{m \pm 1}^{\phi}$$

$$\mp \frac{1}{m R_{0}} \left[r \frac{d \boldsymbol{\xi}_{m}^{r}}{d r} + (1 \mp m) \boldsymbol{\xi}_{m}^{r} - i r \frac{m}{q} \boldsymbol{\xi}_{m}^{\phi} \right],$$

$$(7.28)$$

having dropped higher order coupling terms which are ε^2 times smaller compared to the leading ones.

Upon an inspection of (7.10), we see that the dominant contribution to the compressible part of the perturbed pressure is

$$(m - nq)\Delta p_m = i \frac{B_0^2}{R_0^2} \frac{\gamma^2}{\omega_A^2} (\xi_\theta + q\xi_\phi)_m.$$
 (7.29)

Thus, expressing Δp in terms of the divergence of ξ through (7.9) and (7.28) with $q \sim 1$, we can write

$$\left[\frac{\Gamma p_0}{B_0^2}(m-nq)^2 + \frac{q^2\gamma^2}{\omega_A^2}\right]\xi_m^{\phi} \sim \varepsilon^2 \frac{\gamma^2}{\omega_A^2} \frac{\xi_m^r}{a},$$

where we used the ordering (7.19) for estimating $(\xi_{\vartheta})_m \sim a\xi_m^r$. Contributions due to couplings with sidebands have been dropped as they enter at higher order.¹³ This shows that

$$\xi_m^{\phi} \sim \varepsilon^2 \xi_m^r / a \tag{7.30}$$

at most, either for fast or slow-growing modes. Notice that the smallness of ξ_m^{ϕ} holds true even when $m - nq \sim \varepsilon$, and by comparing with (7.28) this indicates that the flow associated with the dominant mode can be regarded as nearly incompressible. Therefore, from the first expression of (7.27), we can safely set (for many computations we can use $\xi_m^{\phi} = 0$)

¹³ We anticipate that this argument remains valid even for the case of harmonics of equivalent magnitude as described in §7.4.

$$\xi_m^{\vartheta} = -\frac{1}{imr} \left(r \xi_m^r \right)'. \tag{7.31}$$

To obtain Δp_m we plug (7.30) into (7.28) and then multiply by Γp_0 . This shows at once that $r\Delta p_m/B_0^2 \sim \varepsilon^4 \xi_m^r$ at most. Thus, we infer that Δp_m is not an important quantity, so that we may set

$$\Delta p_m = 0. \tag{7.32}$$

Now, analysing the compressibility contribution due to the sidebands, from (7.10) and using (7.30) we obtain

$$\left[\frac{1}{q}(m\pm 1)-n\right]\Delta p_{m\pm 1}\approx iB_0^2\frac{\gamma^2}{\omega_A^2}\xi_{m\pm 1}^{\phi},$$

having assumed that the orderings represented by Eq. (7.19) hold. Under the assumption that $\frac{1}{q}(m \pm 1) - n \sim 1$, we use (7.9) and (7.28) once more, so that the equation above gives

$$\left(\left[\frac{1}{q} (m \pm 1) - n \right]^2 + R_0^2 \frac{\gamma^2}{c_s^2} \right) \Delta p_{m \pm 1} = \pm \frac{B_0^2}{m R_0} \frac{\gamma^2}{\omega_A^2} \left[r \frac{d\xi_m^r}{dr} + (1 \mp m) \xi_m^r \right]$$
(7.33)

where $c_s = \sqrt{\Gamma p_0/\rho_0}$ is the sound speed.¹⁴ It is straightforward to see that $R_0^2 \gamma^2/c_s^2 \sim (\gamma/\omega_A)^2/\beta$.

Although the ordering (7.24) would imply $(\gamma/\omega_A)^2 \sim \beta$, in tokamaks slow growing perturbations usually have $(\gamma/\omega_A)^2/\beta \ll 1$. Consequently, the term proportional to the inverse of the sound speed in the equation above is typically small, and it can be neglected. Notice that this holds even more close to the **marginal stability boundary** for which $\gamma \to 0$. For fast growing modes, which are instead characterised by (7.23), we find that the second term on the left-hand-side of (7.33) scales as $1/\beta$, thence dominating over the first one. Therefore, two limiting expressions of the sideband contributions to Δp are found:

$$\Delta p_{m\pm 1} \approx \begin{cases} \pm \frac{B_0^2}{mR_0} \frac{\gamma^2}{\omega_A^2} \frac{r \frac{d\xi_m^r}{dr} + (1 \mp m)\xi_m^r}{[(m \pm 1)\mu - n]^2}, & \text{slow-growing modes,} \\ \pm \Gamma \beta \frac{B_0^2}{mR_0} \left(r \frac{d\xi_m^r}{dr} + (1 \mp m)\xi_m^r \right), & \text{fast-growing modes.} \end{cases}$$
(7.34)

This shows that $\Delta p_{m\pm 1} \sim \epsilon^3 B_0^2 \xi_m^r/a$ for both fast-growing and slow-growing modes.

We finally need to obtain an expression for $(\sqrt{g}\tilde{B}^{\phi})_m$. Let us analyse slow-growing instabilities first. In such a case plugging (7.9) and (7.25) into (7.12) produces **to leading order in** ε^{15}

¹⁴ Generally $c_s/R_0 < \omega_A$. For a Deuterium plasma with T = 5keV, $n = 10^{20}m^{-3}$, $B_0 = 3T$ and $R_0 = 3m$ one has $\omega_A \approx 1.6 \times 10^6 Hz$ and $c_s/R_0 \approx 3 \times 10^5 Hz$.

¹⁵ To speed up the algebraic manipulations, a useful and intuitive trick consists in taking $r \sim B_0 \sim 1$ and $1/R_0 \sim \varepsilon$.

$$(\sqrt{g}\tilde{B}^{\phi})_{m} = \frac{\sqrt{g}}{R^{2}} \left[\frac{R_{0}}{B_{0}} p_{0}' \xi_{m}^{r} + \langle \frac{J_{0}^{\phi}}{B_{0}^{\phi}} \rangle \frac{(\sqrt{g}\tilde{B}^{r})_{m}}{im} + \frac{n}{m} \langle \frac{g_{\vartheta\vartheta}}{\sqrt{g}} \rangle \frac{(\sqrt{g}\tilde{B}^{r})_{m}'}{im} \right], \quad (7.35)$$

where (7.14) has been used and contributions due to compressibility have been dropped owing to the results above. It is evident that $(\sqrt{g}\tilde{B}^{\phi})_m/B_0$ is ε^2 times smaller than ξ_m^r . We also see that the equation above only depends on ξ_m^r and $(\sqrt{g}\tilde{B}^r)_m$ so that using it in (7.25) allows to express $(\sqrt{g}\tilde{B}^{\vartheta})_m$ as function of ξ_m^r and $(\sqrt{g}\tilde{B}^r)_m$.

For fast-growing instabilities, equation (7.26) will turn out to be accurate enough for the estimation of the perturbation of the toroidal field, whose exact expression is not explicitly required. Therefore, without any harm, we shall formally use (7.35) for fast-growing instabilities as well.

7.3.2 Layer ordering

We are now concerned with the behaviour of a **global instability in** a **neighbourhood of the resonance** r_s for which m - nq = 0. For a fixed toroidal mode number n of the order of unity, suppose that the poloidal spectrum of the perturbation is composed of a dominant mode m accompanied by its sideband harmonics with mode numbers $m \pm 1$. In the derivation presented earlier Eq. (7.16) was assumed to hold. When r_s is approached, however, the perturbation usually develops **strong radial gradients**¹⁶. We only focus on **slow-growing** modes and deploy the following estimates

$$r\frac{d\tilde{f}}{dr} \sim \frac{\tilde{f}}{\varepsilon}, \quad m/q - n \approx -ns\frac{(r - r_s)}{r_s} \sim \varepsilon, \quad \frac{\gamma}{\omega_A} \sim \varepsilon,$$
 (7.36)

where \tilde{f} is a generic perturbed quantity and $s \sim 1$ is the equilibrium magnetic shear at r_s . We refer to (7.36) as the **layer ordering**, and the region near the resonance is called **inertial layer**. The derivation that follows is in many ways similar to the one of the preceding section.

We assume that (7.18) still holds, so that $\tilde{p}_{m\pm 1} \sim \varepsilon \tilde{p}_m$. Now, equation (7.25) is always valid, hence by means of (7.7) and thanks to the layer ordering one has

$$(\sqrt{g}\tilde{B}^{\vartheta})_{m} \sim (\sqrt{g}\tilde{B}^{\phi})_{m} \sim \frac{1}{r\varepsilon}(\sqrt{g}\tilde{B}^{r})_{m} \sim B_{0}\xi_{m}^{r},$$

$$(\sqrt{g}\tilde{B}^{\vartheta})_{m\pm 1} \sim (\sqrt{g}\tilde{B}^{\phi})_{m\pm 1} \sim \frac{1}{r\varepsilon}(\sqrt{g}\tilde{B}^{r})_{m\pm 1} \sim B_{0}\xi_{m}^{r}.$$

$$(7.37)$$

while instead of (7.19) we formally let

$$\xi_{m\pm 1}^{i} \sim \varepsilon \xi_{m}^{i} \quad (i = r, \vartheta, \phi),$$

$$\xi_{m}^{\vartheta} \sim \xi_{m}^{\phi} \sim \frac{1}{r\varepsilon} \xi_{m}^{r}, \quad \xi_{m\pm 1}^{\vartheta} \sim \xi_{m\pm 1}^{\phi} \sim \frac{1}{r} \xi_{m}^{r}.$$

$$(7.38)$$

Let us start by noticing that from the definition of Δp given in (7.9) we have $\Delta p_m \sim \varepsilon B_0^2 \xi_m^r/a$ at most, ¹⁷ and using it in (7.12) shows that

¹⁶ This will be explicitly shown in the following chapters.

¹⁷ This because we take $(\nabla \cdot \boldsymbol{\xi})_m \sim \boldsymbol{\xi}_m^r / \varepsilon$.

 $\sqrt{g}\tilde{B}^{\phi} \sim \varepsilon B_0 \xi_m^r$ at most.

We now rearrange equation (7.8) in a more convenient form to obtain

$$\sqrt{g}\tilde{B}^{\phi} = -f_0' \left[\frac{1}{f_0'} \frac{\partial (f_0' \xi^r)}{\partial r} + \frac{\partial \xi^{\theta}}{\partial \theta} - \frac{1}{q} \frac{\partial \xi^{\phi}}{\partial \theta} \right]. \tag{7.39}$$

This is employed for expressing the ℓ th Fourier projection of the divergence of the fluid displacement as 18

¹⁸ Remember that (7.14) holds.

$$(\nabla \cdot \boldsymbol{\xi})_{\ell} = \frac{d\xi_{\ell}^{r}}{dr} + \langle \frac{\partial \sqrt{g}/\partial r}{\sqrt{g}} \rangle \xi_{\ell}^{r} + i\ell \xi_{\ell}^{\vartheta} - in \xi_{\ell}^{\varphi}$$

$$+ \sum_{\ell' \neq 0} \left[\left(\frac{\partial \sqrt{g}/\partial r}{\sqrt{g}} \right)_{\ell'} \xi_{\ell-\ell'}^{r} + \left(\frac{\partial \sqrt{g}/\partial \vartheta}{\sqrt{g}} \right)_{\ell'} \xi_{\ell-\ell'}^{\vartheta} \right]$$

$$= -\frac{(\sqrt{g}\tilde{B}^{\varphi})_{\ell}}{f_{0}'} + \left(\langle \frac{(\sqrt{g})'}{\sqrt{g}} \rangle - \frac{f_{0}''}{f_{0}'} \right) \xi_{\ell}^{r} + i(\ell\mu - n) \xi_{\ell}^{\varphi}$$

$$+ \sum_{\ell' \neq 0} \left[\left(\frac{\partial \sqrt{g}/\partial r}{\sqrt{g}} \right)_{\ell'} \xi_{\ell-\ell'}^{r} + \left(\frac{\partial \sqrt{g}/\partial \vartheta}{\sqrt{g}} \right)_{\ell'} \xi_{\ell-\ell'}^{\vartheta} \right], \tag{7.40}$$

where we recall that angular brackets indicate the poloidal average.

Imposing that the perturbation of the toroidal magnetic field scales according to the estimate given above, Eq. (7.40) implies that $(\nabla \cdot \xi)_m \sim \xi_m^r$ which then yields $\sqrt{g}\tilde{B}^\phi \sim \varepsilon^2 B_0 \xi_m^r$ (cf. (7.26)). By virtue of the afore-mentioned orderings, using this result in conjunction with (7.39) shows that (7.27) holds. It will be clear later, that the contributions due to $\sqrt{g}\tilde{B}^\phi$ can be dropped near r_s , so that the exact expression of the perturbation of the toroidal field is not required. Hence, without loss of generality, we can use (7.35) both far-from and close-to the resonance.

Therefore, one can approximate (cf. (7.28))

$$(\nabla \cdot \boldsymbol{\xi})_{m} = i \left(\frac{m}{q} - n \right) \boldsymbol{\xi}_{m}^{\phi} + o(\varepsilon \boldsymbol{\xi}_{m}^{r} / r),$$

$$(\nabla \cdot \boldsymbol{\xi})_{m \pm 1} \approx i \left[\frac{1}{q} (m \pm 1) - n \right] \boldsymbol{\xi}_{m \pm 1}^{\phi} \mp \frac{r}{m R_{0}} \left(\frac{d \boldsymbol{\xi}_{m}^{r}}{d r} - i \frac{m}{q} \boldsymbol{\xi}_{m}^{\phi} \right).$$

$$(7.41)$$

We may now write the full expression of (7.29), which remains valid within these orderings as well, yielding

$$\begin{split} & \left[\frac{\Gamma p_0}{B_0^2} (m\mu - n)^2 + \frac{\langle R^2 \rangle}{R_0^2} \frac{\gamma^2}{\omega_A^2} \right] \xi_m^{\phi} = i \frac{\Gamma p_0}{B_0^2} (m\mu - n) \times o(\varepsilon \xi_m^r / r) \\ & - \mu \frac{\gamma^2}{\omega_A^2} \left[\frac{\langle g_{\vartheta\vartheta} \rangle}{R_0^2} \xi_m^{\vartheta} + \sum_{m' \neq 0} \left(\frac{(g_{r\vartheta})_{m'}}{R_0^2} \xi_{m-m'}^r + \frac{(g_{\vartheta\vartheta})_{m'}}{R_0^2} \xi_{m-m'}^{\vartheta} + \frac{(R^2)_{m'}}{R_0^2} \xi_{m-m'}^{\phi} \right) \right]. \end{split}$$

It is implicit that equilibrium quantities must be computed at the resonance. It follows that ξ_m^{ϕ} is not larger than $\varepsilon \xi_m^r/a$ (for both fast and slow-growing instabilities), so that equation (7.31) remains valid. By repeating the same operations which have been employed earlier, one then finds that $\Delta p_m \sim \varepsilon^3 B_0^2 \xi_m^r/a$ at most so that we are allowed to use (7.32).

Recall that c_s is the sound speed which is defined below (7.33).

¹⁹ Contrary to global modes, we do not consider fast-growing localised instabili-

This is similar to the ordering given by the second equation of (7.21).

Finally, for the compressibility arising from the neighbouring sidebands we follow the analysis performed in the preceding section giving

$$\left(\frac{1}{q^2} + R_0^2 \frac{\gamma^2}{c_s^2}\right) \Delta p_{m\pm 1} = \pm \frac{B_0^2 r_s}{m R_0} \frac{\gamma^2}{\omega_A^2} \frac{d\xi_m^r}{dr}.$$
 (7.43)

This is equivalent to (7.33) where on the right-hand-side only terms containing the radial derivative of ξ_m^r have been kept.

In summary, within the layer ordering we can still use (7.30)-(7.32), (7.34) and (7.35) with the replacement $r\frac{d}{dr} \to \frac{r_s}{\varepsilon} \frac{d}{dr}$.

7.4 Auxiliary quantities: Localised modes

A slight modification of the derivation presented in §7.3 is required when **localised modes**, i.e. small-scale perturbations with by $m \sim n \gg 1$, are considered. This is detailed below, where we appropriately carry out the analysis far-from and close-to the resonant points.

7.4.1 Small scale modes far from resonances

As usual, let us fix n and assume that (7.16) holds. Small-scale modes can be viewed as perturbations which are highly localised about their associated resonance. Thus, we may approximate (cf. (7.36))

$$m/q-n\approx -ns\frac{(r-r_m)}{r_m},$$

where r_m denotes the position of the resonance m - nq = 0 and s is the magnetic shear at r_m which is taken to be of the order of unity. Letting $m \sim 1/\varepsilon$ (and also $n \sim 1/\varepsilon$), in the region sufficiently far from the resonance we suppose that $m - nq \sim 1$. The growth rate is assumed to conform to the one of **slow-growing** perturbations and thus is ordered as (cf. (7.24))¹⁹

$$\frac{\gamma}{\omega_A} \sim \varepsilon.$$
 (7.44)

It is now important to understand that the poloidal spectrum of localised perturbations may exhibit a main harmonic, (like **Mercier modes** discussed in chapter 11) or it can be a superposition of multiple modes coupled one to another (as for **Ballooning modes** discussed in chapter 12).

In the former case, (7.18) holds with the spectrum being dominated by the harmonic with poloidal mode number, say, $m \sim n$. From (7.7) and using (7.11), we see that in this region (cf. (7.20))²⁰

$$B_0 \xi_m^r \sim (\sqrt{g} \tilde{B}^r)_m / a \sim (\sqrt{g} \tilde{B}^{\vartheta})_m \sim (\sqrt{g} \tilde{B}^{\phi})_m \tag{7.45}$$

at most. Owing to this scaling we balance each term appearing in Eq. (7.39) by ordering $\xi_m^{\vartheta} \sim \xi_m^{\phi} \sim \xi_m^r/a$. In particular, by comparing with (7.40) as we did in the previous section, to leading order we write (∇ ·

 $(\xi)_m \sim \xi_m^r/a$ (cf. (7.41)) which then gives $\tilde{p}_m \sim \varepsilon^2 B_0^2 \xi_m^r$ and $\tilde{p}_\ell \sim \varepsilon \tilde{p}_m$ for $\ell \neq m$.

Considering now the case when the poloidal spectrum is composed of several modes, since m is large, we may expect that each of these harmonics becomes essentially indistinguishable from one to another (see figure 7.3). We shall therefore replace (7.18) and the first of (7.21) with

$$\xi_{m+1}^{i} \sim \xi_{m-1}^{i} \sim \xi_{m}^{i}, (\sqrt{g}\tilde{B}^{i})_{m+1} \sim (\sqrt{g}\tilde{B}^{i})_{m-1} \sim (\sqrt{g}\tilde{B}^{i})_{m},$$
 (7.46)

having implicitly assumed that we are dealing with modes which have resonances within the plasma. Thus, if (7.46) holds, far from the resonances of the $m, m \pm 1, m \pm 2, \ldots$ modes, we expect to have $\tilde{p}_{\ell} \sim \tilde{p}_{m}$ and

$$B_0 \xi_m^r \sim (\sqrt{g} \tilde{B}^r)_\ell / a \sim (\sqrt{g} \tilde{B}^{\vartheta})_\ell \sim (\sqrt{g} \tilde{B}^{\phi})_\ell, \tag{7.47}$$

where ℓ denotes a generic harmonic. By means of (7.39) and (7.40), an argument similar to the one discussed earlier shows that in this case $(\nabla \cdot \xi)_m \sim \xi_m^r/a$.

One therefore infers that, for localised instabilities featuring either a single main helicity or a multiple equivalent helicities spectrum, the compressible part of the perturbed pressure scales as $\Delta p \sim \varepsilon^2 B_0^2 \xi_m^r/a$ at most.

Plugging these results into (7.12) easily shows that (7.26) and (7.27) remain valid. Note that the two equations of (7.27) appear at the same order if (7.46) applies. It follows that (7.28) holds. Hence, using (7.29) we find $\xi_m^{\phi} \sim \varepsilon^2 \xi_m^r/a$ which is (7.30). As before, this shows that

$$\Delta p_m \sim \varepsilon^4 B_0^2 \xi_m^r / a, \tag{7.48}$$

meaning that in this region the contribution due to compressibility is negligible.

Finally, working out the coupling contributions in (7.12) gives

$$(\sqrt{g}\tilde{B}^{\phi})_{m} = \frac{\sqrt{g}}{R^{2}} \left[\frac{R_{0}}{B_{0}} p_{0}' \xi_{m}^{r} + \frac{n}{m} \langle \frac{g_{\vartheta\vartheta}}{\sqrt{g}} \rangle \frac{(\sqrt{g}\tilde{B}^{r})_{m}'}{im} \right], \tag{7.49}$$

which is (7.35) in the limit of large m. No other Fourier harmonics of ξ^{ϕ} or $\sqrt{g}\tilde{B}^{\phi}$ are needed.

In conclusion, the equations required for the analysis of instabilities with large poloidal mode numbers far from their associated resonances can be simply obtained by taking the $m\gg 1$ limit of those for global modes derived in the previous sections.

7.4.2 The inertial layer of small scale modes

We now investigate the dynamics of localised modes in a neighbourhood of the resonance r_m where $m-nq(r_m)=0$. From (7.16), the mth harmonic is expected to be localised about r_m with a radial extension $\Delta r \sim r/m$. If

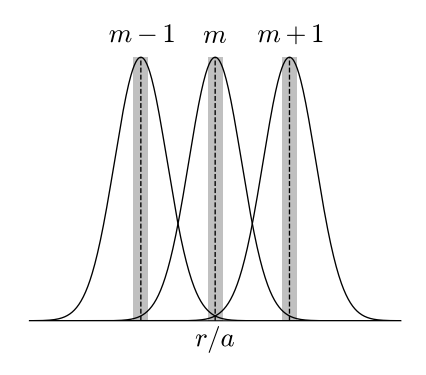


Figure 7.3: Poloidal structure of a perturbation with $m \gg 1$ featuring multiple harmonics. The near resonance region associated with each harmonic is highlighted in grey.

²¹ If the magnetic shear is small, this argument is expected to hold even more due to the increased separation between resonances.

Far from the resonance one has $z \sim 1$.

m is sufficiently large the separation between neighbouring resonances is of the order of 1/ms, that is $(r_{m\pm 1}-r_m)/r_m\sim 1/m$ with $s\sim 1$ (s is the magnetic shear at r_m). Therefore, around r_m we conveniently take each projection (radial, poloidal or toroidal) of the fluid displacement of the sidebands to be ε times smaller compared to the respective one of the dominant mode m as in (7.18). We thus order the magnetic field and the fluid displacement according to (7.37) and (7.38) respectively.

Now we introduce the variable $z = m(r - r_m)/r_m$. In the region close to r_m we let $z \sim \varepsilon$ and deploy a **layer ordering** analogous to (7.36)

$$\frac{d\tilde{f}}{dz} \sim \frac{\tilde{f}}{\varepsilon},\tag{7.50}$$

and let the magnitude of the growth rate to be given by (7.44). Note that this implies $m\mu - n \sim \varepsilon$. According to the orderings above, a quick investigation of (7.40) gives $(\nabla \cdot \xi)_m \sim \xi_m^r/a$ so that $\Delta p_m \sim \varepsilon^2 B_0^2 \xi_m^r/a$. The *m*th Fourier component of equation (7.12) then gives

$$\frac{B_0^2}{R_0^2} \frac{\gamma^2}{\omega_A^2} \xi_{\vartheta} = -\frac{\partial \tilde{p}}{\partial \vartheta} + J_0^{\phi} (\sqrt{g} \tilde{B}^r) - B_0^{\phi} \left(\frac{g_{\phi\phi}}{\sqrt{g}} \frac{\partial \sqrt{g} \tilde{B}^{\phi}}{\partial \vartheta} + i n \tilde{B}_{\vartheta} \right),$$

from which it is immediate to see that $\sqrt{g}\tilde{B}^{\phi}\sim \varepsilon^2 B_0 \xi_m^r$ at most. As in the discussion of the dynamics of global modes near a resonance, this quantity will turn out to be unimportant in the region close to r_m . Using again (7.39), we recover both (7.27) and (7.41). We now basically perform the same operations of section 7.3.2: i) by means (7.29) one first finds (7.42) which implies $\xi_m^{\phi}\approx 0$ also in this case, then ii) we show that $\Delta p_m\approx 0$, and finally iii) we obtain equation (7.43) from which (7.34) follows (terms with radial derivatives being the dominant ones).

Thus, in light of these results auxiliary quantities associated with the perturbed fluid displacement, pressure and toroidal field can be computed from equation (7.30)-(7.32), (7.34) and (7.35) applying the appropriate orderings to the radial derivative and mode number for small and large scale modes far-from and close-to resonances.

7.5 General form of the eigenmode equations

By using the results obtained in the previous sections we can now derive a set of eigenmode equations only involving the perturbed radial fluid displacement. The following analysis will be carried out focussing on **global modes**, i.e. perturbations with $m \sim n \sim 1$. As mentioned in the previous section, the resulting equations can be straightforwardly extended to deal with localised perturbations by letting $m \gg 1$ and employing suitably the orderings discussed earlier. Similarly, the behaviour close to a resonant point is obtained by allowing enhanced radial gradients of the perturbation.

We leave the expression of the quantity $\Delta p_{m\pm 1}$ unspecified: this will be given by either one of (7.34) depending on the ordering of the growth rate and poloidal mode number.

The boxed equations appearing in the following and preceding sections will form the basis for the stability analysis discussed in the next chapters.

7.5.1 Equation for the main mode

We shall analyse equation (7.13) by adopting the *divide et impera* approach. Let us introduce the quantity

$$k_{||} = m\mu - n \text{ with } \mu = 1/q,$$
 (7.51)

where $k_{||}$ is (loosely speaking) referred to as the **parallel wave vector**. The quantity μ is usually called the **rotational transform**. We start from noting that, by means of (7.25) and (7.35), to the leading orders we have²²

$$\begin{split} \left(\sqrt{g}\tilde{J}^{\phi}\right)_{m} &= -\frac{1}{im} \left[\left(\langle \frac{g_{\vartheta\vartheta}}{\sqrt{g}} \rangle \frac{(\sqrt{g}\tilde{B}^{r})'_{m}}{1+h} \right)' - m^{2} \langle \frac{g_{rr}}{\sqrt{g}} \rangle (\sqrt{g}\tilde{B}^{r})_{m} \right] + \\ & \frac{n}{m} \left[\langle \frac{g_{\vartheta\vartheta}}{R^{2}} \rangle \left(\frac{R_{0}}{B_{0}} p'_{0} \xi_{m} + \langle \frac{J_{0}^{\phi}}{B_{0}^{\phi}} \rangle \frac{(\sqrt{g}\tilde{B}^{r})_{m}}{im} \right) \right]' + \sum_{m'\neq 0} C_{m}^{m'}, \quad (7.52) \end{split}$$

having used (5.5) and the fact that $1 - h \approx \frac{1}{1+h}$ with

$$h=\frac{n^2}{m^2}\frac{r^2}{R_0^2}\sim \varepsilon^2.$$

Notice that we retain ε^2 corrections to the dominant terms. The quantity $C_m^{m'}$ accounts for coupling with the sidebands:

$$C_{m}^{m'} = \frac{d}{dr} \left[\left(\frac{g_{r\vartheta}}{\sqrt{g}} \right)_{m'} (\sqrt{g} \tilde{B}^{r})_{m-m'} + \left(\frac{g_{\vartheta\vartheta}}{\sqrt{g}} \right)_{m'} (\sqrt{g} \tilde{B}^{\vartheta})_{m-m'} \right]$$

$$-im \left[\left(\frac{g_{rr}}{\sqrt{g}} \right)_{m'} (\sqrt{g} \tilde{B}^{r})_{m-m'} + \left(\frac{g_{r\vartheta}}{\sqrt{g}} \right)_{m'} (\sqrt{g} \tilde{B}^{\vartheta})_{m-m'} \right].$$
 (7.53)

Proceeding further, from the equilibrium force balance equation 23 we immediately have to leading order

$$\left(\sqrt{g}J_0 \cdot \nabla \frac{\tilde{B}^{\phi}}{B_0^{\phi}}\right)_m = \frac{im}{rB_0}P(\sqrt{g}\tilde{B}^{\phi})_m, \tag{7.54}$$

where

$$P = \left[\frac{R_0}{B_0} p_0' + \frac{k_{||}}{m} \langle \sqrt{g} J_0^{\phi} \rangle \right]. \tag{7.55}$$

 22 Here we used the trick

$$\frac{\sqrt{g}}{R^2} \left\langle \frac{g_{\vartheta\vartheta}}{\sqrt{g}} \right\rangle = \left\langle \frac{g_{\vartheta\vartheta}}{R^2} \right\rangle \approx \frac{r^2}{R_0^2}.$$

²³ That is $p_0'/B_0^{\phi} = \sqrt{g}(J_0^{\vartheta} - J_0^{\phi}/q)$.

Thus, by combining (7.52) and (7.54), a simple algebraic manipulation shows that

$$\left(\sqrt{g}\boldsymbol{B}_{0}\cdot\boldsymbol{\nabla}\frac{\tilde{J}^{\phi}}{B_{0}^{\phi}}-\sqrt{g}\boldsymbol{J}_{0}\cdot\boldsymbol{\nabla}\frac{\tilde{B}^{\phi}}{B_{0}^{\phi}}\right)_{m} = \\
-\frac{k_{||}}{m}\left[\left(\langle\frac{g_{\vartheta\vartheta}}{\sqrt{g}}\rangle\frac{(\sqrt{g}\tilde{B}^{r})'_{m}}{1+h}\right)'-m^{2}\langle\frac{g_{rr}}{\sqrt{g}}\rangle(\sqrt{g}\tilde{B}^{r})_{m}\right] \\
+\frac{nR_{0}}{mB_{0}}\left[\frac{r^{2}p'_{0}}{R_{0}^{2}}\left(ik_{||}\xi_{m}^{r}-\frac{(\sqrt{g}\tilde{B}^{r})_{m}}{f'_{0}}\right)\right]'+\frac{n}{m}\left(\frac{rP}{R_{0}^{2}B_{0}}\right)'(\sqrt{g}\tilde{B}^{r})_{m} \\
-i\left(n\mu'\frac{r^{2}}{R_{0}^{2}}+\frac{mP}{R_{0}B_{0}}\right)\left[\frac{R_{0}}{B_{0}}p'_{0}\xi_{m}^{r}+\langle\frac{J_{0}^{\phi}}{B_{0}^{\phi}}\rangle\frac{(\sqrt{g}\tilde{B}^{r})_{m}}{im}\right]+ik_{||}\sum_{m'\neq 0}C_{m}^{m'}.$$
(7.56)

Note that we did not express $(\sqrt{g}\tilde{B}^r)_m$ in terms of ξ_m^r : this will turn out to be more convenient when analysing resistive MHD stability in chapters 16 and 17.

Let us define the quantity

$$\hat{k}_{||} = \frac{f_0'}{r} k_{||},\tag{7.57}$$

where $k_{||}$ is given by (7.51) and f_0' by (7.14). The relation between $(\sqrt{g}\tilde{B}^r)_m$ and ξ_m^r obtained from (7.7) then reads

$$(\sqrt{g}\tilde{B}^r)_m = irf_0'k_{||}\xi_m^r = ir\hat{k}_{||}\xi_m^r$$

This is employed to recast the first term on the right and side of (7.56) in the more convenient form

$$-i\hat{k}_{||}\left[\langle N\rangle\frac{(\sqrt{g}\tilde{B}^r)'_m}{1+h}\right]' = \frac{1}{r}\frac{d}{dr}\left(\frac{r^2\langle N\rangle}{1+h}\hat{k}_{||}^2\frac{d\xi_m^r}{dr}\right) + \left(\frac{\langle N\rangle(r\hat{k}_{||})'}{1+h}\right)'\hat{k}_{||}\xi_m^r, \tag{7.58}$$

having adopted the notation used in 5.3 to denote the metric coefficients (see Eqs. (5.24)-(5.26)).

The remaining terms in (7.13) are much easier to evaluate. We write the perturbed pressure as $\tilde{p} = \hat{p} + \Delta p$ with

$$\hat{p} = -p_0' \xi^r, \tag{7.59}$$

(7.61)

which is the **convective contribution**. Exploiting (7.32), the terms proportional to the equilibrium current density and perturbed pressure read

 $\left(\sqrt{g}\widetilde{\boldsymbol{B}}\cdot\boldsymbol{\nabla}\frac{J_{0}^{\phi}}{B_{0}^{\phi}}\right)_{m} = \left\langle\frac{J_{0}^{\phi}}{B_{0}^{\phi}}\right\rangle'(\sqrt{g}\widetilde{\boldsymbol{B}}^{r})_{m} + \sum_{m'\neq 0}D_{m}^{m'}, \tag{7.60}$ $\left(\sqrt{g}\boldsymbol{\nabla}\phi\cdot\boldsymbol{\nabla}\frac{1}{B_{0}^{\phi}}\times\boldsymbol{\nabla}\tilde{\boldsymbol{p}}\right)_{m} = -imp_{0}'\left\langle\frac{1}{B_{0}^{\phi}}\right\rangle'\xi_{m}^{r} + \sum_{m'\neq 0}\left[E_{m}^{m'}(\hat{\boldsymbol{p}}) + E_{m}^{m'}(\Delta\boldsymbol{p})\right],$

This is known as Sturm-Liouville form.

Recall that (7.15) holds.

with the functions $D_m^{m'}$ and $E_m^{m'}$, which describe the coupling with other poloidal harmonics, being defined as

$$D_{m}^{m'} = \left(\frac{J_{0}^{\phi}}{B_{0}^{\phi}}\right)_{m'}' (\sqrt{g}\tilde{B}^{r})_{m-m'} + im' \left(\frac{J_{0}^{\phi}}{B_{0}^{\phi}}\right)_{m'} (\sqrt{g}\tilde{B}^{\theta})_{m-m'}, \qquad (7.62)$$

$$E_{m}^{m'}(X) = \left(\frac{1}{B_{0}^{\phi}}\right)_{m'}' i(m-m')X_{m-m'} - im' \left(\frac{1}{B_{0}^{\phi}}\right)_{m'} X_{m-m'}'. \qquad (7.63)$$

Finally, the left hand side of (7.13) is computed by means of (7.27) and (7.30) yielding at leading order

$$\gamma^{2} \left[\frac{\partial}{\partial r} \left(\frac{\rho_{0}}{B_{0}^{\phi}} \xi_{\vartheta} \right) - \frac{\partial}{\partial \vartheta} \left(\frac{\rho_{0}}{B_{0}^{\phi}} \xi_{r} \right) \right]_{m} =$$

$$- \frac{B_{0}}{i m R_{0}} \left[\frac{1}{r} \frac{d}{dr} \left(\frac{\gamma^{2}}{\omega_{A}^{2}} r^{3} \frac{d \xi_{m}^{r}}{dr} \right) - \frac{\gamma^{2}}{\omega_{A}^{2}} \left[(m^{2} - 1) - r \frac{\rho_{0}'}{\rho_{0}} \right] \xi_{m}^{r} \right], \quad (7.64)$$

where we retained mass density radial non uniformities.

Thus, making use of (7.7), (7.14) and (7.15), we collate (7.53), (7.56), (7.58), (7.60)-(7.64) to obtain the **eigenmode equation**, for the dominant harmonic

$$\frac{1}{r}\frac{d}{dr}\left(\frac{r^{2}\langle N\rangle}{1+h}\hat{k}_{||}^{2}\frac{d\xi_{m}^{r}}{dr}\right) + \left\{r\hat{k}_{||}\left[\frac{1}{r}\left(\frac{\langle N\rangle(r\hat{k}_{||})'}{1+h}\right)' - m^{2}\hat{k}_{||}\langle L\rangle - m\frac{f_{0}'}{r}\langle\frac{J_{0}^{\phi}}{B_{0}^{\phi}}\rangle'\right] + m^{2}B_{0}\left[\frac{P^{2}}{R_{0}B_{0}} + \frac{n\mu'}{m}\frac{r^{2}}{R_{0}^{2}}P - nr\frac{k_{||}}{m^{2}}\left(\frac{rP}{R_{0}^{2}}\right)' - p_{0}'\left(\frac{\langle R^{2}\rangle'}{F} - \frac{\langle R^{2}\rangle F'}{F^{2}}\right)\right]\right\}\xi_{m}^{r} + imB_{0}\sum_{m'\neq 0}\left[ik_{||}C_{m}^{m'} + D_{m}^{m'} - E_{m}^{m'}(\hat{p}) - E_{m}^{m'}(\Delta p)\right] \\
= -\frac{B_{0}^{2}}{R_{0}}\left[\frac{1}{r}\frac{d}{dr}\left(\frac{\gamma^{2}}{\omega_{A}^{2}}r^{3}\frac{d\xi_{m}^{r}}{dr}\right) - \frac{\gamma^{2}}{\omega_{A}^{2}}\left[(m^{2} - 1) - r\frac{\rho_{0}'}{\rho_{0}}\right]\xi_{m}^{r}\right]. \tag{7.65}$$

Plasma inertia, that is the growth rate γ , appears on the right hand side of (7.65) and in the $E_m^{m'}(\Delta p)$ terms. These are referred to as **inertial** contributions.

With the particular choice of coordinate system given in chapter 5 for which $\frac{f_0'}{r} = \frac{F}{R_0}$, the **cylindrical limit** is obtained by simply setting (notice that the factor h is actually a **cylindrical contribution**)

$$C_m^{m'} \to 0, \quad D_m^{m'} \to 0, \quad E_m^{m'} \to 0, \quad \langle R^2 \rangle' \to 0,$$

$$\langle L \rangle \to \frac{1}{rR_0}, \quad \langle N \rangle \to \frac{r}{R_0}. \tag{7.66}$$

In this case, letting $\gamma \to 0$ and taking into account ε^2 corrections which do not arise from toroidicity, equation (7.65) reduces to the so called **Newcomb equation**, ²⁴ i.e. the equation for the radial fluid displacement in a straight screw-pinch at marginal stability (that is equation (D.2) in appendix D).

²⁴ From Newcomb (1960). See also Rosenbluth (1958) and Suydam (1958).

For many applications it is useful to isolate the dominant contributions appearing in equation (7.65). These are obtained by writing the toroidal current density in terms of $\hat{k}_{||}$, i.e.

$$m\langle \frac{J_0^{\phi}}{B_0^{\phi}}\rangle = \frac{1}{f_0'} \left([\langle N \rangle r \hat{k}_{||}]' + n[\langle N \rangle f_0']' \right). \tag{7.67}$$

Hence, by means of (7.66) and exploiting the fact that at leading order $f_0'/r = B_0$ (see (7.14)), we get

$$\frac{1}{r} \left(\frac{\langle N \rangle (r\hat{k}_{||})'}{1+h} \right)' - m^2 \hat{k}_{||} \langle L \rangle - m \frac{f_0'}{r} \langle \frac{J_0^{\phi}}{B_0^{\phi}} \rangle' \approx \frac{B_0}{rR_0} (1-m^2) k_{||}. \tag{7.68}$$

Using this result into (7.65) yields

$$\frac{d}{dr}\left(r^3k_{||}^2\frac{d\xi_m^r}{dr}\right) - rk_{||}^2(m^2 - 1)\xi_m^r = 0.$$
 (7.69)

As a final remark, we point out that equation (7.65) can be formally written as

$$\frac{d}{dr}\left(r^3f_1\frac{d\xi_m^r}{dr}\right) - rk_{||}^2(m^2 - 1)\xi_m^r + f_2 = 0,$$

where f_1 and f_2 are some functions of r with $f_1 \sim 1$ and $f_2 \sim \varepsilon^2 r \xi_m^r$, this holding true also for fast growing instabilities with $\gamma/\omega_A \sim 1$.

In summary, the linear dynamics of the dominant mth harmonic is fully described by equations (7.34), (7.51), (7.53), (7.55), (7.57), (7.59), (7.62), (7.63) and (7.65), and its simplified expression given by (7.69). What is missing now is an equation for the sideband harmonics. This is worked out in the next section.

This will turn out to be of crucial importance in the analysis of the m=1 internal kink mode in the next chapter.

Local behaviour about a resonance at marginal stability

Suppose that the radial fluid displacement obeys Eq. (7.69). We are interested in the behaviour of ξ_m^r in proximity of r_s where $k_{||} = 0$. Assume m > 1. Upon introducing the variable $x = (r - r_s)/r_s$, near this point we write

$$\xi_m^r \propto 1 + a_1 x^{\nu} \quad (\nu > 0),$$

and approximate $k_{||} \propto x$. This means that we are looking at perturbations which are not vanishing at r_s . When this form of ξ_m^r is plugged into (7.69) we obtain

$$a_1 v(v+1) x^{v-2} - (m^2 - 1) = 0.$$

This is solved by setting $\nu=2$, meaning that at marginal stability the eigenfunction of an ideal mode obeying (7.69) approaches the resonance with vanishing radial derivative.

7.5.2 Equations for the neighbouring sidebands

The derivation of the equations for the sidebands follows the one employed for the main mode. Luckily, it is much simpler. Let us assume that $m-1 \neq 0$, meaning that we consider m > 1. In line with the arguments of earlier sections, we suppose that the only non-vanishing harmonics are those with poloidal mode numbers m and $m \pm 1$, and the magnitude of the $m \pm 1$ sidebands is ε times smaller compared to that of the mode m. Furthermore, working within the assumption of **slow-growing modes**, inertial corrections can be neglected since they are of higher order. We start from the equivalent of (7.56), where only the leading order contributions are retained. This is

$$\left(\sqrt{g}\boldsymbol{B}_{0}\cdot\boldsymbol{\nabla}\frac{\tilde{J}^{\phi}}{B_{0}^{\phi}}-\sqrt{g}\boldsymbol{J}_{0}\cdot\boldsymbol{\nabla}\frac{\tilde{B}^{\phi}}{B_{0}^{\phi}}\right)_{m\pm1} = -\frac{(m\pm1)\mu-n}{m\pm1}\left[\left(\frac{r}{R_{0}}(\sqrt{g}\tilde{B}^{r})_{m\pm1}^{\prime}\right)^{\prime} - \frac{(m\pm1)^{2}}{rR_{0}}(\sqrt{g}\tilde{B}^{r})_{m\pm1} - i(m\pm1)C_{m\pm1}^{\pm1}\right].$$
(7.70)

Notice that differently from (7.52), corrections due to mode coupling are of the same order as other terms.

It is immediate to verify that $(\sqrt{g} J_0 \cdot \nabla \tilde{B}^{\phi}/B_0^{\phi})_{m\pm 1}$ is negligible compared to other terms and thus it can be dropped. The remaining contributions are

where $D_{m\pm 1}^{\pm 1}$ and $E_{m\pm 1}^{\pm 1}$ are given by (7.62) and (7.63) respectively, and the term proportional to Δp_m vanishes by virtue of (7.30).

Hence, making use of (7.58) and (7.68), the equation for the sidebands can be cast as

$$\frac{1}{r}\frac{d}{dr}\left(r^{3}[(m\pm 1)\mu - n]^{2}\frac{d\xi_{m\pm 1}^{r}}{dr}\right) - [(m\pm 1)^{2} - 1][(m\pm 1)\mu - n]^{2}\xi_{m\pm 1}^{r} + i\frac{R_{0}}{B_{0}}(m\pm 1)\left\{i[(m\pm 1)\mu - n]C_{m\pm 1}^{\pm 1} + D_{m\pm 1}^{\pm 1} - E_{m\pm 1}^{\pm 1}(\hat{p})\right\} = 0.$$
(7.71)

Upon a simple inspection, we shall note that this equation could have been derived directly from (7.65) by replacing $m \to m \pm 1$ and exploiting the fact that $\xi_{m\pm}^r \sim \varepsilon \xi_m^r$ (the ordering of the magnetic field components follows accordingly). This concludes the derivation of the **sideband eigenmode equations** for m > 1.

When m=1, we have to provide an additional equation for $(\sqrt{g}\tilde{B}^{\vartheta})_0$. This is because this quantity cannot be expressed in terms of the radial field through (7.25) due to the appearance of diverging terms proportional to $\frac{1}{m-1}$. Since this affects modes with m=1 only, we leave the

discussion on how to deal with these quantities to the next chapters where the stability properties of such perturbations are addressed.

Each of the next five chapters will be focussing on one of the instabilities mentioned at the beginning of chapter 6.

References

- A. B. Mikhailovskii, **Reviews of Plasma Physics Vol. 9 p. 1** (Ed. M. A. Leontovich), Consultants Bureau (New York, US), 1986.
- A. B. Mikhailovskii, **Instabilities in a Confined Plasma**, Institute of Physics Publishing (Bristol, UK), 1998.
- W. A. Newcomb, Ann. Phys. 10, 232 (1960).
- M. N. Rosenbluth in Proceedings of the Second United Nation International Conference on the Peaceful Uses of Atomic Energy (United Nations Geneva, 1958) Vol. 31, p. 85.
- B. R. Suydam, in Proceedings of the Second United Nation International Conference on the Peaceful Uses of Atomic Energy (United Nations Geneva, 1958) Vol. 31, p. 157.

8

The m = 1 internal kink mode

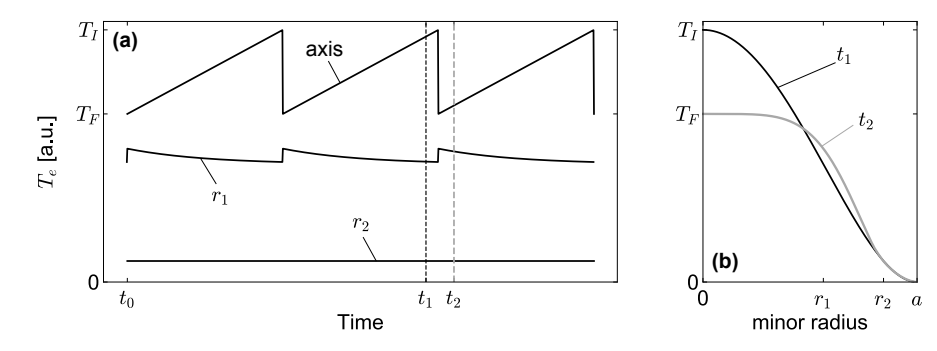
In this chapter we analyse the MHD instability known as the m=1 ideal internal kink mode (or simply internal kink mode). We call **internal mode** any perturbation whose associated radial displacement vanishes at the plasma edge. The typical feature of modes with poloidal mode number **equal to 1** is the fact that at each toroidal section they correspond to a rigid shift of the flux surfaces. This helical perturbation has particular relevance in tokamaks when the poloidal and toroidal mode numbers are equal, that is m=n=1. In such a case, this mode can be driven unstable if a q=1 resonant surface appears within the plasma.

The importance of the m=1 internal kink comes from the fact that it has been associated with the phenomenon, observed basically in all tokamaks, of **sawtooth oscillations** (or sawteeth). These oscillations are quasi-periodic relaxation events which cause a sudden drop in the temperature and density in the centre of the plasma (see figure 8.1). They have been experimentally associated with the growth of a m=n=1 perturbation: during the cycle of this oscillation before the temperature crash, a m=1 internal mode develops when the safety factor on axis is less then unity (q(0) < 1). Although the explanation, albeit rudimentary, of the sawtooth cycle requires a step beyond ideal MHD (this will be elaborated further in chapter 15) the understanding of the linear dynamics of the m=1 ideal internal kink mode proves to be of crucial importance.

This mode has been first studied in cylindrical geometry by Shafranov (1970) and Rosenbluth (1973). However, it was soon realised that the cylindrical description was inadequate, and thus a proper toroidal treatment was presented by Bussac (1975). It was found that the inclusion of toroidal effects cancels out entirely the cylindrical contribution

¹ Sawteeth have a detrimental effect on the energy confinement because of the temperature modulation (this is a serious concern when aiming at ignition), and can potentially trigger other helical perturbations. Nonetheless, sawteeth may help in avoiding accumulation of impurities and fusion ashes (Helium).

Figure 8.1: Example of the time evolution of the electron temperature during a sawtooth oscillation at three different radial locations (a) and the electron temperature radial profile vs minor radius right before and shortly after the temperature drop (b).



leading to the realisation that cylindrical results are in some cases, misleading.

The complete analysis of the internal kink mode requires by far the largest amount of unpleasant algebra compared to any other MHD instability. Since the calculations can be quite involute, here we present, hopefully clear enough, a step-by-step derivation. The calculations we carry out will eventually provide an expression for the growth rate of the mode and its stability boundaries. A brief discussion of the stability of the m = n = 1 mode with a non-monotonic safety factor is also given.

8.1 The general form of the growth rate

Let us take a monotonic safety factor profile with a single m/n resonance, similar the one shown in figure 7.1. An ideal conducting wall is assumed surrounding the plasma, implying that the perturbed fluid displacement at the boundary is vanishing at all orders (cf. (6.16)).

We assume that the spectrum of the perturbed fluid displacement consists of a main harmonic of helicity (1, n) accompanied by ε times smaller sidebands with mode numbers (0, n) and (2, n) respectively. Since the equilibrium is almost circular, it will be clear that no further sidebands are required. For the sake of simplicity we also suppose that at equilibrium $\rho' = 0$ and assume that $\gamma/\omega_A \sim \varepsilon$. Setting m = 1 while keeping *n* generic (so that $k_{||} = \mu - n$), the leading order of (7.65) reads (cf. (7.69))

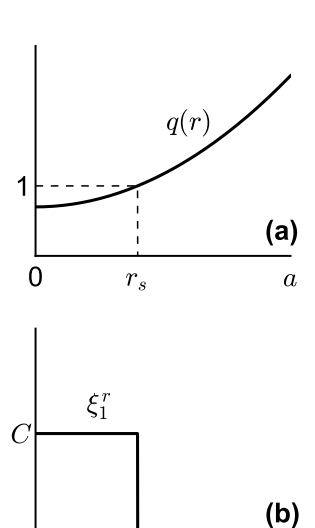
$$\frac{d}{dr}\left(r^3k_{||}^2\frac{d\xi_1^r}{dr}\right) = 0. ag{8.1}$$

Because of the singularity at r_s where q = 1/n, i.e. the **resonance**, we solve the equation above for $r < r_s$ and $r > r_s$ separately. The solution which is finite on the magnetic axis and zero at the plasma edge is

$$\xi_1^r = \begin{cases} C, & r < r_s, \\ 0, & r > r_s, \end{cases}$$
 (8.2)

where C is a constant (cf. Fig. 8.2). An example of the resulting flux surfaces displaced by such a perturbation is shown in figure 8.3.

We now seek a solution of the full equation (7.65) of the form ξ_1^r = $C + X_1$ where $X_1 \sim \varepsilon^2 C$. By means of (7.34) for the slow-growing mode



 r_s

0

Figure 8.2: Safety factor (a) and leading order radial fluid displacement (b) associated with the m = n = 1 internal kink mode.

a

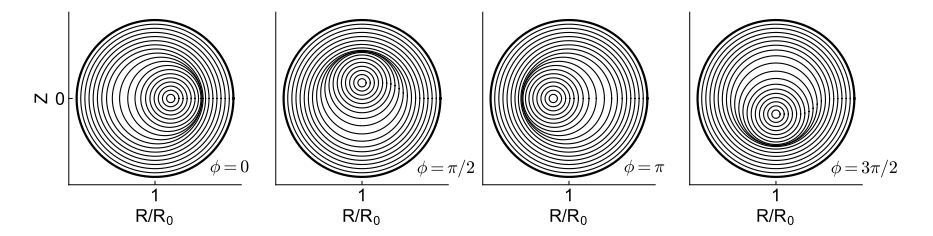


Figure 8.3: Example of the displacement of the flux surfaces due to the m = n = 1 internal kink at various toroidal angles (the Shafranov shift has been neglected).

case, a quick computation shows that at leading order $\Delta p_2 = 0$ and $\Delta p_0' = 0$ both on the left and on the right of r_s . Away from r_s , it is immediate to see that due to the orderings given in §7.2 the inertial contributions in (7.65), viz. $E_1^{\pm 1}(\Delta p)$ and the whole term on the right hand side, cancel (this is seen by plugging Δp_0 and Δp_2 in (7.63)). Thus, to second order in ε Eq. (7.65) is formally written as

$$\frac{1}{r}\frac{d}{dr}\left(r^3k_{||}^2\frac{dX_1}{dr}\right) + UC = 0, (8.3)$$

having defined $U = U_0 + U_{TC} \sim \varepsilon^2$ (TC standing for toroidal coupling) which is obtained from equation (7.65) with

$$U_{0} = \frac{rR_{0}\hat{k}_{||}}{B_{0}^{2}} \left[\frac{1}{r} \left(\frac{\langle N \rangle (r\hat{k}_{||})'}{1+h} \right)' - \hat{k}_{||} \langle L \rangle - \frac{f_{0}'}{r} \langle \frac{J_{0}^{\phi}}{B_{0}^{\phi}} \rangle' \right]$$

$$+ \frac{R_{0}}{B_{0}} \left[\frac{P^{2}}{R_{0}B_{0}} + n\mu' \frac{r^{2}}{R_{0}^{2}} P - nrk_{||} \left(\frac{rP}{R_{0}^{2}} \right)' - p_{0}' \left(\frac{\langle R^{2} \rangle'}{F} - \frac{\langle R^{2} \rangle F'}{F^{2}} \right) \right],$$

$$(8.4)$$

$$U_{TC} = \frac{iR_{0}}{CB_{0}} \sum_{m'=\pm 1} \left[ik_{||} C_{1}^{m'} + D_{1}^{m'} - E_{1}^{m'} (\hat{p}) \right],$$

$$(8.5)$$

where we recall that \hat{p} is given by (7.59).

Up to now, the growth rate γ did not appear in the equations that we presented above due to the fact that the right-hand-side of (7.65) vanishes. This is because $d\xi_1^r/dr=0$ at leading order. However, inertial contributions should not be neglected in the region near the step of ξ_1^r , i.e. close to r_s , where strong radial gradients of the perturbed displacement develop. Indeed, although γ/ω_A is small, in this region $d\xi_1^r/dr$ becomes large and its product with the growth rate can be of order of unity. Therefore, in proximity of r_s we employ the **layer ordering** (7.36), that is

$$r\frac{d\xi_1^r}{dr}\sim \frac{\xi_1^r}{\xi}, \quad k_{||}\approx -nsx,$$

where $s = r_s q_s'$ is the magnetic shear at r_s and $x = (r - r_s)/r_s \sim \varepsilon$. As mentioned in the previous chapter, we refer to the region close to r_s as the **inertial layer**.

² Note that the singularity in r_s appearing in (8.1) and (8.3) is resolved by the inclusion of inertia. At marginal stability plasma inertia is negligible and discontinuities in the perturbed quantities can appear.

³ This argument can be generalised for other instabilities such as Mercier and ballooning modes discussed in chapters 11 and 12.

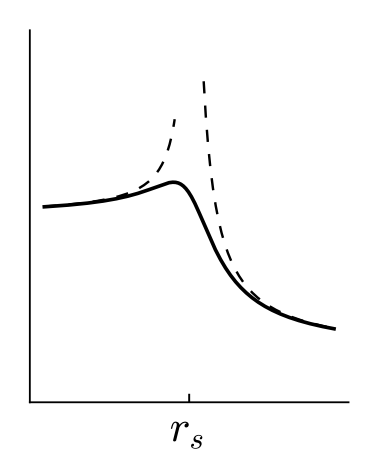


Figure 8.4: Graphical example of the asymptotic matching technique. The layer solution (solid line) joins smoothly on the left and on the right of r_s the external one represented by the dashed line.

If we change the radial coordinate from r to x and deploy the ordering given above, in a neighbourhood of r_s we can reduce (7.65) to the following form²

$$\frac{d}{dx} \left[\left(n^2 s^2 x^2 + (1 + \frac{2}{n^2}) \frac{\gamma^2}{\omega_A^2} \right) \frac{d\xi_m^r}{dx} \right] = 0.$$
 (8.6)

The factor $\frac{2}{n^2}$ originates from the contribution of **plasma compressibility** and is usually referred to as the **inertia enhancement factor** (the box at the end of this section explains more in detail how to include such a term). Let us rescale the Alfvén frequency as $\hat{\omega}_A^2 = \omega_A^2/(1+\frac{2}{n^2})$. Note that the thickness δr of the inertial layer can be estimated by balancing the two terms in the big round brackets in (8.6) giving³

$$\frac{\delta r}{r_s} \sim \frac{\gamma}{ns\hat{\omega}_A}.$$
 (8.7)

The solution of equation (8.6) which reduces to (8.2) for $\omega_A x/\gamma \gg 1$ (i.e. far from r_s) is easily computed and reads

$$\xi_1^r = \frac{C}{2} \left[1 - \frac{2}{\pi} \arctan\left(\frac{nsx}{\gamma/\hat{\omega}_A}\right) \right].$$
 (8.8)

The growth rate is then obtained by requiring that moving away from r_s equation (8.8) matches smoothly (i.e. with a continuous first derivative) the asymptotic behaviour of the solution obtained from (7.65) when r_s is approached. This technique is known as **asymptotic matching**, and a visual example of how this procedure is worked out is shown in figure 8.4.

Far from r_s Eq. (8.8) yields

$$\frac{d\xi_1^r}{dx} \approx -\frac{C\gamma}{\pi ns\hat{\omega}_4 x^2}.$$
 (8.9)

In proximity of the resonance, accounting for regularity of the solution on the magnetic axis, equation (8.3) gives

$$\frac{dX_{1}}{dr} \approx \begin{cases}
-\frac{C}{r_{s}^{3} n^{2} s^{2} x^{2}} \int_{0}^{r_{s} - \epsilon} r U dr, & r < r_{s}, \\
\frac{c_{0}}{r^{3} n^{2} s^{2} x^{2}}, & r > r_{s},
\end{cases}$$
(8.10)

where c_0 is a generic constant of integration and ϵ is an infinitesimal positive quantity with the dimensions of a length (if not specified, the dimensions of ϵ will be clear from the context). Therefore, by comparing (8.9) and (8.10), we finally obtain the expression for the growth rate γ :

$$\frac{\gamma}{\omega_A} = \frac{\pi}{r_s^2 n s \sqrt{1 + \frac{2}{n^2}}} \int_0^{r_s - \epsilon} r U dr. \tag{8.11}$$

Note that the matching for $r > r_s$ is automatically achieved by a suitable choice of c_0 . The relation above shows that $\gamma/\omega_A \sim \varepsilon^2$ for $s \sim 1$.

Although this ordering differs from (7.24), we could have consistently ordered a priori $\gamma/\omega_A\sim\delta,\ rd\xi_1^r/dr\sim\xi_1^r/\delta$ and $x\sim\delta$ with $\delta\sim\varepsilon^2$ yielding the same conclusions. This shows that the typical time-scale of growth of the internal kink is small, and in experiments it usually falls in the range of few milliseconds (with ω_A of the order of some megahertz). Also note that the dependence upon the inverse of the magnetic shear may enhance the growth rate if s is not large at r_s . The **marginal stability boundary**, i.e. the state for which $\gamma = 0$, is identified by the relation

 $\int_{0}^{\tau_{s}-\epsilon} rUdr = 0.$

This could have also been obtained directly by multiplying (8.3) by $r\xi_1^r$ and then integrating from 0 to a.4

Hence, to complete the analysis of the m = 1 internal kink it "only" remains to evaluate the integral in (8.11) by calculating U for $r < r_s$. Unfortunately, this is quite a laborious task.

We tackle the problem as follows: we first derive an expression for the m = 0 and m = 2 satellite harmonics. By means of the resulting expressions for these sidebands, we reduce U_{TC} to a form which depends on C only. We then rearrange the function U_0 separating the cylindrical and toroidal contributions to finally evaluate the integral in (8.11). This eventually leads to the desired expressions for growth rate and stability criterion. We warn the reader that the following sections will contain many mathematical details, which unfortunately cannot be sacrificed if the algebra wants to be understandable.

8.1.1 Inertia enhancement

In this box we show how plasma compressibility, i.e. Δp , modifies inertia. We shall keep m generic. Starting from (7.34) and assuming that the mode grows slowly, we employ the layer ordering (7.36) giving in proximity of the resonant surface r_s

$$\Delta p_{m\pm 1} \approx \pm \frac{q_s^2 B_0^2}{m R_0} \frac{\gamma^2}{\omega_A^2} \frac{d\xi_m^r}{dx},$$

where q_s is the value of the safety factor at r_s . Hence, noting that

$$(1/B_0^{\phi})_{\pm 1} = r/B_0, \tag{8.12}$$

it follows that (7.63) becomes

$$E_m^{\pm 1}(\Delta p) \approx \mp \frac{ir}{B_0} \Delta p'_{m \mp 1}.$$

We thus have

$$imB_0 \sum_{m'=+1} E_m^{m'}(\Delta p) = -\frac{2q_s^2 B_0^2}{R_0} \frac{\gamma^2}{\omega_4^2} \frac{d^2 \xi_m^r}{dx^2}.$$

⁴ Use of (8.1) must be made.

This only part is algebraically formidably long and tedious. Most of the times it is either skipped or presented it in such a compressed way that it is almost impossible to understand what is going on.

Plugging this result into (7.65) yields close to r_s

$$\frac{d}{dx}\left[\left(k_{||}^2+(1+2q_s^2)\frac{\gamma^2}{\omega_A^2}\right)\frac{d\xi_m^r}{dx}\right]=0.$$

Equation (8.6) then follows with $q_s = 1/n$.

8.2 Equations for the satellite harmonics

We require a detailed knowledge of the function U appearing in (8.3). The function U_{TC} depends upon the sideband radial fluid displacements and magnetic field components ($\ell = 0, 2$)

$$\xi_{\ell}^{r}$$
, $(\sqrt{g}\tilde{B}^{r})_{\ell}$, $(\sqrt{g}\tilde{B}^{\vartheta})_{\ell}$

through the coupling coefficients $C_1^{m'}$, $D_1^{m'}$ and $E_1^{m'}$. We refer to the m-1(=0) harmonic as the **lower sideband**, whereas the m+1(=2) mode is the **upper sideband**. Hence, an explicit expression for the satellite harmonics needs to be derived.

8.2.1 Lower $\ell = 0$ sideband

Making use of (7.25) and (7.26), it is immediate to see that $(\sqrt{g}\tilde{B}^r)_0 \sim \varepsilon^2 a B_0 \xi_1^r$, and employing this in the 0th Fourier projection of (7.7) we also get $\xi_0^r \sim \varepsilon^2 \xi_1^r$. Therefore, we can safely set $\xi_0^r = (\sqrt{g}\tilde{B}^r)_0 = 0$. Notice that we could have arrived to the same conclusion by an inspection of (7.71) requiring that ξ_0^r is finite on the axis.

Let us now introduce the quantity

$$l_m = r(\mu - n/m).$$

The expression for $(\sqrt{g}\tilde{B}^{\theta})_0$ is obtained by multiplying (7.12) by $1/B_0^{\phi}$ and then averaging it. Using the fact that $\hat{p}_0 = \Delta p_1 = 0^7$ and under the assumption that $\xi_0^{\theta} \sim \xi_0^{\phi} \sim \varepsilon \xi_1^r$, inertial contributions can be neglected, so that to leading order one has

$$Y_0 \equiv (\sqrt{g}\tilde{B}^{\vartheta})_0 = \frac{R_0 B_0}{r} \left[N_{-1} (l_1 \xi_1^r)' - i l_1 M_{-1} \xi_1^r + \frac{r p_0'}{\mu B_0^2} \xi_1^r \right], \tag{8.13}$$

where we used (7.25) again and

$$(J_0^{\phi}/B_0^{\phi})_{\pm 1} = -q p_0'/B_0^2. \tag{8.14}$$

Hereafter the notation for the metric coefficients follows the one employed in Eqs. (5.25) and (5.26).

⁵ Multiply (7.25) by ℓ , then take $\ell = 0$ and average in ϑ .

⁶ This automatically implies that $\xi_0^r = 0$.

⁷ $\Delta p_1 = 0$ follows from (7.32). Note that from (7.7) one has $(\sqrt{g}\tilde{B}^r)_\ell = iB_0\ell l_\ell \xi_\ell^r$.

Upper $\ell = 2$ sideband

It is clear that (7.7) allows us to write $(\sqrt{g}\tilde{B}^r)_2$ in terms of ξ_2^r . Also, by means of (7.25) and (7.26), the quantity $(\sqrt{g}\tilde{B}^{\theta})_2$ can be written as a function of $(\sqrt{g}\tilde{B}^r)_2$, and thus of ξ_2^r . This yields

$$(\sqrt{g}\tilde{B}^r)_2 = 2iB_0l_2\xi_2^r,$$

 $(\sqrt{g}\tilde{B}^{\vartheta})_2 \approx -\frac{1}{2i}(\sqrt{g}\tilde{B}^r)_2' = -B_0[l_2\xi_2^r]'.$

The equation for ξ_2^r obtained from (7.71) reads

$$\frac{d}{dr} \left(r^3 [2\mu - n]^2 \frac{d\xi_2^r}{dr} \right) - 3r [2\mu - n]^2 \xi_2^r
+ 2i \frac{rR_0}{B_0} \left[i(2\mu - n)C_2^1 + D_2^1 - E_2^1(\hat{p}) \right] = 0.$$
(8.15)

Assume now that the analysis is carried out for $r < r_s$, for which

$$(\sqrt{g}\tilde{B}^r)_1 = iB_0l_1C, \quad (\sqrt{g}\tilde{B}^\vartheta)_1 = -B_0l_1'C.$$

Upon defining

$$\zeta = \Delta' + \frac{r}{2R_0},\tag{8.16}$$

by means of (8.12) and (8.14) it is possible to show that⁸

$$\begin{split} r[D_{2}^{1} - E_{2}^{1}(\hat{p})] &= -2il_{2}r^{2} \left(\frac{p_{0}'}{r\mu B_{0}}\right)' C, \\ ir(2\mu - n)C_{2}^{1} &= -2iB_{0}Cl_{2} \left[\left(N_{1}l_{1}' + iM_{-1}l_{1}\right)' - 2\left(L_{1}l_{1} - iM_{-1}l_{1}'\right) \right] \\ &= i\frac{B_{0}}{R_{0}}l_{2} \left[\left(l_{1}(r\zeta)'\right)' - 2\left(l_{2}'' + \frac{2}{r}(\mu - n)\right)r\zeta + \frac{r^{2}}{R_{0}}\left(l_{2}'' + 2\mu'\right) \right]C, \\ (8.17) \end{split}$$

having used the fact that $M_{-1} = -M_1$, whereas $N_{-1} = N_1$ and $L_1 = L_{-1}$. By expressing p'_0 in terms of ζ through (4.33), after some rearrangements we write the intermediate step

$$\begin{split} r\left[i(2\mu-n)C_{2}^{1}+D_{2}^{1}-E_{2}^{1}(\hat{p})\right] \\ &=2i\frac{B_{0}}{R_{0}}Cl_{2}\left[\left(l_{2}(r\zeta)'\right)'+r\mu'(r\zeta)'+\left(\frac{2n}{r}-2\mu'-\frac{4}{r}\mu\right)r\zeta\right] \\ &=2i\frac{B_{0}}{R_{0}}Cl_{2}\left[\left(r(l_{2}\zeta)'\right)'-4\frac{l_{2}}{r}\zeta-r\zeta\left(\frac{1}{r}(rl_{2})'\right)'\right]. \end{split}$$

Referring to equations (7.58), (7.67) and (7.68) we have the following relations (notice that these can be straightforwardly extended to the case of arbitrary poloidal mode number)

$$l_2[r(l_2X)']' = (rl_2^2X')' + (rl_2')'l_2X,$$

$$\frac{1}{r}(rl_2')' - [\frac{1}{r}(rl_2)']' = \frac{1}{r}(\mu - n/2).$$

The sign on the non-homogeneous term of (8.15) reflects the choice of the parametrisation or R which is $R = R_0 +$ $r\cos\vartheta+\ldots$ In the literature, we can often find it multiplied by a minus factor. This is because in the latter case the poloidal direction is flipped, that is $R = R_0 - r \cos \vartheta + \dots$

⁸ Note that
$$M_{-1} = \frac{i(r\zeta)'}{2R_0}$$
, $N_1 = \frac{r}{R_0} \left(\zeta - \frac{r}{2R_0} \right)$ and $l_1'' = l_2''$.

9 We use the fact that $r\Delta'' + \Delta' + r/R_0 = (r\zeta)'$ so that $\frac{2R_0p_0'}{\mu B_0^2} =$ $-\mu \left[(r\zeta)' + 2\left(1 + \frac{r\mu'}{\mu}\right)\zeta - \left(3 + \frac{r\mu'}{\mu}\right)\frac{r}{R_0} \right]$

When the two results above are plugged into (8.15) we finally obtain

$$\frac{d}{dr} \left(r^{3} [2\mu - n]^{2} \frac{d\xi_{2}^{r}}{dr} \right) - 3r [2\mu - n]^{2} \xi_{2}^{r}$$

$$= \begin{cases}
\left[\frac{d}{dr} \left(r^{3} [2\mu - n]^{2} \frac{d\zeta}{dr} \right) - 3r [2\mu - n]^{2} \zeta \right] C, & r < r_{s}, \\
0, & r > r_{s},
\end{cases}$$
(8.18)

The jump condition for the derivative of ξ_2^r at r_s is obtained by integrating (8.15) across the q=1 surface and exploiting the Dirac-delta singularity of the main mode, i.e. $\frac{d\xi_1^r}{dr}\sim\delta(r-r_s)$ (cf. 8.2)¹⁰ where we implicitly assume that ξ_2^r does not diverge at r_s (an account of the mathematics employed for carrying out these computations is outlined in the box at the end of this section). The only contributing terms come from $\frac{d(\sqrt{g}\tilde{B}^\theta)_1}{dr}$ and $\frac{d(\rho_0'\xi_1^r)}{dr}$, respectively, in C_2^1 and E_2^1 . This yields

$$r_{s} \left[\frac{d\xi_{2}^{r}}{dr} \right] = \frac{2}{n^{2}} \left[nr\mu'\Delta' + \frac{R_{0}p_{0}'}{B_{0}^{2}} \right]_{r_{s}} C = -\left[r\Delta'' + 3\Delta' - \frac{r}{R_{0}} \right]_{r_{s}} C, \quad (8.19)$$

where the right-hand-side of the equation above has to be evaluated at $r = r_s$ and $[\![\cdot]\!] = (\cdot)_{r_s+\epsilon} - (\cdot)_{r_s-\epsilon}$ with $\epsilon \to 0$. The last equality is obtained by means of (4.33). A further integration shows that $[\![\xi_2^r]\!] = 0$, i.e. the upper sideband is continuous at r_s .

We now need to identify the appropriate boundary conditions for ξ_2^r . The sideband ξ_2^r must be finite on the magnetic axis. Furthermore, if no q=2 surface is in the plasma, then $\xi_2^r(a)=0$, otherwise we require that ξ_2^r is regular, meaning finite, at the q=2 resonant surface. Let X_2^i and X_2^e be the solution to the homogeneous equation (8.18) for $r < r_s$ and $r > r_s$ respectively. X_2^i satisfies the regularity condition on the axis, whereas X_2^e fulfils the aforementioned requirements for ξ_2^r either at the plasma boundary or at the resonant q=2 surface. We introduce the quantities (do not confuse the symbols s and \hat{s})

$$b = \frac{r_s}{4} \left[\frac{d}{dr} \ln(X_2^i/r) \right]_{r_s}, \quad c = \frac{r_s}{4} \left[\frac{d}{dr} \ln(X_2^e r^3) \right]_{r_s}, \quad \hat{s} = \frac{\ell_i(r_s)}{2} - \frac{1}{4}, \quad (8.20)$$

where ℓ_i is given by (4.37). By requiring continuity of ξ_2^r at r_s and imposing the jump condition (8.19), we finally obtain

$$\frac{\xi_{2}^{r}}{C} = \begin{cases}
\Delta' + \frac{r}{2R_{0}} + \frac{r_{s}}{R_{0}} \left(\frac{-3/4 + c[3/4 + \hat{s} + \beta_{p}(r_{s})]}{1 + b - c} \right) \frac{X_{2}^{t}(r)}{X_{2}^{t}(r_{s})}, & r < r_{s}, \\
\frac{r_{s}}{R_{0}} \left(\frac{\hat{s} + \beta_{p}(r_{s}) + b[3/4 + \hat{s} + \beta_{p}(r_{s})]}{1 + b - c} \right) \frac{X_{2}^{e}(r)}{X_{2}^{e}(r_{s})}, & r > r_{s}, \\
(8.21)
\end{cases}$$

where use of (4.35) has been made. It is worth noting that some inertial contributions, i.e. terms which depend on γ , may appear at the resonant surface of the m=2 mode if this occurs within the plasma. This is because of the sharp gradient of ξ_2^r at this point (this is analogous to what

 10 Remember that $k_{||} \sim (r-r_{s})$ close to r_{s} and $x\delta(x)=0.$

¹¹ Thanks to the regularity condition at the axis and either at a or at the q=2 surface if it exists in the plasma, we can write

$$\frac{\xi_2^r}{C} = \begin{cases} \zeta + c_1 \frac{X_2^i(r)}{X_2^i(r_s)}, & r < r_s, \\ \frac{X_2^e(r)}{c_2 \frac{X_2^e(r_s)}{X_2^e(r_s)},} & r > r_s, \end{cases}$$

where c_1 and c_2 are two constants.

has been discussed in the previous section about inertia at r_s). However, it is rather immediate to convince ourselves that these corrections which will eventually appear in (8.11) are negligible as they enter at higher order. Therefore, we will ignore them altogether. Now we have all the elements needed to evaluate the integral of the function U.

8.2.3 Integrations across a point

It is rather common to see these sort of integrations, particularly when abrupt steps in the coefficients of the integrated equation appear. To explain how to deal with them let us take the model equation

$$\frac{d}{dr}\left(a_1\frac{df}{dr}\right) + a_2f + \lambda = 0,$$

where r varies from 0 to 1 with r_0 some position within this interval and a_i are regular functions of r which are continuous and different from zero. We take $\lambda(r) = \delta(r - r_0)$ and integrate this equation once yielding

$$a_1f' + F(r) = 0,$$

where $F(r) = \int_0^r (a_2(\varrho)f(\varrho) + \delta(\varrho - r_0)) d\varrho$. It is obvious that if f is non-diverging (i.e. an integral of f exists), then the function F is discontinuous at most at r_0 . Dividing the expression above by a_1 , which is supposed to be non-vanishing, a further integration shows that

$$f + \int_{-\pi}^{\pi} \frac{F(\varrho)}{a_1(\varrho)} d\varrho = const.$$

The continuity of f across r_0 is evident. Note that if $\lambda(r) = \delta'(r - r_0)$, then f becomes discontinuous.

8.3 Evaluation of $\int_0^{r_s} r U_{TC} dr$

In U_{TC} it is more convenient to split individually the contributions from the m-1=0 and m+1=2 harmonics. This is written as $U_{TC}=U_{TC}^{(0)}+U_{TC}^{(2)}$ with

$$egin{aligned} U_{TC}^{(0)} &= rac{iR_0}{CB_0} \left[ik_{||}C_1^1 + D_1^1 - E_1^1(\hat{p})
ight], \ U_{TC}^{(2)} &= rac{iR_0}{CB_0} \left[ik_{||}C_1^{-1} + D_1^{-1} - E_1^{-1}(\hat{p})
ight]. \end{aligned}$$

We shall analyse the contribution from $U_{TC}^{(2)}$ first. A rather tedious algebraic manipulation shows that

$$rU_{TC}^{(2)} = \frac{R_0}{C} \left[\left(l_1 l_2 N_{-1} \frac{d\xi_2^r}{dr} \right)' + T_{12} \frac{d\xi_2^r}{dr} + U_{12} \xi_2^r \right], \tag{8.22}$$

where

$$T_{12} = N_{-1} \left(l_1 l_2' - l_1' l_2 \right) - 3i M_{-1} l_1 l_2 - \frac{n}{2} \frac{r^2 p_0'}{\mu B_0^2},$$

$$U_{12} = l_1 \left(N_{-1} l_2' \right)' - 3i l_1 l_2' M_{-1} - 2l_1 l_2 \left(L_{-1} + i M_{-1}' \right)$$

$$- \frac{r p_0'}{\mu B_0^2} (2\mu - \frac{n}{2}) + l_1 \left(\frac{r p_0'}{\mu B_0^2} \right)',$$

having used (8.12) and (8.14). Note that the terms proportional to the pressure originate from D_1^{-1} and E_1^{-1} . The following relation holds (recall that ζ is given by (8.16)):

$$\begin{split} T_{12}' - U_{12} &= -l_2 \left[(N_{-1}l_1' + iM_{-1}l_1)' - 2(L_1l_1 - iM_{-1}l_1') + r^2 \left(\frac{p_0'}{r\mu B_0^2} \right)' \right] \\ &= \frac{r}{2iB_0C} \left[i(2\mu - n)C_2^1 + D_2^1 - E_2^1(\hat{p}) \right] \\ &= \frac{1}{R_0} \left[\frac{d}{dr} \left(r^3 \left[\mu - \frac{n}{2} \right]^2 \frac{d\zeta}{dr} \right) - 3r \left[\mu - \frac{n}{2} \right]^2 \zeta \right] \equiv \frac{1}{R_0} \mathfrak{L}(\zeta), \end{split}$$

where in obtaining the last line we compared with the right-hand-side of Eq. (8.17). Note that the relation above defines implicitly the operator \mathfrak{L}^{12} Therefore, integrating (8.22) by parts from 0 to $r_s - \epsilon$ with $\epsilon \to 0$ and exploiting (8.18) yields

$$\begin{split} \int_{0}^{r_{s}-\epsilon} r U_{TC}^{(2)} dr &= \frac{R_{0}}{C} \left[\left(T_{12} \xi_{2}^{r} \right) \Big|_{0}^{r_{s}-\epsilon} - \int_{0}^{r_{s}-\epsilon} \left(T_{12}^{\prime} - U_{12} \right) \xi_{2}^{r} dr \right] \\ &= \frac{R_{0}}{C} \left[\left(T_{12} \xi_{2}^{r} \right) \Big|_{r_{s}-\epsilon} - \frac{1}{R_{0}} \int_{0}^{r_{s}-\epsilon} \mathfrak{L}(\zeta) \xi_{2}^{r} dr \right] \\ &= \left[R_{0} T_{12} \frac{\xi_{2}^{r}}{C} - \frac{n^{2} r^{3}}{4} \left(\zeta^{\prime} \frac{\xi_{2}^{r}}{C} - \zeta \frac{(\xi_{2}^{r})^{\prime}}{C} \right) \right]_{r_{s}-\epsilon} - \int_{0}^{r_{s}-\epsilon} \zeta \mathfrak{L}(\zeta) dr. \end{split}$$

From equation (8.21) we write

$$\frac{\xi_2^r}{C}\Big|_{r_s-\epsilon} = \zeta_s + \nu, \quad \frac{(\xi_2^r)'}{C}\Big|_{r_s-\epsilon} = \zeta_s' + \frac{\nu}{r_s}(1+4b),$$

where the subscript s means that the quantity is evaluated at r_s , and ν reads

$$\nu = \frac{r_s}{R_0} \left(\frac{-^3/4 + c[^3/4 + \hat{s} + \beta_p(r_s)]}{1 + b - c} \right).$$

Expressing T_{12} as a function of ζ gives

$$T_{12}\Big|_{r_s} = \frac{n^2 r_s^2}{4R_0} \left(r_s \zeta_s' + 3\zeta_s - \frac{3r_s}{R_0} \right),$$

so that one readily has

$$\begin{split} \int_{0}^{r_{s}-\epsilon} r U_{TC}^{(2)} dr &= \frac{n^{2} r_{s}^{2}}{4} \left[3 \left(\zeta_{s} + \nu \right) \left(\zeta_{s} - \frac{r_{s}}{R_{0}} \right) + \nu \zeta_{s} \left(1 + 4b \right) \right] \\ &+ \int_{0}^{r_{s}-\epsilon} \left[r l_{2}^{2} \zeta'^{2} + 3 \frac{l_{2}^{2}}{r} \zeta^{2} \right] dr. \end{split} \tag{8.23}$$

¹² Equation (8.18) can be written as $\mathfrak{L}(\xi_2^r) = C\mathfrak{L}(\zeta)$ for $r < r_s$.

We now focus on $U_{TC}^{(0)}$. Since $\hat{p}_0 = -p_0'\xi_0^r = 0$, it then follows that $E_1^1(\hat{p}) = 0$. Therefore, by means of (7.53) and (7.62) it is possible to show that

$$rU_{TC}^{(0)} = -\frac{R_0}{CB_0} \left[l_1 (N_1 Y_0)' - i l_1 M_1 Y_0 - \frac{r p_0'}{\mu B_0^2} Y_0 \right]$$

$$= -\frac{R_0}{CB_0} (l_1 N_1 Y_0)' + \frac{R_0}{CB_0} \left[l_1' N_1 + i l_1 M_1 + \frac{r p_0'}{\mu B_0^2} \right] Y_0. \tag{8.24}$$

where Y_0 is given by (8.13). Thus, we have

$$\int_{0}^{r_{s}-\epsilon} r U_{TC}^{(0)} dr = R_{0}^{2} \int_{0}^{r_{s}-\epsilon} \left[l_{1}' N_{1} + i l_{1} M_{1} + \frac{r p_{0}'}{\mu B_{0}^{2}} \right]^{2} \frac{dr}{r}$$

$$= \int_{0}^{r_{s}-\epsilon} r^{3} \left[\frac{n}{2} \left(\zeta' + \frac{3}{r} \zeta - \frac{1}{R_{0}} \right) - \frac{\mu}{R_{0}} \right]^{2} dr, \qquad (8.25)$$

where we exploited the fact that the integration is carried out for $r < r_s$. Therefore, collating (8.23) and (8.25), we eventually obtain

$$\int_{0}^{r_{s}-\epsilon} r U_{TC} dr = \frac{n^{2} r_{s}^{2}}{4} \left[3 \left(\zeta_{s} + \nu \right) \left(\zeta_{s} - \frac{r_{s}}{R_{0}} \right) + \nu \zeta_{s} \left(1 + 4b \right) \right]$$

$$+ \int_{0}^{r_{s}} \left[r l_{2}^{2} \zeta'^{2} + 3 \frac{l_{2}^{2}}{r} \zeta^{2} + r^{3} \left[\frac{n}{2} \left(\zeta' + \frac{3}{r} \zeta - \frac{1}{R_{0}} \right) - \frac{\mu}{R_{0}} \right]^{2} \right] dr.$$
(8.26)

We may let $\epsilon = 0$ in the integral on the right hand side. ¹³ It only remains to evaluate the integral of U_0 . This is discussed in the next section.

Integrals involving the function U_0

The evaluation of the integral of the function U_0 given by (8.4) is a tedious and rather straightforward procedure, which nevertheless requires several mathematical steps. We shall carefully go through each of them in order to make the algebra more transparent.

The strategy for tackling this problem is to write U_0 as a sum of a cylindrical (U_{0c}) and a toroidal (U_{0t}) contribution such that $U_0 = U_{0c}$ + U_{0t} . Let us start by writing

$$\langle L \rangle = \frac{1}{rR_0} (1 + \mathcal{L}), \quad \langle N \rangle = \frac{r}{R_0} (1 + \mathcal{N}),$$

where $\mathcal{L}, \mathcal{N} \sim \varepsilon^2$ and their expressions are obtained from (5.24) and (5.25) reading

$$\mathcal{L} = \frac{9}{4} \frac{r^2}{R_0^2} + 4 \frac{r\Delta'}{R_0} + \frac{\Delta}{R_0} + 2\Delta'^2 + \frac{r^2}{2} \Delta''^2 + \frac{r^2}{R_0} \Delta'' + r\Delta'\Delta'',$$

$$\mathcal{N} = \frac{\Delta'^2}{2} + \frac{3r^2}{4R_0^2} + \frac{\Delta}{R_0}.$$

¹³ This is because there is no domain ambiguity of the quantities under the sign of integration.

Furthermore, we exploit the choice of the parametrisation in chapter 5 for which one has $G = R_0/r$. From this it follows that $f_0'/r = F/R_0$ where F is given by (4.31) and its expression is the same in both cylindrical and toroidal geometry. Hence, by means of (7.67) with m = 1, we obtain

$$\frac{f_0'}{r}\langle\frac{J_0^\phi}{B_0^\phi}\rangle' = \left(\frac{f_0'}{r}\langle\frac{J_0^\phi}{B_0^\phi}\rangle'\right)_{cyl} + \frac{B_0}{R_0}\left[\frac{1}{r}\left(r^2\mu\mathcal{N}\right)'\right]',$$

where the subscript cyl indicates the cylindrical part. A fairly straightforward manipulation shows that the cylindrical and toroidal contributions to U_0 are given, respectively, by

$$U_{0c} = \frac{r\hat{k}_{||}}{B_0^2} \left[\frac{1}{r} \left(\frac{r(r\hat{k}_{||})'}{1+h} \right)' - \frac{\hat{k}_{||}}{r} - R_0 \left(\frac{f_0'}{r} \left\langle \frac{J_0^{\phi}}{B_0^{\phi}} \right\rangle' \right)_{cyl} \right] + \frac{R_0}{B_0} \left[\frac{P^2}{R_0 B_0} + n\mu' \frac{r^2}{R_0^2} P - nrk_{||} \left(\frac{rP}{R_0^2} \right)' + p_0' \frac{R_0^2 F'}{F^2} \right], \tag{8.27}$$

$$U_{0t} = \frac{l_1}{r} \left(r \mathcal{N} l_1' \right)' - \frac{l_1^2}{r^2} \mathcal{L} - l_1 \left[\frac{1}{r} \left(r^2 \mu \mathcal{N} \right)' \right]' - \frac{p_0'}{B_0^2} \langle R^2 \rangle'.$$
 (8.28)

A quick comparison of (7.65), (8.3) and (8.27) with (D.2) and (D.8) shows that we can approximate¹⁴

$$U_{0c} \approx -n^2 \left[\frac{2r p_0'}{B_0^2} - \frac{r^2}{R_0^2} (\mu - n) (\mu + 3n) \right]. \tag{8.29}$$

We now write

$$U_0 = \left(1 - \frac{1}{n^2}\right) U_{0c} + \left(\frac{U_{0c}}{n^2} + U_{0t}\right). \tag{8.30}$$

The computation of the last term in brackets in the equation above concludes the analysis of the stability of the m=1 internal kink mode. This requires few manipulations which will be explained below step-by-step.

First define the integral quantity

$$W = \int_0^{r_s - \epsilon} r \left(\frac{U_{0c}}{n^2} + U_{0t} \right) dr.$$

A little rearrangement shows that (8.28) can be recast as

$$U_{0t} = \left[\mathcal{N} - \mathcal{L} - r \left(r \mathcal{N}' \right)' \right] \frac{l_1^2}{r^2} - l_1 l_1' \mathcal{N}' - n l_1 \left(3 \mathcal{N}' + r \mathcal{N}'' \right) - \frac{p_0'}{B_0^2} \langle R^2 \rangle',$$

and thus, by using (5.21), we can write

$$W = \int_{0}^{r_{s}} dr \left[\frac{r^{3}}{R_{0}^{2}} (\mu - n) (\mu + 3n) - n \frac{l_{1}}{r} \left(r^{3} \mathcal{N}' \right)' + \left[\mathcal{N} - \mathcal{L} - \frac{r}{2} (r \mathcal{N}')' \right] \frac{l_{1}^{2}}{r} + r^{2} R_{0} \frac{p_{0}'}{R_{0}^{2}} \left(\Delta'' + \frac{3\Delta'}{r} - \frac{1}{R_{0}} \right) \right], \quad (8.31)$$

We use the relation $\mu = \frac{l_1}{r} + n$ to express μ' and μ'' as a function of l_1 . Moreover, one has

$$l_1 l_1' \mathcal{N}' = \frac{(r l_1^2 \mathcal{N}')'}{2r} - r \left(r \mathcal{N}'\right)' \frac{l_1^2}{2r^2}.$$

¹⁴ The cylindrical approximation for the safety factor $q = \frac{rB_z}{R_0 \bar{B}_p}$ has been used.

having dropped the infinitesimal quantity ϵ as we did in (8.26).¹⁵ We now express the coefficients appearing in the integral above as a function of ζ (see (8.16)) by means of the following relations:

$$\begin{split} \left(r^{3}\mathcal{N}'\right)' &= \left[\frac{5r^{4}}{4R_{0}^{2}} + \frac{r^{3}\zeta}{2R_{0}} - \frac{r^{4}\zeta'}{2R_{0}} + r^{3}\zeta\zeta'\right]', \\ r\left[\mathcal{N} - \mathcal{L} - \frac{r}{2}(r\mathcal{N}')'\right] &= -\frac{r^{3}}{R_{0}^{2}} - \frac{3(r^{3}\zeta)'}{4R_{0}} + \frac{(r^{4}\zeta')'}{4R_{0}} \\ &- \frac{3}{2}r\zeta^{2} - \frac{r^{3}}{2}\zeta'^{2} - \frac{1}{2}\left(r^{3}\zeta\zeta'\right)', \\ r^{2}R_{0}\frac{p_{0}'}{B_{0}^{2}}\left(\Delta'' + \frac{3\Delta'}{r} - \frac{1}{R_{0}}\right) &= -\frac{r^{3}\mu^{2}}{2}\left(\zeta' + \frac{3\zeta}{r} - \frac{3}{R_{0}}\right)^{2} \\ &- r^{3}\mu\mu'\left(\zeta - \frac{r}{2R_{0}}\right)\left(\zeta' + \frac{3\zeta}{r} - \frac{3}{R_{0}}\right). \end{split}$$

Plugging these formulae into (8.31) yields

$$\begin{split} W &= \int_{0}^{r_{s}} dr \left[n(n-\mu) \left(\frac{r^{4}}{4R_{0}^{2}} + \frac{r^{3}\zeta}{2R_{0}} - \frac{r^{4}\zeta'}{2R_{0}} + r^{3}\zeta\zeta' \right)' \right. \\ &+ \left(\frac{(r^{4}\zeta')'}{4R_{0}} - \frac{3(r^{3}\zeta)'}{4R_{0}} - \frac{3}{2}r\zeta^{2} - \frac{r^{3}}{2}\zeta'^{2} - \frac{1}{2}(r^{3}\zeta\zeta')' \right) \frac{l_{1}^{2}}{r^{2}} \\ &- \frac{r^{3}\mu^{2}}{2} \left(\zeta' + \frac{3\zeta}{r} - \frac{3}{R_{0}} \right)^{2} - r^{3}\mu\mu' \left(\zeta - \frac{r}{2R_{0}} \right) \left(\zeta' + \frac{3\zeta}{r} - \frac{3}{R_{0}} \right) \right]. \end{split}$$
(8.32)

Although (8.32) appears complicated, this equation can be greatly simplified by some integrations by parts and using the following relation

$$\left(\frac{3}{2}r\zeta^{2} + \frac{r^{3}}{2}\zeta'^{2}\right)\frac{l_{1}^{2}}{r^{2}} + \frac{r^{3}\mu^{2}}{2}\left(\zeta' + \frac{3\zeta}{r} - \frac{3}{R_{0}}\right)^{2}$$

$$= 3\frac{l_{2}^{2}}{r}\zeta^{2} + rl_{2}^{2}\zeta'^{2} + r^{3}\frac{n^{2}}{4}\left(\zeta' + \frac{3\zeta}{r}\right)^{2} + \frac{3n^{2}}{4}(r^{2}\zeta^{2})'$$

$$- 3r^{2}\mu\mu'\zeta^{2} + \frac{r^{3}\mu^{2}}{2}\left[\frac{9}{R_{0}^{2}} - \frac{6}{R_{0}}\left(\zeta' + \frac{3\zeta}{r}\right)\right]$$

$$+ \frac{3}{2}\left[r^{2}\left(\mu^{2} - n^{2}\right)\zeta^{2}\right]'.$$

Therefore, with some straightforward manipulations, one has

$$\begin{split} W &= \int_0^{r_s} dr \left[n(n-\mu) \frac{r^3}{R_0^2} + \frac{(r^3 \zeta)'}{4R_0} \left(9\mu^2 + 4n\mu - n^2 \right) - r l_2^2 \zeta'^2 - 3 \frac{l_2^2}{r} \zeta^2 \right. \\ &- r^3 \frac{n^2}{4} \left(\zeta' + \frac{3\zeta}{r} \right)^2 - \frac{3n^2}{4} (r^2 \zeta^2)' - \frac{9r^3}{2R_0^2} \mu^2 + r^3 \mu \mu' \left(\frac{9\zeta}{2R_0} - \frac{3r}{2R_0^2} \right) \right]. \end{split}$$

 15 No ambiguities appear so that the integration can be carried up to r_s without concerns

The two relations below prove to be very useful:

$$\begin{split} \int_0^{r_s} dr \left(n \frac{l_1}{r} + \frac{l_1^2}{2r^2} \right) \frac{(r^4 \zeta')'}{2R_0} \\ &= - \int_0^{r_s} dr \mu \mu' \frac{r^4 \zeta'}{2R_0}, \\ \int_0^{r_s} dr \left(n \frac{l_1}{r} + \frac{l_1^2}{2r^2} \right) (r^3 \zeta \zeta')' \\ &= - \int_0^{r_s} dr \mu \mu' r^3 \zeta \zeta'. \end{split}$$

Note that $\zeta' + 3\zeta/r = (r^3\zeta)'/r^3$.

Since $\mu\mu' = (\mu^2)'/2$, the last term in the expression above can be integrated by parts, and rearranging we get

$$\begin{split} W &= -\frac{3n^2}{4} r_s^2 \zeta_s^2 + \frac{9n^2}{4} \frac{r_s^3}{R_0} \zeta_s - \frac{3n^2}{4} \frac{r_s^4}{R_0^2} - \int_0^{r_s} \left[\frac{3n^2}{4R_0} \left((r^3 \zeta)' - \frac{r^3}{R_0} \right) \right. \\ &+ \left. r^3 \left[\frac{n}{2} \left(\zeta' + \frac{3\zeta}{r} \right) - \frac{\mu + n/2}{R_0} \right]^2 + \frac{r^3}{2R_0^2} (\mu^2 - n^2) + r l_2^2 \zeta'^2 + 3 \frac{l_2^2}{r} \zeta^2 \right] dr. \end{split}$$

The calculation is almost over. By means of (4.37) we can write

$$\frac{1}{2} \int_0^{r_s} dr \frac{r^3}{R_0^2} (\mu^2 - n^2) = \frac{n^2 r_s^4}{2R_0^2} \hat{s}, \tag{8.33}$$

and carrying out the obvious integrations we finally have

$$W = -\frac{3}{4}n^{2}r_{s}^{2}\left(\zeta_{s} - \frac{r_{s}}{2R_{0}}\right)\left(\zeta_{s} - \frac{3r_{s}}{2R_{0}}\right) - \frac{r_{s}^{4}}{2R_{0}^{2}}n^{2}\hat{s}$$

$$-\int_{0}^{r_{s}}\left[rl_{2}^{2}\zeta'^{2} + 3\frac{l_{2}^{2}}{r}\zeta^{2} + r^{3}\left[\frac{n}{2}\left(\zeta' + \frac{3\zeta}{r}\right) - \frac{\mu + n/2}{R_{0}}\right]^{2}\right]dr. \quad (8.34)$$

This concludes the analysis of the integrals appearing in (8.11). The stability of the m=1 internal kink mode can be fully determined by the results contained in equations (8.26) and (8.34). Its discussion is the aim of the next section.

8.5 The stability criterion

By means of (8.30), we are finally able to express the integral in (8.11) as

$$\int_{0}^{r_{s}-\epsilon} rU dr = \left(1 - \frac{1}{n^{2}}\right) \int_{0}^{r_{s}} rU_{0c} dr + \int_{0}^{r_{s}-\epsilon} r\left(\frac{U_{0c}}{n^{2}} + U_{0t} + U_{TC}\right) dr,$$
(8.35)

where U_{0c} in the first integral is obtained from (8.29). If (8.35) is positive instability occurs, whereas stability is achieved when the total integral is negative (cf. (8.11)). Before discussing the full toroidal result, we highlight some properties of the m = n = 1 internal kink mode in a cylinder. In such a geometry $U_{0t} = U_{TC} = 0$, so that the stability is determined by U_{0c} only. Inspecting equation (8.29), it is immediate to see that for any decreasing pressure profile with q < 1 over $0 < r < r_s$ where r_s is some position within the plasma, the integral of U_{0c} is positive. This leads to the conclusion that as long as there is a q = 1 resonance in the plasma the internal kink in a cylinder is always unstable for a monotonically decreasing pressure profile.

We now show that the inclusion of toroidicity opens a window of stability at low pressure. With n generic, plugging (8.26) and (8.34)

That is $p_0' < 0$ and $\mu(0) > 1$.

into (8.35) and writing $\zeta_s = r_s [\beta_p(r_s) + \hat{s} + 3/4]/R_0$ gives the following expression

$$\int_0^{r_s - \epsilon} r U dr = \left(1 - \frac{1}{n^2}\right) \int_0^{r_s} r U_{0c} dr - n^2 \frac{r_s^4}{R_0^2} \delta W_T, \tag{8.36}$$

$$\delta W_T = \frac{8\hat{s}(1+b-c) + 9b(1-c) - 24bc(\beta_p + \hat{s}) - 16c(1+b)(\beta_p + \hat{s})^2}{16(1+b-c)},$$
(8.37)

having employed, for the sake of simplicity, the short hand notation $\beta_b \equiv$ $\beta_p(r_s)$. Letting n=1, the system is stable against the m=1 internal kink mode when $\delta W_T > 0$. This is the so called **Bussac stability criterion**. In general, for $n \neq 1$, it is found that δW_T is numerically smaller compared to the integral involving U_{0c} , so that the stability of modes with n > 1can be described fairly well in cylindrical approximation. In tokamak experiments, however, it is unlikely to have q(0) below 0.7, so that only perturbations with n = 1 turn out to be relevant.

It can be recognised that since the coefficients b, c and \hat{s} depend solely on the current profile distribution (that is the safety factor profile) a critical value of β_p above which the internal kink is unstable may be identified. An example of the numerically computed critical values of $\beta_p(r_s)$ for a q profile of the form

$$q = q_0 \frac{r^2}{\int_0^r 2r(1 - (r/a)^{\nu_1})^{\nu_2} dr}$$
 (8.38)

is shown in figure 8.5 (this corresponds to a current profile $J^{\phi} \propto (1 (r/a)^{\nu_1})^{\nu_2}$). One sees that, contrarily to the cylindrical case, the toroidal internal kink mode is stable for sufficiently low values of β_p .

Unfortunately, although (8.37) is general, it is not of easy interpretation. A simplified stability criterion, and the associated critical β_b , can be obtained for safety factor profiles of the form

$$q = 1 - \Delta q \left[1 - \left(\frac{r}{r_s} \right)^2 \right], \tag{8.39}$$

with $\Delta q \ll 1$ small enough so that there is no q=2 surface within the plasma. Let the functions X_2^i and X_2^e obey the homogeneous equation (8.18). Upon writing

$$X_2^i = x_i + y_i, \quad X_2^e = x_e + y_e$$

with $y_i/x_i \sim y_e/x_e \sim \Delta q$, we set C=0 and expand (8.18) for small Δq with the safety factor given by (8.39). For X_2^i this yields

$$\frac{d}{dr}\left(r^3\frac{dx_i}{dr}\right) - 3rx_i = 0,$$

$$\frac{d}{dr}\left(r^3\frac{dy_i}{dr}\right) - 3ry_i - \frac{4\Delta q}{r_s^2}\left[\frac{d}{dr}\left(r^5\frac{dx_i}{dr}\right) - 3r^3x_i = 0\right].$$

Here we used (4.35) and (4.37) to express all equilibrium quantities as function of β_p and \hat{s} with the latter being defined in section 8.2.2.

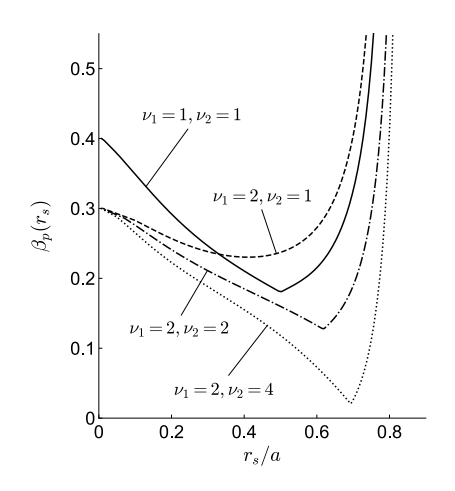


Figure 8.5: Critical β_p versus the position of the q = 1 resonance from Eq. (8.37). The coefficients *b* and *c* have been obtained by solving numerically the homogeneous equation (8.18) with a safety factor of the form (8.38) (Bussac (1975)). Instability occurs for β_b above the corresponding curve. r_s is modified by varying the value of q on axis.

The same applies to X_2^e with the obvious substitutions. It follows that the leading order solutions satisfying the conditions at the magnetic axis and at the plasma boundary are

$$x_i \propto r$$
, $x_e \propto (a/r)^3 - r/a$.

Thus, it is quite easy to see that to first order in Δq one has

$$\begin{split} X_2^i &\propto \frac{r}{r_s} + \frac{2}{3} \Delta q \left(\frac{r}{r_s}\right)^3, \\ X_2^e &\propto \frac{a^3}{r^3} - \frac{r}{a} + \Delta q \left(6\left(\frac{a}{r_s}\right)^3 \frac{r_s}{r} - \frac{2}{3} \frac{r_s}{a} \left(\frac{r}{r_s}\right)^3\right) - \frac{16}{3} \Delta q \left(\frac{a}{r_s}\right)^2 \frac{r}{a}. \end{split}$$

The computation of the parameter b is immediate and gives $b = \Delta q/3$. The quantity c is obtained by expanding $[r(X_2^e)'/X_2^e]_{r_s}$ to first order in Δq so that for sufficiently small r_s/a one has $c \approx 3\Delta q - (r_s/a)^4$. Finally, by means of (8.33) it is straightforward to see that $\hat{s} \approx \Delta q/6$. Plugging these results into (8.37), and neglecting the term $(r_s/a)^4$ in c gives the following **stability criterion**

$$(1 - q(0)) \left(\beta_p^2 - \frac{13}{144}\right) < 0. \tag{8.40}$$

Note that within these approximations, the value of the critical pressure is independent of q(0).

It is worth to point out that stabilisation of the m=1 internal kink mode can be achieved in a high-pressure plasma with $\beta_p \sim 1/\varepsilon$ (Krymskii (1979), Crew (1982), Tokuda (1982), Manickam (1984)). This result is not captured by our analysis which has been carried out within the ordering $\beta_p \sim 1$.

On the (im)possibility of global m > 1 internal modes

Let us assume that the safety factor is of the form shown in figure 8.2-(b) and take q > 1. Apply the standard low- β ordering $\beta \sim r\beta' \sim \varepsilon^2$. The leading order of the **eigenmode equation** for a generic fluid displacement X is formally written as (cf. (7.69))

$$\frac{d}{dr}\left[r^3\left(k_{||}^2+\gamma_n^2\right)\frac{dX}{dr}\right]-r(m^2-1)\left(k_{||}^2+\gamma_n^2\right)X=0,$$

with $\gamma_n^2 = \gamma^2 (1 + 2q^2)/\omega_A^2$ where a constant mass density profile has been chosen. For the sake of simplicity we assume that X is a real valued function. We let $k_{||} \sim m \sim 1$, i.e. we consider global modes. After multiplying the equation above by X and integrating from 0 to a with the boundary condition X(a) = 0 we obtain

$$\gamma_n^2 = -\frac{\int_0^a dr [r^3k_{||}^2|X'|^2 + r(m^2-1)k_{||}^2|X|^2]}{\int_0^a dr [r^3|X'|^2 + r(m^2-1)|X|^2]}.$$

The solution of the equation for y_i and y_e can be found either by applying the method of variation constants or expanding $y = Ar^{\alpha} + Br^{\beta}$.

The right-hand-side is negative (and of the order of unity) indicating stability. This shows that no **global internal** modes with m > 1 are allowed with a monotonic safety factor of the form of Fig. 8.2-(b) and $k_{||} \sim 1$, that is a magnetic shear of order unity, within the low- β ordering. However, if q has a different shape (i.e. $k_{||}$ is ordered differently), or the mode is strongly localised with $m \gg 1$, instabilities with m > 1 can occur (this will be discussed in the next chapters).

8.6 The m=1 internal kink with a hollow q

Configurations with a **non-monotonic** (or **hollow**) *q* profile above unity, having a small or weakly reversed magnetic shear in the core region, are part of the family of the so called **hybrid scenarios**. Although the absence of the q = 1 surface makes them intrinsically sawteeth-free, MHD activity is still observed experimentally. In particular, these scenarios can be affected by m = n = 1 activity which, similar to sawtooth oscillations, can either induce a severe deconfinement of the population of fast particles which are needed to provide the necessary heating power to sustain the fusion reactions (see chapter 1), or lead to a plasma collapse by driving secondary instabilities (or both).

In this section we show how an internal perturbation with mode numbers m = n = 1 can develop even without the presence of a resonant q = 1 surface when the safety factor is hollow and its minimum remains sufficiently close to 1.

Let us consider a safety factor profile as the one depicted in figure 8.6 with its minimum value q_{min} close to 1. The radius r_s is such that $q(r_s) =$ q_{min} . We further assume that the difference between q on axis (q_0) and q_{min} is of order of unity. Following the same steps outlined in (8.1.1) it is easy to see that for n = 1

$$-i\frac{R_0}{B_0}\sum_{m'=+1}E_1^{m'}(\Delta p)=\frac{2\gamma^2}{\omega_A^2}\times\frac{1}{r}\frac{d}{dr}\left(r^3\frac{d\xi_1^r}{dr}\right).$$

Then, the full eigenmode equation for the m = n = 1 internal kink mode is

$$\frac{1}{r}\frac{d}{dr}\left[r^3\left(\frac{1+\mathscr{N}}{1+h}\frac{\hat{k}_{||}^2}{B_0^2}+3\frac{\gamma^2}{\omega_A^2}\right)\frac{d\xi_1^r}{dr}\right]+U_0\xi_1^r+\hat{U}_{TC}=0,\tag{8.41}$$

where U_0 is given by (8.4), and from (8.5) we defined

$$\hat{U}_{TC} = CU_{TC} = \frac{iR_0}{B_0} \sum_{m'=+1} \left[ik_{||} C_1^{m'} + D_1^{m'} - E_1^{m'}(\hat{p}) \right].$$

We consider cases with $0 < \gamma/\omega_A \ll 1$. Since γ is a small number and $k_{||}$ becomes of the order ε when r_s is approached, the leading order solution These configurations are envisaged to be a candidate scenario for continuous tokamak operation. This is because of the high fraction of non inductively generated current and global good confinement.

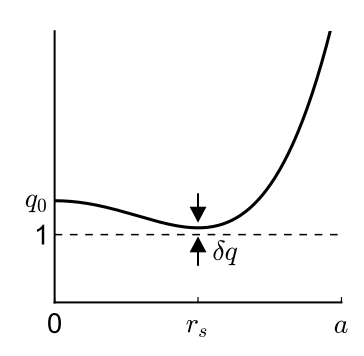


Figure 8.6: Example of an experimentally relevant inverted q profile. Here q_0 denotes the value of the safety factor on the magnetic axis. Note that as the current is increased, q drops and its minimum may dangerously lie close to one.

of equation (8.41) is still given by (8.2). It is easy to convince ourselves that small corrections due to $\mathcal N$ and h in the first term of (8.41) can be dropped. Hence, we let $\mathcal N, h \to 0$ and also approximate $\hat k_{||}/B_0 \approx k_{||}$.

We now multiply (8.41) by $r\xi_1^r$ and integrate from 0 to a. This gives

$$\int_0^a r^3 \left(k_{||}^2 + 3 \frac{\gamma^2}{\omega_A^2} \right) \left| \frac{d\xi_1^r}{dr} \right|^2 dr = \int_0^a r \left(U_0 |\xi_1^r|^2 + \hat{U}_{TC} \xi_1^r \right) dr. \tag{8.42}$$

Let us analyse the right-hand-side first. It is immediate to see that for $r > r_s$ the contribution to the integral due to the term containing U_0 is negligible. Upon defining

$$\hat{U}_{TC}^{(0)} = CU_{TC}^{(0)}$$
, and $\hat{U}_{TC}^{(2)} = CU_{TC}^{(2)}$

a simple inspection of Eqs. (8.13), (8.22) and (8.24) with some integrations by parts shows that

$$\int_0^a r \hat{U}_{TC} \xi_1^r dr \approx C^2 \int_0^{r_s} r (U_{TC}^{(0)} + U_{TC}^{(2)}) dr.$$

Now, because of the step-like nature of the leading order of the radial displacement, we expect that contributions to the left-hand-side of (8.42) should come only from a region close to r_s where ξ_1^r has large gradients. We can therefore approximate the function under the integral sign with its local behaviour close to r_s . Thus, integrating (8.41) from 0 to a radius sufficiently close to r_s gives

$$rac{d \xi_1^r}{d r} pprox - rac{C \int_0^{r_s} r \left(U_0 + U_{TC}
ight) d r}{r_s^3 (k_{||}^2 + 3 rac{\gamma^2}{\omega_A^2})},$$

having exploited the fact that to leading order ξ_1^r is given by (8.2). Using these results, (8.42) transforms into

$$\int_{0}^{a} \frac{\int_{0}^{r_{s}} r(U_{0} + U_{TC}) dr}{r_{s}^{3} \left(k_{||}^{2} + 3\frac{\gamma^{2}}{\omega_{A}^{2}}\right)} dr = 1.$$

With some simple rearrangements, and introducing the variable $z = \omega_A(r - r_s)/(r_s\sqrt{3}\gamma)$ with $\gamma > 0$ the equation above reads

$$\sqrt{3} \frac{\gamma}{\omega_A} \left[\int_{-\infty}^{\infty} \frac{dz}{1 + \omega_A^2 k_{||}^2 / (3\gamma^2)} \right]^{-1} = -\frac{r_s^2}{R_0^2} \delta W_T.$$
 (8.43)

having used (8.36) with δW_T given by (8.37). Near r_s we may expand $k_{||}$ as

$$\frac{k_{||}}{\sqrt{3}\gamma/\omega_A} = \frac{\mu_s - 1}{\sqrt{3}\gamma/\omega_A} + r_s \mu_s' z + \frac{\sqrt{3}}{2} \frac{\gamma}{\omega_A} r_s^2 \mu_s'' z^2 + \dots,$$

Note that ξ_2^r is discontinuous at the q=2 resonance, if this exists within the plasma, where $l_2=0$. Moreover, $l_1\sim \varepsilon$ at r_s .

Note that we allow $k_{||}$ to vary with r.

with the subscript s indicating, as usual, that the quantity must be evaluated at r_s .

When the safety factor is monotonic as the one used in §8.1, we recover the expression of the growth rate given by (8.11) by setting $\mu_s = 1$ and neglecting terms proportional to z^2 or of higher order.

With a non-monotonic safety factor profile instead (cf. figure 8.6), we let $\mu'_s \to 0$ and take $\mu_s < 1$. Thus, the integral on the left-hand-side of (8.43) becomes

$$\int_{-\infty}^{\infty} \frac{dz}{1 + \omega_A^2 k_{||}^2 / (3\gamma^2)} = \int_{-\infty}^{\infty} \frac{dz}{1 + \left(\Delta + \frac{\sqrt{3}}{2} \frac{\gamma}{\omega_A} r_s^2 q_s'' z^2\right)^2}$$

$$= \frac{1}{2i} \int_{-\infty}^{\infty} dz \left(\frac{1}{\Delta + \frac{\sqrt{3}}{2} \frac{\gamma}{\omega_A} r_s^2 q_s'' z^2 - i} - \frac{1}{\Delta + \frac{\sqrt{3}}{2} \frac{\gamma}{\omega_A} r_s^2 q_s'' z^2 + i}\right)$$
(8.44)

where $\Delta = \omega_A (1 - \mu_s)/(\sqrt{3}\gamma) > 0$.

The integrals in the expression above can be evaluated by means of the **residue theorem** accounting for the poles as indicated in Fig. 8.7. This gives

$$\begin{split} \int_{-\infty}^{\infty} \frac{dz}{1 + \omega_A^2 k_{||}^2 / (3\gamma^2)} &= \frac{\pi}{2i\sqrt{A}} \frac{\sqrt{\Delta + i} - \sqrt{\Delta - i}}{\sqrt{1 + \Delta^2}} \\ &= \frac{\pi}{[2A(1 + \Delta^2)(\Delta + \sqrt{1 + \Delta^2})]^{1/2}}, \end{split}$$

with $A = \frac{\sqrt{3}}{2} \frac{\gamma}{\omega_A} r_s^2 q_s^{"}$. By plugging this into (8.43) we finally obtain

$$\frac{r_s\sqrt{q_s''}}{\pi}\bar{\gamma}^{3/2}\left[1+\frac{\delta q}{\bar{\gamma}}\right]^{1/2}=-\frac{r_s^2}{R_0^2}\delta W_T,$$

where $\bar{\gamma}^2 = 3\gamma^2/\omega_A^2 + (\delta q)^2$ having approximated $1 - \mu_s \approx \delta q$. When the safety factor is above unity, the system is stable if $\delta W_T > 0$, while for a given value of $\delta W_T < 0$ instability occurs when $q_{min} < 1 + \delta q_c$. The critical value δq_c which identifies marginal stability is

$$(\delta q_c)^{3/2} = -\frac{\pi r_s}{R_0^2 \sqrt{2q_s''}} \delta W_T.$$

One can extend these findings to negative values of Δ , that is $q_s < 1$, only if the safety factor does not drop too far below 1 such that the separation of the two q = 1 surfaces is not larger than the width of the inertial layer. We stress the point that these results hold as long as $q_0 - q_{min} \sim 1$. When the two values differ only by a small amount, the eigenfunction of the m = 1 harmonic is not given by (8.2) anymore, and a different approach to the stability analysis must be deployed. This case, and its generalisation to perturbations with poloidal and toroidal mode numbers bigger than unity is addressed in the next chapter.

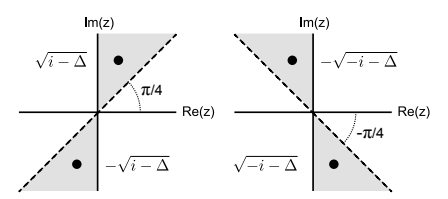


Figure 8.7: The shaded areas indicate the loci of the poles of (8.44) for $\Delta > 0$. Note that we choose the argument of a complex number z = x + iy such that $-\pi < \arg(z) < \pi$ to conform to the negative real axis branch cut, having defined the principal root $\sqrt{z} = \sqrt{|z|}e^{i\arg(z)/2} =$ $\sqrt{\frac{|z|+x}{2}} + i \operatorname{sgn}(y) \sqrt{\frac{|z|-x}{2}}$. Furthermore with $-\infty < \Delta < \infty$ purely real we have $\sqrt{i \pm \Delta} = i\sqrt{-i \mp \Delta}$ and $\sqrt{\Delta + i}\sqrt{\Delta - i} =$ $\sqrt{1+\Delta^2}$.

Defining
$$X = \sqrt{1 + \Delta^2}$$
 we have

$$(X - \Delta)(X + \Delta) = X^2 - \Delta^2 = 1,$$

so that
$$X - \Delta = 1/(X + \Delta)$$
.

The case of two distinct q = 1 resonant surfaces, requires a more convoluted analysis (Hastie (1987), Kuvshinov (1988)) which is not discussed in this report.

References

- M. Abramowitz and I. A. Stegun (eds.), Handbook of Mathematical Functions, Dover Publications (New York, US), 1964.
- M. N. Bussac et al., Phys. Rev. Lett. 35, 1638 (1975).
- G. B. Crew and J. J. Ramos, Phys. Rev. A 26, 1149 (1982).
- A. H. Glasser et al., Phys. Fluids 19, 567 (1976).
- R. J. Hastie et al., Phys. Fluids 30, 1756 (1987).
- A. M. Krymskii and A. B. Mikhailovskii, Fiz. Plazmy 5, 501 (1979) [Sov. J. Plasma Phys. 5, 279 (1979)].
- B. N. Kuvshinov and A. B. Mikhailovskii, Fiz. Plazmy 14, 778 (1988) [Sov. J. Plasma Phys. 14, 457 (1988)].
- J. Manickam, Nucl. Fusion 24, 595 (1984).
- A. B. Mikhailovskii, Reviews of Plasma Physics Vol. 9 p. 1 (Ed. M. A. Leontovich), Consultants Bureau (New York, US), 1986.
- A. B. Mikhailovskii, Instabilities in a Confined Plasma, Institute of Physics Publishing (Bristol, UK), 1998.
- F. Porcelli et al., Plasma Phys. Control. Fusion 38, 2163 (1996).
- M. N. Rosenbluth et al., Phys. Fluids 16, 1894 (1973).
- V. D. Shafranov, Zh. Tekh. Fiz. 40, 241 (1970) [Sov. Phys.-Tech. Phys. 15, 175 (1970)].
- S. Tokuda et al., Nucl. Fusion 22, 661 (1982).
- L. E. Zakharov, Fiz. Plazmy 4, 898 (1978) [Sov. J. Plasma Phys. 4, 503 (1978)].

Infernal modes

Infernal modes are a particular class of internal kink-like perturbations, i.e. helical distortions with a principal poloidal harmonic of helicity say m/n located within the plasma, which can be driven unstable by pressure gradients when the safety factor is flat or the magnetic shear is small over a wide region. The significant reduction of field line bending stabilisation over the broad region of weak magnetic shear (this is due to the first term in (6.19)) allows pressure effects to dominate the dynamics of the perturbation, potentially triggering the instability. The important feature of infernal modes is that, similar to the m=1 internal kink mode with a hollow safety factor, they do not necessarily require an exact q = m/n resonance to occur. An example of safety factor profiles prone to developing infernal modes is given in figure 9.1.

With a flat safety factor over a vast portion of the plasma, even very small pressure gradients can destabilise these perturbations, therefore a careful optimisation of the current and pressure profile must be deployed in order to operate in instability-free conditions. Hence, the aim of this chapter is to describe the driving mechanisms of these perturbations, and to identify the associated (in)stability regions in the appropriate parameter space.

Although infernal modes are more commonly observed in **reversed** shear configurations (an example of a typical ideal MHD perturbation in shear reversed experiments is shown in Fig. 9.2), here we focus primarily on cases in which the safety factor is monotonic and flattened across the whole internal region (cf. profile (a) in Fig. 9.1). Thus, the analysis of the infernal instability is divided into two domains: a core **low-shear** region extending from the magnetic axis to some radius in which the safety factor is flat with with $q \approx m/n$, and an outer **high-shear region**

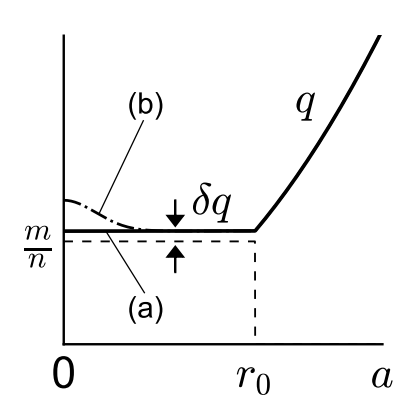
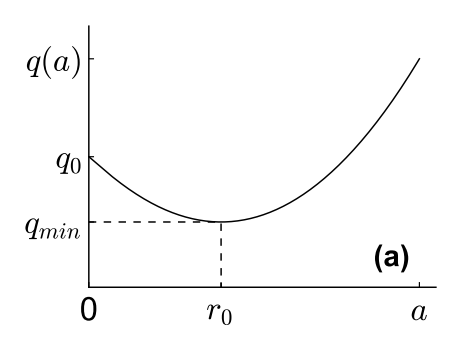


Figure 9.1: Model safety factor profiles, monotonic (solid line, (a)) and weakly reversed (dot-dashed line, (b)), which may be susceptible to infernal modes. Note that these are highly simplified profiles: in experiments the transition of q from flat to sheared at r_0 is smoother.

The m = 1 version of the infernal mode is also known as **quasi-interchange mode**



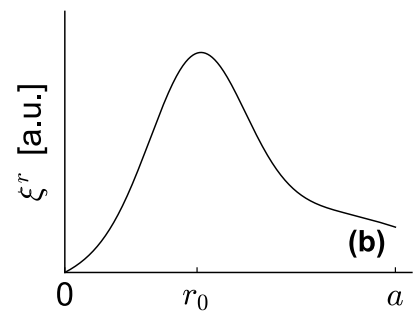


Figure 9.2: Example of experimentally relevant safety factor (a) and fluid fluctuation ξ^r (b) associated with infernal-like perturbations with poloidal mode number m > 1 for $q_{min} > 1$ (see e.g. Manickam (1996), Fredrickson (1996), Okabayashi (1998)).

In the low shear region we still have $\xi^{(0)} \neq 0$.

where the magnetic shear is of order unity. Similar to the analysis of chapter 8, we consider an ideal metallic wall directly interfaced with the plasma, i.e. there is no vacuum gap. We also strictly assume q > 1, so that m = 1 internal kink modes do not develop.

The derivation of the governing equation is carried out separately in the low and high-shear regions by taking the appropriate limiting cases of (7.65) and (7.71). The **dispersion relation**, that is the relation which links growth rate and equilibrium quantities (pressure, current etc.), is then obtained by joining the resulting eigenfunctions at the transition point between low-shear and high-shear regions. To simplify the algebra, we work out the calculations with a highly simplified yet physically relevant pressure profile. These techniques are also applied to address the stability of infernal modes in scenarios with a non-monotonic safety factor. A more detailed analysis of the case when an exact m/n resonance appears in the plasma is briefly discussed at the end of the chapter.

9.1 High-shear region equations

We first examine the region of high shear for which $r\mu' \sim k_{||} \sim 1$, which extends from r_0 to the plasma boundary. We shall consider **global slow-growing modes** for which $\gamma/\omega_A \sim \varepsilon$ (cf. §7.2). Similar to the analysis of the m=1 internal kink mode, we assume that the radial fluid displacement ξ^r can be decomposed in a Fourier series of the form (7.17), that is

$$\xi^{r} = \xi_{m}^{r} e^{i(m\vartheta - n\phi)} + \xi_{m+1}^{r} e^{i[(m+1)\vartheta - n\phi]} + \xi_{m-1}^{r} e^{i[(m-1)\vartheta - n\phi]} + \dots, \tag{9.1}$$

where the sidebands are ordered according to (7.18), i.e. $\xi_{m\pm 1}^r \sim \varepsilon \xi_m^r$, and $m \sim n \sim 1$. Higher order poloidal harmonics are neglected. As usual, we fix the toroidal mode number n (there are no couplings between different n's) and omit to write the subscript n.

According to (7.65) and expansion (9.1), the radial structure of the main mode m is described at leading order by (7.69), whereas sidebands obey equation (7.71). Multiplying (7.69) by ξ_m^r , which is assumed to be a real function of r, and integrating from r_0 to a yields

$$\left(r^{3}k_{||}^{2}\xi_{m}^{r}\frac{d\xi_{m}^{r}}{dr}\right)\Big|_{r_{0}}^{a}-\int_{r_{0}}^{a}\left[r^{3}k_{||}^{2}\left(\frac{d\xi_{m}^{r}}{dr}\right)^{2}+rk_{||}^{2}(m^{2}-1)(\xi_{m}^{r})^{2}\right]dr=0.$$
(9.2)

The ideal conducting wall boundary condition (6.16) dictates $\xi_m^r(a) = 0$. Since $k_{||}(r_0) \sim \varepsilon$ and $k_{||} \sim 1$ for $r_0 < r < a$, the first term in the equation above can be set to zero, and so we are left with an integral of positive definite quantities. Hence, in order for (9.2) to be fulfilled, we must have

$$\xi_m^r = 0$$
, for $r_0 < r < a$. (9.3)

Consequently, because of the vanishing of the dominant harmonic in this region, coupling terms in (7.71) vanish as well. Thence, the sidebands

¹ These can be included if shaping effects, such as elongation and triangularity, are retained.

obey equation

$$\frac{1}{r}\frac{d}{dr}\left(r^{3}[(m\pm 1)\mu - n]^{2}\frac{d\xi_{m\pm 1}^{r}}{dr}\right) - [(m\pm 1)^{2} - 1][(m\pm 1)\mu - n]^{2}\xi_{m\pm 1}^{r} = 0,$$
(9.4)

which is nothing but (7.69) specified for the harmonic $m \pm 1$ instead of m.

Low-shear region equations

In this section we deal with the eigenmode behaviour where q is flattened. Within the low-shear region, we deploy the following ordering

$$\mu' = 0$$
, and $k_{||} = m\mu - n \sim \varepsilon$, (9.5)

and assume that expansion (9.1) still holds. Furthermore, for the sake of simplicity we set $\rho'_0 = 0$. We shall analyse the equations for the sidebands first.

9.2.1 Sidebands

In §7.3 we saw that the contravariant toroidal component of the perturbed magnetic field is ε^2 times smaller than $B_0 \xi_m^r / \sqrt{g}$ (see equation (7.26)). This allows us to write (cf. (7.25))

$$(\sqrt{g}\tilde{B}^{\vartheta})_{\ell} \approx -\frac{1}{i\ell}(\sqrt{g}\tilde{B}^{r})_{\ell}',$$

with $\ell = m, m \pm 1$. Using (7.7) and (9.5) we readily obtain $r(\sqrt{g}\tilde{B}^{\vartheta})_m \sim$ $(\sqrt{g}\tilde{B}^r)_m\sim \varepsilon r B_0 \xi_m^r$. From this, we see that the coefficients $C_{m\pm 1}^{\pm 1}$ and $D_{m\pm 1}^{\pm 1}$ appearing in the equation for the sidebands (7.71) can be neglected: they indeed depend upon the magnetic perturbation of the main mode, and thus are small because $k_{||} \sim \varepsilon$ (cf. (9.5)).

Hence, using the fact that $q \approx m/n$, we obtain

$$\frac{1}{r}\frac{d}{dr}\left(r^3\frac{d\xi^r_{m\pm 1}}{dr}\right) - [(m\pm 1)^2 - 1]\xi^r_{m\pm 1} - i\frac{m^2R_0}{n^2B_0}(m\pm 1)E^{\pm 1}_{m\pm 1}(\hat{p}) = 0. \quad (9.6)$$

Introducing the **ballooning parameter** (see (4.41))

$$\alpha = -\frac{2R_0p_0'q^2}{B_0^2},$$

and making use of Eqs. (7.59) and (7.63),² the equation for the sidebands can be recast in a more compact form as

$$\left[r^{-1\mp 2m} \left(r^{2\pm m} \xi_{m\pm 1}^r\right)'\right]' = \frac{1\pm m}{2} \left[r^{\mp m} \alpha \xi_m^r\right]'. \tag{9.7}$$

As in §8.2, the m-1 and m+1 harmonics are referred to as the **lower** and upper sidebands respectively. We now need an equation for the main mode ξ_m^r . This is derived in the next subsection.

² Recall that $(1/B_0^{\phi})_{\pm 1} = r/R_0$.

With a constant safety factor, we have $\langle \frac{J_0^\phi}{B_0^\phi} \rangle' = 0$ at leading order. Moreover recall that $f_0'/r \approx B_0$ and $\langle N \rangle \approx r/R_0$.

9.2.2 Dominant harmonic

Following the analysis presented in section 7.5.1, the equation for the dominant radial fluid displacement is given by Eq. (7.65). By means of (9.5) and equation (7.55), we may write $P = R_0 p_0'/B_0$. Therefore, using (7.67) we can simplify (7.65) to obtain at leading order

$$\frac{1}{r} \frac{d}{dr} \left[r^{3} \left(k_{||}^{2} + \frac{\gamma^{2}}{\omega_{A}^{2}} \right) \frac{d\xi_{m}^{r}}{dr} \right] - (m^{2} - 1) \left(k_{||}^{2} + \frac{\gamma^{2}}{\omega_{A}^{2}} \right) \xi_{m}^{r}
+ m^{2} \left[\left(\frac{R_{0} p_{0}^{\prime}}{B_{0}^{2}} \right)^{2} - \frac{R_{0} p_{0}^{\prime}}{B_{0}} \left(\frac{\langle R^{2} \rangle^{\prime}}{F} - \frac{\langle R^{2} \rangle F^{\prime}}{F^{2}} \right) \right] \xi_{m}^{r}
+ i m \frac{R_{0}}{B_{0}} \sum_{m^{\prime} \neq 0} \left[D_{m}^{m^{\prime}} - E_{m}^{m^{\prime}}(\hat{p}) - E_{m}^{m^{\prime}}(\Delta p) \right] = 0,$$
(9.8)

where we recall that \hat{p} is defined by (7.59). By employing (7.34) and (7.63) in the limit of small growth rates, the **inertia enhancement** factor is easily computed (cf.section 8.1.1)

$$m\frac{R_0}{B_0} \sum_{m' \neq 0} E_m^{m'}(\Delta p) = i \frac{2m^2 \gamma^2}{n^2 \omega_A^2} \left[\frac{1}{r} \frac{d}{dr} \left(r^3 \frac{d\xi_m^r}{dr} \right) - (m^2 - 1) \xi_m^r \right], \quad (9.9)$$

where we exploited the fact that $q \approx m/n$.

The second line of (9.8) can be simplified by means of (4.31), (4.33) and (5.21) yielding in the limit $s \to 0$

$$F' = \frac{B_0}{q^2} \left(\frac{\alpha}{2} - \frac{2r}{R_0} \right), \quad \langle R^2 \rangle' = -rR_0 \left(\frac{\alpha}{r} + \frac{2}{R_0} \right).$$

This allows us to recast (9.8) as

$$\frac{1}{r}\frac{d}{dr}\left[r^{3}Q\frac{d\xi_{m}^{r}}{dr}\right] + \left[(1-m^{2})Q + \frac{r\alpha}{R_{0}}\left(\frac{n^{2}}{m^{2}} - 1\right) - \frac{\alpha^{2}}{2}\right]\xi_{m}^{r} + i\frac{mR_{0}}{n^{2}B_{0}}\sum_{m'\neq 0}\left[D_{m}^{m'} - E_{m}^{m'}(\hat{p})\right] = 0,$$
(9.10)

where the term Q containing the inertial contribution, namely the growth rate, is given by³

$$Q = \frac{1}{n^2} \left(k_{||}^2 + \frac{\gamma^2}{\omega_A^2} (1 + 2\frac{m^2}{n^2}) \right) \approx \left(\frac{\delta q}{q} \right)^2 + \frac{\gamma^2}{n^2 \omega_A^2} (1 + 2\frac{m^2}{n^2}). \tag{9.11}$$

In the last passage we approximated $q \approx m/n + \delta q$ with $\delta q \ll 1$, conforming to the ordering in (9.5).

For the last term in square brackets on the left-hand-side of Eq. (9.10), a separate treatment is needed depending on whether m=1 or m>1. This is because, as discussed in sections 7.5.2 and 8.2.1, when m=1 the radial displacement of the lower sideband with m-1=0 vanishes and the associated poloidal magnetic perturbation computed from (7.25) exhibits an apparent singularity of the type $\frac{1}{m-1}=\frac{1}{0}$.

³ Note that the higher the q the larger the δq for which $k_{||} \sim \varepsilon$.

Let us analyse the $m \neq 1$ case first. From (7.25) and (7.26) we have

$$(\sqrt{g}\tilde{B}^r)_{m\pm 1} = \pm irB_0 \frac{n}{m} \xi^r_{m\pm 1}, \quad (\sqrt{g}\tilde{B}^{\theta})_{m\pm 1} = -\frac{nB_0}{m(1\pm m)} (r\xi^r_{m\pm 1})'.$$

When these are plugged into $D_m^{m'}$, with the help of (7.59), (8.12) and (8.14) we obtain

$$\sum_{m'\neq 0} \left[D_m^{m'} - E_m^{m'}(\hat{p}) \right] = \frac{i m p_0'}{B_0} \left[\frac{r^{-1-m}}{1+m} \left(r^{2+m} \xi_{m+1}^r \right)' + \frac{r^{-1+m}}{1-m} \left(r^{2-m} \xi_{m-1}^r \right)' \right].$$

Conversely, if m = 1 we follow the same steps employed in §8.2 to show that $\xi_0^r = 0$ while $(\sqrt{g}\tilde{B}^{\vartheta})_0$ is given by (8.13), whose expression at leading order reads

$$(\sqrt{g}\tilde{B}^{\vartheta})_0 = R_0 \frac{mp_0'}{nB_0} \xi_1^r,$$

having taken into account (9.5). Thus, letting $\hat{p}_0 \rightarrow 0$, one has

$$\sum_{m'\neq 0} \left[D_1^{m'} - E_1^{m'}(\hat{p}) \right] = -i \frac{n^2}{4} \frac{B_0}{R_0} \left[\alpha r^{-2} \left(r^3 \xi_2^r \right)' + \alpha^2 \xi_1^r \right].$$

Therefore, we can finally cast equation (0.10) as

$$\begin{split} &\frac{1}{r}\frac{d}{dr}\left[r^{3}Q\frac{d\xi_{m}^{r}}{dr}\right] + \left[(1-m^{2})Q + \frac{r\alpha}{R_{0}}\left(\frac{n^{2}}{m^{2}} - 1\right) - \frac{\alpha^{2}}{2}\right]\xi_{m}^{r} \\ &= \begin{cases} &-\frac{\alpha}{2}\left[\frac{r^{-1-m}}{1+m}\left(r^{2+m}\xi_{m+1}^{r}\right)' + \frac{r^{-1+m}}{1-m}\left(r^{2-m}\xi_{m-1}^{r}\right)'\right], & m > 1, \\ &-\frac{\alpha}{2}\left[\frac{r^{-2}}{2}\left(r^{3}\xi_{2}^{r}\right)' + \frac{\alpha}{2}\xi_{1}^{r}\right], & m = 1. \end{cases} \end{split}$$

$$(9.12)$$

Hence, for infernal modes, the fluid perturbation of the form (9.1) in the low-shear region is completely determined by equations (9.7) and (9.12). We are now ready for the derivation of the **dispersion relation**, which will be aim of the next section.

The dispersion relation 9.3

Let us first note that, since (7.65) does not exhibit singularities if q >m/n in the low-shear region, then ξ_m^r has to be **continuous** in the domain 0 < r < a. Thus, thanks to (9.3), we have $\xi_m^r(r_0) = 0$. We may still suppose that this holds true if the safety factor drops below m/n in the shear-free region as long the condition $|q - m/n| \sim \varepsilon$ is fulfilled in the core so that the singularity at the m/n mode resonance is regularised by inertia (i.e. there is no narrow inertial layer where strong gradients develop). In analogy with the discussion presented in section 8.2.2, a series of successive integrations of (7.71) across r_0 shows that both ξ_{m+1}^r and $d\xi_{m+1}^r/dr$ are continuous at r_0 . As for the m=1 internal kink,

This is a subtle point and it is discussed in the box at the end of this section.

any inertia contribution coming from the resonances associated with the sideband harmonics (the m+1 in our case), if they appear in the plasma, turns out to be negligible. We have now all the elements to compute the dispersion relation.

We shall focus on the m>1 case first. Equation (9.7) can be integrated once giving

$$r^{-1\mp 2m} \left(r^{2\pm m} \xi_{m\pm 1}^r \right)' = L_{\pm} + \frac{1\pm m}{2} r^{\mp m} \alpha \xi_m^r, \tag{9.13}$$

where L_{\pm} are some constants. Multiplying the equation above by $r^{1\pm 2m}$, a further integration yields

$$r^{2\pm m}\xi_{m\pm 1}^r = C_{\pm} + \frac{r^{2\pm 2m}L_{\pm}}{2\pm 2m} + \frac{1\pm m}{2} \int_0^r r^{1\pm m}\alpha \xi_m^r dr, \tag{9.14}$$

where C_{\pm} are two additional constants of integration. It is obvious that regularity on the magnetic axis requires $C_{+} = L_{-} = 0$.

In order to have an expression the constant L_+ , we evaluate (9.13) at r_0 exploiting the fact that $\xi_m^r(r_0) = 0$. This gives

$$L_{+} = r_{0}^{-m} \left(2 + m + \frac{r d\xi_{m+1}^{r} / dr}{\xi_{m+1}^{r}} \Big|_{r_{0}} \right) \xi_{m+1}^{r}(r_{0}).$$

The quantity $\xi_{m+1}^r(r_0)$ is obtained by evaluating (9.14) at r_0 . Combining this result with the expression of L_+ above gives

$$\frac{L_{+}}{1+m} = \frac{1+m}{r_{0}^{2+2m}} \left(\frac{2+m+\hat{c}}{m-\hat{c}}\right) \int_{0}^{r_{0}} r^{1+m} \alpha \xi_{m}^{r} dr, \tag{9.15}$$

where we defined $(\epsilon \to 0)$

$$\hat{c} = \frac{r d\xi_{m+1}^r / dr}{\xi_{m+1}^r} \Big|_{r_0 + \epsilon}.$$

Here \hat{c} is a well defined quantity thanks to the continuity of ξ_{m+1}^r and its derivative at r_0 , and its expression is obtained by solving equation (9.4) for ξ_{m+1}^r with appropriate boundary conditions.⁴ Thus, plugging (9.13) into (9.12) gives

$$\frac{1}{r}\frac{d}{dr}\left[r^{3}Q\frac{d\xi_{m}^{r}}{dr}\right] + \left[(1-m^{2})Q + \frac{r\alpha}{R_{0}}\left(\frac{n^{2}}{m^{2}} - 1\right)\right]\xi_{m}^{r} + \frac{\alpha}{2}\left(\frac{r^{m}L_{+}}{1+m}\right) = 0,$$
(0.16)

where L_+ is given by (9.15).

For m = 1, it is straightforward to show that one obtains precisely (9.16) with the very same definition of L_+ given by (9.15).

Let us note that (9.16) is a linear function of ξ_m^r so that ξ_m^r/A with A some number is still a solution of this equation. We thus divide the equation above by $A = \int_0^{r_0} r^{1+m}/r_0^{2+m} \alpha \xi_m^r dr$ and cast (9.16) as

$$\frac{1}{r}\frac{d}{dr}\left[r^3Q\frac{dX}{dr}\right] + \left[(1-m^2)Q + \frac{r\alpha}{R_0}\left(\frac{n^2}{m^2} - 1\right)\right]X + \alpha\left(\frac{r}{r_0}\right)^m \frac{1+m}{2}\left(\frac{2+m+\hat{c}}{m-\hat{c}}\right) = 0,$$
(9.17)

⁴ That is either $\xi_{m+1}^r(a) = 0$ with no $q = \frac{m+1}{n}$ resonance, or with $\xi_{m+1}^r(r_s)$ finite at the $q = \frac{m+1}{n}$ resonance r_s if it appears in the plasma.

where $X = \xi_m^r/A$. The general procedure to obtain the growth rate consists in first solving (9.17) with the boundary conditions $X(r_0) = 0$ and either X(0) finite for m = 1 or X(0) = 0 for m > 1,5 and then computing the following expression

$$\int_0^{r_0} \frac{r^{1+m}}{r_0^{2+m}} \alpha X dr = \frac{1}{A} \int_0^{r_0} \frac{r^{1+m}}{r_0^{2+m}} \alpha \xi_m^r dr = 1.$$
 (9.18)

To compute the integral above, an exact solution of (9.17) is required which, in general, has a complicated form even for simple pressure profiles. It follows that in most cases the associated dispersion relation is so involved to be of no practical use.

Upon inspecting (9.16), we see that the key physical ingredient characterising the "infernal equations" (9.7) and (9.12) is the presence of a pressure gradient in the low-shear region which drives the coupling between the main mode and its neighbouring sidebands. Now, one notices that (9.18) involves an integral of $\alpha \xi_m^r$. This induces us to conjecture that the exact shape of the pressure gradient is not really fundamental, as this appears under a sign of integration over the whole low-shear region. Thus, in order to simplify the analysis, and yet having a meaningful result, we take a top-hat pressure profile with the step located at $0 < r_p < r_0$ as shown in Fig. 9.3. We denote with p_1 and p_2 the values of the pressure on the magnetic axis and at $r_p < r_0$ respectively. Hence, we write

$$\alpha \approx -2R_0[p_2 - p_1]q^2\delta(r - r_p)/B_0^2 = r_p\delta(r - r_p)\alpha_c$$

where $p_2 < p_1 = p_0(0)$ with $\delta(r)$ indicating the Dirac-delta function of argument r. The expression above defines the parameter

$$\alpha_c = -2\frac{R_0}{r_p} \frac{[p_2 - p_1]}{B_0^2} q^2.$$

Here we shall approximate $q^2 \approx (m/n)^2$.

Thus, instead of using (9.17) and (9.18), we follow an equivalent but slightly more straightforward procedure which requires (9.16) only. Following the mathematical steps indicated in the box at the end of this section, with such a pressure profile, a double integration across r_p shows that ξ_m^r is continuous at this point. Hence, its expression which fulfils the correct boundary conditions at r_p and r_0 is readily obtained

$$\xi_{m}^{r} = \begin{cases} (r/r_{p})^{m-1}, & r < r_{p}, \\ \frac{(r/r_{0})^{m-1} - (r/r_{0})^{-m-1}}{(r_{p}/r_{0})^{m-1} - (r_{p}/r_{0})^{-m-1}}, & r > r_{p}, \end{cases}$$
(9.19)

where, for the sake of simplicity, we normalised ξ_m^r to unity at r_p .

We point out that the eigenfunction of the m = 1 infernal mode differs from the typical top-hat function associated with the internal kink ⁵ This determines the two constants multiplying the two independent solutions of the homogeneous second order differential equation.

Note that this instability driving mechanism is exactly the same as the one of the m = 1 internal kink mode.

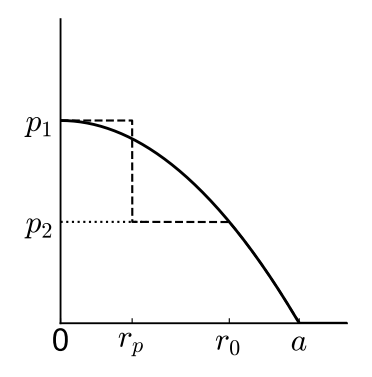
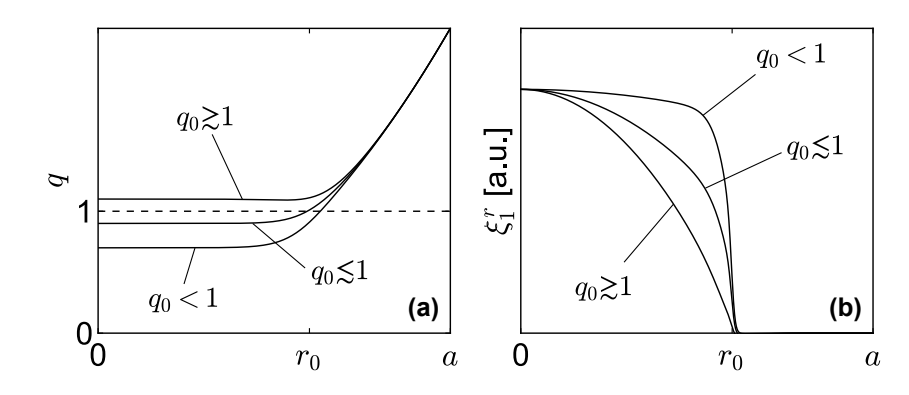


Figure 9.3: Model stepped pressure profile. The location and height of the step may be determined by imposing that the global β and pressure peaking factor have some given values.

Figure 9.4: Safety factor profile (a) and associated eigenfunction of an unstable m=1 mode (b) showing the smooth transition from infernal to kinktype structure of ξ_1^r as the value of q on the axis (q_0) drops below unity (see Hastie (1987) for a full numerical treatment). The horizontal dashed line indicates the q=1 level.



analysed in the previous chapter in that it is smoother. It is worth to point out that in such a case the structure of the eigenfunction of the **unstable** perturbation transitions continuously from infernal to kink-like (i.e. stepped) as q drops below unity and q(0)-1 becomes more negative. This behaviour is shown in figure 9.4.

Thus, exploiting the Dirac-delta behaviour of α and taking $q \approx m/n$, we multiply Eq. (9.16) by r and integrate across r_b yielding

$$r_{p}Q\left[\left[\frac{d\xi_{m}^{r}}{dr}\right]\right]_{r_{p}} + \frac{r_{p}\alpha_{c}}{R_{0}}\left(\frac{n^{2}}{m^{2}} - 1\right) + \alpha_{c}^{2}\frac{1 + m}{2}\left(\frac{2 + m + \hat{c}}{m - \hat{c}}\right)\frac{r_{p}^{2 + 2m}}{r_{0}^{2 + 2m}} = 0, \quad (9.20)$$

where $[\![\cdot]\!]_{r_p} = (\cdot)_{r_p+\epsilon} - (\cdot)_{r_p-\epsilon}$ with ϵ indicating, as usual, an infinitesimally small positive quantity. Using (9.19), one has

$$r_{p} \left[\frac{d\xi_{m}^{r}}{dr} \right]_{r_{p}} = -\frac{2m}{1 - (r_{p}/r_{0})^{2m}}.$$
 (9.21)

It only remains to calculate an expression for \hat{c} . This can be easily obtained by assuming that the safety factor is increasing parabolically in the high-shear region, that is $q = m/n(r/r_0)^2$ for $r > r_0$.⁶ With such a safety factor, the solution of (9.4) reads

$$\xi_{m+1}^{r} = \frac{A_1 \left(\frac{r}{r_s}\right)^m + A_2 \left(\frac{r}{r_s}\right)^{-2-m}}{(m+1)\mu - n},\tag{9.22}$$

where $r_s = r_0 \sqrt{(m+1)/m}$. If $r_s < a$, that is the position of the q=2 resonant surface is inside the plasma, A_1 and A_2 are chosen such that ξ_{m+1}^r is finite at r_s . For the case of $r_s > a$ we instead require that $\xi_{m+1}^r(a) = 0$. This then yields

$$rac{A_2}{A_1} = \left\{ egin{array}{ll} -1, & r_s < a, \\ -\left(rac{a}{r_s}
ight)^{2+2m}, & r_s > a. \end{array}
ight.$$

Therefore, by means of (9.22), the quantity \hat{c} is readily obtained:

$$\hat{c} = \frac{2 + 3m + m\frac{A_2}{A_1}(r_s/r_0)^{2+2m}}{1 + \frac{A_2}{A_1}(r_s/r_0)^{2+2m}}.$$
(9.23)

⁶ This corresponds to the case of vanishing current outside r_0 (see Eq. (4.28)). Notice that we do not consider δq corrections to the expression of \hat{c} as these are of higher order.

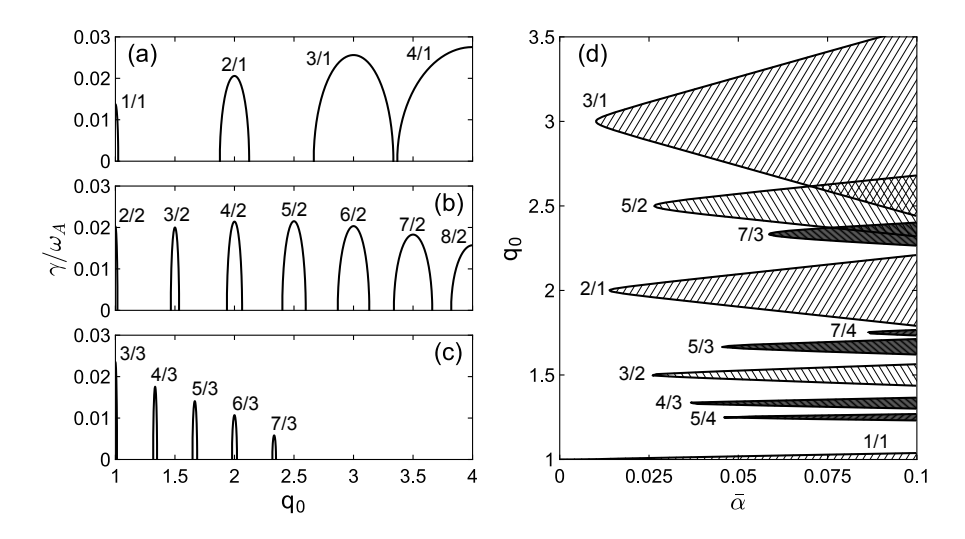


Figure 9.5: Growth rate for n = 1 (a), n = 2 (b) and n = 3 (c) infernal modes with $r_0/a = 0.5$, $R_0 = 10$, $r_p/a = 0.4$, $\bar{\alpha} = \alpha_c/(m/n)^2 = 0.062$. The shaded areas in (d) indicate the instability regions. The mode numbers of the dominant harmonic are indicated.

By plugging (9.11), (9.21) and (9.23) into (9.20) we finally obtain the dispersion relation for the **ideal infernal instability**:

$$\frac{\gamma^{2}}{n^{2}\omega_{A}^{2}}(1+2\frac{m^{2}}{n^{2}}) = \frac{1-\left(\frac{r_{p}}{r_{0}}\right)^{2m}}{2m} \left\{\alpha_{c}^{2}\frac{1+m}{2}\left[\left(\frac{r_{*}}{r_{0}}\right)^{2+2m} - 2\right]\left(\frac{r_{p}}{r_{0}}\right)^{2+2m} - \frac{r_{p}\alpha_{c}}{R_{0}}\left(1-\frac{n^{2}}{m^{2}}\right)\right\} - \left(\frac{\delta q}{m/n}\right)^{2},$$
(9.24)

where either $r_* = r_s$ for $r_s < a$, or $r_* = a$ for $r_s > a$. The growth rates and the associated stability regions obtained from (9.24) are shown in figure 9.5. The destabilising role of the pressure gradient is evident, as well as the field line bending stabilising effect represented by the term proportional to δq^2 . Note that the farther the central q from a rational value, the more stable the system. It should be noted that we allowed negative values of $\delta q < 0$ under the assumption that inertial effects (i.e. γ^2 terms) are strong enough to regularise the singular behaviour at the resonant point where q = m/n. A more detailed discussion on the instability dynamics when q drops even further and inertia regularisation is severely weakened will be discussed later.

This exhausts the analysis of infernal modes of arbitrary m and n mode numbers ($m \ge n$) in scenarios with a monotonically increasing safety factor. In the next section we shall briefly address the problem of infernal stability in hollow q plasmas.

Eigenmode behaviour across steps

By inspecting (7.65), we formally write the equation for the main mode ξ_m^r as

$$\frac{d}{dr}\left(f_1\frac{d\xi_m^r}{dr}\right) - f_2\xi_m^r - f_3 = 0, (9.25)$$

where f_1 is a continuous function, with f_2 and f_3 discontinuous at most. We take $f_1 \neq 0$ everywhere but on the magnetic axis. The infernal ordering assumes that $f_1 \sim f_2 \sim \varepsilon^2$ for $r < r_0$ (low-shear region), whereas $f_1 \sim f_2 \sim 1$ for $r > r_0$ (high-shear region). We let $f_3 \sim \varepsilon^2$ across the whole domain. Integrating (9.25) across r_0 gives

$$\left[f_1 \frac{d\xi_m^r}{dr} \right]_{r_0 - \epsilon}^{r_0 + \epsilon} = 0.$$

Due to the continuity of f_1 , one has $f_1(r_0) \sim \varepsilon^2$ so that this equation does not provide information on the ε^0 order of $d\xi_m^r/dr$ at r_0 . Therefore, $d\xi_m^r/dr$ may be discontinuous at r_0 .

Contrarily, after integrating once (9.25) from 0 to some radius r, we may write

$$\frac{d\xi_m^r}{dr} = \frac{1}{f_1} \int_0^r (f_2 \xi_m^r + f_3) d\varrho,$$

having assumed that this expression is well defined on the magnetic axis. We notice that the right-hand-side of this equation is of order 1 across the whole plasma column. A further integration across r_0 shows that ξ_m^r is continuous at this point.

9.4 Infernal modes with a reversed q > 1

We shall consider a non-monotonic safety factor similar to the one of figures 9.1 (profile b) and 9.2. Let us assume that $q \approx m/n$ for $r_1 < r < r_2$ and focus on modes with m > 1 ($m \neq n$). In analogy with the analysis of §9.1 we multiply (7.69) by ξ_m^r , and integrate from 0 to r_1 and from r_2 to a. This shows that $\xi_m^r = 0$ for $0 < r < r_1$ and for $r_2 < r < a$, and thus implies that the sidebands fulfil equation (9.4) outside the flat-q region.

From (9.13) we obtain

$$\left(r^{2\pm m}\xi_{m\pm 1}^{r}\right)' = L_{\pm}r^{1\pm 2m} + \frac{1\pm m}{2}r^{1\pm m}\alpha\xi_{m}^{r}.$$
 (9.26)

Evaluating the equation above at r_1 and r_2 respectively gives

$$\begin{split} \xi_{m\pm1}^{r}(r_1) &= \frac{r_1^{\pm m} L_{\pm}}{2 \pm m + \hat{c}_{\pm1}}, \quad \text{with} \quad \hat{c}_{\pm1} = \left(r \frac{d\xi_{m\pm1}^{r}/dr}{\xi_{m\pm1}^{r}} \right) \Big|_{r_1}, \\ \xi_{m\pm1}^{r}(r_2) &= \frac{r_2^{\pm m} L_{\pm}}{2 \pm m + \hat{c}_{\pm2}}, \quad \text{with} \quad \hat{c}_{\pm2} &= \left(r \frac{d\xi_{m\pm1}^{r}/dr}{\xi_{m+1}^{r}} \right) \Big|_{r_2}. \end{split}$$

Here, the constants $\hat{c}_{\pm 1}$ and $\hat{c}_{\pm 2}$ are obtained by solving the equation for the sidebands, that is (9.4), in the regions $0 < r < r_1$ and $r_2 < r < a.^7$ The constants L_{\pm} are found by integrating (9.26) from r_1 to r_2 yielding

$$L_{\pm} = \frac{(1 \pm m)^2 (2 \pm m + \hat{c}_{\pm 1}) (2 \pm m + \hat{c}_{\pm 2}) \int_{r_1}^{r_2} r^{1 \pm m} \alpha \xi_m^r dr}{(2 \pm m + \hat{c}_{\pm 1}) (\pm m - \hat{c}_{\pm 2}) r_2^{2 \pm 2m} - (2 \pm m + \hat{c}_{\pm 2}) (\pm m - \hat{c}_{\pm 1}) r_1^{2 \pm 2m}}.$$

⁷ In computing these coefficients one has to take into account possible resonances of the m+1 harmonic. These may occur in either of the regions $0 < r < r_1$ and $r_2 < r < a$.

Contrarily to the case of monotonic safety factor, the constant L_{-} is not vanishing. However, if $r_1/r_2 \rightarrow 0$, (9.15) is recovered with $L_{-} = 0$. By means of (9.26), equation (9.12) becomes (cf. (9.16))

$$\frac{d}{dr} \left[r^{3} Q \frac{d\xi_{m}^{r}}{dr} \right] + r \left[(1 - m^{2}) Q + \frac{r\alpha}{R_{0}} \left(\frac{n^{2}}{m^{2}} - 1 \right) \right] \xi_{m}^{r} + \frac{\alpha}{2} \left(\frac{r^{1+m} L_{+}}{1+m} + \frac{r^{1-m} L_{-}}{1-m} \right) = 0.$$
(9.27)

Analogously to what we did in §9.3 for the derivation of (9.20), we assume that the pressure has a step located at some position $r_1 < r_p < r_2$ such that $\alpha = r_p \delta(r - r_p) \alpha_c$ with α_c defined as before. Normalising $\xi_m^r(r_p) = 1$ for convenience, the dispersion relation is then obtained by integrating equation (9.26) across r_p yielding⁸

⁸ Notice that
$$L_+ \sim \alpha_c$$
.

$$r_{p}Q\left[\left[\frac{d\xi_{m}^{r}}{dr}\right]\right]_{r_{p}}+\frac{r_{p}\alpha_{c}}{R_{0}}\left(\frac{n^{2}}{m^{2}}-1\right)+\frac{\alpha_{c}}{2}\left(\frac{r_{p}^{m}L_{+}}{1+m}+\frac{r_{p}^{-m}L_{-}}{1-m}\right)=0,$$

where instead of (9.21) we have

$$r_{p} \left[\frac{d\xi_{m}^{r}}{dr} \right]_{r_{p}} = -2m \frac{(r_{p}/r_{2})^{2m} - (r_{p}/r_{1})^{2m}}{[1 - (r_{p}/r_{2})^{2m}][1 - (r_{p}/r_{1})^{2m}]}.$$

For sufficiently small r_1/r_2 the dispersion relation above reduces to (9.20).

As for the case of the m=1 internal kink mode with two q=1 resonant surfaces, the stability analysis of scenarios with a hollow safety factor with a broad region of flattened $q\approx 1$ is much more complicated than the one just discussed (Kuvshinov (1989), de Blank (1991)). We point out, however, that if r_1 is either close to r_2 , or sufficiently near to the axis the results of §8.6 or §9.3, respectively, should apply.

We should finally note that instabilities exhibiting an *infernal-type* behaviour, i.e. characterised by a dominant mode of helicity (m, n) with m and n of the order of unity accompanied by two smaller sidebands with poloidal mode numbers $m \pm 1$, can be observed also in scenarios with small but finite magnetic shear as long as the pressure gradient is strong enough to drive **mode coupling**. This is elaborated more in detail in the next section.

9.5 Hybrid kink—infernal perturbations

In the preceding sections, we wrote $q = m/n + \delta q$ in the low-shear region and allowed δq to take positive and negative values. The eigenfunction was assumed to vanish at the transition point between low and high shear regions under the assumption that inertial effects are comparable in amplitude with those associated with field line bending, that is

$$k_{||} \sim \gamma/\omega_A.$$
 (9.28)

⁹ This means that pressure driven toroidal coupling is allowed to still occur at leading order, but inertial effects only matter in a neighbourhood of the q = m/n resonance.

However, if an exact q = m/n resonance appears at some radial position r_s within the plasma, a radical change in the character of the eigenfunction may be expected either close to marginal stability when inertia is small or when δq becomes sufficiently negative so that ordering (9.28) no longer holds (this was hinted in figure 9.4). To treat such a case, we have to tweak the *infernal analysis* outlined in the previous sections.

Let us consider the case of a **monotonically increasing safety factor** in which, for $0 < r < r_s$, both $r\mu'$ and $k_{||}$ are small quantities of order ε while for $r > r_s$ we take $s \sim 1.9$ Furthermore, we keep $\beta \sim \varepsilon^2$ and impose the usual ideal wall boundary conditions at r = a. For simplicity, we focus on marginal stability $(\gamma = 0)$ only and assume q > 1.

In the region of large shear, one still has $\xi_m^r(r > r_s) = 0$ (see (9.3)). Where the magnetic shear is small instead, that is for $0 < r < r_s$, we let the perturbation obey equations (9.7) and (9.12) with (cf. (9.11))

$$Q = k_{||}^2/n^2,$$

where now $k_{||}$ is a function of r. In addition, differently from what has been discussed in §9.3 but analogous to the m=1 internal kink mode, we allow $\xi_m^r(r_s-\epsilon)$ with $\epsilon\to 0$ to be **finite**.

Therefore, we find that integration of (9.7) across r_s yields

$$\left[r^{-1\mp m} \left(r^{2\pm m} \xi_{m\pm 1}^r \right)' \right]_{r_s} = -\frac{1\pm m}{2} \alpha_s \xi_m^r (r_s - \epsilon),$$

having used the notation $\alpha(r_s) = \alpha_s$. It easy to see that $\xi_{m\pm 1}^r$ are continuous at r_s , hence we are left with

$$\left[r\frac{d\xi_{m\pm 1}^r}{dr}\right]_{r_s-\epsilon} = \left[r\frac{d\xi_{m\pm 1}^r}{dr}\right]_{r_s+\epsilon} + \frac{1\pm m}{2}\alpha_s \xi_m^r(r_s - \epsilon). \tag{9.29}$$

This shows that, contrary to the "standard" infernal case, the radial derivatives of the sideband harmonics have a jump at r_s . Notice that this relation bears a close resemblance to (8.19).

Proceeding further, we have that both equations (9.13) and (9.14) still hold with $C_+ = L_- = 0$. Thus, evaluating (9.13) at $r_s - \epsilon$ and using (9.29) gives (cf. (9.3))

$$L_{+} = r_{s}^{-m} (2 + m + \hat{c}) \xi_{m+1}^{r}(r_{s}), \quad \hat{c} = \frac{r d \xi_{m+1}^{r} / dr}{\xi_{m+1}^{r}} \Big|_{r_{s} + \epsilon}.$$

Finally, getting $\xi_{m+1}^r(r_s)$ from (9.14) (again, this is computed at $r_s - \epsilon$) we find that the expression for L_+ is given by (see (9.15))

$$\frac{L_+}{1+m} = \frac{1+m}{r_s^{2+2m}} \left(\frac{2+m+\hat{c}}{m-\hat{c}} \right) \int_0^{r_s-\epsilon} r^{1+m} \alpha \xi_m^r dr.$$

Plugging (9.13) into (9.12) eventually yields the desired equation for ξ_m^r only, namely (9.16). Now, if we adopt the same procedure employed

earlier and exploit linearity, we can recast (9.16) as10

$$\frac{1}{r}\frac{d}{dr}\left(r^{3}\frac{k_{||}^{2}}{n^{2}}\frac{dX}{dr}\right) + \left[(1-m^{2})\frac{k_{||}^{2}}{n^{2}} + \frac{r\alpha}{R_{0}}\left(\frac{n^{2}}{m^{2}} - 1\right)\right]X + \alpha\left(\frac{r}{r_{s}}\right)^{m}\frac{1+m}{2}\left(\frac{2+m+\hat{c}}{m-\hat{c}}\right) = 0,$$

where the normalised fluid displacement X is subject to the condition (9.18))

$$\int_0^{r_s-\epsilon} \frac{r^{1+m}}{r_s^{2+m}} \alpha X dr = 1.$$

This provides a functional relation between, say, q and β at marginal stability. We note that the equation X conforms to is formally the same as (9.17), but the appearance of an exact resonance modifies the boundary condition at r_s which now reads (this is immediately obtained from the equations above)

$$X(r_s - \epsilon) = \frac{R_0}{r_s} \frac{1 + m}{2} \left(\frac{2 + m + \hat{c}}{m - \hat{c}} \right) / \left(1 - \frac{n^2}{m^2} \right). \tag{9.30}$$

We shall now elucidate how the appearance of an exact resonance influences stability even when the magnetic shear is very weak. Let us denote with q_0 the safety factor at the axis and r_s some radial position within the plasma. We take $q = \frac{m}{n}(r/r_s)^2$ for $r > r_s$ (see **sidenote 16** above) so that the constant \hat{c} is fully determined.¹¹ Upon introducing the parameter $\Delta q = q_0 - m/n$, for $r \le r_s$ we choose a safety factor of the form

$$q=q_0,$$

$$q_0>m/n \; (\Delta q \; {
m positive}),$$

$$q=1/\left\{\frac{n}{m}+\left(\frac{1}{q_0}-\frac{n}{m}\right)\left[1-(r/r_s)^{\lambda}\right]\right\}, \qquad q_0< m/n \; (\Delta q \; {
m negative}).$$

When $q_0 > m/n$ we impose $X(r_s) = 0$, otherwise X has to conform to (9.30). With a parabolic pressure profile $p = p_0(1 - r^2/a^2)$ the resulting stability boundaries computed numerically for the m = 2, n = 1 infernal mode are show in figure 9.5. In contrast with fig. 9.5-(d), we see that as q_0 drops below the rational value m/n (= 2/1 in our example) the marginal boundary curve in the $\beta - q_0$ plane is not symmetric with respect to the m/n level and stability is worsened when Δq is negative.

We shall conclude with a brief investigation of the eigenmode radial structure. Computing (9.13) at $r_s - \epsilon$ and using (9.29) yields

$$\left(2-m+\frac{d\xi_{m-1}^r/dr}{\xi_{m-1}^r}\Big|_{r_s+\epsilon}\right)\xi_{m-1}^r(r_s-\epsilon)=0.$$

Since the third term in brackets on the left-hand-side is generally different from zero, one must have $\xi_{m-1}^r(r_s - \epsilon) = 0$. This result in conjunction with the constraint of vanishing radial fluid displacement at the wall requires that $\xi_{m-1}^r = 0$ for $r > r_s$.

¹⁰ Thanks to the smallness of the magnetic shear we approximate

$$\alpha \approx -2 \frac{R_0 p' m^2}{B_0^2 n^2}.$$

We just mention that techniques similar to those we just discussed can be applied to deal with cases with a hollow q as the ones treated in $\S 9.4$.

¹¹ In analogy to (9.23), here we have

$$\hat{c} = \frac{2 + 3m + m\sigma(r_{m+1}/r_s)^{2+2m}}{1 + \sigma(r_{m+1}/r_s)^{2+2m}}.$$

with r_{m+1} denoting the resonance of the m+1 mode where $\sigma=-1$ if $r_{m+1}< a$ and $\sigma=-(a/r_{m+1})^{2+2m}$ otherwise.

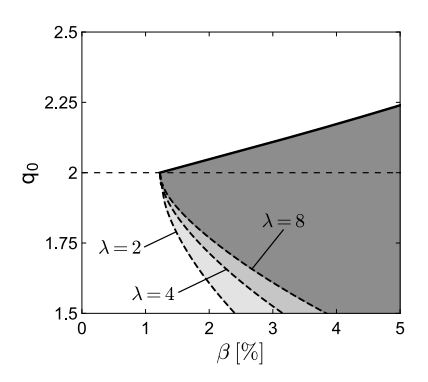


Figure 9.6: Marginal values of q_0 for the infernal mode with a dominant m=2, n=1 harmonic as a function of β defined as in (4.10) with $\sqrt{g} \approx rR_0$. The lower curve has been computed with $r_s=0.6$ and $\epsilon=0.3$ for some different values of λ as indicated. Instability occurs within the shaded areas.

Hence, normalising by $A=\int_0^{r_s-\epsilon}r^{1+m}/r_s^{2+m}\alpha\xi_m^rdr$, the behaviour of the satellite harmonics in the low-shear region conforms to equations (this holds true even when there is no q=/m/n surface)

$$\begin{split} X_{m+1} &= \frac{\xi^r_{m+1}}{A} = \frac{1+m}{2} \left[\left(\frac{r}{r_s} \right)^m \frac{2+m+\hat{c}}{m-\hat{c}} + r^{-2-m} \int_0^r r^{1+m} \alpha X dr \right], \\ X_{m-1} &= \frac{\xi^r_{m-1}}{A} = \frac{m-1}{2} r^{m-2} \left[\int_0^{r_s-\epsilon} r^{1-m} \alpha X dr - \int_0^r r^{1-m} \alpha X dr \right]. \end{split}$$

An example of shape of the radial eigenfunctions when the m/n resonance appears in the plasma is shown in figure 9.7. We see that beyond the standard *infernal* character in which the pressure gradient drives the coupling with the first neighbouring sidebands, the displacement of the dominant harmonic acquires a *kink character* in that, similar to the m=1 internal kink mode, it has an abrupt discontinuity at the position of the $q(r_s)=m/n$ resonance. This induces a jump in the radial derivatives of the satellite harmonics at r_s . The sudden jump in X is gradually smoothened as inertial effects becomes strong enough to remove the singularity at r_s .

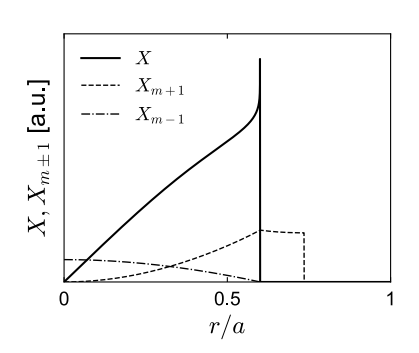


Figure 9.7: Structure of the radial fluid displacements of the m = 2, n = 1 infernal mode computed with the same parameters of Fig. 9.6 with $q_0 = 1.85$.

References

- D. Brunetti et al., Plasma Phys. Control. Fusion 62, 115005 (2020).
- H. J. de Blank and T. J. Schep, Phys. Fluids B 3, 1136 (1991).
- E. D. Fredrickson et al., Phys. Plasmas 4, 1589 (1997).
- C. G. Gimblett et al., Phys. Plasmas 3, 3369 (1996).
- R. J. Hastie and T. C. Hender, Nucl. Fusion 28, 585 (1988).
- H. A. Holties et al., Nucl. Fusion 36, 973 (1996).
- ITER Physics Expert Group on Disruptions, Plasma Control, and MHD and ITER Physics Basis Editors, Nucl. Fusion 39, 2251 (1999).
- B. N. Kuvshinov, Fiz. Plazmy **15**, 910 (1989) [Sov. J. Plasma Phys. **15**, 526 (1989)].
- J. Manickam et al., Nucl. Fusion 27, 1461 (1987).
- J. Manickam et al., "MHD Stability Studies in Reversed Shear Plasmas in TFTR", Proceedings of the 16th International Conference on Fusion Energy (Montreal, Canada, 7–11 October 1996) Vol. 1 p. 453 Paper No. IAEA-CN-64/A5-2, International Atomic Energy Agency (Vienna, AT), 1997.
- M. Okabayashi et al., Nucl. Fusion 38, 1149 (1998).
- T. Ozeki et al., Nucl. Fusion 33, 1025 (1993).
- S. A. Sabbagh et al., Nucl. Fusion 29, 423 (1989).
- S. Takeji et al., Phys. Plasmas 4, 4283 (1997).
- F. L. Waelbroeck and R. D. Hazeltine, Phys. Fluids 31, 1217 (1988).
- C. Wahlberg and J. P. Graves, Phys. Plasmas 14, 110703 (2007).
- L.E. Zakharov, Nucl. Fusion 18, 335 (1978).

10

External kinks

External kink modes are **current driven** instabilities which can develop when the plasma is surrounded by a **vacuum region**. Their effect is to produce a **global** displacement of the plasma column which is non vanishing at the edge. An example of a corrugation of the plasma boundary induced by an external kink for different m poloidal mode numbers is depicted in figures 10.1 and 10.2. Depending on the parallel wave vector associated with the perturbation and the shape of the current profile, these type of instabilities can grow on Alfvénic timescales, that is within **few microseconds**.

Although it is not uncommon to observe high-m external kink modes in the early phase of the discharge (i.e. when the current is ramped-up and the value of the edge safety factor decreases, see (4.29)), long wavelength external kinks, primarily modes with $m \leq 3$, are generally deleterious. In fact, their uncontrolled growth, which typically happens on much shorter timescales than those of the response of feedback controllers, is likely to make the plasma column to touch the surrounding structures, leading eventually to a complete loss of confinement (namely a disruption).

Hence, for steady and safe tokamak operation, these instabilities must be avoided. It is therefore of crucial importance to identify precisely the physical conditions under which external kink modes develop.

This is the aim of this chapter, in which we discuss the conditions favouring the onset of such instabilities, giving particular emphasis to the impact of the shape of the plasma current and the effect of a surrounding **ideally conducting wall**.

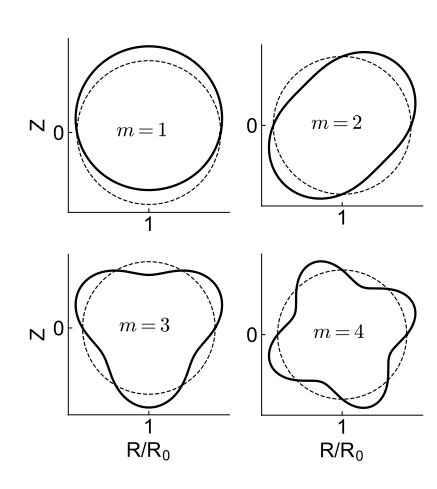


Figure 10.1: Perturbation of the plasma boundary induced by a m = 1, ..., 4 external kink. For a mode with toroidal mode number n the lobes rotate n times for one toroidal revolution (see figure 10.2).

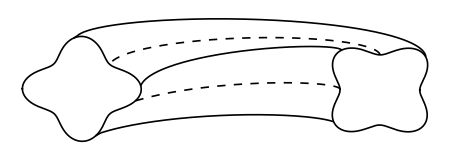


Figure 10.2: Example of the 3D structure of a m = 4, n = 1 external kink perturbation.

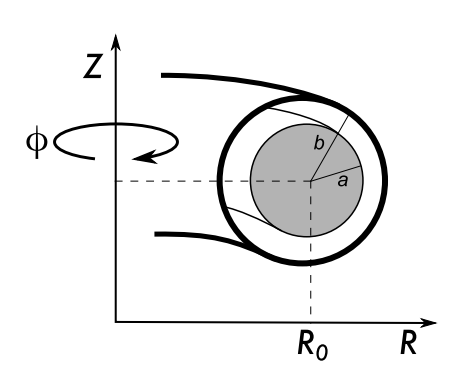


Figure 10.3: Plasma and conducting wall geometry.

10.1 Eigenmode equations

The geometry of the system is shown in figure 10.3. It is assumed the presence of a perfectly conducting wall at position b > a such that $b/R_0 \sim \varepsilon$. The most general Fourier expansion of the radial fluid displacement is

$$\xi^r = \sum_{m,n} \xi_{m,n}^r e^{i(m\vartheta - n\phi)},$$

where all the Fourier components are allowed to be, in principle, of the same order. Let us fix the toroidal number n and, as in §9.1, we take $k_{||} \sim m \sim 1$ with $k_{||}$ given by (7.51). Since coupling between harmonics with different toroidal mode numbers does not occur, we may write

$$\xi^{r} = \sum_{m} \xi_{m}^{r} e^{i(m\vartheta - n\phi)} \quad (n \text{ fixed}), \tag{10.1}$$

having omitted, for the sake of simplicity, to make explicit in ξ_m^r the dependence upon the toroidal mode number n. In order to model the fast timescales typical of the growth rates of current driven external kink instabilities, we let $\gamma/\omega_A \sim 1$ while β effects are kept to be of second order in ε .¹ This highlights the fact that external kink modes are current driven perturbations. Now we shall discuss the governing equations, treating plasma and vacuum regions separately.

Within the plasma, a perturbation of dominant helicity (m, n) obeys (7.65). By means of (7.14), (7.57), (7.67) and approximating $\langle L \rangle \approx 1/(rR_0)$ and $\langle N \rangle \approx r/R_0$, it follows that to leading order the dynamics of the harmonic ξ_m^r in expansion (10.1) is described by

$$\frac{1}{r}\frac{d}{dr}\left[r^{3}\left(k_{||}^{2}+\frac{\gamma^{2}}{\omega_{A}^{2}}\right)\frac{d\xi_{m}^{r}}{dr}\right]-\left[(m^{2}-1)\left(k_{||}^{2}+\frac{\gamma^{2}}{\omega_{A}^{2}}\right)-\frac{\gamma^{2}}{\omega_{A}^{2}}\frac{r\rho_{0}'}{\rho_{0}}\right]\xi_{m}^{r}=0,$$
(10.2)

where we recall that $k_{||}$ is defined in (7.51). Notice that pressure terms do not appear, and no coupling between harmonics with different poloidal mode numbers occurs at this order. The inertia enhancement factor associated with plasma compressibility (cf. (7.34)) is also absent due to the ordering of the growth rate and β which makes this contribution to be ε^2 times smaller compared to the dominant terms. An important point to stress is that contrarily to the m=1 internal kink and infernal modes, it is crucial to include **mass density gradients**.

Focusing now on the vacuum region, the governing equations for the magnetic perturbation are (cf. (6.6))

$$\nabla \times \widetilde{\boldsymbol{B}} = 0$$
, $\nabla \cdot \widetilde{\boldsymbol{B}} = 0$.

This allows us to write the vacuum perturbation as $\widetilde{\pmb{B}} = \nabla \chi$, with χ obeying

$$\nabla^2 \chi = 0. \tag{10.3}$$

¹ Recall that $\omega_A = \frac{B_0}{R_0\sqrt{\rho_0}}$ with normalisation $\mu_0 = 1$.

Expanding χ in a form similar to (10.1), equation (10.3) yields at leading order

$$(r\chi'_m)' - \frac{m^2}{r}\chi_m = 0.$$

It is clear that the large aspect ratio cylindrical approximation proves to be accurate enough. Hence, the description of external kink modes in a torus is exactly the same as the one in a cylinder. Since $\tilde{B}_m^r \approx \chi_m'$, we multiply the expression above by r, and then take the radial derivative to eventually give

$$\left[r\left(\sqrt{g}\tilde{B}_{m}^{r}\right)'\right]' - \frac{m^{2}}{r}\sqrt{g}\tilde{B}_{m}^{r} = 0. \tag{10.4}$$

Imposing the boundary condition (6.13) at the perfectly conducting wall, the solution of (10.4) reads

$$\sqrt{g}\tilde{B}_{m}^{r} \propto \left(\frac{r}{b}\right)^{m} - \left(\frac{b}{r}\right)^{m}.$$
 (10.5)

In the vacuum, the safety factor increases parabolically (cf. Eq. (4.48)) and is continuous at the plasma-vacuum interface a in absence of surface current densities. Hence, we introduce a fictitious vacuum **displacement** ξ_v such that²

$$\sqrt{g}\tilde{B}_{m}^{r} = r[m(a/r)^{2}/q(a) - n]\xi_{v},$$
 (10.6)

where q(a) denotes the value of the safety factor at the plasma boundary. We can thus recast (10.4) as follows

$$\frac{1}{r}\frac{d}{dr}\left[r^3k_{||}^2\frac{d\xi_v}{dr}\right] - (m^2 - 1)k_{||}^2\xi_v = 0.$$
 (10.7)

Since $\rho_0 = 0$ in the vacuum region, we see that ξ_m^r with ξ_v obey the same equation, that is Eq. (10.2). We may therefore identify them employing the symbol ξ_m^r also to denote ξ_v , bearing in mind that the vacuum perturbation is obtained by solving (10.4) for \tilde{B}_m^r . The **dispersion relation** is then derived by joining the plasma and vacuum solutions applying appropriate boundary conditions at the **plasma-vacuum interface**. These calculations are carried out in the next sections.

Necessary condition for instability 10.2

Assume that there are no surface currents at the plasma boundary so that q is continuous at r = a. Boundary condition Eq. (6.7) forces \tilde{B}_m^r , and thus ξ_m^r , to be continuous at the plasma-vacuum interface. Therefore, multiplying (10.2) by r and then integrating across a yields

$$a\left[\left(k_{||}^2 + \frac{\gamma^2}{\omega_A^2}\right) \frac{d\xi_m^r}{dr}\right]_{a=\epsilon}^{a+\epsilon} - \frac{R_0^2 \gamma^2}{B_0^2} \rho_0(a-\epsilon) \xi_m^r(a) = 0, \tag{10.8}$$

In a cylinder one has $g^{rr} = 1$, $g^{\vartheta\vartheta} =$ $1/r^2$, $g^{\phi\phi} = 1/R_0^2$, $g^{r\vartheta} = g^{r\phi} = 0$ and $\sqrt{g} = rR_0$. Note that in such a geometry there is no distinction between rectified and geometric poloidal angles.

We use (6.11) with the condition $\mathbf{n}_0 \cdot \mathbf{B}_0 =$ 0 (it is easily show that the equilibrium field is continuous at r = a).

² Notice that we are not concerned if ξ_v is singular at some locations a < r < b.

where ϵ is, as usual, an infinitesimally small positive quantity. Notice that we allowed radial excursions of the mass density across the plasma boundary, and took $\rho_0(a+\epsilon)=0$ meaning no plasma beyond r=a. A trivial rearrangement of this expression gives

$$a\left(\frac{m}{q(a)}-n\right)^2\left[\frac{d\xi_m^r/dr}{\xi_m^r}\right]_{a-\epsilon}^{a+\epsilon} = \frac{R_0^2\gamma^2}{B_0^2}\rho_0(a-\epsilon)\left(1+a\frac{d\xi_m^r/dr}{\xi_m^r}\bigg|_{a-\epsilon}\right). \quad (10.9)$$

Furthermore, the following relation holds

$$\frac{d}{dr} \left(r^3 \frac{\gamma^2}{\omega_A^2} \frac{d\xi_m^r}{dr} \right) - r \frac{\gamma^2}{\omega_A^2} \left[(m^2 - 1) - r \frac{\rho_0'}{\rho_0} \right] \xi_m^r = r \left[r \frac{\gamma^2}{\omega_A^2} \left(r \xi_m^r \right)' \right]' - m^2 \frac{\gamma^2}{\omega_A^2} r \xi_m^r. \tag{10.10}$$

Thus, if we multiply (10.2) by $r\xi_m^r$ and integrate from 0 to $a-\epsilon$, under the assumption that ξ_m^r is a real valued function, by means of (10.10) we obtain

$$\begin{split} a^{2}|\xi_{m}^{r}|^{2} \Big[a \left(\frac{m}{q(a)} - n \right)^{2} \frac{d\xi_{m}^{r}/dr}{\xi_{m}^{r}} \Big|_{a-\epsilon} + \frac{R_{0}^{2}\gamma^{2}}{B_{0}^{2}} \rho_{0}(a-\epsilon) \left(1 + a \frac{d\xi_{m}^{r}/dr}{\xi_{m}^{r}} \Big|_{a-\epsilon} \right) \Big] \\ - \int_{0}^{a-\epsilon} r k_{||}^{2} \left(r^{2} \left| \frac{d\xi_{m}^{r}}{dr} \right|^{2} + (m^{2}-1) |\xi_{m}^{r}|^{2} \right) dr \\ - \int_{0}^{a-\epsilon} r \frac{\gamma^{2}}{\omega_{4}^{2}} \left(|(r\xi_{m}^{r})'|^{2} + m^{2} |\xi_{m}^{r}|^{2} \right) dr = 0. \end{split}$$

Plugging (10.9) into this equation yields

$$\int_{0}^{a-\epsilon} r \frac{\gamma^{2}}{\omega_{A}^{2}} \left(|(r\xi_{m}^{r})'|^{2} + m^{2} |\xi_{m}^{r}|^{2} \right) dr =$$

$$a^{3} |\xi_{m}^{r}|^{2} \left(\frac{m}{q(a)} - n \right)^{2} \frac{d\xi_{m}^{r}/dr}{\xi_{m}^{r}} \Big|_{a+\epsilon} - \int_{0}^{a-\epsilon} r k_{||}^{2} \left(r^{2} \left| \frac{d\xi_{m}^{r}}{dr} \right|^{2} + (m^{2} - 1) |\xi_{m}^{r}|^{2} \right) dr.$$

$$(10.11)$$

It is thus evident that instability can develop only if the first term on the right-hand-side of the expression above is positive. By means of (10.5) and (10.6) we can easily compute

$$a\frac{d\xi_{m}^{r}/dr}{\xi_{m}^{r}}\Big|_{a+\epsilon} = \frac{2m}{m-nq(a)} - \frac{m+1+(m-1)\left(\frac{a}{b}\right)^{2m}}{1-\left(\frac{a}{b}\right)^{2m}}.$$
 (10.12)

The last term of (10.12) is always negative. Therefore, γ^2 in (10.11) may become positive only if

$$q(a) < \frac{m}{n},\tag{10.13}$$

that is the external kink mode with helicity (m, n) can be made unstable only if its associated resonance occurs in the vacuum. We stress that this is a general result independent of the shape of the current and mass density profiles inside the plasma.

Note that q(a) > m/n is a **sufficient condition** for stability. This translates into a constraint on the plasma current I_p which we recall scales as $I_p \propto 1/q(a)$ (see (4.29)).

Marginal boundaries

The marginal stability boundaries are readily obtained from (10.8) by setting $\gamma = 0$, yielding

$$\left(\frac{m}{q(a)} - n\right)^2 a \left[\frac{d\xi_m^r/dr}{\xi_m^r}\Big|_{a+\epsilon} - \frac{d\xi_m^r/dr}{\xi_m^r}\Big|_{a-\epsilon}\right] = 0.$$
 (10.14)

The first term in the square brackets, which is associated with the vacuum solution, is given by equation (10.12), while the second is obtained from solving (10.2) in the region r < a with vanishing γ . It is worth noting that the marginal boundaries are independent of the shape of the mass density profile.

For generic current profiles, the solution of equation (10.2) is typically tackled numerically. However, an exact analytic solution can be found for a current profile of the form

$$\frac{R_0^2 J^{\phi}}{B_0} = \begin{cases} 2/q_0, & r < r_0, \\ 0, & r > r_0, \end{cases}$$
 (10.15)

with $r_0 \le a$ measuring the extension of the **current channel**. The corresponding q profile is flat and equal to q_0 for $0 < r < r_0$, while $q = q_0(r/r_0)^2$ for $r > r_0$. It is immediate to verify that $r_0/a = \sqrt{q_0/q(a)}$. Integrating (10.2) across r_0 shows that both $d\xi_m^r/dr$ and ξ_m^r are continuous at r_0 . Hence, with such a safety factor profile, the expression of ξ_m^r fulfilling the regularity condition on the magnetic axis is easily obtained and reads

$$\xi_m^r = C \times \begin{cases} (r/r_0)^{m-1}, & r < r_0, \\ \frac{(r/r_0)^{1-m} + (m-1 - nq_0)(r/r_0)^{1+m}}{m - nq}, & r > r_0, \end{cases}$$
(10.16)

where C is a constant. Using this form of the plasma displacement, we can compute

$$\left. a \frac{d\xi_m^r/dr}{\xi_m^r} \right|_{a-\epsilon} = m+1 - \frac{2m}{1+(m-1-nq_0)(a/r_0)^{2m}} + \frac{2nq(a)}{m-nq(a)}. \eqno(10.17)$$

Plugging this result and (10.12) into (10.14) gives⁴

$$\left(\frac{m}{q(a)} - n\right)^2 \left[\frac{1}{1 + (m - 1 - nq_0)(a/r_0)^{2m}} - \frac{1}{1 - \left(\frac{a}{b}\right)^{2m}}\right] = 0.$$
 (10.18)

This equation is satisfied either when q(a) = m/n (cf. (10.13)) or when the term in the square brackets cancels. We shall now analyse separately instabilities with poloidal mode numbers m = 1 and $m \ge 2$.

10.3.1 m = 1 external kinks

We start by noticing that if m = 1 and $a/b \rightarrow 0$, Eq. (10.18) is fulfilled only for q(a) = 1/n. Let us take the equilibrium mass density profile to be a step function, that is (see figure 10.4)

$$\rho_0 \propto H(a-r), \quad \rho_0' \propto \delta(r-a),$$
(10.19)

³ This form of q extends smoothly into the vacuum region.

⁴ If q(a) < m/n, according to (10.28), instability occurs when the term in the square brackets on the left-hand-side of (10.18) is positive.

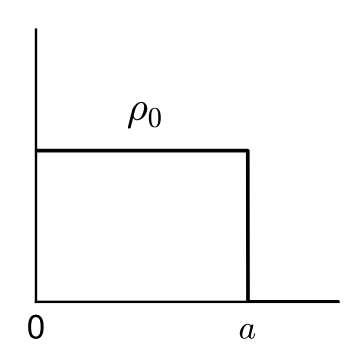


Figure 10.4: Model equilibrium mass density profile for the computation of the external kink stability.

⁵ Exploit the relation $q_0 = q_a(r_0/a)^2$.

This comes from the fact that in the limit of $b \to \infty$ from (10.18) one has $m-1 = nq(a)(r_0/a)^2 < nq(a)$.

where H denotes the Heaviside step function and δ is the Dirac-delta function. With such a mass density profile, the solution of (10.2) for m=1 is $\xi_1^r=const$. This result holds even for $\gamma\neq 0$, and, more importantly, is **completely independent of the shape of the current profile** (with a q profile which is finite on the magnetic axis).

When this expression for the m=1 radial displacement is plugged into (10.11), by means of (10.12) we obtain

$$\frac{\gamma^2}{\omega_A^2} = 2\left(\frac{1}{q(a)} - n\right)^2 \left(\frac{1}{1 - nq(a)} - \frac{1}{1 - \left(\frac{a}{b}\right)^2}\right). \tag{10.20}$$

Notice that this equation could have been equally obtained from (10.9). We see that in the **no-wall limit** $((a/b)^2 \to 0)$ the growth rate γ^2 is always positive for q(a) < 1/n. For the n = 1 mode, which turns out be the most dangerous one, this leads to the celebrated **Kruskal-Shafranov stability criterion**

$$q(a) > 1$$
.

This criterion sets a hard limit on the maximum allowed current that can be carried by the plasma. A window of stability appears for small values of q(a) if an ideal wall with a/b finite surrounds the plasma.

10.3.2 $m \ge 2$ external kinks

In the limit $(a/b)^{2m} \to 0$ and using (10.13), equation (10.18) provides a sufficient condition for stability expressed by the maximum extension of the current channel. This is⁵

$$\left(\frac{r_0}{a}\right)^2 < \frac{m-1}{m}.$$

Since r_0/a has to be smaller than unity, the widest window in q(a) within which instability can develop is identified by the following relation:

$$\frac{m-1}{n} < q(a) < \frac{m}{n}. (10.21)$$

More precisely, whenever q(a) < m/n the plasma is expected to be stable if (see (10.18))

$$\frac{q(a)}{q_0} \ge \frac{nq(a)}{m-1}.\tag{10.22}$$

If wall effects are taken into account, (10.18) yields the instability window

$$\frac{m-1+(r_0/b)^{2m}}{n(r_0/a)^2}< q(a)<\frac{m}{n}.$$

Under the assumption that $(a/b)^{2m} \ll 1$, for a given q(a) < m/n the maximum extension of the current channel required for stability is

$$\left(\frac{r_0}{a}\right)^2 = \frac{m-1}{nq(a)} + \frac{(m-1)^m}{[nq(a)]^{m+1}} \left(\frac{a}{b}\right)^{2m}.$$

The stabilising role of the wall, allowing for a wider current channel, is evident.

An example of the region of instability for safety factor and mass density profiles used in the calculations above in the no-wall limit is shown in figure 10.5. Wider regions of stability can be accessed by allowing the current to have different shapes (Wesson 1978).

10.4 Growth rates

We assume an equilibrium mass density of the form of Eq. (10.19), and the dispersion relation is given by equation (10.9) with $\rho_0(a-\epsilon)=\rho_0(r=0)$. For the particular case of a flat current, (10.9) can be solved analytically (a numerical solution is typically needed for more general current profiles). Setting $\rho_0'=0$ in (10.2), for r< a the radial displacement reads

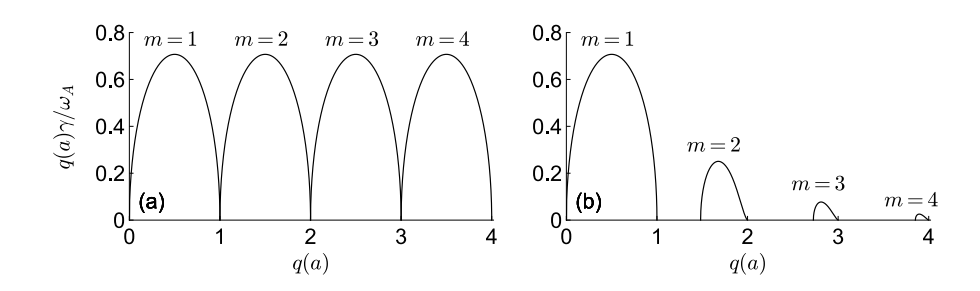
$$\xi_m^r \propto r^{m-1}$$
.

It follows at once that $a\frac{d\xi_m^r/dr}{\xi_m^r}\Big|_{a-\epsilon}=m-1$. Thus, by means of Eq. (10.12) we then have

$$\frac{\gamma^2}{\omega_A^2} = 2\left(\frac{m}{q(a)} - n\right)^2 \left[\frac{1}{m - nq(a)} - \frac{1}{1 - \left(\frac{a}{b}\right)^{2m}}\right].$$
 (10.23)

This expression reduces to (10.20) for m=1. Since $\gamma/\omega_A\sim 1$, it is seen that the instability grows on Alfvénic timescales meaning that for ω_A of the order of megahertz (which is a typical value for currently operating tokamaks) external kinks can grow within few microseconds. Notice that, if $a/b\to 0$, for a given q(a) (with $q_0/q(a)=1$) there are always some m and n mode numbers which yield instability, that is no stable regions can be identified (cf. 10.5). Moreover, one sees that the stabilising effect the ideal wall at fixed a/b becomes less effective as m increases.

However, by comparing with Fig. 10.5, we are induced to infer that more peaked current profiles should mitigate this virulent growth.⁶ This is indeed the case as exemplified by figure 10.6 where the growth rates obtained from the numerical solution of (10.2) for two current profiles, one flat and the other parabolic, are shown.



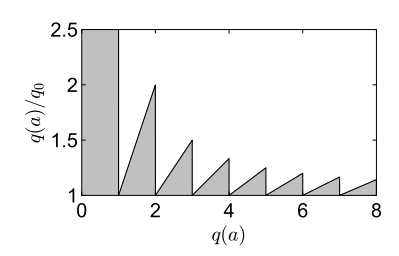


Figure 10.5: Marginal boundaries and expected instability region (shaded area) for the no-wall external kink stability with the stepped current profile. The vertical axis measures the peaking of the current (the flatter the current the more unstable the plasma).

⁶ This is not expected to hold for the m = 1 mode whose growth rate is independent of the shape of q, or current (cf. (10.2)).

Figure 10.6: No wall $(a/b \rightarrow 0)$ growth rate of the n=1 and $m=1,\ldots,4$ modes versus q(a) for a flat mass density profile with the current of the form $R_0^2 J^{\phi}/B_0 = \frac{2}{q_0}(1-(r/a)^2)^{\nu}$ with $\nu=0$ (a) and $\nu=1$ (b). With such a profile one has $q(a)/q_0=1+\nu$. High-m modes are stabilised if the edge current gradient is sufficiently small.

On the instability condition

Let us take a current profile of the form (10.15) and assume that we are close to the stability boundary identified by (10.22) with q(a) far from an integer (that is we focus on a neighbourhood of the oblique lines in figure (10.5) such that $k_{||}(a) \gg R_0^2 \rho_0(0) \gamma^2/B_0^2$). We now write the perturbed plasma displacement as

$$\xi_m^r = X_0 + X_2,\tag{10.24}$$

where both X_0 and X_2 are regular at the magnetic axis with $X_2/X_0 \sim (\gamma/\omega_A)^2$. We expand (10.2) in orders of $(\gamma/\omega_A)^2$ and by means of (10.10) we obtain $(' \equiv d/dr)$

$$\mathfrak{L}(X_0) \equiv \left(r^3 k_{||}^2 X_0'\right)' - r(m^2 - 1) k_{||}^2 X_0 = 0, \tag{10.25}$$

$$\mathfrak{L}(X_2) + r \left[r \bar{\gamma}^2 (r X_0)' \right]' - m^2 \bar{\gamma}^2 r X_0 = 0, \tag{10.26}$$

where $\bar{\gamma}^2 = R_0^2 \rho_0(r) \gamma^2 / B_0^2$. Multiplying (10.26) by X_0 and integrating from 0 to $a - \epsilon$ (ϵ has the usual meaning) yields

$$a^{3}k_{||}^{2}(a)\left[X_{0}X_{2}'-X_{2}X_{0}'\right]_{a-\epsilon} = \int_{0}^{a-\epsilon} X_{0}\mathfrak{L}(X_{2})dr$$

$$= -a^{2}\bar{\gamma}^{2}\left[X_{0}+rX_{0}X_{0}'\right]_{a-\epsilon} + \int_{0}^{a-\epsilon} r\bar{\gamma}^{2}\left(\left[(rX_{0})'\right]^{2}+m^{2}X_{0}^{2}\right)dr, \quad (10.27)$$

having made use of (10.25) with X_0 a real valued function. Plugging ξ_m^r from (10.24) into equation (10.8) gives

$$ak_{||}^{2}(a)\left(\xi_{v}^{\prime}\big|_{a+\epsilon}-X_{0}^{\prime}\big|_{a-\epsilon}\right)-ak_{||}^{2}(a)X_{2}^{\prime}\big|_{a-\epsilon}-\bar{\gamma}^{2}\left[rX_{0}^{\prime}+X_{0}\right]_{a-\epsilon}=0,$$

where, for the sake of clarity, we used ξ_v for denoting the vacuum perturbation (see (10.7)). When this is used in (10.27) to eliminate X_2' we get

$$\begin{split} a^{3}k_{||}^{2}(a)X_{0}(a-\epsilon)\left[\xi_{v}'\right|_{a+\epsilon}-X_{0}'\right|_{a-\epsilon}\right]-a^{3}k_{||}^{2}(a)\left[X_{2}X_{0}'\right]_{a-\epsilon}\\ &=\int_{0}^{a-\epsilon}r\bar{\gamma}^{2}\left(\left[(rX_{0})'\right]^{2}+m^{2}X_{0}^{2}\right)dr. \end{split}$$

Dividing this expression by $X_0(a - \epsilon)\xi_m^r(a)$ and exploiting the fact that $1/\xi_m^r(a) \approx (1 - X_2/X_0)/X_0|_{a-\epsilon}$ with $\xi_m^r(a) = \xi_v(a)$, to leading orders in $(\gamma/\omega_A)^2$ we finally obtain

$$ak_{||}^{2}(a) \left[\frac{d\xi_{v}/dr}{\xi_{v}} \Big|_{a+\epsilon} - \frac{dX_{0}/dr}{X_{0}} \Big|_{a-\epsilon} \right]$$

$$= \frac{1}{a^{2}X_{0}^{2}(a)} \int_{0}^{a-\epsilon} r\bar{\gamma}^{2} \left(\left[(rX_{0})' \right]^{2} + m^{2}X_{0}^{2} \right) dr, \qquad (10.28)$$

having dropped ϵ in the argument of X_0 . It is clear that **instability** occurs when the left-hand-side is positive. This is computed from Eqs. (10.12) and (10.17).

References

- T. J. M. Boyd and J. J. Sanderson, **The Physics of Plasmas**, Cambridge University Press (Cambridge, UK), 2003.
- R. Carruthers and P. A. Davenport, Proc. Phys. Soc. B 70, 49 (1957).
- M. Kruskal and M. Schwarzschild, Proc. R. Soc. Lond. A 223, 348 (1954).
- M. Kruskal and J. L. Tuck, Proc. R. Soc. Lond. A 245, 222 (1958).
- A. B. Mikhailovskii, **Instabilities in a Confined Plasma**, Institute of Physics Publishing (Bristol, UK), 1998.
- V. D. Shafranov, Atomnaya Energiya 1, No 5, 38 (1956) [J. Nucl. Energy 5, 86 (1957)].
- V. D. Shafranov, Zh. Tekh. Fiz. **40**, 241 (1970) [Sov. Phys.-Tech. Phys. **15**, 175 (1970)].
- J. A. Wesson, Nucl. Fusion 18, 87 (1978).
- J. A. Wesson, Tokamaks, Oxford University Press (Oxford, UK), 2011.

Mercier modes

We showed at the end of chapter 8 that in a toroidal plasma at low- β with a monotonic q profile and a **magnetic shear of the order of unity**, no long-wavelength global internal modes are allowed if the q = m/n resonance occurs within the plasma. However, with a small shear, along with infernal modes, **highly localised pressure driven** short wavelength perturbations ($m \gg 1$) can also become unstable.

These instabilities cause a localised ripple of neighbouring flux surfaces yielding an interchange of the associated fluid elements. From this, the name **interchange modes**. Such perturbations, which are typically characterised by a poloidal spectrum with a dominant Fourier harmonic, are found in the literature under many names: in a cylinder these are usually referred to as **Suydam modes**, whereas in a torus they are known as **Mercier modes**, after Suydam (1958) and Mercier (1961) who first described such instabilities in cylindrical and toroidal geometry respectively. Sometimes these perturbations are also called **flute instabilities**. In this chapter, we shall restrict our attention to interchange modes in a tokamak, thus hereafter we will address these instabilities as Mercier modes (we may still have a brief mention to Suydam modes when the specific case of a cylinder is considered which is a trivial reduction of the toroidal one).

Although rarely seen in tokamaks (an example of an interchangetype fluctuation which might be observed in present tokamak experiments is shown in figure 11.1), the techniques employed in the stability analysis of Mercier modes, particularly subtle in some points, are usually employed in the analytical treatment of their resistive counterpart, namely **resistive interchange modes**, and also for the more commonly observed instabilities known as **ballooning modes** (the latter will be

Figure 11.1: Example of an interchangelike perturbation with a core inverted pressure profile and q > 1 (see In (2000)). (a) Safety factor and pressure profiles. (b) Radial fluid displacement of the Mercier instability.

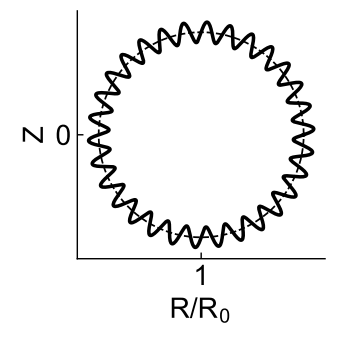
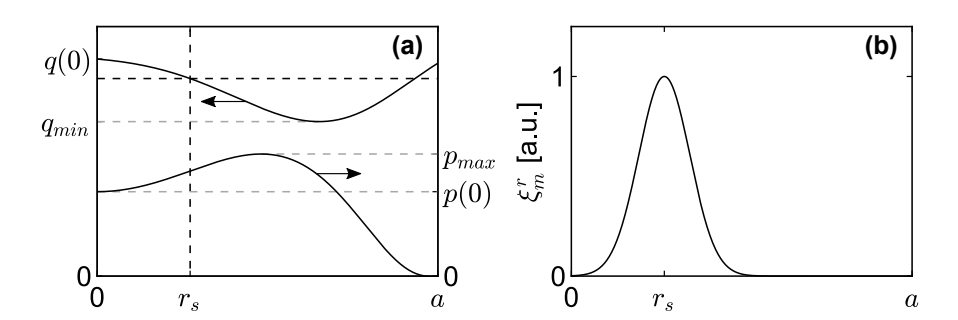


Figure 11.2: Example of the flux surface distortion due to a m = 30 interchange perturbation localised about its resonant surface (indicated by the dashed line). Compare with Fig. 10.1.



discussed in the next chapter even though we will study their stability properties using some alternative methods). Here we present a detailed exposition of the derivation of the eigenmode equations for Mercier modes, and a thorough discussion of the associated stability boundaries and growth rates.

11.1 Eigenmode equation

As for the instabilities analysed in the preceding chapters, the following derivation is based on the results presented in §7.4 and §7.5. As usual, we let $p_0/B_0^2 \lesssim \varepsilon^2$ with $rp_0' \sim p_0$ and look at a single toroidal harmonic at a time with fixed $n \gg 1$. Since $n \gg 1$ and $q \sim 1$, it necessarily follows that $m \gg 1$. These short wavelength perturbations are assumed to be highly localised about their resonant surface r_s for which $k_{||}(r_s) = m\mu(r_s) - n = 0$ (cf. (7.51)). This means that, ideally, the flux surfaces that get distorted by these instabilities are only those in a very narrow neighbourhood around r_s . An example of a flux surface perturbed by an interchange instability is shown in Fig. 11.2.

Following the logical steps discussed in §7.2, we assume that perturbed quantities fulfil the condition

$$\frac{1}{\tilde{f}}\frac{d\tilde{f}}{dx} \sim m \gg 1,\tag{11.1}$$

with $x = (r - r_s)/r_s$. Hence, the mode radial extension is expected to be proportional to $\frac{1}{m}$ so that we order $x \sim 1/m$. From this, we approximate

$$k_{||} \approx -nsx, \tag{11.2}$$

where here s is the magnetic shear at r_s . It follows that $nx \sim 1$ and $k_{||} \sim s$.

Using these estimates and the orderings presented in §7.4, from (7.55) one can write to leading order in $\frac{1}{m}$

$$P pprox rac{R_0}{B_0} p_0',$$

where it is implicitly assumed that $p'_0 = p'_0(r_s)$. The **eigenmode equation** is given by (7.65) which, for the sake of clarity, is reproduced below

for a flat mass density profile $(\rho'_0 = 0)$:

$$\begin{split} &\frac{1}{r}\frac{d}{dr}\left(\frac{r^{2}\langle N\rangle}{1+h}\hat{k}_{||}^{2}\frac{d\xi_{m}^{r}}{dr}\right) + \left\{r\hat{k}_{||}\left[\frac{1}{r}\left(\frac{\langle N\rangle(r\hat{k}_{||})'}{1+h}\right)' - m^{2}\hat{k}_{||}\langle L\rangle - m\frac{f_{0}'}{r}\langle\frac{f_{0}'}{B_{0}'}\rangle'\right] \right. \\ &+ m^{2}B_{0}\left[\frac{P^{2}}{R_{0}B_{0}} + \frac{n\mu'}{m}\frac{r^{2}}{R_{0}^{2}}P - nr\frac{k_{||}}{m^{2}}\left(\frac{rP}{R_{0}^{2}}\right)' - p_{0}'\left(\frac{\langle R^{2}\rangle'}{F} - \frac{\langle R^{2}\rangle F'}{F^{2}}\right)\right]\right\}\xi_{m}^{r} \\ &+ imB_{0}\sum_{m'}\left[ik_{||}C_{m}^{m'} + D_{m}^{m'} - E_{m}^{m'}(\hat{p}) - E_{m}^{m'}(\Delta p)\right] \\ &= -\frac{B_{0}^{2}}{R_{0}}\frac{\gamma^{2}}{\omega_{A}^{2}}\left[\frac{1}{r}\frac{d}{dr}\left(r^{3}\frac{d\xi_{m}^{r}}{dr}\right) - (m^{2} - 1)\xi_{m}^{r}\right], \end{split} \tag{11.3}$$

where \hat{p} is given by (7.59). Notice that we allowed the poloidal spectrum to contain more than one harmonic. It will be clear that, to the required accuracy, we can take

$$\frac{f_0'}{r} \to B_0, \quad \langle L \rangle \to \frac{1}{rR_0}, \quad \langle N \rangle \to \frac{r}{R_0}.$$

We shall now analyse each term in the equation above one by one.

By means of the above-mentioned ordering, and the discussion presented in §7.4, we easily obtain

$$\frac{1}{r}\frac{d}{dr}\left(\frac{r^2\langle N\rangle}{1+h}\hat{k}_{||}^2\frac{d\xi_m^r}{dr}\right)\approx\frac{n^2s^2B_0^2}{R_0}\frac{d}{dx}\left(x^2\frac{d\xi_m^r}{dx}\right).$$

Employing (7.68), the second term on the left-hand-side of (7.65) can be cast to leading order in 1/m as

$$r\hat{k}_{||}\left[\frac{1}{r}\left(\frac{\langle N\rangle(r\hat{k}_{||})'}{1+h}\right)'-m^2\hat{k}_{||}\langle L\rangle-m\frac{f_0'}{r}\langle\frac{J_0^{\phi}}{B_0^{\phi}}\rangle'\right]\approx -\frac{B_0^2}{R_0}(mnsx)^2.$$

Making use of (4.31), (4.33) and (5.21) the third term is rearranged as follows

$$\begin{split} &\frac{P^{2}}{R_{0}B_{0}} + \frac{n\mu'}{m} \frac{r^{2}}{R_{0}^{2}} P - nr \frac{k_{||}}{m^{2}} \left(\frac{rP}{R_{0}^{2}} \right)' - p'_{0} \left(\frac{\langle R^{2} \rangle'}{F} - \frac{\langle R^{2} \rangle F'}{F^{2}} \right) \\ &\approx \frac{R_{0}(p'_{0})^{2}}{R_{0}^{3}} - \frac{srp'_{0}}{q^{2}B_{0}R_{0}} - p'_{0} \left(\frac{\langle R^{2} \rangle'}{F} - \frac{\langle R^{2} \rangle F'}{F^{2}} \right) \\ &\approx \frac{p'_{0}}{B_{0}} \left[\frac{2r}{R_{0}} \left(1 - \frac{1}{q^{2}} \right) + \alpha + 2s\Delta' \right], \end{split}$$
(11.4)

where α is the **ballooning parameter** defined by (4.41) which is ordered as $\alpha \leq \varepsilon$. Note that the expression above is intended to be evaluated at r_s . In cylindrical geometry one has $\langle R^2 \rangle' = 0$, and the following replacement should be made:

$$\frac{p_0'}{B_0}\left[\frac{2r}{R_0}\left(1-\frac{1}{q^2}\right)+\alpha+2s\Delta'\right]\to -\frac{2rp_0'}{R_0B_0q^2}$$

We employ the relations

$$\langle R^2 \rangle' = -R_0 \left(\alpha + 2r/R_0 + 2s\Delta' \right),$$

 $F' = -R_0 B_0 \left[\frac{p'_0}{B_0^2} + \frac{r}{R_0^2 q^2} (2 - s) \right].$

We shall analyse now the inertial contributions exploiting the findings of section 7.4.2. The right-hand-side of (11.3) is readily cast as

$$\frac{1}{r}\frac{d}{dr}\left(\frac{\gamma^2}{\omega_A^2}r^3\frac{d\xi_m^r}{dr}\right) - \frac{\gamma^2}{\omega_A^2}(m^2 - 1)\xi_m^r \approx \frac{\gamma^2}{\omega_A^2}\left(\frac{d^2\xi_m^r}{dx^2} - m^2\xi_m^r\right),$$

while the term involving Δp is obtained from (9.9) and reads

$$-im\frac{R_0}{B_0}\sum_{m'}E_m^{m'}(\Delta p)\approx \frac{2m^2\gamma^2}{n^2\omega_A^2}\left(\frac{d^2\xi_m^r}{dx^2}-m^2\xi_m^r\right).$$

Note that in cylindrical geometry this term does not appear due to the fact that no coupling occurs between harmonics with different poloidal mode numbers. We may point out that for sufficiently small growth rates, inertial contributions should matter only very close to the mode resonance where the radial derivatives of ξ_m^r are expected to become large.

By collating these results together, we obtain

$$\frac{d}{dx}\left(x^{2}\frac{d\xi_{m}^{r}}{dx}\right) - \left\{m^{2}x^{2} + \frac{\alpha}{s^{2}}\left[\frac{r_{s}}{R_{0}}\left(1 - \frac{1}{q^{2}}\right) + \frac{\alpha}{2} + s\Delta'\right]\right\}\xi_{m}^{r} + \frac{\gamma^{2}(1 + 2q^{2})}{n^{2}s^{2}\omega_{A}^{2}}\left(\frac{d^{2}\xi_{m}^{r}}{dx^{2}} - m^{2}\xi_{m}^{r}\right) = -\frac{imR_{0}}{n^{2}s^{2}B_{0}}\sum_{m'}\left[ik_{||}C_{m}^{m'} + D_{m}^{m'} - E_{m}^{m'}(\hat{p})\right].$$
(11.5)

It is clear that, from balancing all terms in the equation above so that they are of similar magnitude, **the magnetic shear must be small** hence we take $s \sim \varepsilon$.

We now analyse the right-hand-side of (11.5), namely the contributions due to couplings with the neighbouring sidebands. Similar to the term which generates the **inertia enhancement** factor, these corrections vanish in a cylinder, thence the following analysis pertains toroidal geometry only. By means of (7.63) and (8.12), one can verify that

$$\frac{mR_0}{n^2 s^2 B_0} E_m^{m'}(\hat{p}) \sim \frac{\alpha}{s^2} \xi_{m\pm 1}^r,$$
 (11.6)

with $m'=\pm 1$ which is valid also when $rd\xi_{m\pm 1}^r/dr\sim m\xi_{m\pm 1}^r$. Explicitly, one has

$$E_m^{\pm 1}(\hat{p}) = -\frac{ip_0'}{B_0} \left(m \xi_{m\pm 1}^r \pm \frac{d \xi_{m\pm 1}^r}{dx} \right).$$

Without loss of generality, we assume that (11.1) holds for the $m \pm 1$ modes as well so that

$$\frac{r}{m\pm 1}\frac{d}{dr}\sim 1. \tag{11.7}$$

Thus, from (7.49) we see that $(\sqrt{g}\tilde{B}^{\phi})_{m\pm 1} \sim B_0 \varepsilon^2 \xi_m^r$ and by means of (7.25) we obtain $r(\sqrt{g}\tilde{B}^{\theta})_{m\pm 1} \sim (\sqrt{g}\tilde{B}^r)_{m\pm 1}$. Hence, we can write

$$(\sqrt{g}\tilde{B}^r)_{m\pm 1} \sim rB_0\xi_{m\pm 1}^r, \quad (\sqrt{g}\tilde{B}^{\vartheta})_{m\pm 1} \sim B_0\xi_{m\pm 1}^r.$$
 (11.8)

Employing (8.14), one has from (7.62)

$$\frac{mR_0}{n^2 s^2 B_0} D_m^{m'} \sim \frac{\alpha}{m s^2} \xi_{m\pm 1}^r.$$
 (11.9)

Due to the smallness of the magnetic shear, it is immediate to recognise that this contribution can be neglected when compared with the one involving $E_m^{m'}$. The remaining term is evaluated using (7.53) which gives

$$\frac{mR_0}{n^2 s^2 B_0} k_{||} C_m^{m'} \sim \frac{\varepsilon}{s} \xi_{m\pm 1}^r.$$
 (11.10)

Thus, since $\varepsilon s/\alpha \ll 1$, we may neglect the contribution arising from (11.10) compared with the one associated with (11.6).

Using the condition $s \ll 1$ once more and thanks to the fact that $\Delta \sim r\alpha$, equation (11.5) can be cast as

$$\begin{split} \frac{d}{dx} \Big((x^2 + \gamma_H^2) \frac{d\xi_m^r}{dx} \Big) - \left[m^2 (x^2 + \gamma_H^2) + \frac{\alpha r}{s^2 R_0} \left(1 - \frac{1}{q^2} \right) + \frac{\alpha^2}{2s^2} \right] \xi_m^r \\ &= \frac{i m R_0}{n^2 s^2 B_0} \sum_{m'} E_m^{m'} (\hat{p}) = -\frac{\alpha}{2 m s^2} \sum_{\pm} \left(m \xi_{m\pm 1}^r \pm \frac{d\xi_{m\pm 1}^r}{dx} \right), \quad (11.11) \end{split}$$

having defined

$$\gamma_H^2 = \frac{\gamma^2 (1 + 2q^2)}{n^2 s^2 \omega_A^2}.$$
 (11.12)

Taking the sidebands $\xi_{m\pm 1}^r$ to be of higher order compared with the harmonic ξ_m^r , they are expected to obey equation (7.71). Since the magnetic shear is small, this equation can be reduced to (9.6) or (9.7). For localised perturbations with $m \gg 1$ this is cast as

$$\left(\frac{d^2}{dx^2} - m^2\right) \xi_{m\pm 1}^r = \pm \frac{m\alpha}{2} \left(\frac{d}{dx} \mp m\right) \xi_m^r,\tag{11.13}$$

which, assuming once again that (11.7) holds, shows that

$$\xi_{m+1}^r \sim \alpha \xi_m^r$$

implying that the right-hand-side of (11.11) is a quantity of order $\frac{\alpha^2}{c^2} \xi_m^r$ Equation (11.13) can be readily integrated giving

$$\left(\frac{d}{dx} + m\right) \xi_{m+1}^r = \frac{m\alpha}{2} \xi_m^r + C_+ e^{mx},$$

$$\left(\frac{d}{dx} - m\right) \xi_{m-1}^r = -\frac{m\alpha}{2} \xi_m^r + C_- e^{-mx}.$$

When these expressions are plugged into (11.11) we obtain

$$\frac{d}{dx}\left((x^2 + \gamma_H^2)\frac{d\xi_m^r}{dx}\right) - \left[m^2(x^2 + \gamma_H^2) + \frac{\alpha r}{s^2 R_0}\left(1 - \frac{1}{q^2}\right)\right]\xi_m^r \\
= -\frac{\alpha}{2ms^2}\left(C_+e^{mx} - C_-e^{-mx}\right).$$

This is essentially the localised $m \gg 1$ limiting case of (9.12) where Q is given by (9.11) with $k_{||} = m\mu - n$.

Note that since $m \gg 1$ one can replace $m \rightarrow m \pm 1$ with no harm.

 $(r/r_s)^m = e^m \ln(r/r_s) \approx e^m \ln(1+x) \approx e^{mx}$

The requirement that ξ_m^r is well localised about its own resonance implies that $C_\pm \to 0$.

Note that we could have obtained the same result by ignoring terms proportional to α^2 under the assumption that the pressure gradient is sufficiently weak. More specifically, taking the ratio between the second and third term in square brackets in (11.11) and asking that the result is small yields $\alpha \ll \varepsilon$. Therefore, in equation (11.11) all the α dependent terms but the one proportional to $(1-1/q^2)$ may be dropped. These conditions are fulfilled by ordering

$$\alpha \sim \varepsilon^{3/2}$$
, $s \sim \varepsilon$.

Thus, changing variable from x to z = mx, the equation which governs the dynamics of Mercier (or Suydam in a cylinder) modes is

$$\frac{d}{dz}\left((z^2 + m^2\gamma_H^2)\frac{d\xi_m^r}{dz}\right) - \left(z^2 + m^2\gamma_H^2 + \hat{U}\right)\xi_m^r = 0,\tag{11.14}$$

where

$$\hat{U} = \begin{cases} -\frac{\alpha r}{s^2 R_0 q^2}, & \text{cylinder,} \\ \frac{\alpha r_s}{s^2 R_0} \left(1 - \frac{1}{q^2}\right), & \text{torus.} \end{cases}$$
(11.15)

Note that we let $\hat{U} \sim 1$. As mentioned earlier, in a cylinder there is no inertia enhancement arising from the sideband compressibility, so that for this case we must perform the replacement $\gamma_H^2 \to \frac{\gamma^2}{n^2 s^2 \omega_A^2}$. Following the same reasoning which led to (8.7), the width of the layer where inertial contributions become relevant is approximately¹

$$\frac{\delta r}{r_s} \sim \frac{\gamma \sqrt{1 + 2(m/n)^2}}{ns\omega_A}.$$
 (11.16)

In the next sections, information on marginal stability boundaries, growth rates and mode radial structure is extracted from the analysis of equation (11.14).

11.2 The Mercier stability criterion

Since $m \gg 1$, the perturbation is highly localised and we may let z to vary from $-\infty$ to $+\infty$. Let us assume ξ_m^r to be a real function. In the limit of $z \to \infty$, Eq. (11.14) reduces to

$$\frac{d}{dz}\left(z^2\frac{d\xi_m^r}{dz}\right) - z^2\xi_m^r = 0,$$

whose solution which decays at infinity is proportional to $\exp(-|z|)/z$. This shows that both ξ_m^r and $z\xi_m^r$ are **square integrable** for $-\infty < z < \infty$

¹ Compared to (8.7), the inertia enhancement factor is generalised to modes with m > 1.

if ξ_m^r is well behaving at the origin. Hence, we multiply (11.14) by ξ_m^r and integrate from $-\infty$ to $+\infty$. This gives

$$m^{2}\gamma_{H}^{2} \int_{-\infty}^{\infty} \left(\left| \frac{d\xi_{m}^{r}}{dz} \right|^{2} + |\xi_{m}^{r}|^{2} \right) dz = - \int_{-\infty}^{\infty} \left[z^{2} \left| \frac{d\xi_{m}^{r}}{dz} \right|^{2} + \left(z^{2} + \hat{U} \right) |\xi_{m}^{r}|^{2} \right] dz.$$
(11.17)

Using Schwarz inequality, we have²

$$\frac{1}{4} \int_{-\infty}^{\infty} |\xi_m^r|^2 dz \le \int_{-\infty}^{\infty} z^2 \left| \frac{d\xi_m^r}{dz} \right|^2 dz,$$

so that

$$m^{2}\gamma_{H}^{2} \int_{-\infty}^{\infty} \left(\left| \frac{d\xi_{m}^{r}}{dz} \right|^{2} + |\xi_{m}^{r}|^{2} \right) dz \le - \int_{-\infty}^{\infty} \left(z^{2} + \hat{U} + \frac{1}{4} \right) |\xi_{m}^{r}|^{2} dz. \quad (11.18)$$

Hence, if $\hat{U} + 1/4 \ge 0$ the right-hand-side of the expression above is always negative, and therefore stability is guaranteed. Note that we could have drawn the same conclusion by using the equality (which holds for a function decreasing as $\exp(-|z|)$ for $z \to \infty$)

$$\int_{-\infty}^{\infty} \left(z^2 \left| \frac{d\xi_m^r}{dz} \right|^2 - \frac{1}{4} |\xi_m^r|^2 \right) dz = \int_{-\infty}^{\infty} \left(z \frac{d\xi_m^r}{dz} + \frac{1}{2} \xi_m^r \right)^2 dz.$$

We may now infer that $\hat{U} + 1/4 = 0$ identifies the marginal stability boundary, that is $\gamma \to 0$ for $\hat{U} \to -\frac{1}{4}$, by arguing that perturbations described by Eq. (11.14) are so localised in space about z = 0, so that the contribution due to the term proportional to z^2 on the right-handside of (11.18) is negligible. It will be indeed proven in the next section that the stability boundary is identified by the relation $\hat{U} + 1/4 = 0$, this eventually leading to the following stability criterion:

$$-\frac{1}{4} \le \begin{cases} \frac{2r_s p_0'(r_s)}{s^2 B_0^2}, & \text{cylinder,} \\ \frac{2r_s p_0'(r_s)}{s^2 B_0^2} \left(1 - q^2\right), & \text{torus.} \end{cases}$$
(11.19)

In toroidal geometry this is known as **Mercier stability criterion**, whereas in a cylinder it takes the name of **Suydam stability criterion**. Note that this is a local criterion, in that it determines stability against localised perturbations at a single resonant surface. Hence, the equilibrium is stable against Mercier (or Suydam) modes if (11.19) is fulfilled at each radial position.

Since in tokamaks the safety factor is usually larger than unity for most of the plasma radius, it is clear from (11.19) why, with a decreasing pressure profile, Mercier modes are rare events. These may still develop in regions where q < 1, but in such cases they are typically overshadowed by the m = 1 internal kink activity (some more detailed considerations on the existence of Mercier modes are discussed in the box at the end of this chapter).

The next section is devoted to the derivation of the dispersion relation, i.e. the growth rate.

² For a square integrable real function f the following relation holds

$$\begin{split} &\frac{1}{4} \left[\int_{-\infty}^{\infty} f^2 dz \right]^2 = \left[\frac{1}{2} \int_{-\infty}^{\infty} z \frac{df^2}{dz} dz \right]^2 \\ &= \left[\int_{-\infty}^{\infty} z f \frac{df}{dz} dz \right]^2 \\ &\leq \left[\int_{-\infty}^{\infty} z^2 \left(\frac{df}{dz} \right)^2 dz \right] \left[\int_{-\infty}^{\infty} f^2 dz \right]. \end{split}$$

In the literature, the criterion (11.19) can be found written as e.g. $D_M < 1/4$, $D_I < 0$ or sometimes $D_I > 0$. It is worth pointing out that plasma shaping can strongly modify this criterion: elongation of the flux surfaces alone is detrimental for stability, whereas adding a small amount of triangularity improves it (Lutjens (1992)).

11.3 Dispersion relation and growth rate

Having established the conditions which allow localised perturbations to be unstable, we now focus on determining their growth rate. This requires a more advanced mathematical treatment, involving the derivation of a dispersion relation through the **asymptotic matching** of approximate solutions. Let us introduce the parameter

$$v = \sqrt{\hat{U} + 1/4}.\tag{11.20}$$

Since (11.19) predicts stability for v > 0, we let $\hat{U} < -1/4$. This means that v is purely imaginary.

We recast equation (11.14) in terms of the variable $y = z/(m\gamma_H)$, with γ_H a positive definite quantity, as

$$\frac{d}{dy}\left((1+y^2)\frac{d\xi_m^r}{dy}\right) - m^2\gamma_H^2\left(1+y^2 + \frac{\hat{U}}{m^2\gamma_H^2}\right)\xi_m^r = 0.$$
 (11.21)

We let γ_H to be small enough so that $\hat{U}/(m^2\gamma_H^2)\gg 1.^3$ Hence, the unity factor in the second term of the left-hand-side of (11.21) can be neglected. The resulting equation is thus analysed in two limiting cases, one for which $y\gg 1$ and the other with $y\lesssim 1$.

Starting with the large y case, ξ_m^r obeys

$$\frac{d}{dy} \left(y^2 \frac{d\xi_m^r}{dy} \right) - m^2 \gamma_H^2 \left(y^2 + \frac{\hat{U}}{m^2 \gamma_H^2} \right) \xi_m^r = 0, \tag{11.22}$$

whose solution which is regular at infinity is

$$\xi_m^r \sim \frac{K_\nu(|z|)}{\sqrt{|z|}},\tag{11.23}$$

where K_{ν} is the modified Bessel function of second kind. We call this the **outer solution**.

In the opposite limit, when $y \leq 1$, Eq. (11.21) reduces to

$$\frac{d}{dy}\left((1+y^2)\frac{d\xi_m^r}{dy}\right) - \hat{U}\xi_m^r = 0.$$
 (11.24)

By letting $X = -y^2$, this is transformed into a hypergeometric differential equation

$$X(1-X)\frac{d^{2}\xi_{m}^{r}}{dX^{2}}+\left(\frac{1}{2}-\frac{3}{2}X\right)\frac{d\xi_{m}^{r}}{dX}+\frac{\hat{U}}{4}\xi_{m}^{r}=0,$$

whose two linearly independent solutions Y_{e} (even) and Y_{o} (odd) are

$$Y_{e} = {}_{2}F_{1}\left(A, B; C; -y^{2}\right),$$

$$Y_{g} = y \times {}_{2}F_{1}(A - C + 1, B - C + 1; 2 - C; -y^{2}),$$
(11.25)

The $\nu = 0$ case is discussed as the limit $\nu \to 0$.

³ This means that we are investigating the behaviour close to the marginal stability boundary, i.e. $\gamma \to 0$.

⁴ These solutions can be analytically continued for Re(X) < 0 in the complex plane. Note that since ${}_2F_1(A,B;C;0) = {}_2F_1(A-C+1,B-C+1;2-C;0) = 1$, it follows that ξ_m^r is well defined for X=0.

where $_2F_1$ is the hypergeometric function and

$$A = \frac{1}{2} \left(\frac{1}{2} - \nu \right), \quad B = \frac{1}{2} \left(\frac{1}{2} + \nu \right), \quad C = 1/2.$$

Therefore, for $y \lesssim 1$ one has

$$\xi_m^r = c_1 Y_e + c_2 Y_o, \tag{11.26}$$

where c_1 and c_2 are some constants. This is referred to as the **inner** solution.

The dispersion relation is obtained by matching asymptotically (11.23) and (11.26) when $1 \ll y \ll \frac{\sqrt{\hat{U}}}{m_{YH}}$ (this procedure is depicted graphically in figure (8.4)). We first note that for $y \ll \frac{\sqrt{\hat{U}}}{m\gamma_H}$ one has $z \ll \sqrt{\hat{U}} \sim 1$. Therefore, we can perform a small argument expansion of (11.23) yielding⁵

$$\xi_m^r \sim |z|^{-\frac{1}{2}-\nu} \left[1 + \frac{\Gamma(-\nu)}{\Gamma(\nu)} \left(\frac{|z|}{2} \right)^{2\nu} \right],$$
 (11.27)

which holds for both z < 0 and z > 0. The asymptotic behaviour of $Y_{e,o}$ is obtained by applying formula (Lebedev (1965))

$${}_{2}F_{1}(a,b;c;-y^{2}) = \left(1+y^{2}\right)^{-a} \frac{\Gamma(c)\Gamma(b-a)}{\Gamma(c-a)\Gamma(b)} {}_{2}F_{1}\left(a,c-b;1+a-b;\frac{1}{1+y^{2}}\right) + \left(1+y^{2}\right)^{-b} \frac{\Gamma(c)\Gamma(a-b)}{\Gamma(c-b)\Gamma(a)} {}_{2}F_{1}\left(c-a,b;1-a+b;\frac{1}{1+y^{2}}\right)$$

to Eqs. (11.26). Thus, by letting $y \gg 1$ we easily get

$$Y_e \sim |z|^{-rac{1}{2}-
u} \left[1 + \Delta_e \left(rac{|z|}{m\gamma_H}
ight)^{2
u}
ight], \quad Y_o \sim |z|^{-rac{1}{2}-
u} \left[1 + \Delta_o \left(rac{|z|}{m\gamma_H}
ight)^{2
u}
ight],$$

where

$$\Delta_{e} = \frac{\Gamma(\nu)\Gamma^{2}(\frac{1}{4} - \frac{\nu}{2})}{\Gamma(-\nu)\Gamma^{2}(\frac{1}{4} + \frac{\nu}{2})}, \quad \Delta_{o} = \frac{\Gamma(\nu)\Gamma^{2}(\frac{3}{4} - \frac{\nu}{2})}{\Gamma(-\nu)\Gamma^{2}(\frac{3}{4} + \frac{\nu}{2})}.$$
 (11.29)

Therefore, it follows that the inner solution behaves asymptotically as

$$\xi_{m}^{r} \propto \begin{cases} |z|^{-\frac{1}{2}-\nu} \left[1 + \left(\frac{|z|}{m\gamma_{H}} \right)^{2\nu} \frac{c_{1}\Delta_{e} + c_{2}\Delta_{o}}{c_{1} + c_{2}} \right], & z > 0, \\ |z|^{-\frac{1}{2}-\nu} \left[1 + \left(\frac{|z|}{m\gamma_{H}} \right)^{2\nu} \frac{c_{1}\Delta_{e} - c_{2}\Delta_{o}}{c_{1} - c_{2}} \right], & z < 0. \end{cases}$$
(11.30)

Matching (11.27) with (11.30) gives

$$\frac{\Delta_e + \frac{c_2}{c_1} \Delta_o}{1 + \frac{c_2}{c_1}} = \left(\frac{m\gamma_H}{2}\right)^{2\nu} \frac{\Gamma(-\nu)}{\Gamma(\nu)} = \frac{\Delta_e - \frac{c_2}{c_1} \Delta_o}{1 - \frac{c_2}{c_1}}.$$
 (11.31)

One can see that this equation can be satisfied only if $c_2/c_1 = 0$ (even ξ_m^r) or $c_2/c_1 \to \infty$ (odd ξ_m^r).

⁵ We use the relation $K_{\nu}(z) \propto I_{-\nu}(z)$ – $I_{\nu}(z)$ where I_{ν} is the modified Bessel function of first kind.

This is valid for $a - b \neq 0, \pm 1, \pm 2, \ldots$ and $c \neq \dots, -2, -1, 0$. Note that here a, b and c denote generic numbers and must not be confused with the plasma or wall

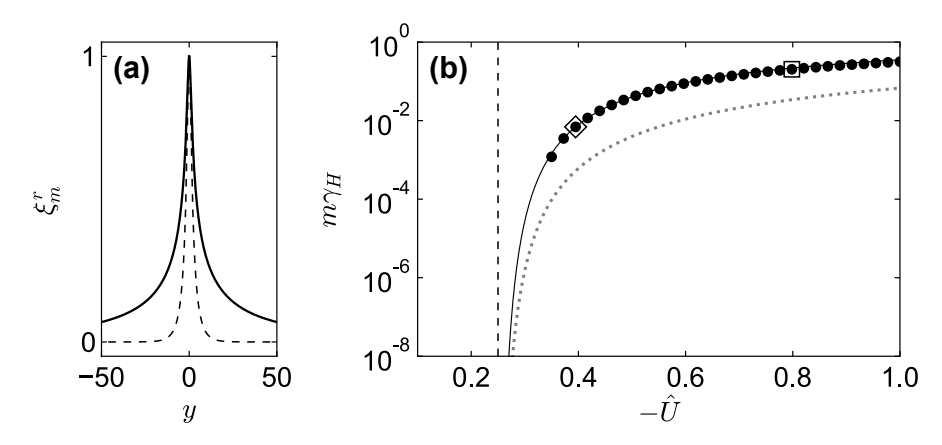


Figure 11.3: Even mode eigenfunctions (a) and growth rates (b). In (a) the solid(dashed) curve is the numerical solution of (11.21) with $-\hat{U} \approx 0.4(0.8)$ corresponding to the diamond(square) in (b). In panel (b) the solid(dotted) line is the growth rate of even(odd) modes computed from Eq. (11.33), whereas the numerical solution for even modes is represented by the dots. The dashed vertical line gives the $-\hat{U} = 1/4$ location.

It is a feature typical of high-m modes to have eigenfunctions with a definite parity: even parity in ξ is called **interchange parity** (or twisting sometimes) whereas odd parity in ξ is referred to as **tearing parity**.⁶

Using the property of the Gamma function $x\Gamma(x) = \Gamma(1+x)$, the resulting dispersion relation then reads

$$\left(\frac{m\gamma_H}{2}\right)^{2\nu} = \begin{cases}
\frac{\Gamma^2(1+\nu)\Gamma^2(\frac{1}{4}-\frac{\nu}{2})}{\Gamma^2(1-\nu)\Gamma^2(\frac{1}{4}+\frac{\nu}{2})}, & \text{even modes,} \\
\frac{\Gamma^2(1+\nu)\Gamma^2(\frac{3}{4}-\frac{\nu}{2})}{\Gamma^2(1-\nu)\Gamma^2(\frac{3}{4}+\frac{\nu}{2})}, & \text{odd modes.}
\end{cases}$$
(11.32)

We shall now express the growth rate associated with even and odd modes in a more explicit form.

Since ν is purely imaginary we write $\nu = i\chi$ with $\chi > 0$. Thus, by exploiting the fact that $x = \exp[\log(x) - 2ik\pi]$ and using (11.12), the growth rate is ⁷

$$\frac{\gamma q \sqrt{1+2q^2}}{s\omega_A} = 2 \exp\left[-\frac{k\pi}{\chi} + \frac{2}{\chi} \arg(\Gamma(1+i\chi)) + \frac{2}{\chi} \arg(\Gamma(\frac{t}{4}-i\frac{\chi}{2}))\right],\tag{11.33}$$

with t=1 for even modes, t=3 for odd modes and $k=0,\pm 1,\pm 2,\ldots$ We first notice that, since the arg function is bounded, $\gamma\to 0$ only when $\chi\to 0$. Hence, by expanding (11.33) for $\chi\ll 1$, we obtain

$$\frac{\gamma q \sqrt{1+2q^2}}{s\omega_A} = 2 \exp\left[-\frac{k\pi}{\chi} + 2\Psi(1) - \Psi(t/4)\right],$$

where Ψ denotes the Digamma function. The ambiguity on the choice of k is resolved by imposing that the growth rate does not present a discontinuity for $\nu \to 0$. From this, it follows that only $k = 1, 2, \ldots$

$$\Gamma(\overline{c}) = \overline{\Gamma(c)}, \quad \log \Gamma(\overline{c}) = \overline{\log \Gamma(c)}.$$

⁶ Note that \tilde{B}^r has opposite parity compared to ξ . It is not uncommon to have parity referring to \tilde{B}^r rather that ξ , and thus the odd(even) parity in \tilde{B} is referred to as interchange(tearing) parity.

⁷ Letting an overbar to denote complex conjugation, the argument of a complex number c is given by $\arg(c) = -i\log\frac{c}{|c|} = -\frac{i}{2}\log\frac{c}{c}$. Note also that the Gamma function fulfils

values are allowed with k = 1 identifying the largest growth rate. We also note that since $\Psi(1/4) < \Psi(3/4)$, even modes grow faster than odd modes. The numerically computed eigenfunction and associated growth rates for Mercier/Suydam modes obtained from (11.21) are shown in figure 11.3 where the comparison with Eq. (11.33) is also given. Finally, the behaviour of the matched inner and outer analytic eigenfunctions from Eqs. (11.27) and (11.27) is depicted in Fig. 11.4, which is also compared with the numerical solution.

Some remarks on Mercier modes existence conditions

Inequality (11.19) poses very strict constraints on the instability window of Mercier modes. It is evident that these perturbations may become unstable if either q < 1 with $p'_0 < 0$, or q > 1 and $p_0' > 0$. The latter case is rarely observed (pressure gradient reversals are unlikely, particularly if in steady state and far from the magnetic axis, cf. Fig. 11.1).

For the $p'_0 < 0$ case, (11.19) suggests that these instabilities can develop only where q drops below unity, and they are mostly unstable in regions of weak magnetic shear, i.e. close to the axis. However, although $\hat{U} \sim 1/s^2$ can become large, γ scales linearly with s (cf. Eq. (11.33)) meaning that Mercier modes developing in these regions are expected to have very small growth rates.

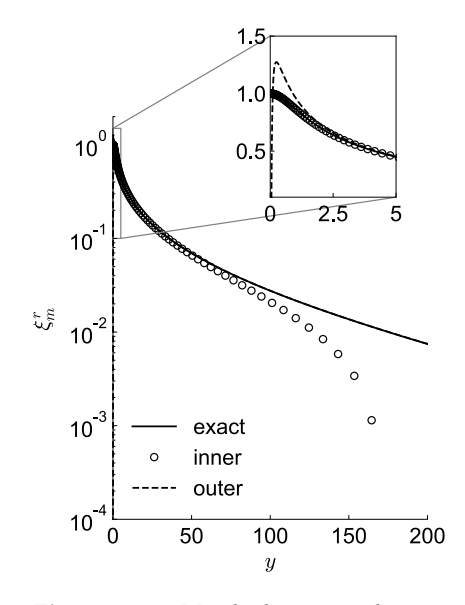


Figure 11.4: Matched inner and outer eigenfunctions compared with the numerically computed solution for the $-\hat{U} \approx 0.4$ case of figure 11.3. Note the linear scale of the y-axis of the inset figure. The exact solution almost overlaps the outer one for large y.

References

- J. M. Greene and J. L. Johnson, Phys. Fluids 5, 510 (1962).
- S. Gupta et al., Phys. Plasmas 9, 3395 (2002).
- Y. In et al., Phys Plasmas 7, 5087 (2000).
- B. B. Kadomtsev and O. P. Pogutse, Dokl. Akad. Nauk SSSR 170, 811 (1966) [Sov. Phys.-Dokl. 11, 858 (1967)].
- R. M. Kulsrud, Phys. Fluids 6, 904 (1963).
- H. Lütjens et al., Nucl. Fusion 32, 1625 (1992).
- C. Mercier, Nucl. Fusion 1, 47 (1960).
- · C. Mercier and H. Luc, Lectures in Plasma Physics: The Magnetohydrodynamic Approach to the Problem of Plasma Confinement in Closed Magnetic Configurations (Commission of the European Communities, Luxembourg), 1974.
- A. B. Mikhailovskii, Instabilities in a Confined Plasma, Institute of Physics Publishing (Bristol, UK), 1998.
- K. Miyamoto, Fundamentals of Plasma Physics and Controlled Fusion, Iwanami Book Service Center (Tokyo, JP), 1997.
- T. Nicolas and K. Ichiguchi, Nucl. Fusion 56, 026008 (2016).
- V. D. Shafranov and E. I. Yurchenko, Zh. Eksp. Teor. Fiz. 53, 1157 (1967) [Sov. Phys.-JETP 26, 682 (1968)].

- L. S. Solov'ev, Zh. Eksp. Teor. Fiz. **53**, 2063 (1967) [Sov. Phys.-JETP **26**, 1167 (1968)].
- T. E. Stringer, Nucl. Fusion 15, 125 (1975).
- B. R. Suydam, in Proceedings of the Second United Nation International Conference on the Peaceful Uses of Atomic Energy (United Nations Geneva, 1958) Vol. 31, p. 157.
- A. A. Ware and F. A. Haas, Phys. Fluids 9, 956 (1966).

12

Ballooning modes

Numerical investigations of the highest attainable pressure in toroidal devices initiated the interest in ballooning modes. These studies showed that as β was increased too much, instabilities bulging in the outer edge of the torus, the tokamak low-field-side (LFS), featuring a mix of poloidal harmonics (**ballooning character**) were triggered. Unless the safety factor profile has broad regions of weak shear¹ the most pessimistic prediction for the maximum achievable pressure is usually dictated by the stability properties of modes with large toroidal mode numbers $(n \to \infty)$. We refer to such perturbations as **ballooning modes**.

Like infernal and Mercier modes, large-*n* balloonings are **pressure driven** instabilities sharing with the former a poloidal spectrum which is a superposition of multiple harmonics, and with the latter a pronounced radial localisation. Differently from infernal instabilities, the spectral content of ballooning modes is much richer in that is composed of a large number of poloidal harmonics of similar amplitude (cf. Fig. 12.1) which results in a much broader radial extension compared to that of Mercier modes (infernal modes can be considered as a particular case of **low**-*n* **ballooning**-type perturbations with a spectrum characterised by three harmonics only). Figure 12.2 shows the interference pattern of several and almost equivalent poloidal harmonics resulting in the bulging in the region of weaker toroidal magnetic field.

In experiments, such type of perturbations are commonly observed in regions where the local reduction of transport² allows large pressure gradients to develop. These are referred to as **transport barriers**. They can form either in the core or at the plasma edge, or both. Internal transport barriers (ITBs) usually develop in scenarios with weak or negative shear, and infernal-type low-*n* precursors are often observed before

¹ In these cases the stabilising effect of field line bending is reduced and infernal-type perturbations are likely to be triggered.

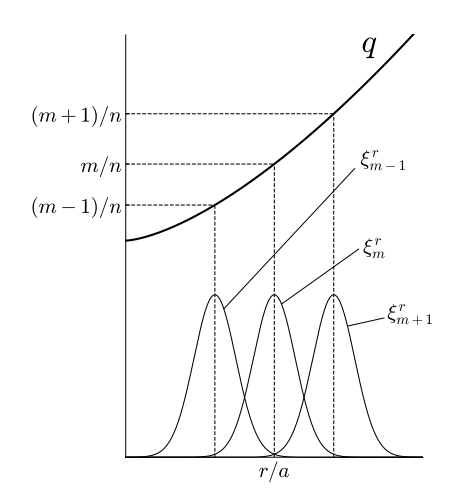


Figure 12.1: Harmonics of a generic fluid displacement ξ for a $n \gg 1$ ballooning-like perturbation.

² This can be of particles, momentum, and heat either for ions or electrons.

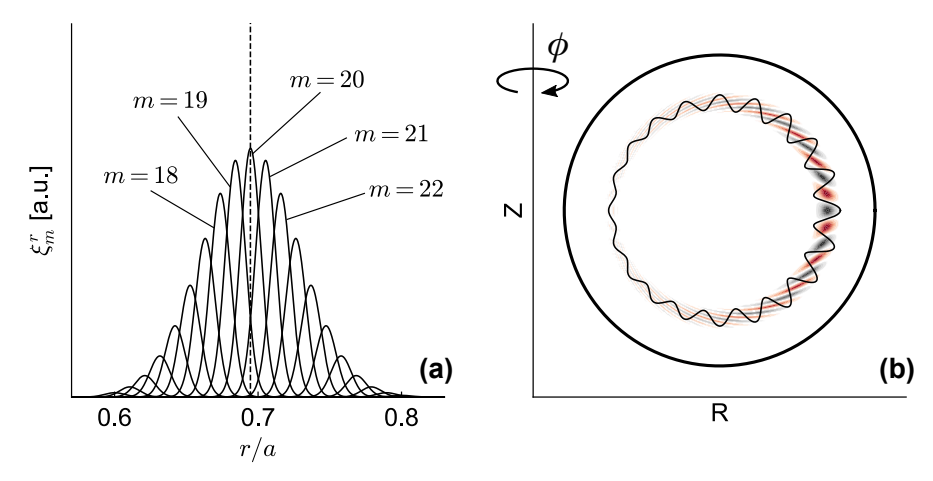


Figure 12.2: Rough example of the structure of a medium-n ballooning mode. The poloidal spectrum in the angle θ (chosen for convenience to be the geometric angle) of the radial fluid displacement consisting of 20 harmonics ranging from m = 10 to m = 30 is shown in (a). In (b) the contours (red for negative and black for positive) of $\xi^r(r,\theta) = \sum_m \xi_m^r(r) \cos(m\theta)$ are shown. The wiggly curve in (b) corresponds to the distorted flux surface at the position highlighted by the vertical dashed line in (a). The interference of the various harmonics forces the distortion of the flux surfaces to be weaker on the high-field-side for all toroidal angles. In a realistic geometry the bulging aligns with the lines of constant straightened angle.

a disruptive plasma termination.

Edge transport barriers (ETBs) are what typically characterise the so called high confinement operating regime (or **H-mode** in short): discovered in the early 80s in the ASDEX tokamak, the plasma was observed to transition spontaneously into a state of improved confinement when a threshold in the externally applied heating power was exceeded. This transition from low to high confinement is known in tokamak jargon as L-H transition. Associated with this confinement enhancement is the formation of strong edge pressure gradients. When the pressure gradient becomes too strong, quasi-periodic relaxation phenomena affecting the edge of the plasma known as Edge Localised Modes (ELMs) may appear.3 Ballooning modes are believed to play an important role in making ELMs occur. Figure 12.3 shows an example of the typical profiles associated with ETBs and ITBs (notice that ETBs and ITBs can occur simultaneously).

The aim of this chapter is therefore to provide a detailed characterisation of the phenomenology of ballooning modes. First we derive an eigenmode equation which accounts for the richness of the poloidal spectrum of ballooning instabilities for the cases of both weak and strong magnetic shear; we then detail various mathematical techniques used for tackling the solution of the eigenmode equation in these two limits. A thorough discussion on mode parity, growth rate and marginal boundaries is finally presented.

³ ELMs, which are ubiquitous in H-mode tokamak plasmas, are periodic bursts relaxing the edge pressure with a filamentary structure accompanied by a sudden particle and energy expulsion associated with large heat fluxes onto the vessel wall. Although ELMs may be helpful for the flushing of the impurities which tend to accumulate in the plasma, the heat loads associated with these events are generally not tolerable for the integrity of the components facing the plasma.

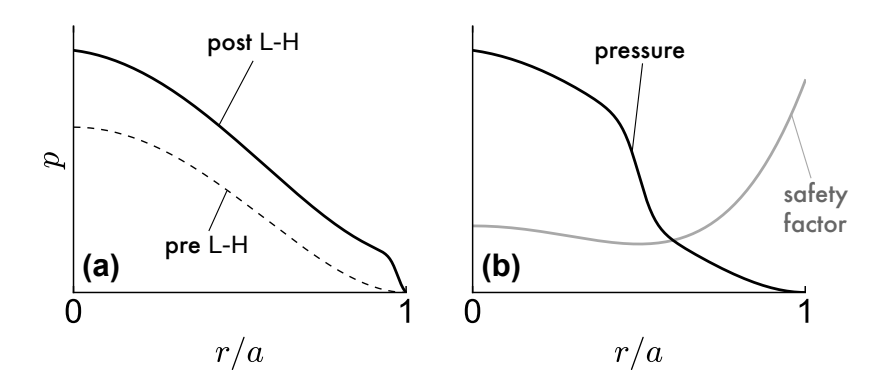


Figure 12.3: Pressure profiles in ETB regimes before and after the L-H transition (a) and in scenarios with ITBs (b). In (b) the shape of a safety factor typically seen in ITB plasmas is also shown.

The ballooning equation 12.1

It is instructive to discuss first the derivation of the ballooning equation in regimes of small pressure gradient and weak magnetic shear (these conditions are usually met near the magnetic axis).

Let us fix the toroidal mode number $n \gg 1$,⁴ and express a generic perturbed quantity \tilde{f} as

$$\tilde{f} = \sum_{m} \tilde{f}_{m} e^{im\vartheta - in\phi}.$$
 (12.1)

After selecting a poloidal harmonic, say the mth, we define $k_{||} = m/q - n$ with r_m denoting the radial position for which $k_{||} = 0$. Similar to the analysis of Mercier modes, we deploy the ordering (11.1):

$$\frac{1}{\tilde{f}_m} \frac{d\tilde{f}_m}{dx} \sim m \sim \varepsilon^{-1} \gg 1 \quad \text{with} \quad x = (r - r_m)/r_m \sim \varepsilon, \tag{12.2}$$

assuming that (11.2) holds with $n \sim m \sim \varepsilon^{-1}$ such that $m/n = q \sim 1$.

According to the discussion in the introduction, we postulate that, and this is the crucial feature which characterises ballooning modes, different Fourier harmonics have similar amplitude. This means that we can order the harmonics appearing in (12.1) as

$$\tilde{f}_m \sim \tilde{f}_{m\pm 1} \sim \tilde{f}_{m\pm 2} \sim \dots$$
 (12.3)

Each of these modes is expected to be localised about its resonant surface with a radial extension of the order of the distance between the two resonances of its first neighbouring sidebands.

The safety factor is expanded around r_m as

$$q \approx \frac{m}{n}(1+sx),$$

where s is the magnetic shear at r_m which is assumed to be constant. It follows that the resonances associated with the $m \pm 1, m \pm 2, \ldots$ modes are equally spaced, and their location is⁵

$$x_{m\pm\ell} = \pm \frac{\ell}{s \, m}, \quad (\ell = 1, 2, \ldots).$$
 (12.4)

⁴ Recall that harmonics with different n behave independently.

⁵ Note that at leading order $(r_{m+1} (r_m)/r_m \approx (r_{m+1}-r_m)/r_{m\pm 1}$.

⁶ Since $m \gg 1$, it is not necessary to specify on which m we restrict our analysis. In reality, as m gets larger the spatial structure of the mode is so small that the MHD single fluid limit becomes inappropriate. One should then refine the analysis by considering, e.g., finite Larmor radius (FLR) effects.

We assume that the poloidal spectrum of the perturbation is composed of a very large but finite number of harmonics. For m and n tending to infinity, the separation between adjacent resonant surfaces becomes infinitesimal and, as long as ℓ increases but remains finite, the position of these resonances practically corresponds to r_m . The associated ballooning perturbation is expected to be highly localised about the q = m/n surface so that the stability analysis can be restricted to a single flux surface at a time, e.g. the one labelled by q. Stability should then be only determined by n and the values of the equilibrium quantities at r_m .

Upon introducing the **ballooning parameter** α defined by (4.41), we now order the pressure and its gradient as $p_0/B_0^2 \sim \varepsilon^2$ and $rp_0' \sim p_0$, such that

$$\alpha \sim \varepsilon \ll 1,$$
 (12.5)

where s is regarded as a small parameter whose ordering is yet to be determined.

In the particular regime of small pressure gradient and weak magnetic shear the ballooning mode analysis is based on equation (11.5) which is reproduced below:

$$\frac{d}{dx}\left(x^{2}\frac{d\xi_{m}^{r}}{dx}\right) - \left\{m^{2}x^{2} + \frac{\alpha}{s^{2}}\left[\frac{r_{m}}{R_{0}}\left(1 - \frac{1}{q^{2}}\right) + \frac{\alpha}{2} + s\Delta'\right]\right\}\xi_{m}^{r} + \gamma_{H}^{2}\left(\frac{d^{2}\xi_{m}^{r}}{dx^{2}} - m^{2}\xi_{m}^{r}\right) = -\frac{imR_{0}}{n^{2}s^{2}B_{0}}\sum_{m'\neq 0}\left[ik_{||}C_{m}^{m'} + D_{m}^{m'} - E_{m}^{m'}(\hat{p})\right], (12.6)$$

where γ_H defined by (11.12).⁷ Because of the assumption of strong localisation of the instability, it is implicit that all equilibrium quantities are to be evaluated at r_m .

We note that the terms proportional to $E_m^{m'}$, $D_m^{m'}$ and $C_m^{m'}$ scale according to (11.6), (11.9) and (11.10) respectively, hence we see that $D_m^{m'}$ is negligible compared to $E_m^{m'}$, the latter also dominating over $C_m^{m'}$ if

$$s \ll \frac{\alpha}{\varepsilon} \sim 1,$$
 (12.7)

having used (12.5) for the last estimate.

Now, according to (12.3), we take the radial displacement of different poloidal harmonics to be of the same order, that is

$$\xi_m^r \sim \xi_{m\pm 1}^r \sim \xi_{m\pm 2}^r \sim \dots, \tag{12.8}$$

each of which with a radial extension $\Delta x \sim \frac{1}{sm}$. From the estimation of the term $E_m^{m'}$, one sees the strength of the coupling between neighbouring sidebands is proportional to α/s^2 . Hence, allowing for (12.8) and assuming that coupling contributions enter at leading order into (12.6), we let

$$\frac{\alpha}{s^2} \sim 1. \tag{12.9}$$

⁷ The inertia enhancement factor due to the sidebands compressibility is obtained using the orderings discussed in §7.4.

By means of (12.5), and in agreement with (12.7), this relation implies

$$s \sim \sqrt{\varepsilon},$$
 (12.10)

showing that the magnetic shear is indeed a small parameter. Note that $sm \sim 1/\sqrt{\varepsilon}$, which still indicates a pronounced localisation of the mode structure. Thus, making use of Eqs. (7.59), (7.63) and (8.12) we obtain

$$\frac{imR_0}{n^2s^2B_0}E_m^{m'}(\hat{p}) = -\frac{\alpha}{2ms^2}\left[m\xi_{m\pm 1}^r \pm \frac{d\xi_{m\pm 1}^r}{dx}\right],\tag{12.11}$$

having exploited the fact that $m \gg 1$.

Simplifying further, we note that the term proportional to $s\Delta'$ in (12.6) can be neglected owing to the smallness of the magnetic shear and due to the fact that $\Delta' \sim \varepsilon$. Hence, the contribution arising from the terms inside the square bracket on the left-hand-side of (12.6) reads

$$\frac{r_m}{R_0}\left(1-\frac{1}{q^2}\right)+\frac{\alpha}{2}.$$

Although this is formally a higher order correction, we retain it because it proves to plays an important role in determining the ballooning stability later on.⁸

Therefore, we collate these findings to write equation (12.6) as

$$\begin{split} \frac{d}{dx} \Big((x^2 + \gamma_H^2) \frac{d\xi_m^r}{dx} \Big) - \left[m^2 (x^2 + \gamma_H^2) + \frac{\alpha r_m}{s^2 R_0} \left(1 - \frac{1}{q^2} \right) + \frac{\alpha^2}{2s^2} \right] \xi_m^r \\ + \frac{\alpha}{2ms^2} \left[\left(m\xi_{m+1}^r + \frac{d\xi_{m+1}^r}{dx} \right) + \left(m\xi_{m-1}^r - \frac{d\xi_{m-1}^r}{dx} \right) \right] = 0. \quad (12.12) \end{split}$$

This equation has exactly the same form of (11.11), which we recall can be viewed as the large m local limit of (9.12), where the only difference lies in the ordering of α/s^2 and the amplitude of the sideband harmonics. It is thus interesting to note that the dynamics of infernal, Mercier and ballooning modes can be essentially described by one equation only in which the *flavour* of the perturbation can be tuned by an appropriate ordering of m and α/s^2 .

Now, in analogy with the derivation presented in §11.3, we can slightly simplify equation (12.12) by dropping some inertial contributions. According to the discussion of section 7.4.2, inertia becomes important in a neighbourhood of r_m where the mth harmonic is expected to develop large gradients while dominating over the sidebands. In this narrow layer, whose thickness is estimated from (11.16), we let (cf. (7.50))

$$r\frac{d\xi_m^r/dr}{\xi_m^r} \gg m, \quad (r - r_m)\frac{d}{dr} \sim 1. \tag{12.13}$$

Within this ordering, using (7.30) and (7.31), which were shown to hold for small scale modes as well, gives

$$-\frac{imR_0}{B_0}\gamma^2 \left[\frac{\partial}{\partial r} \left(\frac{\rho_0}{B_0^{\phi}} \xi_{\vartheta} \right) - \frac{\partial}{\partial \vartheta} \left(\frac{\rho_0}{B_0^{\phi}} \xi_r \right) \right]_m \approx \frac{d}{dx} \left[\frac{\gamma^2}{\omega_A^2} \frac{d\xi_m^r}{dx} \right], \tag{12.14}$$

⁹ Given *m* (large or of order one), the structure of the poloidal spectrum of the radial fluid displacement is roughly determined by balancing terms of the form

$$\frac{d}{dr}\left((r-r_m)^2\frac{d\xi_m^r}{dr}\right)$$
 and $\frac{\alpha}{s^2}\xi_{m\pm 1}^r$,

with r_m denoting either the resonance of the mode (m,n) if this is in the plasma, or some other convenient reference position. It is then evident that as long as $d\xi_m^r/dr \neq 0$, the relative amplitude between adjacent harmonics is proportional to α/s^2 . Note that for the m=1 internal kink mode for which $d\xi_m^r/dr=0$ at leading order, we can still have $\xi_{m\pm 1}^r/\xi_m^r\sim \varepsilon$ even if $\alpha/s^2\sim 1$.

⁸ In real experiments, the aspect ratio is not such a small number, so that the physics contained in this term is expected to have non negligible impact on stability. Note also that these terms remove the singular behaviour of ξ_m^r at x = 0 when $\gamma = 0$ (cf. (12.12)).

¹⁰ At leading order only terms proportional to $\Delta p'_{m+1}$ matter.

where we recall that $\omega_A^2 = B_0^2/(R_0^2\rho_0)$. Similar arguments are invoked to simplify $E_m^{m'}(\Delta p)$, thus yielding (cf. (7.34) and (cf. (11.3))¹⁰

$$-\frac{imR_0}{B_0}\sum_{m'\neq 0}E_m^{m'}(\Delta p)\approx \frac{d}{dx}\left(2q^2\frac{\gamma^2}{\omega_A^2}\frac{d\xi_m^r}{dx}\right). \tag{12.15}$$

Therefore, we may drop the term $m^2\gamma_H^2$ in the second term on the left-hand-side of (12.12) so that the **ballooning equation in the radial coordinate** for small pressure gradient and small magnetic shear may be finally written as

$$\begin{split} \frac{d}{dx} \Big((x^2 + \gamma_H^2) \frac{d\xi_m^r}{dx} \Big) - \left[m^2 x^2 + \frac{\alpha \varepsilon_m}{s^2} \left(1 - \frac{1}{q^2} \right) + \frac{\alpha^2}{2s^2} \right] \xi_m^r \\ + \frac{\alpha}{2ms^2} \left[\left(m \xi_{m+1}^r + \frac{d\xi_{m+1}^r}{dx} \right) + \left(m \xi_{m-1}^r - \frac{d\xi_{m-1}^r}{dx} \right) \right] = 0, \quad (12.16) \end{split}$$

where $\varepsilon_m = r_m/R_0$. In the large *n* limit each of the harmonics composing the spectrum of a ballooning perturbation is expected to obey (12.16). We shall now discuss how to extend this equation to the more experimentally relevant case of α and *s* of the order of unity.

12.1.1 Extending to the $s-\alpha$ equilibrium

The calculations that we present below become relevant when modelling ballooning instabilities located in the edge region of plasmas with ETBs, where both the magnetic shear and the local pressure gradient are fairly large.

Such scenarios are typically described within the $s-\alpha$ equilibrium model (see section 4.3.4) in which large pressure gradients are allowed to exist in a narrow region so that locally $rp_0'/B_0^2 \sim \varepsilon$ while the global pressure remains small, i.e. $p_0/B_0^2 \sim \varepsilon^2$.

Ordering $s \sim \alpha \sim 1$, it was found that $\Delta/a \sim \Delta' \sim \varepsilon$ whereas $r\Delta'' = \alpha$ (cf. (4.40)). From this, Eqs. (4.31) and (5.21) may be written as

$$F' \approx -\frac{R_0 p_0'}{R_0}, \quad \langle R^2 \rangle' \approx -r R_0 \Delta'' = -R_0 \alpha.$$
 (12.17)

The geometry of the equilibrium is determined by the expressions of the metric coefficients given in (5.28). For the sake of simplicity we assume $\alpha = const.$ ¹¹

As before, we fix n (which is a large) and select a poloidal mode number $m \gg 1$ whose associated resonance is located at r_m . Let us consider a region sufficiently far from r_m where (see (11.2) and Fig. 12.4)

$$k_{\parallel} = m\mu - n \approx -nsx \sim 1$$
,

with x defined in (12.2). From (7.7) we immediately see that

$$(\sqrt{g}\tilde{B}^r)_m = -ir_m B_0 n s x \xi_m^r \sim r B_0 \xi^r, \qquad (12.18)$$

¹¹ This is a good approximation as long as the perturbation is radially well localised.

and from (7.25) it follows that

$$(\sqrt{g}\tilde{B}^{\vartheta})_m \sim (\sqrt{g}\tilde{B}^r)_m/r.$$

Furthermore, using the expressions for the metric coefficients given in §5.4 one has $\langle J_0^\phi/B_0^\phi \rangle \sim \varepsilon/r,$ and from (7.49) we obtain

$$(\sqrt{g}\tilde{B}^{\phi})_{m} = \frac{r_{m}p'_{0}}{B_{0}}\xi_{m}^{r} \sim \varepsilon^{2}(\sqrt{g}\tilde{B}^{r})_{m}/r.$$

We now consider the vorticity equation, namely (7.13), in which we require that different Fourier harmonics are equivalent (cf. (7.46) and figure 12.4). Thanks to the ordering of the growth rate (see (7.44)), we ignore, for the moment, inertial effects by setting $\gamma \to 0$ and $\Delta p \to 0$. Thus, by means of the expressions above and using (7.14), (7.54), (7.55)(7.60) and (7.61), the mth Fourier projection of the vorticity equation reads

$$-insx(\sqrt{g}\tilde{J}^{\phi})_{m} + \langle \frac{J_{0}^{\phi}}{B_{0}^{\phi}} \rangle'(\sqrt{g}\tilde{B}^{r})_{m} + \sum_{m'\neq 0} D_{m}^{m'} - im\frac{R_{0}}{B_{0}^{3}}(p'_{0})^{2}\xi_{m}^{r}$$
$$-im\langle \frac{1}{B_{0}^{\phi}} \rangle'\hat{p}_{m} - \sum_{m'\neq 0} E_{m}^{m'}(\hat{p}) = 0, \tag{12.19}$$

where $D_m^{m'}$ and $E_m^{m'}$ are given by (7.62) and (7.63) respectively, with \hat{p} defined by (7.59).

It is easy to see that

$$(\sqrt{g}\tilde{J}^{\phi})_m \sim (\sqrt{g}\tilde{B}^r)_m/r^2, \quad \langle \frac{J_0^{\phi}}{B_0^{\phi}} \rangle' (\sqrt{g}\tilde{B}^r)_m \sim \varepsilon(\sqrt{g}\tilde{B}^r)_m/r^2, \ (J_0^{\phi}/B_0^{\phi})'_{+1} \sim (J_0^{\phi}/B_0^{\phi})'_{+2} \sim \varepsilon/r^2.$$

It follows at once that the terms proportional to $\langle J_0^{\phi}/B_0^{\phi}\rangle'$ and $D_m^{m'}$ in (12.19) can be dropped. Furthermore, from (12.17) one has

$$\langle \frac{1}{B_0^{\phi}} \rangle' = \frac{\langle R^2 \rangle'}{F} - \frac{\langle R^2 \rangle F'}{F^2} = -\frac{\alpha}{B_0} + \frac{R_0 p_0'}{B_0^3}.$$

Hence, equation (12.19) can be written as

$$-insx(\sqrt{g}\tilde{J}^{\phi})_{m}-im\frac{\alpha}{B_{0}}p_{0}'\xi_{m}^{r}-\sum_{m'\neq 0}E_{m}^{m'}(\hat{p})=0. \tag{12.20}$$

The perturbed toroidal current is computed through (7.52) and (7.53) which yields at leading order¹²

$$\begin{split} (\sqrt{g}\,\tilde{J}^\phi)_m &\approx -\,\frac{1}{i\,m} \bigg\{ \, \big[\langle N \rangle (\sqrt{g}\,\tilde{B}^r)_m' \big]' - m^2 \langle L \rangle (\sqrt{g}\,\tilde{B}^r)_m \bigg\} \\ &+ \sum_+ \bigg[2 M_{\mp 1} (\sqrt{g}\,\tilde{B}^r)_{m\pm 1}' - i\,m L_{\mp 2} (\sqrt{g}\,\tilde{B}^r)_{m\pm 2} \bigg], \end{split}$$

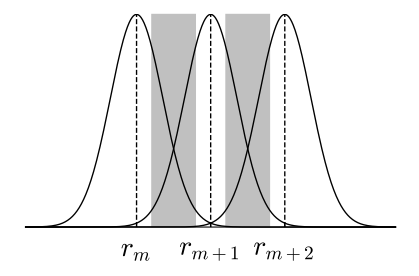


Figure 12.4: Ballooning mode structure with shaded areas indicating the regions where inertial effects are expected to be negligible.

$$(\sqrt{g}\tilde{B}^{\vartheta})_{m\pm\ell}\sim \tfrac{1}{r}(\sqrt{g}\tilde{B}^r)_{m\pm\ell}\sim \tfrac{1}{r}(\sqrt{g}\tilde{B}^r)_m.$$

The term h appearing in (7.52) is approximated from the full expression $h = \langle g_{\vartheta\vartheta}/\sqrt{g}\rangle/G$. We also exploit the fact that $(\ell = 1, 2, \ldots)$

where L, M and N must be evaluated using (5.28).

It remains to get an expression for $E_m^{m'}(\hat{p})$ which is a quantity that depends on $(1/B_0^{\phi})' = (R^2/F)'$. By means of (5.20), we notice that the radial derivative of R^2 generates a term proportional to Δ'' :

$$\frac{dR^2}{dr} = 2R_0 \left(\cos \vartheta - r\Delta'' \sin^2 \vartheta\right).$$

Exploiting the fact that m is large, we obtain

$$\sum_{m'\neq 0} E_m^{m'}(\hat{p}) \approx \frac{i}{B_0} \sum_{\pm} \left(m \hat{p}_{m\pm 1} \pm r \hat{p}'_{m\pm 1} + \frac{m\alpha}{2} \hat{p}_{m\pm 2} \right). \tag{12.21}$$

The inclusion of plasma inertia is almost trivial: these corrections become important only when the resonance is approached so that they can be easily accounted for by allowing terms of the form (12.14) and (12.15).¹³ Thus, collating these results together, and expressing $(\sqrt{g}\tilde{B}^r)_m$ as a function of ξ_m^r through (12.18), one finally has

$$\begin{split} \frac{d}{dx} \left[(x^2 + \gamma_H^2) \frac{d\xi_m^r}{dx} \right] - \left[\left(1 + \frac{\alpha^2}{2} \right) m^2 x^2 + \frac{\alpha^2}{2s^2} \right] \xi_m^r \\ + \frac{\alpha}{2ms^2} \sum_{\pm} \left[m\xi_{m\pm 1}^r \pm \frac{d\xi_{m\pm 1}^r}{dx} + \frac{m\alpha}{2} \xi_{m\pm 2}^r \right] \\ + \frac{xq}{s} \sum_{\pm} \left[\frac{m\alpha^2}{4} (nsx \mp 2\mu) \xi_{m\pm 2}^r \pm \alpha \frac{d[(nsx \mp \mu) \xi_{m\pm 1}^r]}{dx} \right] = 0. \quad (12.22) \end{split}$$

Note that this equation could have been derived directly from (7.65) allowing for enhanced pressure gradients and accounting appropriately for modifications of the equilibrium geometry.

For small α and weak shear with $\alpha/s^2 \sim 1$, Eq. (12.22) reduces to (12.16) when $\varepsilon_m \to 0$. Therefore, by adding the small term proportional to $(1-1/q^2)$, these two equations can be combined into a single one reading

$$\begin{split} \frac{d}{dx} \left[(x^2 + \gamma_H^2) \frac{d\xi_m^r}{dx} \right] - \left[\left(1 + \frac{\alpha^2}{2} \right) m^2 x^2 + \hat{U} + \frac{\alpha^2}{2s^2} \right] \xi_m^r \\ + \frac{\alpha}{2ms^2} \sum_{\pm} \left[m\xi_{m\pm 1}^r \pm \frac{d\xi_{m\pm 1}^r}{dx} + \frac{m\alpha}{2} \xi_{m\pm 2}^r \right] \\ + \frac{xq}{s} \sum_{\pm} \left[\frac{m\alpha^2}{4} (nsx \mp 2\mu) \xi_{m\pm 2}^r \pm \alpha \frac{d[(nsx \mp \mu) \xi_{m\pm 1}^r]}{dx} \right] = 0. \end{split}$$
(12.23)

where α is evaluated at r_m and \hat{U} is the same as (11.15) with the replacement $r_s \to r_m$ that is

$$\hat{U} = \frac{\alpha \varepsilon_m}{s^2} \left(1 - \frac{1}{q^2} \right). \tag{12.24}$$

We shall refer to \hat{U} as the **Mercier correction**, whereas we call (12.23) the **generalised ballooning equation**. Hereafter we only consider cases

Use $(R^2/F)'_{+\ell} \approx (R^2)'_{+\ell}/F$.

 13 By adopting ordering (12.13) we avoid nasty calculations which might appear when $r\rho_0'\rho \sim 1/\varepsilon$. Density gradients of this magnitude are commonly encountered in the region where edge transport barriers develop.

which are **stable against Mercier modes**, hence we take q>1 and $\alpha>0$ such that $\hat{U}>0$. Equation (12.23) can be used to analyse the stability of ballooning modes both in low and high shear regions. Due to the complexity of solving simultaneously a very large number of mutually coupled equations, the problem of the ballooning stability is generally tackled numerically. Luckily, characterising in a more precise manner the underlying assumption of the equivalence of the poloidal harmonics, a great deal of simplification is achieved by representing equation (12.23) in a convenient **Fourier space**. This is elaborated in the next section.

12.2 Fourier space representation

Let us select a radius r_m and a poloidal mode number $m\gg 1$ such that $q(r_m)=m/n$. Suppose that the perturbation of the radial fluid displacement is composed of a large number of harmonics coupled together. Each of these is expected to be centred about its own resonance. Notice that, intuitively because the poloidal mode number is large, if $j\sim 1$ there should be no difference if we refer to the mth or the (m+j)th mode. Thus, one is allowed to assume that these harmonics are **translationally invariant** with period equal to the spacing between neighbouring resonances, that is (cf. (12.4))

$$\xi_m^r(x) = \xi_{m\pm 1}^r(x \pm d) = \dots = \xi_{m\pm \ell}^r(x \pm \ell d) = \dots,$$
 (12.25)

where d = 1/(nqs) and ℓ an integer.¹⁴

In analogy with (11.14), we introduce the variable z = mx so that (12.23) becomes

$$\frac{d}{dz} \left[(z^2 + m^2 \gamma_H^2) \frac{d\xi_m^r}{dz} \right] - \left[\left(1 + \frac{\alpha^2}{2} \right) z^2 + \hat{U} + \frac{\alpha^2}{2s^2} \right] \xi_m^r \\
+ \sum_{\pm} \left[\frac{\alpha}{2s^2} \left(\xi_{m\pm 1}^r \pm \frac{d\xi_{m\pm 1}^r}{dz} + \frac{\alpha}{2} \xi_{m\pm 2}^r \right) \right. \\
+ \frac{zq}{s} \left(\frac{\alpha^2}{4} Y_{m\pm 2} \pm \alpha \frac{dY_{m\pm 1}}{dz} \right) \right] = 0, \tag{12.26}$$

with $Y_{m\pm\ell}=[\mu sz\mp\ell\mu]\xi_{m\pm\ell}^r$. The invariance (12.25) transforms into¹⁵ $\xi_m^r(z)=\xi_{m\pm\ell}^r(z\pm\ell/s)$.

Since m is large (we ideally take the limit $m \to \infty$), the variable z is allowed to vary from $-\infty$ to $+\infty$. Thus, we take the **Fourier transform** of the fluid displacement by defining

$$\xi^*(k) = \int_{-\infty}^{\infty} \xi_m^r(z) e^{-ikz} dz.$$
 (12.27)

The space where $\xi^*(k)$ is defined is referred to as **k-space**. Exploiting

 15 Exploiting this, the eigenfunction at large z obeys

$$\begin{split} 0 &= \frac{d}{dz} \left(z^2 \frac{d\xi_m^r}{dz} \right) - \left(1 + \frac{\alpha^2}{2} \right) z^2 \xi_m^r \\ &+ \frac{\alpha^2}{4} \sum_+ \frac{zq}{s} Y_{m\pm 2} \approx \frac{d}{dz} \left(z^2 \frac{d\xi_m^r}{dz} \right) - z^2 \xi_m^r, \end{split}$$

implying that $\xi_m^r \propto \exp(-|z|)/z$.

¹⁴ Up to this point we do not have any information about the parity of the various functions $\xi_{\ell}^{r}(x)$.

¹⁶ The translational invariance assumption (12.25) can be generalised by taking $\xi_{m\pm\ell}^r(z) = e^{\mp ik_0\ell/s} \xi_m^r(z\mp\ell/s)$. From this, the argument of the oscillating terms (i.e. the sine and cosine) in (12.28) must be replaced with $k/s \to (k+k_0)/s$.

This is due to the **Fourier inversion theorem**.

the invariance (12.25), it follows that

$$\int_{-\infty}^{\infty} \xi_{m\pm\ell}^{r}(z) e^{-ikz} dz = \int_{-\infty}^{\infty} \xi_{m}^{r}(z \mp \ell/s) e^{-ikz} dz = e^{\mp ik\ell/s} \xi^{*}(k),$$

$$\int_{-\infty}^{\infty} Y_{m\pm\ell}(z) e^{-ikz} dz = is\mu\left(\frac{d\xi^{*}(k)}{dk}\right) e^{\mp ik\ell/s},$$

having performed the substitutions $\frac{d}{dz} \rightarrow ik$ and $z \rightarrow i\frac{d}{dk}$.

Hence, by Fourier transforming equation (12.26) to k-space we obtain 16

$$\begin{split} k \left[\left(\frac{d^2}{dk^2} - m^2 \gamma_H^2 \right) (k \xi^*) \right] + \left[\left(1 + \frac{\alpha^2}{2} \right) \frac{d^2}{dk^2} - \hat{U} - \frac{\alpha^2}{2s^2} \right] \xi^* \\ + \frac{\alpha}{2s^2} \left[(e^{-ik/s} + e^{ik/s}) + ik(e^{-ik/s} - e^{ik/s}) + \frac{\alpha}{2} (e^{-2ik/s} + e^{2ik/s}) \right] \xi^* \\ - \frac{d}{dk} \left\{ \left[\frac{\alpha^2}{4} (e^{-2ik/s} + e^{2ik/s}) + \alpha ik(e^{-ik/s} - e^{ik/s}) \right] \frac{d\xi^*}{dk} \right\} = 0. \end{split}$$

By means of Euler's formula and noticing that $1-\cos(2k/s) = 2\sin^2(k/s)$, after some algebra the expression above can be further simplified finally yielding the **ballooning equation in Fourier space** (Connor (1978)):

$$\frac{d}{dk} \left\{ \left[1 + \left(k - \alpha \sin \frac{k}{s} \right)^2 \right] \frac{d\xi^*}{dk} \right\} - \left\{ \hat{U} + m^2 \gamma_H^2 k^2 - \frac{\alpha}{s^2} \left[\cos \frac{k}{s} + \sin \frac{k}{s} \left(k - \alpha \sin \frac{k}{s} \right) \right] \right\} \xi^* = 0.$$
(12.28)

In order for the Fourier transform of ξ_m^r and its inverse to exist, we must have

$$\int_{-\infty}^{\infty} |\xi^*| dk < \infty, \tag{12.29}$$

implying that ξ^* must vanish for $k \to \pm \infty$. Since the Fourier transform preserves parity, even/odd functions in k-space are associated with even/odd functions in real space.

Equation (12.28), with both α and s of the order of unity, is generally solved numerically. Nonetheless, some analytical techniques can be employed when the magnetic shear is either very large or very small. In the latter case, instead of (12.28), we use its limiting expression obtained directly from (12.16) for $s, \alpha \ll 1$ which is

$$\frac{d}{dk} \left[(1+k^2) \frac{d\xi^*}{dk} \right] - \left[\hat{U} + \frac{\alpha^2}{2s^2} + m^2 \gamma_H^2 k^2 - \frac{\alpha}{s^2} \left(\cos \frac{k}{s} + k \sin \frac{k}{s} \right) \right] \xi^* = 0.$$
(12.30)

Although there is a quantitative difference between the results obtained from (12.28) and (12.30), their qualitative behaviour is fairly similar. Moreover, the big advantage of using (12.30) instead of (12.28) is because the mathematical manipulations are much easier to handle, therefore serving as an excellent testbed for learning such techniques. The two cases of large and small magnetic shear are discussed in the next sections.

As just discussed, in this section the analysis is based on (12.30). For our purposes, it is more convenient to write $\xi^* = X/[1+k^2]^{1/2}$ and recast (12.30) as

$$\frac{d^2X}{dk^2} - \left[\frac{\hat{U} + \frac{\alpha^2}{2s^2} + m^2\gamma_H^2k^2 - \frac{\alpha}{s^2}(\cos\frac{k}{s} + k\sin\frac{k}{s})}{1 + k^2} + \frac{1}{(1 + k^2)^2}\right]X = 0. \tag{12.31}$$

This equation features some oscillating terms which depend on k/s. If the magnetic shear is small, they will exhibit rapid oscillations on the scale $2\pi/s$. Therefore, the behaviour of X, and thus of ξ^* , is expected to be composed of a fast oscillation over the variable $\chi=k/s$ superimposed on a more slowly varying function of k.

The method for analysing the marginal boundaries and growth rates associated with (12.30) involves the elimination of the fast oscillations by averaging over their period (averaging method). Let us write (12.31) as

$$\frac{d^2X}{dk^2} - V(k,\chi)X = 0,$$

$$V(k,\chi) = \frac{\hat{U} + \frac{\alpha^2}{2s^2} + m^2\gamma_H^2 k^2 - \frac{\alpha}{s^2}(\cos\chi + k\sin\chi)}{1 + k^2} + \frac{1}{(1 + k^2)^2}.$$
 (12.32)

Introducing the smallness parameter δ , we order

$$s \sim \delta^2$$
, $\alpha \sim \delta$, $\varepsilon_m \sim \delta^3$, $m\gamma_H \sim 1$, (12.33)

and separate the fast and slow length scales by writing

$$\frac{d}{dk} \to \frac{\partial}{\partial k} + \frac{1}{s} \frac{\partial}{\partial \chi}.$$

Note that within this ordering we have $\hat{U} \sim 1$ and $\gamma/\omega_A \sim s$.

The eigenfunction X is expanded as (the deltas in brackets are tags denoting the order of magnitude of the associated term)

$$X = X_0(k) + (\delta)X_1(k,\chi) + (\delta^2)X_2(k,\chi) + (\delta^3)X_3(k,\chi) + \dots, \quad (12.34)$$

with the requirement that the functions X_1, X_2, \ldots vanish when averaged in the variable χ over a period of 2π . Thus, equation (12.32) is solved order by order in δ , from δ^{-3} to δ^{-1} , providing an expression for X_i (i = 1, 2, 3). These are then plugged into the zeroth order (in δ) of (12.32), and averaging over χ yields an equation for X_0 . Let us go through each of these steps one-by-one.

To order δ^{-3} we have

$$\frac{1}{s^2}\frac{\partial^2 X_1}{\partial \chi^2} + \frac{\alpha}{s^2}\frac{(\cos\chi + k\sin\chi)}{1 + k^2}X_0 = 0,$$

whose solution reads

$$X_1 = \frac{\alpha(\cos \chi + k \sin \chi)}{1 + k^2} X_0. \tag{12.35}$$

To the next order we have

$$\frac{1}{s^2} \frac{\partial^2 X_2}{\partial \chi^2} = \frac{\alpha^2 / (2s^2)}{1 + k^2} X_0 - \frac{\alpha}{s^2} \frac{(\cos \chi + k \sin \chi)}{1 + k^2} X_1$$

$$= -\frac{\alpha^2}{2s^2} \left(\frac{(1 - k^2) \cos 2\chi + 2k \sin 2\chi}{(1 + k^2)^2} \right) X_0,$$

where the last passage has been obtained by using (12.35). Again, the integration in χ is trivial and leads to

$$X_2 = \frac{\alpha^2}{8} \left(\frac{(1 - k^2)\cos 2\chi + 2k\sin 2\chi}{(1 + k^2)^2} \right) X_0.$$
 (12.36)

Proceeding further, we get the equation for X_3 by considering the order δ^{-1} of (12.32) which yields

$$\frac{1}{s^2}\frac{\partial^2 X_3}{\partial \chi^2} + \frac{2}{s}\frac{\partial X_1}{\partial k \partial \chi} - \left[\frac{\alpha^2}{2s^2}\frac{X_1}{1+k^2} - \frac{\alpha}{s^2}\frac{(\cos \chi + k \sin \chi)}{1+k^2}X_2\right] = 0.$$

Finally, the equation for X_0 is obtained by averaging (12.32) in χ giving

$$\frac{d^2 X_0}{dk^2} - \left(\frac{\hat{U} + m^2 \gamma_H^2 k^2}{1 + k^2} + \frac{1}{(1 + k^2)^2}\right) X_0 + \frac{\alpha/s^2}{2\pi (1 + k^2)} \int_0^{2\pi} (\cos \chi + k \sin \chi) X_3 d\chi = 0.$$

Carrying out the appropriate integrations¹⁷ we finally get the **eigenvalue** equation for ballooning modes in the limit of small magnetic shear:

$$\frac{d^2X_0}{dk^2} - \left(\frac{\hat{U} + m^2\gamma_H^2k^2}{1 + k^2} + \frac{1 - \frac{\alpha^2}{s} + \frac{7}{32}\frac{\alpha^4}{s^2}}{(1 + k^2)^2}\right)X_0 = 0.$$
 (12.37)

The usual procedure for solving this equation is based on an asymptotic analysis which employs the same techniques developed in §11.3 (Antonsen (1982), Correa-Restrepo (1985)). Here, we shall deploy a simplified method to obtain the desired results.

For the sake of simplicity we take $\hat{U} = 0$, and define

$$b = 1 - \frac{\alpha^2}{s} + \frac{7}{32} \frac{\alpha^4}{s^2}.$$
 (12.38)

Equation (12.37) is then written as

$$\frac{d^2X_0}{dk^2} - \left(\frac{m^2\gamma_H^2k^2}{1+k^2} + \hat{V}(k)\right)X_0 = 0,$$
 (12.39)

with $\hat{V}(k) = b/(1+k^2)^2$. This is similar to a time independent Schrödinger equation with a one dimensional potential.

 17 For a function $f(\chi)$ of period 2π we have

$$\int_0^{2\pi} f \cos \chi \, d\chi = -\int_0^{2\pi} \cos \chi \, \frac{d^2 f}{d\chi^2} \, d\chi,$$
$$\int_0^{2\pi} f \sin \chi \, d\chi = -\int_0^{2\pi} \sin \chi \, \frac{d^2 f}{d\chi^2} \, d\chi.$$

A great deal of simplification can be achieved by i) noticing that due to the smallness of the growth rate the term proportional to $m\gamma_H$ becomes important only at very large k where $\hat{V}(k)$ is negligibly small, and ii) replacing the potential $\hat{V}(k)$ with a Heaviside step function which is vanishing for $|k| > \pi/4$ such that its integral is equal to $\int_0^\infty dk/(1+k^2)^2 = \pi/4$ (see figure 12.5).

By employing these simplifications, equation (12.39) is cast as

$$\frac{d^2X_0}{dk^2} - bX_0 = 0, \quad |k| < \pi/4, \tag{12.40}$$

$$\frac{d^2X_0}{dk^2} - m^2\gamma_H^2X_0 = 0, \quad |k| > \pi/4, \tag{12.41}$$

with the requirement that X_0 is smooth and continuous at $k=\pm\pi/4$ $(\epsilon\to 0)$

$$\left. \frac{dX_0/dk}{X_0} \right|_{\pm \pi/4 - \epsilon} = \frac{dX_0/dk}{X_0} \Big|_{\pm \pi/4 + \epsilon}.$$
 (12.42)

With a positive growth rate ($\gamma_H > 0$), the solutions of (12.40) and (12.41) which are regular at infinity are easily derived and read

$$X_0 = c_1 e^{\sqrt{b}k} + c_2 e^{-\sqrt{b}k},$$
 $|k| < \frac{\pi}{4},$
 $= d_1 e^{-m\gamma_H k},$ $k > \frac{\pi}{4},$
 $= d_2 e^{m\gamma_H k},$ $k < -\frac{\pi}{4},$

where c_1 , c_2 , d_1 , d_2 are some constants. It is evident that smooth matching at $\pm \pi/4$ requires b < 0. The system given by (12.42) is solvable only if X_0 has **definite parity**, that is either even or odd. The odd solution has $c_1/c_2 = d_1/d_2 = -1$, whereas for the even one we have $c_1/c_2 = d_1/d_2 = 1$. Thus, the corresponding growth rates are

$$m\gamma_H = -\sqrt{b} \coth\left(\frac{\pi\sqrt{b}}{4}\right)$$
 (odd),
$$m\gamma_H = -\sqrt{b} \tanh\left(\frac{\pi\sqrt{b}}{4}\right)$$
 (even).

A positive growth rate is found if b < -4 for odd modes or b < 0 for even modes. Since no real α^2/s satisfies the relation b = d for d < -1/7, solutions with odd parity are discarded. We then find that **ballooning** modes of even parity can be unstable for -1/7 < b < 0 with the marginal boundary identified by b = 0 yielding

$$\frac{\alpha^2}{s} = \frac{16}{7} \left(1 \pm \frac{\sqrt{2}}{4} \right). \tag{12.43}$$

According to the equation above, when $\alpha > 0$ ballooning instabilities seem not to occur in regions of negative magnetic shear.

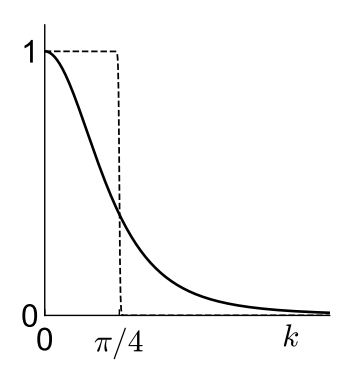


Figure 12.5: Approximation of $1/(1+k^2)^2$ with a step function which yields the same integral for $0 < k < \infty$. Surprisingly, at least for ideal balloonings, this yields fairly accurate results not too different from those obtained by a more precise analysis (see e.g. Strauss (1981)). The latter will be needed in §16.2 for studying ballooning instabilities augmented by resistive effects.

Letting α to take negative values, the marginal boundaries of ballooning modes for small s and $\hat{U}=0$ are independent of the sign of α .

¹⁸ Note that $\int_0^\infty dk/(1+k^2) = \pi/2$. Hence, we substitute $\hat{U}/(1+k^2) \to \hat{U}H(\pi/2-k)$ where H is the **Heaviside step function**.

¹⁹ Within our framework, we could have obtained this result by replacing $\hat{V}(k)$ with an *effective* potential $\hat{V}_{eff}(k) = (b + \hat{U})H(k_{eff} - k)$ with $k_{eff} \sim 1$. In such a case only matching at $|k_{eff}|$ is needed: remarkably, the marginal boundaries do not depend on the choice of k_{eff} . It is important to point out that shaping effects, namely plasma elongation and triangularity, modify the expression of \hat{U} . An elongated plasma with positive triangularity exhibits improved stability at low magnetic shear (Krymskii (1981), Lütjens (1992)).

Solving (12.39) with the inclusion of the Mercier correction $\hat{U}>0$ follows the same procedure described above with the potential \hat{V} now replaced by 18

$$\hat{V} = b + \hat{U},$$
 $|k| < \frac{\pi}{4},$ $|k| < \frac{\pi}{2},$ $|k| < \frac{\pi}{2},$ $|k| > \frac{\pi}{2}.$

Smooth matching at $k = \pi/4$ and $k = \pi/2$ yields the dispersion relation. Also in this case odd modes are discarded if \hat{U} is small, whereas the marginal boundary of even perturbations is given by

$$\sqrt{b+\hat{U}}\tanh\left(\frac{\pi}{4}\sqrt{b+\hat{U}}\right) + \sqrt{\hat{U}}\tanh\left(\frac{\pi}{4}\sqrt{\hat{U}}\right) = 0.$$
 (12.44)

Stability is improved if $0 \le \hat{U} \ll 1$, and ballooning modes of even parity are marginally stable if $b = -2\hat{U}$ (a more refined analysis based on asymptotic matching techniques gives $b = -\hat{U}$). The inclusion of Mercier corrections has a strong stabilising influence at low magnetic shear.

Improved marginal boundaries at low shear

The marginal boundaries identified by (12.43) are not particularly accurate at moderately small shear and pressure gradient. A better estimate can be obtained by using (12.28) instead of (12.30). For the sake of simplicity we set $\hat{U} = 0$.

With the substitution

$$\xi^* = X_0 / \left[1 + \left(k - \alpha \sin \frac{k}{s} \right)^2 \right]^{1/2},$$

and performing the same expansion analysis in the small parameter δ employed in the low shear case, one arrives at the following equation (Hazeltine (1985))

$$\frac{d^2 X_0}{dk^2} - \left(\frac{m^2 \gamma_H^2 k^2}{1 + k^2} + \frac{1}{(1 + k^2)^2} - \frac{2\frac{\alpha^2}{s} - \frac{3}{8}\frac{\alpha^4}{s^2}}{(1 + k^2)^3}\right) X_0 = 0.$$
 (12.45)

The algebra involved in its derivation is rather lengthy and is left as an exercise for the brave reader. We set $c = \frac{3}{8} \frac{\alpha^4}{s^2} - 2 \frac{\alpha^2}{s}$, and, in analogy to what we did earlier, we approximate

$$\frac{1}{(1+k^2)^2} \to H(\frac{\pi}{4}-k), \quad \frac{1}{(1+k^2)^3} \to H(\frac{3\pi}{16}-k),$$

with H the Heaviside step function. Carrying out the appropriate matching at $k=3\pi/16$ and $k=\pi/4$ (cf. (12.42)) yields even and odd eigensolutions, with odd modes to be discarded because

no positive growth rate is found with real α^2/s . The marginal boundaries of even modes are given by the relation

$$\sqrt{c+1}\tanh\left(\frac{3\pi}{16}\sqrt{c+1}\right) + \tanh\frac{\pi}{16} = 0.$$

This equation has solution $c \approx -1.317$, so that the unstable region in the α – s plane lies between by the two parabolae

$$s \approx 0.22\alpha^2$$
, $s \approx 1.3\alpha^2$. (12.46)

An exact solution of (12.45) in the limit $\gamma \to 0$ written in terms of Mathieu functions has been obtained in Dominguez-Vergara (1987) and Fu (1990) (see also Furth (1965) and Miyamoto (1997)).

The large shear case 12.4

Now, we assume that both α and the magnetic shear are of the same order with $s \gg 1$. For this case we shall employ equation (12.28). The stability analysis is approached through the construction of an integral functional which is then evaluated by plugging a convenient trial function (integral approach, Hazeltine (1978) and Pogutse (1979)).

We assume γ positive, even though it is allowed to be arbitrarily small. To explain the idea behind the integral approach let us write a model equation

$$\gamma^2 Q(k)X + \mathcal{L}(X) = 0, \tag{12.47}$$

where Q is a function of k and \mathcal{L} is a linear differential operator such that for two functions X_1 and X_2 which vanish at infinity one has

$$\int_{-\infty}^{\infty} X_1 \mathcal{L}(X_2) dk = \int_{-\infty}^{\infty} X_2 \mathcal{L}(X_1) dk.$$
 (12.48)

We say that \mathcal{L} is self-adjoint.

If we multiply (12.47) by X and integrate from $-\infty$ to $+\infty$, the following expression is obtained

$$\gamma^2 = -\frac{\int_{-\infty}^{\infty} X \mathcal{L}(X) dk}{\int_{-\infty}^{\infty} Q X^2 dk}.$$
 (12.49)

The eigenvalue γ^2 can be viewed as a functional of X. Let X_0 and $X = X_0 + \delta X$ be the solutions of (12.47) with eigenvalue γ_0 and γ respectively²⁰ with both X_0 and δX vanishing at infinity. Omitting to write the bounds of integration and assuming that δX is a small correction to

²⁰ That is $\gamma_0^2 Q X_0 + \mathcal{L}(X_0) = 0$.

 X_0 , from (12.49) we obtain

$$\begin{split} \gamma^2 &= -\frac{\int (X_0 + \delta X) \mathcal{L}(X_0 + \delta X) dk}{\int \mathcal{Q}(X_0 + \delta X)^2 dk} = -\frac{\int X_0 \mathcal{L}(X_0) dk}{\int \mathcal{Q}X_0^2 dk} \left(1 - \frac{\int 2\delta X \mathcal{Q}X_0 dk}{\int \mathcal{Q}X_0^2 dk} + \frac{\int 2\delta X \mathcal{L}(X_0) dk}{\int X_0 \mathcal{L}(X_0) dk}\right) + o(\delta X^2) = \gamma_0^2 + o(\delta X^2), \end{split}$$

having exploited the self-adjointness of the operator \mathcal{L} . This shows that a small deviation δX from the original function X_0 produces a correction of order δX^2 to the original eigenvalue γ_0^2 meaning that even with a rough guess of the eigenfunction one can have a rather good estimate of the true eigenvalue. We say that (12.49) is the **variational principle** for γ^2 in that the first order corrections to the eigenvalue are vanishing, i.e. γ^2 is a stationary point with respect to small variations δX .

Hence, we multiply (12.28) by ξ^* and integrate from $-\infty$ to ∞ . This yields

$$\int_{-\infty}^{\infty} dk \left\{ \left(1 + (k - \alpha \sin \frac{k}{s})^2 \right) \left(\frac{d\xi^*}{dk} \right)^2 + \left[\hat{U} + m^2 \gamma_H^2 k^2 - \frac{\alpha}{s^2} \left(\cos \frac{k}{s} + \sin \frac{k}{s} (k - \alpha \sin \frac{k}{s}) \right) \right] |\xi^*|^2 \right\} = 0.$$
 (12.50)

For the sake of simplicity we take $\hat{U}=0$ and focus on the identification of the marginal stability boundaries, that is we consider the eigenvalue $m^2\gamma_H^2=0$. We have now to guess a sensible trial function to be plugged into this expression.

Let us consider either (12.16) or (12.23) and compare the two terms

$$\frac{d}{dx}\left(x^2\frac{d\xi_m^r}{dx}\right), \quad \frac{\alpha}{ms^2}\frac{d\xi_{m\pm 1}^r}{dx}.$$

The first one is related to the effect of field line bending, while the second measures the strength of **mode coupling**. These must be of the same order. Because of the equivalence of different Fourier harmonics (cf. (12.8)), by letting $d/dx \rightarrow 1/\Delta x$ with Δx denoting the width of the radial harmonic in the x-space and taking $\alpha \sim s$, one has

$$\Delta x \sim \frac{1}{ms}$$
.

In §12.2 we introduced the variable z = mx, so that $\Delta z = m\Delta x \sim 1/s$. It is a well known fact of the Fourier transform that a function strongly localised in z is broadly spread in k and the other way around. This reciprocity of the widths in z and k-space is then represented by

$$\Delta z \Delta k \sim 1$$
.

Because of this, the Fourier transformed function ξ^* is expected to have width $\Delta k \sim s$. Therefore, we choose the following trial function:

$$\xi^* = \exp(-k^2/s^2).$$

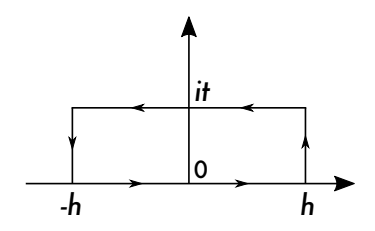


Figure 12.6: The integrals in (12.50) are evaluated with the help of

$$\begin{split} &\int_{-\infty}^{\infty} e^{-y^2} dy = \sqrt{\pi}, \quad \int_{0}^{\infty} y^{z-1} e^{-y} dy = \Gamma(z), \\ &\int_{-\infty}^{\infty} \cos(2ty) e^{-y^2} dy = e^{-t^2} \sqrt{\pi}, \\ &\int_{-\infty}^{\infty} y^2 \cos(2ty) e^{-y^2} dy = e^{-t^2} \frac{\sqrt{\pi}}{2} (1 - 2t^2). \end{split}$$

Noting that $\exp(2ity) = \cos(2ty) + i\sin(2ty)$, the last two expressions are obtained by computing through the residue theorem the integrals of e^{-y^2} and $y^2e^{-y^2}$ over the closed path indicated in the figure with $h \to \infty$. Furthermore one notes that $y\sin(y) = -(d(\cos ay)/da)_{a=1}$.

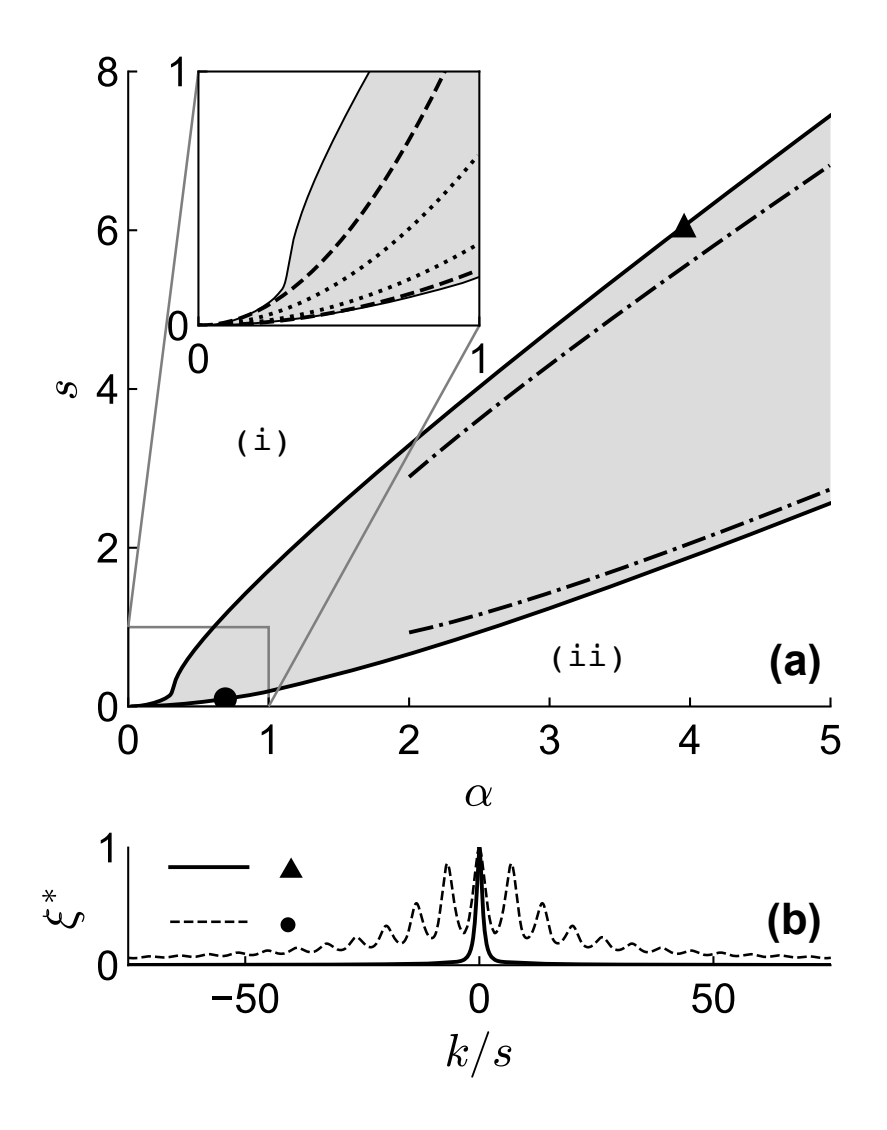


Figure 12.7: (a): Even modes marginal boundaries in the $\alpha - s$ plane computed from (12.43) (dotted), (12.46) (dashed), (12.51) (dot-dashed) and from the numerical solution of (12.28) (continuous line) with boundary condition (12.29) and $\hat{U} = 0$. In (a) the grey area indicates the unstable region. (b): Associated eigenfunctions ξ^* for the high (triangle)/low (dot) shear case.

Note that when this function is transformed back to the real x-space one still obtains a Gaussian. When this is plugged into (12.50), after working out the appropriate integrations (see Fig. 12.6) it is found that the marginal boundaries in the α – s space fulfil the relation

$$s^{2} - \frac{13}{6}e^{-1/8}\alpha s + \frac{4}{3}\left[1 + \alpha^{2}\left(1 - \frac{1}{2\sqrt{e}}\right) - \alpha e^{-1/8}\right] = 0.$$
 (12.51)

Figure 12.7 shows the marginal boundaries identified by (12.46) and (12.51) compared with the ones obtained from the numerical solution of (12.28). One notes two separate regions of stability: the one labelled (i) is called first stability region, while the other labelled (ii) is known as the **second stability region**.

From the existence of the second region of stability we may infer that, starting from an unstable configuration and keeping the magnetic shear fixed, stability can be reached again if the pressure gradient is further increased to sufficiently large values. This is very appealing from the experimental point of view because it indicates the possibility to operate quiescently at high pressure. Now, upon increasing the pressure

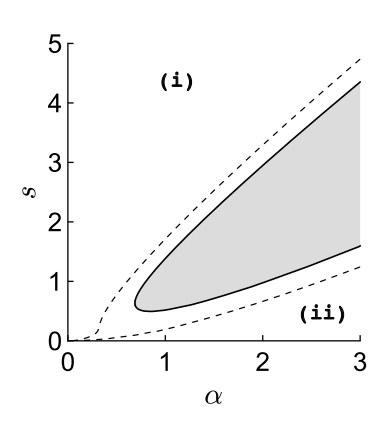


Figure 12.8: Ballooning modes stability region computed with the inclusion of Mercier corrections with $\varepsilon_m(1-1/q^2)=0.2$ (shaded area). The dashed lines are the marginal boundaries computed numerically of Fig. 12.7-(a). Note that the first and second stability regions are now connected.

gradient, large amplitude ballooning modes are likely to occur as soon as the system *hits* the marginal boundary of the first stability region: this prevents the pressure to further build up making the second stability region inaccessible (this argument is invoked to partially explain the cycles of big ELMs). Hence operation at high pressure appears to be impossible to achieve. However, the inclusion of Mercier corrections can "connect" the two stability regions (see equation (12.44) and figure 12.8) so that, at least theoretically, a stable trajectory from region (i) to region (ii) can exist.

References

- M. Abramowitz and I. A. Stegun (eds.), **Handbook of Mathematical Functions**, Dover Publications (New York, US), 1964.
- T. M. Antonsen Jr et al., Plasma Phys. 24, 197 (1982).
- L. Chen et al., Nucl. Fusion 20 901 (1980).
- B. Coppi, Phys. Rev. Lett. 39, 939 (1977).
- J. W. Connor et al., Phys. Rev. Lett. 40, 396 (1978).
- J. W. Connor et al., Phys. Plasmas 5, 2687 (1998).
- N. Dominguez-Vergara, **Stability of Ballooning Modes in Tokamaks with Energetic Particles**, PhD Thesis The University of Texas as Austin (Austin, US), 1987.
- G. Y. Fu et al., Phys. Fluids B 2, 2623 (1990).
- H. P. Furth *et al.*, "Stabilization by Shear and Negative V'", Proceedings of a Conference on Plasma Physics and Controlled Nuclear Fusion Research (Culham, England, 6-10 September 1965) Vol. 1 p. 103 Paper No. CN-21/106, International Atomic Energy Agency (Vienna, AT), 1966.
- S. Gasiorowicz, Quantum Physics, John Wiley & Sons (New York, US), 1974.
- J. M. Greene and M. S. Chance, Nucl. Fusion 21, 453 (1981).
- R. D. Hazeltine and D. Ross, Phys. Fluids 21, 1140 (1978).
- R. D. Hazeltine and J. D Meiss, Phys. Rep. 121, 1 (1985).
- R. D. Hazeltine and J. D Meiss, **Plasma Confinement**, Addison-Wesley Publishing Company (Redwood City, US), 1992.
- A. M. Krymskii, Fiz. Plazmy 7, 678 (1981) [Sov. J. Plasma Phys. 7, 371 (1981)].
- D. Lortz and J. Nührenberg, Phys. Lett. 68A, 49 (1978).
- D. Lortz and J. Nührenberg, Nucl. Fusion 19, 1207 (1979).
- H. Lütjens et al., Nucl. Fusion 32, 1625 (1992).
- A. B. Mikhailovskii and E. I. Yurchenko, Plasma Phys. 24, 977 (1982).
- K. Miyamoto, Fundamentals of Plasma Physics and Controlled Fusion, Iwanami Book Service Center (Tokyo, JP), 1997.
- O. P. Pogutse and E. I. Yurchenko, Fiz. Plazmy 5, 786 (1979) [Sov. J. Plasma Phys. 5, 441 (1979)].
- H. R. Strauss, Phys. Fluids 24, 2004 (1981).
- K. T. Tsang, Phys. Fluids 24, 2017 (1981).

Part IV RESISTIVE STABILITY

13

Resistive MHD in tokamaks: the basics

Up to now, the discussion focussed on MHD instabilities in an ideal plasma. In this framework, plasma resistivity is set to zero, i.e. the conductivity is infinite, so that thanks to the frozen-in theorem any fluid displacement, which may be caused by a perturbation, is glued to the magnetic field. As a consequence, the magnetic topology of the flux surfaces, although distorted, is **preserved**.¹

By allowing for dissipative effects in the form of a small but non vanishing plasma resistivity η , the flux freezing condition is not valid anymore (see §2.2) so that rearrangements of the magnetic topology may occur due to the diffusion of the magnetic flux. In the **Spitzer model**, a fully ionised plasma with a single ion species with charge number Z_i has resistivity (expressed in SI units)

$$\eta = \frac{4\sqrt{2\pi}}{3} \frac{Z_i e_e^2 \sqrt{m_e} \ln \Lambda}{(4\pi\varepsilon_0)^2 (k_B T_e)^{3/2}},$$

where e_e and m_e are the electron charge and mass respectively, $\ln \Lambda$ the Coulomb logarithm, 2 ε_0 the electric permittivity of free space, k_B the Boltzmann constant, and T_e the electron temperature (in Kelvin).

Typically, resistivity is small for temperatures of the order of tens of keV, ³ so that treating the plasma as an ideal conductor is a rather good assumption when describing dynamics which occur on timescales faster that those associated with resistive diffusion. This approximation, however, fails to capture the behaviour of some phenomena observed experimentally which can only be explained by allowing the plasma to be resistive. We refer to these resistivity driven disturbances as **resistive instabilities** or **resistive modes**.

Usually, the onset of such perturbations is observed to occur **below the limits set by ideal MHD**: in other words, a plasma which is *healthy*

¹ Flux surfaces can be deformed but they cannot break: any equilibrium smooth flux surface is mapped continuously into a new smooth and closed one. For any point of the surface the correspondence is 1-to-1.

² This usually takes values around 10.

 $^{^3}$ For a plasma with $T_e \approx 1 keV$, η is comparable to that of Copper at room temperature.

⁴ Commonly observed resistive instabilities in tokamaks are those which break and reconnect the magnetic field lines. This process results in the formation of magnetic islands (see next chapter).

within the ideal framework may still develop instabilities due to dissipation mechanisms (resistivity in our case) leading, consequently, to confinement degradation. The aim of this chapter is thus to provide the basic tools for the description of the perturbed dynamics in a resistive plasma.

Contrary to stability analyses performed with the **ideal MHD** model, one cannot construct a self-adjoint force operator in the form of equation (6.5) meaning that stability approaches based on the exploitation of an energy principle, as the one briefly discussed in chapter 6, cannot, in general, be used.⁵ This also implies that, within a normal mode analysis, the eigenvalues are allowed to be complex valued.

Luckily, most of the machinery developed in the previous chapters, based on the solution of eigenmode differential equations, is what is needed to tackle the problem of resistive stability. Hence, we first write down the fundamental equations of the resistive MHD model appropriately expressed in a toroidally symmetric geometry. After presenting a brief discussion about the regions where resistive effects become important, the set of the resistive equations is simplified accordingly. Finally, we discuss their solution and the structure of the associated eigenfunction from which the growth rate is extracted via an asymptotic matching procedure which will be exploited extensively in the following chapters. We recall that the analysis is carried out in normalised units **with** $\mu_0 = 1$.

Fundamental equations 13.1

For analysing the problem of resistive stability in tokamaks, we borrow some equations from the ideal MHD model of chapter 7: these are Eqs. (7.9) and (7.11)-(7.13) namely the evolution equation for the perturbed pressure, the equation for the divergence of B, the contravariant poloidal projection of the momentum equation and the vorticity equation. For the sake of clarity, we reproduce them below:

$$\tilde{p} = -p_0' \boldsymbol{\xi}^r + \Delta \boldsymbol{p}, \qquad \Delta \boldsymbol{p} = -\Gamma \boldsymbol{p}_0 \boldsymbol{\nabla} \cdot \boldsymbol{\xi}, \tag{13.1}$$

$$\frac{\partial \sqrt{g}\tilde{B}^{\theta}}{\partial \theta} = -\frac{\partial \sqrt{g}\tilde{B}^{r}}{\partial r} - \frac{\partial \sqrt{g}\tilde{B}^{\phi}}{\partial \phi}, \tag{13.2}$$

$$\rho_0 \gamma^2 \xi_{\vartheta} = -\frac{\partial \tilde{p}}{\partial \vartheta} + J_0^{\phi} \left(\sqrt{g} \tilde{B}^r \right) - B_0^{\phi} \left(\frac{g_{\phi\phi}}{\sqrt{g}} \frac{\partial \sqrt{g} \tilde{B}^{\phi}}{\partial \vartheta} - \frac{\partial \tilde{B}_{\vartheta}}{\partial \phi} \right), \tag{13.3}$$

$$\frac{\gamma^{2}}{\sqrt{g}} \left[\frac{\partial}{\partial r} \left(\frac{\rho_{0}}{B_{0}^{\phi}} \xi_{\vartheta} \right) - \frac{\partial}{\partial \vartheta} \left(\frac{\rho_{0}}{B_{0}^{\phi}} \xi_{r} \right) \right] = \boldsymbol{B}_{0} \cdot \boldsymbol{\nabla} \frac{\tilde{J}^{\phi}}{B_{0}^{\phi}} + \tilde{\boldsymbol{B}} \cdot \boldsymbol{\nabla} \frac{J_{0}^{\phi}}{B_{0}^{\phi}} \\
- \boldsymbol{J}_{0} \cdot \boldsymbol{\nabla} \frac{\tilde{B}^{\phi}}{B_{0}^{\phi}} - \boldsymbol{\nabla} \phi \cdot \boldsymbol{\nabla} \frac{1}{B_{0}^{\phi}} \times \boldsymbol{\nabla} \tilde{\boldsymbol{p}}, \tag{13.4}$$

where the perturbed current density is computed by means of (7.6).

⁵ An *extended* resistive energy principle can be derived but only for some special cases (Biskamp (1993)).

We notice that this set of equations is valid in both the ideal and resistive framework. The plasma response is accounted for by allowing for a small, although non-vanishing, resistivity in the induction equation. This is then written as (cf. (2.14))⁶

$$\frac{\partial \boldsymbol{B}}{\partial t} = \boldsymbol{\nabla} \times (\boldsymbol{u} \times \boldsymbol{B}) - \boldsymbol{\nabla} \times (\eta \boldsymbol{J}). \tag{13.5}$$

As an immediate consequence, both equations (7.7) and (7.8) must be augmented by resistive corrections leading to

$$\sqrt{g}\tilde{B}^{r} = \sqrt{g}\boldsymbol{B}_{0} \cdot \nabla \xi^{r} - \frac{1}{\gamma} \left(\frac{\partial (\widetilde{\eta J_{\phi}})}{\partial \vartheta} - \frac{\partial (\widetilde{\eta J_{\vartheta}})}{\partial \phi} \right), \tag{13.6}$$

$$\sqrt{g}\tilde{B}^{\phi} = \sqrt{g}\boldsymbol{B}_{0} \cdot \boldsymbol{\nabla}\xi^{\phi} - \sqrt{g}\boldsymbol{\nabla} \cdot (\boldsymbol{\xi}\boldsymbol{B}_{0}^{\phi}) - \frac{1}{\gamma} \left(\frac{\partial \widetilde{(\eta J_{\theta})}}{\partial r} - \frac{\partial \widetilde{(\eta J_{r})}}{\partial \theta} \right). \quad (13.7)$$

Due to the breaking of the ideal approximation, we must replace (7.10), which is the equation for the compressible contribution of the perturbed pressure, with

$$\rho_0 \gamma^2 \mathbf{B}_0 \cdot \boldsymbol{\xi} = -\tilde{\mathbf{B}}^r \boldsymbol{p}_0' + \mathbf{B}_0 \cdot \boldsymbol{\nabla} \left(\boldsymbol{p}_0' \boldsymbol{\xi}^r - \Delta \boldsymbol{p} \right). \tag{13.8}$$

Thus, the resistive MHD analysis will be entirely based on the set of equations (13.1)-(13.4), (13.6)-(13.8), where, as usual, we assume that the equilibrium is static meaning that there are no mass flows.

Now, as for the ideal case, resistive stability will be studied by Fourier decomposing the perturbation in the cyclic variables, namely the poloidal and toroidal angles. Hence, for our purposes it is useful to write down the poloidal and toroidal Fourier projections of some of the equations listed above. This will turn out to be particularly useful when the impact of toroidicity on resistive modes will be assessed in chapter 17.

Assume that a generic perturbed quantity can be written in a Fourier series as in (6.20), and consider the (ℓ, n) Fourier projection of equations (13.1)-(13.4). Equation (13.2) can be immediately reduced to (7.25)while the covariant poloidal projection of the momentum equation, i.e. (13.3), reads

$$\begin{split} &\frac{\rho_0 \gamma^2}{f_0'} (\sqrt{g} \xi_{\vartheta})_{\ell} = -i\ell \langle \frac{1}{B_0^{\phi}} \rangle \tilde{p}_{\ell} + \langle \frac{J_0^{\phi}}{B_0^{\phi}} \rangle (\sqrt{g} \tilde{B}^r)_{\ell} - i\ell G (\sqrt{g} \tilde{B}^{\phi})_{\ell} \\ &- in \langle N \rangle (\sqrt{g} \tilde{B}^{\vartheta})_{\ell} - \sum_{\ell' \neq 0} \left[\left(\frac{1}{B_0^{\phi}} \right)_{\ell'} i(\ell - \ell') \tilde{p}_{\ell - \ell'} \\ &- \left(\left(\frac{J_0^{\phi}}{B_0^{\phi}} \right)_{\ell'} - in M_{\ell'} \right) (\sqrt{g} \tilde{B}^r)_{\ell - \ell'} + in N_{\ell'} (\sqrt{g} \tilde{B}^{\vartheta})_{\ell - \ell'} \right]. \end{split}$$
(13.9)

We use the notation introduced in chapter 5 for the metric coefficients and recall that angular brackets indicate the operation of poloidal average as defined in (5.18). Proceeding further, the vorticity equation can ⁶ Note that (2.14) implies that with a non zero resistivity an electric field appears at equilibrium which is given by $E_0 = \eta_0 J_0$.

Within the Sptitzer model, we find that $\tilde{\eta} = -3/2\eta_0 \tilde{T}/T_0$. We further assume that

Because of axisymmetry, the toroidal spectral decomposition is trivial (i.e. one simply substitutes $\partial/\partial\phi \rightarrow -in$ with n the toroidal mode number).

be arranged to give

$$\gamma^{2} \left[\frac{\partial}{\partial r} \left(\frac{\rho_{0}}{B_{0}^{\phi}} \xi_{\vartheta} \right) - \frac{\partial}{\partial \vartheta} \left(\frac{\rho_{0}}{B_{0}^{\phi}} \xi_{r} \right) \right]_{\ell} = i [\ell \mu - n] (\sqrt{g} \tilde{J}^{\phi})_{\ell} \\
+ \left\langle \frac{J_{0}^{\phi}}{B_{0}^{\phi}} \right\rangle' (\sqrt{g} \tilde{B}^{r})_{\ell} - \left(\sqrt{g} J_{0} \cdot \nabla \frac{\tilde{B}^{\phi}}{B_{0}^{\phi}} \right)_{\ell} - i \ell \left\langle \frac{1}{B_{0}^{\phi}} \right\rangle' \tilde{p}_{\ell} \\
+ \sum_{\ell' \neq 0} \left[\left(\frac{J_{0}^{\phi}}{B_{0}^{\phi}} \right)'_{\ell'} (\sqrt{g} \tilde{B}^{r})_{\ell-\ell'} + i \ell' \left(\frac{J_{0}^{\phi}}{B_{0}^{\phi}} \right)_{\ell'} (\sqrt{g} \tilde{B}^{\vartheta})_{\ell-\ell'} \\
- \left(\frac{1}{B_{0}^{\phi}} \right)'_{\ell'} i (\ell - \ell') \tilde{p}_{\ell-\ell'} + i \ell' \left(\frac{1}{B_{0}^{\phi}} \right)_{\ell'} \tilde{p}'_{\ell-\ell'} \right], \tag{13.10}$$

where the perturbed current density is given by the relation (cf. (7.52) and (7.53))

$$(\sqrt{g}\tilde{J}^{\phi})_{\ell} = [\langle N \rangle (\sqrt{g}\tilde{B}^{\vartheta})_{\ell}]' - i\ell \langle L \rangle (\sqrt{g}\tilde{B}^{r})_{\ell}$$

$$+ \sum_{\ell' \neq 0} \left\{ [M_{\ell'}(\sqrt{g}\tilde{B}^{r})_{\ell-\ell'} + N_{\ell'}(\sqrt{g}\tilde{B}^{\vartheta})_{\ell-\ell'}]'$$

$$- i\ell [L_{\ell'}(\sqrt{g}\tilde{B}^{r})_{\ell-\ell'} + M_{\ell'}(\sqrt{g}\tilde{B}^{\vartheta})_{\ell-\ell'}] \right\}.$$
(13.11)

The remaining equations, that is (13.6)-(13.8) and the expression for the perturbed pressure, will be discussed later.

Although this set equations appears to have quite a complicated structure, it will be shown that resistive effects become relevant only at very specific locations where the perturbation exhibits strong radial gradients. Allowing for this fact, the stability analysis of resistive modes can be dramatically simplified by deploying an appropriate ordering near these points. This will be addressed in detail in the next two sections.

13.2 Where resistivity matters

For the sake of a qualitative understanding, let us assume that the plasma resistivity is a constant and write the induction equation as

$$\frac{\partial \mathbf{B}}{\partial t} = \mathbf{\nabla} \times (\mathbf{u} \times \mathbf{B}) + \eta_0 \mathbf{\nabla}^2 \mathbf{B}, \tag{13.12}$$

Ignoring the term proportional to u, we see that this equation has the structure of a **diffusion equation for the magnetic field** in the variable x/L where L is some characteristic length. The typical **diffusion time** is then⁸

$$au_{
m diff} = rac{L^2}{\eta_0}.$$

Upon perturbing (13.12), we take the ratio of the last term on the right-hand-side and the one on the left-hand-side to give

$$\frac{|\eta_0 \nabla^2 \widetilde{\boldsymbol{B}}|}{|\partial \widetilde{\boldsymbol{B}}/\partial t|} \sim \frac{\eta_0}{\gamma} \frac{d^2}{dr^2}.$$
 (13.13)

⁸ To convert to SI units one performs the substitution $\eta \to \eta/\mu_0$.

We choose the characteristic length L to be the plasma minor radius (L =a), and introduce a dimensionless parameter S known as the **Lundquist** number9 defined as

$$S \equiv \tau_R \omega_A = \frac{\tau_R}{\tau_A},\tag{13.14}$$

with $\tau_R = a^2/\eta_0$ and $\tau_A = 1/\omega_A = R_0\sqrt{\rho}/B_0$ (τ_A is called the Alfvén time). This quantity estimates the ratio between the resistive diffusion timescales and the Alfvén wave transit speed; in tokamaks this is a large number typically falling within the range of $\sim 10^8 - 10^9$ for plasma temperatures of the order of keV.

Thus, from (13.13) one sees that resistive effects become significant when

$$a^2 \frac{d^2}{dr^2} \sim S \frac{\gamma}{\omega_A}.\tag{13.15}$$

Usually, resistive instabilities in tokamaks grow on timescales of the order of several (tens of) milliseconds. With a typical Alfvén frequency of the order of megahertz, one then finds that $\gamma/\omega_A \sim 10^{-5} - 10^{-4}$. Hence, with the large values of S mentioned earlier, it is evident that (13.15)implies that resistive effects come into play where the perturbation develops strong radial second derivatives.

Consider now for the sake of simplicity a generic perturbed quantity \tilde{f} characterised by a single Fourier harmonic of helicity (m, n), with both m and n of the order of unity and resonance located at r_s . In line with the findings of the previous chapters, we expect large radial gradients to appear in proximity of r_s where $[r_s(\boldsymbol{b}\cdot\boldsymbol{\nabla}\tilde{f})]/\tilde{f}\ll 1$ (\boldsymbol{b} is the unit vector along the equilibrium field). Therefore, according to (13.15), resistivity is going to matter only in a thin layer around this singular point. This is usually referred to as the resistive layer.

Sufficiently far from the resonance instead, the radial gradients of the perturbation are weak so that the dynamics can be described within the ideal approximation. We call this region, where the MHD equations are solved in the $\eta \to 0$ limit, the **ideal region**.

Thus, the stability analysis of resistive perturbations can be simplified as follows: far from the resonance we borrow the results obtained in the previous chapters within the ideal MHD framework, whereas the resistive layer equations are solved only retaining terms which contain higher order derivatives. Now that we have a basic understanding of where and how resistive effects enter into play, we shall proceed by deploying an appropriate ordering aimed to obtain a simplified set of coupled equations suitable for the description the restive layer dynamics. This is discussed in the next section.

Resistive layer orderings 13.3

Let us first flag that because many of the calculations presented below closely follows those of sections 7.3.2 and 7.4.2, some of the mathemati⁹ This is a particular case of the magnetic Reynolds number in a system whose characteristic velocity is the Alfvén one.

cal steps are omitted (the reader is referred to the afore-mentioned sections).

Consider a low- β plasma with $p_0/B_0^2 \sim rp_0'/B_0^2 \sim \varepsilon^2$, and fix, as usual, the toroidal mode number n. Assume that the perturbation can be decomposed in a Fourier series with multiple poloidal harmonics, each of these with a dependence on the toroidal angle and time of the form $\exp(\gamma t - in\phi)$. We further assume that the growth rates are significantly smaller than the typical Alfvén timescales. The analysis is carried out in a narrow region very close to the radius r_s where q = m/n for some poloidal mode number m. Thus, we conveniently take¹⁰

$$\gamma/\omega_A \sim \varepsilon, \quad \frac{r-r_s}{r_s} = x \sim \varepsilon/m.$$
 (13.16)

Denoting with s the magnetic shear at r_s , it follows that

$$m\mu - n \approx -nsx \sim s\varepsilon$$
.

As for the ideal case (see (7.36) and (7.50)), fluctuating quantities are expected to exhibit strong radial excursions in the resistive layer about r_s , hence we take (η_0) is the **equilibrium resistivity**)

$$\frac{\eta_0}{\gamma} \frac{d^2}{dr^2} \sim 1$$
, and $r \frac{d}{dr} \sim \frac{m}{\varepsilon}$. (13.17)

We allow these relations to hold for modes with either $m \sim 1$ or $m \gg 1$.

We now assume that in the resistive layer the spectrum of the disturbance is dominated by the harmonic with poloidal mode number m. Hence, the magnetic perturbation and the fluid fluctuation are assumed to conform to the orderings given in (7.37) and (7.38). It turns out that within these orderings most of the contributions arising from mode coupling, apart from those associated with plasma compressibility, can be treated as negligible corrections. Furthermore, in the layer analysis poloidal harmonics of mode number $m \pm \ell$ with $\ell \ge 2$ are ignored altogether since their amplitude is supposed to be negligibly small compared to the one of the first neighbouring sidebands.

Hence, the mth Fourier projection of (13.6) reads

$$(\sqrt{g}\tilde{B}^{r})_{m} = ir_{s}B_{0}(m\mu - n)\xi_{m}^{r} + \frac{\eta_{0}}{\gamma}\frac{d^{2}(\sqrt{g}\tilde{B}^{r})_{m}}{dr^{2}},$$
(13.18)

where only the terms with higher order derivatives have been retained in the expression for the perturbed current.¹¹ The expressions for other poloidal harmonics are not needed. From (13.7) one has instead (cf. (7.39))

$$\left(1 - \frac{\eta_0 GN}{\gamma} \frac{\partial^2}{\partial r^2}\right) \sqrt{g} \tilde{B}^{\phi} = -f_0' \left(\frac{1}{f_0'} \frac{\partial (f_0' \xi^r)}{\partial r} + \frac{\partial \xi^{\theta}}{\partial \theta} - \mu \frac{\partial \xi^{\phi}}{\partial \theta}\right).$$
(13.19)

We point out that the right-hand-side of the equation above is exact, whereas the left-hand-side has been approximated by only considering its leading contributions.

¹⁰ With such an ordering of the layer radial variable x we can address simultaneously low-m and high-m modes.

¹¹ It is easy to prove that mode coupling only occurs at higher order, so that contributions due to neighbouring sidebands can be safely dropped. It follows that at this stage we can take the cylindrical limit for the terms proportional to the plasma resistivity. A more careful analysis will be deployed in chapter 17.

By means of (13.19) we find that the ℓ th Fourier component of the divergence of ξ can be approximated as (cf. (7.40))

$$\begin{split} (\boldsymbol{\nabla} \cdot \boldsymbol{\xi})_{\ell} &= -\frac{1}{f_{0}'} \left[\left(1 - \frac{\eta_{0} G N}{\gamma} \frac{\partial^{2}}{\partial r^{2}} \right) \sqrt{g} \tilde{B}^{\phi} \right]_{\ell} + \left(\langle \frac{(\sqrt{g})'}{\sqrt{g}} \rangle - \frac{f_{0}''}{f_{0}'} \right) \xi_{\ell}^{r} \\ &+ i (\ell \mu - n) \xi_{\ell}^{\phi} + \sum_{\ell' \neq 0} \left[\left(\frac{\partial \sqrt{g}/\partial r}{\sqrt{g}} \right)_{\ell'} \xi_{\ell-\ell'}^{r} + \left(\frac{\partial \sqrt{g}/\partial \vartheta}{\sqrt{g}} \right)_{\ell'} \xi_{\ell-\ell'}^{\vartheta} \right]. \end{split}$$
 (13.20)

From this, and employing the afore-mentioned orderings for the magnetic perturbation and the fluid displacement, one sees that $(\nabla \cdot \boldsymbol{\xi})_m \sim$ ξ^r/r so that

$$\tilde{p}_m \sim \varepsilon^2 B_0^2 \xi_m^r / r. \tag{13.21}$$

Thus, to leading order in ε , the mth Fourier projection of (13.9) yields explicitly

$$0 = -im \langle \frac{1}{B_0^{\phi}} \rangle \tilde{p}_m - im G(\sqrt{g} \tilde{B}^{\phi})_m - in \langle N \rangle (\sqrt{g} \tilde{B}^{\vartheta})_m,$$

which shows that $(\sqrt{g}\tilde{B}^{\phi})_m \sim \varepsilon^2 B_0 \xi_m^r$. Repeating the same procedure for the $m \pm 1$ harmonics one finds that $(\sqrt{g}\tilde{B}^{\phi})_{m\pm 1}$ is also small. Hence, by plugging these results into (13.19), we see that both (7.27) and (7.41)hold in the resistive layer as well.

Focussing on the parallel projection of the perturbed momentum equation, one has (cf. (7.10) and (13.8))

$$B_0^2 \frac{R^2}{R_0^2} \frac{\gamma^2}{\omega_A^2} \left[\xi^{\phi} + \frac{\mu}{R^2} \left(g_{r\theta} \xi^r + g_{\theta\theta} \xi^{\theta} \right) \right] = -\left(\mu \frac{\partial}{\partial \theta} - i n \right) \tilde{p} - \frac{p_0'}{f_0'} \sqrt{g} \tilde{B}^r.$$
(13.22)

By taking the *m*th Fourier component of this equation we see that ξ_m^{ϕ} ~ $\varepsilon \xi_m^r/r$ at most; it follows that at leading order (cf. (7.31))

$$\xi_m^{\vartheta} \approx -\frac{1}{im} \frac{d\xi_m^r}{dr}.$$
 (13.23)

Exploiting the smallness of the toroidal fluid displacement, from the first of (7.41) we infer that $(\nabla \cdot \boldsymbol{\xi})_m \sim \varepsilon \boldsymbol{\xi}_m^r$ and $\Delta p_m \sim \varepsilon^3 B_0^2 \boldsymbol{\xi}_m^r / r$, thence letting us to set

$$\Delta p_m = 0. \tag{13.24}$$

Retaining only the dominant contributions, the $m \pm 1$ Fourier projections of (13.22) yield

$$\mp i\mu\Delta p_{m\pm 1} = \frac{\rho_0\gamma^2}{f_0'}(\sqrt{g}\boldsymbol{B}_0\cdot\boldsymbol{\xi})_{m\pm 1} \approx B_0^2\frac{\gamma^2}{\omega_A^2}\boldsymbol{\xi}_{m\pm 1}^{\phi}.$$

It is important to stress that corrections due to poloidal harmonics other than the m and $m \pm 1$ are assumed to be small enough so that they have been ignored. By combining this with the second of (7.41) we obtain

$$\left[1 + \frac{q^2 \gamma^2 / \omega_A^2}{\Gamma p_0 / B_0^2}\right] \Delta p_{m \pm 1} \approx \pm \frac{B_0^2 r}{m R_0} \frac{q^2 \gamma^2}{\omega_A^2} \frac{d\xi_m^r}{dr}.$$
 (13.25)

A more precise expression for ξ_m^{ϑ} and ξ_m^{ϕ} will be derived in chapter 16.

 $(m \pm 1)\mu - n \approx \pm \mu$.

Namely the the vorticity equation and the one for the perturbed current.

¹² Here we take $x \sim \delta x$.

If the growth rate is sufficiently small, the second term in the square brackets on the left-hand-side can be dropped, and we recover the usual **inertia enhancement** factor for slow-growing instabilities (the $\beta \to 0$ case with a non vanishing γ will be briefly discussed in the next chapter). This gives the estimate $\tilde{p}_{m\pm 1} \sim \varepsilon^3 B_0^2 \xi_m^r/r$.

We have now all the elements to derive the dynamical equations in the resistive layer. By applying the orderings just discussed to Eqs. (13.10) and (13.11), and recalling that $(1/B_0^{\phi})_{\pm 1} = r/B_0$ we obtain

$$\frac{\gamma^2}{\omega_A^2} \frac{d^2 \xi_m^r}{dx^2} = \frac{nsx}{irB_0} \frac{d^2 (\sqrt{g}\tilde{B}^r)_m}{dx^2} + m \frac{R_0}{B_0^2} \frac{d}{dx} \left(\tilde{p}_{m-1} - \tilde{p}_{m+1} \right). \tag{13.26}$$

Finally, employing the expression for the compressible contribution to the perturbed pressure, we reduce (13.18) and (13.26) to the following system of coupled linear equations:

$$\left[1 - \frac{\eta_0}{r_s^2 \gamma} \frac{d^2}{dx^2}\right] \frac{(\sqrt{g}\tilde{B}^r)_m}{i r_s B_0} = -n s x \xi_m^r, \tag{13.27}$$

$$\frac{\gamma^2}{\omega_A^2} (1 + 2q_s^2) \frac{d^2 \xi_m^r}{dx^2} = \frac{nsx}{ir_s B_0} \frac{d^2 (\sqrt{g} \tilde{B}^r)_m}{dx^2},$$
 (13.28)

where $q_s = m/n$ and s is the magnetic shear at the resonance. A more refined analysis of the layer equations including higher order toroidal effects will be presented in chapter 17.

Equations (13.27) and (13.28) govern the leading order dynamics in the resistive layer whose radial thickness can be estimated as follows: let us write $d^2/dx^2 \sim 1/(\delta x)^2$. From (13.27) and using (13.17), the order of magnitude of the magnetic perturbation is $(\sqrt{g}\tilde{B}^r)_m/irB_0 \sim ns\xi_m^r\delta x$. Plugging this into (13.28) yields (8.7). Relation (13.15) can be written as $1/(\delta x)^2 \sim S\frac{\gamma}{\omega_A}$, and when this is combined with (8.7) we find that the approximate width of the resistive layer around r_s is

$$\delta x \sim \left(\frac{\sqrt{1+2q_s^2}}{nsS}\right)^{1/3}.$$
 (13.29)

For tokamak-relevant values of *S* one finds that $\delta x \ll 1$.

We point out that our analysis assumes that the mode resonance occurs well inside the plasma. This implies that the boundary conditions at the plasma edge, either with or without a vacuum gap, are those discussed in section 6.1.1 within ideal MHD framework. The next section will be devoted to the construction of the resistive layer solution.

13.4 Solution of the resistive layer equations

Equations (13.27) and (13.28) can be reduced to a single one by deploying an appropriate **Fourier transform** in the radial variable x.¹³ Let us

¹³ One can in principle avoid using the Fourier transform and obtain a single fourth order differential equation for $(\sqrt{g}\tilde{B}^r)_m$.

introduce a smallness parameter $\epsilon_R > 0$ whose definition will be given later, and define

 $y=\frac{x}{\epsilon p}$.

If ϵ_R is sufficiently small, moving away from the resistive layer we may allow y to vary from $-\infty$ to $+\infty$.

Upon defining the k-space Fourier quantities

$$\psi^* = \int_{-\infty}^{\infty} (\sqrt{g}\tilde{B}^r)_m e^{-iky} dy, \quad \xi^* = \int_{-\infty}^{\infty} \xi_m^r e^{-iky} dy,$$
 (13.30)

the induction and vorticity equations, namely Eqs. (13.27) and (13.28), now read

$$\left(1 + \frac{\eta_0}{r_s^2 \gamma} \frac{k^2}{\epsilon_R^2}\right) \psi^* = r_s B_0 n s \epsilon_R \frac{d\xi^*}{dk},$$

$$\frac{\gamma^2}{\omega_A^2} (1 + 2q_s^2) k^2 \xi^* = \frac{n s}{r_s B_0} \epsilon_R \frac{d}{dk} \left(k^2 \psi^*\right).$$
(13.31)

When combined together, these give

$$\frac{d}{dk} \left(\frac{k^2}{1 + V k^2 / \epsilon_R^2} \frac{d\xi^*}{dk} \right) - \frac{\gamma^2}{\omega_A^2} \frac{(1 + 2q_s^2)}{n^2 s^2} \frac{k^2}{\epsilon_R^2} \xi^* = 0, \tag{13.32}$$

having defined for convenience

$$V=\frac{\eta_0}{r_s^2\gamma}.$$

We choose as smallness parameter

$$\epsilon_R = S^{-1/3}/m \tag{13.33}$$

where

$$S = \frac{r_s^2 \omega_A}{\eta_0},\tag{13.34}$$

is the Lundquist number introduced earlier with the replacement $a \rightarrow r_s$. Then, equation (13.32) is cast as 14

$$\frac{d}{dk} \left(\frac{k^2}{1 + V_e k^2} \frac{d\xi^*}{dk} \right) - Q k^2 \xi^* = 0, \tag{13.35}$$

where

$$V_e = \frac{m^2}{\gamma/\omega_A} S^{-1/3}, \quad Q = \frac{\gamma^2}{s^2 \omega_A^2} q_s^2 (1 + 2q_s^2) S^{2/3}.$$
 (13.36)

It is worth noting that (13.35) is independent of the sign of the magnetic shear. Hence, when solving the equation above, we have to bear in mind that any time that s appears this actually means |s|.

Now, similar to what we saw in the analysis of ballooning instabilities, we must require $\xi^*(k) \to 0$ for $k \to \infty$ in order to have its Fourier inverse $\xi_m^r(r)$ to exist. Since (13.35) is singular at k=0, we first find We select a narrow interval about the resonance whose boundaries in the variable y, that is the one which is Fourier transformed, effectively become $\pm \infty$. In such a case, the Fourier transform is well defined.

¹⁴ Note that if we choose $\epsilon_R = 1/m$ when m is large, the Fourier variable k corresponds to that of §12.2.

a solution for k > 0. Following Mikhailovskii (1998), we introduce the variable $\zeta = (QV_e)^{1/2}k^2$ and write $\xi^* = e^{-\zeta/2}Y(\zeta)$ so that equation (13.35) transforms into

$$\zeta \frac{d^2 Y}{d\zeta^2} + \left(\frac{1}{2} - \zeta + \frac{1}{1 + \zeta/M_t}\right) \frac{dY}{d\zeta} - \left(\frac{M_t + 1}{4} + \frac{1}{2(1 + \zeta/M_t)}\right) Y = 0,$$
(13.37)

having defined

$$M_t = (Q/V_e)^{1/2}. (13.38)$$

The particular solution to this equation which decays for ζ (and hence k) going to infinity is

$$Y(\zeta) = U\left(\frac{M_t + 5}{4}, \frac{3}{2}, \zeta\right) + \frac{2}{M_t}U\left(\frac{M_t + 1}{4}, \frac{1}{2}, \zeta\right),\tag{13.39}$$

where U denotes the **confluent hypergeometric function**. The box at the end of the chapter shows by direct substitution that this expression solves (13.37). The explicit solution procedure for a more general case is outlined in Correa-Restrepo (1982), and it will be briefly discussed at the end of section 16.3.3.

To extend the solution of (13.35) to the k < 0 plane, from (13.39) we generate even and odd solutions valid in the whole domain $-\infty < k < \infty$ by defining $\xi^*(-k) = \xi^*(k)$ and $\xi^*(-k) = -\xi^*(k)$.

In order to obtain the dispersion relation, the solution in the resistive layer has to be matched with the one computed in the ideal region. Hence we need to obtain from ξ^* the corresponding asymptotic behaviour in real space far from r_s , i.e. for large y. Let us write the Fourier inverse of $\xi^*(k)$:

$$\xi_m^r(y) = \frac{1}{2\pi} \int_{-\infty}^{\infty} \xi^*(k) e^{iky} dk.$$
 (13.40)

By expanding the even and odd solutions $\xi^*(k)$ in a power series in k we obtain

$$\xi^* \propto \begin{cases} 1 + \frac{\Delta_R}{|k|} + \sum_{\ell=1}^{\infty} a_{\ell} |k|^{\ell}, & \text{even,} \\ \left(1 + \frac{\Delta_R}{|k|} + \sum_{\ell=1}^{\infty} a_{\ell} |k|^{\ell}\right) \operatorname{sgn}(k), & \text{odd,} \end{cases}$$
(13.41)

where a_{ℓ} are some numerical coefficients and the resistive layer parameter Δ_R is defined as (Γ is the Gamma function)

$$\Delta_R = -\frac{\sqrt{M_t/V_e}}{2(M_t - 1)} \frac{\Gamma\left(\frac{M_t + 3}{4}\right)}{\Gamma\left(\frac{M_t + 5}{4}\right)}.$$
 (13.42)

Applying definition (13.40), we inverse Fourier transform each of the terms appearing in the expansion series (13.41). In doing this, we use the following formulae (Lighthill (1958))¹⁵

$$1 \to \delta(y),$$

$$\frac{1}{k} \to \frac{i}{2} \operatorname{sgn}(y),$$

$$\frac{1}{|k|} \to -\frac{1}{\pi} \left(\ln|y| + C \right),$$

$$\operatorname{sgn}(k) \to -\frac{1}{i\pi y},$$

$$(13.43)$$

where C is an arbitrary constant.

Noticing that the inverse Fourier transform of the terms appearing under the sign of sum in (13.41) yields contributions which decay faster than 1/y, hence negligible for $y \gg 1$, we finally find that the even and odd solutions in the resistive layer behave asymptotically in real space for large y as

$$\xi_{m,\text{even}}^r \propto \delta(y) - \frac{\Delta_R}{\pi} \left(\ln |y| + C \right),$$

 $\xi_{m,\text{odd}}^r \propto -\frac{1}{i\pi y} + \frac{i}{2} \Delta_R \operatorname{sgn}(y).$

An example of the shape of the odd solution both in k and real (y) space is shown in figure 13.1.

It is worth mentioning that the most general solution of the equation kf(k)=0 is $f \propto \delta(k)$. Hence, since $k^2d\xi^*/dk=kd(k\xi^*)/dk-k\xi^*$, the function $\xi^* \propto \delta(k)$ is also a solution of (13.35). When this is transformed back to real space, a constant will be generated which for convenience is absorbed in the C factor of the expression above. We point out that for $y \neq 0$ (and hence $x \neq 0$) the Dirac-delta function appearing in the even solution can be ignored.

Thus, with a trivial rearrangement, the expressions above are conveniently written in terms of the variable x as follows:

$$\xi_{m,\text{even}}^r \propto 1 + \frac{1}{\hat{C}} \ln|x|, \qquad (13.44)$$

$$\xi_{m,\text{odd}}^r \propto \frac{1}{x} \left(1 + \frac{m\pi\Delta_R}{2} S^{1/3} |x| \right),$$
 (13.45)

having replaced the constant C with another arbitrary constant \hat{C} . The eigenfunction in the resistive layer is then written as a **linear combination of even and odd solutions** whose asymptotic behaviour conforms to (13.44) and (13.45) respectively.

The growth rate and the structure of the eigenfunction are both determined by matching the resistive layer solution with the one obtained in the ideal region. This will be studied in detail in the next chapters, where we will analyse the resistive stability properties of both global and localised perturbations, namely

· tearing modes,

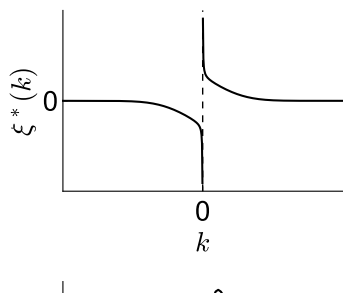
 15 In the notation of Lighthill (1958) one defines the Fourier transform, here denoted by an asterisk, of the function f as

$$f^*(\hat{k}) = \int_{-\infty}^{\infty} f(\hat{x}) e^{-2\pi i \hat{k} \hat{x}} d\hat{x}.$$

The following relations hold:

$$\begin{split} & \left[\frac{1}{\hat{x}}\right]^* = -i\pi \, \mathrm{sgn}(\hat{k}), \quad [\mathrm{sgn}(\hat{x})]^* = \frac{1}{i\pi \hat{k}}, \\ & \left[\frac{1}{|\hat{x}|}\right]^* = -2 \left(\ln |\hat{k}| + C\right), \quad [1]^* = \delta(\hat{k}), \\ & [\hat{x}^{\ell} \, \mathrm{sgn}(\hat{x})]^* = \frac{2(n!)}{(2\pi i \hat{k})^{\ell+1}}, \quad [\hat{x}^{\ell}]^* = \frac{\delta^{(\ell)}(\hat{k})}{(-2\pi i)^{\ell}}, \end{split}$$

where ℓ is a positive integer and C an arbitrary constant. For our purposes, by comparing with (13.40), we identify $\hat{x} \rightarrow k/(2\pi)$ and $\hat{k} \rightarrow -\gamma$.



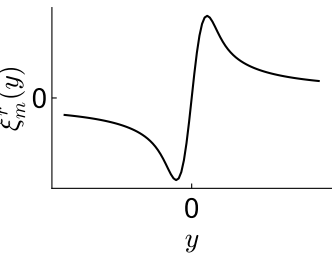


Figure 13.1: Example of the shape of odd $\xi^*(k)$ and corresponding $\xi^r_m(r)$ for $M_t \ll 1$.

- m = 1 resistive kink,
- resistive interchange modes,
- resistive ballooning modes,

External kink and infernal modes do not require a resonance in the plasma to become unstable, so they do not need a resistive treatment.¹⁶ A slight refinement of the resistive layer equations is needed for resistive interchange and ballooning modes; this will be thoroughly detailed in chapter 16.

¹⁶ Infernal modes may be analysed within the resistive framework by allowing for resistive effects at the resonance of the upper sideband. On the contrary, hybrid kink-infernal perturbations have a dominant harmonic which exhibits an exact resonance. In such a case one can include effects associated with resistivity in a similar fashion to the m = 1 resistive kink.

On the resistive layer solution

Here we show by direct substitution that (13.39) solves (13.37). Let us start by calling $h = (M_t + 1)/4$ and define

$$U_1 = U\left(h+1,\frac{3}{2},\zeta\right), \quad U_2 = U\left(h,\frac{1}{2},\zeta\right).$$

By writing $Y = U_1 + \frac{2}{M_t}U_2$ and exploiting the fact that U_1 and U_2 solve respectively

$$\zeta \frac{d^2}{d\zeta^2} U_1 + \left(\frac{3}{2} - \zeta\right) \frac{dU_1}{d\zeta} - (h+1)U_1 = 0, \tag{13.46}$$

$$\zeta \frac{d^2}{d\zeta^2} U_2 + \left(\frac{1}{2} - \zeta\right) \frac{dU_2}{d\zeta} - hU_2 = 0,$$
 (13.47)

equation (13.37) is then cast as

$$\frac{1}{1+\zeta/M_t}\frac{d}{d\zeta}\left(U_1+\frac{2}{M_t}U_2\right)-\frac{dU_1}{d\zeta}+U_1-\frac{U_1+\frac{2}{M_t}U_2}{2(1+\zeta/M_t)}=0.$$

After multiplying this by $1 + \zeta/M_t$ we obtain

$$\frac{2}{M_t}\frac{dU_2}{d\zeta} - \frac{\zeta}{M_t}\frac{dU_1}{d\zeta} + \left(\frac{1}{2} + \frac{\zeta}{M_t}\right)U_1 - \frac{U_2}{M_t} = 0.$$

Since $U_1 = -\frac{1}{\hbar}dU_2/d\zeta$, this reduces to (13.47), thus proving that (13.39) is a solution of (13.37).

References

- M. Abramowitz and I. A. Stegun (eds.), Handbook of Mathematical Functions, Dover Publications (New York, US), 1964.
- D. Biskamp, **Nonlinear Magnetohydrodynamics**, Cambridge University Press (Cambridge, UK) 1993.
- A. Bondeson and J. R. Sobel, Phys. Fluids 27, 2028 (1984).
- B. Coppi et al., Nucl. Fusion 6, 101 (1966).

- D. Correa-Restrepo, Z. Naturforsch. A 37, 848 (1982).
- $\bullet \ \ M.\,J.\,Lighthill, \textbf{Introduction to Fourier Analysis and Generalised Functions},$ CUP (Cambridge, UK), 1958.
- F. Pegoraro and T. J. Schep, Plasma Phys. Control. Fusion 28, 647 (1986).
- F. Porcelli, Phys. Fluids 30, 1734 (1987).
- A. B. Mikhailovskii, Instabilities in a Confined Plasma, Institute of Physics Publishing (Bristol, UK), 1998.

14

Tearing modes

As mentioned in the previous chapter, one of the must striking effects of letting the plasma to be resistive is that the magnetic topology can be rearranged. This permits the breaking and reconnection of the magnetic field lines which then produces regions of isolated flux tubes known as **magnetic islands**. In tokamaks (and other toroidal confinement devices), the structure of magnetic islands consists of nested flux surfaces centred about a secondary magnetic axis (see fig. 14.1). These revolve helically around the plasma column following this secondary magnetic axis, and eventually close on themselves after an integer number of poloidal and toroidal turns. Typically, in experiments, magnetic islands rotate dragged by flow of the bulk plasma.

In presence of such perturbations, **transport** of energy and particles across the plasma is enhanced, and the temperature is equilibrated within the island. Further worsening of confinement may arise from the overlap of neighbouring island chains causing the magnetic field to become **stochastic**. A schematic depiction of the deterioration of the plasma performance due to the presence of one or more magnetic islands is shown in figure 14.2.

Although the reduction in performance is highly undesirable, some actuators can be put in place to mitigate it. However, it is not uncommon to observe a reduction (in the lab frame) of the rotation frequency of magnetic islands, eventually locking onto the surrounding structures (this is usually referred to as **mode locking**): in such a case, the island amplitude grows to such an extent that a catastrophic loss of confinement, i.e. a disruption, is often triggered (typically for islands with helicity 2/1). Therefore, for safe device operation and to preserve machine integrity, once should reduce as much as possible the likelihood of such

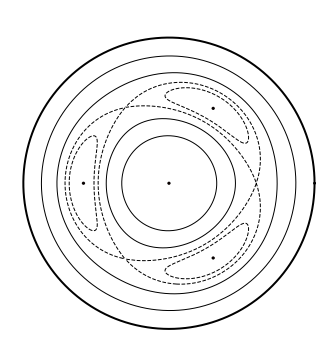


Figure 14.1: Example of the poloidal structure of a m = 3 island chain.

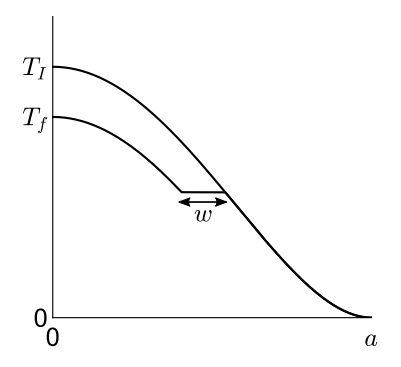


Figure 14.2: Core temperature decrease due to the presence of one or more magnetic islands creating a "belt" of width w where temperature is flattened. The subscript I stands for initial and f for final.

¹ The seed might be generated by, e.g., linear coupling between poloidal harmonics of fluid or magnetic perturbations, or through a non-linear interaction of disparate plasma fluctuations. The non-linear growth of the island width is usually algebraic, i.e. it grows with some power of time. Experimentally, once detected, there is margin to apply actuators to control or suppress the growth of NTMs.

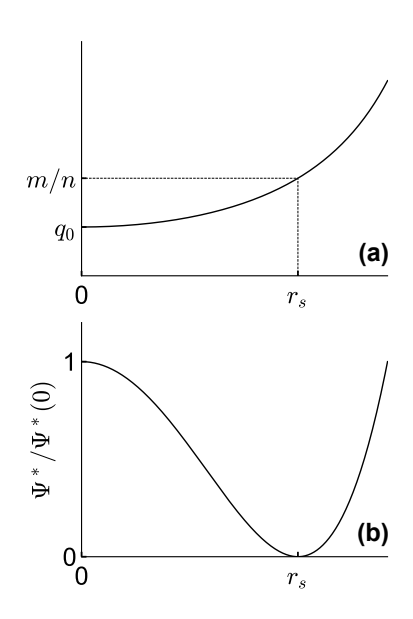


Figure 14.3: Example of monotonic safety factor with resonance m/n at position r_s (a) and corresponding helical flux defined by (14.1).

events. To this purpose, we need to i) understand the physical mechanisms which drive the formation of magnetic islands, and ii) identify the associated regions of stability.

In its simplest form, the instability which is responsible for the formation of magnetic islands is the so called **tearing mode**. Tearing modes are single helicity perturbations driven unstable by the **gradient** of the toroidal current density, i.e. these are **current driven** instabilities with evolution timescales of the order of several tens of milliseconds (longer than those of ideal modes which usually grow within few milliseconds or less). Linearly unstable tearing modes are referred to as **classical** or **spontaneous**, and this chapter is devoted to a thorough exposition of their linear stability properties.

Magnetic islands may also form in a linearly tearing stable configuration when a "seed" appears, whose growth in amplitude is sustained non-linearly by local pressure gradients. These are known in the literature as **neoclassical tearing modes** (NTMs).¹ Although of high experimental relevance, we will not address neither the physics of the seeding nor the non-linear evolution of NTMs.

Thus, this chapter is structured as follows: we first briefly discuss how the magnetic flux is modified by the presence of local small perturbations and how this rearrangement yields magnetic islands. Subsequently, the **tearing equation**, namely the equation that determines the global structure of the eigenfunction, is derived and solved analytically for a very idealised, though insightful, safety factor profile. Then, the growth rate is obtained by means of the asymptotic matching techniques discussed in the previous chapter. Finally, the stability of few more general q profiles, including non-monotonic ones, is examined mainly from a numerical point of view. The effects of the plasma pressure on the growth rate of unstable tearing modes are briefly discussed.

14.1 The reconnected flux

To gain more insight on the consequences of the violation of the flux conservation, and thus on the structure of the flux surfaces subject to small perturbations, we shall analyse a simple case of a large aspect ratio tokamak equilibrium with a monotonic safety factor (the details of whether or not a vacuum gap surrounds the plasma are not important).

We start by noting that in straight field line coordinates, the equilibrium magnetic field can be conveniently written as (cf. (4.4))

$$\boldsymbol{B} = \nabla \Phi(r) \times \nabla \vartheta - \nabla \psi(r) \times \nabla \phi,$$

where the toroidal flux Φ is given by (4.6). After selecting two integers m and n such that $q(r_s) = m/n$ at some position r_s , we introduce the **helical flux** Ψ^* defined as (see Fig. 14.3)

$$\Psi^* = \int_{r_r}^r \left(\psi' - \frac{n}{m} \Phi' \right) dr, \tag{14.1}$$

and the **helical coordinate** χ

$$\chi = \vartheta - \frac{n}{m}\phi.$$

Using these two quantities, the equilibrium field is recast as

$$\boldsymbol{B} = \nabla \Phi \times \nabla \chi - \nabla \Psi^* \times \nabla \phi \equiv \nabla \Phi \times \nabla \chi + \boldsymbol{B}^*.$$

This expression implicitly defines the **auxiliary field** B^* . One sees that $\Psi^* \sim (r - r_s)^2$ in a neighbourhood of the resonance, so that the poloidal component of B^* changes sign moving from the left to the right of r_s . It will be clear that it is this auxiliary field that undergoes reconnection. We now allow for a small flux perturbation of the form $\tilde{\psi}_m = \tilde{\psi}(r) \cos m\chi$ which is obviously associated with the appearance of a radial magnetic field. Following the results of the previous chapters, we expect the perturbation of the toroidal flux to be ε^2 times smaller than $\tilde{\psi}_m$, thence Φ is assumed to retain its equilibrium value. It then follows that the perturbed magnetic field is $\widetilde{\boldsymbol{B}} = -\nabla \widetilde{\psi}_m \times \nabla \phi$. It is easy to see that

$$(\boldsymbol{B} + \widetilde{\boldsymbol{B}}) \cdot \nabla(\boldsymbol{\Psi}^* + \widetilde{\boldsymbol{\psi}}_m) = 0,$$

indicating that the total flux $\Psi_{\text{tot}}^* = \Psi^* + \tilde{\psi}_m$ labels the **perturbed mag**netic surfaces.

By expanding Ψ^* about r_s and assuming that $\tilde{\psi}$ is almost constant around this narrow region, the flux surfaces for which $\Psi_{\mathrm{tot}}^* = \mathit{const}$ are parametrised by

$$r - r_s = \sqrt{2 \frac{\Psi_{\text{tot}}^* - \tilde{\psi} \cos m \chi}{d^2 \Psi^* / dr^2 |_{r_s}}}.$$

An example of the structure of the reconnected flux is shown in figure 14.4. Similar to the dynamics of particles in a magnetic field (cf. appendix A), the expression above provides a functional relation between r and the helical angle χ which gives the trajectory (or **orbit**) of the magnetic field lines. One sees that in the $r-\chi$ plane field lines have **open** and closed orbits, and the two domains are divided by a so called mag**netic separatrix**. Assuming that $d^2\Psi^*/dr^2|_{r_s}$ and $\tilde{\psi}$ are both negative, the value of the helical flux at the separatrix is $\Psi^*_{tot} = \tilde{\psi}$ and this can be used to estimate the maximum width w of the magnetic island yielding

$$r_{\rm sep}(\chi = \pi/m) - r_s = \frac{w}{2} = 2\sqrt{\frac{\tilde{\psi}}{d^2\Psi^*/dr^2|_{r_s}}}.$$

Notice that these results hold if the magnetic perturbation is sufficiently small, while more complex behaviours are observed in realistic geometries.

In ideal MHD such a rearrangement of the structure of the helical flux in the plasma2 does not occur because of the requirement of the finiteness of the radial fluid displacement at the resonance, which forces the radial magnetic perturbation to be **vanishing** at this point (cf. (7.7)).

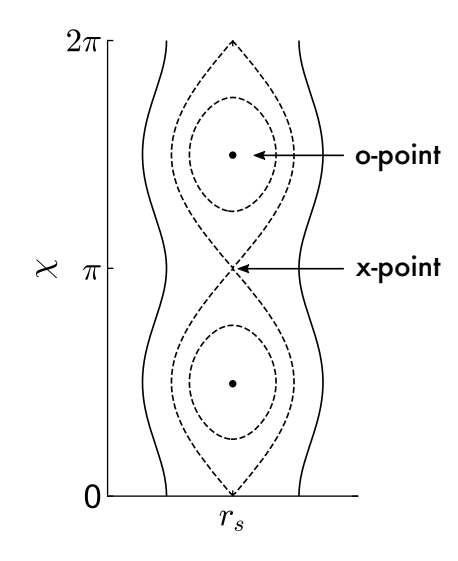


Figure 14.4: Contours of Ψ_{tot}^* about a resonance r_s where $q(r_s) = m/n$ after adding a helical perturbation with mode numbers m = 2 and n = 1 (here both $d^2\Psi^*/dr^2|_{r_s}$ and $\tilde{\psi}$ are negative). The o and x-points, denoting respectively the local extrema of the total flux and the locii of intersection of the magnetic separatrix, are indicated.

² When we discussed external kink modes in chapter 10, we allowed for a non-vanishing magnetic fluctuation in the vacuum (cf. (10.5)). This means that external kinks effectively produce magnetic islands in vacuum. Notice that the vacuum is sometimes modelled as a plasma with infinite resistivity.

14.2 The tearing equation

As discussed in $\S13.4$, the resistive stability analysis is based on the **asymptotic matching** of the solution obtained in the region far from r_s where plasma inertia and resistivity are negligible, with the one computed in proximity of the resonance, that is within the resistive layer. The asymptotic behaviour of the latter when moving away from r_s has been solved in the preceding chapter, so it remains to compute the solution in the ideal region.

Far from the resonance we can use the set of ideal MHD equations of chapter 7 specifically (7.7), which links the magnetic and fluid perturbations, and (7.65). The latter, after dropping contributions from mode coupling and inertia, and retaining only the higher order terms can be reduced to (7.69), i.e. the cylindrical approximation proves to be sufficient for the required accuracy. It follows that, to leading order, the equations governing the dynamics in the ideal region of the magnetic and fluid perturbation characterised by a single Fourier harmonic of helicity (m, n) are

$$\tilde{\psi}_m \equiv (\sqrt{g}\tilde{B}^r)_m = irB_0 k_{||} \xi_m^r, \tag{14.2}$$

$$\frac{d}{dr}\left(r^3k_{||}^2\frac{d\xi_m^r}{dr}\right) - rk_{||}^2(m^2 - 1)\xi_m^r = 0,\tag{14.3}$$

where $k_{||} = m\mu - n$ as usual. Finiteness of ξ_m^r has to be imposed at the magnetic axis, and appropriate boundary conditions must be applied at r = a, depending whether or not a vacuum region surrounds the plasma. As already noted earlier, the equation of ξ_m^r is singular where $k_{||} = 0$. For the sake of simplicity, we assume for the moment that there is only one position r_s for which $k_{||}(r_s) = 0$ (a generalisation to cases with multiple resonances will be discussed in §14.5).

Hence, equation (14.3) is solved separately for $r < r_s$ and $r > r_s$, and matching it with (13.44) and (13.45) eventually yields the growth rate. It will be shown that the linear stability of a tearing mode of helicity (m, n) is determined by the sign of the quantity³

$$r_s \Delta' \equiv \left[\frac{r}{\tilde{\psi}_m(r)} \frac{d\tilde{\psi}_m(r)}{dr} \right]_{r_s - \epsilon}^{r_s + \epsilon},$$
 (14.4)

where ϵ is an infinitesimally small positive quantity with the dimensions of a length. The quantity Δ' , not to be confused with the derivative of the Shafranov shift, is called the tearing stability index. It is important to stress again that in the tearing analysis the radial magnetic perturbation is allowed to be different from zero at the resonance.

Rather than solving (14.3), tearing stability is more often analysed in terms of its equivalent form written in terms of $\tilde{\psi}_m$ which is

$$\frac{d}{dr}\left(r\frac{d\tilde{\psi}_m}{dr}\right) - \frac{m^2}{r}\tilde{\psi}_m - \frac{mR_0}{k_{||}}\left(\frac{d}{dr}\langle\frac{J_0^{\phi}}{B_0^{\phi}}\rangle\right)\tilde{\psi}_m = 0, \tag{14.5}$$

Either analytic or numerical.

³ This is often referred to this as the **log-arithmic jump** of the magnetic fluctuation across the resonance.

where the last term is computed from (7.67) in the **cylindrical limit**. This is commonly called the **tearing equation**, and it can be derived directly from (7.13) by just considering its dominant terms:

$$\boldsymbol{B}_0 \cdot \boldsymbol{\nabla} \frac{\widetilde{J}^{\phi}}{B_0^{\phi}} + \widetilde{\boldsymbol{B}} \cdot \boldsymbol{\nabla} \frac{J_0^{\phi}}{B_0^{\phi}} = 0.$$

Equation (14.5) allows for a slightly more transparent identification of the behaviour of the perturbation near the resonant point. In a neighbourhood of r_s where $k_{||} \approx -nsx$ with $x = (r - r_s)/r_s$, we may approximate this equation as

$$\frac{d^2\tilde{\psi}_m}{dx^2} - \frac{\lambda}{x}\tilde{\psi}_m = 0, \quad \lambda = -\frac{mr_sR_0}{ns}\frac{d}{dr}\langle \frac{J_0^{\phi}}{B_0^{\phi}}\rangle. \tag{14.6}$$

Few integrations show that close to the resonance the behaviour of $\tilde{\psi}_m$ is

$$\frac{\tilde{\psi}_m(x)}{\tilde{\psi}_m(r_s)} = 1 + c_+ x + \lambda x \ln x, \qquad r > r_s,$$

$$= 1 + c_- x + \lambda x \ln |x|, \qquad r < r_s,$$
(14.7)

where c_{\pm} are some constants. We then find that $(1_{4}.4)$ can be expressed as

$$r_s\Delta'=c_+-c_-.$$

Notice that the logarithmic term in $\tilde{\psi}_m$, and thus the singular behaviour of $\tilde{\psi}'_m$, disappears when there are no current gradients at r_s .

The solution of (14.3), or equivalently (14.5), is generally computed numerically. However, exact analytic solutions can be found for some model safety factors. In the next section we present a detailed analysis of (14.3) for the simple case of a step current profile, which is similar to the one employed in the analysis of external kink modes of chapter 10. Although very crude, the analysis performed with this model safety factor is able to capture many important features of the tearing dynamics in tokamaks.

Eigenfunction and growth rate for the step 14.3 current model

Let us consider a toroidal plasma separated by a vacuum region from an ideally conducting wall located at b > a. We say that the wall is at infinity when $a/b \ll 1$. Assume now a safety factor profile of the form

$$q = \begin{cases} q_0, & r < r_0, \\ q_0 \left(\frac{r}{r_0}\right)^2, & r > r_0, \end{cases}$$
 (14.8)

with $q_0 < m/n$. Note that q extends parabolically into the vacuum region (see §4.4). This corresponds to a stepped current of the form given ⁴ A method for analysing the stability of tearing modes based on the WKB approximation has been presented in Hegna and Callen (1993).

⁵ Recall that if the metallic wall is directly interfaced with the plasma, the boundary condition at the edge becomes $\xi_m^r(a) = 0$.

⁶ The trick to simplify the calculation is to write the eigenfunction in the outer region in the form

$$\xi_m^r \sim \frac{1}{k_{||}} \left[\left(\frac{r}{r_s} \right)^{m-1} + A_{\pm} \left(\frac{r}{r_s} \right)^{-m-1} \right],$$

where \pm stands for $r \ge r_s$.

by (10.15); we recall that $r_0 \le a$ measures the radial extension of the current, i.e the current channel. The reason for using such an idealised profile is that, although other exact analytic solutions can be found with smooth profiles, this choice of q allows for straightforward algebraic manipulations yet yielding meaningful results.⁴

With this safety factor profile, the two independent solutions of (14.3) are readily found so that

$$\xi_m^r(r) = \frac{1}{k_{||}} \left(c_1 \left(\frac{r}{r_0} \right)^{m-1} + c_2 \left(\frac{r}{r_0} \right)^{-m-1} \right), \tag{14.9}$$

where c_1 and c_2 are some numbers. Notice that $k_{||}$ is constant for $r < r_0$. A double integration of $(1_4.3)$ across r_0 shows that $\xi_m^r(r)$ is continuous and smooth at this position. We require $\xi_m^r(r)$ to be finite at the magnetic axis, whereas the interface conditions at the plasma-vacuum boundary are those given by $(10.12).^5$ The position of the resonant surface associated with the mode (m, n) is

$$r_s = r_0 \sqrt{\frac{m}{nq_0}},\tag{14.10}$$

and is always assumed to occur within the plasma. Therefore, by means of (14.9), we readily obtain the following system

$$\xi_{m}^{r}(r) \propto \begin{cases} \left(\frac{r}{r_{0}}\right)^{m-1}, & 0 < r < r_{0}, \\ \frac{1}{k_{||}} \left[\left(\frac{r}{r_{0}}\right)^{m-1} + \frac{1}{m-1-nq_{0}} \left(\frac{r}{r_{0}}\right)^{-m-1}\right], & r_{0} < r < r_{s}, \quad (14.11) \\ \frac{1}{k_{||}} \left[\left(\frac{r}{a}\right)^{m-1} - \left(\frac{b}{a}\right)^{2m} \left(\frac{r}{a}\right)^{-m-1}\right], & r_{s} < r < a. \end{cases}$$

The constants which multiply the first and second expressions must be chosen in order to ensure that ξ_m^r is continuous at r_0 . We shall call (14.11) the **outer region solution** or **outer solution**.

In a neighbourhood of the resonance, it is rather immediate to show that the eigenfunction behaves as^6

$$\xi_{m}^{r} = -\frac{\hat{c}_{1}}{x} \left(1 + \frac{m + \frac{1}{2} - (m - \frac{1}{2})A_{-}}{1 + A_{-}} x \right), \quad r < r_{s},$$

$$= \frac{\hat{c}_{2}}{x} \left(1 + \frac{m + \frac{1}{2} - (m - \frac{1}{2})A_{+}}{1 + A_{+}} x \right), \quad r > r_{s},$$
(14.12)

where \hat{c}_1 and \hat{c}_2 are some other constants, and

$$A_{-} = \frac{(r_0/r_s)^{2m}}{m - 1 - nq_0}, \quad A_{+} = -(b/r_s)^{2m}. \tag{14.13}$$

The solution we just obtained has now to be matched smoothly with the one computed in the resistive layer. We start by noting that because of our choice of the safety factor the quantity λ introduced in equation (14.6) in the previous section is vanishing, so that the outer region solution does not exhibit any logarithmic behaviour near r_s . Therefore, in (13.44) we take $\hat{C} \rightarrow \infty$.

Let us call

$$\Delta_{\pm} = \frac{m + \frac{1}{2} - (m - \frac{1}{2})A_{\pm}}{1 + A_{\pm}}.$$
 (14.14)

Equation (14.4) written in terms of these quantities becomes

$$r_{\rm s}\Delta'=\Delta_{\perp}-\Delta_{-}$$

Since Δ_{-} diverges when m = 1 (for any n), here we restrict the analysis to modes with m > 1 (the m = 1 tearing mode will be studied in detail in the next chapter). Hence, on the left and right of the resonance we write

$$c_{e} - \frac{c_{o}}{|x|} \left(1 + \frac{m\pi\Delta_{R}}{2} S^{1/3} |x| \right) = \frac{\hat{c}_{1}}{|x|} \left(1 - \Delta_{-} |x| \right), \quad r < r_{s}, \tag{14.15}$$

$$c_e + \frac{c_o}{|x|} \left(1 + \frac{m\pi\Delta_R}{2} S^{1/3} |x| \right) = \frac{\hat{c}_2}{|x|} (1 + \Delta_+ |x|), \quad r > r_s,$$
 (14.16)

where c_e and c_o are two constants which multiply (13.44) and (13.45) respectively. The relations above guarantee smooth matching on the left and on the right of the resonance between the outer solution and the resistive layer one, the latter written asymptotically as a linear combination (13.44) and (13.45). Summing and subtracting (14.15) and (14.16) produces:

$$2c_e = \frac{\hat{c}_1 + \hat{c}_2}{|x|} + \hat{c}_2 \Delta_+ - \hat{c}_1 \Delta_-,$$

$$2\frac{c_o}{|x|} \left(1 + \frac{m\pi \Delta_R}{2} S^{1/3} |x| \right) = \frac{\hat{c}_2 - \hat{c}_1}{|x|} + \hat{c}_2 \Delta_+ + \hat{c}_1 \Delta_-.$$

It follows that balancing the powers of |x| requires

$$\hat{c}_1 + \hat{c}_2 = 0, \quad 2c_o = \hat{c}_2 - \hat{c}_1,$$

$$2c_e = \hat{c}_2 \Delta_+ - \hat{c}_1 \Delta_-, \quad c_o m \pi \Delta_R S^{1/3} = \hat{c}_2 \Delta_+ + \hat{c}_1 \Delta_-.$$
(14.17)

By means of equation (13.42), the **dispersion relation** is written as

$$\frac{(\gamma/\omega_A)^{5/4}}{1 - M_t} \frac{\Gamma\left(\frac{M_t + 3}{4}\right)}{\Gamma\left(\frac{M_t + 5}{4}\right)} = \frac{2}{\pi} \frac{r_s \Delta'}{S^{3/4}} \sqrt{\frac{ms/q_s}{(1 + 2q_s^2)^{1/2}}}$$
(14.18)

where M_t is given by (13.38) and explicitly reads

$$M_t = \left(\frac{\gamma}{\omega_A}\right)^{3/2} \frac{q_s S^{1/2}}{s \, m} \sqrt{1 + 2q_s^2}. \tag{14.19}$$

We anticipate that the dispersion relation for other resistive instabilities retains the same structure, with the ideal limit obtained by setting ⁷ For more generic q profiles, logarithmic terms of the form of the ones discussed in §14.2 appear. These are automatically matched with the inner layer solution by a suitable choice of \hat{C} .

Recall that $q_s = m/n$.

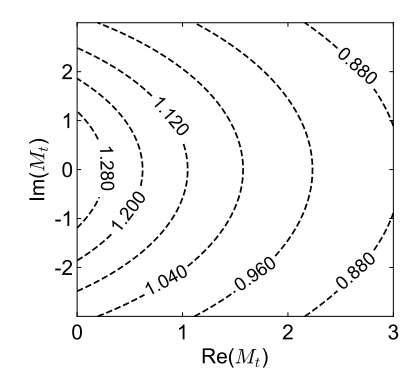


Figure 14.5: Contour levels of $|\Gamma\left(\frac{M_t+1}{4}\right)/\Gamma\left(\frac{M_t+5}{4}\right)|$ as a function of the real and imaginary parts of M_t . Note we restricted the plot to the $Re(M_t) > 0$ half-plane.

⁸ The solution of $x^{5/4} = 1$ is x = 1, whereas $x^{5/4} = -1$ is solved by $x \approx -0.81 \pm 0.59i$. These results can be obtained via a graphical analysis through Nyquist techniques (see chapter 17).

 $M_t \to \infty$. For tearing modes, (14.18) can be simplified further; let's see how. We saw in §14.1 that magnetic islands can be induced by allowing for a small and slowly varying (spatially) magnetic perturbation in proximity of the resonance r_s . Upon comparing (14.2) with (14.12), we choose to focus on cases for which Δ_\pm are not too large, which in turn implies that $r_s\Delta'$ is not big either. Then, the right-hand-side of (14.18) is small since, typically, $S \gg 1$.

We further notice that the absolute value of $\Gamma\left(\frac{M_t+1}{4}\right)/\Gamma\left(\frac{M_t+5}{4}\right)$ does not exhibit strong variations when M_t , as a complex quantity, varies within quite a broad range (see Fig. 14.5). Hence, by balancing the left and right-hand-side of (14.18) we expect M_t and thus γ/ω_A to be small. Therefore, by taking the $M_t \ll 1$ limit, the dispersion relation (14.18) can be reduced to

$$\left(\frac{\gamma}{\omega_A}\right)^{5/4} = \frac{2}{\pi} \frac{\Gamma\left(\frac{5}{4}\right)}{\Gamma\left(\frac{3}{4}\right)} \frac{r_s \Delta'}{S^{3/4}} \sqrt{\frac{ms/q_s}{(1+2q_s^2)^{1/2}}}.$$
 (14.20)

For such a case instability occurs when⁸

$$\Delta' > 0. \tag{14.21}$$

This is known as the **tearing instability criterion**. For $r_s\Delta' \sim 1$, the growth rate of tearing perturbations scales as $S^{-3/5}$, hence, with Lundquist numbers of the order of $10^8 - 10^9$, we see that these instabilities are associated with timescales of the order of **several tens of milliseconds**, thus they exhibit a much slower growth compared to ideal modes.

Having established the conditions for the appearence of a tearing instability through Eq. (14.21), we shall now investigate more in detail the structure of Δ' associated with the model q given by (14.8). Although the analysis is based on a highly idealised profile, several important physical conclusions can be drawn from this simple model.

By means of (14.13) and (14.14), one has

$$r_s \Delta' = -2m \frac{A_+ - A_-}{(1 + A_+)(1 + A_-)}$$

$$= -2m \frac{m - 1 - nq_0 + (r_0/b)^{2m}}{[1 - (r_s/b)^{2m}][m - 1 - nq_0 + (r_0/r_s)^{2m}]}$$

$$= -2m \left(\frac{1}{1 - (r_s/b)^{2m}} - \frac{(r_0/r_s)^{2m}}{m - 1 - nq_0 + (r_0/r_s)^{2m}} \right). \tag{14.22}$$

From this expression we observe that:

i) For m sufficiently large at fixed q_0 , one finds $\Delta' = -2m/r_s$ with $-\Delta_+ \approx \Delta_- \approx m$. Hence, in a typical tokamak plasma with $q_0 \sim 1$ and q(a) around 3 or 4, **high-m tearing modes are expected to be stable**. One arrives to the same result for m finite by letting $b \to \infty$ (no wall) and $r_0/r_s \to 0$ (large gap between resonance and current channel).

9 Note that $nq_0 = m(r_0/r_s)^2$.

- ii) The denominators on the second line of (14.22) is always positive, so that the sign of Δ' is determined by $m-1-nq_0+(r_0/b)^{2m}$, more specifically $\Delta'>0$ if $(r_0/a)^{2m}=[q_0/q(a)]^m<(1-m+nq_0)(b/a)^{2m}$.
- iii) In the limit $b/a \to \infty$, a mode with poloidal mode number m is unstable when $\sqrt{(m-1)/m} < r_0/r_s$. Since $m-1-nq_0+(r_0/r_s)^{2m}=m[1-(r_0/r_s)^2]-1+(r_0/r_s)^{2m}$, we find that Δ' diverges when $r_s\to r_0$, that is the closer the resonance to the current gradient the more unstable the system.
- iv) If b = a, another singularity in Δ' is found when $r_s \to a$ but in this case $\Delta' \to -\infty$ showing the strong stabilising effect of an ideal wall when the resonance approaches a.

An example of the regions of positive Δ' in the $q_0 - [q_0/q(a)]$ plane are shown in figure 14.6.

Point iii) highlights the fact that for $m \sim 1$ the stability of tearing modes is dictated by the **global gradient** of the current density, not necessarily by the gradient at the resonance position. Large m modes instead are well localised about r_s , hence their stability properties are determined by the local current gradient near the resonance.

We finally point out that the values of Δ_{\pm} dictate the structure of the eigenfunction in the resistive layer. This, indeed, can be inferred by evaluating the relative strength of the even and odd solutions from (14.17) yielding

$$\frac{c_e}{c_o} = \frac{\Delta_+ + \Delta_-}{2}.\tag{14.23}$$

It is clear that the **odd** part of the radial fluid displacement dominates when $\Delta_+ \approx -\Delta_-$. Typically, the tearing mode eigenfunction in the resistive layer (i.e. in real space) has a shape similar to that shown in figure 13.1. When this happens, we say that the eigenfunction has a **tearing character**.

14.4 The numerical solution of the tearing equation for generic profiles

Since tearing stability is entirely determined by Δ' , the analysis boils down to the computation of the shape of ξ_m^r or $\tilde{\psi}_m$ in the ideal region (cf. (14.3) and (14.5)).

So far we dealt with a highly idealised current density profile which allowed analytically tractable algebraic manipulations. Although many important physical effects can be deduced from such a simplified analysis, this is not suited for describing realistic situations characterised by safety factor profiles with more generic shapes. Unfortunately, even in the simplest case of a low- β large aspect ratio tokamak of circular cross section for which the fluid/magnetic perturbation is described by (14.3)

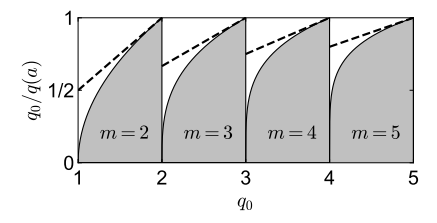


Figure 14.6: The shaded areas show the regions of positive tearing stability index for several poloidal harmonics with n=1 and b=a. We indicate which poloidal harmonic is unstable in the corresponding region. The m/n resonance of the corresponding modes lies in the vacuum for values of $q_0/q(a)$ above the dashed lines.

 $^{^{10}}$ One can still employ the cylindrical limit at low β with weak shaping, meaning that mode coupling effects can be dropped altogether.

 $^{11}~\lambda$ defined in (14.6) is finite at the axis. In particular

$$\frac{mR_0}{k_{||}} \langle \frac{J_0^{\phi}}{B_0^{\phi}} \rangle' = \frac{m}{m\mu - n} \left[\frac{1}{r} \left(\frac{r^2}{q} \right)' \right]'.$$

This quantity only depends on mode numbers and the safety factor profile.

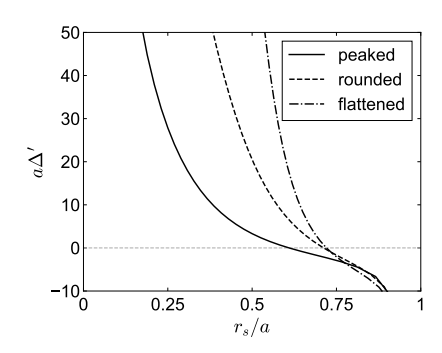


Figure 14.7: Values of Δ' for the m=2, n=1 mode for the peaked, rounded and flattened model computed with $x_b=2$ assuming an ideal wall directly interfaced with the plasma. Note that $a\Delta' \rightarrow -\infty$ as the ideal wall is approached.

and (14.5), it is not typically possible to write an exact analytic solution with a generic q, so that a numerical procedure is usually sought.

Numerical schemes typically focus on the solution of (14.5) since $\tilde{\psi}_m$, contrarily to ξ_m^r , does not diverge at the resonance, although its derivative may present a logarithmic singularity as discussed in §14.2. Given the shape of the current density, i.e. the safety factor, this equation is solved separately on the left and on the right of the resonance constraining $\tilde{\psi}_m$ to be continuous at r_s . The behaviour in proximity of the magnetic axis is of the form $\tilde{\psi}_m \propto r^m$ as easily seen from (14.5), whereas at the plasma edge the boundary conditions depend on the presence (or absence) of a vacuum region separating the plasma from the surrounding metallic structures: if an ideally conducting metallic wall is directly interfaced with the plasma we require $\tilde{\psi}_m(a) = 0$, while with the wall at distance b > a from the plasma one imposes (cf. (10.12))

$$\frac{rd\tilde{\psi}_m/dr}{\tilde{\psi}_m}\bigg|_a = \bigg[\frac{1}{k_{||}}\frac{d(rk_{||})}{dr}\bigg]_{a-\epsilon} + \frac{2m}{m-nq(a)} - \frac{m+1+(m-1)\left(\frac{a}{b}\right)^{2m}}{1-\left(\frac{a}{b}\right)^{2m}},\tag{14.24}$$

where we used the fact that $q \propto r^2$ in the vacuum region (see §4.4).

When the boundary conditions allow to have an explicit expression for $\tilde{\psi}_m$ and $d\tilde{\psi}_m/dr$ at one of the two endpoints of the interval where (14.5) is solved, one can set a **Cauchy initial value problem**, otherwise a scheme based on the **shooting method** is employed. Once $\tilde{\psi}_m$ is obtained for $r < r_s$ and $r > r_s$, the computation of Δ' is typically accomplished by fitting $d\tilde{\psi}_m/dr$ in a neighbourhood of r_s with a function of the form $c_1 + c_2 \ln x$ with c_1 and c_2 two parameters.

We shall now report few numerical results on tokamak tearing stability based on two widely used safety factor parametrisations. One has been discussed by Furth et al. (1973) and reads

$$q = q_0 \left[1 + \left(x_b \frac{r}{a} \right)^{a_F} \right]^{b_F}. \tag{14.25}$$

With this shape of q at fixed x_b , the flattening or peaking of the associated current density profile is controlled by the parameters a_F and b_F . In the work by Furth et al. (1973), three different cases labelled *peaked*, *rounded* and *flattened* models have been analysed corresponding, respectively, to the following values of a_F and b_F :

	a_F	b_F
peaked	2	1
rounded	4	1/2
flattened	8	1/4

The values of the tearing stability index of the m = 2, n = 1 mode for the three models listed in the table above are shown in figure 14.7, where

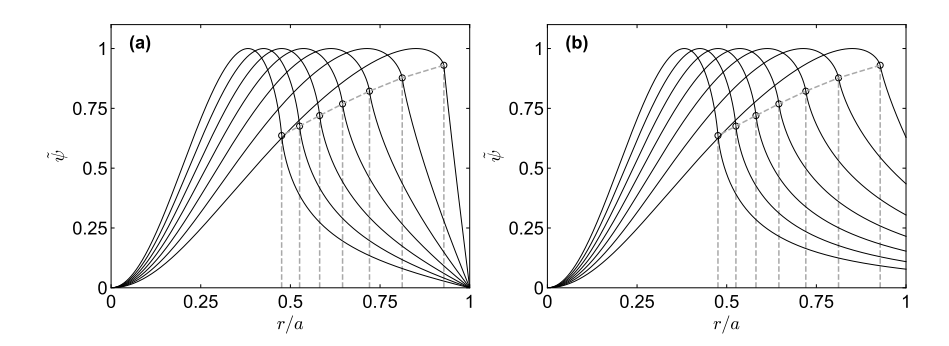


Figure 14.8: Shape of the m=2, n=1 tearing mode eigenfunction for the peaked model for different radial locations of the resonant surfaces with (a) a wall directly interfaced with the plasma, and (b) in the no wall limit. Here $x_b=2$. Notice the divergence of the derivative of $\tilde{\psi}_m$ as the resonance is approached.

the position of the resonance has been modified by varying the value of q_0 . The associated eigenfunction computed for the peaked model with and without $(a/b \rightarrow 0)$ a wall directly interfaced with the plasma is shown in Fig. 14.8 for different locations of the resonance. In the notation of Furth et al. (1973) one has the following identifications

$$(r_0\Delta')_{\text{Furth}} \to \frac{1}{x_b}(a\Delta'), \quad (x_s)_{\text{Furth}} \to x_b r_s/a.$$

In line with the result obtained for the stepped model of \$14.3, the numerical computation also finds that large m instabilities have a negative tearing stability index:

$$\Delta' \approx -\frac{2m}{r_{\rm s}},\tag{14.26}$$

We shall now analyse tearing stability with another parametrisation of the safety factor (Yu (1996)):

$$q = q_0 \frac{r^2}{\int_0^r 2r[1 - (r/a)^2]^{g_1}[1 + \alpha_D(r/a)^2]^{g_2} dr}.$$
 (14.27)

Notice that this parametrisation is also capable of dealing with non-monotonic shapes of the current profile, and it will be employed in the next section when discussing the stability of tearing modes with multiple resonant surfaces associated with same q value. The simple case with $g_1=1$ and $g_2=\alpha_D=0$ yields a parabolic current density profile $J^\phi=J_0(1-r^2/a^2)$, and the resulting stability has been analysed by Wesson (2011) (see figure 14.9).

Summarising, the study of tearing stability in tokamaks can be reduced, in its simplest form, to the analysis of the solution of a single differential equation, namely Eq. (14.5). The inclusion of additional effects such as plasma shaping, finite β and mode coupling is a much more complicated task which requires more advanced/refined techniques which we do not discuss.

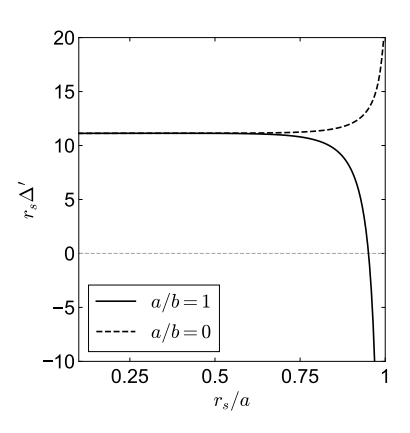


Figure 14.9: Tearing stability index for the m=2, n=1 mode with and without an ideal wall surrounding directly the plasma computed using the q profile given in (14.27) with $g_1=1$ and $g_2=\alpha_D=0$. Note that differently from Fig. 14.7, here the quantity $r_s\Delta'$ is plotted

On the β dependence of the inertia enhancement

Let us consider a mode of helicity (m,n) for which $\Delta'>0$. We further assume that β effects are weak enough not to affect $\tilde{\psi}_m$, so that we regard Δ' to be β independent. By means of Eq. (13.25), the inertia enhancement factor reads

$$\left(\frac{\gamma^2}{\omega_A^2} \to \frac{\gamma^2}{\omega_A^2} \left(1 + \frac{2q_s^2}{1 + q_s^2 \frac{\gamma^2/\omega_A^2}{\Gamma_{bo}/B_s^2}}\right) \equiv \frac{\gamma^2}{\omega_A^2} I_{\gamma},$$

where the equilibrium quantities are evaluated at the resonant surface of the (m, n) mode. For $r_s\Delta'$ not too large, plugging this result into (14.20) shows that the growth rate of the tearing mode scales as

$$\frac{\gamma}{\omega_A} \propto \frac{(r_s \Delta')^{4/5}}{S^{3/5}} I_{\gamma}^{-1/5}.$$

Since $\Delta'>0$ by hypothesis, the growth rate at zero β is finite with $I_{\gamma}\to 1$. When finite pressure effects are taken into account, in the limit $\beta\gg\gamma^2/\omega_A^2$ one gets $I_{\gamma}\to 1+2q_s^2$.

Thus, upon defining $\hat{\beta} = \Gamma p_0/B_0^2$, it is straightforward to obtain the limiting cases

$$rac{\gamma}{\omega_A} \propto rac{(r_s \Delta')^{4/5}}{S^{3/5}} \Big(1 - rac{2}{5} rac{\hat{eta} S^{6/5}}{C_0^2 (r_s \Delta')^{8/5}} \Big), \quad rac{\hat{eta}}{\gamma^2 / \omega_A^2} \ll 1,$$
 $\propto rac{(r_s \Delta')^{4/5}}{S^{3/5}} (1 + 2q_s^2)^{-1/5}, \qquad \qquad rac{\hat{eta}}{\gamma^2 / \omega_A^2} \gg 1,$

where in writing the first line we exploited the fact that $\gamma/\omega_A \sim (r_s\Delta')^{4/5}/S^{3/5}$.

14.5 Double tearing modes

It is not unusual in tokamaks to have non-monotonic current profiles associated with hollow safety factors. ¹² In these situations, multiple radii with identical q values may appear so that a magnetic perturbation with helicity (m, n) can *resonate* at different radial positions inducing magnetic islands to form at these points. Cases with three or more radii associated with the same value of q are much more unlikely, therefore we focus our attention on hollow safety factors with a shape similar to that shown in Fig. 4.7. Resistive perturbations with a tearing character featuring two resonant locations are called **double tearing modes**.

For fixed m and n, let us denote with r_1 and r_2 the radial locations of the two resonances where q = m/n with $r_1 < r_2$. For the sake of simplicity, we assume the **plasma to be directly interfaced with an ideal wall**. Although an analytical treatment can be deployed, we shall

¹² This may happen, e.g., during the current ramp-up in the early stage of the plasma discharge. Particle impurities accumulating in the core can also produce hollow current profiles.

approach the problem of double tearing stability in a manner which is more easily implemented in numerical schemes. We start by writing the solution of equation (14.5) as a combination of two basis functions ψ_1 and ψ_2 , the former defined in the interval $0 < r < r_2$ and the latter in $r_1 < r < a$, such that $\psi_1(r_2) = \psi_2(r_1) = 0$. The shape of these two basis functions is shown in figure 14.10. The ideal wall boundary condition at the plasma edge dictates $\tilde{\psi}_m(a) = 0$. Normalising $\tilde{\psi}_m(r_1) = 1$, the eigenfunction of equation (14.5) is then expressed as

$$\begin{split} \tilde{\psi}_m &= \frac{\psi_1}{\psi_1(r_1)}, & 0 < r < r_1, \\ &= \frac{\psi_1 + \sigma \psi_2}{\psi_1(r_1)}, & r_1 < r < r_2, \\ &= \sigma \frac{\psi_2}{\psi_1(r_1)}, & r_2 < r < a, \end{split}$$

where σ is a numerical coefficient and continuity of the magnetic fluctuation at both resonances has been imposed.

Now, analogously to (14.4), we define the logarithmic jumps of $\tilde{\psi}_m$ at r_1 and r_2 , that is

$$\Delta_{1}' = \frac{\psi_{1}' + \sigma \psi_{2}'}{\psi_{1}(r_{1})} \Big|_{r_{1} + \epsilon} - \frac{\psi_{1}'}{\psi_{1}(r_{1})} \Big|_{r_{1} - \epsilon},$$

$$\Delta_{2}' = \frac{\psi_{2}'}{\psi_{2}(r_{2})} \Big|_{r_{2} + \epsilon} - \frac{\psi_{1}' + \sigma \psi_{2}'}{\sigma \psi_{2}(r_{2})} \Big|_{r_{2} - \epsilon}.$$

Matching with the solutions in the two resistive layers around r_1 and r_2 , as we did for equation (14.18) in §14.3, ¹³ formally gives

$$\Delta_{R,1}^*(\gamma) \equiv m\pi \Delta_{R,1} S_1^{1/3} = r_1 \Delta_1',
\Delta_{R,2}^*(\gamma) \equiv m\pi \Delta_{R,2} S_2^{1/3} = r_2 \Delta_2',$$
(14.28)

where $\Delta_{R,i}$ is computed according to (13.42) with the subscript 1(2) indicating that the associated quantity must be evaluated at $r_1(r_2)$. The radial dependence of the Lundquist number is because $S \sim 1/\eta \sim T^{3/2}$.

It now remains to determine σ and thus the growth rate γ . Upon defining

$$\begin{split} \Delta'_{11} &= \frac{\psi'_{1}}{\psi_{1}(r_{1})}\Big|_{r_{1}+\epsilon} - \frac{\psi'_{1}}{\psi_{1}(r_{1})}\Big|_{r_{1}-\epsilon}, \\ \Delta'_{22} &= \frac{\psi'_{2}}{\psi_{2}(r_{2})}\Big|_{r_{2}+\epsilon} - \frac{\psi'_{2}}{\psi_{2}(r_{2})}\Big|_{r_{2}-\epsilon}, \\ \Delta'_{12} &= \frac{\psi'_{2}}{\psi_{2}(r_{2})}\Big|_{r_{1}+\epsilon}, \\ \Delta'_{21} &= -\frac{\psi'_{1}}{\psi_{1}(r_{1})}\Big|_{r_{2}-\epsilon}, \end{split} \tag{14.29}$$

where ϵ has the same meaning as in (14.4), the matching conditions (14.28) can be written as

$$\Delta_{R,1}^{*}(\gamma) - r_{1}\Delta_{11}' = \sigma r_{1}\Delta_{12}' \frac{\psi_{2}(r_{2})}{\psi_{1}(r_{1})},$$

$$\Delta_{R,2}^{*}(\gamma) - r_{2}\Delta_{22}' = \frac{1}{\sigma} r_{2}\Delta_{21}' \frac{\psi_{1}(r_{1})}{\psi_{2}(r_{2})}.$$

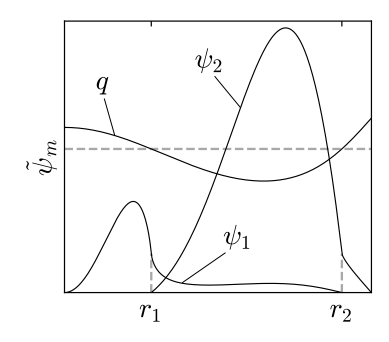


Figure 14.10: Example of the basis functions ψ_1 and ψ_2 , and the associated hollow safety factor.

¹³ The same matching procedure outlined earlier, i.e. (14.17), remains valid. It is important to keep in mind that we will have different expressions for the coefficients Δ_{\pm} depending on whether these are evaluated at r_1 or r_2 .

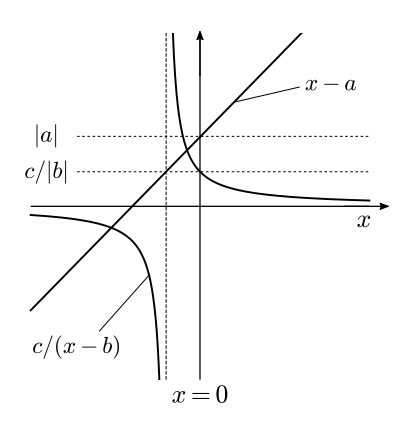


Figure 14.11: Graphical representation of the dispersion relation (14.32) for a < 0 and b < 0. All the other cases are found by either translating horizontally the hyperbola, or moving vertically the x - a line.

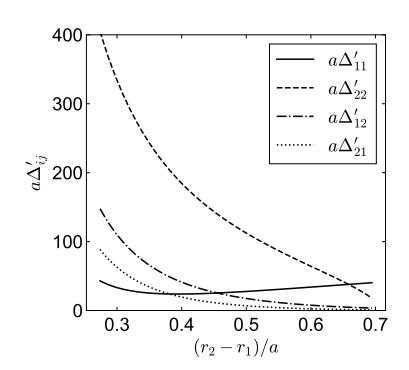


Figure 14.12: Numerical values of $a\Delta'_{ij}$ for the m=2, n=1 mode as a function of the relative distance of the two resonances r_1 and r_2 , with a safety factor of the form (14.27) with $q_0=2.3$, and $g_1=g_2=3$. The parameter α_D has been varied within the range 1.75-2.5 (Yu (1996)). An ideally conducting wall is at position r=a. Relation (14.31) has been verified to hold.

Multiplying these two together yields the following dispersion relation

$$\left(\Delta_{R,1}^*(\gamma) - r_1 \Delta_{11}'\right) \left(\Delta_{R,2}^*(\gamma) - r_2 \Delta_{22}'\right) = r_1 r_2 \Delta_{12}' \Delta_{21}'. \tag{14.30}$$

We now notice that both ψ_1 and ψ_2 satisfy equation (14.5), from which we immediately obtain

$$\begin{split} \frac{d}{dr} \bigg(r \psi_2 \frac{d\psi_1}{dr} \bigg) - r \frac{d\psi_1}{dr} \frac{d\psi_2}{dr} - \bigg[\frac{m^2}{r} + \frac{mR_0}{k_{||}} \bigg(\frac{d}{dr} \langle \frac{J_0^{\phi}}{B_0^{\phi}} \rangle \bigg) \bigg] \psi_1 \psi_2 &= 0, \\ \frac{d}{dr} \bigg(r \psi_1 \frac{d\psi_2}{dr} \bigg) - r \frac{d\psi_1}{dr} \frac{d\psi_2}{dr} - \bigg[\frac{m^2}{r} + \frac{mR_0}{k_{||}} \bigg(\frac{d}{dr} \langle \frac{J_0^{\phi}}{B_0^{\phi}} \rangle \bigg) \bigg] \psi_1 \psi_2 &= 0. \end{split}$$

By equating these expressions and integrating from r_1 to r_2 one then finds that

$$r_1 \frac{\psi_2'(r_1 + \epsilon)}{\psi_2(r_2)} = -r_2 \frac{\psi_1'(r_2 - \epsilon)}{\psi_1(r_1)}.$$
 (14.31)

This relation implies that $\Delta'_{12}\Delta'_{21} \geq 0$ so that the right-hand-side of (14.30) is positive or zero. By means of this result, several conclusions can be now drawn from (14.30) by visualising it graphically. For simplicity we only consider the limit of **small growth rate** for which, similarly to (14.20), one can approximate $\Delta^*_{R,i} = K_i(\gamma/\omega_A)^{5/4}$ with K_i a positive coefficient.

Let us write equation (14.30) in the following form:

$$x - a = \frac{c}{x - b}.\tag{14.32}$$

where $x = (\gamma/\omega_A)^{5/4}$, $a \propto r_2\Delta'_{11}$ $b \propto r_2\Delta'_{22}$ and c > 0 a constant. The left-hand-side of this equation describes a straight line with positive slope, while the right-hand-side traces a hyperbola. A real solution for γ exists any time the straight line crosses the hyperbola in the x > 0 half-plane.

One then finds that the system in unstable whenever

$$\Delta'_{11} > 0$$
, and $\Delta'_{22} > 0$,

or

$$\Delta'_{11}\Delta'_{22} < 0.$$

Conversely, when Δ'_{11} and Δ'_{22} are both negative, instability only occurs when $\Delta'_{11}\Delta'_{22} < \Delta'_{12}\Delta'_{21}$. This is intuitively depicted in Fig. 14.11. Therefore, the stability analysis of double tearing modes reduces to the computation of the Δ'_{ij} coefficients, and thence checking their sign and relative amplitude. Figure 14.12 gives an example of the values of $a\Delta'_{ij}$ obtained numerically from the solution of (14.5) with a safety factor of the form (14.27). An alternative **graphical approach** which can be employed for determining the stability of the double tearing mode is based on Nyquist techniques (these will be used in chapter 17).

One notices from Fig. 14.12 that Δ_{ij} increases as the distance between the resonances is reduced. When Δ_{ij} becomes sufficiently large,

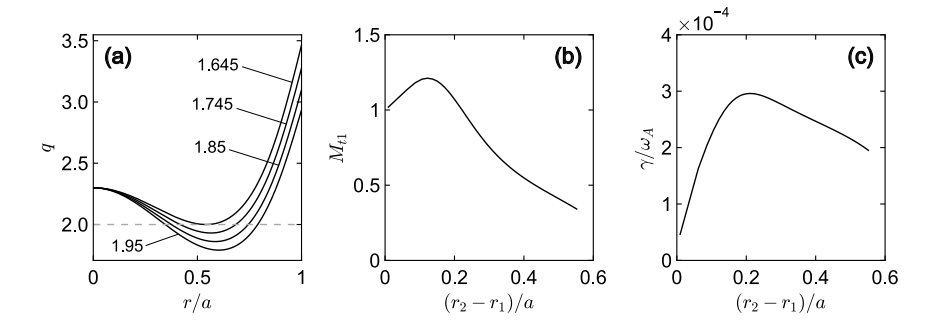


Figure 14.13: Safety factor profiles (a) used for the computation of M_{t1} (b) and growth rate (c) from equation (14.33). For the calculation we employed the same parameters of Fig. 14.12 having set $S_1 = S_2 = 10^8$ with the plasma directly interfaced with an ideal wall. The distance between the two resonances is controlled by varying α_D from 1.645 to 2.14 (this is indicated in (a)). In (c) only the largest growth rate (largest positive root) is shown.

we cannot approximate $\Delta_{R,i}^* \propto (\gamma/\omega_A)^{5/4}$ anymore, and the full resistive response at the two layers expressed by (14.18) should be used. This leads to the following dispersion relation (cf. (14.30))

$$\left(\frac{M_{t1}}{1 - M_{t1}} \frac{\Gamma((M_{t1} + 3)/4)}{\Gamma((M_{t1} + 5)/4)} - \frac{r_1 \Delta'_{11}}{C_1}\right) \times \left(\frac{M_{t2}}{1 - M_{t2}} \frac{\Gamma((M_{t2} + 3)/4)}{\Gamma((M_{t2} + 5)/4)} - \frac{r_1 \Delta'_{22}}{C_2}\right) = r_1 r_2 \frac{\Delta'_{12} \Delta'_{21}}{C_1 C_2},$$
(14.33)

where by means of (13.36) and (13.38) we defined (assume for the sake of simplicity a constant mass density profile)

$$C_{1} = \frac{\pi}{2} \left(\frac{n|s_{1}|S_{1}}{\sqrt{1 + 2(m/n)^{2}}} \right)^{1/3}, \qquad C_{2} = C_{1} \left(\frac{|s_{2}|S_{2}}{|s_{1}|S_{1}} \right)^{1/3},$$

$$M_{t1} = \left(\frac{\gamma}{\omega_{A}} \right)^{3/2} \frac{\sqrt{1 + 2(m/n)^{2}}}{n|s_{1}|} S_{1}^{1/2}, \qquad M_{t2} = M_{t1} \frac{|s_{1}|}{|s_{2}|} \sqrt{\frac{S_{2}}{S_{1}}}.$$

Equation (14.33) can be solved for M_{t1} from which the value of γ is extracted.

As shown in figure 14.13-(b), M_{t1} becomes of order of unity when the separation between the two resonances is very small. In such a case one finds that $\gamma \sim |s_1|^{2/3} S_1^{1/3}$. Since $|s_1|$ approaches zero as the resonant points get closer, it follows that the growth rate is negligibly small when $r_1 \rightarrow r_2$ (see Fig. 14.13-(c)). We shall nevertheless stress that the manipulations outlined above are valid as long as the distance between the two resonances is larger than the resistive layer width.

References

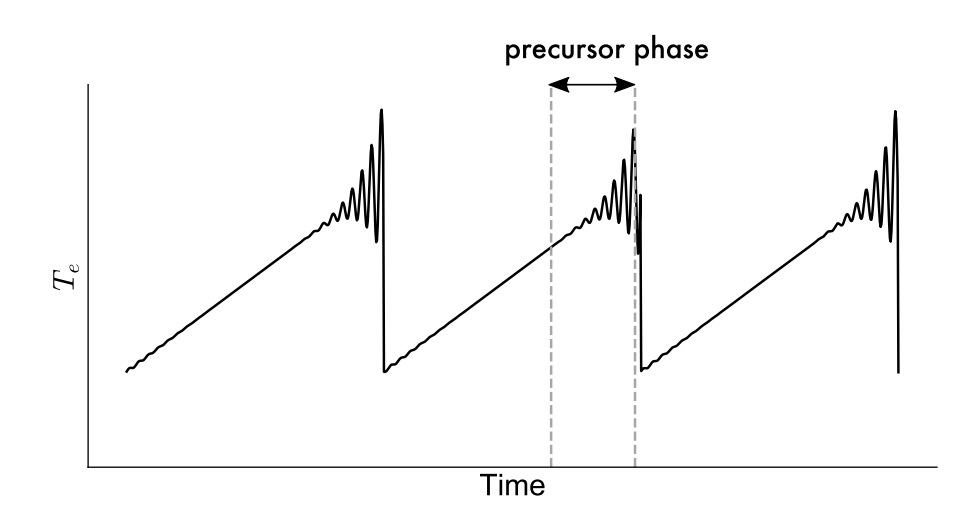
• B. Coppi et al., Nucl. Fusion 6, 101 (1966).

- R. L. Dewar, and M. Persson, Phys. Fluids B 5, 4273 (1993).
- R. Fitzpatrick, Phys. Plasmas 2, 825 (1995).
- H. P. Furth et al., Phys. Fluids 6, 459 (1963).
- H. P. Furth et al., Phys. Fluids 16, 1054 (1973).
- S. Günter et al., Nucl. Fusion 40, 1541 (2000).
- C. C. Hegna and J. D. Callen, Phys. Plasmas 1, 2308 (1994).
- T. C. Hender et al., Nucl. Fusion 27, 1389 (1987).
- Y. Ishii et al., Phys. Plasmas 7, 4477 (2000).
- B. B. Kadomtsev and O. P. Pogutse, Zh. Eksp. Teor. Fiz. **65**, 575 (1973) [Sov. Phys.-JETP **38**, 283 (1974)].
- B. N. Kuvshinov and A. B. Mikhailovskii, Fiz. Plazmy **16**, 1102 (1990) [Sov. J. Plasma Phys. **16**, 639 (1990)].
- R. J. La Haye, Phys. Plasmas 13, 055501 (2006).
- S. Migliuolo, Nucl. Fusion 33, 1721 (1993).
- Y. Nishimura et al., Phys. Plasmas 5, 4292 (1998).
- J. A. Wesson, Tokamaks, Oxford University Press (Oxford, UK), 2011.
- Q. Yu, Phys. Plasmas 3, 2898 (1996).

15

The m = 1 resistive mode

We mentioned in chapter 8 that the cyclic events known as sawtooth oscillations are linked to the appearance of a global instability with poloidal mode number m=1 when the safety factor on the magnetic axis is less than unity. During these periodic cycles, a slow ramp in temperature is followed by a rapid drop (crash) usually after the onset of a m=n=1 mode which may exhibit a structure similar to that of an internal kink. The time occurring between the onset of the m=n=1 mode and the temperature crash is called **precursor phase** (see figure 15.1). After the crash, due to enhanced **transport** across flux surfaces, the temperature and mass density profiles become flat (cf. Fig. 8.1) approximately up to the radial position of the q=1 radius of the pre-crash safety factor (we denote this radius with $r_{q=1}$). The current density changes as well, leading to either a **complete** or a **partial** flattening of the safety factor profile within the region extending from the magnetic axis to $r_{q=1}$. An example of the shape of q is shown in Fig. 15.2.



¹ In tokamak jargon, **complete (or full) reconnection** refers to cases when q is completely flattened across the core, otherwise we talk about **incomplete (or partial) reconnection**. The onset of a tearing-like fluctuation is often observed right after the temperature crash.

Figure 15.1: Time evolution of the electron temperature on the magnetic axis in presence of a MHD precursor right before the crash during a sawtooh cycle.

In ideal MHD flux surfaces may be displaced but not torn, so that transport across them is expected to be weak. It follows that ideal instabilities should not yield a temperature and current redistribution as is observed during sawteeth cycles. The simplest effect that may be invoked to account for such dynamics is the **breaking** and **reconnection** of the magnetic flux surfaces, which thus requires some amount of plasma resistivity to occur.

Hence, in this short chapter we address the problem of the stability of the m=1 resistive mode, i.e. the resistive counterpart of the internal kink perturbation studied in chapter 8. It is important to stress that although the m=1 resistive instability is sought to be a key player in the dynamics of the sawtooth oscillation, here we do not attempt to provide an exhaustive picture of the sawtooth phenomenon whose explanation requires a far more advanced treatment which is not captured by our basic analysis.

This chapter is structured as follows: after obtaining the correct asymptotic behaviour of the m=1 eigenfunction near the q=1 resonance, we derive a simple dispersion relation which is expressed in a form similar to Eq. (14.18). Various limiting cases are then analysed, thoroughly detailing for each of those the associates growth rate and mode structure. We then detail more accurately the smooth transition of the character of the m=1 perturbation, from tearing to kink-like, when the marginal stability boundary of the m=1 ideal internal kink is approached. Finally, we present a brief discussion on the coupling of the 1/1 and the 2/1 modes.

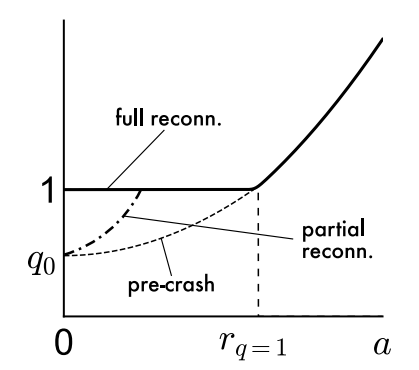


Figure 15.2: Example of safety factor profile before (pre) the crash and after a full and partial reconnection.

15.1 The dispersion relation

Let us take a perturbation with poloidal and toroidal mode numbers m=n=1. As usual, we consider a monotonically increasing safety factor with the q=1 resonance located at some position r_s within the plasma (cf. Fig. 7.1). The magnetic shear is of the order of unity. Most of the calculations which are required to obtain the dispersion relation have already been presented in chapters 8 and 14, so that it is sufficient to give a brief summary of those results.

In the outer region far from r_s , the m = 1 eigenfunction is written as

$$\xi_1^r = \xi_\infty + X_1 \quad r < r_s,$$

= X_1 , $r > r_s$,

where ξ_{∞} is a constant and $X_1/\xi_{\infty} \sim \varepsilon^2$. When the resonance is approached, the derivative of the eigenfunction behaves as in (8.10). This expression can be integrated, and, without loss of generality, we may

write

$$\xi_{1}^{r} = \begin{cases} \xi_{\infty} \left(1 + \frac{\int_{0}^{r_{s}} rU dr}{r_{s}^{2} s^{2} x} \right) = \xi_{\infty} \left(1 - \frac{r_{s}^{2} \delta W_{T}}{R_{0}^{2} s^{2} x} \right), & r < r_{s}, \\ \frac{c \, nst}{x}, & r > r_{s}, \end{cases}$$
(15.1)

where the quantity δW_T is defined by equation (8.36) and cnst is some constant which does not need to be specified. The eigenfunction given by Eq. (15.1) can be cast in a form similar to (14.12) as

$$\xi_{1}^{r} = \frac{\hat{c}_{1}}{|x|} (1 - \Delta_{-}|x|), \quad r < r_{s},
= \frac{\hat{c}_{2}}{|x|} (1 + \Delta_{+}|x|), \quad r > r_{s},$$
(15.2)

having defined

$$\Delta_{-} = -\frac{R_0^2 s^2}{r_s^2 \delta W_T}, \text{ and } \Delta_{+} = 0,$$
(15.3)

where \hat{c}_1 and \hat{c}_2 are some multiplicative constants.

The **dispersion relation** is immediately obtained from the matching conditions (14.15), (14.16) and (14.17), and reads (cf. (14.18))

$$\frac{3^{1/4}S^{3/4}}{\sqrt{s}} \frac{(\gamma/\omega_A)^{5/4}}{M_t - 1} \frac{\Gamma\left(\frac{M_t + 3}{4}\right)}{\Gamma\left(\frac{M_t + 5}{4}\right)} = -\frac{2}{\pi} \frac{R_0^2 s^2}{r_s^2 \delta W_T} \equiv \frac{2}{\lambda_H}.$$
 (15.4)

We recall that M_t is given by (13.38) in which we have to set $m=n=q_s=1$. Here we introduced the quantity λ_H , commonly found in the literature, which is a measure of the stability of the **ideal** m=1 mode: the m=1 ideal internal kink mode is unstable when λ_H is positive, and marginally stable for $\lambda_H=0$. The stability of the resistive mode depends on the value of λ_H , and various limiting case will be investigated in detail in the next subsections.

15.1.1 The ideal limit

Let us first define the normalised quantity

$$\hat{\lambda}_H = \lambda_H \left(\frac{sS}{\sqrt{3}}\right)^{1/3}.\tag{15.5}$$

By means of (14.19) we rearrange equation (15.4) as

$$\frac{M_t - 1}{M_t^{5/6}} \frac{\Gamma\left(\frac{M_t + 5}{4}\right)}{\Gamma\left(\frac{M_t + 3}{4}\right)} = \frac{\hat{\lambda}_H}{2}.$$
 (15.6)

For positive and sufficiently large λ_H such that $\hat{\lambda}_H \gg 1$ one must have $M_t \to \infty$. Expanding the expression above for M_t large yields $M_t^{2/3} = \hat{\lambda}_H$ which can be written as

$$\frac{\gamma}{\omega_A} = \frac{s\lambda_H}{\sqrt{3}}.$$

This is equivalent to (8.11), that is the growth rate of the m=1 ideal internal kink mode. One sees that in the unstable region of the m=1 ideal internal kink mode resistivity does not play any significant role.

15.1.2 The m = 1 resistive internal kink

Let us now look at the $\lambda_H \approx 0$ case. It follows that the right-hand-side of (15.6) is very small, thus implying that the left-hand-side is small too. This can only be accomplished if $M_t \approx 1$ which yields the growth rate

$$\frac{\gamma}{\omega_A} = \frac{s^{2/3}}{(3S)^{1/3}}. (15.7)$$

For typical values of the Lundquist number in tokamaks, this gives $\gamma/\omega_A \sim 10^{-4}-10^{-3}$, indicating that the time-scale of the growth of the instability is of the order of few milliseconds.

We can be slightly more precise, and from (15.4) we write

$$M_t = 1 + (\gamma/\omega_A)^{5/4} \lambda_H \frac{3^{1/4} S^{3/4}}{\sqrt{s\pi}}.$$

If λ_H is sufficiently small, we can solve this expression perturbatively for γ , eventually giving

$$\frac{\gamma}{\omega_A} = \frac{s^{2/3}}{(3S)^{1/3}} \left[1 + \frac{2}{3} \frac{\lambda_H}{\sqrt{\pi}} \left(\frac{sS}{\sqrt{3}} \right)^{1/3} \right].$$

This shows that stability is improved as λ_H becomes more negative. Note that this equation can also be written as

$$M_t^{2/3} = 1 + \frac{2}{3} \frac{\hat{\lambda}_H}{\sqrt{\pi}}.$$
 (15.8)

The shape of the associated eigenfunction is now easily obtained. Setting $M_t = 1$ in (13.39), one finds that

$$Y(\zeta) = \frac{2}{\sqrt{\zeta}},$$

so that the even and odd solutions in k-space read

$$\xi^* = \frac{e^{-V_e k^2/2}}{|k|} \quad \text{(even)},$$

$$= \frac{e^{-V_e k^2/2}}{k} \quad \text{(odd)},$$

where $V_e = m^2 (1 + 2q_s^2)^{1/3}/(ns)^{2/3} = (3/s^2)^{1/3}$ has been computed by plugging (15.7) into (13.36).

Let us first focus on the behaviour in real (y) space, as defined in §13.4, of the even solution. By expanding in k the first of (15.9) we obtain a power series of the form (cf. (13.41))

$$\xi^* \propto \frac{1}{|k|} \left(1 - V_e k^2 / 2 + \ldots \right),$$

where only the first term in brackets is needed. Asymptotic matching with (15.1) requires $C \to \infty$ in the expression for the Fourier transform of 1/|k| given in (13.43), so that the even solution in real space is simply a constant. The Fourier transform of the odd solution yields the *error function*, 2 that is

$$\frac{1}{2\pi} \int_{-\infty}^{\infty} \frac{e^{-V_e k^2/2}}{k} e^{iky} dk = \frac{i}{2} \operatorname{erf}\left(\frac{y}{\sqrt{2V_e}}\right). \tag{15.10}$$

Therefore, we can write the even and odd functions in real space as

$$\xi_1^r = 1$$
 (even),
$$= \operatorname{erf}\left(\frac{y}{\sqrt{2V_e}}\right) \quad \text{(odd)},$$

It follows that the solution in the resistive layer which matches asymptotically the one computed in the outer region is

$$\xi_1^r = \frac{\xi_\infty}{2} \left(1 - \operatorname{erf}\left(\frac{y}{\sqrt{2V_e}}\right) \right).$$
 (15.11)

When this expression is plugged into (13.28), the radial perturbation of the magnetic field reads

$$(\sqrt{g}\tilde{B}^r)_1 \propto \frac{y}{\sqrt{2V_e}} \operatorname{erf}\left(\frac{y}{\sqrt{2V_e}}\right) - \frac{y}{\sqrt{2V_e}} + \frac{e^{-y^2/(2V_e)}}{\sqrt{\pi}},\tag{15.12}$$

where, as boundary condition, we imposed that $(\sqrt{g}\tilde{B}^r)_1$ vanishes for $y \to +\infty$: this is because in the ideal region $(\sqrt{g}\tilde{B}^r)_1 \propto k_{||}\xi_1^r$, and since ξ_1^r is vanishing, the magnetic perturbation must be zero as well. Notice that this determines both of the constants of integration originating from the solution of (13.28). One notices that, contrary to ideal MHD results, the magnetic perturbation at the q=1 resonance is not vanishing i.e. $(\sqrt{g}\tilde{B}^r)_1(r_s) \neq 0$. A rearrangement of the magnetic topology of the magnetic flux is therefore allowed, so that magnetic islands may form as discussed in the previous chapter (see Fig. 15.3).

15.1.3 The m = 1 reconnecting mode

We now investigate the $\lambda_H < 0$ case with $|\lambda_H| \sim 1$, i.e. we assume to carry out the analysis in the region of stability of the ideal internal kink mode. It is obvious that for large values of the Lundquist number, the left-hand-side of (15.6) is large. Let us first note that if we take $M_t \gg 1$ the right-hand-side of (15.6) becomes proportional to γ which must then be equal to a negative quantity thus indicating stability. Hence, the only possibility for having an unstable mode is to take $M_t \ll 1$. We therefore obtain the m=1 equivalent of the dispersion relation for tearing modes (14.20), that is

$$\left(\frac{\gamma}{\omega_A}\right)^{5/4} = \frac{2}{|\lambda_H|} \frac{\Gamma\left(\frac{5}{4}\right)}{\Gamma\left(\frac{3}{4}\right)} \frac{\sqrt{s}}{3^{1/4} S^{3/4}}.$$

² The error function is defined as $\operatorname{erf}(x) = \frac{2}{\sqrt{\pi}} \int_0^x e^{-t^2} dt$. To obtain (15.10), one uses the **convolution theorem** which states that the Fourier transform of the product of two functions f and g is the convolution of the product of their transform. Denoting

$$\hat{h}(y) = \frac{1}{2\pi} \int_{-\infty}^{\infty} h(k)e^{iky}dk,$$

the convolution theorem is written as

$$\widehat{(fg)}(y) = \int_{-\infty}^{\infty} \widehat{f}(\tau)\widehat{g}(y-\tau)d\tau.$$

We set $f(k) = e^{-V_e k^2/2}$ and g(k) = 1/k, and the resulting integrals are evaluated following the caption of Fig. 12.6.

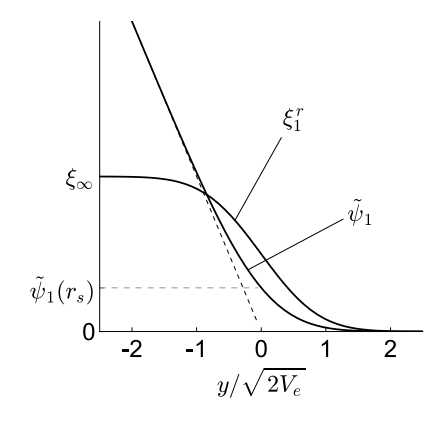


Figure 15.3: Radial shape of ξ_1^r and $\tilde{\psi}_1 \equiv (\sqrt{g}\tilde{B}^r)_1$ in the resistive layer. Here we borrow the notation from (14.2).

The growth rate of this instability scales as $S^{-3/5}$, showing that it grows on tearing timescales which are much slower than those of the modes analysed in the previous sections.

Since we have been able to find a positive growth rate for any value of λ_H , we then infer that the m=1 resistive mode is always unstable when there is a q=1 surface in the plasma (see Fig. 15.4-(a)). One should note, however, that in a realistic situation additional effects, not captured by our analysis, can contribute to the stability of the mode: further stabilisation may indeed arise from two-fluid (FLR) or kinetic corrections, and also from other effects associated with toroidicity (a brief account of the latter will be given in chapter 17).

We shall finally discuss the spatial structure of the m=1 resistive perturbation. The character of this instability is dictated by M_t , namely its growth rate (this is computed at fixed plasma parameters such has Lundquist number and magnetic shear). In order to see the change in shape of the layer eigenfunction as M_t is varied, we express γ/ω_A and V_e in terms of M_t as (cf. (13.36) and (13.38))

$$\frac{\gamma}{\omega_A} = \left(\frac{msM_t}{S^{1/2}q_s\sqrt{1+2q_s^2}}\right)^{2/3},$$

$$V_e = \left(\frac{m^2q_s\sqrt{1+2q_s^2}}{s}\right)^{2/3} M_t^{-2/3} \equiv A^2M_t^{-2/3},$$
(15.13)

where the constant A > 0, implicitly defined in the latter of the two equations above, is a quantity of the order of unity. Note that we must take $m = q_s = 1$ in the expressions above.

By making use of (13.40), we now want to transform to real space in the variable y/A the even and odd solutions generated by (13.39) for arbitrary M_t (cf. §13.4). The even solution is expanded according to (13.41), and, in analogy with the discussion of section 15.1.2, we find that in real space this is a constant.³ Focussing on the odd solutions, by means of two expressions above, we have

$$\xi_{\text{odd}}^* = e^{-M_t^{1/3} A^2 k^2 / 2} \left[U\left(\frac{M_t + 5}{4}, \frac{3}{2}, M_t^{1/3} A^2 k^2\right) + \frac{2}{M_t} U\left(\frac{M_t + 1}{4}, \frac{1}{2}, M_t^{1/3} A^2 k^2\right) \right] \operatorname{sgn}(k). \quad (15.14)$$

Its inverse Fourier transform is performed numerically, and figure 15.4-(b) summarises the results of this computation: the change in character of the eigenfunction when M_t becomes smaller than unity becomes evident. We say that the odd fuction acquires a **tearing character** when $M_t \ll 1$. The global structure (in real space) of the eigenfunction is finally obtained by combining together the even and odd solutions in order to fulfil the correct boundary conditions at $y/A = \pm \infty$. This is detailed in the next section.

³ This holds also for tearing perturbations with m > 1 computed with the step-current profile employed in the analysis of $\S14.3$ (compare with (13.44)).

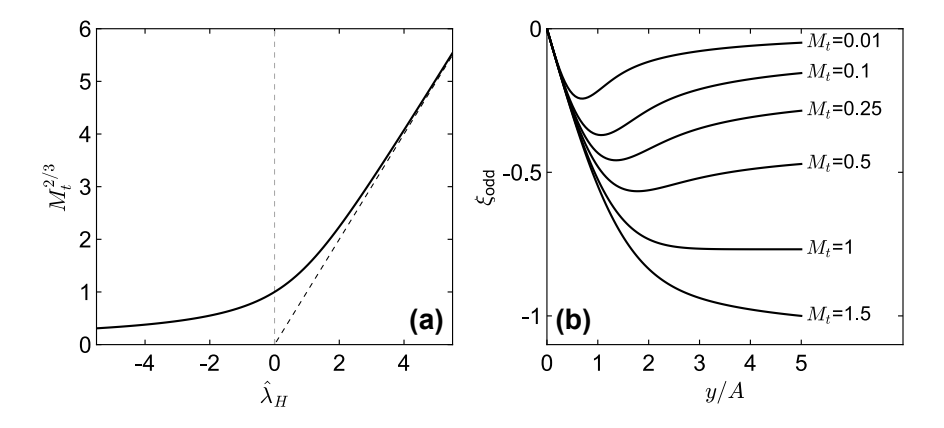


Figure 15.4: (a): Dependence of $M_t^{2/3} \propto$ γ upon $\hat{\lambda}_H$ obtained from the numerical solution of (15.6). The oblique black dashed line denotes the growth rate of the m = 1 ideal mode. (b): Resistive layer odd solution in real space for different values of the parameter M_t .

On the relative amplitude of the even and odd solu-

For the m=1 mode we found that $\Delta_+=0$ and $\Delta_-\sim \varepsilon^{-2}\gg 1$ for δW_T of the order of unity or less (cf. (15.3)). If one then uses (14.23), it seems that the even solution in the resistive layer always dominates over the odd one. Using the constants c_e and c_o , however, may be misleading in that they only measure the relative amplitude of the large-y expansions of the layer solutions, i.e. Eqs. (13.44) and (13.45).

To resolve this ambiguity, let us take $\xi_1^r = c_e \xi_{\text{even}} + i \hat{c}_o \xi_{\text{odd}}$ where $\xi_{\text{even}} = 1$ and

$$\xi_{\text{odd}} = \frac{1}{2\pi} \int_{-\infty}^{\infty} \xi_{\text{odd}}^*(k) e^{iky} dk,$$

with $\xi_{\rm odd}^*$ given by (15.14). For $0 < k \ll 1$, from (15.14) we have to leading order

$$\xi_{\text{odd}}^* = \frac{2\sqrt{\pi}(1 - M_t)}{M_t\Gamma\left(\frac{M_t + 3}{4}\right)} \left(1 + \frac{\Delta_R}{|k|}\right) \text{sgn}(k),$$

so that taking the large y limit of the inverse Fourier transform of ξ_{odd}^* yields (cf. (13.45))

$$\xi_{\text{odd}} = \frac{2i(1 - M_t)\epsilon_R}{\sqrt{\pi}M_t\Gamma\left(\frac{M_t + 3}{4}\right)} \times \frac{1}{x}\left(1 + \frac{m\pi\Delta_R}{2}S^{1/3}|x|\right),\,$$

where we recall that $\epsilon_R = 1/(mS^{1/3})$. A comparison with (14.15) and (14.16) shows that

$$c_o = \frac{2(M_t - 1)\epsilon_R}{\sqrt{\pi}M_t\Gamma\left(\frac{M_t + 3}{4}\right)}\hat{c}_o.$$

Thus, plugging this result into (14.23) gives

$$\frac{c_e}{\hat{c}_o/A} = \frac{\sqrt{\pi}(M_t-1)}{M_t \Gamma\left(\frac{M_t+3}{4}\right)} \hat{\lambda}_H^{-1}.$$

The singularity at $\hat{\lambda}_H = 0$ is removed thanks to (15.8).

According to the discussion in the previous section one has $A = (\sqrt{3}/s)^{1/3}$.

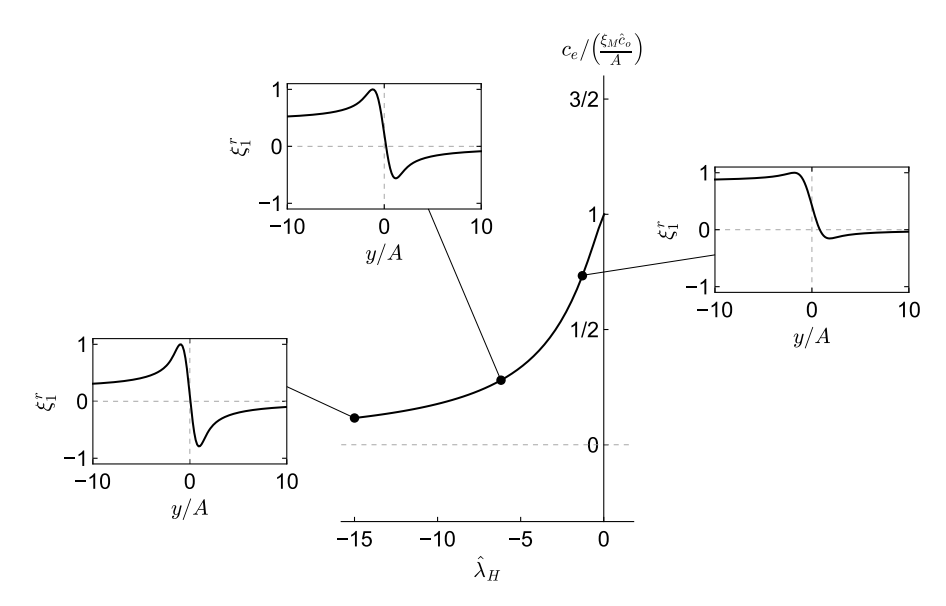


Figure 15.5: Ratio of the multiplying constants of the even (c_e) and odd $(\xi_M \hat{c}_o/A)$ solutions as function of the variable y/A. The insets show the structure of the normalised eigenfunction ξ_1^r in the resistive layer. For large and negative $\hat{\lambda}_H$ the eigenfunction is mainly odd.

Now, when ξ_1^r is written in terms of the variable y/A, it reads

$$\xi_1^r = c_e - \left(\frac{\hat{c}_o}{A}\xi_{\rm M}\right) \times \frac{1}{2\pi\xi_{\rm M}} \int_{-\infty}^{\infty} \xi_{\rm odd}^*(x) \sin\left(x\left(\frac{y}{A}\right)\right) dx,$$

where $\varkappa=Ak$ and $\xi_{\rm M}$ is the maximum value in the *y*-domain taken by function $\frac{1}{2\pi}\int_{-\infty}^{\infty}\xi_{\rm odd}^*(\varkappa)\sin\left(\varkappa(y/A)\right))d\varkappa$. We therefore take the function (bounded between -1 and 1)

$$\frac{1}{2\pi \mathcal{E}_{\mathrm{M}}} \int_{-\infty}^{\infty} \xi_{\mathrm{odd}}^{*}(\mathbf{x}) \sin\left(\mathbf{x}\left(\frac{\mathbf{y}}{A}\right)\right) d\mathbf{x}$$

to be the odd solution in the resistive layer. The quantity $\hat{c}_o \xi_{\rm M}/A$ now measures the odd contribution to the full linear eigenfunction. Since we constructed an odd solution which is comparable in magnitude with the even one, the quantity $Ac_e/(\hat{c}_o \xi_{\rm M})$ represents a good estimate of their mutual strength. Its behaviour as a function of $\hat{\lambda}_H$ is shown in Fig. 15.5.

15.2 Interacting resistive layers

The linear dynamics of the 1/1 mode, either ideal or resistive, depends crucially on the coupling with its first neighbouring sidebands. A mutual interaction between the q=1 and the q=2 layers, if the latter is within the plasma, will then occur. We now make the following considerations: the dynamics at the q=2 surface is expected to have an effect on the global stability of the n=1 perturbation, namely growth rate and marginal boundaries, while the amplitude of the 1/1 harmonic will dictate the structure of the 2/1 magnetic perturbation. In this section we shall analyse more in detail such behaviours.

Our starting point is the expression for δW_T as given in (8.37) where the coefficients b, c and \hat{s} are defined by Eq. (8.20). We decompose the factor c as $c = c_I + c_R$ where c_I is independent of γ and η . A more precise definition of these quantities will be given later. Plugging this into (8.37) gives

$$\delta W_T = \delta W_I - \left(\frac{c_R/(1+b-c_I)}{1-c_R/(1+b-c_I)}\right) \delta W_R,$$

having defined δW_I and δW_R as

$$\delta W_{I} = \frac{\hat{s}}{2} + \frac{9b(1 - c_{I}) - 24bc_{I}(\beta_{p} + \hat{s}) - 16c_{I}(1 + b)(\beta_{p} + \hat{s})^{2}}{16(1 + b - c_{I})},$$

$$\delta W_{R} = \frac{\left[\frac{3}{4}b + (1 + b)(\beta_{p} + \hat{s})\right]^{2}}{(1 + b - c_{I})}.$$
(15.15)

Upon conveniently introducing the quantities

$$\hat{\lambda}_I = -\left(\frac{sS}{\sqrt{3}}\right)^{1/3} \frac{\pi r_s^2 \delta W_I}{s^2 R_0^2}, \qquad \hat{\lambda}_R = \left(\frac{sS}{\sqrt{3}}\right)^{1/3} \frac{\pi r_s^2 \delta W_R}{s^2 R_0^2},$$

where s and S are the magnetic shear and the Lundquist number computed at the q = 1 surface labelled by r_s , the dispersion relation (15.6) becomes

$$\frac{M_t - 1}{M_t^{5/6}} \frac{\Gamma\left(\frac{M_t + 5}{4}\right)}{\Gamma\left(\frac{M_t + 3}{4}\right)} - \frac{\hat{\lambda}_I}{2} = \frac{c_R/(1 + b - c_I)}{1 - c_R/(1 + b - c_I)} \frac{\hat{\lambda}_R}{2}.$$
 (15.16)

Notice that equilibrium quantities appearing in M_t have to be evaluated at $r_{\rm s}$.

We now consider a safety factor profile of the form (see (14.8))

$$q = q_0,$$
 $r < r_0,$
= $(r/r_s)^2,$ $r > r_0.$

We take $q_0 < 1$ and also $r_s < a/\sqrt{2}$ so that the q = 2 surface located at $r = r_2$ is within the plasma. It is easily shown that $r_2/r_s = \sqrt{2}$ and $r_0/r_s = \sqrt{q_0}$ while s = 2 for $r > r_0$. Thus, employing (4.37) and (14.11), we find that the expressions for the coefficients \hat{s} and b are

$$\hat{s} = -\frac{1}{2} \ln q_0, \qquad b = \frac{1 - q_0}{1 - q_0(1 - q_0)},$$

both of which are greater than zero. The tearing stability index of the 2/1 mode computed in the cylindrical limit according to the analysis of the preceding chapter, is (see Eq. (14.22))

$$r_2\Delta_c' = -\frac{16(1-q_0)}{1+(3-q_0)(1-q_0)} + \frac{4}{1-(b_w/r_2)^4}.$$

where b_w is the radial position of an ideally conducting wall. For $q_0 < 1$ the quantity above is always negative thus indicating that the classical 2/1 tearing mode is stable.

Since q(a) > 2 and thus $q(a)/q_0 > 2$, a quick comparison with figure 10.5 shows that external kink modes are stable.

Now, following the calculations of 14.3 (see in particular **sidenote** 6) we may write X_2^e as

$$X_{2}^{e} \propto \left[\frac{r}{r_{2}} + A_{-} \left(\frac{r}{r_{2}}\right)^{-3}\right] / (2\mu - 1), \qquad r_{s} < r < r_{2},$$

$$\propto \left[\frac{r}{r_{2}} + A_{+} \left(\frac{r}{r_{2}}\right)^{-3}\right] / (2\mu - 1), \qquad r > r_{2}, \qquad (15.17)$$

where $A_{+} = -(b_w/r_2)^4$ and A_{-} , still undetermined, contains the contributions from inertia and resistivity at the q = 2 surface. Thus, by means of the equation above, the quantity c is readily obtained

$$c = \frac{2 + 4A_{-}}{1 + 4A_{-}}. (15.18)$$

Letting $x = (r - r_2)/r_2$, as r_2 is approached one has (cf. (14.12))

$$X_2^e(r \to r_2 - \epsilon) \propto \frac{1}{x} + \Delta_-, \quad X_2^e(r \to r_2 + \epsilon) \propto \frac{1}{x} + \Delta_+,$$

where, in analogy with (14.14), we defined

$$\Delta_{\pm} = \frac{\frac{5}{2} - \frac{3}{2}A_{\pm}}{1 + A_{\pm}}.\tag{15.19}$$

Matching with the inner layer solution of the q=2 resonance yields a dispersion similar to (14.18) that is

$$\Delta_* \equiv \frac{\pi}{2} \left(\frac{2}{3} S_2 \right)^{1/3} \frac{M_{t2}^{5/6}}{1 - M_{t2}} \frac{\Gamma((M_{t2} + 3)/4)}{\Gamma((M_{t2} + 5)/4)} = \Delta_+ - \Delta_-, \tag{15.20}$$

where the subscript 2 means that the corresponding quantity has to be evaluated at r_2 . Equation (15.20) is now combined with (15.19) to obtain an expression for A_- which reads

$$A_{-} = \left(\frac{4A_{+}}{1 + A_{+}} + \Delta_{*}\right) / \left(\frac{4}{1 + A_{+}} - \Delta_{*}\right). \tag{15.21}$$

Thus, if we let δW_I to denote the growth rate of the ideal internal kink as given in §8.5, we consistently set $c_I = \lim_{A_- \to -1} c.^4$ It then follows that $c_I = 2/3$, whereas the correction containing the q = 2 layer response reads

$$c_R = \frac{4}{3} \left(\frac{1 + A_-}{1 + 4A_-} \right) = \frac{16/3}{3\Delta_* + 4(1 + 4A_+)/(1 + A_+)}.$$

A quick computation finally yields

$$\frac{c_R/(1+b-c_I)}{1-c_R/(1+b-c_I)} = \frac{16/3}{(1+3b)(\Delta_*-r_2\Delta_c')}.$$

Therefore, combining this result with equation (15.16) eventually gives

$$\frac{1}{\varphi(M_t)} - \frac{\hat{\lambda}_I}{2} = -\frac{8\hat{\lambda}_R/(3c_0)}{(1+3b)(\varphi(M_{t2}) + r_2\Delta_c'/c_0)},\tag{15.22}$$

⁴ This is equivalent to letting the response at the q = 2 resonance to be ideal in the limit of very small growth rates.

where $c_0 = \frac{\pi}{2}(2S_2/3)^{1/3}$ and the function φ is defined as

$$\varphi(M) = \frac{M^{5/6}}{M-1} \frac{\Gamma((M+3)/4)}{\Gamma((M+5)/4)}.$$

Let us study (15.22) more carefully. If we keep S_2 finite and let $S \to \infty$, i.e. the response at the q=1 surface is ideal, the left-hand-side of (15.22) is computed in the limit $M_t \to \infty$. Thus, by letting $\gamma \to 0$, one can identify the marginal boundary

$$\delta W_I + \frac{8\delta W_R/3}{r_2\Delta_c'(1+3b)} = 0.$$

Since $\delta W_R > 0$ and $r_2 \Delta'_c < 0$ with our choice of the safety factor, resistivity at the q=2 surface yields a critical β_p lower than the one obtained from the fully ideal computation.

Now assume $S < \infty$ and, for the sake of simplicity, take $M_{t2} = M_t.5$ It is easy to see that if $\hat{\lambda}_I \approx 0$ then $M_t \approx 1$ which is the growth rate of the m = 1 resistive kink mode studied earlier. The important difference compared to what has been discussed in the previous sections is that a non-vanishing radial magnetic perturbation is allowed at the q=2surface. This occurs even if the tearing stability index associated with the 2/1 mode is negative meaning that a 2/1 magnetic island, dragged by the 1/1 mode, may develop.

To quantify the amplitude of the magnetic perturbation at r_2 , following the procedure of section 15.1.4, we first write the 2/1 radial fluid displacement in its corresponding resonant resistive layer as

$$\xi_2^r(y) = c_e - c_o \frac{\sqrt{\pi} M_t \Gamma\left(\frac{M_t + 3}{4}\right)}{2i(M_t - 1)\epsilon_R} \frac{1}{2\pi} \int_{-\infty}^{\infty} \xi_{\text{odd}}^*(k) e^{iky} dy,$$

$$y = \frac{r - r_2}{\epsilon_R r_2}, \quad \epsilon_R = \frac{1}{2S_2^{1/3}},$$
(15.23)

where c_e and c_o are the constants of Eqs. (14.15) and (14.16) while ξ_{odd}^* is defined by (15.14). The quantity A is computed according to (15.13) with $m=q_s=s=2$ and n=1. Furthermore, we let $\xi^*=\frac{1}{2\pi}\int_{-\infty}^{\infty}\xi_2^r(y)e^{-iky}dy$ and find that the odd contribution to ξ^* is

$$(\xi^*)_{\text{odd}} = -c_o \frac{\sqrt{\pi} M_t \Gamma\left(\frac{M_t + 3}{4}\right)}{2i(M_t - 1)\epsilon_R} \xi^*_{\text{odd}}(k). \tag{15.24}$$

The magnetic perturbation associated with ξ^* in k-space is referred to as ψ^* .

Far from the q=2 resonance, we use (8.21) and (15.17) to obtain at leading order

$$\begin{split} \xi_2^r(r \to r_2 - \epsilon) \approx & \frac{C_{11} r_s}{2 R_0} \left(\frac{\hat{s} + \beta_p(r_s) + b[^3/_4 + \hat{s} + \beta_p(r_s)]}{1 + b - c} \right) \times \\ & \times \left(\frac{1 + A_-}{(r_s/r_2) + A_-(r_2/r_s)^3} \right) \frac{1}{|x|} \left(1 - \Delta_-|x| \right), \end{split}$$

With a generic q profile, Eq. (15.22) can be formally cast as (Connor (1988))

$$\frac{1}{\varphi(M_t)}-A=-\frac{B^2}{\varphi(M_{t2})+r_2\Delta_\epsilon'/c_0}.$$

It is worth to point out that the dispersion relation of two generic interacting inertial/resistive layers retains essentially the same structure although different expressions for A, B, c_0 and $r_2\Delta'_c$ must be employed.

analogy discussed in \$1_{4.5}, one has $M_{t2}/M_{t1} = \frac{|s_1|}{|s_2|} \sqrt{\frac{s_2(1+2q_2^2)}{s_1(1+2q_1^2)}} \text{ with the}$ subscripts 1 and 2 referring to the resonances at r_1 and r_2 respectively.

The Fourier transform of an even/odd real valued function is an even purely real/odd purely imaginary function in kspace.

where C_{11} is the amplitude of the 1/1 harmonic and $\epsilon \to 0$. Thus, by following the matching rules (14.17) we can identify

$$\hat{c}_{1} = -c_{o} = \frac{C_{11}r_{s}}{2R_{0}} \left(\frac{\hat{s} + \beta_{p}(r_{s}) + b[^{3}/_{4} + \hat{s} + \beta_{p}(r_{s})]}{1 + b - c} \right) \times \frac{1 + A_{-}}{(r_{s}/r_{2}) + A_{-}(r_{2}/r_{s})^{3}}.$$
(15.25)

The quantity A_- is obtained from (15.21) which, in the limit $b_w/a \to \infty$ with $M_t \approx 1$, yields

$$1 + A_{-} = -\frac{4}{\Delta_{*}} \approx \frac{2A(M_{t} - 1)}{\sqrt{\pi}S_{2}^{1/3}}.$$

We recall that the constant A is defined in (15.13) with the aforementioned substitutions.

We now exploit the fact that in k-space ξ^* vanishes at infinity and use the first of (13.31) to write

$$(\sqrt{g}\tilde{B}^r)_2(0) = \frac{1}{2\pi} \int_{-\infty}^{\infty} \psi^*(k) dk = \frac{r_2 B_0 V_e}{\pi S_2^{1/3}} \int_{-\infty}^{\infty} \frac{k \xi^*(k)}{(1 + V_e k^2)^2} dk.$$

One notices that in the expression above only the odd contribution to ξ^* is needed. Hence, after setting $M_t \approx 1$ and using (15.24), we finally obtain

$$\frac{(\sqrt{g}\tilde{B}^r)_2(0)}{ir_2B_0} = \frac{C_{11}r_2}{R_0} \left(\frac{\hat{s} + \beta_p(r_s) + b[^3/4 + \hat{s} + \beta_p(r_s)]}{1 + b - c_I} \right) \frac{A\sqrt{2}}{3\sqrt{\pi}S_2^{1/3}}.$$

References

- M. Abramowitz and I. A. Stegun (eds.), **Handbook of Mathematical Functions**, Dover Publications (New York, US), 1964.
- G. Ara et al., Ann. Phys. 112, 443 (1978).
- B. Connor et al., Phys. Fluids 31, 577 (1988).
- B. Coppi et al., Nucl. Fusion 6, 101 (1966).
- B. Coppi et al., Fiz. Plazmy 2, 961 (1976) [Sov. J. Plasma Phys. 2, 533 (1976)].
- R. J. Hastie et al., Phys. Fluids 30, 1756 (1987).
- S. Migliuolo, Nucl. Fusion 33, 1721 (1993).
- F. Porcelli, Phys. Fluids 30, 1734 (1987).

Remember that when $M_t = 1$ the function ξ_{odd}^* as defined in (15.14) becomes

$$\xi_{\text{odd}}^* = 2e^{-A^2k^2/2}/(Ak).$$

16

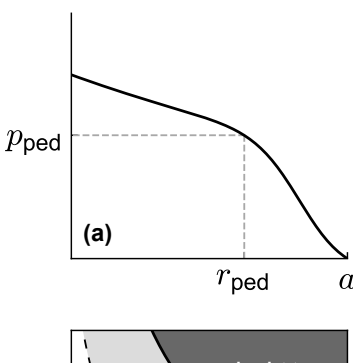
Localised resistive instabilities

In this chapter we investigate the effect of plasma resistivity on the dynamics of two types of localised perturbations, namely **resistive ballooning** and **resistive interchange modes**.

Resistive ballooning modes are likely to appear in regions of steep pressure gradients and large plasma collisionality. These condition are usually met in proximity of the plasma edge when the pressure gradient starts to build up at the H-mode entry (see Figs. 12.3 and 16.1). It is common in this regime to observe high frequency, small amplitude Edge Localised Modes (ELMs) which appear well below the ideal ballooning limit (this is the maximum achievable pressure beyond which ideal ballooning modes become unstable). These event are commonly labelled as **type-III ELMs**. The frequency of type-III ELMs decreases with increased injected power, and in some cases they seem to occur below a threshold in the electron temperature suggesting the possible role of plasma resistivity. Resistive ballooning modes are supposed to play an important role in explaining the appearance of type-III ELMs.

Other localised perturbations discussed in this chapter are resistive interchange modes, namely the resistive counterpart of Mercier modes. These instabilities may be associated with a soft β limit not so catastrophic to terminate the plasma discharge but serious enough to degrade plasma performance. Although the stability criteria associated with resistive interchange modes are less stringent than those of Mercier perturbations, we will see that tokamaks operating with monotonically increasing safety factors are quite resilient against such types of instabilities.¹

Similar to their corresponding ideal perturbations, both resistive interchange and ballooning modes are **pressure driven** instabilities where



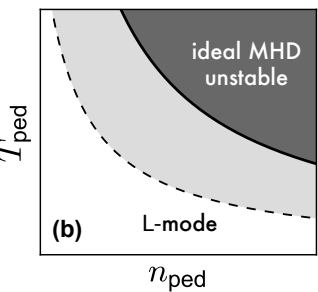


Figure 16.1: (a): H-mode edge pressure profile. (b) Example of the stability diagram of the edge region expressed in terms of density and temperature at $r_{\rm ped}$ (hyperbolae denote isobars) at fixed positive magnetic shear. The H-mode is accessed above the black dashed line. Type-III ELMs may appear in the region highlighted in light grey.

¹ Resistive interchange modes could pose a concern to stability in plasma discharges of long duration with a reversed magnetic shear. A more precise characterisation of the relevance of such instabilities will be given in the next chapter.

the poloidal spectrum of the former is composed of one dominant harmonic, while the latter features multiple equivalent modes.

The aim of this chapter is therefore to provide an approximate yet meaningful discussion of the linear dynamics of these perturbations detailing the mathematical techniques employed in their modelling. Firstly, we derive a set of eigenmode equations which properly account for resistive effects when dealing with localised instabilities. Subsequently, we will focus separately on the two aforementioned perturbations discussing in detail their stability properties.

16.1 Governing equations

Let us fix the poloidal and toroidal mode numbers m and n, both **much** larger than unity and such that $m/n \sim 1$. The associated resonance for which q = m/n is at position r_s , and we define $x = (r - r_s)/r_s$. We now identify two regions: one far from the resonance such that

$$mx \sim 1, \tag{16.1}$$

and a narrow layer about r_s whose radial extension is such that

$$mx \sim \varepsilon \ll 1.$$
 (16.2)

These orderings conform to (12.2) and (13.16) respectively. In analogy with the notation employed earlier, we call the former the **outer region** (also known as **ideal region**) and the latter the **resistive layer** (or simply **layer**) **region**. Furthermore, we assume to deal with **slow-growing** instabilities such that $\gamma/\omega_A \sim \varepsilon$.² Resistive effects are only allowed in the layer region.

Since we are dealing with highly localised perturbations, following (11.2) the expression of the parallel wave vector defined in (7.51) can be approximated as

$$k_{||} = m\mu - n \approx -nsx,$$

where s is the magnetic shear at r_s and $\mu = 1/q$ with $q \sim 1$; this expression is assumed to hold in the outer and layer regions.

Thus, according to (13.18), in the resistive layer close to the resonance the magnetic perturbation with mode number m obeys (η_0 is the equilibrium resistivity)

$$\left(1 - \frac{\eta_0}{r_s^2 \gamma} \frac{d^2}{dx^2}\right) (\sqrt{g}\tilde{B}^r)_m = -ir_s B_0 n s x \xi_m^r.$$
(16.3)

Close to r_s we allow the second term in brackets on the left-hand-side to be of the order of unity. Far from the resonance, instead, the radial gradients of the perturbation are weaker so that resistive corrections become negligible. Therefore, the equation for the radial field in the outer region is obtained from (16.3) by simply setting $\eta_0 \to 0$. Sideband

Note that the magnitude of $(\sqrt{g}\tilde{B}^r)_m$ is proportional to $sr_sB_0\xi_m^r$.

² Although we adopt the same slow-growing ordering of ideal modes, resistive perturbations are expected to grow on much longer timescales.

Having established a link between the magnetic perturbation and the fluid displacement, we now need an equation for the latter. For this purpose we formally start from the **vorticity equation**, i.e. Eq. (13.4), and apply the orderings for small scale modes far from resonance presented in §7.4.³ The dynamics in the resistive layer is obtained by simply allowing radial derivatives of the perturbed quantities to be the dominant ones. Since the perturbation is supposed to be highly localised, throughout this chapter, equilibrium quantities are evaluated at the resonance r_s . With the definition of the **ballooning parameter** given in (4.41) which is $(q_s = m/n)$

$$\alpha = -\frac{2R_0 p_0' q_s^2}{B_0^2},$$

for the sake of simplicity and similar to §12.1, we consider a configuration with $\alpha \ll 1$ and $s \ll 1$ such that (12.5), (12.7) and (12.9) hold. We further assume p_0' **constant**.

Let us start by taking the mth component of (13.22). We recall that the contribution coming from Δp_m , that is the compressible part of the perturbed pressure associated with the harmonic m, is small both close to and far from r_s (cf. (7.48) and (13.24)), hence it can be neglected. Therefore, recalling that \hat{p} is given by (7.59), we can approximate

$$B_0^2 \frac{\gamma^2}{\omega_A^2} \xi_m^{\phi} \approx -i(m\mu - n)\hat{p}_m - \frac{p_0'}{f_0'} (\sqrt{g}\tilde{B}^r)_m$$

$$= -\frac{p_0'}{f_0'} \frac{\eta_0}{r_s^2 \gamma} \frac{d^2}{dx^2} (\sqrt{g}\tilde{B}^r)_m. \tag{16.4}$$

Notice that contrary to the ideal case, there is **no exact cancellation** between the magnetic fluctuation and the radial fluid displacement. Then, from the first of (7.27) we have

$$\xi_{m}^{\vartheta} = -\frac{1}{imr} \left(r \xi_{m}^{r} \right)' - \frac{n}{m} \frac{p_{0}'}{B_{0}^{3}} \frac{\eta_{0}}{r_{s}^{3} \gamma^{3} / \omega_{A}^{2}} \frac{d^{2}}{dx^{2}} (\sqrt{g} \tilde{B}^{r})_{m}, \tag{16.5}$$

where we approximated $f_0' \approx r_s B_0$ (cf. (7.14)). We retain the second term on the right-hand-side even though it is smaller compared to the first one (this will help with some calculations in the next chapter).

Because of the smallness of the growth rate, the inertial contribution on the left-hand-side of (13.4) is easily computed by applying the layer ordering (13.17) and using (16.5). In doing that, corrections due to mode coupling with satellite harmonics are ignored and we get

$$\gamma^{2} \left[\frac{\partial}{\partial r} \left(\frac{\rho_{0}}{B_{0}^{\phi}} \xi_{\vartheta} \right) - \frac{\partial}{\partial \vartheta} \left(\frac{\rho_{0}}{B_{0}^{\phi}} \xi_{r} \right) \right]_{m} \approx \frac{iB_{0}}{mR_{0}} \frac{\gamma^{2}}{\omega_{A}^{2}} \frac{d^{2} \xi_{m}^{r}}{dx^{2}} - \frac{n}{m} \frac{p_{0}'}{R_{0} B_{0}^{2}} \frac{\eta_{0}}{r_{s}^{2} \gamma} \frac{d^{3}}{dx^{3}} (\sqrt{g} \tilde{B}^{r})_{m}.$$
 (16.6)

³ This procedure loosely follows the one employed in the derivation of the Mercier and ideal ballooning modes equation in sections 11.1 and 12.1.1.

Remember that we normalised $\mu_0 = 1$.

We now look at the right-hand-side of (13.4).

In the limit of large m and under the assumption of small shear, we approximate (7.55) as $P \approx \frac{R_0}{B_0} p_0'$ so that by means of (7.56), which is valid within both the ideal and resistive MHD framework, we write

$$\left(\sqrt{g}\mathbf{B}_{0}\cdot\nabla\frac{\tilde{J}^{\phi}}{B_{0}^{\phi}}-\sqrt{g}\mathbf{J}_{0}\cdot\nabla\frac{\tilde{B}^{\phi}}{B_{0}^{\phi}}\right)_{m} = \frac{nsx}{r_{s}mR_{0}}\left[\frac{d^{2}}{dx^{2}}(\sqrt{g}\tilde{B}^{r})_{m}\right] - m^{2}(\sqrt{g}\tilde{B}^{r})_{m} - m^{2}(\sqrt{g}\tilde{B}^{r})_{m}\right] - \frac{n}{m}\frac{p_{0}'}{R_{0}B_{0}^{2}}\frac{\eta_{0}}{r_{s}^{2}\gamma}\frac{d^{3}}{dx^{3}}(\sqrt{g}\tilde{B}^{r})_{m} - im\frac{R_{0}}{B_{0}^{3}}(p_{0}')^{2}\xi_{m}^{r}. \quad (16.7)$$

Notice that in the expression above we retained terms proportional to the plasma pressure, whereas contributions of the form $k_{||}C_m^{m'}$ have been neglected as they only yield small corrections to the term in square brackets on the right-hand-side; these are in fact proportional to the magnetic shear, and they become small when s is small. A similar argument is invoked to drop the term proportional to the equilibrium current gradient, that is the second one on the right-hand-side of (13.4).4

From equations (7.61), (7.63) and (12.11), we exploit once more the fact that Δp_m is negligible, so that the term involving the perturbed pressure is written as

$$\left(\sqrt{g} \nabla \phi \cdot \nabla \frac{1}{B_0^{\phi}} \times \nabla \tilde{p} \right)_m \approx i m \frac{p_0'}{B_0} \left[\frac{2r}{R_0} \left(1 - \frac{1}{q_s^2} \right) + \alpha - \frac{R_0 p_0'}{B_0^2} \right] \xi_m^r$$

$$+ \frac{i n^2 B_0 \alpha}{2m^2 R_0} \sum_{\pm} \left(m \xi_{m \pm 1}^r \pm \frac{d \xi_{m \pm 1}^r}{dx} \right) + \sum_{m' = \pm 1} E_m^{m'} (\Delta p),$$
 (16.8)

where, again, contributions scaling with s have been dropped thanks to the smallness of the magnetic shear. In analogy to the ideal case (see §12.3), we keep the contribution in the square brackets of (16.8), which, although smaller than other terms, plays an important role in determining ballooning stability at small shear.

It remains to compute $\sum_{m'=\pm 1} E_m^{m'}(\Delta p)$, and for this knowledge of $\Delta p_{m\pm 1}$ is required. By means of (13.22) and using (13.18) we approximate

$$B_0^2 \frac{\gamma^2}{\omega_A^2} \xi_{m\pm 1}^{\phi} = -\frac{p_0'}{B_0} \frac{\eta_0}{r_s^3 \gamma} \frac{d^2}{dx^2} (\sqrt{g} \tilde{B}^r)_{m\pm 1} \mp i \mu_s \Delta p_{m\pm 1}, \tag{16.9}$$

where $\mu_s = 1/q_s = n/m$. Note that this expression guarantees that the ideal results are recovered in the limit $\eta_0 \to 0$. The left-hand-side of this expression is expected to become important only in the narrow resistive layer around the resonance where the perturbation develops strong radial gradients. Hence, assuming that (16.2) holds, from (16.4) we order $\xi_m^{\phi} \sim \frac{1}{rB_0} (\sqrt{g} \tilde{B}^r)_m \sim \varepsilon \xi_m^r$ so that we may drop ξ_m^{ϕ} in (7.41) to obtain

$$\xi_{m\pm 1}^{\phi} \approx iq_s \left(\pm \frac{\Delta p_{m\pm 1}}{\Gamma p_0} - \frac{1}{mR_0} \frac{d\xi_m^r}{dx}\right).$$

Thus, plugging this expression of $\xi_{m\pm 1}^{\phi}$ into (16.9) gives (cf. (13.25))

$$\pm \Delta p_{m\pm 1} = \frac{B_0^2}{mR_0} \frac{q^2 \gamma^2}{\omega_A^2} \frac{d\xi_m^r}{dx} + i q_s \frac{p_0'}{B_0} \frac{\eta_0}{r_s^3 \gamma} \frac{d^2}{dx^2} (\sqrt{g}\tilde{B}^r)_{m\pm 1}, \qquad (16.10)$$

⁴ Notice that $\langle J_0^\phi/B_0^\phi\rangle'\sim s\varepsilon/r^2$, and, according to the results of §11.1 and §12.1, the factors $D_m^{m'}$ are also small.

having neglected terms proportional to $(\gamma/\omega_A)^2/\beta$ under the assumption that the growth rate is sufficiently small. Finally, from (7.63), we approximate

$$E_m^{\pm 1}(\Delta p) = \frac{i}{B_0} \left(\pm \frac{d\Delta p_{m\pm 1}}{dx} + m\Delta p_{m\pm 1} \right). \tag{16.11}$$

Thus, upon defining the variable z = mx and introducing the quantity $A = s\mu_s r_s B_0$, we combine equations (16.6)-(16.8), (16.10) and (16.11) to yield⁵

$$m^{2}\gamma_{H}^{2}\frac{d^{2}\xi_{m}^{r}}{dz^{2}} = -\frac{iz}{A}\left(\frac{d^{2}}{dz^{2}}(\sqrt{g}\tilde{B}^{r})_{m} - (\sqrt{g}\tilde{B}^{r})_{m}\right) + \left(\hat{U} + \frac{\alpha^{2}}{2s^{2}}\right)\xi_{m}^{r}$$

$$-\frac{\alpha}{2s^{2}}\sum_{\pm}\left(\xi_{m\pm1}^{r} \pm \frac{d\xi_{m\pm1}^{r}}{dz}\right)$$

$$+i\frac{\alpha}{2sA}\frac{m^{2}\eta_{0}}{r_{s}^{2}\gamma}\sum_{\pm}\left[\frac{d^{3}}{dz^{3}}(\sqrt{g}\tilde{B}^{r})_{m\pm1} \pm \frac{d^{2}}{dz^{2}}(\sqrt{g}\tilde{B}^{r})_{m\pm1}\right],$$
(16.12)

where γ_H and \hat{U} are defined respectively by (cf. (11.12) and (12.24))

$$\gamma_H^2 = \frac{\gamma^2 (1 + 2q_s^2)}{n^2 s^2 \omega_A^2}, \qquad \hat{U} = \frac{\alpha r_s}{s^2 R_0} \left(1 - \frac{1}{q_s^2} \right). \tag{16.13}$$

As in chapter 12, we refer to \hat{U} as the **Mercier contribution**. Equations (16.3) and (16.12) form the basis of the stability analysis for resistive ballooning and resistive interchange modes whose linear dynamics will be thoroughly investigated in the next two sections. It is worth to point out that these two equations have been written in such a way that they are valid both in the ideal and resistive layer regions.

16.2 Resistive ballooning modes

16.2.1 The eigenmode equation

The logic lying behind the analysis of resistive ballooning modes closely follows the one employed in chapter 12. This means that i) we deploy the assumption of **translational invariance** of the radial fluid displacement and magnetic perturbation expressed mathematically in a way similar to (12.25), and ii) we exploit this to write a single eigenmode equation in a convenient **Fourier space**. The growth rate is finally obtained through an asymptotic analysis of the resulting eigensolution.

Since m is large,⁶ the variable z appearing in (16.12) is allowed to vary from $-\infty$ to $+\infty$. Therefore, defining the **Fourier transform** of ξ_m^r and $(\sqrt{g}\tilde{B}^r)_m$ as in (13.30), from equations (16.3) and (16.12) we readily

⁵ Recall that all equilibrium quantities appearing in this expression need to be evaluated at r_s .

⁶ We actually take the $m \to \infty$ limit.

⁷ Recall that the translational invariance of a generic quantity X in the form of (12.25) implies that

$$\int_{-\infty}^{\infty} X_{m\pm 1}(z)e^{-ikz}dz = e^{\mp ik/s}X^*(k).$$

obtain⁷

$$\begin{split} \left(1+\bar{V}k^2\right) &\frac{\psi^*}{A} = \frac{d\xi^*}{dk}, \\ &\frac{d}{dk}\left((1+k^2)\frac{\psi^*}{A}\right) - \left[\hat{U} + \frac{\alpha^2}{2s^2} + m^2\gamma_H^2k^2 - \frac{\alpha}{s^2}\left(\cos\frac{k}{s} + k\sin\frac{k}{s}\right)\right]\xi^* \\ &- \frac{\alpha}{s}\bar{V}\left(k^3\cos\frac{k}{s} - k^2\sin\frac{k}{s}\right)\frac{\psi^*}{A} = 0, \end{split}$$

having introduced the quantity

$$\bar{V}=\frac{m^2\eta_0}{r_s^2\gamma}.$$

These two equations are combined together to finally give the **eigen-mode equation for resistive ballooning modes**:

$$\frac{d}{dk} \left(\frac{1+k^2}{1+\bar{V}k^2} \frac{d\xi^*}{dk} \right) - \left[\hat{U} + \frac{\alpha^2}{2s^2} + m^2 \gamma_H^2 k^2 - \frac{\alpha}{s^2} \left(\cos \frac{k}{s} + k \sin \frac{k}{s} \right) \right] \xi^* - \frac{\alpha}{s} \frac{\bar{V}k^2}{1+\bar{V}k^2} \left(k \cos \frac{k}{s} - \sin \frac{k}{s} \right) \frac{d\xi^*}{dk} = 0.$$
(16.14)

Notice that this equation is valid over the whole domain $-\infty < k < \infty$. Treating the magnetic shear as a small quantity, the dispersion relation, i.e. the growth rate, is obtained by performing a *double* **two scale analysis** for $k \lesssim 1$ and $k \gg 1$.

16.2.2 The growth rate

For the sake of simplicity and facilitate the algebra, we drop the Mercier contribution, that is we set $\hat{U} = 0$. Let us deploy the following ordering:

$$s \sim \delta^2$$
, $\alpha \sim \delta$, $\bar{V} \sim m^2 \gamma_H^2 \sim \epsilon_n^2 \sim \delta^4$,

where ϵ_{η} is some small parameter. Typically, resistive instabilities grow on much slower timescales compared to those of ideal modes, and this is reflected by our choice of the ordering of the growth rate.

When $k \sim 1$, exploiting the smallness of \bar{V} , we may drop the resistive terms and inertial contributions so that Eq. (16.14) is reduced to (12.30).⁸ Letting $\xi^* = X/[1+k^2]^{1/2}$ and expanding X as in (12.34), we follow the exact same techniques discussed in §12.3 to derive an equation for the non-oscillating (averaged) part of the eigenfunction $\xi_0^* = X_0/[1+k^2]^{1/2}$. This yields (cf. (12.37))

$$\frac{d}{dk}\left((1+k^2)\frac{d\xi_0^*}{dk}\right) + \frac{\lambda^2}{1+k^2}\xi_0^* = 0, \quad \lambda^2 = \frac{\alpha^2}{s} - \frac{7}{32}\frac{\alpha^4}{s^2}.$$

The associated even and odd solutions are (Strauss (1981))

$$\xi_{\text{even}}^* = \cos[\lambda \arctan(k)], \quad \xi_{\text{odd}}^* = \sin[\lambda \arctan(k)].$$

Compare this with (12.33)

⁸ This corresponds to considering the ideal region far from r_s in real space.

One then finds that for large k these behave as

$$\xi_{\text{even}}^* \propto 1 + \frac{\hat{\Delta}_{\ell}}{|k|},$$

$$\xi_{\text{odd}}^* \propto \left(1 + \frac{\hat{\Delta}_{0}}{|k|}\right) \operatorname{sgn}(k),$$
(16.15)

with the coefficients $\hat{\Delta}_{e}$ and $\hat{\Delta}_{o}$ defined by

$$\hat{\Delta}_e = \lambda \tan(\frac{\pi}{2}\lambda),$$

$$\hat{\Delta}_o = -\lambda \cot(\frac{\pi}{2}\lambda).$$

We now consider the large k limit where resistive corrections become important.⁹ After setting $k = \hat{k}/\epsilon_{\eta}$ with $\hat{k} \sim 1$, we define the "periodic" variable $\chi = k/s$ appearing in the arguments of the sine and cosine functions in equation (16.14) and write

$$\frac{d}{d\hat{k}} \left(\frac{\hat{k}^2 + \epsilon_{\eta}^2}{1 + \bar{V}\hat{k}^2 / \epsilon_{\eta}^2} \frac{d\xi^*}{d\hat{k}} \right) - \left[\frac{\alpha^2}{2s^2} + m^2 \gamma_H^2 \frac{\hat{k}^2}{\epsilon_{\eta}^2} - \frac{\alpha}{s^2} \left(\cos \chi + \frac{\hat{k}}{\epsilon_{\eta}} \sin \chi \right) \right] \xi^* - \frac{\alpha}{s} \frac{\bar{V}\hat{k}^2 / \epsilon_{\eta}^2}{1 + \bar{V}\hat{k}^2 / \epsilon_{\eta}^2} \left(\hat{k} \cos \chi - \epsilon_{\eta} \sin \chi \right) \frac{d\xi^*}{d\hat{k}} = 0.$$
(16.16)

We treat \hat{k} and χ as independent variables, thus allowing us to transform the differential operator $d/d\hat{k}$ into

$$\frac{d}{d\hat{k}} = \frac{\partial}{\partial \hat{k}} + \frac{1}{\epsilon_{\eta} s} \frac{\partial}{\partial \chi}.$$

In analogy with (12.34) we expand ξ^* as

$$\xi^* = \xi_0^*(k) + (\delta^3)\xi_1^*(k,\chi) + (\delta^5)\xi_2^*(k,\chi) + \dots,$$

where the order of ξ_i^* ($i=0,1,\ldots$) is given by the δ -coefficients in brackets. As in the analysis of ideal ballooning modes, we require that $\int_0^{2\pi} \xi_i^* d\chi = 0$ for $i \geq 1$. Hence, to the first two leading orders, (16.16) yields

$$\begin{split} &\frac{1}{\epsilon_{\eta}^{2}s^{2}}\frac{\hat{k}^{2}}{1+\bar{V}\hat{k}^{2}/\epsilon_{\eta}^{2}}\frac{\partial^{2}\xi_{1}^{*}}{\partial\chi^{2}}=-\frac{\alpha}{s^{2}}\frac{\hat{k}}{\epsilon_{\eta}}\xi_{0}^{*}\sin\chi,\\ &\frac{1}{\epsilon_{\eta}^{2}s^{2}}\frac{\hat{k}^{2}}{1+\bar{V}\hat{k}^{2}/\epsilon_{\eta}^{2}}\frac{\partial^{2}\xi_{2}^{*}}{\partial\chi^{2}}=-\frac{\alpha}{s^{2}}\xi_{0}^{*}\cos\chi. \end{split} \tag{16.17}$$

The integration of these two equations is trivial showing that $\xi_1^* \sim \sin \chi$ and $\xi_2^* \sim \cos \chi$. Now, taking into account the non-vanishing contributions, we find that at leading order the average in χ of (16.16) yields

$$\begin{split} \frac{\partial}{\partial \hat{k}} \left(\frac{\hat{k}^2}{1 + \bar{V}\hat{k}^2/\epsilon_{\eta}^2} \frac{\partial \xi_0^*}{\partial \hat{k}} \right) - \left[\frac{\alpha^2}{2s^2} + m^2 \gamma_H^2 \frac{\hat{k}^2}{\epsilon_{\eta}^2} \right] \xi_0^* + \frac{\alpha}{s^2} \frac{\hat{k}}{\epsilon_{\eta}} \langle \xi_1^* \sin \chi \rangle_{\chi} \\ - \frac{\alpha}{s^2} \frac{\bar{V}\hat{k}^3/\epsilon_{\eta}^3}{1 + \bar{V}\hat{k}^2/\epsilon_{\eta}^2} \langle \cos \chi \frac{\partial \xi_1^*}{\partial \chi} \rangle_{\chi} = 0, \end{split}$$

⁹ That is we are analysing the resistive layer region in real space.

$$\frac{\partial}{\partial \hat{k}} \left(\frac{\hat{k}^2}{1 + \bar{V}\hat{k}^2 / \epsilon_n^2} \frac{\partial \xi_0^*}{\partial \hat{k}} \right) - m^2 \gamma_H^2 \frac{\hat{k}^2}{\epsilon_n^2} \xi_0^* = 0.$$
 (16.18)

If one chooses $\epsilon_{\eta} = S^{-1/3}$, this equation is formally equivalent to (13.35). Correspondingly, the asymptotic small \hat{k} behaviour of the (*regular*) solution which is not diverging at infinity is determined by equation (13.41) where the replacement $k \to \hat{k}$ has to be performed.

we finally obtain the large-k averaged resistive ballooning equation

Therefore, matching the regular solution of (16.18) with (16.15) yields the dispersion relation

$$\frac{\hat{\Delta}_{e} + \frac{\hat{c}_{o}}{\hat{c}_{e}} \hat{\Delta}_{o}}{1 + \frac{\hat{c}_{o}}{\hat{c}_{e}}} = \frac{\Delta_{R}}{\epsilon_{\eta}} = \frac{\hat{\Delta}_{e} - \frac{\hat{c}_{o}}{\hat{c}_{e}} \hat{\Delta}_{o}}{1 - \frac{\hat{c}_{o}}{\hat{c}_{e}}}, \tag{16.19}$$

where Δ_R is given by (13.42) with V_e , Q and M_t defined in (13.36) and (13.38). Here \hat{c}_e and \hat{c}_o are constants multiplying ξ_{even}^* and ξ_{odd}^* , respectively, given by (16.15).

The expression above has the same structure of (11.31), and is solved by setting either $\hat{c}_o/\hat{c}_e=0$ or $\hat{c}_o/\hat{c}_e=\infty$. Therefore, in analogy to earlier calculations for ideal localised instabilities, we immediately find that resistive ballooning modes have **definite parity**: **even** perturbations have $\hat{c}_o/\hat{c}_e=0$, whereas **odd** ones are obtained by setting $\hat{c}_o/\hat{c}_e=\infty$. It follows that the growth rate for odd and even resistive ballooning modes is given by

$$\frac{M_t^{5/6}}{(1 - M_t)} \frac{\Gamma\left(\frac{M_t + 3}{4}\right)}{\Gamma\left(\frac{M_t + 5}{4}\right)} = \frac{2m}{c_0 S^{1/3}} \hat{\Delta}_o, \tag{odd},$$

$$=\frac{2m}{c_0 S^{1/3}}\hat{\Delta}_{e}, \qquad \text{(even)}, \qquad (16.21)$$

where $c_0 = (ns/\sqrt{1+2q_s^2})^{1/3}$. The behaviour of $\hat{\Delta}_e$ and $\hat{\Delta}_o$ as a function of α^2/s for positive shear is shown in figure 16.2. The ideal limit is obtained by letting $M_t \to \infty$ (care has to be taken when dealing with the odd solution and when λ becomes imaginary for the even one, see Strauss (1981)).

Now, analysing the linear stability of resistive odd modes, we see that the right-hand-side of (16.20) is small if S is large, so that the dispersion relation is analogous to the one which we obtained earlier for tearing perturbations. Hence odd parity resistive ballooning modes are unstable when $\hat{\Delta}_o > 0$, that is within the instability region of even ideal perturbations. We conclude that these modes are of minor relevance due to the fact that their instability window coincides with that of ideal balloonings, and because they grow on tearing-like timescales $(\gamma/\omega_A \sim S^{-3/5})$ which are much slower than those of ideal perturbations.

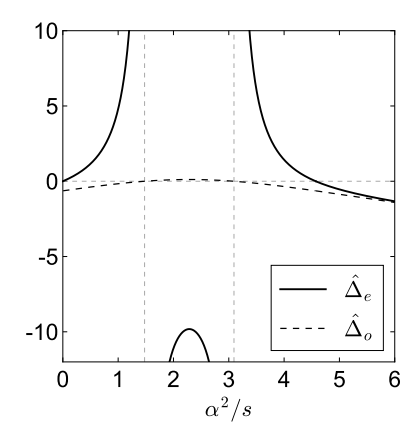


Figure 16.2: Parameters $\hat{\Delta}_{\ell}$ and $\hat{\Delta}_{\theta}$ versus α^2/s . The ideal ballooning marginal boundaries are denoted by the vertical lines (cf. (12.43)).

Resistive balloonings of even parity, instead, become unstable for

$$0 < \alpha^2/s < \frac{16}{7} \left(1 - \frac{\sqrt{2}}{4} \right),$$

and

$$\frac{16}{7}\left(1+\frac{\sqrt{2}}{4}\right) < \alpha^2/s < \frac{32}{7}$$

meaning that they are unstable throughout the whole first stability region as well as in a small portion of the second stability region of ideal balloonings. The quantity $\hat{\Delta}_{\ell}$ becomes very large when $\lambda \approx 1$, i.e. in proximity of the marginal boundary of ideal ballooning modes (these are identified by the relation $\lambda = 1$). It follows that the growth rate of the associated resistive instability is given by $M_t \approx 1$: this is basically equivalent to the dispersion relation of the m=1 resistive internal kink analysed earlier, yielding the fast scaling $\gamma/\omega_A \sim S^{-1/3}$. Sufficiently far from the ideal marginal boundaries, i.e. in the regions of stability of ideal ballooning modes, $\hat{\Delta}_{\ell}$ is of the order of unity and the structure of (16.21) becomes essentially equivalent to (14.20), yielding slow-growing perturbations with growth rates exhibiting a dependence upon the Lundquist number of the type $S^{-3/5}$, that is tearing-like.

The instability regions of resistive ballooning modes in the α -s plane are shown in Figure 16.3. We briefly point out that if **Mercier corrections** are taken into account, resistive stability can be greatly improved (Strauss (1981) and Correa-Restrepo (1982)), and the corresponding marginal boundaries are schematically depicted in Fig. 16.4. This stabilisation mechanism is associated with curvature effects in the resistive layer region, and is analogous to the one yielding the modified tearing stability criterion discussed in the next chapter.

16.3 Resistive interchange modes

As for ballooning instabilities, the analysis of resistive interchange modes is based on equation (16.12). Let r_s be the resonant point of the harmonic with poloidal and toroidal mode numbers m and n, respectively, such that $q(r_s) = m/n$ and assume that the magnetic shear is small. Differently from resistive balloonings, the analysis of interchange modes does not encompass more resonances other than r_s . We assume the mth harmonic is well localised about this point and its amplitude is taken to be much larger than the one of the sidebands with poloidal mode number $m \pm 1$.

This argument is corroborated by the fact that, if the radial extension of the mode m is proportional to 1/m (cf. (11.1)) and the separation between r_s and the resonances of the first neighbouring sidebands is $\frac{1}{sm}$ (cf. (12.4)), the smallness of the magnetic shear prevents the resonances

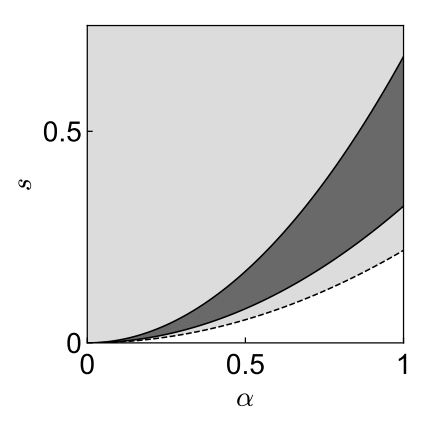


Figure 16.3: The area shaded in dark grey is unstable against ideal and odd resistive balloonings, while even resistive ballooning modes are found to be unstable in the region coloured in light grey.

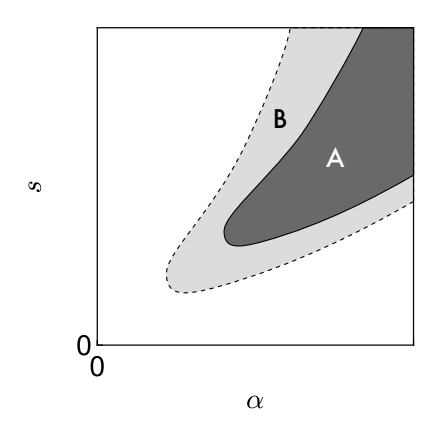


Figure 16.4: Instability regions for ideal (region A) and resistive ballooning modes (region B) of even parity when Mercier corrections are taken into account. The resistive marginal boundaries eventually coincide with the ideal ones if the resistivity is small enough.

of the satellite harmonics to occur in the vicinity of the region where the mode $m \gg 1$ is localised.

Hence, evaluating the $m \pm 1$ Fourier component of (13.18) in proximity of r_s yields

$$\xi_{m\pm 1}^r = \mp \frac{i}{\mu_s r_s B_0} \left(1 - \frac{m^2 \eta_0}{r_s^2 \gamma} \frac{d^2}{dz^2} \right) (\sqrt{g} \tilde{B}^r)_{m\pm 1}.$$

When this expression is plugged into (16.12) we obtain

$$m^{2} \gamma_{H}^{2} \frac{d^{2} \xi_{m}^{r}}{dz^{2}} = -\frac{iz}{A} \left(\frac{d^{2}}{dz^{2}} (\sqrt{g} \tilde{B}^{r})_{m} - (\sqrt{g} \tilde{B}^{r})_{m} \right) + \left(\hat{U} + \frac{\alpha^{2}}{2s^{2}} \right) \xi_{m}^{r} + i \frac{\alpha}{2sA} \sum_{+} \left[\frac{d}{dz} (\sqrt{g} \tilde{B}^{r})_{m\pm 1} \pm (\sqrt{g} \tilde{B}^{r})_{m\pm 1} \right].$$
 (16.22)

We now assume that ordering (7.37) holds. Thus exploiting the smallness of the toroidal component of the perturbed magnetic field and using (7.25), we find that the $m \pm 1$ projections of (13.10) can be approximated to leading orders as $(cf. (11.13))^{10}$

$$\left(\frac{d^2(\sqrt{g}\tilde{B}^r)_m}{dz^2} - (\sqrt{g}\tilde{B}^r)_m\right) = i(\mu r_s B_0) \frac{\alpha}{2} \left(\frac{d\xi_m^r}{dz} \mp \xi_m^r\right),$$
(16.23)

having dropped, as usual, contributions due to Δp_m .

In analogy to what we did for ideal Mercier modes, we integrate the expression above once and set to zero the constants of integration to guarantee localisation of ξ_m^r . Upon combining (16.22) and the solution of (16.23), we transform to k-space (cf. (13.30)) the resulting expression to obtain the following **eigenmode equation for resistive interchange modes**

$$\frac{d}{dk} \left(\frac{1+k^2}{1+\bar{V}k^2} \frac{d\xi^*}{dk} \right) - \left(\hat{U} + m^2 \gamma_H^2 k^2 \right) \xi^* = 0.$$
 (16.24)

Equation (16.24) is studied by performing a **two scale analysis** in a similar fashion to what has been discussed in the preceding section, where here retaining the Mercier contribution proves to be essential. We point out that for $\bar{V} \to 0$, Eq. (16.24) is equivalent to the Fourier transform of (11.14) where the small inertial contributions which are not multiplied by k^2 are dropped (these have been indeed proved to be unimportant for determining ideal stability).

16.3.1 $k\lesssim 1$ eigenfunction

Let us first consider the $k \lesssim 1$ region, for which inertial and resistive effects can be ignored. In such a case, equation (16.24) reduces to

$$\frac{d}{dk}\left((1+k^2)\frac{d\xi^*}{dk}\right) - \hat{U}\xi^* = 0.$$
 (16.25)

Noticing that this has exactly the same structure of (11.24), we introduce the quantity ν as defined in (11.20) which is

$$v = \sqrt{\frac{1}{4} + \hat{U}}.$$

¹⁰ This is analogous to the derivation presented in section 7.5.2.

The system is supposed to be stable against Mercier modes so that we take $0 < \nu < 1$. We refer to the solution of (16.25) as the **ideal solution** and its asymptotic behaviour for large k is immediately found from (11.30) giving

$$\xi^* \propto |k|^{-\frac{1}{2}-\nu} \left(1 + \frac{c_e \Delta_e + c_o \Delta_o}{c_e + c_o} |k|^{2\nu} \right), \quad k > 0,$$

$$\propto |k|^{-\frac{1}{2}-\nu} \left(1 + \frac{c_e \Delta_e - c_o \Delta_o}{c_e - c_o} |k|^{2\nu} \right), \quad k < 0,$$
(16.26)

where Δ_{e} and Δ_{o} are defined in (11.29) and c_{e} and c_{o} are some constants multiplying the even and odd solutions respectively. We point out that when $\nu > 1$, the asymptotic behaviour of the solution of (16.25) is not given by Eq. (16.26) anymore leading to important consequences which will be discussed later.¹¹

To obtain the dispersion relation it remains to analyse the solution in the large k region: this requires few mathematical manipulations which are detailed in the next subsection.

16.3.2 $k \gg 1$ eigenfunction

We first write $\hat{U} = \tau(\tau + 1)$ choosing

$$\tau = -\frac{1}{2} + \nu. \tag{16.27}$$

Since 0 < v < 1, τ varies between -1/2 and 1/2. We assume that k is large and introduce the variable $\hat{k} = k/S^{1/3}$ such that \hat{k} is taken to be of the order of unity. Contrary to the $k \sim 1$ case, we retain resistive and inertial effects, so that (16.24) can be approximated as

$$\frac{d}{d\hat{k}} \left(\frac{\hat{k}^2}{1 + V_e \hat{k}^2} \frac{d\xi^*}{d\hat{k}} \right) - \left(\tau(\tau + 1) + Q\hat{k}^2 \right) \xi^* = 0, \tag{16.28}$$

where V_e and Q are defined in (13.36). Repeating the procedure outlined in §13.4, we define the variable $\zeta = M_t V_e \hat{k}^2$ with M_t given by (13.38) and write $\xi^* = \zeta^{\tau/2} e^{-\zeta/2} Y(\zeta)$. After some algebra, equation (16.28) becomes (cf. (13.37))

$$\zeta \frac{d^2 Y}{d\zeta^2} + \left(\frac{1}{2} + \tau - \zeta + \frac{1}{1 + \zeta/M_t}\right) \frac{dY}{d\zeta} - \left(h + \frac{1 + \tau/M_t}{2(1 + \zeta/M_t)}\right) Y = 0, \quad (16.29)$$

having defined

$$h = \frac{(M_t + \tau)(M_t + \tau + 1)}{4M_t}.$$

Following Correa-Restrepo (1982), we write

$$Y = \frac{d\mathscr{U}}{d\zeta} - \frac{2h}{M_t + \tau}\mathscr{U},$$

¹¹ Let p_i (i=0,1,...) some constants. By means of (11.28), for v>1 not an integer such that $v\neq 3/2$ the behaviour of ξ^* in the large k limit for both the even and odd solution is

$$\xi^* \propto |k|^{\nu - 1/2} \left(1 + p_0/k^2 \right), \quad (*)$$

while if v = 3/2 we have

$$\xi_{\text{even}}^* \propto k + \frac{p_1}{k^2}, \quad \xi_{\text{odd}}^* \propto k.$$

Let now ν be a positive integer and instead of (11.28) use the transformation formula

$$F(a, b; c; z) = (1 - z)^{-a} F(a, c - b; c; \frac{z}{z - 1}),$$

with $|\arg(1-z)| < \pi$. Also in this case even and odd solutions behave similarly: when $\nu = 2, 3, \ldots$ we find the same asymptotics as in (*), whereas for $\nu = 1$ one has

$$\xi^* \propto |k|^{1/2} \left(1 + \frac{p_2}{k^2} (1 + p_3 \ln |k|) \right).$$

and find that the function $\mathscr U$ obeys **Kummer's equation** (see the box at the end of the chapter)

$$\zeta \frac{d^2 \mathcal{U}}{d\zeta^2} + \left(\frac{1}{2} + \tau - \zeta\right) \frac{d \mathcal{U}}{d\zeta} - h \mathcal{U} = 0, \tag{16.30}$$

whose solutions are written in terms of the **confluent hypergeometric** functions M and U (we follow the notation of Abramowitz and Stegun (1964)). Thus, the solution of (16.28) for $\hat{k} > 0$ which does not diverge at infinity is

$$\xi^* = \zeta^{\tau/2} e^{-\zeta/2} \left[U \left(h + 1, \tau + \frac{3}{2}, \zeta \right) + \frac{2}{M_t + \tau} U \left(h, \tau + \frac{1}{2}, \zeta \right) \right]. \quad (16.31)$$

Even and odd solutions are constructed in the domain $-\infty < k < \infty$ by setting $\xi^*(-k) = \xi^*(k)$ and $\xi^*(-k) = -\xi^*(k)$ (see §13.4).

Eventually, the asymptotic behaviour of ξ^* when \hat{k} approaches zero is readily obtained:

$$\xi^* \propto |\hat{k}|^{\tau} \left[1 + (M_t V_e)^{-1/2 - \tau} \frac{\Gamma\left(\frac{1}{2} + \tau\right)}{\Gamma\left(-\frac{1}{2} - \tau\right)} \left(\frac{M_t + \tau}{M_t - 1 - \tau} \right) \times \frac{\Gamma\left(\frac{1}{4}(M_t + 3 - 2\tau + \tau(\tau + 1)/M_t)\right)}{\Gamma\left(\frac{1}{4}(M_t + 5 + 2\tau + \tau(\tau + 1)/M_t)\right)} |\hat{k}|^{-1 - 2\tau} \right].$$

The **dispersion relation** is finally obtained by matching this expression with (16.26). Similar to ideal Mercier and resistive ballooning modes, resistive interchange instabilities exhibit definite parity, either even or odd, and the growth rate conforms to

$$(M_t V_e)^{-\frac{1}{2}-\tau} \left(\frac{M_t + \tau}{M_t - 1 - \tau} \right) \frac{\Gamma\left(\frac{1}{4}(M_t + 3 - 2\tau + \tau(\tau + 1)/M_t)\right)}{\Gamma\left(\frac{1}{4}(M_t + 5 + 2\tau + \tau(\tau + 1)/M_t)\right)}$$

$$= \frac{\Gamma^2(1 - \nu)\Gamma^2(\frac{t}{4} + \frac{\nu}{2})}{\Gamma^2(1 + \nu)\Gamma^2(\frac{t}{4} - \frac{\nu}{2})} S^{-2\nu/3}, \qquad (16.32)$$

where t = 1 for even modes and t = 3 for the odd ones.¹²

Before embarking on the analysis of the dispersion relation, we remark that when $\tau \geq 1/2$, that is $\nu \geq 1$ the small k expansion of (16.31) yields

$$\xi^* \propto |k|^{-3/2} \left(1 + a_0 (1 + a_1 \ln |k|) k^2 \right), \qquad (\tau = 1/2),$$

 $\propto |k|^{-1/2 - \nu} \left(1 + a_2 k^2 \right), \qquad (\tau > 1/2),$

with a_i (i=0,1,2) some constants. By comparing with the asymptotic behaviour of the ideal solution described in the **sidenote 11** in this chapter, one comes to the conclusion that, generally, it is not possible to match the solutions of (16.25) and (16.28). This means that no unstable modes can be constructed for $\tau \ge 1/2$ (Correa-Restrepo (1982)).

¹² The dispersion relation for ideal Mercier modes is easily recovered by taking $M_t \to \infty$.

16.3.3 Growth rate and stability boundary

Assume that τ is sufficiently far away from either -1/2 or 1/2. In the limit of S large and ν not too small, the right-hand-side of (16.32) is a very small number. Therefore, this relation is satisfied when M_t fulfils the following condition¹³

$$M_t + 1 + 2\tau + \tau(\tau + 1)/M_t = -4\ell, \quad \ell = 0, 1, 2, \dots$$
 (16.33)

The most unstable case is associated with the $\ell=0$ level and gives $M_t=-\tau$ which, by means of (14.19), yields the growth rate

$$\frac{\gamma}{\omega_A} = \left(\frac{-s\,n\tau}{\sqrt{1+2q_s^2}}\right)^{2/3} S^{-1/3},\tag{16.34}$$

where we recall that $q_s = m/n$. One sees that a growing instability requires $\tau < 0$. We can be slightly more precise on the estimation of the growth rate. Assume $-1/2 < \tau < 0$ with τ neither too small nor too close to -1/2, and formally write (16.32) as $f(M_t) = S^{-2\nu/3}/\Delta_{RI}(t) \ll 1$ where

$$\Delta_{RI}(t) = \frac{\Gamma^2 (1+\nu) \Gamma^2 (\frac{t}{4} - \frac{\nu}{2})}{\Gamma^2 (1-\nu) \Gamma^2 (\frac{t}{4} + \frac{\nu}{2})}.$$
 (16.35)

By performing a series expansion of $f(M_t)$ around $M_t = -\tau$ we obtain

$$M_t = - au - rac{2
u m^{2
u}}{\Gamma(1-
u)} rac{(- au)^{
u/3}}{\Delta_{RI}(t)} \Biggl(rac{\sqrt{1+2q_s^2}}{nsS}\Biggr)^{2
u/3}.$$

Since $\Delta_{RI}(1) > \Delta_{RI}(3)$ as shown in figure 16.5, we find that even modes grow faster than the odd ones, although their growth rates differ by a rather small amount.

If $\tau = 0$, the right-hand-side of (16.32) is still a small number, being actually zero for even modes due to the divergence of the Gamma function at $\nu = 1/2$. Therefore, Eq. (16.32) can be reduced to a form which is equivalent to the dispersion relation of tearing perturbations, that is (cf. (14.20))

$$\left(\frac{\gamma}{\omega_A}\right)^{5/4} = -\frac{m}{\Delta_{RI}} \frac{\Gamma\left(\frac{5}{4}\right)}{\Gamma\left(\frac{3}{4}\right)} \sqrt{\frac{ns}{(1+2q_s^2)^{1/2}}} S^{-3/4}.$$
(16.36)

Because $\Delta_{RI} > 0$ for odd modes, we conclude that no instability develops when $\tau = 0$. We thus infer that resistive interchange modes, either even or odd, only occur when $\tau < 0$.

A more general case in which the magnetic shear is allowed to be of the order of unity will be briefly discussed in the next chapter. ¹³ There are actually two solubility conditions, that is

$$\begin{split} M_t + \tau &= 0, \\ M_t + 1 + 2\tau + \tau(\tau+1)/M_t &= -4\ell, \end{split}$$

with $\ell = 1, 2, \dots$ For the second one we used the fact that $5 + 4\ell = 4(\ell + 1) + 1$. These can be combined to yield (16.33).

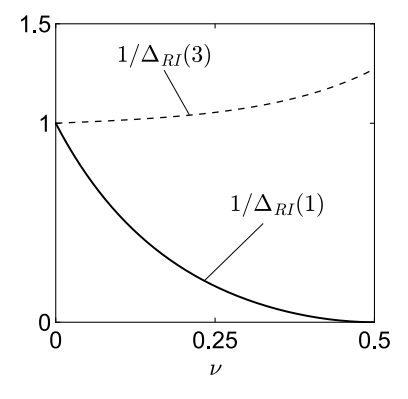


Figure 16.5: Values of the inverse of $\Delta_{RI}(t)$ for t=1 (even modes) and t=3 (odd modes) as function of the parameter $0 < \nu < 1/2$ which corresponds to $-1/2 < \tau < 0$.

On the solution of equation (16.29)

We first note that if \hat{L} is a differential operator in the variable ζ and the function $\mathscr U$ is such that $\hat{L}\mathscr U=0$, then the following relation holds

$$\frac{d}{d\zeta}\hat{L}\mathcal{U} + f(\zeta)\hat{L}\mathcal{U} = 0, \qquad (16.37)$$

with $f(\zeta)$ a generic function. Upon writing \hat{L} as

$$\hat{L} = \zeta \frac{d^2}{d\zeta^2} + (A - \zeta) \frac{d}{d\zeta} - B, \qquad (16.38)$$

with A and B some constants, equation (16.37) becomes

$$\zeta \frac{d^3 \mathcal{U}}{d\zeta^3} + \left[A + 1 - \zeta + \zeta f(\zeta) \right] \frac{d^2 \mathcal{U}}{d\zeta^2} - \left[B + 1 + f(\zeta)(\zeta - A) \right] \frac{d \mathcal{U}}{d\zeta} - Bf(\zeta) \mathcal{U} = 0.$$
 (16.39)

Now, letting $Y = e^{a\zeta} \frac{d}{d\zeta} \left(e^{-a\zeta} \mathcal{U} \right) = \frac{d\mathcal{U}}{d\zeta} - a\mathcal{U}$ where a is some number, equation (16.29) then reads

$$\zeta \frac{d^{3} \mathcal{U}}{d\zeta^{3}} + \left[\frac{1}{2} + \tau - (a+1)\zeta + \frac{1}{1+\zeta/M_{t}} \right] \frac{d^{2} \mathcal{U}}{d\zeta^{2}} \\
- \left[a \left(\frac{1}{2} + \tau - \zeta + \frac{1}{1+\zeta/M_{t}} \right) + h + \frac{1+\tau/M_{t}}{2(1+\zeta/M_{t})} \right] \frac{d \mathcal{U}}{d\zeta} \\
+ a \left[h + \frac{1+\tau/M_{t}}{2(1+\zeta/M_{t})} \right] \mathcal{U} = 0.$$
(16.40)

A quick comparison between (16.39) and (16.40) shows that

$$A = \frac{1}{2} + \tau, \quad B = h, \quad a = \frac{2h}{M_t + \tau},$$

$$f(\zeta) = -\frac{1}{M_t} \left(\frac{M_t + \tau + 1}{2} + \frac{1}{1 + \zeta/M_t} \right).$$

Equation (16.30) then follows from (16.38).

References

- M. Abramowitz and I. A. Stegun (eds.), Handbook of Mathematical Functions, Dover Publications (New York, US), 1964.
- A. V. Chankin and G. Saibene, Plasma Phys. Control. Fusion 41, 913 (1999).
- J. W. Connor, Plasma Phys. Control. Fusion 40, 531 (1998).
- B. Coppi et al., Nucl. Fusion 6, 101 (1966).
- D. Correa-Restrepo, Z. Naturforsch. A 37, 848 (1982).
- D. Correa-Restrepo, Plasma Phys. Control. Fusion 27 565 (1985).

- A Erdélyi (ed.), Higher Transcendental Functions Volume I, McGraw-Hill Book Company (New York, US), 1953.
- G. Y. Fu et al., Phys. Fluids B 2, 2623 (1990).
- M. Furukawa et al., Nucl. Fusion 39, 2077 (1999).
- A. H. Glasser et al., Phys. Fluids 18, 875 (1975).
- R. J. Hastie et al., Phys. Plasmas 10, 4405 (2003).
- A. W. Leonard, Phys. Plasmas 21, 090501 (2014).
- A. B. Mikhailovskii, Instabilities in a Confined Plasma, Institute of Physics Publishing (Bristol, UK), 1998.
- R. Sartori et al., Plasma Phys. Control. Fusion 46, 723 (2004).
- A. Sykes et al., Plasma Phys. Control. Fusion 29, 719 (1987).
- H. R. Strauss, Phys.Fluids 24, 2004 (1981).
- H. Zohm, Plasma Phys. Control. Fusion 38, 105 (1996).

17

Curvature effects in the resistive layer

So far, toroidicity effects, apart from those yielding inertia enhancement, have been taken into account, in a rather approximate manner and for the very specific case of small magnetic shear, only for the analysis of resistive ballooning and resistive interchange modes. In contrast, the non-ideal stability of tearing and m = 1 kink modes has been basically carried out in the cylindrical limit. However, toroidal corrections, also known as **curvature effects**, play an important role in the determination of resistive stability, thence we need to devise an alternative procedure to properly include them independently of the strength of the magnetic shear.

In deriving the resistive layer equations presented in chapter 13 the magnitude of the radial gradients of the perturbations was assumed to be of the order of the inverse aspect ratio. Within this approximation, by retaining the leading order contributions only, most of the effects induced by toroidicity have been missed.

The alternative strategy, which guarantees that curvature effects are properly included, is to introduce an additional smallness parameter δ much smaller than ε , the inverse aspect ratio, and let the radial derivatives of perturbed quantities to be as large as $1/\delta$. Assuming this to hold, then i) the resistive MHD equations are expanded in δ , and ii) a further expansion in ε to second order is performed (when needed) yielding, formally, expressions of the form

$$(f + \varepsilon^2 g + \ldots) + o(\delta) = 0.$$

If δ is small enough, all the relevant physics is contained in the dominant term in δ , and toroidal corrections enter the equations to order ε^2 .

Having outlined the skeleton of the procedure we want to adopt, this

A more general derivation of the resistive layer equations is given in appendix ${\bf F}$

$$\omega_A^{-1} = \tau_A = R_0 \sqrt{\rho}/B_0.$$

The estimation of the thickness of the inertial-resistive layer given by (13.29) suggests that, for $s, m, n \sim 1$ and typical tokamak values of the Ludquist number, the smallness parameter δ has to be much smaller than ε .

chapter is organised as follows: we first introduce the resistive layer ordering for the perturbed pressure, fluid displacement and magnetic field. Subsequently, a set of simplified expressions for some relevant physical quantities are obtained. We then proceed to write the induction and vorticity equations in a form similar to (13.27) and (13.28) but augmented by toroidal effects. These equations are equivalent to the ones known in the literature as the **Glasser-Greene-Johnson** (or **GGJ** in short) equations, but computed in the limit of large aspect ratio for a circular tokamak. Following the same procedure presented in §13.4, we merge these equations into a single one by transforming them in Fourier space. Modifications to stability due to curvature effects will be finally discussed for some of the resistive perturbations analysed in earlier chapters.

17.1 Toroidal layer orderings

We consider a low- β plasma such that $\beta \sim \varepsilon^2$. The equilibrium is assumed, for the sake of simplicity, to be **up-down symmetric** as described in chapter 5. Perturbations depend on time and on the toroidal angle as $\exp(\gamma t - in\phi)$ with n denoting, as usual, the toroidal mode number. Let r_s be radial position where $q(r_s) = m/n \equiv q_s$ with m and n both positive.

As discussed in chapter 13, we allow resistive effects to become important only in a narrow region close to the resonance r_s where perturbations are expected to develop large radial gradients. Upon introducing the parameter δ , and letting resistive perturbations to grow on much slower timescales than those of ideal modes, we deploy the following ordering (cf. (13.17))

$$\gamma/\omega_A \sim \delta, \quad \frac{r - r_s}{r_s} = x \sim \frac{\delta}{m},$$

$$r\frac{d}{dr} \sim \frac{m}{\delta}, \quad \frac{\eta_0}{\gamma} \frac{d^2}{dr^2} \sim 1, \quad \delta \ll \varepsilon^2,$$
(17.1)

where the ordering of the radial derivatives is assumed to hold when these are acting on perturbed quantities. As usual, η_0 denotes the equilibrium resistivity. From this, in a neighbourhood of r_s the parallel wave vector can be approximated as $k_{||} = m\mu - n \approx -nsx \sim \delta$ where s is the magnetic shear at the position of the resonance. Besides, we take the numbers m and n to be as large as $1/\varepsilon$ at most. Finally, in the remainder of this chapter equilibrium quantities are implicitly supposed to be evaluated at the resonance r_s .

We now assume that in the thin layer around the resonance the radial component of the fluid disturbance is dominated by the harmonic with poloidal mode number m so that we take

$$\xi_{m+\ell}^r \sim \delta \varepsilon^\ell \xi_m^r. \tag{17.2}$$

The reason for the multiplicative factor proportional to ε can be intuitively motivated by the fact that the poloidal spectrum is expected to

be centred about the *m*th harmonic, with the magnitude of higher order modes coupled through toroidicity gradually decreasing with some powers of the inverse aspect ratio.

Since the divergence of the magnetic field is zero, we conveniently order

$$(\sqrt{g}\tilde{B}^{\vartheta})_{m} \sim (\sqrt{g}\tilde{B}^{\phi})_{m} \sim \frac{1}{r\delta}(\sqrt{g}\tilde{B}^{r})_{m} \sim B_{0}\xi_{m}^{r},$$

$$(\sqrt{g}\tilde{B}^{\vartheta})_{m\pm\ell} \sim (\sqrt{g}\tilde{B}^{\phi})_{m\pm\ell} \sim \frac{1}{r\delta}(\sqrt{g}\tilde{B}^{r})_{m\pm\ell} \sim \varepsilon^{\ell}B_{0}\xi_{m}^{r},$$

$$(17.3)$$

whereas the magnitudes of the poloidal and toroidal projections of the fluid perturbation are

$$\xi_{m}^{\vartheta} \sim \xi_{m}^{\phi} \sim \frac{1}{r\delta} \xi_{m}^{r},$$

$$\xi_{m \pm \ell}^{\vartheta} \sim \xi_{m \pm \ell}^{\phi} \sim \frac{\varepsilon^{\ell}}{r\delta} \xi_{m}^{r}.$$
(17.4)

The consistency of these orderings will later be evident.

The left-hand-side of the parallel projection of the perturbed momentum equation, that is Eq. (13.22), is of order $\delta B_0^2 \xi_m^r$ at most, hence by taking the m and $m \pm \ell$ Fourier components of this equation we have

$$\tilde{p}_m \sim B_0^2 \xi_m^r, \quad \tilde{p}_{m \pm \ell} \sim \delta B_0^2 \xi_m^r / r.$$
 (17.5)

In particular, by balancing each of the terms appearing in the mth projection of (13.22) such that they have comparable magnitude, we can further refine the ordering of the compressible part of the pressure and the toroidal projection of the fluid displacement as

$$\Delta p_m \sim \varepsilon^2 B_0^2 \xi_m^r / r, \quad \xi_m^\phi \sim \frac{\varepsilon^2}{r \delta} \xi_m^r.$$
 (17.6)

The latter will be proven to hold a posteriori.

Now, for many calculations, it is more convenient to express a generic perturbed quantity \tilde{f} as a sum of a **resonant** and **non-resonant** part, that is

$$\tilde{f} = e^{im\vartheta - in\phi} \left(\tilde{f}_m(r) + \tilde{f}_{NR}(r,\vartheta) \right),$$

with the subscript NR standing for non-resonant. Explicitly, one has

$$\tilde{f}_{NR}(r,\vartheta) = \sum_{\ell \neq 0} \tilde{f}_{m+\ell}(r)e^{i\ell\vartheta}.$$
 (17.7)

This sum is assumed to be convergent, and because of this we may order

$$\tilde{f}_{NR} \sim \text{the largest of } \tilde{f}_{m+\ell} \text{ with } \ell \neq 0.$$
 (17.8)

It is evident that, by definition, $\langle \tilde{f}_{NR} \rangle = 0$ where angular brackets denote the poloidal average as defined by (5.18). With this decomposition of the perturbation, the action of the parallel gradient reads

$$e^{-im\vartheta+in\phi}\frac{\sqrt{g}}{f_0'}\boldsymbol{B}_0\cdot\boldsymbol{\nabla}\tilde{f}=i(m\mu-n)\left(\tilde{f}_m+\tilde{f}_{NR}\right)+\mu\frac{\partial\tilde{f}_{NR}}{\partial\vartheta}.$$
 (17.9)

Note that for a generic quantity A one has

$$A_{m} = \langle e^{-im\vartheta + in\phi} A \rangle,$$

$$A_{NR} = e^{-im\vartheta + in\phi} A - A_{m}.$$

The programme of the next sections is to apply the orderings above to work out the expressions of some physical quantities to be employed in the derivation of the resistive layer dynamical equations, specifically for the radial component of the fluid displacement and the magnetic perturbation of the resonant Fourier harmonic.

17.2 Fields, displacements and pressure

To achieve the aforementioned objective, knowledge is needed about some auxiliary quantities, such as the form of the fluctuation of the toroidal field or the non-resonant contribution to the perturbed pressure. This section is therefore devoted to work out these expressions. To keep the algebra sufficiently clear, we carry out the analysis for the toroidal field, fluid displacements and perturbed pressure separately.

17.2.1 Perturbed magnetic field

Exploiting (17.5), we see that the leading contribution (in δ) to the $m \pm \ell$ Fourier projection of equation (13.10) reads

$$\mu(\sqrt{g}\tilde{J}^{\phi})_{m\pm\ell} + (1/B_0^{\phi})_{\ell} \tilde{p}'_m = 0, \tag{17.10}$$

with the perturbed toroidal current written as (cf. (13.11))

$$(\sqrt{g}\tilde{J}^{\phi})_{m\pm\ell} = \langle N \rangle (\sqrt{g}\tilde{B}^{\vartheta})'_{m\pm\ell} + \sum_{m'\neq 0} N_{m'} (\sqrt{g}\tilde{B}^{\vartheta})'_{m\pm\ell-m'}, \tag{17.11}$$

having employed the notation of §5.3 to denote the metric coefficients. Only the $m\pm 1$ components are needed, so that combining (17.10) and (17.11) and keeping the dominant terms in ε produces

$$\langle N \rangle (\sqrt{g}\tilde{B}^{\vartheta})'_{m\pm 1} = -[N_1(\sqrt{g}\tilde{B}^{\vartheta})_m + q(1/B_0^{\phi})_1 \,\tilde{p}_m]'.$$
 (17.12)

By integrating this equation, a constant would appear which, to conform to (17.3), is ordered as $\varepsilon B_0 \xi_m^r$. We set this constant to zero for the moment (we will elaborate later on the consequences of having this quantity not vanishing) and write

$$Y \equiv (\sqrt{g}\tilde{B}^{\vartheta})_{m\pm 1} = -\frac{N_1}{\langle N \rangle} (\sqrt{g}\tilde{B}^{\vartheta})_m - q \frac{(1/B_0^{\varphi})_1}{\langle N \rangle} \tilde{p}_m \sim \varepsilon B_0 \xi_m^r.$$
 (17.13)

After selecting the mth Fourier component of (13.9) and using (17.5) to drop contributions from the satellite harmonics to the perturbed pressure, we obtain

$$\begin{split} 0 &= -im \langle \frac{1}{B_0^{\phi}} \rangle \tilde{p}_m - imG(\sqrt{g}\tilde{B}^{\phi})_m - in \langle N \rangle (\sqrt{g}\tilde{B}^{\vartheta})_m \\ &- in \sum_{m' \neq 0} N_{m'} (\sqrt{g}\tilde{B}^{\vartheta})_{m-m'}, \end{split}$$

Thanks to the up-down symmetry, we have $(1/B_0^\phi)_\ell = (1/B_0^\phi)_{-\ell}$. Analogous arguments apply to other quantities.

 $^{^1}$ Contributions coming from other harmonics are ε times smaller and so they are dropped.

which is exact at leading order in δ . Thus, using (17.13) and retaining the dominant corrections in ε yields

$$(\sqrt{g}\tilde{B}^{\phi})_{m} \approx -\frac{r\tilde{p}_{m}}{B_{0}} + \mu \frac{r^{2}}{R_{0}^{2}} \frac{(\sqrt{g}\tilde{B}^{r})'_{m}}{im},$$
 (17.14)

which easily shows that $(\sqrt{g}\tilde{B}^{\phi})_m \sim \varepsilon^2 B_0 \xi_m^r$.

Now, by means of the orderings discussed in §17.1, the $m \pm \ell$ Fourier projection of (13.9) is written as

$$0 = m \left(\frac{1}{B_0^{\phi}}\right)_{\ell} \tilde{p}_m + (m \pm \ell) G(\sqrt{g}\tilde{B}^{\phi})_{m \pm \ell}$$

$$+ n \langle N \rangle (\sqrt{g}\tilde{B}^{\vartheta})_{m \pm \ell} + n \sum_{m' \neq 0} N_{m'} (\sqrt{g}\tilde{B}^{\vartheta})_{m \pm \ell - m'},$$

$$(17.15)$$

where use of (17.5) has been made again. Plugging (17.10) and (17.11) into this expression dictates that the perturbation of the toroidal field associated with the non-resonating harmonics scales as $\varepsilon^3 B_0 \xi_m^r$ at most, therefore we can set

$$(\sqrt{g}\tilde{B}^{\phi})_{m\pm\ell} = 0. \tag{17.16}$$

Thus, under the assumption that (17.8) holds, we conveniently write $(\sqrt{g}\tilde{B}^{\phi})_{\rm NR}=0$. We point out that if the constant of integration in (17.13) is allowed we end up with the following modified expressions of the perturbed toroidal field

$$(\sqrt{g}\tilde{B}^{\phi})_{m\pm\ell} = const, (\sqrt{g}\tilde{B}^{\phi})_{NR} = D(\vartheta),$$
 (17.17)

where D is a function of the poloidal angle.

17.2.2 Poloidal and toroidal displacements

Let us assume that (17.8) holds, i.e. the magnitude of the non-resonant part of the perturbation is the same as the one of the non-resonant Fourier harmonic of lowest order (in ε). Thus, we employ the orderings (17.2)-(17.5) and (17.8) to write

$$\tilde{p}_{NR} \sim \delta B_0^2 \xi_m^r / r, \quad \xi_{NR}^r \sim \delta \varepsilon \xi_m^r,$$

$$\xi_{NR}^{\vartheta} \sim \xi_{NR}^{\varphi} \sim \frac{\varepsilon}{r \delta} \xi_m^r.$$
(17.18)

Owing to the smallness of the toroidal perturbation of the magnetic field (see (17.14) and (17.16)), we take the m and $m \pm \ell$ projections of equation (13.19), which for our purposes proves to be accurate enough, yielding to leading order (in δ)

$$\xi_{m}^{\vartheta} = \mu \xi_{m}^{\phi} - \frac{1}{i m f_{0}^{r}} \frac{d(f_{0}^{r} \xi_{m}^{r})}{dr} + o(\varepsilon^{2} \xi_{m}^{r}/r),$$

$$\xi_{m \pm \ell}^{\vartheta} - \mu \xi_{m + \ell}^{\phi} = o(\varepsilon^{\ell} \xi_{m}^{r}/r).$$
(17.19)

When $m \pm \ell = 0$ with m > 0 we need to be more careful. One first notices that, by means of (17.5), equation (17.15) gives

$$0 = m \left(\frac{1}{B_0^{\phi}}\right)_{-m} \tilde{p}'_m + n(\sqrt{g}\tilde{J}^{\phi})_0. \quad (\clubsuit)$$

We now take the covariant radial projection of (7.1) which, upon linearisation, yields to leading order in δ

$$\frac{\tilde{p}'}{B_0^{\phi}} = -\frac{\partial G \sqrt{g} \tilde{B}^{\phi}}{\partial r} - \mu \sqrt{g} \tilde{J}^{\phi}.$$

By averaging in ϑ and using (a) in conjunction with (17.5), we obtain $(\sqrt{g}\,\tilde{B}^\phi)_0'=0$ which conforms to (17.17). This result is rather general and applies to any geometry, i.e. not necessarily updown symmetric.

Exploiting (17.7), we readily find

$$\xi_{NR}^{\vartheta} = \mu \xi_{NR}^{\phi} + o(\varepsilon \xi_m^r / r), \tag{17.20}$$

where the small terms in this equation are supposed to have zero poloidal average.

Now, the non-resonant contribution to the divergence of the fluid displacement reads

$$\begin{split} (\nabla \cdot \boldsymbol{\xi})_{\mathrm{NR}} &= \frac{\partial \boldsymbol{\xi}_{\mathrm{NR}}^{r}}{\partial r} + i m \boldsymbol{\xi}_{\mathrm{NR}}^{\vartheta} - i n \boldsymbol{\xi}_{\mathrm{NR}}^{\phi} + \left(\frac{1}{\sqrt{g}} \frac{\partial \sqrt{g}}{\partial r} - \langle \frac{1}{\sqrt{g}} \frac{\partial \sqrt{g}}{\partial r} \rangle \right) \boldsymbol{\xi}_{m}^{r} \\ &+ \frac{1}{\sqrt{g}} \frac{\partial \sqrt{g}}{\partial r} \boldsymbol{\xi}_{\mathrm{NR}}^{r} - \langle \frac{1}{\sqrt{g}} \frac{\partial \sqrt{g}}{\partial r} \boldsymbol{\xi}_{\mathrm{NR}}^{r} \rangle + \frac{\partial \boldsymbol{\xi}_{\mathrm{NR}}^{\vartheta}}{\partial \vartheta} \\ &+ \frac{\partial \sqrt{g}}{\partial \vartheta} \frac{\left(\boldsymbol{\xi}_{m}^{\vartheta} + \boldsymbol{\xi}_{\mathrm{NR}}^{\vartheta}\right)}{\sqrt{g}} - \langle \frac{\partial \sqrt{g}}{\partial \vartheta} \frac{\boldsymbol{\xi}_{\mathrm{NR}}^{\vartheta}}{\sqrt{g}} \rangle. \end{split} \tag{17.21}$$

From (17.18) and the definition of the compressible part of the perturbed pressure, we immediately see that $(\nabla \cdot \xi)_{NR} \sim \delta$ so that (17.20) and (17.21) yield at leading order in δ :²

$$o(r\xi_m^r) = \frac{\partial}{\partial \vartheta} \left(\sqrt{g} \xi_{NR}^{\vartheta} \right) + \frac{\partial \sqrt{g}}{\partial \vartheta} \xi_m^{\vartheta} - \langle \frac{\partial \sqrt{g}}{\partial \vartheta} \xi_{NR}^{\vartheta} \rangle \sqrt{g}.$$

Averaging in ϑ shows that the last term in angular brackets on the right-hand-side is of higher order (in δ) compared with the other contributions, and a further integration in ϑ finally yields

$$\mu \xi_{\rm NR}^{\phi} = \xi_{\rm NR}^{\theta} = \left(\frac{1/\sqrt{g}}{\langle 1/\sqrt{g} \rangle} - 1\right) \xi_{m}^{\theta}. \tag{17.22}$$

We now turn our attention to the expression of the toroidal displacement of the dominant mode. Let us first note that to the leading orders in the parameter δ we have

$$\frac{\sqrt{g}}{f_0'} \mathbf{B}_0 \cdot \boldsymbol{\xi} = e^{im\vartheta - in\phi} \left[g_{\phi\phi} \left(\boldsymbol{\xi}_m^{\phi} + \boldsymbol{\xi}_{NR}^{\phi} \right) + \mu g_{\vartheta\vartheta} \left(\boldsymbol{\xi}_m^{\vartheta} + \boldsymbol{\xi}_{NR}^{\vartheta} \right) \right] \\
= e^{im\vartheta - in\phi} \left[g_{\phi\phi} \left(\boldsymbol{\xi}_m^{\phi} - q \boldsymbol{\xi}_m^{\vartheta} \right) + \frac{G + \mu^2 N}{\langle 1/\sqrt{g} \rangle} q \boldsymbol{\xi}_m^{\vartheta} \right], \tag{17.23}$$

where we used (17.22) for expressing the non-resonant part of the poloidal and toroidal perturbed fluid displacement. The mth Fourier projection of (13.22) can be written as

$$\frac{B_0^2}{R_0^2 f_0'} \frac{\gamma^2}{\omega_A^2} \left(\sqrt{g} \boldsymbol{B}_0 \cdot \boldsymbol{\xi} \right)_m = -i \left(m\mu - n \right) \tilde{p}_m - \frac{p_0'}{f_0'} (\sqrt{g} \tilde{B}^r)_m.$$

Thus, by plugging (17.23) into this expression and using the first of (17.19) we obtain

$$\xi_{m}^{\phi} = \frac{q}{im} \left(1 - \frac{\langle R^{2} \rangle \langle 1/\sqrt{g} \rangle}{G + \mu^{2} \langle N \rangle} \right) \frac{d\xi_{m}^{r}}{dr} - \frac{\langle 1/\sqrt{g} \rangle}{G + \mu^{2} \langle N \rangle} \frac{R_{0}^{2}/B_{0}^{2}}{\gamma^{2}/\omega_{A}^{2}} \left[i \left(m\mu - n \right) \tilde{p}_{m} + \frac{p_{0}'}{f_{0}'} (\sqrt{g}\tilde{B}^{r})_{m} \right]. \tag{17.24}$$

² Recall that $m\mu - m \sim \delta$.

A fairly easy computation performed employing the metric coefficients of chapter 5 shows that the order of this quantity conforms to (17.6).

$$1 - \frac{\langle R^2 \rangle \langle R^{-2} \rangle}{1 + \mu^2 \langle N \rangle / G} \approx \frac{r^2}{R_o^2} (\mu^2 - 2).$$

17.2.3 Perturbed pressure

The non-resonant part of (13.22) upon derivation along the radial variable reads

$$\frac{\rho_0 \gamma^2}{f_0'} (\sqrt{g} \mathbf{B}_0 \cdot \mathbf{\xi})_{\text{NR}}' = -\mu \frac{\partial \tilde{p}_{\text{NR}}'}{\partial \vartheta} - \frac{p_0'}{f_0'} (\sqrt{g} \tilde{\mathbf{B}}')_{\text{NR}}'. \tag{17.25}$$

Since the magnetic field is divergence-free and thanks to (17.16), it is immediate to verify that to leading orders in ε we have

$$\begin{split} (\sqrt{g}\tilde{B}^r)'_{\mathrm{NR}} &= [(\sqrt{g}\tilde{B}^r)_{m+1}e^{i\vartheta} + (\sqrt{g}\tilde{B}^r)_{m-1}e^{-i\vartheta}]' \\ &= -i[(m+1)(\sqrt{g}\tilde{B}^{\vartheta})_{m+1}e^{i\vartheta} + (m-1)(\sqrt{g}\tilde{B}^{\vartheta})_{m-1}e^{-i\vartheta}] \\ &= -2i[m\cos\vartheta + i\sin\vartheta]Y. \end{split}$$

Note that harmonics of mode number $m \pm \ell$ with $\ell > 1$ have been discarded since they are expected to become progressively smaller as ℓ increases.³ Notice also that an additional function of ϑ (only) would appear if we allowed for the constants of integration in (17.13). For the moment we set this constant to zero.

To the accuracy required in the following calculations, it is sufficient to approximate $\xi_m^{\theta} \approx -\frac{1}{im} d\xi_m^r/dr$ so that by means of (17.23) a straightforward computation shows that the inertial contribution can be written

$$\frac{1}{f_0'}(\sqrt{g}\boldsymbol{B}_0\cdot\boldsymbol{\xi})_{\rm NR} = \frac{q}{i\,m}\left[\left(R^2-\langle R^2\rangle\right)-\mu^2\frac{N-\langle N\rangle}{\langle 1/\sqrt{g}\rangle}\right]\frac{d\xi_m^r}{dr}.$$

Thus, collating these results together finally yields an expression for the non-resonant part of the perturbed pressure

$$\frac{\partial \tilde{p}'_{NR}}{\partial \vartheta} = 2iq \frac{p'_0}{f'_0} [m\cos\vartheta + i\sin\vartheta] Y
- \frac{B_0^2}{R_0^2} \frac{\gamma^2}{\omega_A^2} \frac{q^2}{im} \left(R^2 - \langle R^2 \rangle - \mu^2 \frac{N - \langle N \rangle}{\langle 1/\sqrt{g} \rangle} \right) \frac{d^2 \xi_m^r}{dr^2}.$$
(17.26)

We shall now investigate the order of magnitude of Δp_m . For this, we explicitly compute the resonant part of the divergence of ξ which is

$$(\nabla \cdot \xi)_{m} = \frac{d\xi_{m}^{r}}{dr} + \langle \frac{1}{\sqrt{g}} \frac{\partial \sqrt{g}}{\partial r} \rangle \xi_{m}^{r} + im\xi_{m}^{\theta} - in\xi_{m}^{\theta}$$
$$+ \langle \frac{\partial \sqrt{g}}{\partial r} \frac{\xi_{NR}^{r}}{\sqrt{g}} \rangle + \langle \frac{\partial \sqrt{g}}{\partial \theta} \frac{\xi_{NR}^{\theta}}{\sqrt{g}} \rangle. \tag{17.27}$$

Exploiting the fact that the perturbation of the toroidal magnetic field is small, we may write the non-resonant contribution to equation (13.19) as

$$\frac{\partial \xi_{\text{NR}}^r}{\partial r} + i m \left(\xi_{\text{NR}}^{\vartheta} - \mu \xi_{\text{NR}}^{\phi} \right) + \frac{\partial}{\partial \vartheta} \left(\xi_{\text{NR}}^{\vartheta} - \mu \xi_{\text{NR}}^{\phi} \right) = 0.$$

³ This can be inferred from (17.10)-(17.13), from which the expected dependence on the inverse aspect ratio is of the form given in (17.3).

The right-hand-side is actually a function of order $\varepsilon^3 \xi_m^r / r$ which, for the accuracy required in our analysis, can be safely set to zero. When this expression in plugged in (17.21), to leading order in δ we get

$$0 = i(m\mu - n)\xi_{NR}^{\phi} + \mu \frac{\partial \xi_{NR}^{\phi}}{\partial \vartheta} + \left(\frac{1}{\sqrt{g}} \frac{\partial \sqrt{g}}{\partial r} - \left\langle \frac{1}{\sqrt{g}} \frac{\partial \sqrt{g}}{\partial r} \right\rangle \right) \xi_{m}^{r} + \frac{\partial \sqrt{g}}{\partial \vartheta} \frac{\left(\xi_{m}^{\vartheta} + \xi_{NR}^{\vartheta}\right)}{\sqrt{g}} - \left\langle \frac{\partial \sqrt{g}}{\partial \vartheta} \frac{\xi_{NR}^{\vartheta}}{\sqrt{g}} \right\rangle.$$
(17.28)

If we multiply by \sqrt{g} and average in ϑ the following expression is ob-

$$0 = i(m\mu - n)\langle\sqrt{g}\xi_{NR}^{\phi}\rangle + \langle\frac{\partial\sqrt{g}}{\partial\vartheta}\left(\xi_{NR}^{\vartheta} - \mu\xi_{NR}^{\phi}\right)\rangle + \left(\langle\frac{\partial\sqrt{g}}{\partial r}\rangle - \langle\sqrt{g}\rangle\langle\frac{1}{\sqrt{g}}\frac{\partial\sqrt{g}}{\partial r}\rangle\right)\xi_{m}^{r} - \langle\sqrt{g}\rangle\langle\frac{\partial\sqrt{g}}{\partial\vartheta}\frac{\xi_{NR}^{\vartheta}}{\sqrt{g}}\rangle.$$
(17.29)

Upon using (17.20) and (17.22), we find that $\langle \frac{\partial \sqrt{g}}{\partial \theta} \frac{\xi_{NR}^{\theta}}{\sqrt{g}} \rangle$ is a quantity of order $\varepsilon^2 \xi_m^r/r$. Thus, by combining the first of (17.19) with (17.27) and using (17.22) we easily obtain4

$$\begin{split} (\nabla \cdot \xi)_{m} &= \left(\langle \frac{1}{\sqrt{g}} \frac{\partial \sqrt{g}}{\partial r} \rangle - \frac{f_{0}^{\prime\prime}}{f_{0}^{\prime}} \right) \xi_{m}^{r} + i(m\mu - n) \xi_{m}^{\phi} \\ &+ \langle \frac{\partial \sqrt{g}}{\partial \vartheta} \frac{\xi_{\text{NR}}^{\vartheta}}{\sqrt{g}} \rangle + o(\varepsilon^{2} \xi_{m}^{r}/r) \sim \varepsilon^{2} \xi_{m}^{r}/r, \end{split}$$

implying that $\Delta p_m \sim \varepsilon^4 B_0^2 \xi_m^r/r$ at most. Because of this, we conveniently set

$$\Delta p_m = 0, \tag{17.30}$$

meaning that, to the required accuracy, corrections due to Δp_m do not enter into play.

We now have all the elements to write the induction and vorticity equations in a form equivalent to that of Eqs. (13.27) and (13.28) but augmented by curvature effects. Since the algebra is slightly involute, the derivation of each of the two equations is carried out separately.

The resistive layer equations 17.3

Induction equation 17.3.1

Instead of (13.18), the leading contributions in the small parameter δ to the induction equation obtained from (13.6) are easily worked out to give

$$\sqrt{g}\tilde{B}^{r} = f_{0}^{r} \left(\mu \frac{\partial}{\partial \vartheta} - i n \right) \xi^{r} - \frac{\eta_{0} G}{\gamma} \frac{\partial}{\partial r} \left[\frac{\partial}{\partial \vartheta} (N \sqrt{g} \tilde{B}^{\vartheta}) - i n N \sqrt{g} \tilde{B}^{\varphi} \right].$$
(17.31)

⁴ Recall that to leading order

$$\begin{split} \sqrt{g} &= rR_0 \Big(1 + \frac{2r}{R_0} \cos \vartheta + o(\varepsilon^2) \Big), \\ f_0' &= rB_0 \Big(1 + o(\varepsilon^2) \Big). \end{split}$$

The mth Fourier component of this equation reads

$$(\sqrt{g}\tilde{B}^{r})_{m} = if_{0}'(m\mu - n)\xi_{m}^{r}$$
$$-i\frac{\eta G}{\gamma} \left[\langle N \rangle [m(\sqrt{g}\tilde{B}^{\vartheta})_{m} - n(\sqrt{g}\tilde{B}^{\varphi})_{m}]' + 2mN_{1}Y' \right]. \quad (17.32)$$

By means of (17.30) and exploiting the smallness of the toroidal field, we immediately find that the perturbation of the poloidal magnetic field associated with the neighbouring sidebands can be approximated to leading orders in ε as⁵

$$Y = \frac{N_1}{\langle N \rangle} \frac{(\sqrt{g}\tilde{B}^r)'_m}{im} + q \frac{R_0 p'_0}{B_0} \xi_m^r.$$
 (17.33)

Since Y appears under the sign of radial derivation, the constants that would appear from the integration of (17.12) are annihilated. Therefore, using this result in conjunction with Eqs. (17.14)-(17.16), equation (17.32) can be recast as

$$\begin{split} \left[1 - \frac{\eta_0 G\langle N \rangle}{\gamma} \left(1 - \frac{2N_1^2}{\langle N \rangle^2}\right) \frac{d^2}{dr^2}\right] (\sqrt{g}\tilde{B}^r)_m \\ &= i f_0' (m\mu - n) \xi_m^r - i p_0' \frac{\eta_0 G\langle N \rangle}{\gamma} \mathcal{H} \frac{d\xi_m^r}{dr}, \end{split}$$

where the quantity \mathcal{H} is defined as

$$\mathscr{H} = 2mq \frac{N_1}{\langle N \rangle^2} (1/B_0^{\phi})_1 \approx 2mq \frac{N_1}{\langle N \rangle^2} (r/B_0). \tag{17.34}$$

Notice that contributions of order ε^3 or smaller have been ignored.

Without loss of generality, thanks to the smallness of the term proportional to the perturbed pressure, we can rescale the resistivity to write the **resistive-layer induction equation** as

$$\left[1 - \frac{\eta_R}{\gamma} \frac{d^2}{dr^2}\right] (\sqrt{g}\tilde{B}^r)_m = i f_0'(m\mu - n) \xi_m^r - i p_0' \frac{\eta_R}{\gamma} \mathcal{H} \frac{d\xi_m^r}{dr}. \quad (17.35)$$

Finally, using this equation along with (17.30) into Eq. (17.24) allows us to find a simplified expression for the toroidal displacement of the main mode, which, to leading order in ε , reads

$$\xi_{m}^{\phi} = \frac{q}{im} \left(1 - \frac{\langle R^{2} \rangle \langle 1/\sqrt{g} \rangle}{G + \mu^{2} \langle N \rangle} \right) \frac{d\xi_{m}^{r}}{dr} - \frac{p_{0}^{r} \omega_{A}^{2}}{r_{s} B_{0}^{3} \gamma^{2}} \left(\frac{\eta_{R}}{\gamma} \right) (\sqrt{g} \tilde{B}^{r})_{m}^{"}.$$
 (17.36)

To close the system, we need to derive an equation for ξ_m^r : this is the aim of the next subsection.

⁵ Remember that $(1/B_0^{\phi})_1 \approx r/R_0$, $\langle N \rangle \approx r/R_0$ and $N_1 \approx r\Delta'/R_0$.

$$\eta_R = \eta_0 G\langle N \rangle \left(1 - \frac{2N_1^2}{\langle N \rangle^2} \right).$$

Motivating the ordering of $\xi_{m+\ell}^r$

To leading order in δ , the $m\pm 1$ Fourier projection of (17.31) yields

$$\begin{split} &\left(1-\frac{\eta_0 G\langle N\rangle}{\gamma}\frac{d^2}{dr^2}\right)(\sqrt{g}\tilde{B}^r)_{m\pm1}=\pm i\mu f_0'\xi_{m\pm1}^r\\ &-i\frac{\eta_0 G}{\gamma}\frac{d}{dr}\left[N_1((m\pm1)(\sqrt{g}\tilde{B}^\vartheta)_m-n(\sqrt{g}\tilde{B}^\phi)_m)\right]. \end{split}$$

We now exploit the fact that the toroidal field is ε^2 times smaller than the poloidal one, and take the radial derivative of this equation to obtain

$$\bigg(1-\frac{\eta_0G\langle N\rangle}{\gamma}\frac{d^2}{dr^2}\bigg)Y=\mp\frac{\mu f_0'}{m\pm1}\frac{d\xi_{m\pm1}^r}{dr}+\frac{\eta_0GN_1}{\gamma}\frac{d^2}{dr^2}(\sqrt{g}\tilde{B}^\vartheta)_m.$$

Thanks to (17.1), (17.3) and (17.33), ordering (17.2) then follows. The $m \pm \ell$ harmonics are expected to become progressively smaller as ℓ increases.

17.3.2 Vorticity equation

We first isolate the leading orders in δ in (13.10), so that the vorticity equation may be written as

$$\begin{split} \frac{\gamma^2}{\omega_A^2} \frac{B_0^2}{R_0^2 f_0'} \frac{d}{dr} (g N \xi^{\vartheta})_m &= i (m \mu - n) (\sqrt{g} \tilde{J}^{\phi})_m - \left(\sqrt{g} J_0 \cdot \nabla \frac{\tilde{B}^{\phi}}{B_0^{\phi}} \right)_m \\ &- i m \langle \frac{1}{B_0^{\phi}} \rangle' \tilde{p}_m + \langle \frac{\partial}{\partial \vartheta} \left(\frac{1}{B_0^{\phi}} \right) \tilde{p}_{NR}' \rangle + i \sum_{m' \neq 0} \left[m' \left(\frac{J_0^{\phi}}{B_0^{\phi}} \right)_{m'} (\sqrt{g} \tilde{B}^{\vartheta})_{m-m'} \right]. \end{split}$$

$$(17.37)$$

When performing the expansion in the inverse aspect ratio, we only need to compute corrections which appear up to order ε^3 . Each of the terms in the equation above is analysed separately.

It is immediate to see that thanks to (17.33) (see also (17.13)), the term with the equilibrium current yields⁶

$$\sum_{m'\neq 0} m' \left(\frac{J_0^{\phi}}{B_0^{\phi}}\right)_{m'} (\sqrt{g}\tilde{B}^{\vartheta})'_{m-m'} \approx \left[\left(\frac{J_0^{\phi}}{B_0^{\phi}}\right)_1 - \left(\frac{J_0^{\phi}}{B_0^{\phi}}\right)_{-1} \right] Y' = 0.$$
 (17.38)

Exploiting the smallness of the sidebands' toroidal field, one has (cf. (7.54) and (7.55))

$$\left(\sqrt{g}\boldsymbol{J}_{0}\cdot\boldsymbol{\nabla}\frac{\tilde{B}^{\phi}}{B_{0}^{\phi}}\right)_{m}\approx im\frac{R_{0}p_{0}^{\prime}}{rB_{0}^{2}}(\sqrt{g}\tilde{B}^{\phi})_{m},$$

having approximated $f_0' \approx r B_0$. The toroidal current density, which is

⁶ This is because J_0^{ϕ}/B_0^{ϕ} is symmetric in ϑ , so that $(J_0^{\phi}/B_0^{\phi})_1 = (J_0^{\phi}/B_0^{\phi})_{-1}$. Notice that these two quantities are of order ε^2/r .

computed to the leading order in ε from (17.11) by taking $\ell = 0$, reads

$$\begin{split} (\sqrt{g}\tilde{J}^{\phi})_{m} \approx & \frac{d}{dr} \left[\langle N \rangle (\sqrt{g}\tilde{B}^{\vartheta})_{m} + 2N_{1}Y \right] \\ = & -\frac{d}{dr} \left[\langle N \rangle \left(\frac{(\sqrt{g}\tilde{B}^{r})'_{m}}{im(1 + \mu^{2}r^{2}/R_{0}^{2})} - \mu \frac{rp'_{0}}{B_{0}} \xi_{m}^{r} \right) - 2N_{1}Y \right], \end{split}$$

where we used the expression of the toroidal field perturbation given by (17.14) and exploited the smallness of the *m*th projection of the compressible contribution to the perturbed pressure (cf. (17.30)). Thus, by putting these results together, equation (17.37) can be cast in the following form

$$\frac{\gamma^2}{\omega_A^2} \frac{B_0^2}{R_0^2} (gN\xi^{\vartheta})'_m = -if'_0(m\mu - n) \left[\frac{\langle N \rangle (\sqrt{g}\tilde{B}^r)''_m}{im(1 + \mu^2 r^2/R_0^2)} - \langle N \rangle \mu \frac{rp'_0}{B_0} \frac{d\xi_m^r}{dr} - 2N_1 Y' \right] - im \frac{R_0 p'_0}{B_0} (\sqrt{g}\tilde{B}^{\phi})_m + imr B_0 p'_0 \langle \frac{1}{B_0^{\phi}} \rangle' \xi_m^r - \langle \sqrt{g} \frac{\partial \tilde{p}'_{NR}}{\partial \vartheta} \rangle.$$
(17.39)

Now, upon defining $P = R_0 p_0'/B_0$ (cf. (7.55)) and using (17.14) in conjunction with (17.30) and (17.35), we obtain the following relation

$$\begin{split} &-f_0'(m\mu-n)\langle N\rangle \mu \frac{rp_0'}{B_0}\frac{d\xi_m^r}{dr} + m\frac{R_0p_0'}{B_0}(\sqrt{g}\tilde{B}^\phi)_m \approx \\ &+ mrR_0\left(\mu\mu'\frac{r^2}{R_0^2} + \frac{P}{R_0B_0}\right)p_0'\xi_m^r - ip_0'\frac{\mu r^2}{R_0B_0}\frac{\eta_R}{\gamma}(\sqrt{g}\tilde{B}^r)_m'''. \end{split}$$

Again, only the leading order contributions in ε have been retained. From equations (17.19), (17.22) and (17.36) a quick calculation shows that to the required accuracy one has

$$\begin{split} \frac{\gamma^2}{\omega_A^2} \frac{B_0^2}{R_0^2} (gN\xi^{\vartheta})_m' &= \frac{\gamma^2}{\omega_A^2} \frac{B_0^2}{R_0^2} \Big[\langle gN \rangle \xi_m^{\vartheta} + \langle gN \xi_{\mathrm{NR}}^{\vartheta} \rangle \Big]' \\ &\approx - p_0' \frac{\mu r^2}{R_0 B_0} \frac{\eta_R}{\gamma} (\sqrt{g} \tilde{B}^r)_m''' - \frac{B_0^2 \gamma^2}{i m R_0^2 \omega_A^2} \left(\frac{\langle \sqrt{g} N \rangle \langle R^2 \rangle}{G + \mu^2 \langle N \rangle} \right) \frac{d^2 \xi_m^r}{dr^2}. \end{split}$$

By means of (17.26), another easy manipulation shows that the term proportional to the non-resonant part of the perturbed pressure reads

$$\begin{split} \frac{d}{dr} \langle \sqrt{g} \frac{\partial \tilde{p}_{\rm NR}'}{\partial \vartheta} \rangle &\approx \frac{d}{dr} \Big[2 i \, m \, q \, \frac{r p_0'}{B_0} Y \\ &- \frac{B_0^2}{R_0^2} \frac{\gamma^2}{\omega_A^2} \frac{q^2}{i \, m} \langle \sqrt{g} \left(R^2 - \langle R^2 \rangle - \mu^2 \frac{N - \langle N \rangle}{\langle 1/\sqrt{g} \rangle} \right) \rangle \frac{d^2 \xi_m^r}{d \, r^2} \Big]. \end{split} \tag{17.40}$$

Thus, when all these quantities that we have just computed are in-

serted into (17.39) we obtain the following equation

$$\begin{split} &-\frac{B_{0}^{2}}{R_{0}^{2}}\frac{\gamma^{2}}{\omega_{A}^{2}}\frac{r^{3}R_{0}}{m}\left(1+2q^{2}+\ldots\right)\frac{d^{2}\xi_{m}^{r}}{dr^{2}}\\ &=f_{0}'(m\mu-n)\left(\frac{\langle N\rangle(\sqrt{g}\tilde{B}^{r})_{m}''}{im(1+\mu^{2}r^{2}/R_{0}^{2})}-2N_{1}Y'\right)\\ &+mrB_{0}p_{0}'\left[\frac{R_{0}}{B_{0}}\left(\mu\mu'\frac{r^{2}}{R_{0}^{2}}+\frac{P}{R_{0}B_{0}}\right)-\langle\frac{1}{B_{0}^{\phi}}\rangle'\right]\xi_{m}^{r}+2mq\frac{rp_{0}'}{B_{0}}Y+\Theta,\quad(17.41) \end{split}$$

where the dots on the left-hand-side indicate small corrections of order ε^2 and Θ is a constant which accounts for those originating from (17.38) and (17.40). By using equations (17.33) and (17.34), we find that

$$\frac{\langle N \rangle (\sqrt{g}B^r)_m^{\prime\prime}}{im(1+\mu^2r^2/R_0^2)} - 2N_1Y^{\prime} \approx -ic_0\Big((\sqrt{g}\tilde{B}^r)_m^{\prime\prime} - i\mathcal{H}p_0^{\prime}\frac{d\xi_m^r}{dr}\Big),$$

$$c_0 = \frac{\langle N \rangle}{m}\Big(\frac{1}{1+\mu^2r^2/R_0^2} - \frac{2N_1^2}{\langle N \rangle^2}\Big).$$

Dividing (17.41) by c_0 and explicitly writing the factor $\langle 1/B_0^{\phi} \rangle'$ through (7.15) with F' and $\langle R^2 \rangle'$ given by (4.31) and (5.21) respectively (cf. (11.4)), the **resistive-layer vorticity equation** is finally given by

$$\frac{\gamma^{2}}{\omega_{A}^{2}} \frac{B_{0}^{2}}{R_{0}^{2}} \Lambda_{i} \frac{d^{2} \xi_{m}^{r}}{dr^{2}} = i f_{0}^{\prime} (m\mu - n) \left[(\sqrt{g} \tilde{B}^{r})_{m}^{\prime\prime} - i \mathcal{H} p_{0}^{\prime} \frac{d \xi_{m}^{r}}{dr} \right]
+ i \mathcal{H} p_{0}^{\prime} (\sqrt{g} \tilde{B}^{r})_{m}^{\prime} - 2m^{2} R_{0} p_{0}^{\prime} \left[\frac{r}{R_{0}} \left(1 - \frac{1}{q^{2}} \right) + s \Delta^{\prime} \right] \xi_{m}^{r} + \Theta, \quad (17.42)$$

where $\Lambda_i = r^2 R_0^2 (1 + 2q^2 + ...)$ with an obvious rescaling of Θ .

In summary, the linear dynamics in the resistive layer which takes into account curvature effects, for both $m \sim 1$ and $m \gg 1$ instabilities, is fully determined by equations (17.35) and (17.42) where use of (17.30) and (17.34) has been made. These are equivalent to the **Glasser-Greene-Johnson (GGJ) equations** (Glasser *et al.* (1975)) evaluated for of large aspect ratio circular tokamak. Obtaining the eigensolution of these equations is the aim of the next section.

17.4 The eigensolution

The following analysis closely follows that of §13.4. We start by approximating $m\mu - n \sim -nsx$ where the variable x is defined in (17.1). Written in terms of x, equations (17.35) and (17.42) become respectively

$$(q_s = m/n)$$

$$\begin{split} &\left[1-\frac{\eta_R}{r_s^2\gamma}\frac{d^2}{dx^2}\right](\sqrt{g}\tilde{B}^r)_m=-if_0'nsx\xi_m^r-ir\mathcal{H}p_0'\frac{\eta_R}{r_s^2\gamma}\frac{d\xi_m^r}{dx},\\ &\frac{\gamma^2}{\omega_A^2}\frac{B_0^2}{R_0^2}\Lambda_i\frac{d^2\xi_m^r}{dx^2}=-if_0'nsx\left[\frac{d^2(\sqrt{g}\tilde{B}^r)_m}{dx^2}-ir_s\mathcal{H}p_0'\frac{d\xi_m^r}{dx}\right]\\ &+ir_s\mathcal{H}p_0'\frac{d(\sqrt{g}\tilde{B}^r)_m}{dx}-2m^2r_s^2R_0p_0'\left[\frac{r_s}{R_0}\left(1-\frac{1}{q_s^2}\right)+s\Delta'\right]\xi_m^r+\Theta. \end{split}$$

In both of the two equations above it is implicitly assumed that equilibrium quantities which do not depend on x must be evaluated at r_s .

We now introduce the variable

$$y=\frac{x}{\epsilon_R}$$

where $0 < \epsilon_R \ll 1$ is a smallness parameter which will be conveniently defined later. If ϵ_R is sufficiently small, moving away from the resistive layer we allow y to vary from $-\infty$ to $+\infty$. Thus, we define the **Fourier transform** of the magnetic perturbation and the fluid displacement as

$$\psi^* = \int_{-\infty}^{\infty} (\sqrt{g}\tilde{B}^r)_m e^{-iky} dy, \quad \xi^* = \int_{-\infty}^{\infty} \xi_m^r e^{-iky} dy,$$

so that the induction and vorticity equations transformed to k-space then read (we use the same conventions of **sidenote 15** of \$13.4)

$$\left(1 + V \frac{k^2}{\epsilon_R^2}\right) \psi^* = A \epsilon_R \frac{d\xi^*}{dk} + EV \frac{k}{\epsilon_R} \xi^*,$$

$$-\frac{\gamma^2}{\omega_A^2} \frac{B_0^2}{R_0^2} \Lambda_i \frac{k^2}{\epsilon_R^2} \xi^* = A \epsilon_R \frac{d}{dk} \left(-\frac{k^2}{\epsilon_R^2} \psi^* + E \frac{k}{\epsilon_R} \xi^* \right)$$

$$- E \frac{k}{\epsilon_R} \psi^* + U \xi^* + 2\pi \Theta \delta(k),$$
(17.43)

having defined the following quantities

$$\begin{split} V &= \frac{\eta_R}{r_s^2 \gamma}, \quad A = f_0' \, n s, \quad E = r_s \mathcal{H} p_0', \\ U &= -2 m^2 r_s^2 R_0 p_0' \left[\frac{r_s}{R_0} \left(1 - \frac{1}{q_s^2} \right) + s \Delta' \right]. \end{split}$$

Let us outline the solution approach: as in §13.4, equations (17.43) are combined into a single one for ξ^* , which is found to be singular at k=0 regardless of the value of Θ . Subsequently even and odd solutions are obtained by extending appropriately to negative values of k the eigenfunction defined for k>0.

Therefore, let $\Theta \rightarrow 0$ for the moment (the $\Theta \neq 0$ case is briefly

Do not confuse the symbol H with the Heaviside step function. Although the magnitude of H^2 is ε^2 times smaller compared to other contributions, we retained it for ease of comparison with the results found in the literature.

discussed at the end of this section) and define

$$H = -\frac{E}{A} \approx -2q_s^2 \frac{R_0 p_0'}{s B_0^2} \Delta' + \dots,$$

$$D_R = H^2 - H - \frac{\alpha r_s}{s^2 R_0} \left(1 - \frac{1}{q_s^2} \right),$$

$$\hat{Q} = \frac{\gamma^2}{\omega_A^2} \frac{B_0^2}{R_0^2} \frac{\Lambda_i}{A^2} \approx \frac{\gamma^2}{\omega_A^2} \left(\frac{1 + 2q_s^2}{n^2 s^2} + \dots \right),$$

where α is the ballooning parameter given by (4.41) and the dots denote corrections of order ε^2 compared to the leading contribution. Combining Eqs. (17.43) thus yields

$$\begin{split} \frac{d}{dk}\left(\frac{k^2}{1+Vk^2/\epsilon_R^2}\frac{d\xi^*}{dk}\right) + \left[H\frac{d}{dk}\left(\frac{k}{1+Vk^2/\epsilon_R^2}\right)\right. \\ & - \frac{H^2}{1+Vk^2/\epsilon_R^2} + D_R - \hat{Q}\frac{k^2}{\epsilon_R^2}\right]\xi^* = 0. \end{split}$$

By taking the smallness parameter ϵ_R to be defined as in (13.33) with the Lundquist number S given by (13.34) with the substitution $\eta_0 \to \eta_R$, the equation above then becomes

$$\frac{d}{dk}\left(\frac{k^2}{1+V_ek^2}\frac{d\xi^*}{dk}\right) + \left[H\frac{d}{dk}\left(\frac{k}{1+V_ek^2}\right) - \frac{H^2}{1+V_ek^2} + D_R - Qk^2\right]\xi^* = 0,$$
(17.44)

having specified (cf. (13.36) and (13.38))

$$V_e = \frac{m^2}{\gamma/\omega_A} S^{-1/3}, \quad Q = \frac{\gamma^2}{s^2 \omega_A^2} q_s^2 (1 + 2q_s^2) S^{2/3} \quad M_t = \sqrt{\frac{Q}{V_e}}.$$

The solution of (17.44) is sought by basically following the same procedure outlined in section 16.3.2.

We start by introducing the quantity (see (16.27))

$$\tau = -\frac{1}{2} + \sqrt{\frac{1}{4} + H^2 - H - D_R} = -\frac{1}{2} + \nu,$$

where $v = \sqrt{\hat{U} + 1/4}$ (cf. (11.20)) with the definition of \hat{U} given in (16.13). As in the previous chapter, we assume that $-1/2 < \tau < 1/2$. If we write $\xi^* = \zeta^{\tau/2} e^{-\zeta/2} Y(\zeta)$ with $\zeta = M_t V_e k^2$, some algebra shows that (17.44) transforms into

$$\zeta \frac{d^2Y}{d\zeta^2} + \left(\frac{1}{2} + \tau - \zeta + \frac{1}{1 + \zeta/M_t}\right) \frac{dY}{d\zeta} - \left(\hat{h} + \frac{1 + (\tau + H)/M_t}{2(1 + \zeta/M_t)}\right) Y = 0,$$

where the quantity \hat{h} is given by

$$\hat{h} = \frac{1}{4} \left(M_t + 2\tau + 1 - \frac{D_R}{M_t} \right).$$

⁷ It is expected that no instability can be constructed for $\tau > 1/2$.

Employing the tricks discussed at the end of chapter 16, after some straightforward manipulations, one then finds that (cf. (16.31))

$$\xi^* = \zeta^{\tau/2} e^{-\zeta/2} \left[U\left(\hat{h} + 1, \tau + \frac{3}{2}, \zeta\right) + \frac{2U\left(\hat{h}, \tau + \frac{1}{2}, \zeta\right)}{M_t + \tau + H} \right],$$

where U is the **confluent hypergeometric function** which decays for $\zeta \to \infty$. Thus, for small k, the behaviour of the eigensolution is of the form

$$\xi^* \propto |k|^{\tau} \left[1 + \Delta_R^* |k|^{-1-2\tau} \right], \tag{17.45}$$

$$\Delta_R^* = (M_t V_e)^{-1/2-\tau} \frac{\Gamma\left(\frac{1}{2} + \tau\right)}{\Gamma\left(-\frac{1}{2} - \tau\right)} \times \frac{\Gamma\left(\frac{1}{4}(M_t + 3 - 2\tau - D_R/M_t)\right) (M_t + \tau + H)}{\Gamma\left(\frac{1}{4}(M_t + 5 + 2\tau - D_R/M_t)\right) (M_t - 1 - \tau + H)}. \tag{17.46}$$

Transforming to real y space is an easy task,⁸ so that the layer solution written in terms of the variable x reads (recall that ϵ_R is defined by (13.33))

$$\begin{split} \xi_{m}^{r} & \propto \frac{1}{|x|^{1+\tau}} \left(1 + \frac{c_{e} \Delta_{e}^{*} + c_{o} \Delta_{o}^{*}}{c_{e} + c_{o}} \left| \frac{x}{\epsilon_{R}} \right|^{1+2\tau} \right), \qquad r > r_{s}, \\ & \propto \frac{1}{|x|^{1+\tau}} \left(1 + \frac{c_{e} \Delta_{e}^{*} - c_{o} \Delta_{o}^{*}}{c_{e} - c_{o}} \left| \frac{x}{\epsilon_{R}} \right|^{1+2\tau} \right), \qquad r < r_{s}, \end{split}$$
(17.47)

where c_e and c_o are some constants multiplying the even and odd solutions respectively, and we defined the coefficients

$$\Delta_{e}^{*} = -\cot\left(\frac{\pi}{2}\tau\right) \frac{\Gamma(-\tau)}{\Gamma(1+\tau)} \Delta_{R}^{*} = \frac{\pi \csc^{2}\left(\frac{\pi}{2}\tau\right)}{2\Gamma^{2}(1+\tau)} \Delta_{R}^{*},$$

$$\Delta_{o}^{*} = -\tan\left(\frac{\pi}{2}\tau\right) \frac{\Gamma(-\tau)}{\Gamma(1+\tau)} \Delta_{R}^{*} = \frac{\pi \sec^{2}\left(\frac{\pi}{2}\tau\right)}{2\Gamma^{2}(1+\tau)} \Delta_{R}^{*}.$$
(17.48)

Equations (17.46) and (17.47) give the resistive layer response including effects arising from toroidal curvature. It should be emphasised that these results apply to the case of an almost circular up-down symmetric tokamak, while the generalisation to a more complex, yet axisymmetric, geometry is discussed in appendix F.

To get the dispersion relation, the resistive-layer eigenfunction has to be matched with the outer solution. The latter is obtained from (17.35) and (17.42) in which inertial and resistive effects are dropped. If $\Theta=0$ this eventually leads to $(f_0'\approx r_s B_0)$

$$\frac{d}{dx}\left(x^2\frac{d\xi_m^r}{dx}\right) = \frac{r_s\alpha}{s^2R_0}\left(1 - \frac{1}{q^2}\right)\xi_m^r \equiv \hat{U}\xi_m^r,\tag{17.49}$$

⁸ Employing Lighthill's notation of **sidenote 15** of §13.4, we have

$$\begin{aligned} \left[|\hat{\mathbf{x}}|^{\alpha} \right]^* &= \frac{2 \cos\left[\frac{\pi}{2} (\alpha + 1)\right]}{(2\pi |\hat{k}|)^{\alpha + 1}} \alpha!, \\ \left[|\hat{\mathbf{x}}|^{\alpha} \operatorname{sgn}(\hat{\mathbf{x}}) \right]^* &= -\frac{2i \sin\left[\frac{\pi}{2} (\alpha + 1)\right]}{(2\pi |\hat{k}|)^{\alpha + 1}} \alpha! \operatorname{sgn}(\hat{k}), \end{aligned}$$

with α any real number where $\alpha! = \Gamma(\alpha + 1)$. In the notation used this report we identify $\hat{x} = k/(2\pi)$ and $\hat{k} = -y$. Note that the higher order terms that would appear in (17.45) lead to small corrections in the $y \to \infty$ limit.

When dealing with tearing modes one defines $r_s\Delta'=A_2+A_1$ which reduces to (14.4) in the zero β limit. Indeed, for x>0 one has $x^\epsilon=e^{\epsilon\ln x}\approx 1+\epsilon\ln x$ when $\epsilon\to0$.

where, as usual, equilibrium quantities must be evaluated at r_s . The asymptotic behaviour of the ideal solution when the resonance is approached then reads

$$\xi_m^r \propto |x|^{-\frac{1}{2}-\nu} + A_1|x|^{-\frac{1}{2}+\nu}, \qquad r < r_s,$$

$$\propto |x|^{-\frac{1}{2}-\nu} + A_2|x|^{-\frac{1}{2}+\nu}, \qquad r > r_s,$$
(17.50)

with A_1 and A_2 two constants. This shows that (17.47) and (17.50) can be matched asymptotically.

If Θ is allowed to be different from zero, it is easy to see that $\xi^*(k) \propto \frac{2\pi\Theta\delta(k)/A^2}{H-H^2+D_R}$ is a solution of (17.44). According to Glasser (1975), this represents the exact solution $\xi_m^r \propto const.$ and $(\sqrt{g}\tilde{B}_m^r) \propto x$ which is independent of the resistivity and Q, and thus it would correspond to a non-local ideal instability. We do not consider this case, hence hereafter we set $\Theta=0$.

17.5 Stability criteria modified by curvature

The aim of this final section is to analyse how the stability of some of the resistive perturbations studied in the previous chapters is affected by curvature effects. Let us assume, for the sake of simplicity, that $H \ll 1$ meaning that the magnetic shear does not get as small as ε^2 .

According to (17.50), the behaviour of the solution in the ideal region when the resonance is approached is of the form

$$\xi_m^r \propto |x|^{-1-\tau} \left(1 + A_1 |x|^{1+2\tau}\right), \qquad r > r_s,$$

$$\propto |x|^{-1-\tau} \left(1 + A_2 |x|^{1+2\tau}\right), \qquad r < r_s.$$

Matching this expression with (17.47) requires

$$\frac{c_e \Delta_e^* + c_o \Delta_o^*}{c_e + c_o} = \epsilon_R^{1+2\tau} A_1,$$

$$\frac{c_e \Delta_e^* - c_o \Delta_o^*}{c_e - c_o} = \epsilon_R^{1+2\tau} A_2.$$

From the second relation we obtain an expression for the ratio c_o/c_e which this is then plugged into the first one to finally yield the **dispersion** relation (Glasser (1984))

$$\epsilon_R^{-2-4\tau} \Delta_e^* \Delta_o^* + A_1 A_2 - \frac{1}{2} \epsilon_R^{-1-2\tau} (\Delta_e^* + \Delta_o^*) (A_1 + A_2) = 0.$$
 (17.51)

Bearing in mind (17.48), given A_1 and A_2 , the equation above can be viewed as a quadratic expression for Δ_R^* which, after some straightforward rearrangements, can eventually be cast as

$$\left(\frac{\pi\epsilon_R^{-1-2\tau}\Delta_R^*}{\Gamma^2(1+\tau)}\right)^2 + \frac{A_1A_2}{\csc^2(\pi\tau)} - (A_1 + A_2)\frac{\pi\epsilon_R^{-1-2\tau}\Delta_R^*}{\Gamma^2(1+\tau)} = 0.$$
(17.52)

Thence in the following we shall show how this dispersion relation can be used to extract the growth rate of the m=1 resistive kink, interchange and tearing modes.

17.5.1 m = 1 resistive kink

When m = n = 1 we set $A_1 = 0$ and $A_2 = -\pi/\lambda_H$ with $\tau = 0.9$ Equation (17.51) then leads to (cf. (15.6))

$$M_t^{1/6} \frac{M_t - 1 + H}{M_t + H} \frac{\Gamma\left(\frac{1}{4}(M_t + 5 - D_R/M_t)\right)}{\Gamma\left(\frac{1}{4}(M_t + 3 - D_R/M_t)\right)} = \frac{\hat{\lambda}_H}{2},$$

where $\hat{\lambda}_H$ is given by (15.5). For a monotonically decreasing pressure profile and s > 0, in a neighbourhood of the marginal boundary of the ideal kink mode ($\hat{\lambda}_H \approx 0$) the growth rate takes the form¹⁰

$$M_t = 1 - H + \frac{\hat{\lambda}_H}{\sqrt{\pi}}.$$

Toroidal curvature has a stabilising role by reducing the growth rate through the factor H. Cases with large and negative $\hat{\lambda}_H$ are addressed in the discussion of tearing modes.

Resistive interchange modes

High-*m* modes generally have definite parity, so that we take $A_1 = A_2 = A$ where the exact expression of A is not required. It follows that (17.51)can be written as

$$(\epsilon_R^{-1-2\tau}\Delta_\ell^* - A)(\epsilon_R^{-1-2\tau}\Delta_\ell^* - A) = 0.$$

The growth rate for even and odd modes is obtained by setting to zero one of the two terms on the left-hand-side at a time. 11

Using the identity

$$D_R = H^2 - H - \tau(\tau + 1)$$

the dispersion relation for interchange perturbations can be recast in a form similar to (16.32), that is

$$\frac{4M_t(M_tV_e)^{-\frac{1}{2}-\tau}}{M_t^2 - (1+\tau-H)^2} \frac{\Gamma\left(\frac{1}{4}(M_t + 3 - 2\tau - D_R/M_t)\right)}{\Gamma\left(\frac{1}{4}(M_t + 1 + 2\tau - D_R/M_t)\right)} \propto S^{-2\nu/3}, \qquad (17.53)$$

where information about mode parity is contained in the terms we omitted to write on the right-hand-side.

Similar to the calculations of section 16.3.3, we assume to be stable against Mercier modes $(-1/2 < \tau)$ and thanks to the fact that the Lundquist number is large we postulate that the right-hand-side of (17.53) is small (this requires ν being not too small). Hence, the roots of this equation are expected to be close to the poles of the Gamma function in the denominator so that the growth rate is given by 12

$$M_t = -\left(\frac{1}{2} + \tau + 2\ell\right) + \left[\left(\frac{1}{2} + \tau + 2\ell\right)^2 + D_R\right]^{1/2}, \quad \ell = 0, 1, \dots$$

⁹ Notice than (17.45) reduces to (13.41) with the replacement $\Delta_R \to \Delta_R^*$.

Note that in this case H > 0 with $H^2 \ll H$, meaning that $D_R < 0$.

¹¹ The dispersion relation (16.32) is recovered from (17.51) by letting $A_1 =$ $A_2 = (m/2)^{2\nu} \Gamma(-\nu) \Gamma(\nu)$ and matching (16.26) with (17.45), where in the former we must replace $k \to kS^{1/3}$. Notice indeed, that the Fourier transform defined in §16.2 with the substitution $k \to kS^{1/3}$ becomes the same as the one defined in §17.4

¹² The large M_t solution is discarded since it corresponds to ideal instability.

From this relation and exploiting the smallness of H, we infer that interchange modes are unstable when

$$0 < D_R \approx -\frac{\alpha \Delta'}{s} - \frac{\alpha r_s}{s^2 R_0} \left(1 - \frac{1}{q^2} \right),$$

with the largest growth rate attained for $\ell=0$. According to the expression above, configurations with a monotonically **decreasing pressure profile** and a **reversed magnetic shear**, i.e. exhibiting regions where s < 0, may be prone to developing resistive interchange instabilities (Furukawa (1999)). Notice that in the derivation above we did not impose any ordering on the magnetic shear.

17.5.3 Tearing modes

Let us assume $0 < |\tau| \ll 1$ and $D_R < 0$. The second term on the left-hand-side of (17.51) is of order τ^2 so that it can be dropped if τ is sufficiently small. Hence, by means of (17.46), the dispersion relation becomes

$$(M_t V_e)^{-1/2-\tau} \frac{\Gamma\left(\frac{1}{4}(M_t + 3 - 2\tau - D_R/M_t)\right)(M_t + \tau + H)}{\Gamma\left(\frac{1}{4}(M_t + 5 + 2\tau - D_R/M_t)\right)(M_t - 1 - \tau + H)}$$

$$= \epsilon_R^{1+2\tau} \Gamma^2(1+\tau) \frac{\Gamma(-\frac{1}{2} - \tau)}{\pi\Gamma(\frac{1}{2} + \tau)} r_s \Delta' \equiv -\Delta_{ext}, \qquad (17.54)$$

where we defined $r_s\Delta' = A_1 + A_2$ which is assumed to be a quantity of the order of unity.

Further simplification can be achieved by assuming

$$\epsilon \sim \tau \sim H \sim D_R \ll M_t \ll 1$$
,

where ϵ is some smallness parameter. Expanding the left-hand-side of (17.54) to first order in ϵ and then taking the $M_t \ll 1$ limit eventually yields¹³

$$\sqrt{\frac{M_t}{V_e}} \frac{\Gamma(3/4)}{\Gamma(5/4)} \left(1 - \frac{\pi D_R}{4M_t} \right) = \Delta_{ext}.$$
 (17.55)

Although we took $D_R \ll M_t$, later we let these two quantities to have comparable magnitude. The equation above can be conveniently rearranged in the form

$$f \equiv a\gamma_*^{5/4} + b\gamma_*^{-1/4} - \Delta_{ext} = 0, \tag{17.56}$$

where $\gamma_* = \gamma/\omega_A$ with a and b given by

$$a = \frac{\Gamma(3/4)}{\Gamma(5/4)} \frac{S^{5/12}}{m} \sqrt{\frac{q_s \sqrt{1 + 2q_s^2}}{sm}},$$

$$b = \frac{\Gamma(3/4)}{\Gamma(5/4)} \frac{S^{-1/12}}{m} \sqrt{\frac{sm}{q_s \sqrt{1 + 2q_s^2}}} \frac{\pi |D_R|}{4}.$$

This typically holds in configurations with positive shear and monotonically decreasing pressure profile.

Note that (14.20) is recovered for $\tau = H = D_R = 0$.

¹³ Here one has $D_R \approx -H - \tau$. Terms of the form $\ln(M_t V_e)$ are neglected compared to those which have a dependence of the type M_t^{-1} .

We want to determine if equation (17.56) has some **complex** solutions with $Re(\gamma/\omega_A) > 0$. This problem is best tackled by employing **Nyquist** techniques.

Let's consider in the complex γ_* -plane the contour C obtained by joining together the paths C_i (i = 1, ..., 4) as shown in figure 17.1. No poles of f are within the interior of C. Furthermore, allowing $R \to \infty$ and $d \to 0$ permits the whole half-plane with $\gamma_* > 0$ to be encircled by C. We now define the function g as

$$g = a\gamma_*^{5/4} + b\gamma_*^{-1/4},$$

and denote with f(C) and g(C) the image of C through the mappings fand g respectively. Adding a constant factor to g moves g(C) horizontally in the Re(g) - Im(g) plane: therefore the shape of f(C) is obtained from g(C) translating it by the amount Δ_{ext} (forwards if $\Delta_{ext} < 0$ or inwards $\Delta_{ext} > 0$).

In the limit of $R \to \infty$, the image of C_1 is obtained by setting $\gamma_* =$ Re^{it} with $-\frac{\pi}{2} < t < \frac{\pi}{2}$ so that

$$g(C_1) = aR^{5/4}e^{i5t/4}.$$

Conversely, letting $\gamma_* = de^{-it}$ with $d \to 0$ we obtain

$$g(C_3) = bd^{-1/4}e^{it/4}$$
.

The paths C_2 and C_4 are parametrised by $\gamma_* = ze^{\pm i\pi/2}$ (plus sign for C_2 and minus sign for C_4) with z varying between d and R following the orientation shown in Fig. 17.1. This yields

$$g(C_2) = \left(-az^{5/4}\sin\frac{\pi}{8} + bz^{-1/4}\cos\frac{\pi}{8}\right) + i\left(az^{5/4}\cos\frac{\pi}{8} - bz^{-1/4}\sin\frac{\pi}{8}\right),$$

$$g(C_4) = \left(-az^{5/4}\sin\frac{\pi}{8} + bz^{-1/4}\cos\frac{\pi}{8}\right) - i\left(az^{5/4}\cos\frac{\pi}{8} - bz^{-1/4}\sin\frac{\pi}{8}\right).$$

It is immediate to see that $g(C_4) = \overline{g(C_2)}$. We find that $g(C_2)$ crosses the real axis in the Re(g) - Im(g) plane at

$$Re(g) = \frac{\cos \frac{\pi}{4}}{\cos \frac{\pi}{8}} \left(ab^5 \cot \frac{\pi}{8} \right)^{1/6} \equiv z_1 > 0,$$

and intersects the imaginary axis in

$$Im(g) = \frac{\cos\frac{\pi}{4}}{\sin\frac{\pi}{8}} \left(ab^5 \tan\frac{\pi}{8}\right)^{1/6} \equiv z_2 > 0.$$

A qualitative behaviour of g(C) is shown in figure 17.2.

With the contour C given above, the Cauchy's argument principle states that if f(C) encircles (counterclockwise) the origin in the Re(f) – Im(f) plane N times, with N a positive integer, then there exist N roots of the equation f = 0 with positive γ_* . In order for this to happen, one

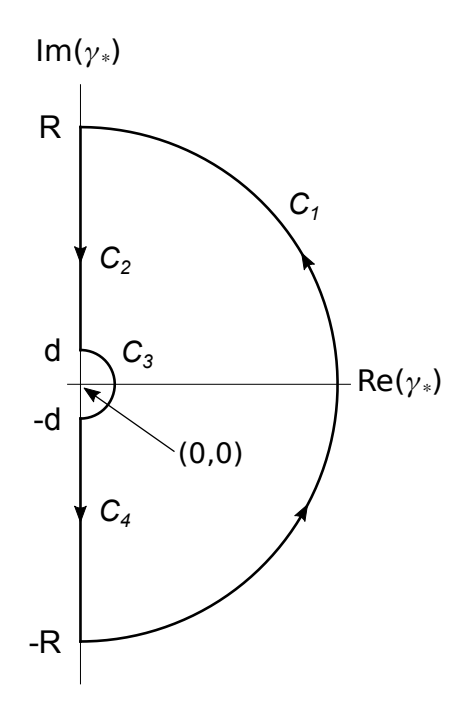


Figure 17.1: Contour C in the complex γ_* plane. We let $R \to \infty$ and $d \to 0$ so that all points with $Re(\gamma_*) > 0$ are enclosed by C. Note that this contour avoids the origin which is the pole of the functions f and g.

Recall that the overbar denotes complex conjugation.

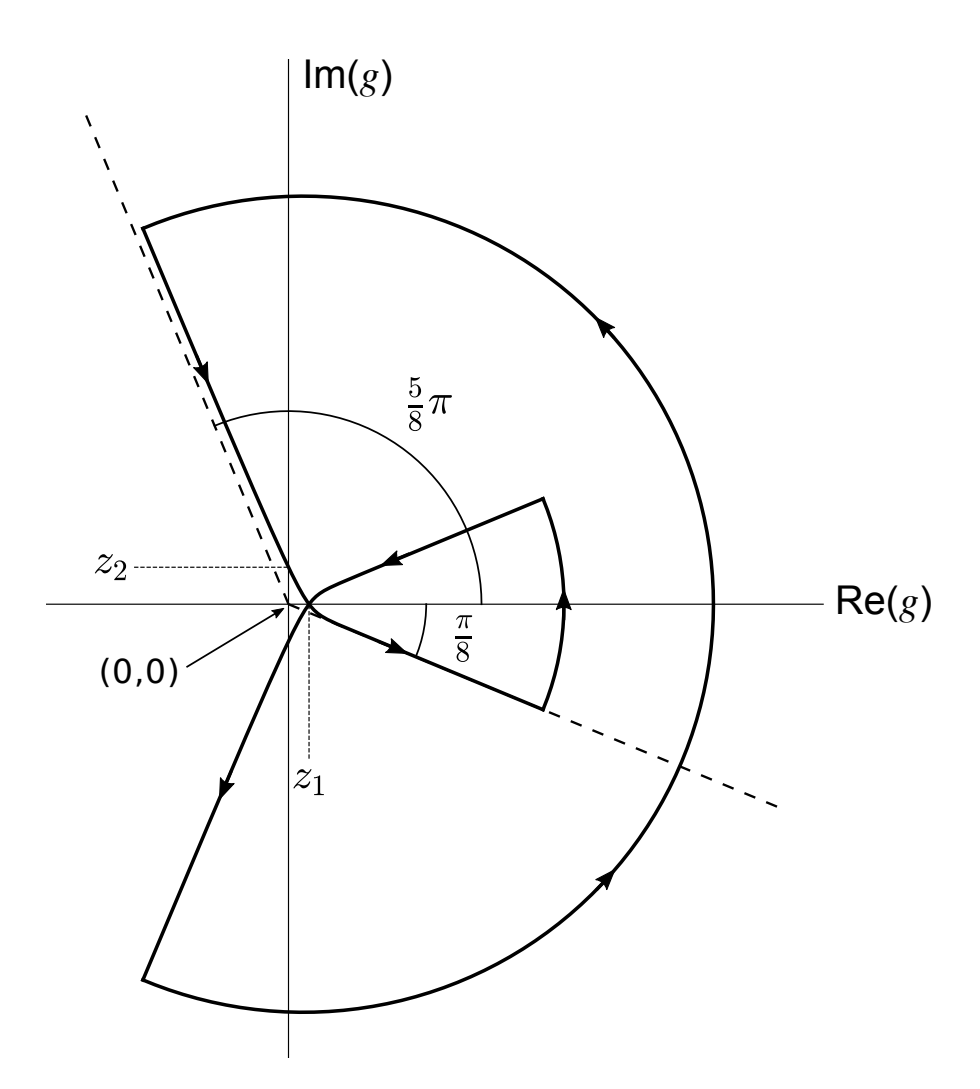


Figure 17.2: Qualitative example of the mapping of the contour C in the Re(g) - Im(g) plane. In drawing this figure we took $d > (b/a)^4 R^{-5}$, which ensures that the radius of the arc associated with the path C_3 is smaller than the one associated with C_2 . If we shift the plot by a finite amount such that the origin is encircled by g(C), one sees that $\operatorname{Ind}_{g(C)}(0) = 2$ when $R \to \infty$.

must have $\Delta_{ext} > z_1$. Letting $\tau \to 0$ in the expression of Δ_{ext} , it follows that instability can occur only if (Glasser (1975))¹⁴

$$r_s \Delta' > 2\pi \frac{\Gamma(3/4)}{\Gamma(1/4)} \frac{(nsS)^{1/3}}{(1+2q_s^2)^{1/6}} \left(\frac{\pi}{4}|D_R|\right)^{5/6} \frac{\cos\frac{\pi}{4}}{\cos\frac{\pi}{8}} \left(\cot\frac{\pi}{8}\right)^{1/6},$$
 (17.57)

having used the fact that $m/q_s = n$. This is the **modified instability criterion for tearing modes**. Numerical analyses (Hender (1987)) confirmed the validity of this result. Larger values of $r_s\Delta'$ are needed for the instability to happen as S is increased. At very large S the resistive marginal boundary is very close to the ideal one.

It is worth mentioning that a dispersion relation similar to (17.57) can also be obtained for resistive ballooning modes (Strauss (1981), Correa-Restrepo (1982)).

$$\frac{r_s V_s}{X_0} = \frac{(nsS)^{1/3}}{(1 + 2q_s^2)^{1/6}},$$

and Δ' in this report corresponds to Δ in Glasser (1975). Notice also that

$$2\frac{\cos\frac{\pi}{4}}{\cos\frac{\pi}{8}}\left(\cot\frac{\pi}{8}\right)^{1/6}=\frac{\sqrt{2}}{\sin\frac{\pi}{8}}\left(\tan\frac{\pi}{8}\right)^{5/6}.$$

¹⁴ In the notation of Glasser (1976) one

Cauchy's argument principle

Nyquist graphical analysis is based on the following theorem of complex analysis. Let C be a closed contour (oriented counterclockwise) in the complex plane without intersections and take a function f which is **holomorphic** on C and its interior except for a set of isolated points (the poles of the function). If f does not have zeroes or poles on C then the following holds

$$\operatorname{Ind}_{\Gamma}(0) = \frac{1}{2\pi i} \int_{C} \frac{f'(z)}{f(z)} dz = N - P,$$

where N and P are the number of zeros and poles of f in the interior of C respectively counted according to their multiplicity. The **winding number** $\operatorname{Ind}_{\Gamma}(0)$ is an integer which gives the total number of times the curve $\Gamma = f \circ C$, which is the image of C through the function f, winds counterclockwise around the origin in the $\operatorname{Re}(f) - \operatorname{Im}(f)$ plane. The curve Γ is also called f(C). Hence, letting C to be a contour which encloses points on the right half-plane, if P = 0 and $\operatorname{Ind}_F(0) \neq 0$ the theorem above guarantees that f = 0 for some points inside C. i.e. with positive real part (these roots may have a non-vanishing imaginary part).

A plane closed curve with no selfintersections (simple) is said to be counterclockwise oriented if the curve interior is always on the left when travelling along the curve itself.

References

- M. Abramowitz and I. A. Stegun (eds.), Handbook of Mathematical Functions, Dover Publications (New York, US), 1964.
- B. Coppi et al., Nucl. Fusion 6, 101 (1966).
- D. Correa-Restrepo, Z. Naturforsch. A 37, 848 (1982).
- M. Furukawa et al., Nucl. Fusion 39, 2077 (1999).
- A. H. Glasser et al., Phys. Fluids 18, 875 (1975).
- A. H. Glasser et al., Phys. Fluids 19, 567 (1976).
- A. H. Glasser et al., Phys. Fluids 27, 1225 (1984).
- J. M. Greene, **Introduction to Resistive Instabilities** (LRP 114/76), École Polytechnique Fédérale de Lausanne, (Lausanne Switzerland), 1976.
- T. C. Hender et al., Nucl. Fusion 27, 1389 (1987).
- J. L. Johnson and J. M. Greene, Plasma Phys. 9, 611 (1967).
- S. E. Kruger et al., Phys. Plasmas 5, 4169 (1998).
- S. Lang, Complex Analysis, Spinger-Verlag (New York, US), 1999.
- A. B. Mikhajlovskij, Nucl. Fusion 15, 95 (1975).
- A. B. Mikhailovskii, Instabilities in a Confined Plasma, Institute of Physics Publishing (Bristol, UK), 1998.
- W. Rudin, Real and Complex Analysis, McGraw-Hill (Singapore, SG), 1987.
- H. R. Strauss, Phys.Fluids 24, 2004 (1981).

Part V APPENDICES



Particle motion in a tokamak-like magnetic field

In this appendix we discuss the importance of a helical field for particle confinement, thus showing why a toroidal current is needed. This is accomplished by analysing particle trajectories in a tokamak-like magnetic field.

Let us assume that a helical field winds around toroidally concentric nested surfaces (**magnetic surfaces**) of **circular cross section**. We employ the right-handed orthogonal coordinate system (r, θ, ϕ) introduced in section 3.1.2. In this coordinates the velocity vector has components $\mathbf{v} = (dr/dt, rd\theta/dt, Rd\phi/dt)$ where $R = R_0 + r\cos\theta$. We assume that the radial magnetic field is vanishing $(B_{\rm rad} \equiv B_r = 0)$, while the toroidal and poloidal components are $(B_0 > 0)$

$$B_{
m tor} \equiv B_{\phi} = rac{R_0 B_0}{R}, \quad B_{
m pol} \equiv B_{ heta} = rac{r B_0}{R \, q(r)}.$$

The latter expression, with q a generic function of r, follows from the divergence-free condition of the magnetic field. The function q is assumed to be positive definite. To leading order one has $B \approx B_{\rm tor}$ with the magnetic field stronger for $\theta = \pi$ and weaker at $\theta = 0$.

Neglecting the electric field, the particle kinetic energy and magnetic moment are conserved (cf. (1.1)), and the trajectory of the **guiding centre** is described by the projections of (1.4) along the radial, poloidal and toroidal directions. This yields for a particle with charge e_s and

¹ This corresponds to the safety factor parameter discussed in §4.1.

mass m_s

$$\begin{split} \frac{dr}{dt} &\approx -\frac{m_s(v_\perp^2 + 2v_{||}^2)}{2e_s B_0 R_0} \sin \theta \equiv -v_b \sin \theta, \\ r\frac{d\theta}{dt} &\approx \frac{rv_{||}}{R_0 q} - \frac{m_s(v_\perp^2 + 2v_{||}^2)}{2e_s B_0 R_0} \cos \theta \equiv \frac{rv_{||}}{R_0 q} - v_b \cos \theta, \\ R\frac{d\phi}{dt} &\approx v_{||}, \end{split} \tag{A.1}$$

The particle Larmor radius is assumed to be small compared to the characteristic length of the system.

having ordered $q \sim 1$, $\epsilon = r/R_0 \ll 1$ and $v_b/(\epsilon v_{||}) \sim \epsilon \ll 1$. Because $B_{\rm pol}/B_{\rm tor} \sim \epsilon \ll 1$, it follows at once that corrections of the order of the Larmor radius entering the expression for $d\phi/dt$ can be neglected (they are ϵ times smaller than those appearing in dr/dt and $rd\theta/dt$). For obtaining the particle trajectory projected onto the poloidal plane we just need the first two of (A.1). From the equation for dr/dt, we infer that the departure of the orbit from the surface of radius r is expected to be small, so that the analysis may be carried out on a single magnetic surface at a time.

Let us ignore, for the moment, Larmor radius corrections to $d\theta/dt$. A particle experiences the poloidal non-uniformities of the magnetic field during its motion, and it may undergo *mirror effects* moving into regions of stronger field, similar to what discussed in section 1.2.1 for the case of open configurations. This means that an angle θ_* for which $v_{||} = 0$, and the particle is **reflected**, can exist. Reflection occurs if (see (1.3) with $B_{\text{max}} = B_0(1 + \epsilon)$)

$$\frac{\mathscr{E}}{\mu B_0} < 1 + \epsilon.$$

Particles fulfilling this condition which bounce poloidally back and forth between $-\theta_*$ and θ_* are called **trapped**, otherwise they are said to be **passing**.² From (1.1), we may now express the parallel velocity as

$$v_{||} = \pm \sqrt{\frac{2\mu B_0}{m_s} \epsilon \left(2x^2 - 1 + \cos\theta\right)}, \quad \text{with} \quad x^2 = \frac{\mathscr{E} - \mu B_0(1 - \epsilon)}{2\mu B_0 \epsilon}. \quad (A.2)$$

Passing particles have $x^2 > 1$, whereas if $0 < x^2 < 1$ the particle will be reflected when the angle θ_* (or $-\theta_*$) is approached.³ Since $1 - \cos \theta = 2\sin^2\frac{\theta}{2}$, it is easy to see that $\sin \theta_*/2 = \kappa$.

Hence, taking the ratio of dr/dt over $d\theta/dt$ in (A.1) gives

$$\frac{dr}{d\theta} \approx \mp \frac{q}{2\Omega_s} \frac{v_{\perp}^2 + 2v_{||}^2}{\sqrt{\frac{2\mu B_0}{m_s}\epsilon}} \frac{\sin \theta}{\sqrt{2\chi^2 - 1 + \cos \theta}},\tag{A.3}$$

having defined the **cyclotron frequency** $\Omega_s = e_s B_0/m_s$. Noticing that

$$\frac{m_s(v_\perp^2 + 2v_{||}^2)}{2} = \mu B_0 \left[1 + 2\epsilon \left(2x^2 - 1 + \frac{1}{2}\cos\theta \right) \right] \tag{A.4}$$

² A passing particle is still "caged" by the magnetic field.

³ Since $\frac{\mathscr{E}}{\mu B_0}|_{\min} \approx 1 - \epsilon$, it follows that $0 < \chi^2 < \infty$.

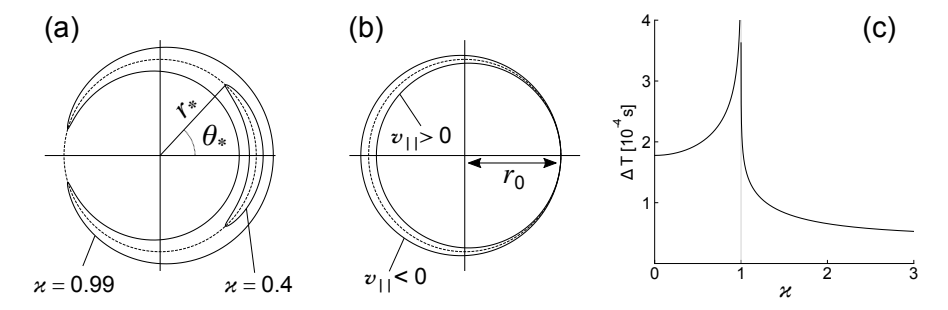


Figure A.1: Trapped (a) and passing (b) ion orbits for a deuteron of energy $\mathcal{E} = 10keV$ with $\epsilon = 0.1$, $B_0 = 3T$ and q = 2. In this case $r_* = r_0 = 0.3a$ where a = 1m is the minor radius of the device with $R_0 = 3.\overline{3}m$. The associated transit time ΔT as a function of the parameter x is shown in (c). Note that the transit time diverges when x approaches unity.

is approximately constant if ϵ is sufficiently small, and assuming that q and ϵ do not change significantly to the relevant order, equation (A.3) can be readily integrated giving

$$r = \pm \frac{q}{\Omega_s} \frac{v_\perp^2 + 2v_{||}^2}{\sqrt{\frac{2\mu B_0}{m_s} \epsilon}} \sqrt{2\varkappa^2 - 1 + \cos\theta} + const. \tag{A.5}$$

This provides a functional relation between r and θ .

For passing particles we expand (A.5) for $\varkappa\gg 1$, and obtain in the $\epsilon\ll 1$ limit

$$egin{aligned} r-r_0 &pprox rac{q}{2\Omega_s} rac{v_\perp^2 + 2v_{||}^2}{v_{||}} \left(\cos heta - 1
ight) \ &= \pm rac{q}{2\Omega_s} \sqrt{rac{\mathscr{E}}{m_s \epsilon}} \left(rac{1 + 4\epsilon arkappa^2}{arkappa \sqrt{1 + 2\epsilon arkappa^2}}
ight) \left(\cos heta - 1
ight), \end{aligned}$$

with r_0 denoting the radial position of the particle at $\theta = 0$. Here we exploited (A.2) to express μB_0 as a function of \mathscr{E} and \varkappa .

Assuming that $\theta=0$ at t=0, the time Δt required for the particle to complete a poloidal turn, which we call **transit time**, is calculated by integrating the second expression in (A.1), that is $d\theta/dt \approx v_{||}/(R_0q)$, with the parallel velocity given by (A.2). This yields

$$\frac{\varkappa}{R_0 q} \sqrt{\frac{\mu B_0 \epsilon}{m_s}} \Delta t = \int_0^{\pi} \frac{d\theta}{\sqrt{1 - \varkappa^{-2} \sin^2 \frac{\theta}{2}}} = 2K \left(\frac{1}{\varkappa}\right),$$

where K is the complete elliptic integral of the first kind (for the definition of the elliptic integrals see **sidenote 24** in section 4.4.1).

For a trapped particle ($\chi^2 < 1$) let r_* be the radius of the circular surface on which the reflection point with angle θ_* lies. After setting $\epsilon \ll 1$ in (A.4), equation (A.5) becomes

$$r - r_* \approx \pm \frac{q}{\Omega_s} \sqrt{\frac{2\mu B_0}{m_s \epsilon} \left(2x^2 - 1 + \cos\theta\right)}.$$
 (A.6)

Figure A.2: Example of the trajectory of a trapped particle showing toroidal precession

Exploiting the properties of the complete and incomplete elliptic integrals of the first kind we have

$$\begin{split} & \int_0^{\theta_*/2} \frac{dy}{\sqrt{1-\varkappa^{-2}\sin^2 y}} = \\ & \int_0^{\sin\frac{\theta_*}{2}} du [(1-u^2)(1-\varkappa^{-2}u^2)]^{-1/2} = \\ & \varkappa \int_0^1 dz [(1-z^2)(1-\varkappa^2z^2)]^{-1/2} = \\ & \varkappa \int_0^{\pi/2} \frac{dy}{\sqrt{1-\varkappa^2\sin^2 y}} \equiv \varkappa K(\varkappa). \end{split}$$

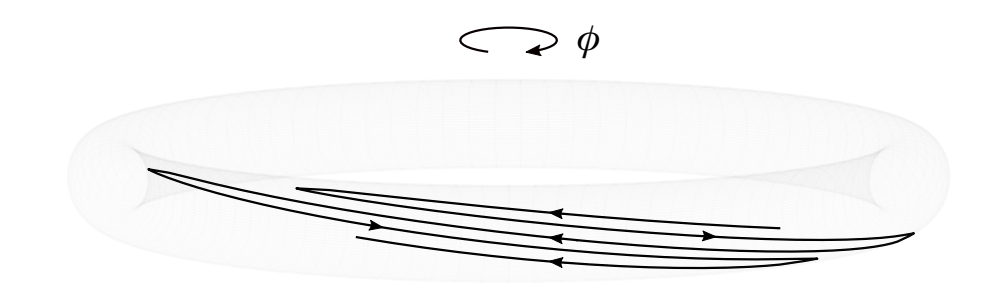
Notice that the integral over a closed particle orbit is

$$\oint Ad\theta = \int_{-\theta_*}^{\theta_*} Ad\theta + \int_{\theta_*}^{-\theta_*} Ad\theta,$$

where the second integral on the right-hand-side is performed after the reflection. If A=1 or $A=\cos\theta$ the total integral is zero. while if $A=\pm f(\cos\theta)$, i.e. it changes sign after the reflection point θ_* along the orbit, one has

$$\oint Ad\theta = 4 \int_0^{\theta_*} f(\cos \theta) d\theta$$

having exploited the fact that f is an even function of θ .



Trapped particle orbits are called **banana orbits**. The largest radial excursion is attained by marginally trapped particles with $\kappa^2 = 1 - \delta$ and $\delta \ll 1$; since $2\mu B_0/m_s \approx v_\perp^2$ it follows that $r - r_* \sim q r_{L,s}/\sqrt{\epsilon}$ where $r_{L,s}$ is the particle Larmor radius defined in section 1.2.1. Note the radial departure of **deeply passing** particles with $\kappa \to \infty$ is $\sqrt{\epsilon}$ times smaller (in order of magnitude) than the one of trapped ones. Finally, as we did for passing particles, we assume that $\theta = 0$ at t = 0 and integrate $d\theta/dt$ to get the oscillation period Δt along the closed trajectory:

$$\frac{\varkappa}{4R_0q}\sqrt{\frac{\mu B_0\epsilon}{m_s}}\Delta t = \int_0^{\theta_*/2} \frac{dy}{\sqrt{1-\varkappa^{-2}\sin^2 y}} = \varkappa K(\varkappa). \tag{A.7}$$

Typical poloidal plane orbit projections and transit time of trapped and passing particles are shown in figure A.1.

We shall now focus on the motion in the toroidal direction. Taking the ratio of the third over the second equation in (A.1) gives

$$\frac{d\phi}{d\theta} = \frac{R_0 q}{R} \left(1 + \frac{\frac{v_b q}{\epsilon} \cos \theta}{v_{||} - \frac{v_b q}{\epsilon} \cos \theta} \right).$$

For well passing particles the parallel velocity is large compared with v_b and never vanishes, so that the toroidal angular position steadily increases in time and the associated trajectory is a helix that wraps around the magnetic surface.

For trapped particles the situation requires a more careful analysis. Letting $\kappa < 1$ with $\epsilon \ll 1$, from (A.4) we may approximate $v_b \approx \frac{\mu B_0}{m_s \Omega_s R_0} \approx const.$ Thus, expanding both q and R around r_* we have to leading order

$$\frac{d\phi}{d\theta} \approx q_* \left(1 - \epsilon_* \cos \theta + s_* \frac{r - r_*}{r_*} + \frac{q_* v_b}{\epsilon_* v_{||}} \cos \theta \right), \tag{A.8}$$

where $q_*=q(r_*)$, $s_*=[(rdq/dr)/q]_{r_*}$ and $\epsilon_*=r_*/R_0$. In the equation above $v_{||}$ has to be evaluated at r_* as well. By means of (A.2) and (A.6), this equation can be easily integrated and the result expressed in terms of the elliptic integrals of the first and second kind. Let $\Delta\phi=\oint (d\phi/d\theta)d\theta$ denote the increase of the toroidal angle after a trapped particle closed orbit period. From (A.6) we have $r-r_*\sim [R_0/(\Omega_s\epsilon)]^{1/2}\sqrt{v_b}$, hence if $v_b\to 0$ in (A.8) then $\Delta\phi=0$, i.e. the particle bounces back and forth in the toroidal direction with a zero average toroidal drift.

However, with $v_b \neq 0$ one finds

$$\begin{split} \Delta\phi &= \frac{4q_*^2}{r_*\Omega_s}\sqrt{\frac{\mu B_0}{2\epsilon_* m_s}} \times \\ &\times \left[\int_0^{\theta_*} \frac{\cos\theta}{\sqrt{2\varkappa^2 - 1 + \cos\theta}} d\theta + 2s_* \int_0^{\theta_*} \sqrt{2\varkappa^2 - 1 + \cos\theta} d\theta \right] \\ &= \frac{8q_*^2}{r_*\Omega_s} \sqrt{\frac{\mu B_0}{\epsilon_* m_s}} K(\varkappa) \left[\frac{E(\varkappa)}{K(\varkappa)} - \frac{1}{2} + 2s_* \left(\frac{E(\varkappa)}{K(\varkappa)} - 1 + \varkappa^2 \right) \right], \end{split}$$

where E(x) is the complete elliptic integral of the second kind. This shows that there is an **average precession in the toroidal direction** (see figure A.2). The associated mean velocity is obtained by evaluating $\Delta \phi/\Delta t$ with Δt from (A.7).

Notice that particle trajectories will be modified by the inclusion of electric fields and collisions.

References

- M. Abramowitz and I. A. Stegun (eds.), Handbook of Mathematical Functions, Dover Publications (New York, US), 1964.
- R. Balescu, Transport Processes in Plasmas Vol. 2 Neoclassical Transport Theory, North-Holland (Amsterdam, NL), 1988.
- H. L. Berk and A. A. Galeev, Phys. Fluids 10, 441 (1967).
- T. J. M. Boyd and J. J. Sanderson, **The Physics of Plasmas**, Cambridge University Press (Cambridge, UK), 2003.
- A. A. Galeev and R. Z. Sagdeev, Zh. Eksp. Teor. Fiz. **53**, 348 (1967) [Sov. Phys.-JETP **26**, 233 (1968)].
- P. Helander and D. J. Sigmar, Collisional Transport in Magnetized Plasmas, Cambridge University Press (Cambridge, UK), 2005.
- B. B. Kadomtsev and O. P. Pogutse, Zh. Eksp. Teor. Fiz. **51**, 1734 (1966) [Sov. Phys.-JETP **24**, 1172 (1967)].
- A. I. Morozov and L. S. Solov'ev, Reviews of Plasma Physics Vol. 2 p. 201 (Ed. M. A. Leontovich), Consultants Bureau (New York, US), 1966.
- W. M. Stacey, Fusion Plasma Physics, Wiley (New York, US), 2012.

$$\begin{split} &\int_0^{\frac{\theta_*}{2}} \sqrt{\varkappa^2 - \sin^2\theta} d\theta = \varkappa \int_0^{\varkappa} \frac{\sqrt{1 - \varkappa^{-2} t^2}}{\sqrt{1 - t^2}} dt = \\ &\varkappa^2 \int_0^1 \frac{\sqrt{1 - z^2}}{\sqrt{1 - \varkappa^2 z^2}} dz = \varkappa^2 \int_0^{\pi/2} \frac{\cos^2\theta d\theta}{\sqrt{1 - \varkappa^2 \sin\theta^2}} \\ &= E(\varkappa) + (\varkappa^2 - 1)K(\varkappa). \end{split}$$

In the last equality one uses $\cos^2 \theta = 1 - \sin^2 \theta$.

B

Tokamak GCP equilibrium

Here we discuss tokamak equilibrium within the anisotropic GCP model presented in chapter 2 (see §2.4). Although the problem of plasma anisotropy is not addressed in this report, we nevertheless think that it is useful to summarise clearly and simply some of the techniques involved in its analysis.

We start with (2.15) which can be cast as

$$\frac{d}{dt}\bar{f_s}(\boldsymbol{x},v_{||},\mu,t) = \frac{\partial \bar{f_s}}{\partial t} + \frac{d\boldsymbol{x}}{dt} \cdot \frac{\partial \bar{f_s}}{\partial \boldsymbol{x}} + \frac{dv_{||}}{dt} \frac{\partial \bar{f_s}}{\partial v_{||}} = 0,$$

having defined b = B/B and

$$\begin{split} \frac{d\mathbf{x}}{dt} &= \mathbf{u}_{\perp} + v_{||}\mathbf{b}, \\ \frac{dv_{||}}{dt} &= v_{||}\mathbf{u}_{\perp} \cdot (\mathbf{b} \cdot \nabla \mathbf{b}) - \mathbf{b} \cdot \nabla \left(\mu B + \frac{e_s}{m_s} \Phi_E - \frac{u_{\perp}^2}{2}\right). \end{split}$$

Here $\mu = v_{\perp}^2/2B$. We change coordinates from $v_{||}$ to $\epsilon_s(\mathbf{x}, v_{||}, \mu, t)$, to be defined later, yielding

$$\frac{d}{dt}\bar{f_s}(\mathbf{x},\epsilon_s,\mu,t) = \frac{\partial \bar{f_s}}{\partial t} + \frac{d\mathbf{x}}{dt} \cdot \frac{\partial \bar{f_s}}{\partial \mathbf{x}} + \left(\frac{\partial \epsilon_s}{\partial t} + \frac{d\mathbf{x}}{dt} \cdot \frac{\partial \epsilon_s}{\partial \mathbf{x}} + \frac{dv_{||}}{dt} \frac{\partial \epsilon_s}{\partial v_{||}}\right) \frac{\partial \bar{f_s}}{\partial \epsilon_s} = 0,$$
(B.1)

having exploited the conservation of the magnetic moment Eq. (2.16). We choose

$$\epsilon_s = \frac{1}{2}v_{||}^2 + \mu B_0,$$
 (B.2)

where B_0 is the equilibrium magnetic field. As a matter of notation, equilibrium quantities are indicated by the subscript o.

We stress the fact that the choice of ϵ_s is not unique. With this definition of ϵ_s , it immediately follows that (recall that x, $v_{||}$ and μ are

independent variables)

$$\frac{\partial \epsilon_s}{\partial t} = 0, \quad \nabla \epsilon_s = \mu \nabla B_0, \quad \frac{\partial \epsilon_s}{\partial v_{||}} = v_{||}.$$

Using the expressions above into (B.1) gives

$$\frac{\partial \bar{f}_{s}}{\partial t} + (\boldsymbol{u}_{\perp} + v_{||}\boldsymbol{b}) \cdot \nabla \bar{f}_{s} + \left[(\boldsymbol{u}_{\perp} + v_{||}\boldsymbol{b}) \cdot \nabla \mu B_{0} + v_{||} \left(v_{||}\boldsymbol{u}_{\perp} \cdot (\boldsymbol{b} \cdot \nabla \boldsymbol{b}) - \boldsymbol{b} \cdot \nabla E_{s} \right) \right] \frac{\partial \bar{f}_{s}}{\partial \epsilon_{s}} = 0,$$
(B.3)

where $E_s = \mu B + \frac{\ell_s}{m_s} \Phi_E - \frac{u_\perp^2}{2}$. For an equilibrium with no flows we take $\partial/\partial t = 0$, $\boldsymbol{u}_\perp = 0$ and $\Phi_{E0} = 0^1$ so that equation (B.3) dictates

$$\boldsymbol{b}_0 \cdot \boldsymbol{\nabla} \bar{f}_{s0} = 0, \tag{B.4}$$

that is $\bar{f}_{s0} = \bar{f}_{s0}(\psi, \epsilon_s, \mu)$ where ψ is the equilibrium poloidal flux. Let us introduce the parallel gradient operator $\nabla_{||} = \boldsymbol{b}_0 \cdot \boldsymbol{\nabla}$. Hereafter we consider a globally neutral static plasma consisting of electrons with charge -e and ions with charge +e.

To determine the expressions for $p_{||0}$ and $p_{\perp 0}$ it is more convenient to transform the integrals in Eqs. (2.18) into integrals in $d\mu$ and $d\epsilon_s$. In doing so, we invert (B.2) to obtain

$$v_{\parallel} = \pm \sqrt{2\left(\epsilon_s - \mu B_0\right)},\tag{B.5}$$

where μ is allowed to vary from 0 to ∞ . Hence, at fixed μ , one has $v_{||}dv_{||}=d\epsilon_s$ and since $v_{||}^2$ ranges from 0 to ∞ then ϵ_s varies from its minimum value $\epsilon_{s,min}=\mu B_0$ to ∞ . This yields

$$\int d^3 \mathbf{v} = 2\pi \int_0^\infty d\mathbf{v}_\perp \mathbf{v}_\perp \int_{-\infty}^\infty d\mathbf{v}_{||} \mathbf{v}_{||} = \sum_{\sigma} 2\pi \int_0^\infty d\mu \int_{\epsilon_{s,min}}^\infty d\epsilon_s \frac{\mathbf{B}_0}{|\mathbf{v}_{||}|},$$

where $\sigma = +1$ for $v_{||} > 0$ and $\sigma = -1$ for $v_{||} < 0$. It follows that the parallel and perpendicular pressure can be written as

$$p_{||0} = \sum_{\sigma,s} 2\pi m_s \int_0^\infty d\mu \int_{\epsilon_{s,min}}^\infty d\epsilon_s B_0|v_{||}|\bar{f}_{s0},$$

$$p_{\perp 0} = \sum_{\sigma} 2\pi m_s \int_0^\infty d\mu \int_{\epsilon_{s,min}}^\infty d\epsilon_s \frac{\mu B_0^2}{|v_{||}}\bar{f}_{s0}.$$

Because $\nabla_{||}\bar{f}_{s0}=0$, it is easy to see that

$$\nabla_{||} p_{||0} = (p_{||0} - p_{\perp 0}) \frac{\nabla_{||} B_0}{B_0}, \tag{B.6}$$

having used (cf. (B.5))

$$abla_{||}(B_0|v_{||}) = |v_{||}|\nabla_{||}B_0 - \frac{B_0}{|v_{||}|}\nabla_{||}(\mu B_0).$$

¹ If equilibrium flows are allowed, then $\Phi_{E0} \neq 0$. This is because the parallel and perpendicular components of the electric field decouple as they appear at different orders in m_s/e_s .

In order to make the action of the parallel gradient operator on $1/|v_{||}|$ analytically manageable, we first note that

$$\int_{\epsilon_{s,min}}^{\infty} d\epsilon_s \frac{\bar{f}_{s0}}{|v_{||}|} = |v_{||}|\bar{f}_{s0}|_{\epsilon_{min}}^{\infty} - \int_{\epsilon_{s,min}}^{\infty} d\epsilon_s |v_{||}| \frac{\partial \bar{f}_{s0}}{\partial \epsilon_s}.$$

If \bar{f}_{s0} decreases faster than $1/|v_{||}|$ for $\epsilon_s \to \infty$, the first term on the right-hand-side of the equation above vanishes since $|v_{||}|(\epsilon_{s,min}) = 0$. Therefore we may recast the perpendicular pressure as

$$p_{\perp 0} = -\sum_{\sigma,s} 2\pi m_s \int_0^\infty d\mu \int_{\epsilon_{s,min}}^\infty d\epsilon_s |v_{||} |\mu B_0^2 \frac{\partial \bar{f}_{s0}}{\partial \epsilon_s}.$$

Following a procedure similar to the one used above for $p_{||0}$, we get

$$\nabla_{||} p_{\perp 0} = \left(2p_{\perp 0} + C \right) \frac{\nabla_{||} B_0}{B_0}, \tag{B.7}$$

where C is defined by

$$C = \sum_{\sigma,s} 2\pi m_s \int_0^\infty d\mu \int_{\epsilon_{s,min}}^\infty d\epsilon_s \frac{\mu^2 B_0^3}{|v_{||}|} \frac{\partial \bar{f}_{s_0}}{\partial \epsilon_s}.$$

Given the expressions for $p_{\parallel 0}$ and $p_{\perp 0}$, the macroscopic MHD equilibrium is then determined by (2.17). A quick computation shows that (cf. section 2.4.2)

$$0 = -\nabla p_{\perp 0} + \left(1 - \hat{\Delta}\right) \mathbf{J}_0 \times \mathbf{B}_0 - \hat{\Delta} \nabla B_0^2 / 2 - \mathbf{B}_0 \left(\mathbf{B}_0 \cdot \nabla \hat{\Delta}\right), \tag{B.8}$$

with $\hat{\Delta} = (p_{\parallel 0} - p_{\perp 0})/B_0^2$. Let use introduce a toroidal coordinate system (r, θ, ϕ) as the one used in §4.3 with r a flux variable with the dimensions of a length, θ a generic poloidal angle and ϕ the toroidal angle. The system is axisymmetric so that $\partial/\partial\phi = 0$ for any equilibrium scalar quantity. With a magnetic field of the form (cf. (4.4))³

$$\mathbf{B} = B_{\phi 0}(r, \theta) \nabla \phi - \nabla \psi(r) \times \nabla \phi$$

with ψ denoting the equilibrium poloidal flux, the covariant projection of (B.8) along ϕ gives

$$(1 - \hat{\Delta})\sqrt{g}J_0^r = B_{\phi 0}\frac{\partial \hat{\Delta}}{\partial \theta},$$

from which we infer $J_0^r \neq 0$. This equation yields

$$\frac{1}{B_{\phi 0}} \frac{\partial B_{\phi 0}}{\partial \theta} = \frac{1}{1 - \hat{\Lambda}} \frac{\partial \hat{\Delta}}{\partial \theta},$$

which can be easily integrated showing that $(1 - \hat{\Delta})B_{\phi 0}$ is a flux function. The projection of (B.8) along e_r can be regarded as a generalisation of the Grad-Shafranov equation (4.14) to anisotropic systems.

² This has to be the case for an integrable distribution function in the domain $-\infty < v_{||} < \infty$.

We use the fact that ϵ_s is an independent variable, so that the parallel gradient commutes with the symbol of derivation with respect to ϵ_s .

³ Notice that we require $B_0^r = 0$.

⁴ Other forms for \bar{f}_{s0} can be used, depending on the nature of the problem under consideration.

We can use either ψ or r as a flux label.

As an explicit example, we choose \bar{f}_{s0} to be a bi-Maxwellian distribution function,⁴ that is

$$\bar{f}_{s0} = \frac{m_s^{3/2} n_{s0}}{(2\pi k_B)^{3/2} T_{\perp s} \sqrt{T_{||s}}} \exp \left[-\frac{m_s}{2k_B} \left(\frac{v_{||}^2}{T_{||s}} + \frac{v_{\perp}^2}{T_{\perp s}} \right) \right].$$

where m_s is the particle mass, k_B the Boltzmann constant, n_{s0} the equilibrium number density with $T_{||s}$ and $T_{\perp s}$ the parallel and perpendicular temperatures of the species s (both taking their respective equilibrium values with the subscript zero omitted for simplicity). It is usually assumed that $T_{||s}$ is a flux function due to the strong parallel heat conduction. We further assume $T_{||i} = T_{||e} = T_{||}$ and $T_{\perp i} = T_{\perp e} = T_{\perp}$. It is easy to see that the equation above can be recast in the form

$$\bar{f}_{s0} = F_s(\psi) \exp \left[-\frac{m_s}{k_B} \left(\frac{\mu}{\hat{\mu}_s(\psi)} + \frac{\epsilon_s}{\hat{\epsilon}_s(\psi)} \right) \right],$$

thus fulfilling (B.4) where ϵ_s is given by (B.2) with the following identifications:

$$\hat{\epsilon}_s = T_{||}, \quad \frac{1}{B_0 \hat{\mu}_s} = \frac{1}{T_\perp} - \frac{1}{T_{||}}, \quad \frac{m_s^{3/2} n_s}{(2\pi k_B)^{3/2} T_{\perp s} \sqrt{T_{||s}}} = F_s.$$
 (B.9)

It is evident that both n_{s0} and T_{\perp} must depend upon the poloidal angle, with n_{s0}/T_{\perp} a flux function. Using this form of the distribution function, a little algebra shows that

$$C = -2p_{\perp 0}\frac{T_{\perp}}{T_{||}}.$$

Quasineutrality $\sum_s e_s n_s = 0$ implies that $n_i = n_e = n_0$. Moreover, $p_{||0} = 2n_0T_{||}$ and $p_{\perp 0} = 2n_0T_{\perp}$. Thus, multiplying (B.6) by T_{\perp} and plugging the result into (B.7) shows that $n_0 \propto T_{\perp}$, so that

$$\frac{n_0}{\hat{n}_0(\psi)} = \frac{T_\perp}{T_{\perp}(\psi)},\tag{B.10}$$

as expected from (B.q). Using this result into (B.7) gives⁵

$$T_{\perp} = \frac{B_0 T_{||}}{B_0 - \Theta(y_l)},$$
 (B.11)

where $\Theta(\psi)$ is an arbitrary function which measures the degree of anisotropy. Thus, a GCP tokamak equilibrium with a **bi-Maxwellian distribution** function is fully determined by equations (B.6)-(B.8) and (B.10)-(B.11).

References

- H. J. de Blank, **Theory of the m=1 kink mode in toroidal plasmas**, PhD Thesis Rijksuniversiteit (Utrecht, NL), 1990.
- D. Dobrott and J. M. Greene, Phys. Fluids 13, 2391 (1970).

⁵ Here we exploit the fact that

$$\label{eq:planeta} \mathbf{\nabla}_{||} \boldsymbol{p}_{\perp 0} = 4 \hat{n}_0 \frac{T_\perp}{T_{||}(\psi)} \mathbf{\nabla}_{||} T_{\perp 0}.$$

- J. P. Freidberg, **Ideal MHD**, Cambridge University Press (Cambridge, UK), 2014.
- R. Iacono et al., Phys. Fluids B 2, 1794 (1990).
- A. B. Mikhailovskii, **Instabilities in a Confined Plasma**, Institute of Physics Publishing (Bristol, UK), 1998.

C

General proof of the self-adjointness of the ideal MHD force operator

An explicit proof of the self-adjointness of the force operator for an ideal isotropic plasma, also including a vacuum region separating the plasma from an ideal metallic wall is presented. Instead of exploiting the energy conservation in ideal MHD, as it has been done in chapter 6, we proceed with a direct, although rather tedious, algebraic method.

We start by dotting (6.5) with η (a generic fluid perturbation), and integrate it over the plasma volume V. After a little algebra we obtain

$$\begin{split} \int_{V} \boldsymbol{\eta} \cdot \boldsymbol{F}(\boldsymbol{\xi}) dV &= -\int_{V} \Big(\Gamma p_{0}(\boldsymbol{\nabla} \cdot \boldsymbol{\xi}) (\boldsymbol{\nabla} \cdot \boldsymbol{\eta}) + \frac{1}{\mu_{0}} \boldsymbol{Q}(\boldsymbol{\xi}) \cdot \boldsymbol{Q}(\boldsymbol{\eta}) \\ &+ (\boldsymbol{\xi} \cdot \boldsymbol{\nabla} p_{0}) (\boldsymbol{\nabla} \cdot \boldsymbol{\eta}) - \boldsymbol{\eta} \cdot \boldsymbol{J}_{0} \times \boldsymbol{Q}(\boldsymbol{\xi}) \Big) dV \\ &- \int_{\Sigma} (\boldsymbol{\eta} \cdot \boldsymbol{n}_{0}) \Big(\tilde{p} + \frac{\boldsymbol{B}_{0} \cdot \boldsymbol{Q}(\boldsymbol{\xi})}{\mu_{0}} \Big) d\Sigma \end{split} \tag{C.1}$$

where $Q(\xi) = \nabla \times (\xi \times B)$ and n_0 is the unit vector normal to the unperturbed plasma-vacuum surface Σ . In obtaining the surface integral we used the fact that

$$\mathbf{n}_0 \cdot \mathbf{B}_0 = 0. \tag{C.2}$$

Here $\tilde{p} = \tilde{p}(\xi)$ as given by Eqs. (6.3) in section 6.1. We recast (C.1) as

$$-\int_{V} \boldsymbol{\eta} \cdot \boldsymbol{F}(\boldsymbol{\xi}) dV = \delta W_{P} + \delta W_{V},$$

We try to keep all the relevant mathematical steps in order to make the derivation more transparent.

where

$$\delta W_{P} = \int_{V} \left(\Gamma p_{0}(\nabla \cdot \boldsymbol{\xi})(\nabla \cdot \boldsymbol{\eta}) + \frac{1}{\mu_{0}} \boldsymbol{Q}(\boldsymbol{\xi}) \cdot \boldsymbol{Q}(\boldsymbol{\eta}) + (\boldsymbol{\xi} \cdot \nabla p_{0})(\nabla \cdot \boldsymbol{\eta}) - \boldsymbol{\eta} \cdot \boldsymbol{J}_{0} \times \boldsymbol{Q}(\boldsymbol{\xi}) \right) dV, \qquad (C.3)$$

$$\delta W_{V} = \int_{\Sigma} (\boldsymbol{\eta} \cdot \boldsymbol{n}_{0}) \left(\tilde{p} + \frac{\boldsymbol{B}_{0} \cdot \boldsymbol{Q}(\boldsymbol{\xi})}{\mu_{0}} \right) d\Sigma. \qquad (C.4)$$

We now show that both δW_P and δW_V are symmetric by swapping ξ and η . This will prove that F is **self-adjoint**.

Symmetric form for δW_P

The parallel component of the vector η does not appear in the last two term of δW_P . In fact, by writing $\eta = \eta_{\perp} + \eta_{||} B_0$ we immediately have

$$\xi \cdot \nabla p_0(\nabla \cdot \eta_{||} \mathbf{B}_0) - \eta_{||} \mathbf{B}_0 \cdot \mathbf{J}_0 \times \mathbf{Q}(\xi)$$

$$= (\xi \cdot \nabla p_0) \mathbf{B}_0 \cdot \nabla \eta_{||} + \eta_{||} \mathbf{Q}(\xi) \cdot \mathbf{J}_0 \times \mathbf{B}_0 = \mathbf{B}_0 \cdot \nabla (\eta_{||} \xi \cdot \nabla p_0)$$

which vanishes when integrated over the plasma volume thanks to (C.2). Using the equilibrium force balance equation (4.1) we write

$$\mathbf{J}_0 = \sigma \mathbf{B}_0 + \frac{\mathbf{B}_0 \times \nabla p_0}{B_0^2},\tag{C.5}$$

where $\sigma = \mathbf{J}_0 \cdot \mathbf{B}_0 / B_0^2$ so that

$$-\boldsymbol{\eta}_{\perp} \cdot \boldsymbol{J}_{0} \times \boldsymbol{Q}(\boldsymbol{\xi}) = -\sigma \boldsymbol{Q}(\boldsymbol{\xi}) \cdot \boldsymbol{\eta}_{\perp} \times \boldsymbol{B}_{0} - (\boldsymbol{\eta}_{\perp} \cdot \boldsymbol{\nabla} \boldsymbol{p}_{0}) \frac{\boldsymbol{B}_{0} \cdot \boldsymbol{Q}(\boldsymbol{\xi})}{B_{0}^{2}}. \quad (C.6)$$

Let us introduce the curvature vector x defined as

$$\mathbf{x} = \boldsymbol{b} \cdot \nabla \boldsymbol{b} = -\boldsymbol{b} \times \nabla \times \boldsymbol{b},$$

with $\mathbf{b} = \mathbf{B}_0/|\mathbf{B}_0|$. The last equality holds due to the fact that $\mathbf{b} \cdot \mathbf{b} = 1$. We notice that

$$\nabla \cdot \boldsymbol{\eta}_{\perp} = -\frac{1}{B_0^2} \left[\boldsymbol{B}_0 \cdot \boldsymbol{Q}(\boldsymbol{\eta}) + \boldsymbol{\eta}_{\perp} \cdot \nabla \left(\mu_0 \boldsymbol{p}_0 + B_0^2 \right) \right]$$
$$= -\frac{1}{B_0^2} \left[\boldsymbol{B}_0 \cdot \boldsymbol{Q}(\boldsymbol{\eta}) - \boldsymbol{\eta}_{\perp} \cdot \nabla \mu_0 \boldsymbol{p}_0 \right] - 2\boldsymbol{\eta}_{\perp} \cdot \varkappa. \tag{C.7}$$

Thus, plugging (C.6) and (C.7) into (C.3) yields

$$\delta W_{P} = \int_{V} \left(\Gamma p_{0}(\nabla \cdot \boldsymbol{\xi})(\nabla \cdot \boldsymbol{\eta}) + \frac{1}{\mu_{0}} \boldsymbol{Q}(\boldsymbol{\xi}) \cdot \boldsymbol{Q}(\boldsymbol{\eta}) \right)$$

$$- \frac{1}{B_{0}^{2}} \left[(\boldsymbol{\xi} \cdot \nabla p_{0})(\boldsymbol{B}_{0} \cdot \boldsymbol{Q}(\boldsymbol{\eta})) + (\boldsymbol{\eta} \cdot \nabla p_{0})(\boldsymbol{B}_{0} \cdot \boldsymbol{Q}(\boldsymbol{\xi})) \right]$$

$$+ \frac{\mu_{0}}{B_{0}^{2}} (\boldsymbol{\xi} \cdot \nabla p_{0})(\boldsymbol{\eta} \cdot \nabla p_{0})$$

$$- \sigma \boldsymbol{Q}(\boldsymbol{\xi}) \cdot \boldsymbol{\eta} \times \boldsymbol{B}_{0} - 2(\boldsymbol{\xi} \cdot \nabla p_{0})(\boldsymbol{\eta} \cdot \boldsymbol{x}) \right) dV, \qquad (C.8)$$

Here we list some useful relations:

$$\begin{split} & \boldsymbol{\nabla} \left(\mu_0 \boldsymbol{p}_0 + \frac{B_0^2}{2} \right) = B_0^2 \boldsymbol{\times} + \boldsymbol{b} (\boldsymbol{b} \cdot \boldsymbol{\nabla} \frac{B_0^2}{2}), \\ & \boldsymbol{\eta}_\perp = \frac{\boldsymbol{B}_0 \times (\boldsymbol{\eta}_\perp \times \boldsymbol{B}_0)}{B_0^2}, \\ & \boldsymbol{\nabla} \cdot \boldsymbol{J}_0 = \boldsymbol{B}_0 \cdot \boldsymbol{\nabla} \boldsymbol{\sigma} - 2 \frac{\boldsymbol{B}_0}{B_0^2} \cdot (\boldsymbol{\nabla} \boldsymbol{p}_0 \times \boldsymbol{\times}). \end{split}$$

where we dropped the subscript \bot in η since the projections automatically pick out its perpendicular component. Now we introduce the quantity

$$\hat{\Delta} = -\sigma \mathbf{Q}(\boldsymbol{\xi}) \cdot \boldsymbol{\eta} \times \mathbf{B}_0 - 2(\boldsymbol{\xi} \cdot \boldsymbol{\nabla} p_0)(\boldsymbol{\eta} \cdot \boldsymbol{\varkappa}) + \sigma \mathbf{Q}(\boldsymbol{\eta}) \cdot \boldsymbol{\xi} \times \mathbf{B}_0 + 2(\boldsymbol{\eta} \cdot \boldsymbol{\nabla} p_0)(\boldsymbol{\xi} \cdot \boldsymbol{\varkappa}).$$

If we show that the integral of $\hat{\Delta}$ over the volume V is vanishing, it necessarily follows the last two terms in (C.8) are symmetric by interchanging $\boldsymbol{\xi}$ and $\boldsymbol{\eta}$. A short computation shows that

$$\hat{\Delta} = \nabla \cdot [\sigma(\boldsymbol{\eta} \times \boldsymbol{B}_0) \times (\boldsymbol{\xi} \times \boldsymbol{B}_0)] - \nabla \sigma \cdot (\boldsymbol{\eta} \times \boldsymbol{B}_0) \times (\boldsymbol{\xi} \times \boldsymbol{B}_0) - 2(\boldsymbol{\xi} \times \boldsymbol{\eta}) \cdot (\nabla \boldsymbol{p}_0 \times \boldsymbol{x}) = \nabla \cdot [\sigma \boldsymbol{\eta} \cdot (\boldsymbol{\xi} \times \boldsymbol{B}_0) \boldsymbol{B}_0] + \boldsymbol{\xi} \times \boldsymbol{\eta} \cdot [\boldsymbol{B}_0(\boldsymbol{B}_0 \cdot \nabla \sigma) - 2(\nabla \boldsymbol{p}_0 \times \boldsymbol{x})].$$

We now split the last term of the equation above into its parallel and perpendicular components, yielding

$$\hat{\Delta} = \nabla \cdot [\sigma \boldsymbol{\eta} \cdot (\boldsymbol{\xi} \times \boldsymbol{B}_0) \boldsymbol{B}_0] + \boldsymbol{\xi} \times \boldsymbol{\eta} \cdot \boldsymbol{B}_0 \left[\boldsymbol{B}_0 \cdot \nabla \sigma - 2 \frac{\boldsymbol{B}_0}{B_0^2} \cdot (\nabla \boldsymbol{p}_0 \times \boldsymbol{x}) \right] - 2(\boldsymbol{\xi} \times \boldsymbol{\eta}) \times \boldsymbol{B}_0 \cdot \frac{(\nabla \boldsymbol{p}_0 \times \boldsymbol{x}) \times \boldsymbol{B}_0}{B_0^2}.$$
(C.9)

When integrated over the plasma volume, the first term of (C.9) vanishes due to (C.2). The second term is proportional to $\nabla \cdot J_0$ and thence is zero. The last term vanishes too since ∇p_0 and \times are both perpendicular to B_0 . Therefore, δW_P is symmetric in exchanging ξ with η .

Symmetric form for δW_V

As in section 6.1.1, we assume that the displaced surface moves with a normal velocity $n \cdot u$, and we set the analysis in a reference frame moving with the plasma surface. Let the subscript M denote quantities in the moving frame. By applying the appropriate Galilean transformations one transforms these quantities back in the original fixed reference frame.

Let the subscript v indicate a vacuum quantity. In the vacuum there are no sources so that we use the Coulomb gauge in which $\widetilde{\boldsymbol{E}}_v = -\partial \boldsymbol{A}/\partial t$ with $\widetilde{\boldsymbol{B}}_v = \nabla \times \boldsymbol{A}$. Since in the plasma $\widetilde{\boldsymbol{E}}_M = \widetilde{\boldsymbol{E}} + \boldsymbol{u} \times \boldsymbol{B}_0 = 0$, we must have $\widetilde{\boldsymbol{E}}_{vM} = 0$ as well, so that Eq. (6.9) gives

$$0 = \boldsymbol{n}_0 \times \widetilde{\boldsymbol{E}}_{vM} = \boldsymbol{n}_0 \times \left(\widetilde{\boldsymbol{E}}_v + \boldsymbol{u} \times \boldsymbol{B}_{v0} \right),$$

where this condition can be supposed to be fulfilled at the unperturbed boundary because \widetilde{E}_{vM} is a first-order perturbed quantity. Therefore, we obtain

$$\mathbf{n}_0 \times \mathbf{A} = -(\mathbf{n}_0 \cdot \boldsymbol{\xi}) \mathbf{B}_{v0}. \tag{C.10}$$

This has not to be confused with the same symbol used in App. B.

We now use the jump condition of the total pressure at the plasma-vacuum boundary. Hence, we perturb (6.10) and evaluate it at position $r_p = r_{eq} + \xi$. This yields

$$\tilde{p} + \boldsymbol{\xi} \cdot \boldsymbol{\nabla} \left(p_0 + \frac{B_0^2}{2\mu_0} \right) + \frac{\boldsymbol{B}_0 \cdot \widetilde{\boldsymbol{B}}}{\mu_0} = \boldsymbol{\xi} \cdot \boldsymbol{\nabla} \left(\frac{B_{v0}^2}{2\mu_0} \right) + \frac{\boldsymbol{B}_{v0} \cdot \widetilde{\boldsymbol{B}}_v}{\mu_0},$$

and the following expression is produced:

$$\delta W_V = \int_{\Sigma} (\boldsymbol{\eta} \cdot \boldsymbol{n}_0) \boldsymbol{\xi} \cdot \left[\boldsymbol{\nabla} \left(\frac{B_{v0}^2}{2\mu_0} \right) - \boldsymbol{\nabla} \left(\boldsymbol{p}_0 + \frac{B_0^2}{2\mu_0} \right) \right] d\Sigma +$$

$$\int_{\Sigma} (\boldsymbol{\eta} \cdot \boldsymbol{n}_0) \frac{\boldsymbol{B}_{v0} \cdot \widetilde{\boldsymbol{B}}_v}{\mu_0} d\Sigma.$$

Thanks to (6.10), the tangential jump of the total pressure is continuous, i.e. $\mathbf{n}_0 \times [\![\nabla (p_0 + B_0^2/2\mu_0)]\!] = 0.1$ This allows us to write

$$\delta W_V = \int_{\Sigma} (\boldsymbol{\eta} \cdot \boldsymbol{n}_0) (\boldsymbol{\xi} \cdot \boldsymbol{n}_0) \boldsymbol{n}_0 \cdot \left[\nabla \left(\frac{B_{v0}^2}{2\mu_0} \right) - \nabla \left(\boldsymbol{p}_0 + \frac{B_0^2}{2\mu_0} \right) \right] d\Sigma + \int_{\Sigma} (\boldsymbol{\eta} \cdot \boldsymbol{n}_0) \frac{B_{v0} \cdot \widetilde{B}_v}{\mu_0} d\Sigma.$$

The final step consists in considering $\widetilde{\boldsymbol{B}}_{v}$ as a function of $\boldsymbol{\eta}$ and $\boldsymbol{\xi}$ thanks to the boundary condition at the displaced plasma surface. Hence, we write $\widetilde{\boldsymbol{B}}_{v}(\boldsymbol{\xi}) = \nabla \times \boldsymbol{A}(\boldsymbol{\xi})$ with $\nabla \times [\nabla \times \boldsymbol{A}(\boldsymbol{\xi})] = 0$. The same applies to $\widetilde{\boldsymbol{B}}_{v}(\boldsymbol{\eta})$ with the obvious substitutions. Using the interface conditions (C.10) yields

$$\int_{\text{Vac}} \widetilde{\boldsymbol{B}}_{v}(\boldsymbol{\xi}) \cdot \widetilde{\boldsymbol{B}}_{v}(\boldsymbol{\eta}) dV = \int_{\text{Vac}} \nabla \cdot \left[\boldsymbol{A}(\boldsymbol{\eta}) \times \nabla \times \boldsymbol{A}(\boldsymbol{\xi}) \right] dV =$$

$$- \int_{\Sigma} \boldsymbol{n}_{0} \cdot \left[\boldsymbol{A}(\boldsymbol{\eta}) \times \widetilde{\boldsymbol{B}}_{v}(\boldsymbol{\xi}) \right] d\Sigma = \int_{\Sigma} (\boldsymbol{n}_{0} \cdot \boldsymbol{\eta}) \boldsymbol{B}_{v0} \cdot \widetilde{\boldsymbol{B}}_{v}(\boldsymbol{\xi}) d\Sigma$$

where the subscript Vac means that the integration is carried out over the vacuum region, and the minus sign appearing after the second equality is because the volume of the vacuum region is outside the plasma surface Σ . This shows that also δW_V is symmetric in exchanging \mathcal{E} and η .

References

- I. B. Bernstein, Handbook of Plasma Physics Vol. 1: Basic Plasma physics, edited by A. A. Galeev and R. N. Sudan p. 421 (Eds. M. N. Rosenbluth and R. Z. Sagdeev), North-Holland (Amsterdam, NL), 1983.
- J. P. Freidberg, **Ideal MHD**, Cambridge University Press (Cambridge, UK), 2014.
- A. H. Glasser, Ballooning Modes in Axisymmetric Toroidal Plasmas, Lecture 3, Plasma Physics Laboratory Princeton University (Princeton New Jersey, US).

¹ This is because $\mu_0 p_0 + B_0^2/2 - B_{v0}^2/2 = 0$ everywhere on Σ, so that $\mathbf{n}_0 \times \nabla (\mu_0 p_0 + B_0^2/2 - B_{v0}^2/2) = 0$.

- J. P. Goedbloed and S. Poedts, **Principles of Magnetohydrodynamics With Applications to Laboratory and Astrophysical Plasmas**, Cambridge University Press (Cambridge, UK), 2004.
- B. B. Kadomtsev, Reviews of Plasma Physics Vol. 2 p. 153 (Ed. M. A. Leontovich), Consultants Bureau (New York, US), 1966.

The screw-pinch eigenmode equation

Let us first present the derivation of the eigenmode equation for the radial fluid displacement in a straight screw-pinch at marginal stability $(\gamma \to 0)$ following the procedure outlined in §7.5. This is known as the Newcomb equation (see section 7.5.1). Each symbol associated with physical quantities appearing here has the same meaning as in chapter 7.

We start by recalling that in a cylinder the metric coefficients read (cf section 3.1.1) $g_{rr}=1$, $g_{\theta\theta}=r^2$, $g_{r\theta}=g_{r\phi}=0$, $\sqrt{g}=rR_0$, where R_0 , the *major radius*, is a constant. The **equilibrium relation** may be written as

$$rR_0p_0'/f_0' = -F' - \mu\sqrt{g}J_0^{\phi},$$

where $f_0' = rF/R_0$ (cf. (7.14)) and F is given by (4.4) with $\mu = 1/q$. The toroidal current takes the form

$$\frac{J_0^{\phi}}{B_0^{\phi}} = \frac{R_0}{mf_0'} \left[\frac{r^2}{R_0^2} (\hat{k}_{||} + n \frac{f_0'}{r}) \right]',$$

with $\hat{k}_{||} = \frac{f_0'}{r} k_{||}$ and $k_{||} = m\mu - n$. We assume that the **plasma is an ideal conductor** so that (cf. 7.7)

$$\sqrt{g}\tilde{B}^r = \sqrt{g}\boldsymbol{B}_0 \cdot \boldsymbol{\nabla}\xi^r = f_0' \left(\mu \frac{\partial}{\partial \theta} + \frac{\partial}{\partial \phi} \right) \xi^r.$$
 (D.1)

With a perturbation depending on θ and ϕ as $e^{i(m\theta-n\phi)}$, in analogy with the derivation of (7.35), we find that

$$(\sqrt{g}\tilde{B}^{\phi})_{m} = \frac{r/R_{0}}{1+h} \left[\frac{rR_{0}}{f_{0}'} p_{0}' \xi_{m}^{r} + \frac{J_{0}^{\phi}}{B_{0}^{\phi}} \frac{(\sqrt{g}\tilde{B}^{r})_{m}}{im} + \frac{n}{m^{2}} \frac{r}{R_{0}} \frac{(\sqrt{g}\tilde{B}^{r})_{m}'}{i} \right],$$

with $h = \frac{n^2}{m^2} \frac{r^2}{R_0^2}$. Contrary to (7.35), the expression above is exact. Since equilibrium quantities in cylindrical geometry do not depend upon the

The procedure we follow here is not necessarily the simplest for deriving the eigenmode equation, but it is useful for comparison with the calculations employed in the previous chapters.

¹ Recall that in cylindrical geometry poloidal and toroidal Fourier modes behave independently. Moreover, at marginal stability $\tilde{p} = -p_0'\xi^r$ (cf. (7.9) and (7.10)).

angular variable θ , we drop the symbol of poloidal average (the comparison with the expressions derived in chapter 7 is straightforward).

Following the same steps presented in §7.5, the eigenmode equation is obtained from the vorticity equation (7.13). First, we get

$$\begin{split} \left(\sqrt{g}\,\tilde{J}^{\phi}\right)_{m} &= -\frac{1}{im} \Bigg[\left(\frac{r}{R_{0}}\,\frac{(\sqrt{g}\,\tilde{B}^{r})'_{m}}{1+h}\right)' - \frac{m^{2}}{rR_{0}}(\sqrt{g}\,\tilde{B}^{r})_{m} \Bigg] \\ &+ \frac{n}{m} \Bigg[\frac{r^{2}/R_{0}^{2}}{1+h} \left(\frac{rR_{0}}{f_{0}'}p_{0}'\xi_{m} + \frac{J_{0}^{\phi}}{B_{0}^{\phi}}\frac{(\sqrt{g}\,\tilde{B}^{r})_{m}}{i\,m}\right) \Bigg]', \end{split}$$

and, in analogy with (7.54), we have

$$\left(\sqrt{g}\boldsymbol{J}_{0}\cdot\boldsymbol{\nabla}\frac{\tilde{B}^{\phi}}{B_{0}^{\phi}}\right)_{m}=\frac{i\,m}{f_{0}^{\,\prime}}\left(\frac{rR_{0}}{f_{0}^{\,\prime}}\boldsymbol{p}_{0}^{\prime}+\frac{k_{||}}{m}\sqrt{g}J_{0}^{\phi}\right)(\sqrt{g}\,\tilde{B}^{\phi})_{m}=\frac{i\,mP_{c}}{f_{0}^{\,\prime}}(\sqrt{g}\,\tilde{B}^{\phi})_{m},$$

where P_c is the cylindrical analogue of (7.55) and is defined as

$$P_c = \frac{\sqrt{g}}{f_0'} p_0' + (\mu - n/m) \sqrt{g} J_0^{\phi}.$$

Combining these two expressions and exploiting the independence upon θ of the equilibrium gives

$$\begin{split} \sqrt{g} \left(\boldsymbol{B}_{0} \cdot \boldsymbol{\nabla} \frac{\tilde{J}^{\phi}}{B_{0}^{\phi}} - \boldsymbol{J}_{0} \cdot \boldsymbol{\nabla} \frac{\tilde{B}^{\phi}}{B_{0}^{\phi}} \right)_{m} &= -\frac{k_{||}}{m} \left[\left(\frac{r}{R_{0}} \frac{(\sqrt{g}\tilde{B}^{r})'_{m}}{1+h} \right)' - \frac{m^{2}}{rR_{0}} (\sqrt{g}\tilde{B}^{r})_{m} \right] \\ &+ \frac{n}{m} \left(\frac{r^{2}/R_{0}^{2}}{f_{0}'(1+h)} P_{c} \right)' (\sqrt{g}\tilde{B}^{r})_{m} - i \frac{r/R_{0}}{1+h} \left(n\mu' \frac{rP_{c}}{R_{0}} + \frac{mP_{c}^{2}}{f_{0}'} \right) \boldsymbol{\xi}_{m}^{r}. \end{split}$$

Finally, we easily obtain

$$\begin{split} \left(\sqrt{g}\,\widetilde{\boldsymbol{B}}\cdot\boldsymbol{\nabla}\frac{J_0^\phi}{B_0^\phi}\right)_m &= i\left(\frac{J_0^\phi}{B_0^\phi}\right)'r\hat{k}_{||}\boldsymbol{\xi}_m^r,\\ \left(\sqrt{g}\,\boldsymbol{\nabla}\phi\cdot\boldsymbol{\nabla}\frac{1}{B_0^\phi}\times\boldsymbol{\nabla}\tilde{\boldsymbol{p}}\right)_m &= i\,mp_0'\frac{R_0^2F'}{F^2}\boldsymbol{\xi}_m^r. \end{split}$$

We stress the fact that these expressions are exact.

By means of (7.58) with $N=r/R_0$ and using (D.1), at marginal stability the eigenmode equation for a mode of helicity (m,n) in a screw-pinch reads

 $\frac{1}{r}\frac{d}{dr}\left(\frac{r^{3}k_{||}^{2}}{1+h}\frac{d\xi_{m}^{r}}{dr}\right) + \left[\left(\frac{r(r\hat{k}_{||})'}{1+h}\right)' - m^{2}\hat{k}_{||}\right]\hat{k}_{||}\xi_{m}^{r}$ $- m\frac{R_{0}f_{0}'}{r}\left[\left(\frac{J_{0}^{\phi}}{B_{0}^{\phi}}\right)' + \frac{n}{m}\left(\frac{r^{3}p_{0}'/R_{0}}{(f_{0}')^{2}(1+h)}\right)' + \frac{nk_{||}}{m^{2}}\left(\frac{r^{2}/R_{0}^{2}}{1+h}\frac{J_{0}^{\phi}}{B_{0}^{\phi}}\right)'\right]r\hat{k}_{||}\xi_{m}^{r}$ $+ \left[\frac{m}{1+h}\left(n\mu'r^{2}p_{0}' + mP_{c}^{2}\right) + m^{2}p_{0}'\frac{f_{0}'}{r}\frac{R_{0}^{3}F'}{F^{2}}\right]\xi_{m}^{r} = 0. \tag{D.2}$

This equation is easily compared with (7.65).

It is easily shown that the following relations hold

$$\begin{split} \left(\frac{J_0^{\phi}}{B_0^{\phi}}\right)' + \frac{m}{n} \left(\frac{hrR_0p_0'}{(f_0')^2(1+h)}\right)' + \frac{k_{||}}{n} \left(\frac{hJ_0^{\phi}/B_0^{\phi}}{1+h}\right)' \\ &= \left(\frac{J_0^{\phi}/B_0^{\phi}}{1+h}\right)' - \frac{m}{n} \left(\frac{h}{1+h}\frac{F'}{f_0'}\right)' - \frac{m}{n}\frac{\mu'h}{1+h}\frac{J_0^{\phi}}{B_0^{\phi}}, \\ \frac{f_0'}{r} \left(\frac{J_0^{\phi}/B_0^{\phi}}{1+h}\right)' &= \frac{mR_0}{n} \left[\frac{(h\hat{k}_{||})'}{nr(1+h)} + \frac{(hF/R_0)'}{r(1+h)}\right]' - \frac{F'}{R_0}\frac{J_0^{\phi}/B_0^{\phi}}{1+h}. \end{split}$$

When these are plugged into (D.2) some simple grouping yields

$$\frac{1}{r}\frac{d}{dr}\left(\frac{rh\hat{k}_{||}^2}{1+h}\frac{d\xi_m^r}{dr}\right) + \mathcal{G}\xi_m^r = 0, \tag{D.3}$$

where $\mathscr{G} = \sum_{i=1}^{4} A_i$ having defined

$$\begin{split} A_1 &= \left\{ \frac{n^2}{m^2 R_0^2} \left[\left(\frac{r(r\hat{k}_{||})'}{1+h} \right)' - m^2 \hat{k}_{||} \right] - r \left(\frac{(h\hat{k}_{||})'}{r(1+h)} \right)' \right\} \hat{k}_{||}, \\ A_2 &= -\frac{n}{R_0} \left[\left(\frac{(hF)'}{r(1+h)} \right)' - F \left(\frac{hF'}{r(1+h)F} \right)' \right] r \hat{k}_{||}, \\ A_3 &= \frac{n^2 F'}{R_0^2} \left(\frac{rR_0}{f_0'} p_0' + \frac{k_{||}}{m} \frac{\sqrt{g} J_0^{\phi}}{1+h} \right) = \frac{n^2 F'}{R_0^2} \left(P_c - \frac{k_{||}}{m} \frac{h \sqrt{g} J_0^{\phi}}{1+h} \right), \\ A_4 &= \frac{\mu' h}{1+h} \frac{nm}{R_0^2} F P_c + \frac{n^2}{R_0^2} \frac{P_c^2}{1+h}. \end{split}$$

A simplified expression for $\mathscr G$ can be found. Let us first write the toroidal field as $B_z=F/R_0$ and introduce the poloidal field B_p such that $\mu=R_0B_p/(rB_z)$ and $\hat k_{||}=B_z(m\mu-n).^2$ It is possible to prove that

$$A_4 = \frac{n^3/R_0^2}{mB_z(1+h)} \left[R_0 B_z' + \frac{n}{m} (rB_p)' \right] \left[\left(2B_z + rB_z' \right) B_p + \frac{m}{n} R_0 B_z B_z' \right],$$

and using this result, after some little algebra, one gets

$$A_3 + A_4 = \frac{2n^3}{m^2} \frac{B_p/R_0^2}{1+h} [mR_0B_z' + n(rB_p)'] + \frac{nh}{1+h} (B_z')^2 (m\mu - n).$$

Proceeding further, we have

$$A_2 = \left[-\frac{n^3/m^2}{1+h} \left(2\frac{rB_z'}{R_0^2} + \frac{r^2}{R_0^2} \frac{(B_z')^2}{B_z} \right) + \frac{4n^5}{m^4} \frac{r^2}{R_0^4} \frac{B_z}{(1+h)^2} \right] B_z(m\mu - n),$$

which eventually leads to

$$\begin{split} A_2 + A_3 + A_4 &= \frac{2n^2}{r^2} B_p(rB_p)' - \frac{n^2}{r} \left[\frac{m^2 B_p^2 - n^2 B_z^2 r^2 / R_0^2}{m^2 (1+h)} \right]' \\ &+ \frac{2n^4}{R_0^2 m^2} \frac{h B_z^2 - B_p^2}{(1+h)^2} - \frac{2n^2}{r^2 (1+h)} [B_p^2 + h B_z^2] + \frac{4n^3 h B_z^2 (m\mu - n)}{m^2 R_0^2 (1+h)^2}. \end{split} \tag{D.4}$$

 $f_0'/r = R_0 B_0^{\phi} = F/R_0.$

$$\begin{split} \sqrt{g}J_0^\phi &= \frac{m^2R_0^2}{n^2}(hB_p/r)',\\ \mu' &= R_0\left(\frac{B_p'}{rB_z} - \frac{B_p}{r^2B_z} - \frac{B_pB_z'}{rB_z^2}\right)\\ P_c &= -\left[R_0B_z' + \frac{n}{m}(rB_p)'\right]. \end{split}$$

² By means of the **equilibrium relation**, the following relations prove to be extremely useful in the manipulation of the coefficients A_i :

Finally, a quick calculation shows that

$$A_1 = \left(\frac{n^2}{m^2 R_0^2} \frac{1+3h}{(1+h)^2} - \frac{n^2}{R_0^2}\right) \hat{k}_{||}^2.$$
 (D.5)

Hence, grouping together the terms proportional to $1/(1+h)^2$ in (D.4) and (D.5) and expressing μ in terms of B_p and B_z , a bit tedious calculation finally gives³

$$\mathcal{G} = -\frac{n^2}{R_0^2} \hat{k}_{||}^2 + \frac{2n^2}{r^2} B_p(rB_p)' - \frac{n^2}{r} \left[\frac{m^2 B_p^2 - n^2 B_z^2 r^2 / R_0^2}{m^2 (1+h)} \right]' - \frac{n^2 (mR_0 B_p + nrB_z)^2}{m^2 r^2 R_0^2 (1+h)}.$$
 (D.6)

We can write \mathscr{G} in a more convenient form by using the equilibrium relation $B_p B_p' = -p_0' - \frac{B_p^2}{r} - B_z B_z'$. Distributing the derivative on the numerator and denominator of the third term in (D.6) yields

$$\begin{split} \mathcal{G} &= -\frac{n^2}{R_0^2} \hat{k}_{||}^2 - \frac{2n^2}{r} \frac{h p_0'}{1+h} + \frac{2n^2}{r^2} \frac{B_p^2 + h B_z^2}{1+h} \\ &+ \frac{n^2}{r} \left[\frac{m^2 B_p^2 - n^2 B_z^2 r^2 / R_0^2}{m^2 (1+h)^2} \right] h' - \frac{n^2 (m R_0 B_p + n r B_z)^2}{m^2 r^2 R_0^2 (1+h)}. \end{split}$$

If we now combine the first, third and fifth terms of the expression above, the function \mathscr{G} in equation (D.3) can be finally written as

$$\mathscr{G} = -h \frac{m^2 - 1 + m^2 h}{r^2 (1+h)} \hat{k}_{||}^2 - \frac{2n^2}{r} \frac{h p_0'}{1+h} + \frac{n^2}{r} \left(\frac{m^2 B_p^2 - n^2 B_z^2 r^2 / R_0^2}{m^2 (1+h)^2} \right) h'. \quad (D.7)$$

One notes that $r^2\mathscr{G}/B_z^2$ is expressed as a sum of ε^2 and ε^4 terms.

For the case of the m=1 mode, the dominant contribution of order ε^2 cancels out, so that to leading order $\mathscr G$ is given by

$$\mathscr{G} \approx -\frac{n^4 B_z^2}{R_0^2} \left[\frac{2r p_0'}{B_z^2} - \frac{B_p^2}{B_z^2} (1 - nq) (1 + 3nq) \right], \tag{D.8}$$

with $q = rB_z/(R_0B_p)$. This result is used in the discussion of the stability properties of the m=1 internal kink mode in toroidal geometry (cf. chapter 8).

The Hain-Lüst equation

We shall now obtain the **Hain-Lüst equation**, which is the screw-pinch eigenmode equation extended to the case of non-vanishing inertia. This is more easily accomplished by following a different procedure compared

 3 This is the result given in Newcomb (1960).

to the one used in the section above. Let us start by writing the following equilibrium relations for a straight screw-pinch

$$\begin{split} \sqrt{g} J_0^{\theta} &= -R_0^2 (B_0^{\phi})', \quad \sqrt{g} J_0^{\phi} &= (r^2 B_0^{\theta})', \\ p_0' &= R_0^2 B_0^{\phi} (B_0^{\phi})' - B_0^{\theta} (r^2 B_0^{\theta})', \\ B^2 &= r^2 (B_0^{\theta})^2 + R_0^2 (B_0^{\phi})^2. \end{split} \tag{D.9}$$

Furthermore, it is convenient to define (**do not misinterpret** this F with the covariant ϕ component of the magnetic field)

$$F_{||} = mB_0^{\theta} - nB_0^{\phi}, \quad D = mR_0^2B_0^{\phi} + nr^2B_0^{\theta}, \quad H = m^2R_0^2 + n^2r^2.$$

As before, the fluid displacement is expanded as $\xi(r,\theta,\phi) = \xi(r)e^{i(m\theta-n\phi)}$, and the same applies to other perturbed quantities. Our starting point are the linearised radial and toroidal covariant components of the momentum equation, and its projection along the total \boldsymbol{B} field. They read (cf. (7.1) and (7.10))

For the sake of simplicity, we omit to write the subscript m when referring to the harmonic of helicity (m, n).

$$\begin{split} \rho_0 \gamma^2 \xi^r &= -\tilde{p}' - R_0^2 B_0^{\phi} (\tilde{B}^{\phi})' - B_0^{\theta} (r^2 \tilde{B}^{\theta})' \\ &+ i F_{||} \tilde{B}^r - R_0^2 (B_0^{\phi})' \tilde{B}^{\phi} - (r^2 B_0^{\theta})' \tilde{B}^{\theta}, \end{split} \tag{D.10}$$

$$\rho_0 \gamma^2 R_0^2 \xi^{\phi} = i n \tilde{p} + i B_0^{\theta} (m R_0^2 \tilde{B}^{\phi} + n r^2 \tilde{B}^{\theta}) + R_0^2 (B_0^{\phi})' \tilde{B}^{r}, \tag{D.11}$$

$$\rho_0 \gamma^2 (r^2 B_0^{\theta} \xi^{\theta} + R_0^2 B_0^{\phi} \xi^{\phi}) = i F_{||} (\Gamma p_0 \nabla \cdot \xi), \tag{D.12}$$

where $\tilde{p} = -p_0' \xi^r - \Gamma p_0 \nabla \cdot \xi$. We now introduce the variables $X = \xi^r$, $Y = B_0^{\phi} \xi^{\theta} - B_0^{\theta} \xi^{\phi}$ and $Z = \Gamma p_0 \nabla \cdot \xi$. The perturbed pressure and the components of the magnetic field are thus written as

$$\begin{split} \tilde{p} &= -p_0'X - Z, \quad \tilde{B}^r = iF_{||}X \\ \tilde{B}^\theta &= -\frac{1}{r}(B_0^\theta rX)' - inY, \quad \tilde{B}^\phi = -\frac{1}{r}(B_0^\phi rX)' - imY, \end{split}$$

whereas the divergence of ξ explicitly reads

$$\frac{Z}{\Gamma p_0} = \frac{1}{r} (rX)' + \frac{i}{B_0^{\phi}} (mY + F_{||} \xi^{\phi}). \tag{D.13}$$

When equations (D.11) and (D.12) are written in terms of X, Y and Z they become

$$\rho_0 \gamma^2 R_0^2 \xi^{\phi} = 2inr(B_0^{\theta})^2 X - iB_0^{\theta} D \frac{(rX)'}{r} + B_0^{\theta} HY - inZ,$$

$$\frac{\rho_0 \gamma^2}{B_0^{\phi}} \left(r^2 B_0^{\theta} Y + B^2 \xi^{\phi} \right) = iF_{||} Z.$$

An easy calculation shows that by employing (D.13) to eliminate ξ^{ϕ} , the two equations above take the following form

$$DZ = -B^{2}D\frac{(rX)'}{r} + 2nrB^{2}B_{0}^{\theta}X - i\left(B^{2}H + r^{2}R_{0}^{2}\rho_{0}\gamma^{2}\right)Y, \qquad (D.14)$$

$$\left(F_{||}^{2} + \frac{\rho_{0}\gamma^{2}B^{2}}{\Gamma h_{0}}\right)Z = \rho_{0}\gamma^{2}\left(B^{2}\frac{(rX)'}{r} + iDY\right). \qquad (D.15)$$

$$\nabla \cdot \boldsymbol{\xi} = \frac{1}{r} (r \boldsymbol{\xi}^r)' + i m \boldsymbol{\xi}^{\theta} - i n \boldsymbol{\xi}^{\phi},$$

If one multiplies equation (D.15) by D and uses (D.14), it is possible to obtain an expression for Y just involving X that is

$$i\Delta Y = 2nrB_0^{\theta}\Phi X - D\Omega \frac{(rX)'}{r}, \tag{D.16}$$

having conveniently defined

$$\begin{split} \Omega &= F_{||}^2 + \rho_0 \gamma^2 \Big(1 + \frac{B^2}{\Gamma p_0} \Big), \qquad \Phi &= F_{||}^2 + \frac{\rho_0 \gamma^2 B^2}{\Gamma p_0}, \\ \Delta &= \frac{\rho_0^2 \gamma^4 r^2 R_0^2}{\Gamma p_0} + H \Big[F_{||}^2 + \rho_0 \gamma^2 \Big(1 + \frac{B^2}{\Gamma p_0} \Big) \Big]. \end{split}$$

We finally recast (D.10) in terms of the variables X, Y and Z to get

$$\rho_0 \gamma^2 X = \left(Z + B^2 \frac{(rX)'}{r} + iDY \right)' - \left(F_{||}^2 + 2r B_0^{\theta} (B_0^{\theta})' \right) X + 2inr B_0^{\theta} Y.$$

Hence, using (D.15) and (D.16), after little algebra we eventually obtain the **Hain-Lüst eigenmode equation**

$$\begin{split} \frac{d}{dr} \Big(r^2 R_0^2 \frac{\Omega}{\Delta} (F_{||}^2 + \rho_0 \gamma^2) \frac{(rX)'}{r} \Big) - \Big[F_{||}^2 + \rho_0 \gamma^2 + 2r B_0^{\theta} (B_0^{\theta})' \\ - 2nr \Big(\frac{\Omega}{\Lambda} D B_0^{\theta} \Big)' - 4n^2 r^2 (B_0^{\theta})^2 \frac{\Phi}{\Lambda} \Big] X &= 0. \end{split}$$

With some efforts, it can be shown that in the $\gamma \to 0$ limit this expression reduces to the Newcomb equation (see (D.6)).

References

- J. P. Freidberg, **Ideal MHD**, Cambridge University Press (Cambridge, UK), 2014.
- K. Hain and R. Lüst, Z. Naturforsch. A 13, 936 (1958).
- W. M. Manheimer and C. Lashmore-Davies, MHD Instabilities in Simple Plasma Configuration (Accession Number: ADA144936), Naval Research Laboratory (Washington DC, US), 1984.
- K. Miyamoto, Fundamentals of Plasma Physics and Controlled Fusion, Iwanami Book Service Center (Tokyo, JP), 1997.
- W. A. Newcomb, Ann. Phys. 10, 232 (1960).

In **cylindrical geometry** the physical poloidal field B_p is related to B^θ through the relation

$$B_p = \frac{\boldsymbol{B} \cdot \boldsymbol{\nabla} \theta}{|\boldsymbol{\nabla} \theta|}.$$

Similar relations can be obtained for B_{θ} and the toroidal projections.

Е

External kinks in a cylinder with a resistive wall

From the analysis of external kink modes presented in chapter 10, we saw that stability can be improved by surrounding the plasma with an ideally conducting wall. Better stability properties are indeed achieved because magnetic diffusion in the vacuum is avoided, and flux compression prevents the development of the instability. If the wall has a finite amount of resistivity, however, the magnetic field can diffuse through the wall, and an external instability can develop.

We shall now discuss briefly the dynamics of external kink modes allowing for wall resistivity. Let us consider a **cylindrical plasma column** of radius a surrounded by a resistive wall at distance b > a. We employ cylindrical coordinates (r, ϑ, ϕ) with associated metric tensor coefficients $g_{rr} = 1$, $g_{\vartheta\vartheta} = r^2$, $g_{\phi\phi} = R_0^2$, $g_{r\vartheta} = g_{r\phi} = 0$ and $\sqrt{g} = rR_0$. As in chapter 10, the vacuum magnetic perturbation is written as $\widetilde{\boldsymbol{B}} = \nabla \chi$, with χ obeying (10.3). Similar to Eq. (10.1), we expand χ in a Fourier series to give for the mth harmonic

$$(r\chi'_m)' - \frac{m^2}{r} \left(1 + \frac{n^2 r^2}{m^2 R_0^2}\right) \chi_m = 0,$$

where $m \sim 1$ and the prime denotes, as usual, the radial derivative. Imposing the radial component of the magnetic field to vanish at infinity, the solution of the equation above is written as

$$\chi_{m} = \begin{cases} c_{1}K_{m}\left(\frac{nr}{R_{0}}\right) + c_{2}I_{m}\left(\frac{nr}{R_{0}}\right), & a < r < b, \\ c_{3}K_{m}\left(\frac{nr}{R_{0}}\right), & r > b, \end{cases}$$
 (E.1)

We use the relations

$$\begin{split} I_m'(r) &= \frac{1}{2} \left(I_{m+1}(r) + I_{m-1}(r) \right), \\ K_m'(r) &= -\frac{1}{2} \left(K_{m+1}(r) + K_{m-1}(r) \right), \end{split}$$

noticing that for large r one has $I_m(r) \sim e^r/\sqrt{r}$ and $K_m(r) \sim e^{-r}/\sqrt{r}$.

¹ That is $\tilde{B}^{\phi} \to 0$. In fact, the toroidal projection of the vacuum field $\tilde{B} = \nabla \chi$ is ε^2 smaller compared to the radial and poloidal ones. This ordering is assumed to hold within the wall as well.

It is easy to see that $\sqrt{g}\tilde{B}_m^r$ must be continuous across the wall (cf. 8.2.3).

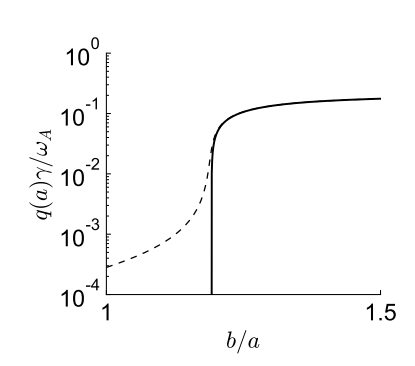


Figure E.1: Growth rate of the m=2=n=1 mode vs ideal (solid line) and resistive (dashed line) wall position for a current profile of the form $R_0^2 J^\phi/B_0 = \frac{2}{q_0}(1-(r/a)^2)$ with q(a)=1.8 (q(0)=q(a)/2). We used the parameters $\eta_w=5\times 10^{-7}\Omega m$ (of the order of the electrical resistivity of stainless steel) with $\omega_A=10^6 s^{-1}$, a=1m and d/a=0.01.

where I_m and K_m are the modified Bessel functions of the first and second kind, and c_i (i = 1, 2, 3) some constants.

Inside the wall one has $\boldsymbol{E} = \eta_w \boldsymbol{J}$ where η_w , the characteristic wall resistivity, is constant. Using Faraday's law one obtains $\partial \boldsymbol{B}/\partial t = -\eta_w \nabla \times \boldsymbol{J}$. It is customary to neglect the toroidal component of the perturbed magnetic field, so that from the divergence-free condition of \boldsymbol{B} one has $\tilde{B}_m^{\vartheta} = -\frac{1}{imr}(r\tilde{B}_m^r)'$. Hence, we obtain

$$\frac{\partial \sqrt{g}\tilde{B}^{r}}{\partial t} = -\eta_{w} \left(\frac{\partial R_{0}^{2} \tilde{J}^{\phi}}{\partial \vartheta} - \frac{\partial r^{2} \tilde{J}^{\vartheta}}{\partial \phi} \right) = \eta \left[\frac{1}{r} \frac{d}{dr} \left(r \frac{d(\sqrt{g}\tilde{B}_{m}^{r})}{dr} \right) - \frac{m^{2}}{r^{2}} \sqrt{g}\tilde{B}_{m}^{r} \right]. \tag{E.2}$$

We now deploy the **thin wall approximation**: the wall is assumed to have thickness $d \ll b$ such that $r(\tilde{B}_m^r)' \sim \tilde{B}_m^r b/d \gg \tilde{B}_m^r$. Now, taking the time dependence of the perturbation of the form $\exp(\gamma t)$, equation (E.2) can be simplified as follows:

$$\gamma \tau_w \tilde{B}_m^r = b^2 (\tilde{B}_m^r)^{\prime\prime},$$

with $\tau_w = \frac{b^2 \mu_0}{\eta_w}$ denoting a **characteristic diffusion time**. By integrating this equation across the wall, one gets

$$\gamma \tau_w d\tilde{B}_m^r(b) = b^2 \llbracket (\tilde{B}_m^r)' \rrbracket_b,$$

where $[\![(\cdot)]\!]_b = (\cdot)_{b+\epsilon} - (\cdot)_{b-\epsilon}$ with $\epsilon \to 0$. Using this result and the fact that $\tilde{B}_m^r = \chi_m'$, from (E.1) we have

$$\tilde{B}_{m}^{r} = C \times \begin{cases} \frac{K'_{m} \left(\frac{nr}{R_{0}}\right) + c_{2}/c_{1}I'_{m} \left(\frac{nr}{R_{0}}\right)}{K'_{m} \left(\frac{nb}{R_{0}}\right) + c_{2}/c_{1}I'_{m} \left(\frac{nb}{R_{0}}\right)}, & a < r < b, \\ \frac{K'_{m} \left(\frac{nr}{R_{0}}\right)}{K'_{m} \left(\frac{nb}{R_{0}}\right)}, & r > b, \end{cases}$$
(E.3)

where C is a generic constant and

$$\frac{c_2}{c_1} = \frac{[K_m'(z)]^2 \gamma \tau_w d/b^2}{I_m'(z) K_m''(z) - K_m'(z) I_m''(z) - K_m'(z) I_m'(z) \gamma \tau_w d/b^2},$$

with $z = nb/R_0$ (recall that the radial derivative is with respect to the variable r not z).

For $z \ll 1$ and m integer, one has $K_m(z) \approx \frac{(m-1)!}{2} (z/2)^{-m}$ and $I_m(z) \approx \frac{1}{m!} (z/2)^m$, so that

$$I'_m(z)K''_m(z) - K'_m(z)I''_m(z) \approx m^2/b^3, \quad K'_m(z)I'_m(z) \approx -m/(2b^2).$$

Therefore, it follows that

$$\frac{c_2}{c_1} \approx \frac{[2^{m-1}(m-1)!z^{-m}]^2 \gamma \tau_w d/b}{1 + \gamma \tau_w d/(2mb)}.$$

Plugging this into (E.3) gives

$$ilde{B}_m^r \sim r^{-m-1} \left[1 - rac{\gamma au_w d/(2mb)}{1 + \gamma au_w d/(2mb)} \left(rac{r}{b}
ight)^{2m}
ight],$$

which reduces to (10.5) for $\tau_w \to \infty$ (ideal wall). Let us call

$$D = \frac{\gamma \tau_w d/(2mb)}{1 + \gamma \tau_w d/(2mb)}.$$
 (E.4)

Note that D < 1 for $\gamma > 0$. We consider cases with γ real. Hence, introducing the fictitious vacuum displacement ξ_v as in §10.1 (the same notation is used), it easily follows that (cf. (10.12))

$$\frac{r\xi_v'}{\xi_v}\Big|_{a+\epsilon} = \frac{2m}{m - nq(a)} - \frac{m+1 + (m-1)D(a/b)^{2m}}{1 - D(a/b)^{2m}}.$$
 (E.5)

The last term on the right-hand-side of (E.5) is always negative for D < 1, so that by comparing it with (10.11) we infer that also in the case of a resistive wall surrounding the plasma the equilibrium can be unstable to an external kink perturbation of helicity (m, n) only if q(a) < m/n, that is if (10.13) is fulfilled.

Solving (10.9) yields the stability boundary and the growth rates, the former obtained by setting D=0 (i.e. $\gamma\to 0$). From (E.5), it is immediate to verify that **the marginal boundary is independent of** b. In fact, this stability boundary coincides with the one obtained for a cylinder surrounded by an ideally conducting wall in the limit $a/b\to 0$, i.e. wall far from the plasma (**no-wall limit**). This means that if the plasma is no-wall external-kink unstable, a resistive wall does not suppress the instability, though it can reduce considerably the growth rate (see Fig. E.1).

The growth rate can be computed analytically for flat current and mass density profiles both vanishing for a < r < b. Following the procedure outlined in §10.1, and using $a\frac{d\xi_m^r/dr}{\xi_m^r}\Big|_{a=\epsilon} = m-1$, by means of (10.9) we obtain a cubic equation for γ

$$\frac{\gamma^2}{\omega_A^2} = 2\left(\frac{m}{q(a)} - n\right)^2 \left[\frac{1}{m - nq(a)} - \frac{1}{1 - D(a/b)^{2m}}\right],$$
 (E.6)

where D depends upon the growth rate according to (E.4). The numerical solution of the dispersion relation Eq. (10.9) with (10.12) replaced by (E.5) is show in figure E.2, and confirms the necessity of condition (10.13) to be fulfilled for stability.

References

 M. Abramowitz and I. A. Stegun (eds.), Handbook of Mathematical Functions, Dover Publications (New York, US), 1964. One can introduce a typical wall diffusion time defined as $\hat{\tau}_w = \mu_0 db/\eta_w$.

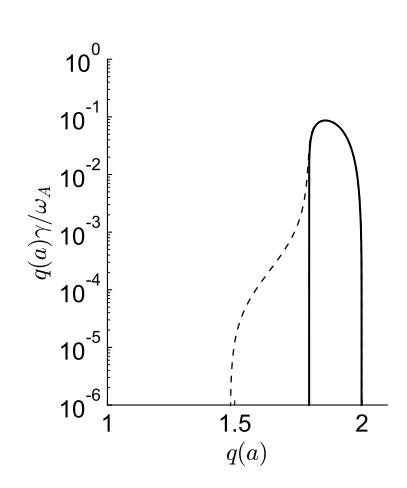


Figure E.2: Growth rate of the m=2=n=1 mode for an ideal (thick solid line) and resistive (thin dashed line) wall at position b/a=1.2. The current profile and other parameters are as in Fig. E.1. The mode is stable in the limit of $a/b \rightarrow 0$ (no wall) for $q(a) \approx 1.482$.

- C. G. Gimblett, Nucl. Fusion 26, 617 (1986).
- K. Miyamoto, Plasma Physics for Controlled Fusion, Science and Culture Publishing (Tokyo, JP), 2012.
- L. E. Zakharov and S. V. Putvinskii, Fiz. Plazmy **13**, 118 (1987) [Sov. J. Plasma Phys. **13**, 68 (1987)].

F

A more general derivation of the resistive layer equations

In chapter 17 we carried out the resistive layer analysis for a circular tokamak through a double expansion in two smallness parameters retaining toroidicity effects to second order in the inverse aspect ratio. Here, the derivation of the resistive layer equations is generalised for the case of a generic axisymmetric configuration fully retaining curvature effects.

Our starting point is the set of equations (13.1)-(13.5) and (13.8). Next, we deploy the following orderings (cf. (17.1), (17.3) and (17.4))

$$\frac{\tilde{p}}{p_0} \sim \frac{\xi^r}{r}, \quad \frac{\gamma}{\omega_A} \sim \delta, \quad r \frac{\partial A_0}{\partial r} \sim A_0, \quad r \frac{\partial \tilde{A}}{\partial r} \sim \frac{\tilde{A}}{\delta}, \quad \frac{r - r_s}{r_s} = x \sim \delta, \\
\frac{\eta_0}{r_s^2 \gamma} \sim \delta^2, \quad \xi^{\vartheta} \sim \xi^{\phi} \sim \frac{\xi^r}{r \delta}, \quad \sqrt{g} \tilde{B}^{\vartheta} \sim \sqrt{g} \tilde{B}^{\phi} \sim \frac{\sqrt{g} \tilde{B}^r}{r \delta} \sim B_0 \xi^r,$$
(F.1)

where the subscript 0 and a tilde denote equilibrium and perturbed quantities respectively, and δ is a small parameter. As usual, r_s denotes the radius at which $q(r_s) = m/n$.

As in §17.1, perturbations are decomposed into a resonant and non-resonant part so that the action of the parallel gradient is given by (17.9). Recalling that $\tilde{p} = -p_0'\xi^r + \Delta p$, equation (13.8) yields

$$\rho_0 \gamma^2 \sqrt{g} \mathbf{B}_0 \cdot \boldsymbol{\xi} = -\sqrt{g} \tilde{\mathbf{B}}^r \boldsymbol{p}_0' - f_0' \left[i(m\mu - n) \tilde{\boldsymbol{p}} + e^{im\vartheta - in\phi} \mu \frac{\partial \tilde{\boldsymbol{p}}_{NR}}{\partial \vartheta} \right].$$

Since $(m\mu - n) \approx -nsx \sim \delta$, we immediately have $\tilde{p}_{NR} \sim \delta \tilde{p}_m$. From this, similar to (17.10), the leading order contribution to (13.4) is

$$\mu \frac{\partial}{\partial \vartheta} (\sqrt{g} \tilde{J}^{\phi})_{\rm NR} + \tilde{p}'_m \frac{\partial}{\partial \vartheta} \left(\frac{1}{B_0^{\phi}} \right) = 0.$$

Contrary to the analysis of chapter 17, here just a single expansion in the layer parameter δ will be performed. We also recall that this is a local analysis, hence equilibrium quantities are assumed to be evaluated at the resonance position, i.e. at r_s .

Recall that $\langle A_{NR} \rangle = 0$.

The equation above can be easily integrated to give

$$(\sqrt{g}\tilde{J}^{\phi})_{\rm NR} = -q\left(\frac{1}{B_0^{\phi}} - \langle \frac{1}{B_0^{\phi}} \rangle\right)\tilde{p}_m'. \tag{F.2}$$

Let us now write the perturbed toroidal current as

$$\sqrt{g}\tilde{J}^{\phi} = \frac{\partial}{\partial r} \left(N e^{im\vartheta - in\phi} [(\sqrt{g}\tilde{B}^{\vartheta})_m + (\sqrt{g}\tilde{B}^{\vartheta})_{NR}] \right), \tag{F.3}$$

from which (note that to dominant orders radial derivatives actually act on the perturbation)

$$(\sqrt{g}\,\tilde{J}^{\phi})_{m} = \langle N \rangle (\sqrt{g}\,\tilde{B}^{\vartheta})_{m}' + \langle N(\sqrt{g}\,\tilde{B}^{\vartheta})_{NR}' \rangle.$$

Therefore, by means of (F.2), one can write

$$\begin{split} N[(\sqrt{g}\tilde{B}^{\vartheta})'_{m} + (\sqrt{g}\tilde{B}^{\vartheta})'_{\mathrm{NR}}] \\ &= \langle N \rangle (\sqrt{g}\tilde{B}^{\vartheta})'_{m} + \langle N (\sqrt{g}\tilde{B}^{\vartheta})'_{\mathrm{NR}} \rangle - q \Big(\frac{1}{B_{0}^{\phi}} - \langle \frac{1}{B_{0}^{\phi}} \rangle \Big) \tilde{p}'_{m}. \end{split}$$

If we divide by N and average in ϑ , an equation for $\langle N(\sqrt{g}\tilde{B}^{\vartheta})'_{\rm NR}\rangle$ is obtained. Eventually, this leads to

$$\sqrt{g}\tilde{J}^{\phi} = \frac{e^{im\vartheta - in\phi}}{\langle 1/N \rangle} \left[(\sqrt{g}\tilde{B}^{\vartheta})'_m + q \left(\langle \frac{1}{NB_0^{\phi}} \rangle - \langle \frac{1}{N} \rangle \frac{1}{B_0^{\phi}} \right) \tilde{p}'_m \right]. \tag{F.4}$$

A comparison with (F.3) easily yields

$$(\sqrt{g}\tilde{B}^{\vartheta})_{NR} = \left(\frac{1/N}{\langle 1/N \rangle} - 1\right)(\sqrt{g}\tilde{B}^{\vartheta})_{m} + q\frac{1/N}{\langle 1/N \rangle} \left(\left\langle \frac{1}{NB_{0}^{\varphi}} \right\rangle - \left\langle \frac{1}{N} \right\rangle \frac{1}{B_{0}^{\varphi}} \right) \tilde{p}_{m} + C(\vartheta), \tag{F.5}$$

where $C(\vartheta)$ is a periodic function of ϑ with vanishing poloidal average.

Furthermore, because of the smallness of \tilde{p}_{NR} , from (13.3) we find that

$$G\frac{\partial}{\partial \vartheta}(\sqrt{g}\tilde{B}^{\phi}) = -e^{im\vartheta - in\phi} \left(\frac{im}{B_0^{\phi}} \tilde{p}_m + inN[(\sqrt{g}\tilde{B}^{\vartheta})_m + (\sqrt{g}\tilde{B}^{\vartheta})_{NR}] \right).$$

Plugging (F.5) into the expression above produces

$$\left(G + \frac{\mu^2}{\langle 1/N \rangle}\right) (\sqrt{g}\tilde{B}^{\phi})_m = \frac{\mu(\sqrt{g}\tilde{B}^r)'_m}{i\,m\langle 1/N \rangle} - \frac{\langle 1/(NB_0^{\phi})\rangle}{\langle 1/N \rangle}\tilde{p}_m - \mu\langle NC(\vartheta)\rangle, \quad (F.6)$$

where the last term on the right-hand-side has to be considered as a constant. One then has

$$(\sqrt{g}\tilde{B}^{\vartheta})_{m} + (\sqrt{g}\tilde{B}^{\vartheta})_{NR} = \frac{G/N}{\langle G/N \rangle + \mu^{2}} \left[-\frac{1}{im} (\sqrt{g}\tilde{B}^{r})'_{m} + q \left(\left\langle \frac{1}{NB_{0}^{\phi}} \right\rangle - \left\langle \frac{1}{N} \right\rangle \frac{1}{B_{0}^{\phi}} - \frac{\mu^{2}}{GB_{0}^{\phi}} \right) \tilde{p}_{m} + \frac{\langle G/N \rangle + \mu^{2}}{G/N} C(\vartheta) - \mu^{2} \frac{\langle NC(\vartheta) \rangle}{G} \right].$$
(F.7)

The divergence-free condition of \boldsymbol{B} implies (cf. (7.25))

$$\begin{split} (\sqrt{g}\tilde{B}^{\theta})_{m} &= -\frac{1}{im}(\sqrt{g}\tilde{B}^{r})'_{m} + \frac{n}{m}(\sqrt{g}\tilde{B}^{\phi})_{m}, \\ &\frac{\partial}{\partial r}(\sqrt{g}\tilde{B}^{r})_{\mathrm{NR}} + \left(im + \frac{\partial}{\partial \theta}\right)(\sqrt{g}\tilde{B}^{\theta})_{\mathrm{NR}} \\ &- in(\sqrt{g}\tilde{B}^{\phi})_{\mathrm{NR}} = 0. \quad (\bigstar) \end{split}$$

Hence, allowing for (F.3) the relation above yields

$$(\sqrt{g}\tilde{f}^{\phi})_{m} = -\frac{G}{\langle G/N \rangle + \mu^{2}} \frac{(\sqrt{g}\tilde{B}^{r})_{m}^{\prime\prime}}{im} + q \left(\frac{G\langle \frac{1}{NB_{0}^{\phi}} \rangle}{\langle G/N \rangle + \mu^{2}} - \langle \frac{1}{B_{0}^{\phi}} \rangle \right) \tilde{p}_{m}^{\prime}. \quad (F.8)$$

Finally, if we use (17.10) and (17.11) into (17.15) we see that $(\sqrt{g}\tilde{B}^{\phi})'_{m\pm\ell}=0$, thus suggesting

$$(\sqrt{g}\tilde{B}^{\phi})_{NR} = D(\vartheta), \tag{F.9}$$

having used (17.7) with D some function of the poloidal angle.

Now, we want to express $(\sqrt{g}\tilde{B}^r)_m$ as a function of ξ_m^r and \tilde{p}_m . To achieve our purpose, we shall take the contravariant radial projection of the induction equation which is (17.31). If one considers the dominant contributions, it is easy to see that $\xi_{NR}^r \sim \delta \xi_m^r$. Therefore, we employ (F.8) to work out the resonant component of (17.31) giving

$$\begin{split} &\left[1 - \frac{\eta_0 G\langle N \rangle}{\gamma} \left(\frac{G/\langle N \rangle + \mu^2}{\langle G/N \rangle + \mu^2}\right) \frac{d^2}{dr^2}\right] (\sqrt{g} \tilde{B}^r)_m = i f_0' (m\mu - n) \xi_m^r \\ &- i m q \frac{\eta_0 G\langle N \rangle}{\gamma} \left(\langle \frac{1}{N B_0^{\phi}} \rangle \frac{G/\langle N \rangle + \mu^2}{\langle G/N \rangle + \mu^2} - \frac{1}{\langle N \rangle} \langle \frac{1}{B_0^{\phi}} \rangle \right) \tilde{p}_m'. \end{split} \tag{F.10}$$

To close the system, it is now necessary to determine the equations for the resonant radial fluid displacement and perturbed pressure.

Staring with the expressions for the poloidal and toroidal fluid displacements, these are obtained from the contravariant poloidal and toroidal projections of the induction equation (13.5) which, to the accuracy we need, read $(i=\vartheta,\phi)$

$$\left(1 - \frac{\eta_0 GN}{\gamma} \frac{\partial^2}{\partial r^2}\right) (\sqrt{g}\tilde{B}^i) = \sqrt{g} \boldsymbol{B}_0 \cdot \nabla \xi^i - \sqrt{g} \nabla \cdot (\boldsymbol{\xi} \boldsymbol{B}_0^i).$$
(F.11)

Because of the ordering of the perturbed pressure (see (F.1)) it follows that $\nabla \cdot \boldsymbol{\xi} \sim 1$, therefore to leading order equations (F.11) give

$$\mu \partial_{\vartheta} \xi_{\mathrm{NR}}^{\phi} = \partial_{\vartheta} \xi_{\mathrm{NR}}^{\vartheta} = \sqrt{g} \Big(\xi_{m}^{\vartheta} + \xi_{\mathrm{NR}}^{\vartheta} \Big) \partial_{\vartheta} (1/\sqrt{g}),$$

whose solution is given by Eq. (17.22) that is

$$\mu \xi_{\rm NR}^{\phi} = \xi_{\rm NR}^{\theta} = \left(\frac{1/\sqrt{g}}{\langle 1/\sqrt{g} \rangle} - 1\right) \xi_{m}^{\theta}. \tag{F.12}$$

One also finds that Eq. (F.11) with $i=\phi$, can be written as (13.19) showing that to leading order in δ we have (cf. (17.19))

$$\xi_m^{\vartheta} = \mu \xi_m^{\phi} - \frac{1}{im} \frac{d\xi_m^r}{dr}.$$
 (F.13)

Repeating the calculations of section 17.2.2 shows that ξ_m^{ϕ} is given by equation (17.24), thus determining completely ξ_m^{ϑ} which is

$$\xi_{m}^{\vartheta} = -\frac{\langle 1/\sqrt{g} \rangle}{G + \mu^{2} \langle N \rangle} \times \left[\frac{\langle R^{2} \rangle}{im} \frac{d\xi_{m}^{r}}{dr} + \mu \frac{R_{0}^{2}/B_{0}^{2}}{\gamma^{2}/\omega_{A}^{2}} \left(i(m\mu - n) \tilde{p}_{m} + \frac{p_{0}'}{f_{0}'} (\sqrt{g} \tilde{B}^{r})_{m} \right) \right]. \tag{F.14}$$

The result is exact to leading order in δ . For $(\sqrt{g}\tilde{B}^{\phi})_0$ we use the same arguments discussed at the end of section 17.2.1.

¹ Notice that $\sqrt{g} \tilde{J}^{\phi} = (N \sqrt{g} \tilde{B}^{\vartheta})'$.

² Recall that $\Delta p = -\Gamma p_0 \nabla \cdot \boldsymbol{\xi}$.

We now seek the equation for ξ_m^r . In analogy with section 17.3.2, the resonant part of the vorticity equation reads

$$\begin{split} &\frac{\rho_{0}\gamma^{2}}{f_{0}^{\prime}}\left\langle gN(\xi_{m}^{\vartheta}+\xi_{\mathrm{NR}}^{\vartheta})\right\rangle^{\prime}=i(m\mu-n)(\sqrt{g}\tilde{J}^{\phi})_{m}+\left\langle (\sqrt{g}\tilde{B}^{\vartheta})_{\mathrm{NR}}\frac{\partial}{\partial\vartheta}\left(\frac{J_{0}^{\phi}}{B_{0}^{\phi}}\right)\right\rangle \\ &-\left[\frac{\sqrt{g}}{f_{0}^{\prime}}\left(J_{0}^{\vartheta}\frac{\partial}{\partial\vartheta}+J_{0}^{\phi}\frac{\partial}{\partial\varphi}\right)(\sqrt{g}\tilde{B}^{\phi})\right]_{m}-im\left\langle \frac{1}{B_{0}^{\phi}}\right\rangle^{\prime}\tilde{p}_{m}+\left\langle \tilde{p}_{\mathrm{NR}}^{\prime}\frac{\partial}{\partial\vartheta}\left(\frac{1}{B_{0}^{\phi}}\right)\right\rangle. \end{split} \tag{F.15}$$

Using (F.6) and (F.9), one can verify that the term proportional to the toroidal magnetic field gives to leading order in δ

$$\left[\sqrt{g}\left(J_{0}^{\vartheta}\frac{\partial}{\partial\vartheta}+J_{0}^{\phi}\frac{\partial}{\partial\phi}\right)(\sqrt{g}\tilde{B}^{\phi})\right]_{m}^{\prime}=\frac{\mu p_{0}^{\prime}\langle1/B_{0}^{\phi}\rangle}{\langle G/N\rangle+\mu^{2}}\left((\sqrt{g}\tilde{B}^{r})_{m}^{\prime}-imq\langle\frac{1}{NB_{0}^{\phi}}\rangle\tilde{p}_{m}\right)^{\prime}.\tag{F.16}$$

It is easily recognised that the second term on the right-hand-side of (F.15) can be recast as

$$\left\langle (\sqrt{g}\tilde{B}^{\vartheta})_{\rm NR} \frac{\partial}{\partial \vartheta} \left(\frac{J_0^{\phi}}{B_0^{\phi}} \right) \right\rangle = q \frac{p_0'}{f_0'} \left\langle \frac{1}{B_0^{\phi}} \frac{\partial}{\partial \vartheta} (\sqrt{g}\tilde{B}^{\vartheta})_{\rm NR} \right\rangle. \tag{F.17}$$

Thanks to (17.25), the contribution due to the non-resonant perturbed pressure becomes (use (\bigstar))

$$\left\langle \tilde{p}_{NR}^{\prime} \frac{\partial}{\partial \vartheta} \left(\frac{1}{B_{0}^{\phi}} \right) \right\rangle^{\prime} = q \frac{\rho_{0} \gamma^{2}}{f_{0}^{\prime}} \left\langle \frac{1}{B_{0}^{\phi}} (\sqrt{g} \boldsymbol{B}_{0} \cdot \boldsymbol{\xi})_{NR}^{\prime} \right\rangle^{\prime}$$
$$- q \frac{p_{0}^{\prime}}{f_{0}^{\prime}} \left\langle \frac{1}{B_{0}^{\phi}} \left(i m (\sqrt{g} \tilde{B}^{\vartheta})_{NR} + \frac{\partial}{\partial \vartheta} (\sqrt{g} \tilde{B}^{\vartheta})_{NR} \right) \right\rangle^{\prime}, \tag{F.18}$$

where in the last averaged term it is only necessary to compute the first contribution which, by means of (F.7), reads

$$\begin{split} \left\langle \frac{(\sqrt{g}\tilde{B}^{\vartheta})_{\mathrm{NR}}}{B_{0}^{\phi}} \right\rangle' &= -\frac{G}{\langle G/N \rangle + \mu^{2}} \Big(\langle \frac{1}{NB_{0}^{\phi}} \rangle - \langle \frac{1}{B_{0}^{\phi}} \rangle \langle \frac{1}{N} \rangle \Big) \frac{(\sqrt{g}\tilde{B}^{r})_{m}^{\prime\prime}}{im} \\ &+ q \Big(\frac{\langle G/(NB_{0}^{\phi}) \rangle + \mu^{2} \langle 1/B_{0}^{\phi} \rangle}{\langle G/N \rangle + \mu^{2}} \langle \frac{1}{NB_{0}^{\phi}} \rangle - \langle \frac{1}{N(B_{0}^{\phi})^{2}} \rangle \Big) \tilde{p}_{m}^{\prime}. \end{split} \tag{F.19}$$

Now, making use of (17.23) and (F.13) shows that

$$\frac{1}{f_0'}(\sqrt{g}\boldsymbol{B}_0\cdot\boldsymbol{\xi})_{\rm NR} = \frac{q}{i\,m}\left(R^2 - \langle R^2\rangle\right)\frac{d\xi_m^r}{dr} + \mu\frac{N - \langle N\rangle}{\langle 1/\sqrt{g}\rangle}\xi_m^{\vartheta}$$

which then allows us to simplify the inertial contributions appearing in (F.15) as follows

$$\begin{split} \frac{\rho_{0}\gamma^{2}}{f_{0}^{\prime}} \left[\frac{\langle \sqrt{g}N \rangle}{\langle 1/\sqrt{g} \rangle} \xi_{m}^{\vartheta} - \left\langle \frac{(\sqrt{g}\mathbf{B}_{0} \cdot \boldsymbol{\xi})_{\text{NR}}}{\mu B_{0}^{\vartheta}} \right\rangle \right]^{\prime} &= q^{2} \frac{\rho_{0}\gamma^{2}}{imf_{0}^{\prime}} \left[\frac{\langle R^{2} \rangle^{2}}{G + \mu^{2} \langle N \rangle} - \frac{\langle R^{4} \rangle}{G} \right] \frac{d^{2}\xi_{m}^{r}}{dr^{2}} \\ &- \frac{\mu \langle 1/B_{0}^{\vartheta} \rangle}{G/\langle N \rangle + \mu^{2}} \left(i(m\mu - n) \tilde{p}_{m} + \frac{p_{0}^{\prime}}{f_{0}^{\prime}} (\sqrt{g}\tilde{B}^{r})_{m} \right)^{\prime}. \end{split} \tag{F.20}$$

The following equilibrium relations prove to be very useful

$$\begin{split} &\langle \frac{1}{B_0^\phi} \rangle p_0' = \langle \sqrt{g} \, J_0^\vartheta \rangle - \mu \langle \sqrt{g} \, J_0^\phi \rangle, \\ &\frac{\partial}{\partial \vartheta} \Big(\frac{J_0^\phi}{B_0^\phi} \Big) = - q \, \frac{p_0'}{f_0'} \, \frac{\partial}{\partial \vartheta} \Big(\frac{1}{B_0^\phi} \Big). \end{split}$$

$$\langle gN(\xi_m^{\vartheta} + \xi_{NR}^{\vartheta}) \rangle = \frac{\langle \sqrt{g}N \rangle}{\langle 1/\sqrt{g} \rangle} \xi_m^{\vartheta}$$

Thence, by collating (F.8) and (F.16)-(F.20), the vorticity equation (F.15) can be eventually rearranged in the following form

$$\begin{split} q^2 \frac{\rho_0 \gamma^2}{i m f_0'} \Big[\frac{\langle R^2 \rangle^2}{G + \mu^2 \langle N \rangle} - \frac{\langle R^4 \rangle}{G} \Big] \frac{d^2 \xi_m^r}{dr^2} &= -\frac{G(m \mu - n)/m}{G/\langle N \rangle + \mu^2} \times \\ \times \Big[\frac{G/\langle N \rangle + \mu^2}{\langle G/N \rangle + \mu^2} (\sqrt{g} \tilde{B}^r)_m'' - i m q \Big(\langle \frac{1}{N B_0^{\phi}} \rangle \frac{G/\langle N \rangle + \mu^2}{\langle G/N \rangle + \mu^2} - \frac{1}{\langle N \rangle} \langle \frac{1}{B_0^{\phi}} \rangle \Big) \tilde{p}_m' \Big] \\ &+ q \frac{p_0'}{f_0'} \frac{G}{G/\langle N \rangle + \mu^2} \Big(\langle \frac{1}{N B_0^{\phi}} \rangle \frac{G/\langle N \rangle + \mu^2}{\langle G/N \rangle + \mu^2} - \frac{1}{\langle N \rangle} \langle \frac{1}{B_0^{\phi}} \rangle \Big) (\sqrt{g} \tilde{B}^r)_m' \\ &+ i m \Big(\frac{\mu \mu' \langle 1/B_0^{\phi} \rangle}{G/\langle N \rangle + \mu^2} - \langle \frac{1}{B_0^{\phi}} \rangle' - q^2 \frac{p_0'}{f_0'} \Big(\frac{G\langle \frac{1}{N B_0^{\phi}} \rangle^2}{\langle G/N \rangle + \mu^2} - \langle \frac{1}{N \langle B_0^{\phi}} \rangle \Big) \Big) \tilde{p}_m + \Theta, \end{split}$$
(F.21)

where Θ is some constant.

It only remains to provide an expression for the resonant perturbed pressure. Let us write (F.11) as (cf. (13.19))

$$\Pi^{\vartheta} \equiv \left(1 - \frac{\eta_{0}GN}{\gamma} \frac{\partial^{2}}{\partial r^{2}}\right) \frac{\sqrt{g}\tilde{B}^{\vartheta}}{\psi'_{0}} = -\left(\frac{1}{\psi'_{0}} \frac{\partial(\psi'_{0}\xi^{r})}{\partial r} - q \frac{\partial}{\partial \phi} \left(\xi^{\vartheta} - \mu \xi^{\phi}\right)\right), \tag{F.22}$$

$$\Pi^{\phi} \equiv \left(1 - \frac{\eta_{0}GN}{\gamma} \frac{\partial^{2}}{\partial r^{2}}\right) \frac{\sqrt{g}\tilde{B}^{\phi}}{f'_{0}} = -\left(\frac{1}{f'_{0}} \frac{\partial(f'_{0}\xi^{r})}{\partial r} + \frac{\partial}{\partial \vartheta} \left(\xi^{\vartheta} - \mu \xi^{\phi}\right)\right). \tag{F.23}$$

From (F.12), i.e. (17.22), it is obvious that $(\xi^{\theta} - \mu \xi^{\phi})_{NR} \sim \xi_m^r/r$, hence if we subtract the non-resonant parts of (F.22) and (F.23) it easily follows that to the relevant orders

$$\frac{\partial}{\partial \theta} (\xi_{NR}^{\theta} - \mu \xi_{NR}^{\phi}) = \Pi_{NR}^{\theta} - \Pi_{NR}^{\phi}. \tag{F.24}$$

When the non-resonant contribution of (F.23) is plugged into (17.21),³ by multiplying by \sqrt{g} and averaging in ϑ , we immediately obtain (cf. (17.28) and (17.29))

$$\begin{split} \langle \sqrt{g} \Pi_{\mathrm{NR}}^{\phi} \rangle = & i (m \mu - n) \langle \sqrt{g} \xi_{\mathrm{NR}}^{\phi} \rangle + \left(\langle \frac{\partial \sqrt{g}}{\partial r} \rangle - \langle \sqrt{g} \rangle \langle \frac{1}{\sqrt{g}} \frac{\partial \sqrt{g}}{\partial r} \rangle \right) \xi_{m}^{r} \\ & - \langle \sqrt{g} \frac{\partial}{\partial \vartheta} \left(\xi_{\mathrm{NR}}^{\vartheta} - \mu \xi_{\mathrm{NR}}^{\phi} \right) \rangle - \langle \sqrt{g} \rangle \langle \frac{\partial \sqrt{g}}{\partial \vartheta} \frac{\xi_{\mathrm{NR}}^{\vartheta}}{\sqrt{g}} \rangle. \end{split}$$

It therefore follows that by making use of (F.24) one has

$$\langle \frac{\partial \sqrt{g}}{\partial \vartheta} \frac{\xi_{\mathrm{NR}}^{\vartheta}}{\sqrt{g}} \rangle = i(m\mu - n) \frac{\langle \sqrt{g} \xi_{\mathrm{NR}}^{\varphi} \rangle}{\langle \sqrt{g} \rangle} + \left(\frac{\langle \sqrt{g} \rangle'}{\langle \sqrt{g} \rangle} - \langle \frac{1}{\sqrt{g}} \frac{\partial \sqrt{g}}{\partial r} \rangle \right) \xi_{m}^{r} - \frac{\langle \sqrt{g} \Pi_{\mathrm{NR}}^{\vartheta} \rangle}{\langle \sqrt{g} \rangle}.$$

Thus, if we plug the quantity above into (17.27) and deploy the definition of perturbed pressure, by means of the resonant contribution of

³ Explicitly, (F.23) yields

$$\begin{split} \frac{\partial \xi_m^r}{\partial r} + i m (\xi_m^\vartheta - \mu \xi_m^\phi) \\ + \frac{f_0^{\prime\prime}}{f_0^\prime} \xi_m^r &= -\Pi_m^\phi, \\ \frac{\partial \xi_{\mathrm{NR}}^r}{\partial r} + i m (\xi_{\mathrm{NR}}^\vartheta - \mu \xi_{\mathrm{NR}}^\phi) \\ + \frac{\partial}{\partial \vartheta} (\xi_{\mathrm{NR}}^\vartheta - \mu \xi_{\mathrm{NR}}^\phi) &= -\Pi_{\mathrm{NR}}^\phi \end{split}$$

Equation (F.22) can be arranged similarly.

(F.23) we eventually obtain

$$\begin{split} -\frac{\tilde{p}_{m} + p_{0}' \xi_{m}^{r}}{\Gamma p_{0}} &= (\nabla \cdot \xi)_{m} = \left(\frac{\langle \sqrt{g} \rangle'}{\langle \sqrt{g} \rangle} - \frac{f_{0}''}{f_{0}'}\right) \xi_{m}^{r} \\ &+ i(m\mu - n) \left(\xi_{m}^{\phi} + \frac{\langle \sqrt{g} \xi_{NR}^{\phi} \rangle}{\langle \sqrt{g} \rangle}\right) - \left(\Pi_{m}^{\phi} + \frac{\langle \sqrt{g} \Pi_{NR}^{\vartheta} \rangle}{\langle \sqrt{g} \rangle}\right). \end{split}$$

Here we list some useful relations:

$$\begin{split} \Pi_{\mathrm{NR}}^{\vartheta} &= \frac{(\sqrt{g}\tilde{B}^{\vartheta})_{\mathrm{NR}}}{\psi_0'} - \frac{\eta_0 G}{\gamma \psi_0'} \frac{\partial}{\partial r} (\sqrt{g}\tilde{J}^{\phi})_{\mathrm{NR}}, \\ \Pi_m^{\phi} &= \left(1 - \frac{\eta_0 G \langle N \rangle}{\gamma} \frac{d^2}{dr^2}\right) \frac{(\sqrt{g}\tilde{B}^{\phi})_m}{f_0'}, \\ \frac{f_0''}{f_0'} &= \frac{\langle \sqrt{g} \rangle'}{\langle \sqrt{g} \rangle} - \frac{\langle 1/B_0^{\phi} \rangle'}{\langle 1/B_0^{\phi} \rangle'}, \\ \langle \frac{1}{(B_0^{\phi})^2} \rangle &= \frac{\langle R^4 \rangle}{(Gf_0')^2}, \quad \langle \frac{1}{B_0^{\phi}} \rangle^2 = \frac{\langle R^2 \rangle^2}{(Gf_0')^2}, \\ \frac{R_0^2/B_0^2}{\gamma^2/\omega_4^2} &= \frac{1}{\rho_0 \gamma^2}. \end{split}$$

Using (F.10) to express $[(m\mu - n)\xi_m^r]'$, by means of (F.2), (F.6), (F.13), (F.14) and (F.19), after some manipulations it can be shown that the equation above can be finally arranged as

$$\begin{split} &-\frac{\tilde{p}_{m}+p_{0}'\xi_{m}^{r}}{\Gamma p_{0}}=\frac{qG/\langle 1/B_{0}^{\phi}\rangle}{G/\langle N\rangle+\mu^{2}}\Big[\langle \frac{1}{NB_{0}^{\phi}}\rangle \frac{G/\langle N\rangle+\mu^{2}}{\langle G/N\rangle+\mu^{2}}-\frac{1}{\langle N\rangle}\langle \frac{1}{B_{0}^{\phi}}\rangle \Big]\frac{(\sqrt{g}\tilde{B}^{r})_{m}'}{imf_{0}'}\\ &-\left(\frac{q}{f_{0}'}\right)^{2}\frac{\eta_{0}G}{\gamma\langle R^{2}\rangle}\Big[\frac{\langle R^{4}\rangle}{G}-\frac{\langle R^{2}\rangle^{2}}{G+\mu^{2}\langle N\rangle}\Big]\tilde{p}_{m}''-\frac{ip_{0}'}{f_{0}'\rho_{0}\gamma^{2}}\frac{(m\mu-n)(\sqrt{g}\tilde{B}^{r})_{m}}{\langle \sqrt{g}\rangle(G+\mu^{2}\langle N\rangle)}\\ &+\frac{(m\mu-n)^{2}}{\langle \sqrt{g}\rangle(G+\mu^{2}\langle N\rangle)}\frac{R_{0}^{2}/B_{0}^{2}}{\gamma^{2}/\omega_{A}^{2}}\tilde{p}_{m}+\Big[\frac{\langle 1/B_{0}^{\phi}\rangle'}{\langle 1/B_{0}^{\phi}\rangle}-\frac{\mu\mu'\langle N\rangle}{G+\mu^{2}\langle N\rangle}\Big]\xi_{m}^{r}\\ &-\frac{q^{2}}{\langle \sqrt{g}\rangle}\Big(\frac{G\langle 1/(NB_{0}^{\phi})\rangle^{2}}{\langle G/N\rangle+\mu^{2}}-\langle \frac{1}{N(B_{0}^{\phi})^{2}}\rangle\Big)\tilde{p}_{m}+\Sigma, \end{split} \tag{F.25}$$

where Σ is another constant whose value is not important.

In conclusion, the resistive layer dynamics is determined by the closed system of equations represented by (F.10), (F.21) and (F.25). These reduce to (17.30), (17.35) and (17.42) in the limit of a thin tokamak (see next section).

Recovering the GGJ equations

For completeness, we shall show that the layer equations that we have just derived are equivalent to those of Glasser (1975). We first define the quantities

$$\begin{split} &\Lambda_* = q^2 \left[\frac{\langle R^4 \rangle}{G} - \frac{\langle R^2 \rangle^2}{G + \mu^2 \langle N \rangle} \right], \quad \zeta = G \langle N \rangle \frac{G / \langle N \rangle + \mu^2}{\langle G / N \rangle + \mu^2}, \quad \eta_R = \eta_0 \zeta, \\ &Q_0 = \left[\frac{s^2 m^2 (f_0')^2 \eta_R}{q^2 r_s^2 (G + \mu^2 \langle N \rangle)} \frac{\zeta}{\rho_0 \Lambda_*} \right]^{1/3}, \quad \Psi_0 = \frac{q^2 r_s^2 Q_0^2 (G + \mu^2 \langle N \rangle)^{1/2}}{s^2 m^2 (f_0')^2 \eta_R} \sqrt{\frac{\rho_0 \Lambda_*}{\zeta}}, \end{split}$$

and then we multiply the induction, vorticity and pressure equations by the following factors:

$$\frac{\Psi_0}{i} \times (\text{F.10}), \quad \frac{ir_s^2 q^2}{\zeta} \left(\frac{G + \mu^2 \langle N \rangle}{ms^2 f_0'} \right) \times (\text{F.21}), \quad \frac{(f_0')^2 \zeta \langle \sqrt{g} \rangle}{p_0' \Lambda_*} \times (\text{F.25}).$$

Therefore, upon introducing the variables

$$\begin{split} Q &= \gamma/Q_0, \quad \Xi = \xi_m^r, \quad \Psi = \frac{\Psi_0}{i} (\sqrt{g} \tilde{B}^r)_m, \quad \Upsilon = -\tilde{p}_m/p_0', \\ X &= \frac{f_0'(m\mu - n)}{Q_0(G + \mu^2 \langle N \rangle)^{1/2}} \sqrt{\frac{\zeta}{\rho_0 \Lambda_*}}, \end{split}$$

after some tedious algebra the resistive equations can be presented in the form chosen by Glasser (1975) which is

$$\begin{split} &\frac{d^2\Psi}{dX^2}-H\frac{d\Upsilon}{dX}=Q(\Psi-X\Xi),\\ &Q^2\frac{d^2\Xi}{dX^2}-QX^2\Xi+QX\Psi+H\frac{d\Psi}{dX}+(E+F)\Upsilon+\hat{\Theta}=0,\\ &\frac{1}{Q}\frac{d^2\Upsilon}{dX^2}-\frac{X^2}{Q^2}\Upsilon-G_*\Upsilon+(G_*-KE)\Xi+\frac{X}{Q^2}\Psi-K\left(H\frac{d\Psi}{dX}+F\Upsilon\right)+\hat{\Sigma}=0, \end{split}$$

where $\hat{\Theta}$ and $\hat{\Sigma}$ are some rescaled constants and the parameters E, F, G_* , H and K are defined as⁴

$$\begin{split} E &= \frac{q^2 r_s^2 p_0'}{s^2 f_0' \zeta} (G + \mu^2 \langle N \rangle) \left(\frac{\mu \mu' \langle 1/B_0^{\phi} \rangle}{G/\langle N \rangle + \mu^2} - \left\langle \frac{1}{B_0^{\phi}} \right\rangle' \right), \\ F &= \frac{q^4 r_s^2}{s^2 \zeta} \left(\frac{p_0'}{f_0'} \right)^2 (G + \mu^2 \langle N \rangle) \left(\langle \frac{1}{N(B_0^{\phi})^2} \rangle - \frac{G \langle 1/(NB_0^{\phi}) \rangle^2}{\langle G/N \rangle + \mu^2} \right), \\ G_* &= \frac{(f_0')^2 \zeta \langle \sqrt{g} \rangle}{\Gamma p_0 \Lambda_*}, \quad H &= \frac{q^2 r_s p_0'}{s f_0'} \left(\langle \frac{1}{NB_0^{\phi}} \rangle - \frac{1}{\langle N \rangle} \langle \frac{1}{B_0^{\phi}} \rangle \frac{\langle G/N \rangle + \mu^2}{G/\langle N \rangle + \mu^2} \right), \\ K &= \left(\frac{s \zeta (f_0')^2}{q r_s p_0'} \right)^2 \left[\Lambda_* (G + \mu^2 \langle N \rangle) \right]^{-1}. \end{split}$$

Letting V(r) be the volume enclosed by the surface labelled by r, we have $V(r) - V(r_s) = V'(r_s)(r - r_s) = 4\pi^2 \langle \sqrt{g} \rangle (r - r_s)$, so that our radial variable X can be written as

$$X = -\frac{V(r) - V(r_s)}{X_0}, \quad X_0 = 4\pi^2 \langle \sqrt{g} \rangle \frac{r_s Q_0}{ns f_0'} (G + \mu^2 \langle N \rangle)^{1/2} \sqrt{\frac{\rho_0 \Lambda_*}{\zeta}}.$$

Thus, compared to Glasser (1975), we have flipped the sign of X and Ψ . The large aspect ratio limiting expressions of some of the quantities listed above, upon using the metric coefficients presented in §5.3, read

$$\begin{split} \Lambda_* &\simeq r_s^3 R_0 (1+2q^2), \quad Q_0 \simeq \left(\frac{(snB_0)^2 \eta_0}{(r_s R_0)^2 \rho_0 (1+2q^2)} \right)^{1/3}, \\ X_0 &\simeq 4\pi^2 \frac{(R_0 r_s)^{4/3} \eta_0^{1/3}}{(snB_0)^{1/3}} [\rho_0 (1+2q^2)]^{1/6}, \\ E &\simeq \frac{2q^2 r_s p_0'}{s^2 B_0^2} \left[1 - \frac{1}{q^2} + s \frac{R_0}{r_s} \Delta' - \frac{R_0^2 p_0' q^2}{r_s B_0^2} \left(1 + \frac{1}{2q^2} \right) \right], \\ F &\simeq 2 \frac{(R_0 p_0' q^2)^2}{s^2 B_0^4} \left(1 + \frac{1}{2q^2} \right), \quad G_* &\simeq \frac{B_0^2}{\Gamma p_0 (1+2q^2)}, \\ H &\simeq -\frac{2q^2 R_0 p_0'}{s B_0^2} \Delta', \quad K &\simeq \frac{s^2 B_0^4}{(q R_0 p_0')^2} \Big/ (1+2q^2). \end{split}$$

⁴ The Mercier criterion for stability is written as

$$D_I \equiv E + F + H - \frac{1}{4} < 0,$$

whereas resistive interchange modes are stable if

$$D_R \equiv E + F + H^2 < 0.$$

These criteria assess stability of each flux surface against such localised perturbations.

Notice that $(m\mu - n) = -nsx$ and $V(r) = 2\pi \int_0^r dr \int_0^{2\pi} d\theta \sqrt{g}$.

To facilitate the comparison with Glasser (1976), we recall that from (4.26) and (4.34) one has

$$R_0 \Delta' \frac{r^3}{q^2} = \int_0^r \left(\frac{r^3}{q^2} - 2 \frac{r^2 R_0^2 p_0'}{B_0^2} \right) dr.$$

References

- B. Coppi et al., Nucl. Fusion 6, 101 (1966).
- A. H. Glasser et al., Phys. Fluids 18, 875 (1975).
- A. H. Glasser et~al., Phys. Fluids ${f 19}$, 567~(1976).
- $\bullet\,$ J. L. Johnson and J. M. Greene, Plasma Phys. 9, 611 (1967).
- S. E. Kruger *et al.*, Phys. Plasmas **5**, 4169 (1998).

Symbols

Here we provide a list of commonly used symbols. For some of these quantities, the page where their definition can be found is also indicated.

Physical constants

k_B	Boltzmann constant
$oldsymbol{arepsilon}_0$	vacuum permittivity
μ_0	vacuum permeability
e	proton charge

Special functions

opecial functions	
Γ	Gamma function
Ψ	Digamma function
K	complete elliptic integral of first kind
E	complete elliptic integral of second kind
$_2F_1$	hypergeometric function
U	(Kummer's) confluent hypergeometric function
M	(Tricomi's) confluent hypergeometric function
$I_{ u}$	modified Bessel function of first kind
$K_{ u}$	modified Bessel function of second kind
H	Heaviside step function

Geometry

Geometry	
(R, Z, ϕ)	cylindrical coordinate system
	(right handed, ϕ clockwise from above)
(r, θ, ϕ)	toroidal coordinate system (right handed,
	θ counterclockwise in the poloidal plane, ϕ clockwise from above)
(r,ϑ,ϕ)	straightened toroidal coordinate system (right handed,
	ϑ counterclockwise in the poloidal plane, ϕ clockwise from above)
r	radial variable, 32
heta	generic poloidal angle, 32
ϑ	rectified poloidal angle, 55
ϕ	geometric toroidal angle, 32
\sqrt{g}	Jacobian, 24, 38
a	minor radius, 38
R_0	major radius, 27, 37
arepsilon	inverse aspect ratio, 39
Δ	Shafranov shift, 38

Operations

$\overline{(\cdot)}$	complex conjugation
$\llbracket \cdot rbracket$	jump across a point, 106
$' \equiv \frac{d}{dr}$ or $\frac{\partial}{\partial r}$	radial derivative, 40
$\langle \cdot \rangle$	poloidal average, 61
~	similar order indicator, 30

Other quantities

```
mass density
ρ
T
                        temperature
                        pressure
þ
                        resistivity
η
                        toroidal rotation
\Omega
\boldsymbol{B}
                        magnetic field
\boldsymbol{B}
                        modulus of the magnetic field
                        modulus of the magnetic field on the magnetic axis, 34
B_0
                        covariant toroidal magnetic field, 32
F
ψ
                        poloidal flux, 33
Φ
                        toroidal flux, 33
                        radial derivative of the toroidal flux, 82
                        safety factor, 34, 56
q
                        rotational transform, 93
μ
                        ratio of kinetc over magnetic pressure, 34, 43
β
                        magnetic shear, 42
s
                        ballooning parameter 45
\alpha
\mathcal{S}
                        Lundquist number, 179
                        Mach number, 52
M
                        Larmor radius, 6
r_L
                        cyclotron frequency (species s), 18
\Omega_s
                        Alfvén frequency, 84
\omega_A
                        growth rate, 73
r_s (or r_m)
                        resonance of the mode (m, n), 76
                         "wave vector" of the mode (m, n), 93
k_{||}
```

Summary table for internal ideal MHD

gradient and magnetic shear ratio, and the poloidal mode number. It is implicit that for large scale perturbations (m \sim 1), α and s have to be considered as global parameters, while for Summary of the expected character of internal ideal perturbations depending on pressure short wavelength modes they take their associated local value. In this report we did not discuss high- β tokamak global instabilities.

	m = 1	$m\gtrsim 1$	$m\gg 1$
$\alpha/s^2 \sim \varepsilon$	internal kink		
$\alpha/s^2 \sim 1/\varepsilon$	infernal	nal	Mercier
$\alpha/s^2 \sim 1$	high-β tokama	nigh-β tokamak global modes	ballooning

Index

∇B drift, 7	contravariant, 24	bi-Maxwellian, 266
1.1 (1	basis, 25, 32	Maxwellian, 18
adiabatic index, 13	components of the metric tensor,	dominant mode, 83
Alfvén	24	double tearing mode, 200
eigenmodes, 79	convective derivative, 13	
frequency, 84	convolution, 77	$E \times B$ drift, 7
speed, 84	theorem, 209	Edge Localised Mode, 217
time, 179	coordinate lines, 24	Edge Localised Modes (ELMs), 69,
wave, 179	coordinates	156, 172
Alfvénic timescales, 133, 139	curvilinear, 23	eigenmode equations, 79
anomalous resistivity, 17	orthogonal cylindrical, 26	eigenvalue, 73, 80
asymptotic matching, 102	orthogonal toroidal, 27	electric permittivity, 175
auxiliary field, 191	Coulomb	elliptic integral, 51
average binding energy, 3	gauge, 271	first kind, 259
averaging method, 165	logarithm, 175	second kind, 261
ballooning	covariant, 24	energy confinement time, 4
equation, 160	basis, 25, 32	energy conservation, 269
equation, 100 equation in Fourier space, 164	components of the metric tensor,	energy principle, 74, 176
	24	equilibrium
generalised equation, 162	crash, 205	β limit, 43, 51
limit, 217	current	stable, 69
modes, 155	channel, 137, 194	static, 31, 70, 80
parameter, 45 banana orbits, 260	driven instability, 133	unstable, 69
,	hole, 41	error function, 209
basis function, 201	loop, 51	Euler's formula, 164
Bessel function, 150, 151, 282 Boltzmann	curvature, 36	external kink, 133
	effects, 233	, 30
constant, 13, 175, 266	radius, 27, 42	fast-growing modes, 84
kinetic equation, 12	vector, 270	field line bending, 75, 76, 119
boundary conditions, 72, 81, 106	curvature drift, 8	first stability region, 171, 225
Bussac stability criterion, 113	cyclotron frequency, 258	FLR model, 19
Cartesian coordinate, 24	ion, 18	fluid
Cauchy	cylindrical	displacement, 70, 80
argument principle, 251	approximation, 27	flute instabilities, 143
initial value problem, 198	coordinates, 32, 36	flux
Christoffel symbols, 26	geometry, 27	compression, 48, 281
classical tearing modes, 190	geometry, 27	conservation, 190
closure, 12	Debye length, 13	freezing, 14, 175
fluid, 13	Deuterium, 4	label, 32
cofactor, 24	diagonal unit tensor, 16	surface, 32
collision time, 18	diffusion	tube, 189
complex conjugation, 73	equation, 178	flux conserving tokamak, 43
compressibility, 81	time, 178, 282	force balance, 31, 39, 41
confinement	Digamma function, 152	force operator, 176
inertial, 5	Dirac-delta, 106, 125, 138	Fourier
magnetic, 5	dispersion relation, 120	harmonics, 75
confluent hypergeometric function,	disruption, 69, 133, 189	inverse, 183
184, 228, 247	distribution function, 11	inversion theorem, 164
104, 220, 24/	distribution function, 11	I mversion encorem, 104

projection, 77	internal inductance, 43	contribution, 221
series, 75	internal kink, 96, 99, 119, 205, 278	correction, 162, 225
space, 163, 221	internal mode, 99	modes, 143
transform, 163	inverse aspect ratio, 39	stability criterion, 149
frozen-in theorem, 14, 76, 175	iron core, 7	metric coefficients, 61
functional, 169	isobars, 32	metric tensor, 24
fusion ashes, 69	isothermal flux surface, 52, 70	MHD
rusion asies, og	isotropic plasma, 269	ideal equations, 13
Galilean transformations, 71, 271	isotropic plasma, 209	ideal model, 13
Gamma function, 152, 184, 229	Jacobian, 24	conservation laws, 14
Gaussian pillbox, 71	Jucobian, 2 4	drift model, 18, 19
GGJ equations, 234, 244, 290	kinetic	force operator, 71
global modes, 82	energy, 257	model, 11
Grad-Shafranov equation, 31, 36	pressure, 13, 71	resistive equations, 17
growth rate, 73	Kruskal-Shafranov criterion, 138	resistive model, 17
guiding centre, 6, 257	Kummer's equation, 228	minor radius, 38
GCP model, 20	1 1 1 1 1 1 1 1 1 1 1 1 1 1 1 1 1 1 1 1	mirror
GCP model, 18	L-H transition, 156	criterion, 6
gyro-phase angle, 20	Laplace transform, 72	field, 6
gyro-radius, 6, 18	large aspect ratio, 39	mode coupling, 78, 85
5/10 144145, 0, 10	Larmor radius, 6, 258, 260	mode locking, 189
H-mode, 156, 217	Lawson criterion, 4	modified tearing instability criterion,
Hain-Lüst equation, 278, 280	layer ordering, 88, 92	225, 252
heating	Levi-Civita symbol, 26	momentum equation, 14, 176
neutral beam injection (NBI), 9	linearisation, 70	monochromatic, 78, 83
radio-frequency (RF), 9	linearised MHD equations, 80	multi-fluid equations, 12
Heaviside step function, 138, 167	localised modes, 82	muti naid equations, 12
helical	logarithmic jump, 192	neoclassical tearing modes, 190
coordinate, 191	Lorentz transformation, 71	Newcomb equation, 95, 275
field, 257	low-field-side, 7, 155	no-wall limit, 138, 283
flux, 190	low-shear region, 119	non-linearity, 70
helicity, 75	lower sideband, 104, 121	non-monotonic, 128
high-field-side, 7, 155	Lundquist number, 179, 183, 246	normal mode analysis, 72, 176
high-pressure plasma, 114		Nyquist, 196, 202, 251
high-shear region, 119	m = 1 reconnecting mode, 209	
hollow safety factor, 115	m = 1 resistive mode, 206	Ohm's law, 17
hoop force, 43, 44	Mach number, 52	Ohmic heating, 8
hybrid scenarios, 115	magnetic	orbit theory, 5
hypergeometric	axis, 32, 189	outer region, 218
differential equation, 150	bottle, 5	
function, 51, 151	diffusion, 175, 281	parallel gradient, 75
	flux, 8, 190, 209	parity, 156
ideal region, 179, 218	islands, 17, 175, 189	particle
ignition, 4	mirror, 5	confinement, 257
induction equation, 17, 177	moment, 6, 20, 257, 263	loss cones, 6
inertia, 95	pressure, 34, 71	passing, 258
enhancement, 102, 182	reconnection, 17	trajectory, 257
inertial	separatrix, 191	trapped, 258
contribution, 95	shear, 76	pitch
layer, 88, 101	surface, 31, 32	angle, 55
infernal modes, 119	topology, 175, 189, 209	field line, 55
instability	magnetic islands, 189	plasma, 4
ideal, 69	magneticshear, 42	current, 8
resistive, 69	main mode, 83	frequency, 13
integral approach, 169	major radius, 27, 37, 275	rotation, 52
interchange	marginal stability boundary, 18, 73	plasma β , 34
modes, 143	Mathieu functions, 169	plasma-vacuum boundary, 71
parity, 152	Mercier	poloidal

plasma β , 43	satellite harmonics, 79, 83	thin wall appro
average, 61	sawtooth oscillation, 99, 205	tokamak, 3
field, 8	Schrödinger equation, 166	toroidal
field coils, 7	Schwarz inequality, 149	(ring) functi
flux, 33	screw-pinch, 41, 79, 275	coupling, 78
mode number, 75	second stability region, 171, 225	flux, 33
spectrum, 75, 83	self-adjoint operator, 73, 169	magnetic fiel
Poynting vector, 15	separatrix, 43	mode numbe
pre-Maxwell equations, 13	Shafranov shift, 31, 38	toroidal
precession, 261	shaping parameters, 38	field coils, 7
precursor phase, 205	shooting method, 198	transit time, 25
	sidebands, 79, 83	translational in
quantum number, 77, 83	slow-growing modes, 84	transport barri
quasi-interchange, 120	small scale modes, 84	edge (ETB),
roding oo	small-scale modes, 82	internal (ITI
radius, 32 reconnection	solenoid, 7	trial function,
complete, 205	Solov'ev equilibrium, 31, 36	Tritium, 4
incomplete, 205	sound speed, 87	twisting parity,
rectified poloidal angle, 55	spectrum, 73	type-III ELMs,
rectifying parameter, 60	Spitzer model, 17, 175	tyre tube force,
residue theorem, 117	stability equations, 79	
resistance, 8	stellarator, 6	upper sideband
resistive	stochastic, 189	
instability, 175	straight field line coordinate system,	vacuum perme
mode, 175	56, 79	variational prin
resistive ballooning modes, 217	Sturm-Liouville, 94	vertical field, 9
averaged equation, 224	surface current, 48, 71	Vlasov equation volume average
resistive interchange modes, 143, 217	Suydam	_
resistive internal kink, 208	modes, 143	vorticity equati
resistive layer, 179, 233, 244	stability criterion, 149	wall
resistivity, 8, 17		diffusion tim
resonance, 76	tearing	ideal, 43, 71
resonant surface, 76	equation, 190, 193	resistive, 71,
reversed field pinch, 6	instability criterion, 196	resistivity, 28
Reynolds number, 179	mode, 190	wave vector, 76
rotational transform, 93	parity, 152	parallel, 93
200000000000000000000000000000000000000	stability index, 192, 199	WKB approxin
$s - \alpha$ equilibrium model, 46, 64, 160	tearing modes, 248	
safety factor, 31, 34, 56	thermal velocity, 13	X-point, 43, 51

```
pproximation, 282
inctions, 49
g, 78
c field, 7
ımber, 75
ls, 7
e, 259
al invariance, 163, 221
arrier, 155
ΤΒ), 156
(ITB), 155
on, 169
rity, 1<u>5</u>2
LMs, 217
orce, 43, 44
band, 104, 121
rmeability, 13
principle, 170
ld, 9, 43, 49, 51
nation, 12, 20
erage, 34
quation, 81, 176
time, 283
3, 71, 133, 193, 198
71, 281
y, 282
r, 76
93
roximation, 194
```